BENTHIC HABITATS OF THE EXTENDED FAIAL ISLAND SHELF AND THEIR RELATIONSHIP TO GEOLOGIC, OCEANOGRAPHIC AND INFRALITTORAL BIOLOGIC FEATURES

Fernando Tempera

A Thesis Submitted for the Degree of PhD at the University of St. Andrews

2009

BENTHIC HABITATS OF THE EXTENDED FAIAL ISLAND SHELF AND THEIR RELATIONSHIP TO GEOLOGIC, OCEANOGRAPHIC AND INFRALITTORAL BIOLOGIC FEATURES

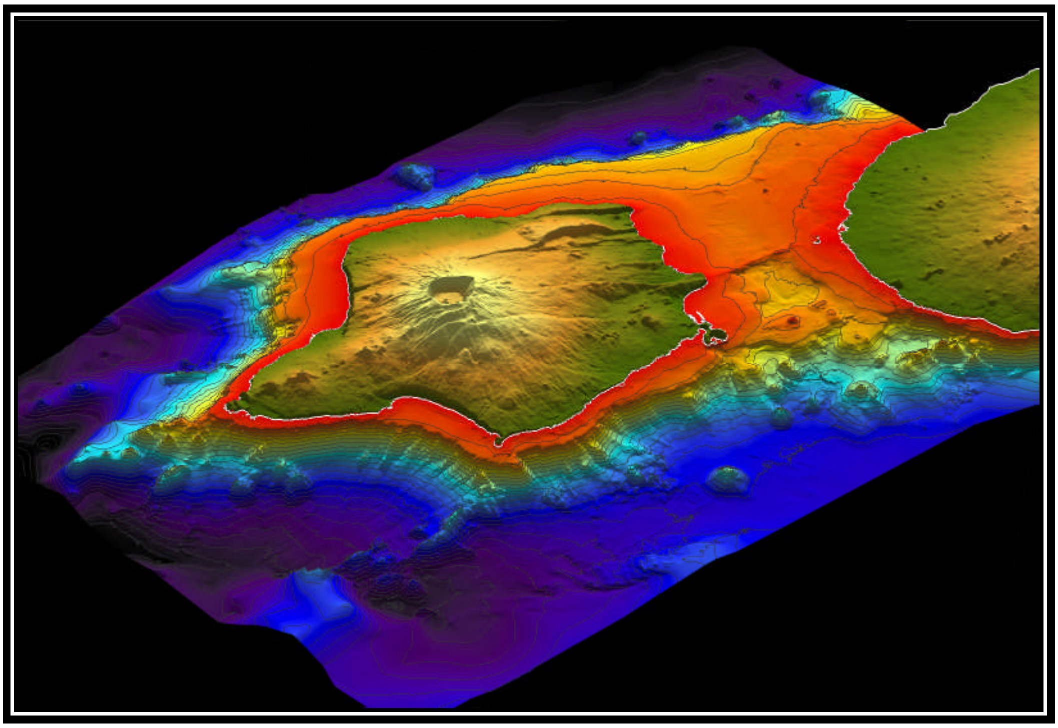

FERNANDO TEMPERA

A THESIS SUBMITTED FOR THE DEGREE OF DOCTOR OF PHILOSOPHY

SCHOOL OF GEOGRAPHY AND GEOSCIENCES

University of St Andrews

OCTOBER 2008

FUNDING DECLARATION

The Foundation for Science and Technology funded this work by means of a PhD grant (ref. SFRH/BD/12885/2003).

FCT
Fundação para a Ciência e a Tecnologia
MINISTÉRIO DA CIÊNCIA E DO ENSINO SUPERIOR

Ciência.Inovação 2010
Programa Operacional Ciência e Inovação 2010
MINISTÉRIO DA CIÊNCIA, TECNOLOGIA E ENSINO SUPERIOR

EUROPEAN UNION/UNIÃO EUROPEIA
STRUCTURAL FUNDS/FUNDOS ESTRUTURAIS

GOVERNO DA REPÚBLICA PORTUGUESA

"Tudo no mundo está dando resposta, o que demora é o tempo das perguntas."
José Saramago *in Memorial do Convento*

(Everything in the world is offering answers, it is questioning that takes time.)

Abstract

This thesis presents a new template for multidisciplinary habitat mapping that combines the analyses of seafloor geomorphology, oceanographic proxies and modelling of associated biologic features.

High resolution swath bathymetry of the Faial and western Pico shelves is used to present the first state-of-the-art geomorphologic assessment of submerged island shelves in the Azores. Solid seafloor structures are described in previously unreported detail together with associated volcanic, tectonic and erosion processes.

The large sedimentary expanses identified in the area are also investigated and the large bedforms identified are discussed in view of new data on the local hydrodynamic conditions. Coarse-sediment zones of types hitherto unreported for volcanic island shelves are described using swath data and *in situ* imagery together with sub-bottom profiles and grainsize information. The hydrodynamic and geological processes producing these features are discussed.

New oceanographic information extracted from satellite imagery is presented including yearly and seasonal sea surface temperature and chlorophyll-*a* concentration fields. These are used as proxies to understand the spatio-temporal variability of water temperature and primary productivity in the immediate island vicinity. The patterns observed are discussed, including onshore-offshore gradients and the prevalence of colder/more productive waters in the Faial-Pico passage and shelf areas in general. Furthermore, oceanographic proxies for swell exposure and tidal currents are derived from GIS analyses and shallow-water hydrographic modelling.

Finally, environmental variables that potentially regulate the distribution of benthic organisms (seafloor nature, depth, slope, sea surface temperature, chlorophyll-*a* concentration, swell exposure and maximum tidal currents) are brought together and used to develop innovative statistical models of the distribution of six macroalgae *taxa* dominant in the infralittoral (articulated Corallinaceae, *Codium elisabethae*, *Dictyota* spp., *Halopteris filicina*, *Padina pavonica* and *Zonaria tournefortii*). Predictive distributions of these macroalgae are spatialized around Faial island using ordered logistic regression equations and raster fields of the explanatory variables found to be statistically significant.

This new approach represents a potentially highly significant step forward in modelling benthic communities not only in the Azores but also in other oceanic island shelves where the management of benthic species and biotopes is critical to preserve ecosystem health.

PRELIMINARY DECLARATIONS

I, Fernando Nuno Costa Tempera, hereby certify that this thesis, which is approximately 62,000 words in length, has been written by me, that it is the record of work carried out by me and that it has not been submitted in any previous application for a higher degree.

Date Signature of candidate

I was admitted as a research student in October 2003 and as a candidate for the degree of Doctor of Philosophy in October 2004; the higher study for which this is a record was carried out in the University of St Andrews between 2003 and 2008.

Date Signature of candidate

Supervisor Declaration

I hereby certify that the candidate has fulfilled the conditions of the Resolution and Regulations appropriate for the degree of Doctor of Philosophy in the University of St Andrews and that the candidate is qualified to submit this thesis in application for that degree.

Date Signature of supervisor

COPYRIGHT DECLARATION

In submitting this thesis to the University of St Andrews I understand that I am giving permission for it to be made available for use in accordance with the regulations of the University Library for the time being in force, subject to any copyright vested in the work not being affected thereby. I also understand that the title and abstract will be published, and that a copy of the work may be made and supplied to any bona fide library or research worker, that my thesis will be electronically accessible for personal or research use, and that the library has the right to migrate my thesis into new electronic forms as required to ensure continued access to the thesis. I have obtained any third-party copyright permissions that may be required in order to allow such access and migration.

Date Signature of candidate

Acknowledgements

To my family for all their continued motivation.

I am especially grateful to my two supervisors: Dr. Richard Bates and Dr. Ricardo Serrão Santos.

Richard kindly accepted to supervise my work at St Andrews and continually offered me his scientific and personal support as well as critical surveying equipment. His suggestions were always constructive and his comments greatly improved this work. He is particularly acknowledged for allowing me great freedom to pursue my own ideas and in the process learn about so many subjects.

Ricardo provided me with a challenging research environment as well as personal support, work opportunities and logistic means to pursue my research at the Azores. Much of the funding necessary to take the fieldwork ahead originated from research programmes coordinated by him. I also owe Ricardo my uninterrupted integration in ongoing and submitted projects at DOP/UAç.

To Dr. Neil Mitchell for introducing me to the joy of using multibeam technology to image the seafloor, receiving me in Cardiff and providing his experienced input throughout the writing up of the "geomorphology" chapters.

To Ana Meirinho for her kind-hearted support in the run-up to this PhD.

To Ana Wegier for helping keep me sane during the final and hard months of the PhD with her never-ending tenderness.

To Dr. Ana Martins and Miguel Figueiredo for providing the AVHRR and SeaWiFS satellite imagery datasets for the study area.

To Dr. Igor Bashmachnikov for all his suggestions while analysing the results derived from the satellite imagery, summarizing the information available about ocean currents impinging on Faial's vicinity and for sharing current meter data collected by the mid-passage mooring.

To Dr. Rui Quartau for providing complementary data on sediment grainsize, sub-bottom profiles and general discussions on island shelf geology.

To Dr. Jack Jarvis for his support with setting up the current model in TELEMAC and general encouragement.

To Dr. Monique MacKenzie, Dr. Peteke Feijten, Dr. Maarten Van Ham, Filipa Samarra, Dr. David Manley, Dr. Zhiqiang Feng and Dr. Robin Flowerdew for their support with Statistical Modelling techniques and software.

To Dr. Marji Puotinen (University of Wollongong) for her precious collaboration in extracting the fetch data for the vicinity of Faial using her AML™ Arc-Info™ script.

To Pedro Mata and Dr. Fernando Carvalho (Instituto de Meteorologia, Portugal) for kindly providing the swell statistics dataset.

To Clint Blight, Sonja Heinrich, Geert Aarts, Mónica Silva, Louise Cunningham and all the others from SMRU and Gatty Marine Lab for their continued support.

To Frederico Cardigos, Miguel Machete, Pedro Afonso, Carla Gomes, Cláudia Oliveira, Inês Seabra, Telmo Morato, Filipe Porteiro, Ana Colaço and Andreia Henriques for their general encouragement and for keeping me in touch with everything happening in the Azores and particularly at DOP/UAç.

To Meghann Ormond, Ruth Mottram, Philippa Ascough, Henrik Friis, Alix Cage, Jamie McCreath, Xiaoqi Feng, Lixun Liu and all the other postgraduate colleagues I have had the pleasure of sharing postgraduate rooms with.

To Dr. Ruth Robinson for all the general encouragement and challenging GIS enquiries.

To Colin Cameron, Alan Vaughan and Paulo Castro for their help with solving many annoying IT issues.

To Ricardo Medeiros for his permanent availability to help with the collation, digitising and sharing of geographic information where requested and his endurance while managing all the GIS demand throughout my absence from DOP/UAç.

To Jorge Fontes, Vanessa Santos, Jaen Nieto Amat, Ricardo Delgado and Pedro Frade for their help with the dives.

To David Abecasis and Manuela Ramos for their help during the ROV and drop-down camera surveys.

To Maria Carvalho for her patience in obtaining all those papers and general encouragement.

To Mara Schmiing for inspiring my return to the Azores.

To Renato Bettencourt and Norberto Serpa for the resourceful RIBs management and their general support in DOP's diving section.

To all the crew of RVs *Arquipélago* and *Águas Vivas* for their competence and ability in ensuring the survey goals, enjoyable journeys and safe returns to shore.

To Paul Byham and Submetrix for their kind and always helpful support during the surveys using the Swathplus system and subsequent data processing.

To all the various boat skippers from DOP's ribs and rented vessels, namely Filipe Goulart.

To Dr. António Pascoal, Dr. Paulo Oliveira, Dr. Carlos Silvestre, Luís Sebastião and all the others in the ISR team who supported and inspired this work during the missions in the Azores and my visits to Lisbon.

To Dr. Jon Davies, Dr. Craig Brown and Dr. David Connor for helping me identify a supervisor and a university to make my PhD with in the UK.

To Eng. Sónia Santos (DRA-Azores) for the kind loaning a substitute DGPS during the 2004 survey.

To Guilherme Soares (DRRF-Azores) for supplying DGPS post-processing files.

To Thierry Schmitt for all his support during my stay in Cardiff.

To Dermot Goodwill for the PG suite with a great view towards the sunset.

To all the general office, scientific staff and students both at SGG and DOP for being available when help was needed and for maintaining such a supportive environment.

I am grateful to the Portuguese Foundation for Science and Technology (FCT) for awarding me a PhD grant (SFRH/BD/12885/2003).

The field research was funded by the projects:

MARÉ - Integrated Management of Coastal and Marine Areas in the Azores (Life-Nature B4-3200/98/509);

MAROV - Coastal Marine Habitats, Thematic Mapping of the Seabed using GIS, AUV (Autonomous Underwater Vehicles) & ASV (Autonomous Surface Vehicles). (PDCTM/P/MAR/15249/1999);

OGAMP - Management of Marine Protected Areas in Macaronesia (Azores, Canaries and Madeira) (INTERREG IIIb - MAC/4.2/A2 2001);

MARMAC - Knowledge, Promotion and Valorisation for a Sustainable Use of Marine Protected Areas in Macaronesia (INTERREG IIIb - 03/MAC/4.2/A2 2004);

MAYA - Development of a Miniaturized Autonomous Underwater Vehicle for Habitat Mapping (AdI/POSI/2003);

GEMAS – Assessment, Management and Monitoring of Underwater Sands around the islands of Faial, Pico and São Miguel (DROTRH contract);

MARINOVA - Marine Aquaculture and Artificial Reefs: New models of integrated production (INTERREG IIIb - MAC/4.2/M11).

Fieldwork in the no-go zone of Monte da Guia marine protected area was conducted under license of the Environment Directorate of the Regional Government of the Azores.

The use of the subaerial topographic data produced by the Instituto Geográfico do Exército (IGeoE) was conceded by the Environment Directorate of the Regional Government of the Azores in the scope of project MARÉ (Life-Nature B4-3200/98/509).

Last but not least, thanks to all of those I surely forgot to mention above.

TABLES OF CONTENTS

CHAPTER 1 - GENERAL INTRODUCTION

CHAPTER 2 - AZORES GEOLOGICAL FRAMEWORK

CHAPTER 3 - SEAFLOOR DIVERSITY AND ASSOCIATED PROCESSES ON THE VOLCANIC ISLAND SHELF OF FAIAL ISLAND AND NEIGHBOURING PASSAGE (AZORES, NE ATLANTIC)

Page

CHAPTER 4 - LARGE SEDIMENTARY BEDFORMS AND ASSOCIATED CURRENTS IN THE FAIAL-PICO PASSAGE (AZORES, NE ATLANTIC)

Page

CHAPTER 5 - RIPPLED SCOUR DEPRESSIONS AND SORTED BEDFORMS ON THE VOLCANIC ISLAND SHELF OF FAIAL (AZORES, NE ATLANTIC)

Page

CHAPTER 6 - SPATIAL PATTERNS OF SEA SURFACE TEMPERATURE AND CHLOROPHYLL-*A* AROUND FAIAL ISLAND (AZORES, NE ATLANTIC) FROM SATELLITE IMAGERY

Page

CHAPTER 7 - PREDICTIVE MODELLING OF CHARACTERISTIC ALGAE DISTRIBUTIONS AROUND FAIAL ISLAND AND NEIGHBOURING PASSAGE (AZORES, NE ATLANTIC)

Page

CHAPTER 8 - MAIN CONCLUSIONS

CHAPTER 9 – FINAL DISCUSSION

CHAPTER 10 - FUTURE WORK

APPENDIX I - ESTIMATION OF SWELL EXPOSURE AROUND FAIAL ISLAND

APPENDIX II - SPECIFICATIONS OF THE TIDAL-FORCED SHALLOW-WATER OCEANOGRAPHIC MODEL USED FOR FAIAL ISLAND

Page

APPENDIX III - RELATIONSHIP RETWEEN DEPENDENT AND INDEPENDENT VARIABLES

APPENDIX IV - TRANSFORMATION OF THE EXPLANATORY VARIABLES

INDEX OF FIGURES

CHAPTER 1 - GENERAL INTRODUCTION

CHAPTER 2 - AZORES GEOLOGICAL FRAMEWORK

CHAPTER 3 - SEAFLOOR DIVERSITY AND ASSOCIATED PROCESSES ON THE VOLCANIC ISLAND SHELF OF FAIAL ISLAND AND NEIGHBOURING PASSAGE (AZORES, NE ATLANTIC)

CHAPTER 4 - LARGE SEDIMENTARY BEDFORMS AND ASSOCIATED CURRENTS IN THE FAIAL-PICO PASSAGE (AZORES, NE ATLANTIC)

Page

CHAPTER 5 - RIPPLED SCOUR DEPRESSIONS AND SORTED BEDFORMS ON THE VOLCANIC ISLAND SHELF OF FAIAL (AZORES, NE ATLANTIC)

Page

CHAPTER 6 - SPATIAL PATTERNS OF SEA SURFACE TEMPERATURE AND CHLOROPHYLL-*A* AROUND FAIAL ISLAND (AZORES, NE ATLANTIC) FROM SATELLITE IMAGERY

Page

CHAPTER 7 - PREDICTIVE MODELLING OF CHARACTERISTIC ALGAE DISTRIBUTIONS AROUND FAIAL ISLAND AND NEIGHBOURING PASSAGE (AZORES, NE ATLANTIC)

Page

CHAPTER 8 - MAIN CONCLUSIONS

CHAPTER 9 – FINAL CONCLUSION

CHAPTER 10 - FUTURE WORK

APPENDIX I - ESTIMATION OF SWELL EXPOSURE AROUND FAIAL ISLAND

Page

APPENDIX II - SPECIFICATIONS OF THE TIDAL-FORCED SHALLOW-WATER OCEANOGRAPHIC MODEL USED FOR FAIAL ISLAND

APPENDIX III - RELATIONSHIP RETWEEN DEPENDENT AND INDEPENDENT VARIABLES

APPENDIX IV - TRANSFORMATION OF THE EXPLANATORY VARIABLES

INDEX OF TABLES

CHAPTER 1

1. General introduction

Due to ever increasing anthropogenic activities in coastal areas, impacts on the seafloor demand far more comprehensive assessments of submerged geological features and their associated biological communities than previous studies have undertaken. In the Azores the requests for such information arise mostly from assessments of geological hazards and environmental impacts together with coastal zone management initiatives such as prioritisation of sites for nature conservation and zoning of marine protected areas (MPAs).

Thorough environmental assessments cannot be pursued without high resolution bathymetric information for the vicinity of the islands or seamount tops, where most human activities and impacts are concentrated. However most of the base data for the Azores originate from nautical charts produced by the Portuguese Navy Hydrographic Institute based on single-beam and lead-line surveys often executed several decades ago. The shallow coastal areas in these maps are generally depicted at scales of 1:100,000 to 1:50,000 with only harbour entrances represented in more detail (1:10,000 to 1:5,000). This low sounding resolution and scarcity of information on the nature of the seafloor nature limits the scale at which the submerged island geology and habitats can thereby be resolved. As a result, geological patterns and processes occurring in the immediate island vicinity are very poorly described, inhibiting the reconstruction of how island shelves and flanks evolved and the identification of potential submerged geological hazards.

Recent projects such as MAROV, GEMAS and MAYA have greatly added to the scientific knowledge of some Azores islands through the application of modern hydrographical and geophysical technologies for surveying shallow areas (e.g., pencil beam, side scan and multibeam sonars as well as seismic reflection profilers). In 2003-2004, surveys using multibeam and phase-measuring sonars were conducted around Faial, Pico and São Jorge islands (Mitchell et al., 2003) which provided the first state-of-the-art topographic data on Azores island shelves and slopes. The data collected on Faial's shelf and neighbouring channel to Pico (for the purpose of this thesis designated the "extended Faial shelf") constitute the foundation for this thesis. Analyses presented in the following chapters represent the first comprehensive effort to use high resolution bathymetric and backscatter data to understand the underwater geomorphology of the

Azores islands themselves. Solid seafloor structures associated with volcanic, tectonic and erosion processes are described along with bedforms identified in areas covered by sediment.
The thesis builds on multidisciplinary research and thus attempts to link seafloor mapping from the geologic perspective with issues of benthic ecology.

An overview of the coastal ecology of the Azores has been given by Morton et al. (1998), who review littoral and shallow sublittoral biotopes found in the archipelago based on their own data and previous research. Among the works that inform it is that of Hawkins et al. (1990), who first outlined zonation schemes of intertidal and shallow subtidal assemblages in the Azores. Ever since, other works have been published such as Tittley & Neto (2000) and Wallenstein et al. (2007), which suggest a provisional list of infralittoral algal assemblages.

This thesis is naturally informed by these studies, but a wealth of unpublished species distribution information collated by numerous subtidal surveys executed during projects MARÉ, OGAMP and MARMAC is brought together for the first time. These new datasets, collected using visual surveys of rocky bottom assemblages, provide an exceptional source from which to assess the relationships between benthic species abundances and major environmental parameters known to vary around the coast.

The final chapter of this thesis attempts to provide statistical models based on environmental information produced during the course of this study to derive continuous predictive maps of species distribution at an island scale. A selection of macroalgae that dominate subtidal biotopes is used for this purpose.

2. Objectives

The main focus of the thesis is to present an integrated approach for mapping of underwater geological features and distributions of associated benthic species using a combination of geophysical techniques and *in situ* observations.

Specific objectives include:

- Characterization of the shelf seafloor discriminating between rocky seafloor and sedimentary beds using geophysical surveys;
- Analysis of the geomorphology of solid seafloor areas and their relationship to geologic formation processes;

- Analysis of current-induced sedimentary features;
- Mapping of a series of major environmental factors known to regulate the occurrence and abundance of subtidal macroalgae, including oceanographic parameters;
- Investigation of macroalgae distributions with respect to major environmental variables;
- Production of statistical models of biological distributions in the rocky infralittoral based on major environmental variables and spatial representation of the predictive models obtained;
- Development of an articulated multidisciplinary approach to the exploration and mapping of the seabed for geological and ecological studies.

3. Study area

The area within the archipelago of the Azores that has been chosen for this study is the seafloor immediately surrounding the island of Faial and the neighbouring passage that separates it from the island of Pico. A wide range of environmental conditions are encompassed within this 30km×15km area. The shelf surrounding these islands extends for distances of between 140m and 4km from the shore. The shelf seafloor includes sediments, boulder fields and bedrock expanses with varying degrees of complexity and slope. Exposure to hydrologic forces also varies substantially along the coast with large sections being exposed to the full force of prevailing wind and swells and other areas exhibiting sheltered conditions. This environmental variation results in a diverse set of representative biotopes and species that offer varied technologic and analytic opportunities. The biodiversity of the area is well catalogued and considerable datasets have been accumulating on the spatio-temporal variations in the occurrence and abundance of benthic species.

As a result of this geomorphologic and ecologic variety, the area is of great relevance for nature conservation and is generally accounted as maintaining a good conservation status. Over the last two decades it has received marine conservation classifications that include (i) zones designated under the Azores Network of Protected Areas, (ii) five Special Areas of Conservation (SACs - Natura 2000 network), (iii) one OSPAR marine protected area and (iv) one long-term biodiversity research reference site (project BIOMARE).

4. Organization of the thesis

The thesis is organized as series of chapters of which the analytical ones are presented in a paper format. The content articulation between the different chapters is illustrated in Figure 1 together with information fluxes among chapters.

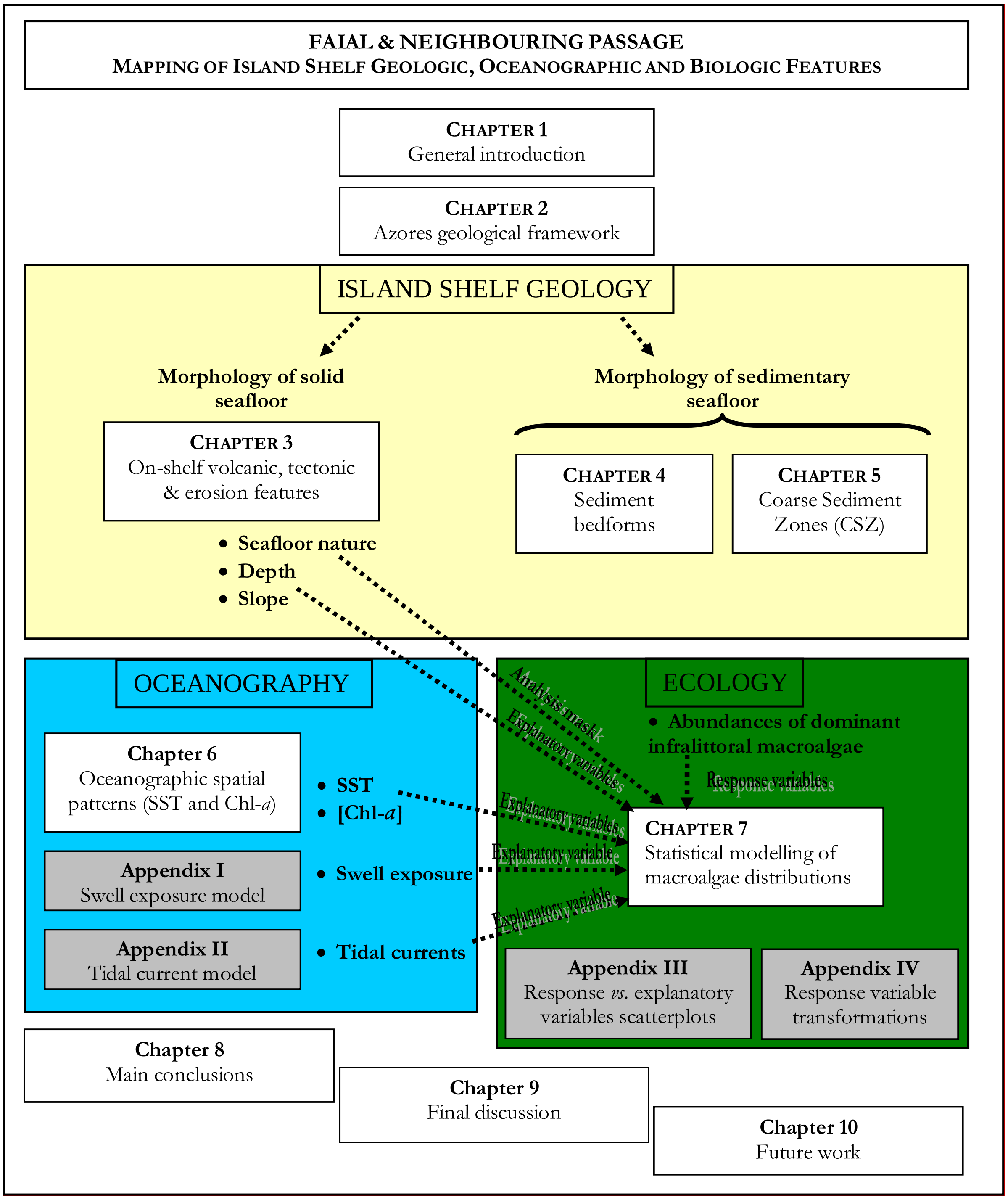

Figure 1: Diagram of the thesis composition and flows of results between chapters.

Following the current introductory chapter (**Chapter 1**), a general overview of the Azores region geology is presented in **Chapter 2**. More exhaustive overviews of the geology and ecology are given in later relevant chapters both to preserve the integrity of the paper format chosen and to maintain relevance to the specifics of each chapter.

Chapter 3 introduces the new high resolution bathymetry and backscatter dataset acquired using swath systems on the shelf of Faial and neighbouring passage to Pico. Based on this information the solid seafloor diversity and associated processes are comprehensively analysed for an Azorean island shelf for the first time, whilst saving sediment beds for separate analyses in Chapters 4 and 5. Bottom-type interpretations based on ground-truthing data provided by *in situ* imagery and sediment grab sampling from a drop-down camera and a remotely operated vehicle (ROV) are presented in all three chapters.

Chapter 4 has a specific geographic focus on the large expanses of sedimentary seafloor identified in the Faial-Pico passage, where these type of seafloor exhibited signs of a high dynamics. Within this chapter, prominent bedforms are described for the study area for the first time which suggest powerful hydrodynamic conditions. The general characteristics of several sediment wave fields are described and sediment transport patterns inferred. Current velocities are computed based on bedform geometry and contrasted to new information on local currents derived from a mid-passage oceanographic mooring and CTD surveys carried out in the area.

In **Chapter 5** the coarse-sediment zones (CSZ), a well-delimited sedimentary feature identified off eastern Faial Island, are investigated. These CSZ conform to descriptions found in the literature of "rippled scour depressions" and "sorted bedforms", which were hitherto unreported for volcanic island shelves. This section presents high resolution bathymetry, backscatter images and *in situ* video imagery of the features, together with sub-bottom profile data and sediment grainsize information collected in the area. Three CSZ morphological types are identified from the general shape, relief, size and orientation to the shoreline. The origin of the coarse material and the driving forces for its surficial exposure are discussed in view of different hydrodynamic and sedimentologic processes as well as the local geological history.

In **Chapter 6** different proxies of other environmental variables that potentially regulate the distribution of benthic organisms living on temperate shelves are presented. For benthic research purposes, information about oceanographic variability should ideally pertain to the near-bottom layer. However, data available from sampling using *in situ* data-loggers and shipboard surveys has insufficient resolution to produce a spatio-temporal model of the thermal and ocean colour

variability at the scale of Faial. As an alternative, this chapter extracts spatio-temporal patterns of Sea Surface Temperature (SST) and Surface Chlorophyll-*a* Concentration from AVHRR and SeaWiFS satellite imagery as first order approximations of seawater temperature and primary productivity patterns. It is postulated that this approach is valid in as much as near-surface properties can be coupled to sub-surficial structure in temperate areas, particularly when mixing is induced along the water column throughout winter or in areas of shoaling topography (e.g., coastal upwelling on island shelf areas). "Whole area" cycles and statistics are analysed for SST and chl-*a* and their correlation discussed. Yearly and seasonally-averaged fields are obtained for both parameters and their general zonation discussed, namely the onshore-offshore gradients and the prevalence of colder/more productive waters in coastal areas and in the Faial-Pico passage.
Chapter 7 collates environmental variables presented in previous chapters (seafloor nature, depth, slope, SST and Chl-a concentration) and variables resulting from simple GIS analyses (swell exposure; **Appendix I**) and oceanographic models (maximum tidal currents; **Appendix II**). Data from surveys of benthic biological assemblages conducted in the study area are introduced that represent the response variables in statistical models. The chapter proceeds to identify which combinations of major environmental variables (depth, slope, swell exposure, maximum tidal currents, SST and chl-*a* concentration) best explain the variation of abundance of six dominant macroalgae taxa characteristic of rocky infralittoral biotopes (articulated Corallinaceae, *Codium elisabethae*, *Dictyota* spp., *Halopteris filicina*, *Padina pavonica* and *Zonaria tournefortii*) by using ordered logistic regression statistical models. Modelled distribution predictions are spatialized for the rocky infralittoral substrate around Faial using the final model equations and the continuous raster fields for the environmental variables found to be statistical significant.

Chapter 8 summarizes the conclusions of the analytical chapters demonstrating the advances made in the current thesis.

Chapter 9 dicusses the achievement of the ultimate goal of developing an articulated multidisciplinary approach to the exploration and mapping of the seabed for geological and ecological studies.

Chapter 10 presents a series of suggestions for further work based on the new knowledge acquired and the issues detected throughout the study.

5. References

5.1. Literature

Mitchell, N.C., T. Schmitt, E. Isidro, F. Tempera, F. Cardigos, J.C. Nunes & J. Figueiredo (2003). Multibeam sonar survey of the central Azores volcanic islands. *InterRidge News*, 12(2): 30-32.

Morton, B., J.C. Britton & A.M.F. Martins (1998). *Coastal Ecology of the Azores*. Sociedade Afonso Chaves, Ponta Delgada

Hawkins, S.J., L.P. Burnay, A.I. Neto, R. Tristão da Cunha & A.M. Frias Martins (1990). A description of the zonation patterns of molluscs and other important biota on the South coast of São Miguel, Azores. *Açoreana*, 2: 21-38.

Tittley, I., & A.I. Neto (2000). A provisional classification of algal characterized rocky shore biotopes in the Azores. *Hydrobiologia*, 440 (1): 19-25.

Wallenstein, F. F. M. M., A. I. Neto, N. V. Álvaro & C. I. Santos (2007). Algae based biotopes of the Azores (Portugal): spatial and seasonal variation. *Aquatic Ecology*. Online first paper. DOI: 10.1007/s10452-007-9134-y.

5.2. Projects:

GEMAS - Assessment, Management and Monitoring of Underwater Sands around the Islands of Faial, Pico and São Miguel (DROTRH contract).

MARÉ - Integrated Management of Coastal and Marine Areas in the Azores (Life-Nature B4-3200/98/509).

MARMAC - Knowledge, Promotion and Valorisation for a Sustainable Use of Marine Protected Areas in Macaronesia (INTERREG IIIb - 03/MAC/4.2/A2 2004).

MAROV - Coastal Marine Habitats, Thematic Mapping of the Seabed Using GIS, AUV (Autonomous Underwater Vehicles) & ASV (Autonomous Surface Vehicles). (PDCTM/P/MAR/15249/1999).

MAYA - Development of a Miniaturized Autonomous Underwater Vehicle for Habitat Mapping (AdI/POSI/2003).

OGAMP - Management of Marine Protected Areas in Macaronesia (Azores, Canaries and Madeira) (INTERREG IIIb - MAC/4.2/A2 2001).

CHAPTER 2

1. Azores geological framework

The Azores is an archipelago of nine islands situated in the North Atlantic. The islands spread across an extent of 617km and are aligned along major tectonic lineaments generally trending WNW-ESE (Figure 1).

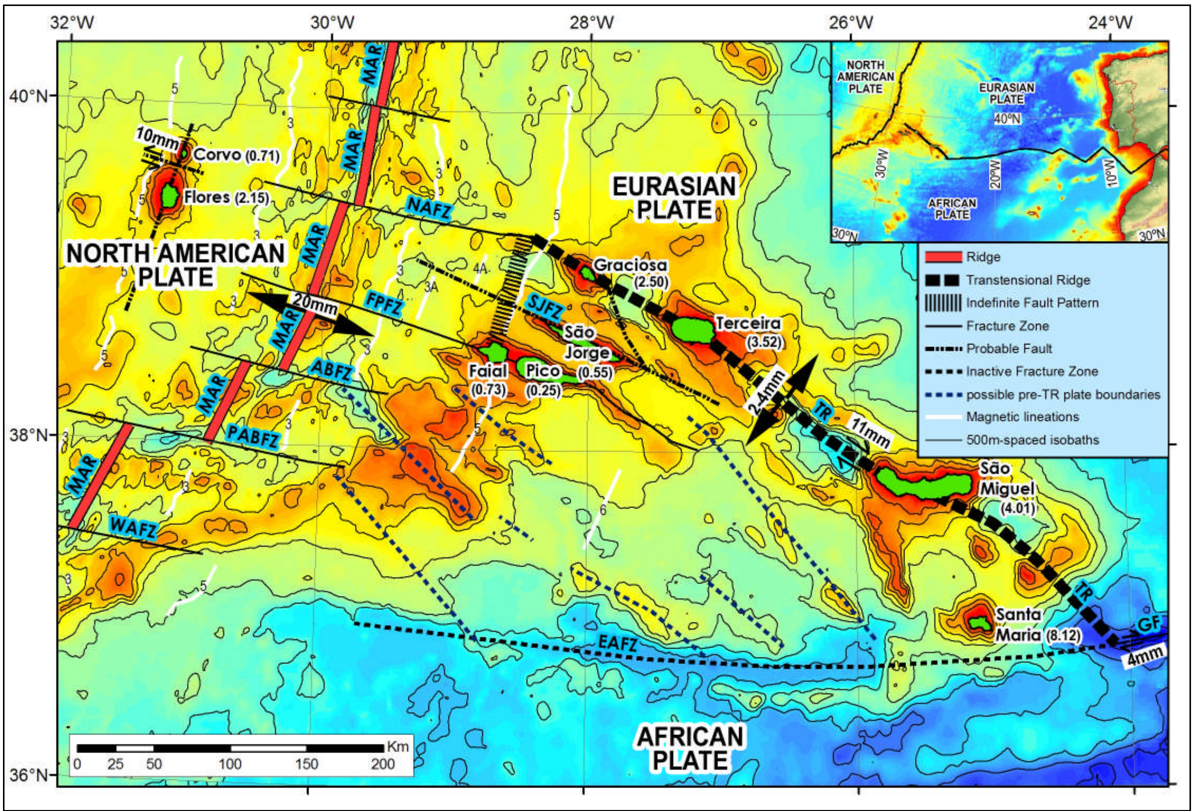

Figure 1: General geotectonic framework of the Azores archipelago (adapted from Montesinos et al., 2003; Vogt & Jung, 2004; Nunes et al., 2006). Corvo and Flores tectonics is adapted from Azevedo & Portugal Ferreira (2006) who provide also the compilation of earliest radiometric ages obtained from subaerial material in each island. Tectonic displacement rates are in mm per year and are adapted from Buforn et al. (1988), DeMets et al. (1994), Fernandes et al. (2004), Vogt & Jung (2004) and Azevedo & Portugal Ferreira (2006). Magnetic lineations are adapted from Cannat et al. (1999) and Vogt & Jung (2004). Bathymetric background is from Lourenço et al. (1998). Bathymetric contour spacing is 500m. ABFZ = Açor Bank Fracture Zone; EAFZ = East Azores Fracture Zone; FPFZ = Faial–Pico Fracture Zone; MAR = Mid-Atlantic Ridge; NAFZ = North Azores Fracture Zone; PABFZ = Princess Alice Bank Fracture Zone; GF = GLORIA Fault; SJFZ = São Jorge Fracture Zone; TR = Terceira Rift; WAFZ = West Azores Fracture Zone.

All islands rise from volcanic edifices sitting on a rugged elevation roughly delineated by the 2000-m depth contour and named the Azores Plateau (Needham & Francheteau, 1974). The maximum radiometric ages of the islands exhibit no systematic age progression otherwise expected of ocean floor moving relative to a discrete mantle hotspot (Feraud et al., 1980).

The Azores plateau contains the triple junction (ATJ) between the North American (NA), Eurasian (EUR) and African plates (AF) (Searle, 1980; Forjaz, 1983; Luís et al., 1994; Lourenço et al., 1998) and occupies an area of 5.8×10^6 km^2 (Nunes et al., 2006).

The main tectonic features in the region are (i) the Mid-Atlantic Ridge (MAR), which crosses the Azores Plateau trending approximately North-South and (ii) the Terceira Rift (TR) which strikes WNW-ESE to NW-SE and defines the NE margin of the plateau (Lourenço et al., 1998; Madeira & Brum da Silveira, 2003, Faria et al., 2003; Vogt & Jung, 2004).

The Azorean section of the MAR is a spreading centre that separates the NA plate from the EUR and AF plates at a rate ranging from 23 mm/yr on the north to 20 mm/yr on the south (DeMets et al., 1994; Fernandes et al., 2004).

TR is an ultra-slow spreading ridge which is thought to operate as the present EUR-AFR plate boundary along much of its extent (Vogt & Jung, 2004). Because it strikes obliquely to the relative motion of these two plates, deformation along this structure is transtensional with an extensional component of 2-4mm/yr (Searle, 1980; Luís et al., 1998; Vogt & Jung, 2004) and a dextral strike-slip movement of ca. 11mm/yr (Ribeiro, 2002). The SE end of TR connects to the Gloria Fault, a section of the EUR-AFR plate boundary that behaves as an E-W dextral strike-slip fault moving 4 mm/yr (DeMets et al., 1990).

From a geodynamical perspective, such rates suggest a differential eastward displacement of the Eurasian and African plates. The resultant deformation has caused the chipping of successive blocks from the SW corner of the EUR and northward migration of the ATJ (Lourenço et al., 1998). The sequence of relic EUR-AFR plate boundaries generated by this process is expressed in the WNW-ESE trending tectonic and volcanic structures parallel to the Terceira Rift (Luís et al., 1994; Vogt & Jung, 2004). Luís et al. (1994) suggest that this intense tectono-magmatic interplay (where new faults in the crust would provide ascent pathways for mantle material) explains the construction of the Azores Plateau. However, various works (see Gente et al., 2003, for a recent review) have gathered geochemical and geophysical evidence (basalt geochemistry, elevated spreading ridge and gravity anomaly) indicating the Azores Plateau results from a ridge-hotspot interaction (Cannat et al., 1999).

Despite all the studies, the fine scale geometry of the deformation presently associated with the EUR-AF boundary at the triple junction is still unclear. Recent GPS kinematic studies by Fernandes et al. (2006) show that Graciosa (the northernmost island of the central group) has a motion matching the predicted stable EUR behaviour, while Santa Maria (the southeastern-most island) has a motion matching the predicted stable AF behaviour. Given that all other intervening sites displayed an intermediate behaviour, the EUR-AF boundary in the Azores region ought to be placed within a lithospheric band, passing through São Miguel, Terceira and the Faial-Pico Fracture Zone, that would diffusely accommodate the differential plate movements (Fernandes et al., 2006). This results in the present triple junction being located at the Faial-Pico alignment with the MAR (Luís et al., 1994).

2. References

Azevedo, J.M.M. & M.R. Portugal Ferreira (2006). The volcanotectonic evolution of Flores Island, Azores (Portugal). *Journal of Volcanology and Geothermal Research*, 156(1-2): 90-102.

Buforn, E., A. Udías & M.A. Colombas (1988). Seismicity, source mechanisms and tectonics of the Azores–Gibraltar plate boundary. *Tectonophysics*, 152: 89-118.

Cannat, M., A. Briais, C. Deplus, J. Escartin, J. Georgen, J. Lin, S. Mercouriev, C. Meyzen, M. Muller, G. Pouliquen, A. Rabain & P. da Silva (1999). Mid-Atlantic Ridge - Azores hotspot interactions: along-axis migration of a hotspot derived event of enhanced magmatism 10 to 4 Ma ago. *Earth and Planetary Science Letters*, 173(3): 257-269.

DeMets, C., R.G. Gordon, D.F. Argus & S. Stein (1990). Current plate motions. *Geophysical Journal International*, 101: 425-478.

DeMets, C., R.G. Gordon, D.F. Argus & S. Stein (1994). Effect of recent revisions to the magnetic reversal time scale on estimates of current plate motions. *Geophysical Research Letters*, 21: 2191-2194.

Faria, C., T. Ferreira, J.L. Gaspar & F. Sousa (2003). Tectonic structures revealed by CO2 soil diffuse degassing anomalies at Faial Island (Azores). *Geophysical Research Abstracts*, 5: 13119.

Feraud, G., I. Kaneoka & C.J. Allegre (1980). K/Ar ages and stress pattern in the Azores: dynamic implications. *Earth and Planetary Science Letters*, 46: 275-286.

Fernandes, R.M.S., L. Bastos, B.A.C. Ambrosius, R. Noomen, S. Matheussen & P. Baptista (2004). Recent geodetic results in the Azores Triple Junction region. *Pure and Applied Geophysics*, 161(3): 683-699.

Fernandes, R.M.S., L. Bastos, J.M. Miranda, N. Lourenço, B.A.C. Ambrosius, R. Noomen & W. Simons (2006). Defining the plate boundaries in the Azores region. *Journal of Volcanology and Geothermal Research*, 156: 1-9.

Forjaz, V.H. (1983). Azores tectonic sketch. *Unpublished Research Report.* Centro de Vulcanologia INIC, Ponta Delgada. 1 p.

Gente, P., J. Dyment, M. Maia & J. Goslin (2003). Interaction between the Mid-Atlantic Ridge and the Azores hot spot during the last 85 Myr: emplacement and rifting of the hot spot-derived plateaus. *Geochemistry, Geophysics and Geosystems*, 4 (10): 1-23.

Lourenço, N., J.M. Miranda, J.F. Luís, A. Ribeiro, L.A.J. Mendes-Victor, J. Madeira, and H.D. Needham (1998). Morpho-tectonic analysis of the Azores Volcanic Plateau from a new bathymetric compilation of the area. *Marine Geophysical Researches*, 20(3): 141-156.

Luís, J.F., J.M. Miranda, A. Galdeano, P. Patriat, J.C. Rossignol & L.A.M. Victor (1994). The Azores triple junction evolution since 10 Ma from an aeromagnetic survey of the Mid-Atlantic Ridge. *Earth and Planetary Science Letters*, 125: 439-459.

Luís, J.F., J.M. Miranda, A. Galdeano & P. Patriat (1998). Constraints on the structure of the Azores spreading center from gravity data. *Marine Geophysical Researches*, 20: 157-170.

Madeira, J., & A. Brum da Silveira (2003). Active tectonics and first paleoseismological results in Faial, Pico and S. Jorge islands (Azores, Portugal). *Annals of Geophysics*, 46: 733-761.

Montesinos, F.G., A.G. Camacho, J.C. Nunes, C.S. Oliveira, & R. Vieira (2003). A 3-D gravity model for a volcanic crater in Terceira Island (Azores). *Geophysical Journal International*, 154(2): 393-406.

Needham, H.D. & J. Francheteau (1974). Some characteristics of the rift valley in the Atlantic Ocean near 36° 48 North. *Earth and Planetary Science Letters*, 22: 29-43.

Nunes J.C., A. Camacho, Z. França, F.G. Montesinos, M. Alves, R. Vieira, E. Velez, & E. Ortiz (2006). Gravity anomalies and crustal signature of volcano-tectonic structures of Pico Island (Azores). *Journal of Volcanology and Geothermal Research*, 156: 55-70.

Ribeiro, A. (2002). *Soft Plate and Impact Tectonics*. Springer, Berlin. 324 pp.

Searle, R. (1980). Tectonic pattern of the Azores spreading centre and triple junction. *Earth and Planetary Science Letters*, 51: 415-434.

Vogt, P.R. & W.Y. Jung (2004). The Terceira Rift as hyperslow, hotspot dominated oblique spreading axis: a comparison with other slow spreading plate boundaries. *Earth and Planetary Science Letters*, 218: 77-90.

CHAPTER 3

SEAFLOOR DIVERSITY AND ASSOCIATED PROCESSES ON THE VOLCANIC ISLAND SHELF OF FAIAL ISLAND AND NEIGHBOURING PASSAGE (AZORES, NE ATLANTIC)

Abstract

Faial and Pico are two islands located in the central group of the Portuguese archipelago of the Azores (Northeast Atlantic). Both islands are estimated to have emerged during the Pleistocene (800 and 270 ky BP respectively) and are located east of the Mid-Atlantic Ridge. A 5 km-wide shelf unites both islands creating a unique shallow water structure in an archipelago where seafloor elsewhere between islands typically exceeds depths of 1000 m. This submerged isthmus underwent subaerial exposure at least during the Middle and Upper Pleistocene glaciations.

The present paper focuses on analysing the extension and surficial geomorphology of the shelf around Faial island and neighbouring passage to Pico down to 200 meter depth based on swath bathymetry and ground-truthed backscatter data.

Shelf width and depth at shelf edge are shown to vary significantly around the study area reflecting the distinct ages, tectonic histories and on-shelf sedimentation patterns of the geologic edifices composing the islands.

A complex pattern of tectonic, volcanic and erosion features was interpreted from acoustically high backscattering areas on the shelf and validated by ROV and drop-down camera imagery, sub-bottom profiles and sediment grab samples. The most important elements characterized were (i) tectonic faults expressed on the seafloor surface, (ii) the submerged evidence of fissural volcanic activity associated with some of these faults, (iii) a variety of lava flow morphologies penetrating the present waterline, (iv) boulder slopes generated by coastal erosion, (v) a basin in the southern half of the Faial-Pico passage and (vi) cliff palaeo-shorelines.

Keywords: volcanic island shelves; geomorphology; Faial; Pico; Azores.

TABLE OF CONTENTS

1. Introduction

The Azores region (Northeast Atlantic) has been a prominent target in the effort to map mid-ocean ridges. The presence of the triple junction between the Mid-Atlantic Ridge and the Eurasia-Africa plate boundary, together with the various geophysical anomalies associated with it, have been primary motivations for the studies.

A review of the analysed swath datasets highlights that most of the surveys (e.g., Searle, 1980; Lourenço et al., 1998; Cannat et al., 1999; Ligi et al., 1999; Gente et al., 2003; Stretch et al., 2006) have concentrated on deep-sea areas where higher swath efficiency is obtained due to the wider areas insonified in a single passage.

In these circumstances, the best-available sources of topographic information for shallow-water have been the publicly-available hydrographical charts, produced on the basis of lead-line and single-beam echosounding surveys. Because of their broad scale, low sounding resolution and scarcity of information on seafloor nature, only a crude perception of the submerged geology of the islands can be extracted. Geologic patterns and processes occurring in the island vicinity are therefore very poorly described, hampering not only the scientific understanding of the emplacement and erosion histories of individual islands (for other regions see, e.g., Menard, 1983 or Moore, 1987) but also compromising the mapping of potential geologic hazards.

In 2003 and 2004, this generalized lack of high resolution geomorphologic information was partially filled through swath sonar surveys conducted around the islands of Faial, Pico and São Jorge (Mitchell et al., 2003). The new data revealed a multitude of geomorphologic features on the surveyed slopes and shelves that have only started to be described in Mitchell et al. (2008).

The current paper focuses on the swath bathymetry and backscatter data acquired on the shelf of Faial and neighbouring passage to Pico. It constitutes the first work to analyse systematically the underwater geomorphology of an Azorean island shelf using modern hydrographical surveying technologies. High resolution topography and backscatter images are used to provide an overview of the most important surficial morphology and textural patterns observed down to the shelf edge. Submerged features associated with tectonic, volcanic and erosion processes are highlighted and a substrate map is derived that later informs the mapping of rocky infralittoral biological distributions (Chapter 7).

Bottom-type interpretation is based on ground-truthing data provided by sediment grab sampling and *in situ* imagery from a drop-down camera and a remotely operated vehicle (ROV). Published information about the adjoining sub-aerial geology is used to complement the understanding of the underwater geomorphology.

In addition to its geomorphologic interest, the study area is also of great relevance for nature conservation. As a result of its good conservation status and particular ecological conditions, the site is classified under the Natura 2000, the OSPAR and the BIOMARE networks of protected areas (Tempera et al., 2001). Therefore, the results of this study are also of relevance for the mapping of benthic habitats in a most accessible, sensitive and frequently used area.

2. Background

2.1. Faial and Pico geologic setting

The islands of Faial and Pico are emplaced in an area of diffuse plate boundary dominated by tectonic blocks trending 120º and 150º. Both islands are thought to have emerged during the Pleistocene (Feraud et al., 1980; Chovelon, 1982) and their volcanism is closely associated with the underlying tectonic framework. The geologic complexes of the two islands and their general chronology are presented in Figure 1.

Faial island has an area of 173.1 km^2 and presently reaches an altitude of 1,043 m above sea level (a.s.l.). The plan-view shape of the coastline is approximately pentagonal with a maximum length of 21 km and a width of 14 km (França et al., 2003). This shape is the result of volcanism predominantly associated with dextral faults striking WNW-ESE (100-120º) (Madeira & Brum da Silveira, 2003).

The emergence of the island is estimated at about 800 kyr BP (Féraud et al, 1980) with the development of a composite volcano of the Ribeirinha Complex on the NE of the island probably centred over the present Pedro Miguel graben (Coutinho, 2000).

After the activity in the Ribeirinha Complex ceased, a stratovolcano started to build on the western flank of the Ribeirinha complex at about 470 kyr BP, which originated the Cedros Complex. The upper unit of this complex is named the Caldeira Formation and corresponds to trachytic eruptions that capped large expanses of the island during the last 16 kyr (Madeira, 1998). This edifice features a central caldera formed over the last 1,600 years.

A B

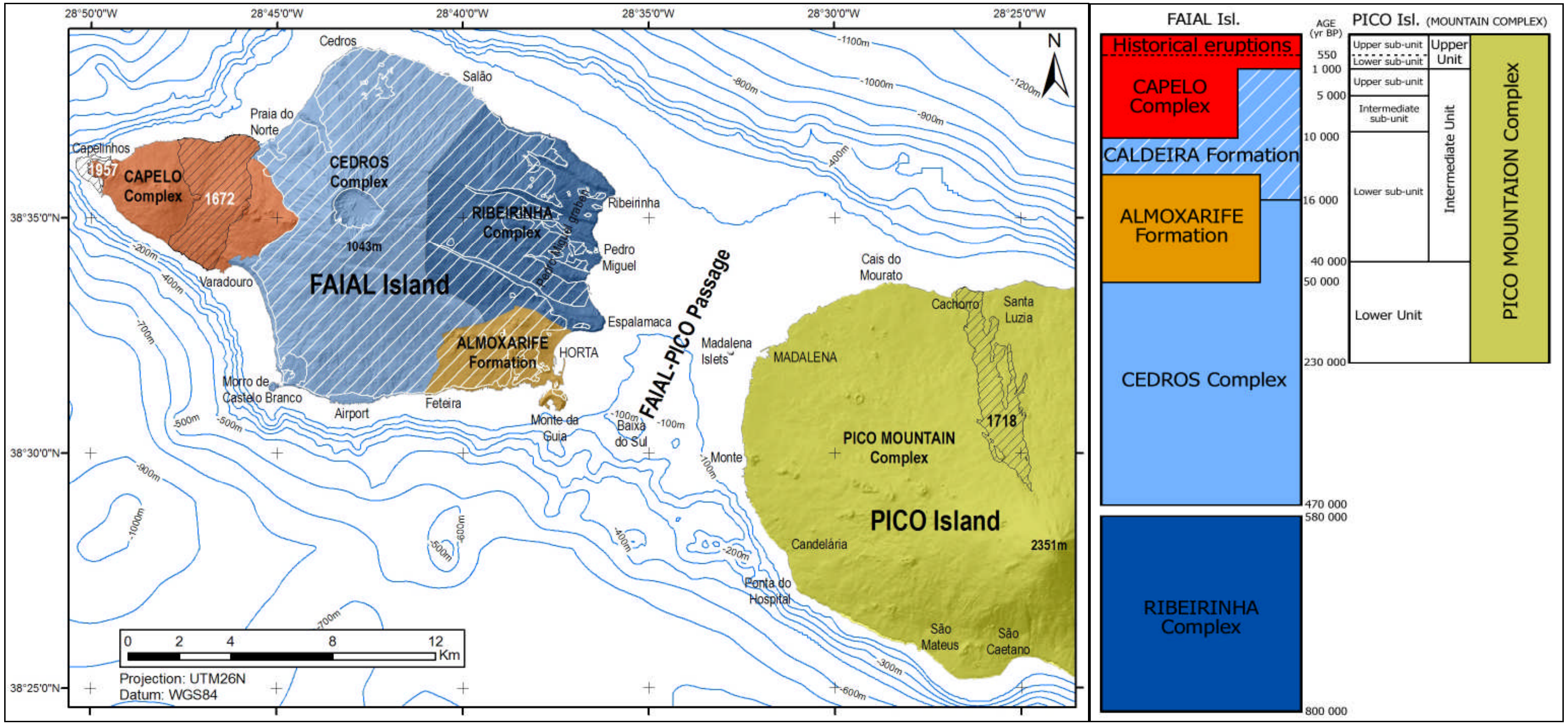

Figure 1: A. Geomorphologic complexes of Faial and Pico and general bathymetry. Historic eruptions are represented in a pattern of black stripes and labelled with the year. B. Stratigraphy of Faial and western Pico [adapted from Madeira (1998), Pacheco (2001) and Nunes (1999)]

The SE of Faial is composed of the Almoxarife Formation - a flattened sector formed by basaltic fissural eruptions. This unit comprises Hawaiian/Strombolian scoria cones and lava flows as well as the Monte da Guia Surtseyan cone (Madeira, 1998). Absolute ages for this formation are scarce and of poor quality (0.03 ± 0.02 Ma in Féraud et al., 1980).

The Capelo complex – a peninsula developing to the W of the Cedros Complex - is the youngest edifice of the island. It is composed of an alignment of basaltic Hawaiian, Strombolian and Surtseyan cones formed by fissural volcanism younger than 10 kyr. Two eruptions occurred in this complex since the island was colonized in the 15th century: Cabeço do Fogo in 1672-73 and Capelinhos in 1957-58 (França et al., 2003; Madeira & Brum da Silveira, 2003).

Pico is the youngest island in the archipelago with a maximum radiometric age of 300 kyr (Chovelon, 1982). It is the second largest with an area of 447.7 km^2 and is composed of 3 distinct edifices: two central volcanoes and one fissural volcanic zone (Madeira, 1998; Nunes, 1999). For the sake of the present study only the western-most edifice – the Pico Mountain Complex (PMC) – is of interest as it constitutes the whole eastern margin of the Faial-Pico passage. PMC dominates the island with a peak altitude of 2,351 m (a.s.l.), representing the highest altitude found along the Mid-Atlantic Ridge. The complex is a composite stratovolcano estimated to have emerged 240 kyr BP (Nunes et al., 1998, 2006). The cone is the result of numerous Hawaiian and Strombolian-type eruptions taking place both at the summit and at numerous parasitic cones distributed over its flanks (França et al., 2003). Three of these eruptions took place in the 18th century but they are located outside the study area. Lava flows are chiefly of basalts (~78%) and subordinate hawaiites (~20%) but a few Surtseyan eruptions also occurred such as in the tuff cones of Cabeço Debaixo da Rocha and Madalena Islets (França et al, 2003, 2006).

A passage which is 6 km-wide in its narrowest section currently separates Faial and Pico. Large expanses of this inter-island shelf are shallower than 100 m and a sill straddling between the Espalamaca headland (Faial island) to Madalena (Pico island) bears a maximum depth of 63 m. The flanks of this shelf drop steeply to depths of 1500 m on the north and 900 m on the south.

The depths found in the passage and the ages obtained for the islands that surround it suggest the submerged connecting shelf passage would have acted as a sub-aerial isthmus during the sea level regressions associated with recent glacial periods. The geology of this submerged area have been only been briefly tackled by Berthois (1953), Zbyszewski et al. (1963) and Nunes (1999; reporting on data from the GeoAçores/89 expedition). Together they highlighted some general geomorphologic characteristics such as (i) the prolongation of the WNW-ESE trend of the tectonic features associated with the Pedro Miguel graben, (ii) the "Espalamaca-Madalena Islets" ridge, (iii) the shallower depths of the northern half of the passage compared to the southern half (hypothesized as an underwater caldera) and (iv) the existence of mid-passage submerged Surtseyan cones.

2.2. Faial and Pico oceanographic setting

The Faial-Pico area is subject to prevailing swells from NW and W (Figure 2) as derived by Carvalho (2003) from a long-term (1989-2002) output of the MAR3G wave model (Oliveira Pires and Carvalho, 1996).

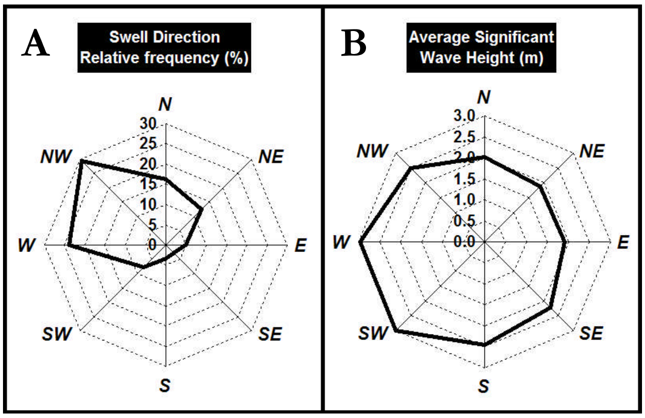

Figure 2: Direction spectrum and average swell height in Central Azores (adapted from Carvalho, 2003). A. Relative frequency of swell. B. Average significant wave height. Graphs use the meteorologic convention ("from") for directions.

Tides reach maximum ranges of only 1.5 m (Instituto Hidrográfico, 2005) and are deemed as the main driver of water flows affecting the local shelves. Fine scale data on the currents are scarce but anecdotal data indicates they are typically stronger around headlands and within the passage, where open ocean waters are vertical and horizontally funnelled. A shallow-water model of the currents induced by tides within the inter-island passage suggested maximum vertically-averaged tidal currents of 0.6 m/s in the passage (Duarte, 1997). Subsequent research by Simões et al. (1997) reported a good fit of the model with observations collected by ADCP (Acoustic Doppler Current Profiler) throughout a tide cycle and produced profiles showing maximum currents of 1.1 m/s near the surface and 0.5 m/s near the bottom.

3. Methods

Swath sonars are acoustic remote sensing tools that currently allow mapping the seafloor at resolutions between a few decimetres and 10 meters, depending on water depth. These systems operate by ensonifying a strip of seafloor across the survey ship track and detecting the bottom echo at more than a hundred intervals along each across-track sweep.

The technique relies on accurately determining travel times of the acoustic pulses from the sonar transceiver to the submerged target (usually the seafloor) and combining these measurements with highly accurate information of the position, heading and attitude of the sonar transceiver, tide height and sound velocity profile at the time of each pulse. Accurate X, Y and Z coordinates can thereby be computed for each individual echo received from the seafloor.

Systems calculate the depth of the sea bed at any discrete point on the across track acoustic sweep by determining two variables: the slant range (or distance between the acoustic transducer and the point on the seafloor) and the angle of the direct acoustic path from transducer to the point on the sea bed. Beam-forming and phase-measuring sonars differ in the fact that whilst in the former the return time of the reflected signal is measured at a particular angle, in the latter the angle of the reflected signal is measured at a particular time.

Both systems typically provide two kinds of data: bathymetric data and "acoustic backscatter" (i.e., the amount of sound returned off the bottom). Whilst bathymetrical info can be used to represent the topography of the seafloor in high resolution, backscatter is used to map the geologic nature of the seafloor, and is particularly reliable if interpreted in conjunction with ground-truthing imagery, geological samples and seismic profiles of the seafloor.

3.1. Data collection and processing

Survey tracks totalling 1,227 km were completed around the island of Faial and neighbouring passage to Pico, corresponding to an effective surveying time of 138h 07m.

The main survey was conducted in the autumn 2003 used a Reson 8160 beam-forming swath sonar mounted on RV *Arquipélago*. The target areas were essentially the island slopes of São Jorge, Faial and Pico, and the inter-island shelf that unites the latter two.

A complementary survey was carried out in the summer 2004 to cover the nearshore gaps left by the beam-forming sonar survey around Faial and western Pico, using a Submetrix 2000 phase-measuring sonar installed on RL *Águas Vivas*.

The data processing of both datasets was conducted by the author of this thesis.

A summary of the equipment, data processing methods and extension of the two surveys is presented in Table 1.

Table 1: Characterization of the swath survey equipment, areal coverage and data processing methods.

SWATH SYSTEM:	BEAM-FORMING SONAR	PHASE-MEASURING SONAR
TIME OF SURVEY	Autumn 2003	Summer 2004
PARTNERSHIP	Univ. of Azores – Cardiff Univ.	Univ. of Azores – Univ. of St Andrews
VESSEL	RV *Arquipélago* (25 m)	RV *Águas Vivas* (11 m)
SONAR	Reson 8160 (81-P processor)	Submetrix 2000
TRANSCEIVER	50 kHz; 150º (126 beams); bow-mount	117 kHz; 300º; bow-mount
MOTION REFERENCE UNIT	Applanix POS/MV 220, (attitude; orientation ; PPS time tagging)	TSS DMS 05 (attitude)
GPS	CSI wireless DGPS Max (with EGNOS corrections)	CSI wireless DGPS Max (with EGNOS corrections); Trimble Pathfinder Pro XRS (postprocessed); regular Garmin GPS
SVP	Navitronic SVP25	Navitronic STD Plus 646
TIDAL CORRECTIONS	Valeport 740 water level measurements	Portuguese Hydrographical Institute online tide tables
GENERAL AREA SURVEYED	slopes of São Jorge, Faial and Pico islands; Faial-Pico passage	nearshore of Faial island and western coast of Pico
SURVEY TRACK LENGTH IN STUDY AREA	695 km	532 km
SURVEY DURATION IN STUDY AREA	88h 40m	49h 27m
AVERAGED SURVEY SPEED	4.8 kts	5.9 kts
BATHYMETRY POST-PROCESSING	CARIS HIPS & SIPS ® v. 5.x	Swathplus ® v.2.04; CARIS HIPS & SIPS ® v. 5.4
BACKSCATTER POST-PROCESSING	CARIS HIPS & SIPS ® v. 5.x	Sonarweb Pro v. 3.16
BINNING OF POST-PROCESSED DATA	20 m and 5 m grids	20 m and 5 m grids
BACKSCATTER MOSAIC RESOLUTION	1 m	1 m

3.1.1. Beam-forming sonar survey

Due to limitations in ship time, survey lines were spaced at intervals that have not always guaranteed overlap between adjacent lines. However, the resulting data holes are small and do not compromise the overall geomorphologic interpretations.

The swath survey covered the slopes of the islands of São Jorge, Faial, Pico and the shelf between the latter two but the analyses produced in this work focus solely on the data collected on the shelf of Faial and neighbouring passage to Pico.

3.1.2. Phase-measuring sonar survey

Additional bathymetric and backscatter data were acquired in the nearshore of Faial island and western coast of Pico using a phase-measuring sonar. This survey was aimed to covering nearshore data gaps left by the previous beam-forming sonar survey due to limitations in safely operating the 25 m vessel in shallow water. Given the narrower surveying angle that characterizes the fixed-angle beam-forming systems, the wider angle of phase-measuring systems was considered as an advantage in shallow waters as it is permitted covering broader strips of seafloor, requiring less survey lines and consequently shorter ship time.

DGPS-accurate positioning was obtained by post-processing. Only 27% of the phase-measuring sonar survey was completed with a DGPS level of positioning accuracy despite efforts to retrieve an equivalent accuracy level by GPS post-processing. The regular GPS precision characterizing the remaining data was still deemed sufficient for the scale at which features were analysed. According to DoD (2001), regular GPS has featured an horizontal accuracy of ~8 m ($RMS_{95\%}$) subsequent to Selective Availability discontinuation.

3.1.3. Backscatter

The variation in the intensity of the reflected acoustic energy (i.e., backscatter) was recorded in both the beam-forming and phase-measuring sonar surveys. These acoustic patterns are useful in highlighting aspects of geologic features such as bottom nature and texture which are not perceptible from the rendering of bathymetric data only (Todd et al., 1999).

CARIS HIPS & SIPS was used to process the swath sonar backscatter and produce mosaics at a resolution of 1 m^2. Processing included both geometric corrections (bottom tracking, removal of altitude and slant range correction using the *Height source* option) and elementary radiometric compensation (*Beam pattern* option).

Phase-measuring sonar backscatter data were imported into Sonarweb Pro v. 3.16 where geometric corrections and time varied gain radiometric compensation were applied. The quality of phase-measuring sonar backscatter was generally better than that of beam-forming sonar. Final mosaics were assembled using the “shine-through” algorithm and a resolution of 1 m^2.

3.2. Ground-truthing

Validation data for the interpretation of acoustic data as seafloor types was provided by (i) imagery collected with the ROV and drop-down camera, and (ii) GIS-based superimposition of complementary information. The latter included point data from earlier surficial geologic sampling, data from seismic reflection surveys and local maps of the adjacent subaerial geology.

3.2.1. *In situ* seafloor imagery

Visual ground-truthing of the seafloor in the form of video imagery was accomplished using a VideoRay Explorer ROV (summer 2004) and a Tritech MD4000 drop-down camera (summer 2005).

A minimum of two locations representative of each physiographic/acoustic signatures (e.g., large boulders, small boulders and cobbles, lava flows, irregular beds, eroded stratified structures, coarse sediments, fine sediments) was sampled.

The ROV operations were conducted to maximum depths of roughly 60 m, while the vessel was at anchor. A 2-3 kg weight attached to the tether 11 m away from the ROV was used to minimize current-induced drifts and dampen swell movements. The drop-down camera was operated down to 180 m depth. Survey transects were aimed at obtaining vertical profiles along slopes and traverse different seafloor types while the vessel was left to drift. The altitude of the system from the seafloor varied due to obstacle avoidance procedures and a hopping strategy aimed at obtaining both close ups of the biologic benthic coverage and wider views of the seabed. For most of the survey, the camera was positioned at 2 m from the substrate which was enough to easily describe the seafloor down to depths of ca. 100 m due to good sunlight penetration (clear oceanic waters) and good performance of the camera in low light conditions. In deeper areas, illumination relied on two camera L.E.D. lights which provided sufficient light for distances to the ground smaller than 1 m.

Since neither the ROV nor the drop-down camera were deployed with an underwater positioning system (e.g., USBL), the position of the lowered system was usually approximated with the position of the boat. When cable drag and/or divergence between boat drift and current direction shift moved the camera away from the boat, annotations of the length of cable let out and a visual estimate of the cable slanting angle to the vertical were used to calculate a lag correction using simple trigonometric formulae.

3.2.2. Seafloor sampling

Data from earlier box coring and grab surveys (Quartau et al., 2002, 2003, 2005; Isidro et al., 2006), summarized in the form of point shapefiles with completed attribute tables, were used to validate and establish the nature of the seafloor and grainsize of the sediments mapped acoustically. Information about 50 locations sampled either in 2002 (Duncan box-corer) or 2004 (Van Veen grab) was scattered throughout the study area down to a maximum depth of 80 m.

Publicly available hydrographical charts and an historic expedition report (Richard, 1934) provided an additional source of information on surficial bottom nature. Despite the large number of locations sampled within the study area (1,612 in hydrographical charts plus 4 in the expedition report), these older data had limited reliability given (i) the age of the surveys (much data in charts date back to the 1940's and those in the expedition report to the late 19th and early 20th centuries), (ii) the sampling technique utilized (armed sounding leads) and (iii) bias of the sampling towards shallow areas near and harbour vicinity.

3.2.3. Sub-bottom profiling

Results of sub-bottom profiling were kindly provided by Dr. Rui Quartau and used to refine the interpretation of the geomorphologic structures. The survey comprised a grid of parallel transects normal to the shore and spaced at 400 to 800 m intervals. Transects were generally run between the 10-m and 80-m depths, with occasional tracks extending to around 120 m. A complementary validation line was surveyed around both islands that cut across the previous grid along the 30-m depth contour.

The dataset was acquired in July 2001 and July 2002 and included sub-bottom profiles collected with two systems:

- an EG&G 230-1 Uniboom boomer (0.7-8 kHz);
- a Datasonics CAP-6000W chirp sonar system (1.5-10 kHz sweep).

The boomer produced a nominal resolution of 1-1.5 m and a maximum sub-bottom penetration of 60 m. The seismic reflection data were both printed onto paper in real time (using an EPC 4603 plotter) and stored in audio cassettes (using a TASCAM 234 recorder) that were later digitized into SEG-Y files. The lack of a stabilized power during the 2001 FAPI-1 survey introduced significant electric noise in the data obtained. This resulted in low signal-to-noise ratios and had a significantly impact on the quality of the sub-bottom imagery.

The chirp was operated in a configuration that provided a nominal resolution of 10-12 cm and a maximum sub-bottom penetration of 5 m. Digital data were stored in SEG chirp sonar data files which were later converted into SEG-Y.

SEG-Y seismic files were post-processed using SPW (Parallel Geoscience Corp., version 1.8.19) to remove artifacts and enhance the signal to noise ratio. The resulting navigation and seismic files were converted into formats used in Landmark environments and imported into Openworks and Seisworks projects were they were interpreted. The sediment thickness interpreted from the profiles were used to produce interpolated grids of sand deposit thickness (Quartau et al., 2002, 2003).

Uncorrected depth-below-vessel was acquired concurrently with the seismic surveys using a hull-mounted KODEN CVS-821 single-beam echosounder.

3.3. Geographic Information System

A geographic information system built within ArcGIS 9.1 ® ESRI was used to display and analyse the bathymetric grids and backscatter mosaics resulting from the processing described in 3.1. Slope rasters were derived from the regular bathymetric grids.

Semi-transparent greyscaled slope maps were used to convey a rotation-invariant perception of seafloor steepness on colour-coded plane views of large areas and enhance morphologic detail during feature delineation. Surfer ® Golden Software was used to produce exaggerated shaded relief maps of smaller areas.

Processed backscatter mosaics were imported into ArcMap in the form of geotiff files (exported from CARIS HIPS & SIPS) and jpg+jpw files (exported from SonarWeb Pro). These mosaics were plotted with an inverted greyscale where black corresponded to the highest backscatter and white to the lowest.

Digitizing of new interpreted information and extraction of quantitative features (e.g., distances, areas, depths) for shelf features was also performed in ArcMap.

The GIS was also instrumental in comparing the new swath datasets to existing ground-truthing information (e.g., location of sub-bottom profiles and grab samples) and maps of the subaerial geology (e.g.: Serralheiro et al., 1989; Nunes, 1999).

3.4. Shelf width, depth at edge and apparent widening rate

An objective criterion hereafter named analytic shelf edge (ASE) was applied to delineate the shelf outer limit. This criterion was based on setting the transition between shelf and slope along the 5º (to the horizontal) slope contour (Lundblad et al., 2006). Digitizing of this limit was made at a scale of 1:15,000 individually for each sector of the subaerial geologic edifices defined in the literature and resulted in a shapefile of equally-spaced (50 m) points distributed over the ASE.

Depth at shelf edge was obtained by intersecting the ASE point shapefile with a 20 m resolution bathymetric grid.

Shelf width was extracted for each shelf sector as an average of the distances between the ASE points and the closest point in the shoreline of the related subaerial geologic edifice. Geologic edifice shorelines were generalized before these computations to exclude protruding "on shelf volcanoes" such as Morro de Castelo Branco, Monte da Guia and Capelinhos. Given the atypically close to the shelf edge location of the latter, this procedure was deemed necessary to avoid biasing width measurement.
The apparent widening rate was computed as the ratio between the average shelf width and the age of the related subaerial edifice.

3.5. Geomorphologic features

The bathymetric and backscatter maps were visually inspected in the GIS environment aiming at identifying and interpreting distinct seafloor types and relevant geomorphologic structures.

3.5.1. Seafloor types

A classification of seabed nature has been made based on distinctive patterns expressed in the bathymetry and on tonal and textural properties of the backscatter (Blondel & Burton, 1997). In the depiction used for backscatter, smooth-surfaced sandy substrates appear light grey and homogeneous as they are relatively weak scatterers of the insonification energy. Contrastingly, rocky habitats show the darkest patterns due to their high reflectivity. Texture in both types of substrate is dependent on how the surfaces of these substrates are oriented and organized, reflecting different amounts of energy back to the transceiver at fine scales.
A polygon layer was digitized in ArcMap that segments the seafloor in its two major nature classes: hard seafloor and sediments.

3.5.2. Palaeo-shorelines

Long submerged cliffs parallel to contour lines were interpreted as probable palaeo-shorelines. They were identified by overlaying 5-m spaced depth contours over a two-colour coded slope map ($<5^o$ and $\geq 5^o$). The 5º threshold was considered as the significant palaeo-shoreline indicator in view of the scale of the grids and the risk of some trivial structures and artefacts confounding the analysis if a lower value was used.
Digitizing of the palaeo-shorelines was made at the cliff base and resulted in a polyline shapefile. This was converted into equally-spaced point arrays that were intersected with the 5 m resolution bathymetric grid to obtain the average depth per palaeo-shoreline stretch.

4. Results

4.1. Survey extension

The extension of the shelf covered by swath surveys is shown in Figure 3 along with the location of ground-truthing observations made using the ROV and the drop-down camera.

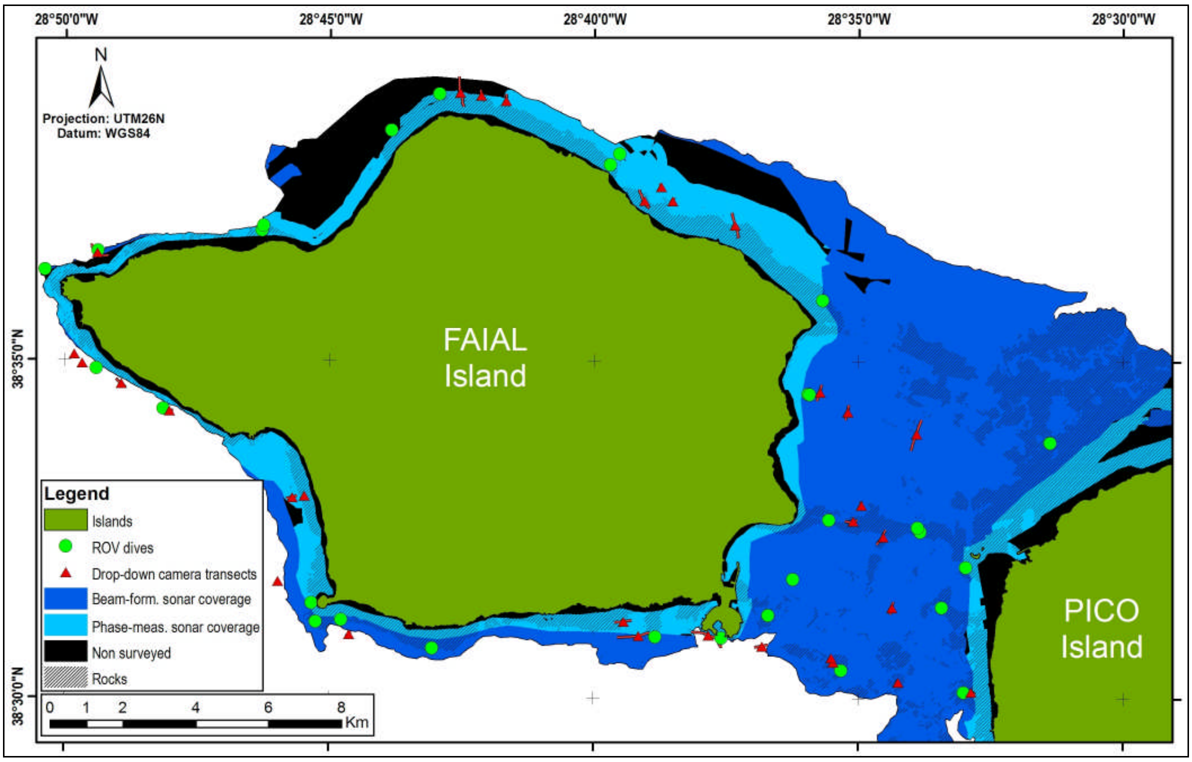

Figure 3: On-shelf survey extension and location of ground-truthing observations using the ROV and the drop-down camera. Shoreline follows the hydrographical chart datum (Portuguese Hydrographic Institute).

4.2. Bathymetry

A bathymetry binned at 20 m resolution of the island shelves and flanks is shown in Figure 4 that combines the results of the beam-forming and phase-measuring sonar surveys. For completeness at this small scale, data gaps on the shelf were filled by interpolation (natural neighbour algorithm) with information digitized from official hydrographical sounding sheets (where available) and from published hydrographical charts (source: IH). Island topography (source: IGeoE) was added to illustrate geomorphologic connections between the underwater and subaerial structures. A sense of rotation-invariant shading is achieved by superimposing semi-transparent grayscale-coded slope maps onto colour-filled contour maps.

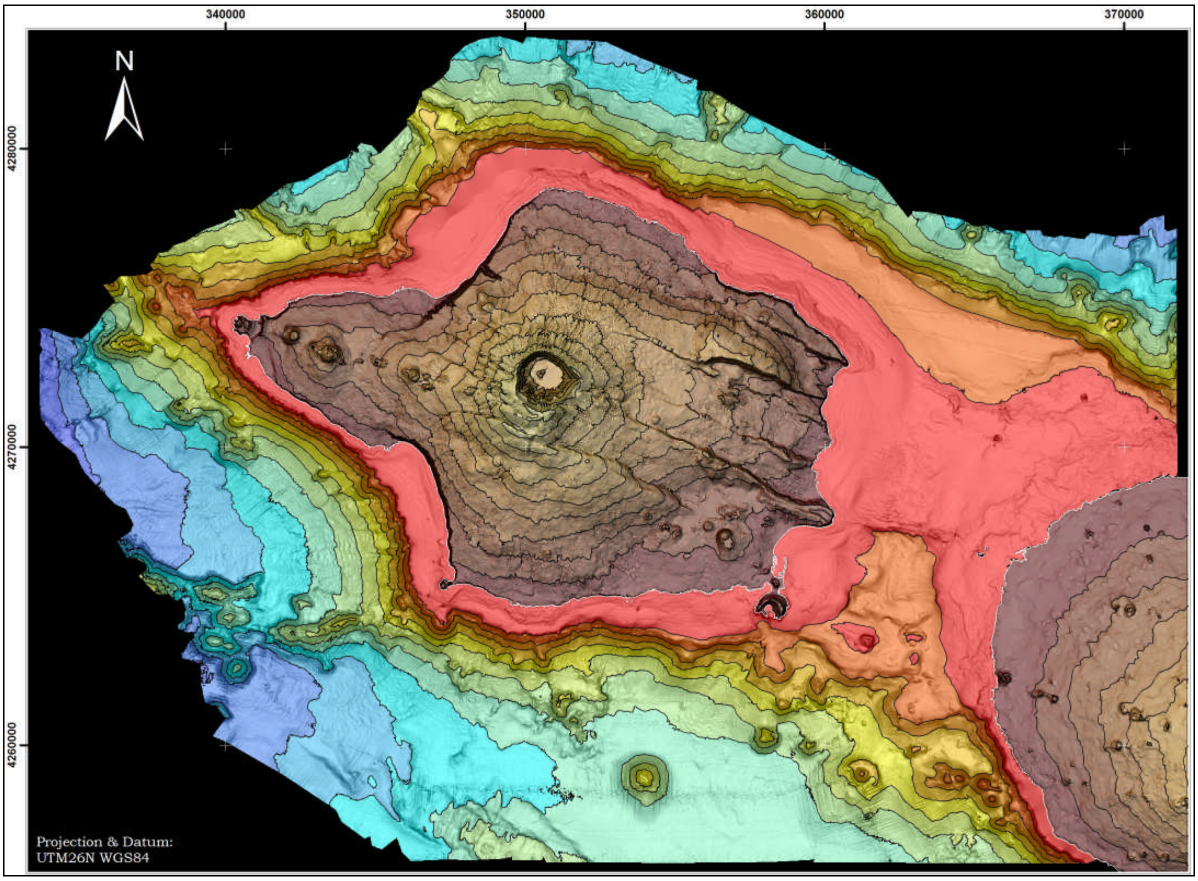

Figure 4: Bathymetry and topography of the study area combining the beam-forming and phase-measuring sonar survey data (20 m grid resolution) with IGeoE altimetry. Contour interval is 100 m. White line is shoreline.

Maps with higher detail are presented in Figure 5 to Figure 9 for different sectors of the study area. Survey data artefacts are visible on the underwater relief maps such as (i) along-track corrugations due to insufficient attitude correction of the original sonar data or slight movements of the transducer array during vessel motion, (ii) swath edge mismatches caused by imperfect correction for sound velocity variation within the water column and (iii) central ridging caused by overcompensation of the roll offset of the phase-measuring transducers. This pervasive noise has readily identifiable characteristics and seafloor features are easily discriminated from it.

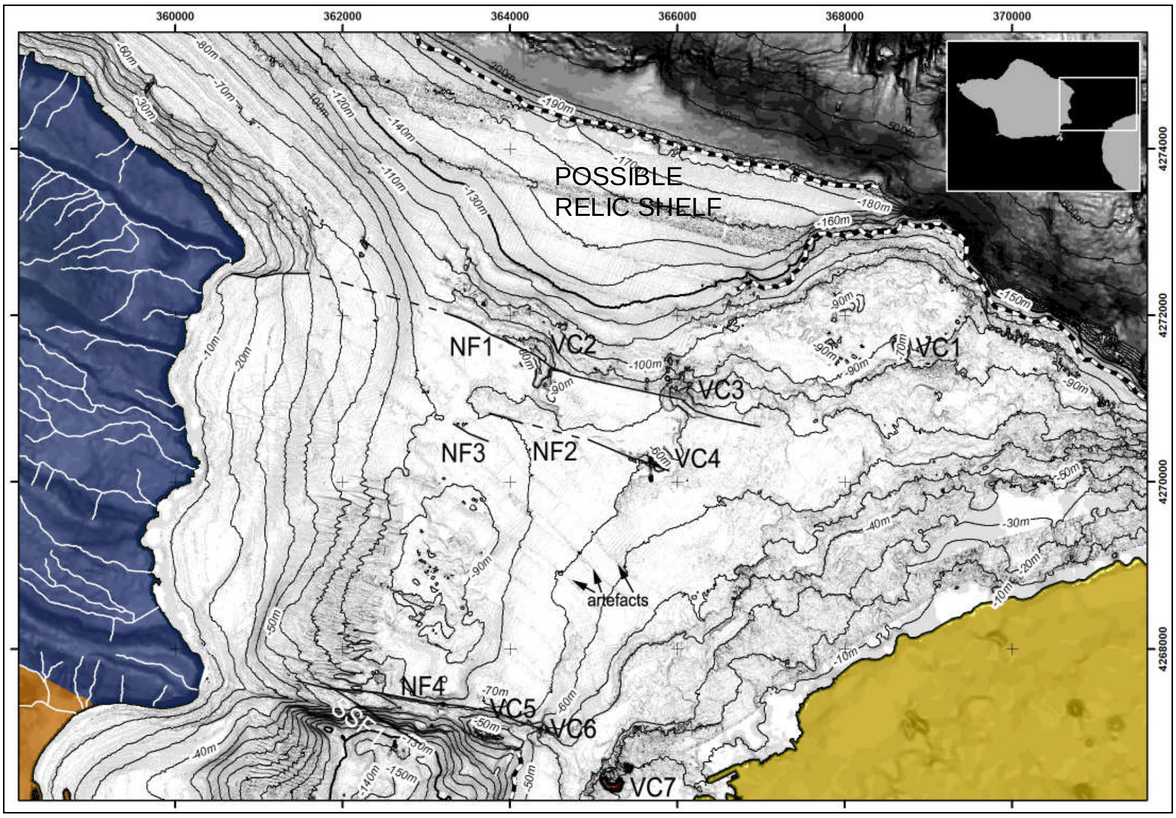

Figure 5: Northern part of the Faial-Pico passage. The contour interval is 10 m to depths of 200 m and thereafter 100 m. Dashed black and white line represents analytic shelf edge (ASE). VC1 to VC7 are volcanic centres detailed in 4.4.5. Features of note include the Espalamaca-Madalena ridge near the bottom of the picture (along NF4), a submerged lava series on northwestern Pico, the shallower depths of the northern part of the passage compared to the basin south of the ridge, the on-shelf extension of the subaerial faulting from eastern Faial (NF1 to NF4) and a possible subsided relic shelf partially surmounted by a later shelf edge from the northwestern sector of the Pico Mountain Complex.

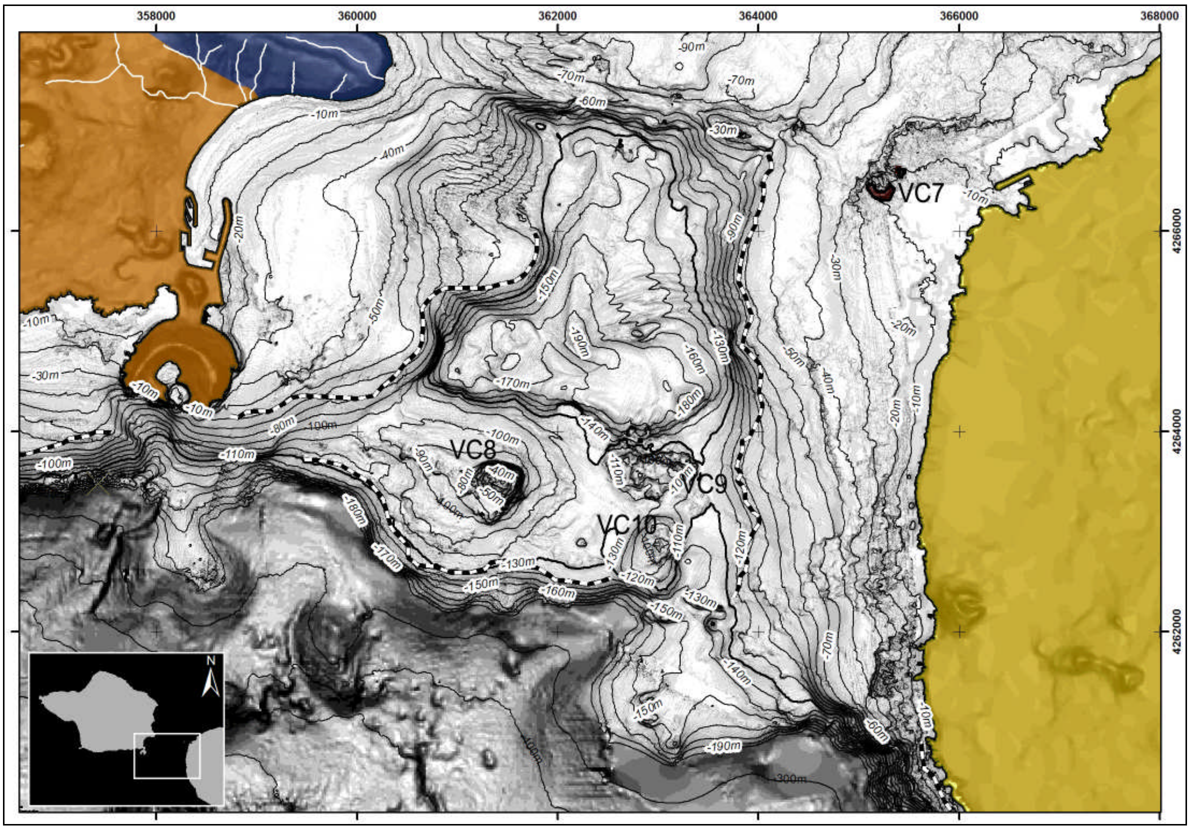

Figure 6: Southern part of the Faial-Pico passage and southern Faial. Features of note include the Baixa do Sul edifice (with surmounting cones at VC8, VC9 and VC10) straddling the southern part of the passage and closing a basin to its northern flank. The two shelf edges that border the eastern and western flanks of the basin are likely older than the formation of the Baixa do Sul edifice. Symbology as previous caption.

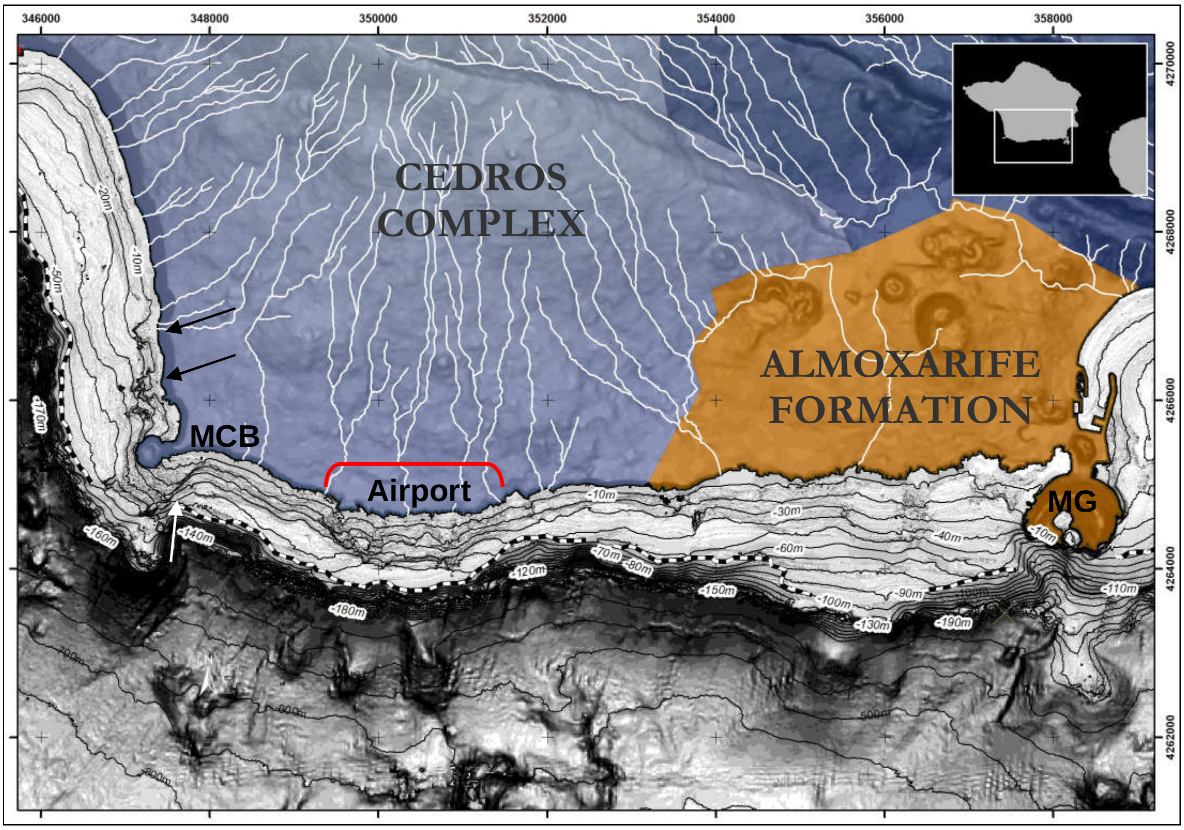

Figure 7: Southern Faial from Morro de Castelo Branco (MCB) to Monte da Guia (MG). Features of note include the irregular topography south the airport, interpreted as a large lavaflow (red bracket), the SW-NE-oriented cliff SW of MCB (white arrow) and possible lava fronts on the N of MCB (black arrows). Symbology as Figure 5.

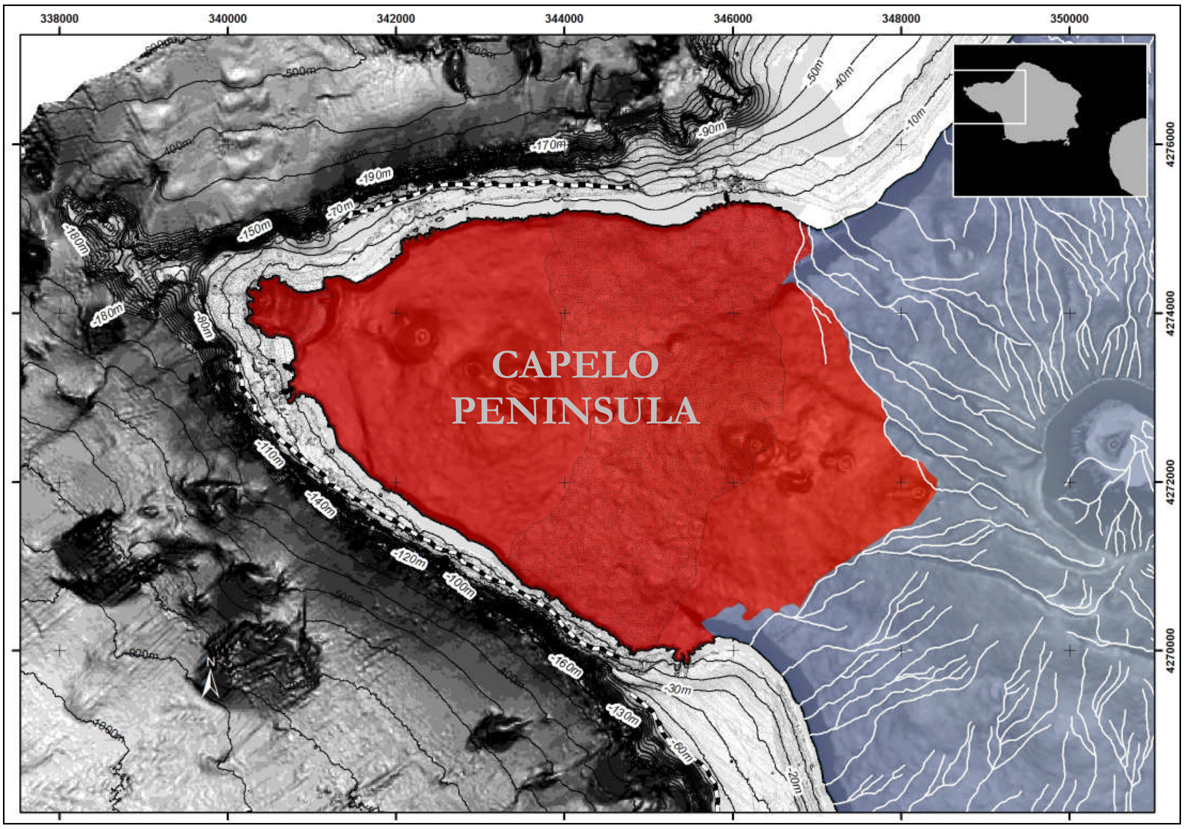

Figure 8: Capelo peninsula on western Faial. Features of note include the narrow shelf around the peninsula and its rugged topography which is conferred by an abundance of lava flows crossing the shelf. Symbology as Figure 5.

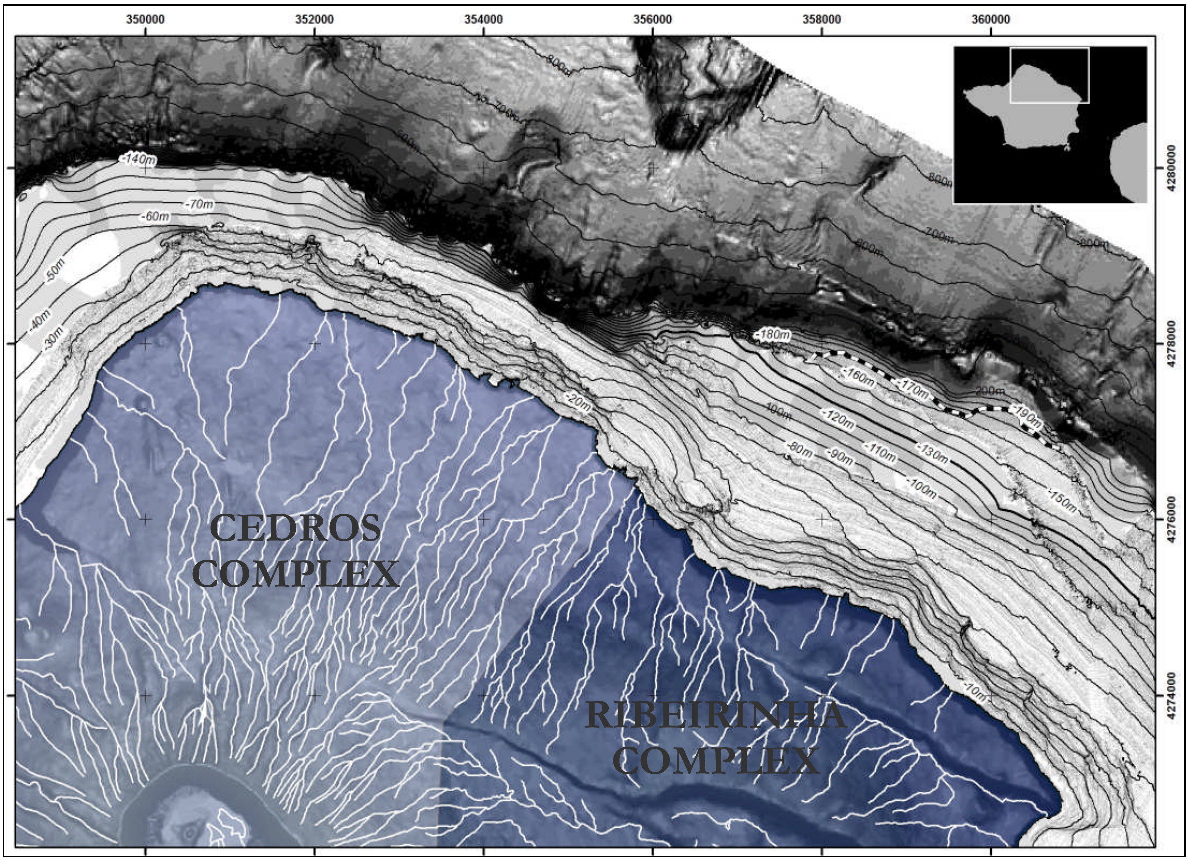

Figure 9: Northern Faial. Features of note include the nearshore boulder slopes and the smoother sedimentary deposit at their base. Some residual bedrock outcrops stand out amongst the boulders. Symbology as Figure 5.

4.3. Seafloor nature

The seafloor down to the shelf edge was classified according to its hard or soft nature based mainly on the backscatter response (Figure 10). Hard substrates accounted for 32% of the shelf area, the remaining 68% having been interpreted as sediments.

Backscatter quality, and thus the ability to distinguish backscatter regions, significantly declined over the island slopes due to increasing water depth and an inability to adequately compensate for the artefacts generated by considerable across track changes in grazing angle associated with surveying parallel to the steep seafloor.

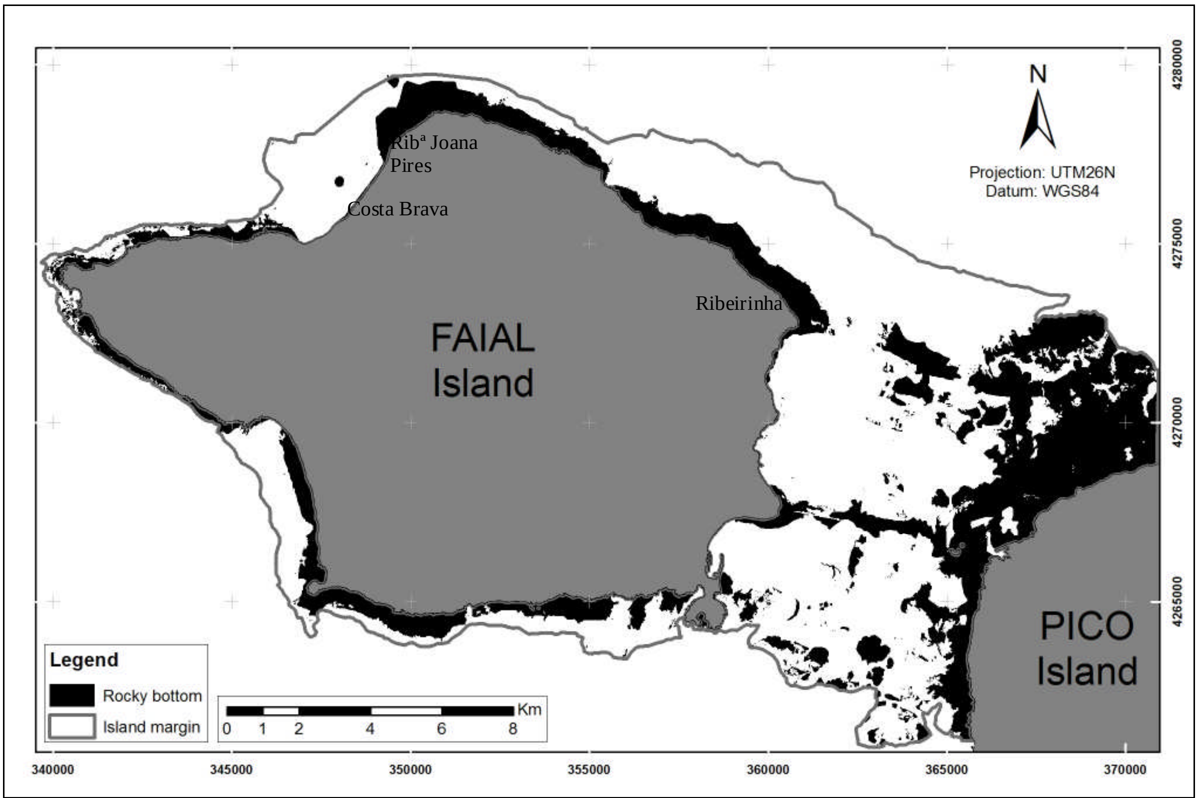

Figure 10: Segmentation of the shelf according to seafloor nature (black = rock; white = sediment).

4.4. Geomorphologic features

Analysis of bathymetry and backscatter revealed a variety of geomorphologic structures and seabed types. These are described below and illustrations are provided of their topographic and/or textural expression.

4.4.1. Shelf extent

The high resolution and coverage obtained from the surveys allowed the construction of a bathymetric grid from which an appraisal of the main characteristics of the shelves in the study area was possible. Figure 11 illustrates the extent of the different shelf sectors and their depth at shelf edge around Faial and western Pico.

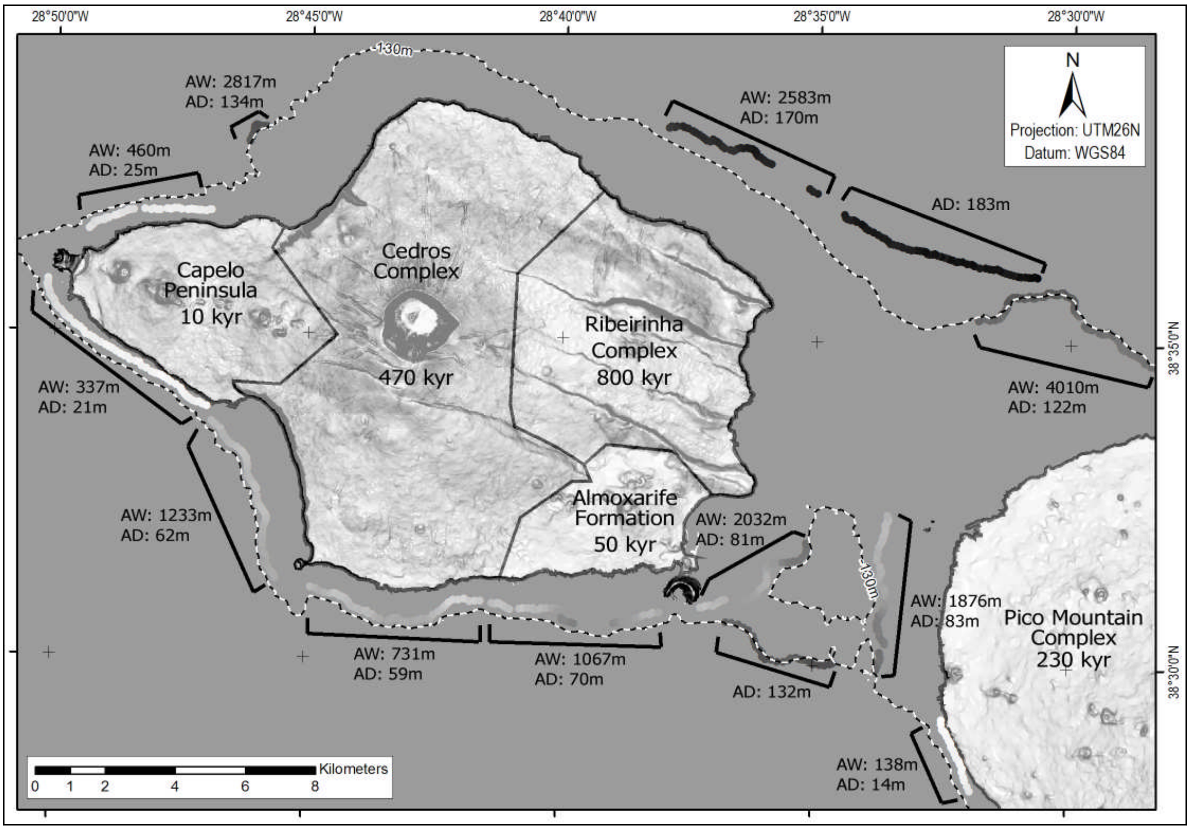

Figure 11: Average shelf width (AW) and depth at edge (AD) around Faial island and western Pico. Islands are segmented into edifices and their respective subaerial maximum ages are shown. Identified shelf edges are coloured in gray-scale reflecting its depth (black – deeper; white - shallower). In long stretches of northern Faial, the swath surveys poorly covered the shelf edge. The 130 m depth contour is shown to represent the sea level at the most recent glacial maxima.

4.4.1.1. Shelf width

The two widest shelf sectors were found to the NW of Faial and NW of Pico, with widths of 2,817 m and 4,010 m, respectively. Around the Ribeirinha complex (the oldest edifice in the study area) the shelf averaged a width of 2,583 m. Capelo peninsula, the youngest part of Faial island, exhibited a thin shelf with a width averaging only 460 m on the more exposed north side and 337 m on the less exposed southern shore.

Western Pico is dominated by the shelf uniting it to Faial but it was still possible to identify shelf edges to the North, West and Southwest that varied considerably in width. The thinnest shelf in the study area was identified on the SW of the Pico Mountain Complex and averaged 138 m width. Contrastingly, NW Pico exhibited the widest shelf sector, which averaged 4,010 m width.

4.4.1.2. Analytical shelf edge depth

Depths of the shelf edge also varied considerably between the different sectors. The deepest values were obtained off the Ribeirinha Complex and on the northern margin of the Faial-Pico passage at between 170 and 180 m. Average depths along the southern margin of Faial were between 59 and 70 m. The shelf edge off the Capelo Peninsula was at depths as shallow as 21-25 m that should reflect its very recent emplacement (10 kyr). The shallowest shelf edge (averaging 14 m) was found on the SW of the Pico Mountain Complex. The edge off NW Pico averaged 122 m depth, roughly coinciding with sea level during the most recent Glacial Maxima.

Gaps in the data off the northern and northwestern Faial margin largely prevented an accurate determination of the shelf width and depth of the sectors of the Cedros Complex most exposed to wave action. A small segment of the margin surveyed in this area exhibited an average width of 2,817 m and an average depth of 134 m. On the northern sector of the Cedros Complex the shelf is narrower, considering the location of the 130 m depth contour (which elsewhere closely encompasses the interpreted shelf edge) relative to the coastline.

4.4.1.3. Apparent rates of shelf widening

The apparent rates of shelf widening (hereafter termed ARoSW) were computed from shelf width divided by the maximum age of the adjacent geologic edifice (Figure 12-A). The resulting values show that older edifices display ARoSW much smaller than the younger edifices (Figure 12-B). Since the age assumed for each subaerial edifice is not necessarily representative of the actual age of the range of growth stages of all the sectors around it, the diversity of growth rates could be partly an artefact of incomplete age information. For instance, the widening rate computed for Pico Mountain Complex SW is 0.6 km/Myr while that of Pico Mountain Complex NW is 17.4 km/Myr), a difference of two orders of magnitude.

A

Geologic edifice sector	Apparent rates of shelf widening (km/Myr)
Faial island	
Ribeirinha N	3.2
Almoxarife SE	40.6
Almoxarife S	21.3
Cedros S	1.6
Cedros SW	2.6
Capelo S	33.7
Capelo N	46.0
Cedros W	6.0
Pico island	
Pico Mountain SW	0.6
Pico Mountain W	8.2
Pico Mountain NW	17.4

B

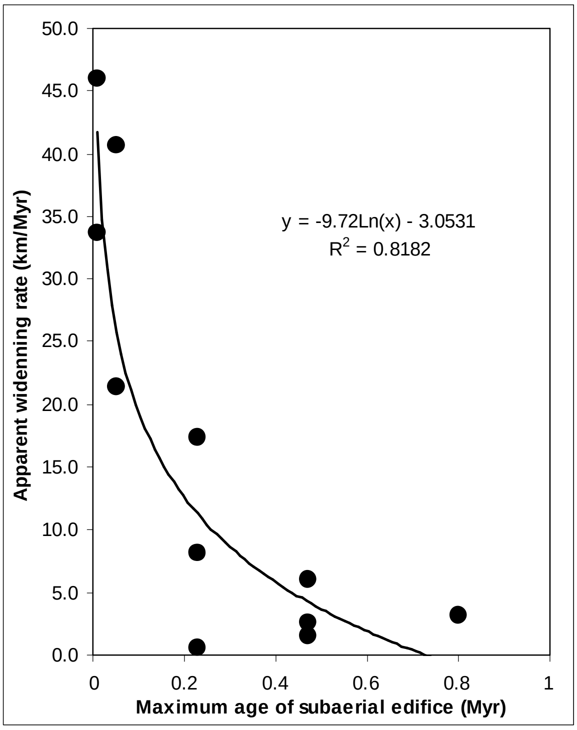

Figure 12: Apparent rates of shelf widening (ARoSW). A. ARoSW by shelf sector ordered in a clockwise direction. B. Scatterplot of ARoSW *versus* maximum age of adjacent subaerial edifice.

The non-linear relationship between these two variables for the age interval available in the study area was fit with a log-linear equation *ARoSW=-9.72ln(Age)-3.0531* (R^2=0.82). The fitted curve underestimates *ARoSW* in older shelves since it is not likely that widening stops for edifices older than 0.73 Myr.

4.4.2. Marginal island shelf erosion by mass movements

Mass movements on Faial's margin were detected that locally affect the extent of the shelf. The major event in the study area is a slump off Monte da Guia (Figure 13). The multiple concave slump scarps which are observed to the SSW of Monte da Guia may represent the record a retrogressive failure succession that removed parts of the island slope until, due to loss of support, the uppermost slump removed the island margin and part of the southern flank of Monte da Guia Surtseyan cone. The central axis of this latest slump is towards SE and part of the debris is thought to have flowed against the rise to the south of Monte da Guia. However, the bulk of the flows seems to have been directed to the SW. The run-out of this mass movement succession attains a depth of 750 m and extends across a flow-wise distance exceeding 6 km (measured from the sub-aerial scarp down to the deepest down-bowed isobaths identifiable on the debris fan surface). A few large blocks are scattered within the flow.

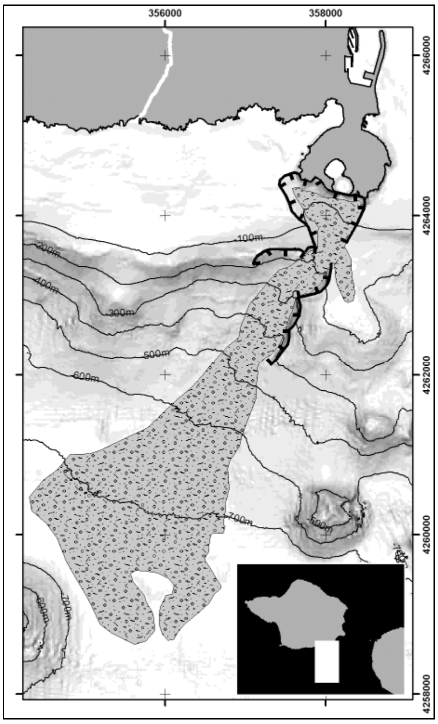

Figure 13: Monte da Guia landslide scarps and debris fan

Considerable gullying was also found on the Cedros Complex shelf edge off Praia do Norte (Figure 15-F). On its SW flank, between Varadouro and Morro de Castelo Branco, this complex exhibits multiple slump scallops but no large gullies (Figure 14-B). Despite its oldest age, the Ribeirinha complex margin (along with the northern part of the passage) displayed little evidence of mass wasting erosion (Figure 15-E). The recent Almoxarife Formation (Figure 14-A) and the very young Capelo Peninsula also showed an absence of large gullies (Figure 14-C and D).

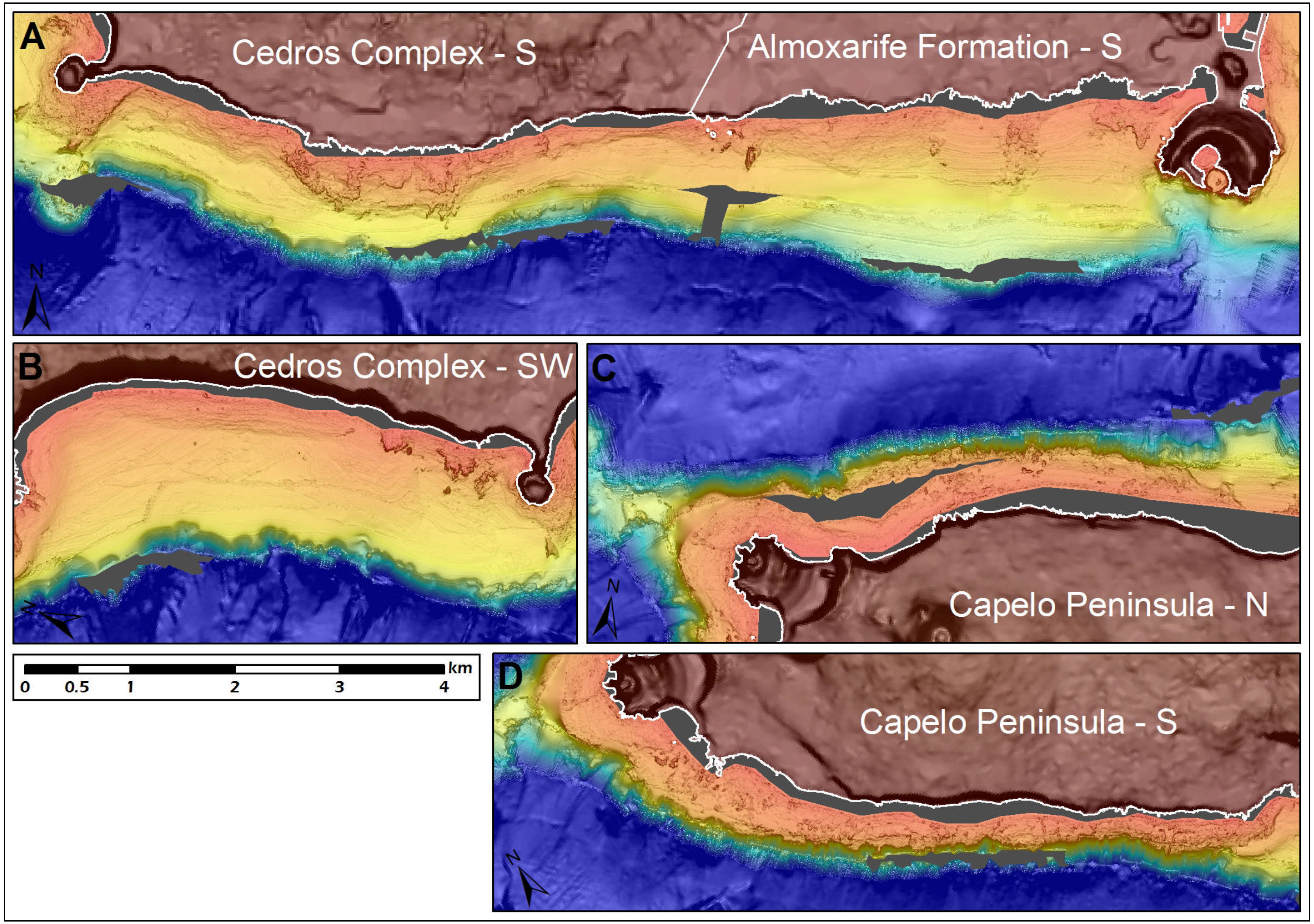

Figure 14: Aspect of marginal erosion of the south (A) and western (B to D) sectors of Faial shelf.

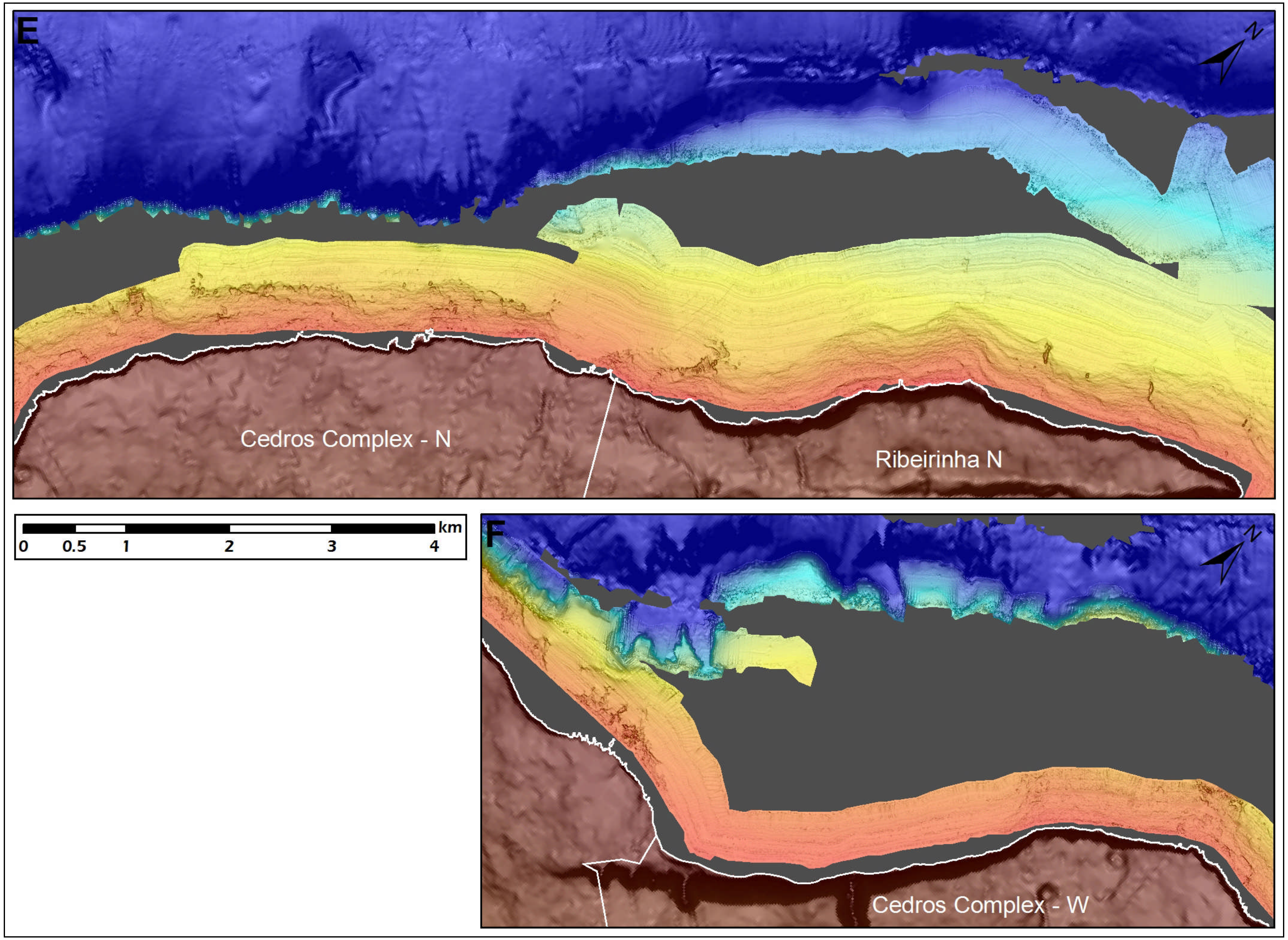

Figure 15: Aspect of marginal erosion of the north (A) and north-western (B) sectors of Faial shelf.

4.4.3. Palaeo-shorelines

Faial island shelf exhibited few potential palaeo-shorelines. Only minor cliff sections at the level of the latest glacial maxima lowstands 120-130 m bpsl were identified off the southern shore (Figure 34). Contrastingly, palaeo-shorelines were mapped in greater abundance off western Pico and a few small stretches along the southern flank of Baixa do Sul ridge (Figure 16).

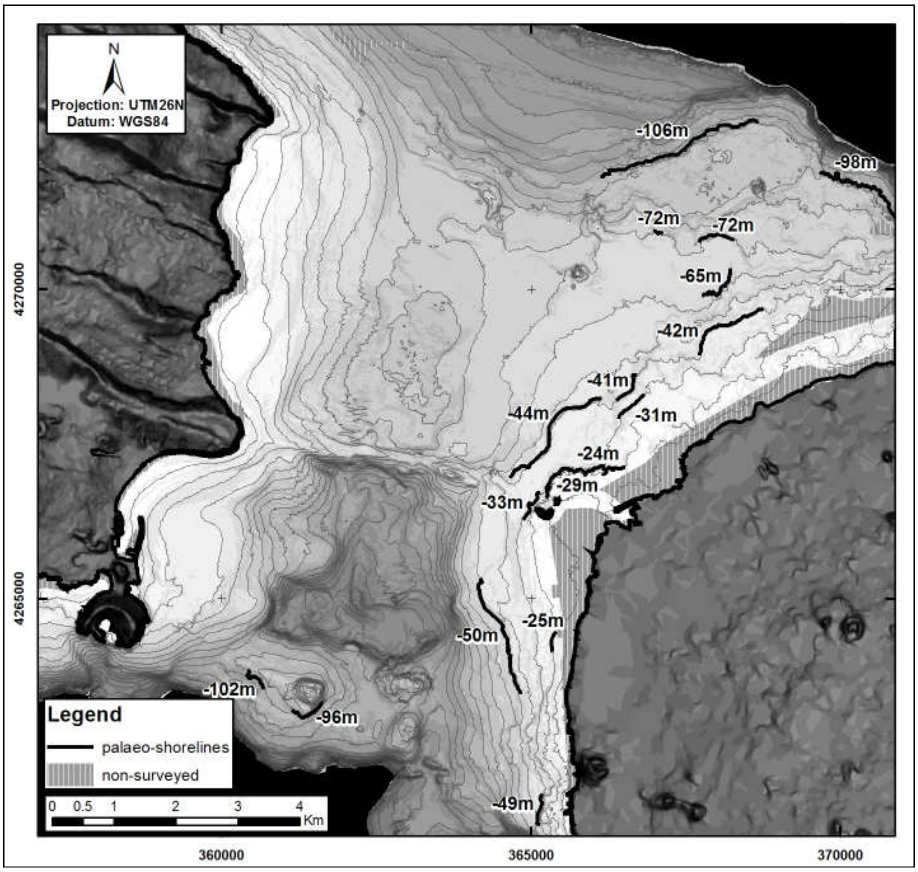

Figure 16: Location of potential palaeo-shorelines in the Faial-Pico passage.

A total linear extent of 20.3 km was mapped for palaeo-shorelines in the Faial-Pico passage, with individual lengths ranging between 190 m and 3.1 km. Detailed plan views of these palaeo-shorelines are shown in Figure 17 and Figure 19. A 3-D perspective of one of these palaeo-shorelines is shown in Figure 18-A. Many of these shorelines display marginal erosion in the shape of small narrow indentations which conform to *type IV* plunging cliffs described by Borges (2003) for lava flow shores (Figure 18-B).

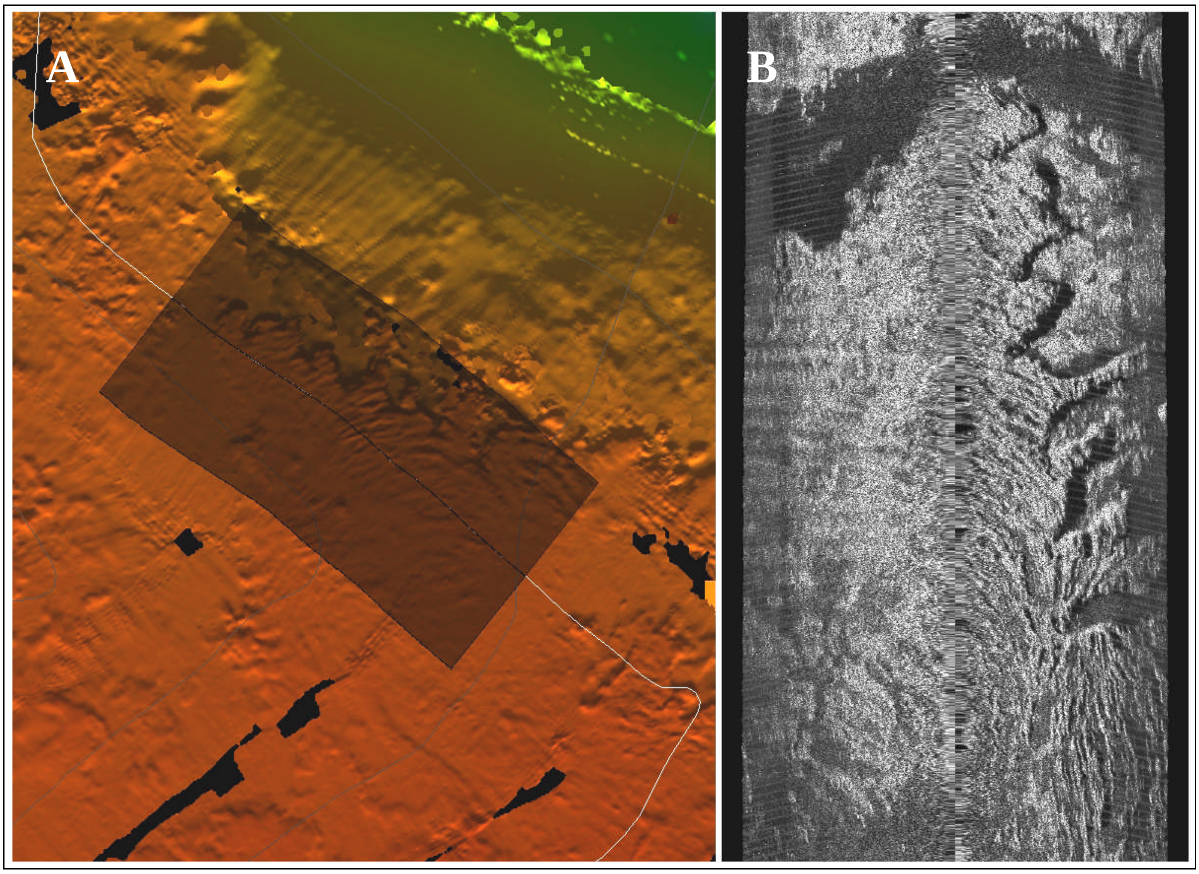

Figure 17: Cliff palaeo-shoreline NW of Pico with a base at 98 m depth. A. Shaded relief with superimposed swath survey track lines. B. Backscatter image of the darkened area in A. Features of note include the preserved ropy texture of the upper surface of the wave-quarried lava front.

A

B

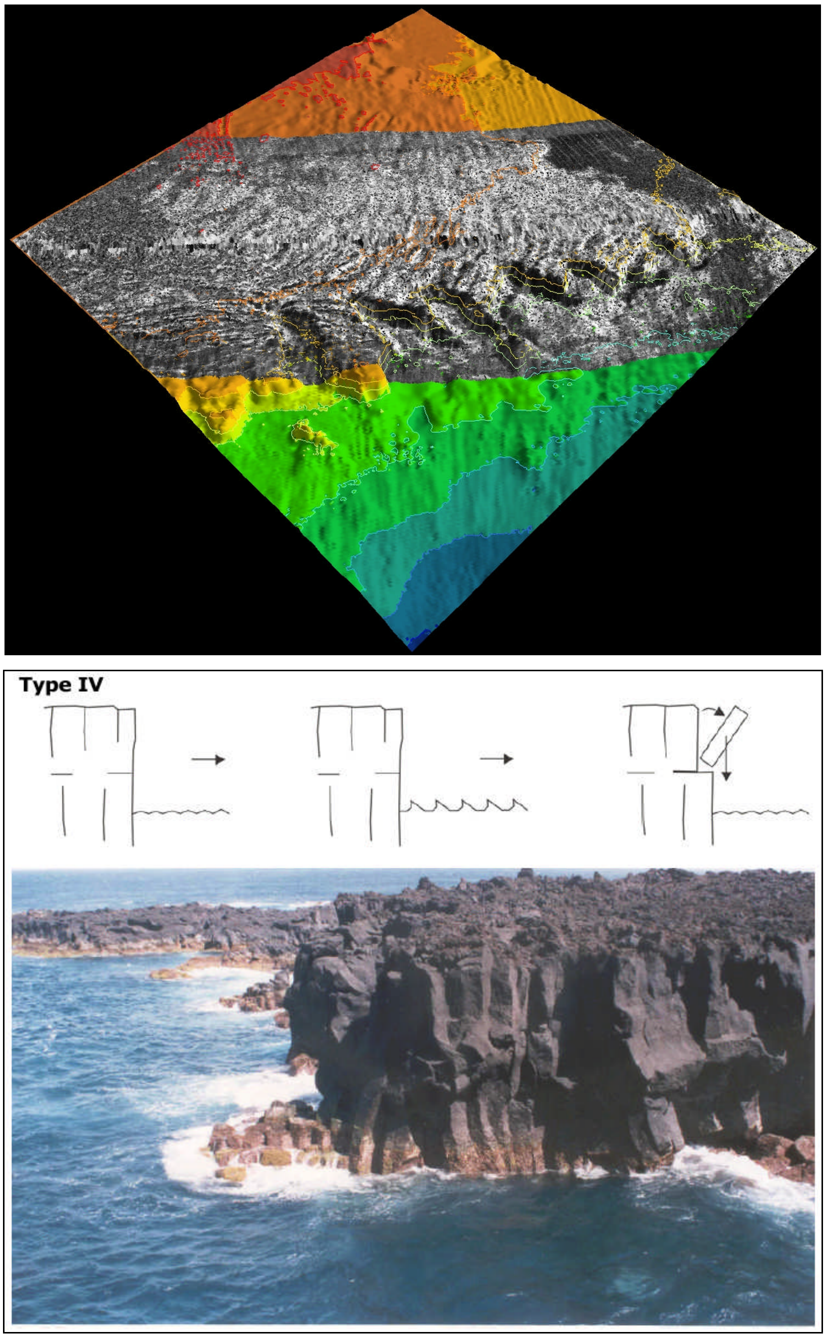

Figure 18: A. 3-D perspective of the previous feature with colour-coded relief draped with a strip of backscatter data. In the backscatter images, light tones represent high backscatter and dark tones represent low backscatter and shadows. The scarps of the indentations are approximately 10-m high. B. Evolution and aspect of a *type IV* shoreline identical to the identified palaeo-shoreline (adapted from Borges, 2003).

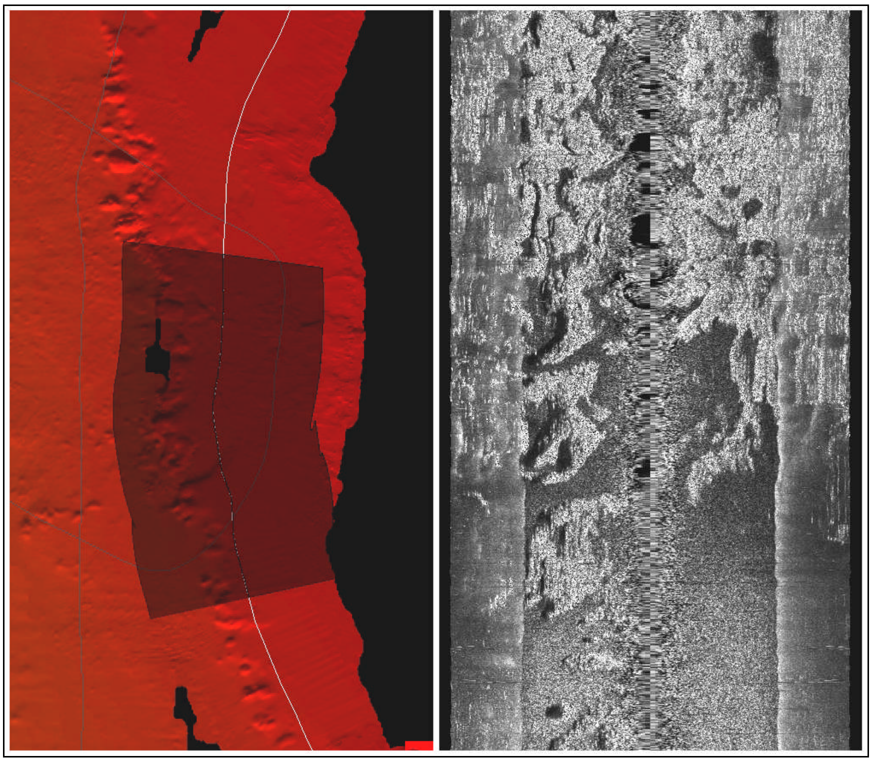

Figure 19: Cliff palaeo-shoreline to the W of Pico with a base at 50 m depth. A. Shaded relief with superimposed swath survey track lines. B. Backscatter image of the darkened area in A. Features of note include the higher degree of sedimentation (dark grey tones) and absence of a ropy texture in comparison with the example presented in Figure 17.

4.4.3.1. Vertical location of palaeo-shorelines

The location of the palaeo-shorelines below present sea-level is quantitatively analysed taking into account their extent at different bathymetric levels.

Since the average depth (122 m) of the shelf edge on the north-western sector of the Pico Mountain Complex (section 4.4.1) indicated no major recent isostatic variation and most of the palaeo-shorelines analysed are located in this sector, the bathymetric location of features could be straightforwardly related to an eustatic Holocene sea-level curve.

The bathymetric distribution of the cliff palaeo-shoreline bases (red dashes) on this area is plotted in Figure 20 alongside a global eustatic sea level curve for the last 22 kyr.

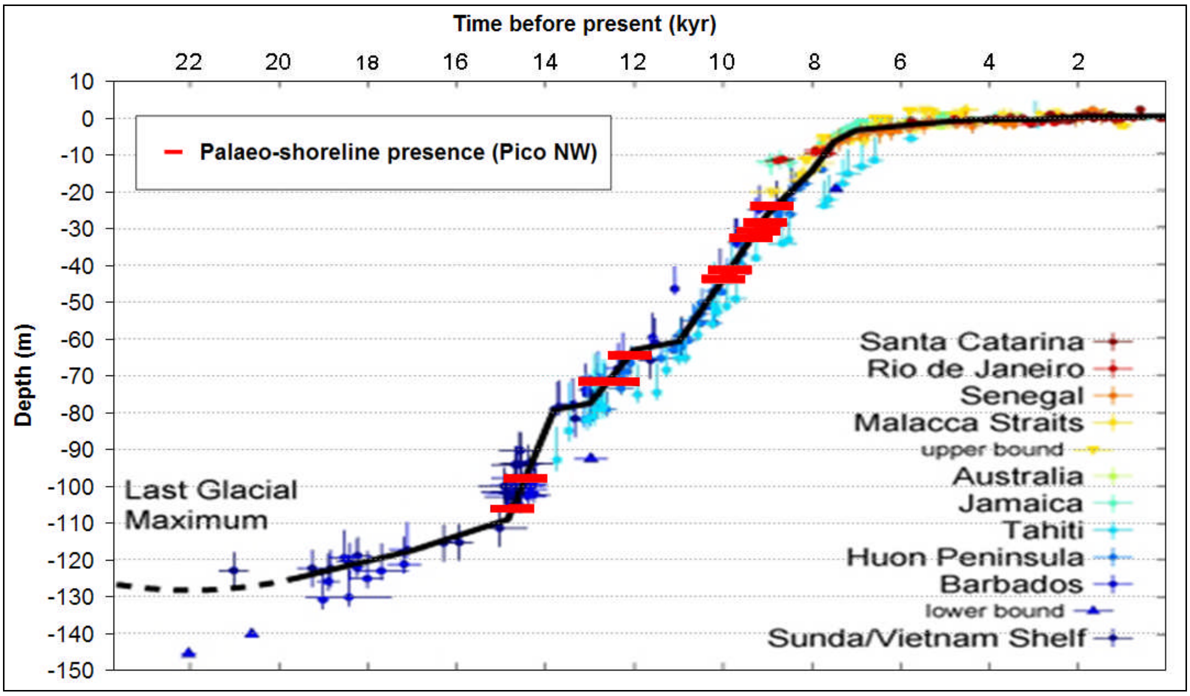

Figure 20: Palaeo-shoreline bathymetric location (red dashes) plotted over a curve of Holocence sea-level rise (black line) based on Fleming et al. (1998).

Palaeo-shorelines occurred at vertical locations (-106 m, -98 m, -72 m, -65 m, -44 m, -42 m, -41 m, -33 m, -31 m, -29 m and -24 m) that corresponded to periods of fast sea-level rise during the Holocene. None was visible at bathymetric levels corresponding to the sea level standstills identified for the same period. It is also worth-noting that the deepest palaeo-shoreline approximately coincides with the period when sea-level rise intensified at 110 m depth b.p.s.l. No records of palaeo-shorelines were noted at depths less than 20 m due to extensive gaps in data over the shallowest areas.

4.4.4. Boulder slopes

Boulder slopes are a major feature of Faial's nearshore. Such slopes develop mostly at the base of tall cliffs developing by action of surf erosion as Borges (2003) has previously described in a physiographic study of the Azores coastlines.

The most extensive boulder accumulations within the study area were located on the north coast of Faial (i.e., the Ribeirinha and Cedros volcanic edifices), from the mouth of the Ribeira de Joana Pires to Ponta da Ribeirinha. On this stretch of coast they reached a maximum width of 860 m (off Ponta da Ribeirinha) measured from the present shoreline. An underwater image of the large boulders composing these areas is shown in Figure 21.

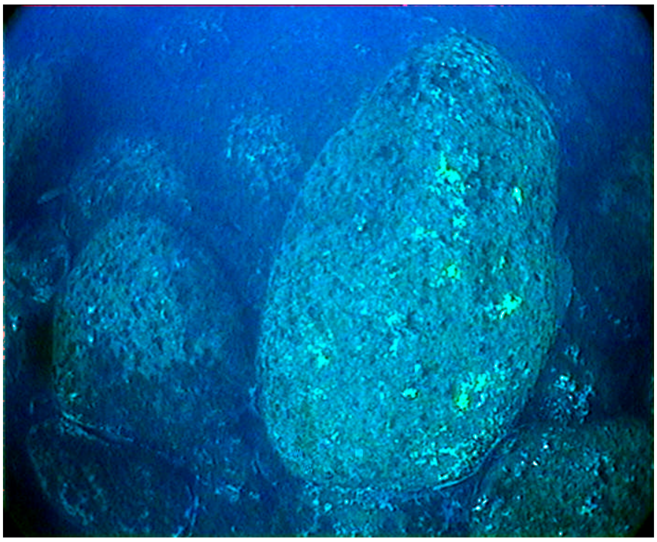

Figure 21: Underwater aspect of boulder slope.

Successive small terraces which trend parallel or oblique to the shoreline and dip diagonally across bathymetric contours were identified on some of these boulders slopes. These are particularly well developed on the NE coast of Faial (Figure 22) where they extend down to depths of 55 m. The terraces are better developed on the SE leeside of protrusions and their vertical spacing varies between 6 and 20 m. The boulders on these terraces are often partially submerged in sand.

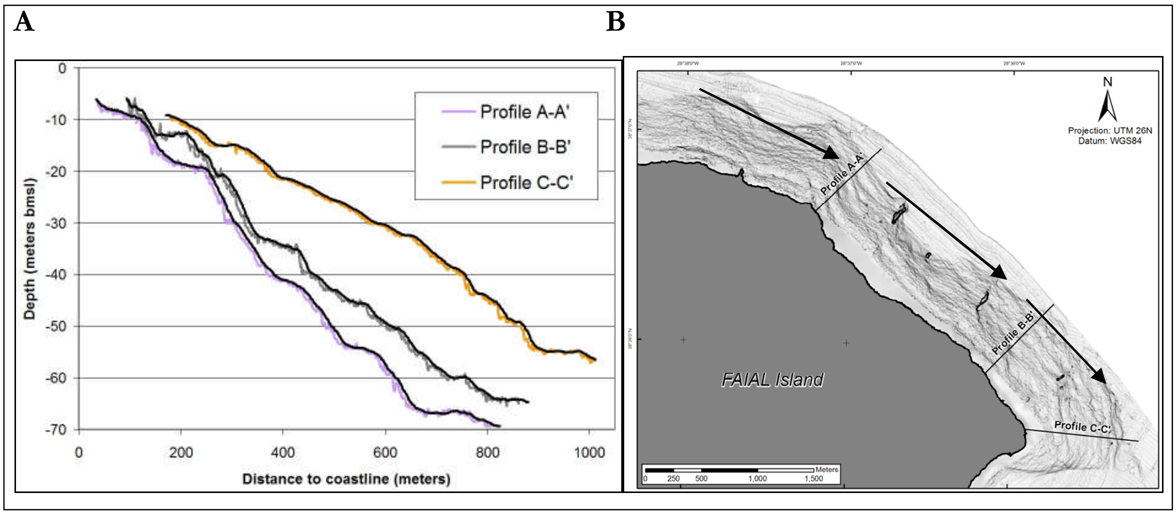

Figure 22: Dipping terraces on the boulder slopes of NE Faial. A. Shore normal profiles of the boulder slope down to the sediment plain. Vertical exaggeration is 10×. B. Location of extracted profiles over colour coded bathymetry shaded by semitransparent grayscale-coded slope map. Arrows represent probable nearshore sediment drift predicted from prevailing swell direction. Three small elongate structures are identifiable normal to the coast that may represent basalt dykes.

4.4.5. Submerged volcanic cones

The occurrence of Surtseyan eruptive centres throughout the Faial-Pico passage was previously reported by Nunes (1999) for locations such Baixa do Norte, Baixa do Sul and the Madalena Islets.

The detailed swath bathymetry confirms these and other cones and furthermore reveals their fine-scale morphology (Figure 23). In addition, other on-slope volcanic centres can be identified (in Figure 4, and in higher detail in Figure 5 to Figure 9) but only the on-shelf volcanic ones are analysed in the present work. With the exception of VC1, the cones are clearly associated with the WNW-ESE normal faults that extend from eastern Faial.

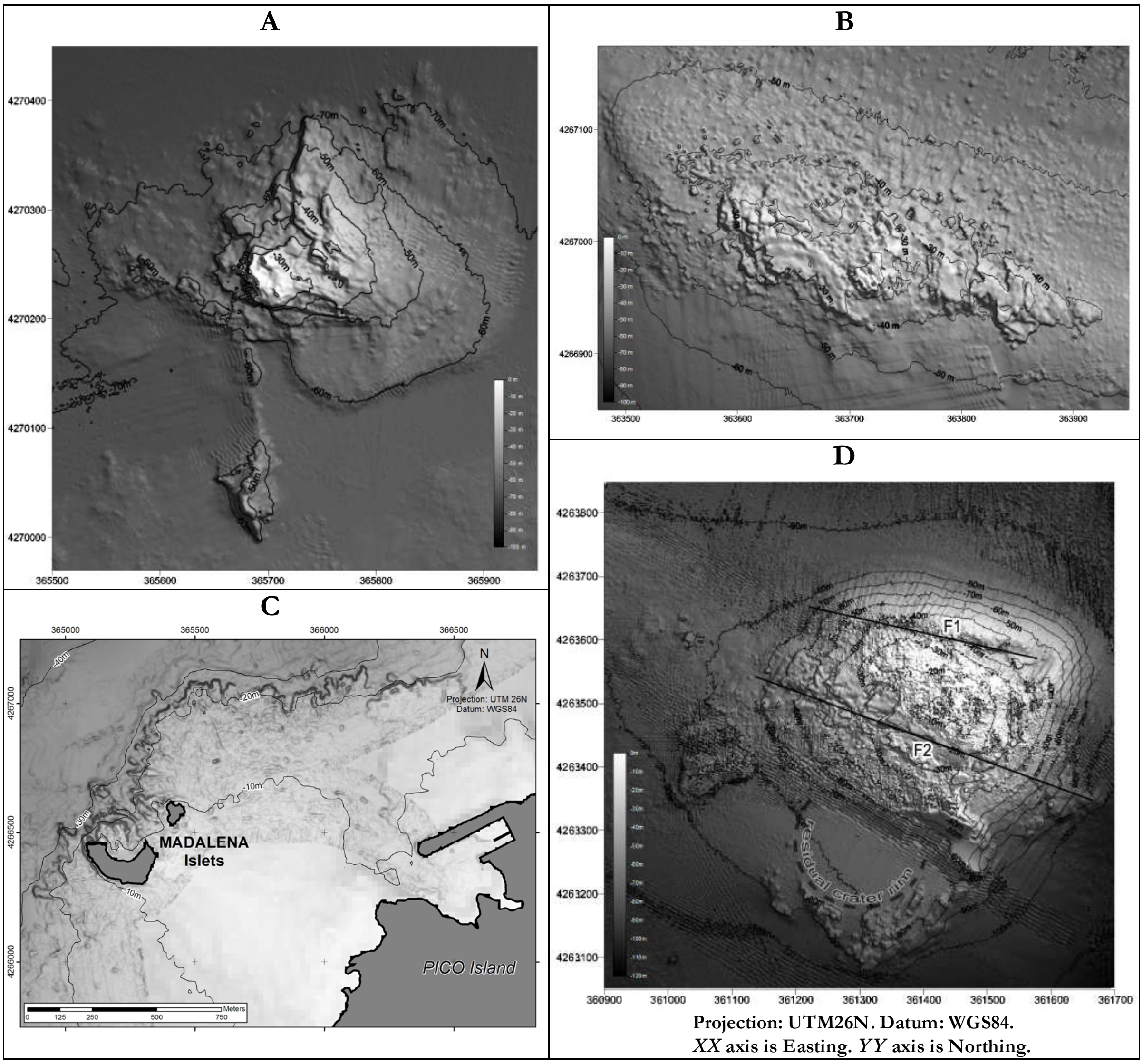

Figure 23: Submerged volcanic cones from the Faial-Pico passage. A. VC4 - Baixa da Barca; B. VC5 - Baixa do Norte; C. Madalena Islets; D. VC8 - Baixa do Sul.

The Baixa do Sul ridge is the largest identifiable volcanic centre in the passage area (Figure 6). The complex is sited on a WNW-ESE extension to a tectonic weakness noted on shore but its emplacement can be considered independent from the subaerial complexes identified on the neighbouring islands. The shallowest cone surmounting this edifice (VC8 - Baixa do Sul) is shown on Figure 23-D. The rim of a round crater that has been filled with sediment is identified on its southern flank, at an approximate depth of 80 m. To the north of this, a cone extends to depths of only 7 m which is truncated by two dominant, sub-parallel lines of weakness presumed to be faults trending WNW-ESE (F1 and F2). Observations made *in situ* by scuba-divers indicated these lines of weakness are marked by pot-holes and erosional notches. Some of the latter are a few meters in diameter which is not surprising given the exposure of the site to oceanic storms.

Although Baixa do Sul is a Surtseyan tuff cone (Nunes, 1999), drop down camera images along the ridge showed pillow lavas on VC10 (Figure 24) revealing that upper parts the Baixa do Sul ridge were emplaced subaqueously. No imagery was acquired on VC9 but the bulbous morphology suggested even more clearly stacks of mega-pillows with a lesser sediment coating which may denote a younger age.

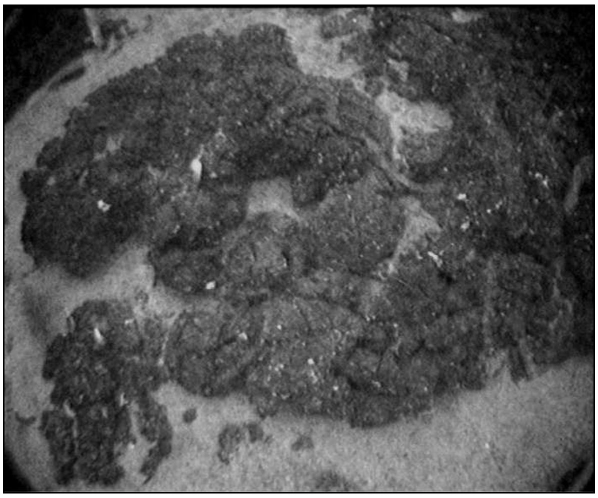

Figure 24: Drop down camera images of VC10 showing pillow lavas. Note the bulbous shape and the cracked surfaces created by cooling-induced contraction.

Two small volcanic cones in the northeast part of the passage, VC4 (Baixa da Barca) and VC5 (Baixa do Norte), are shown in Figure 23-A and B, respectively. The northwestern half of VC4 displays a higher degree of dismantling, which is likely explained by its open exposure to the prevailing swells from the NW during periods of lower sea level. No crater is readily identifiable in VC4 but a possible fissural extrusion with a N-S orientation stems from the SW flank and extends for 200 m. VC5 displays an elongated morphology that suggests it to be one of the fissural eruptive centres that contributed to building the Espalamaca-Madalena ridge. Ground-truthing by scuba diving and ROV showed that some persistent blocks constitute the shallowest peaks but the surroundings are dominated by boulders.

The underwater bathymetry further revealed that the southern Madalena islet (Ilhéu Deitado) forms a cone that appears independent from the northern Madalena islet (Ilhéu em Pé), which may represent part of a different crater further to the north which may have been draped by the lava flows that surround the islets.

Further heavily eroded cones may be present amongst the boulder slopes of northern Faial. These are relatively resilient features exhibiting a heavily eroded tilted stratification (Figure 25-A) that shows signs of a concentric arrangement. In a drop-down camera deployment (ref. DDC#15) aimed at one of these features close to the northernmost tip of Faial, fragments of columnar basalt were imaged that further support the idea of a dismantled cone (Figure 25-B to D).

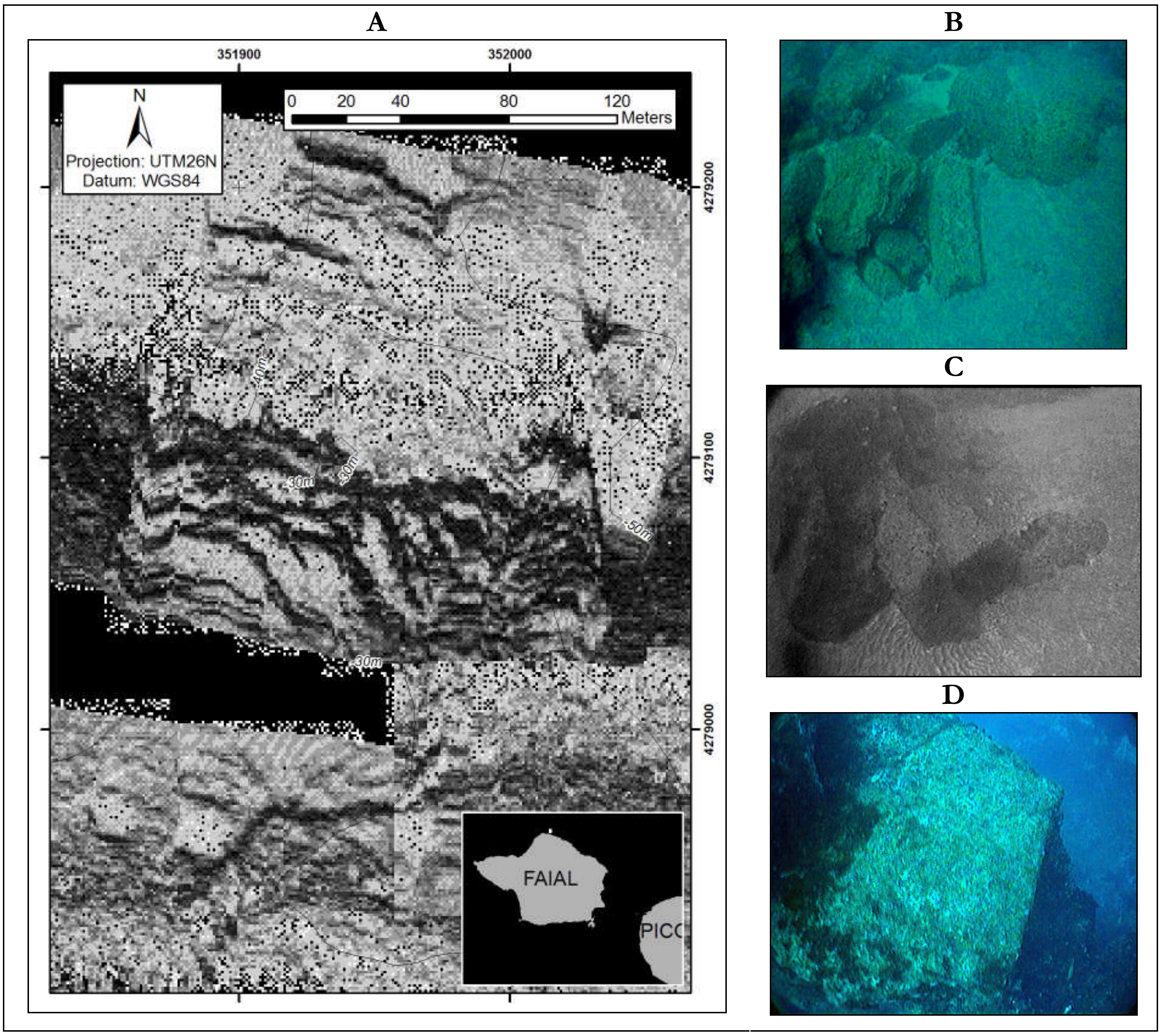

Figure 25: Possible heavily eroded cones amongst the boulder slopes of northern Faial. A. Backscatter mosaic displaying dismantled tilted layering. B and C - Pieces of broken columnar basalt. D – Top view of *in situ* columnar basalt.

4.4.6. Lava flows

Lava flows extending over to the seafloor could be identified on the nearshore of both Pico and Faial (Figure 26). They are distinguished from palaeo-shorelines because the latter are typically parallel to bathymetric contours while the former tended to cross cut the contours.

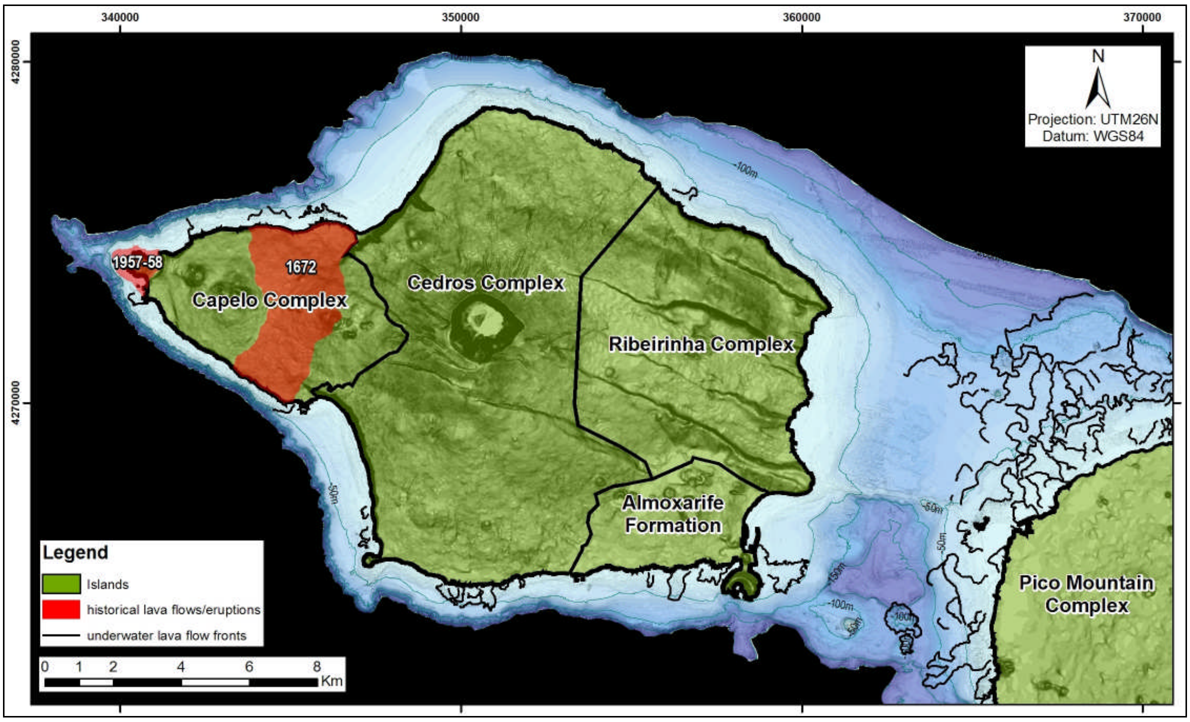

Figure 26: Lava flow fronts identifiable on the shelf of Faial and western Pico.

A variety of backscatter patterns corresponding to lava flows are shown in Figure 27 to Figure 30. The most characteristic lava flow sequence was found on northwestern Pico, where a lava series has been extruded over the shelf exhibiting multiple superimposed lava benches (Figure 27-A). This sequence extends from the northeastern-most tip of the study area down to the village of Madalena, across approximately 7 km of coastline. The southern-most of these flows surrounded the Surtseyan cone of Madalena Islets, which almost became a steptoe.

Further south along the coast of Pico, lava flows are also a prevailing feature, although they are not so numerous (Figure 27-B and Figure 28-A).

Around Faial, lava flows were prominent around the recent Capelo peninsula although individual fronts and margins where difficult to distinguish (Figure 14-C and D). Other examples exist on the Almoxarife Formation and on the S and SW of the Cedros Complex. Some of these are shown in Figure 28-B, Figure 29 and Figure 30.

Two stacks of pillow lavas were identified as lava flows on the eastern side of the Baixa do Sul ridge.

A

B

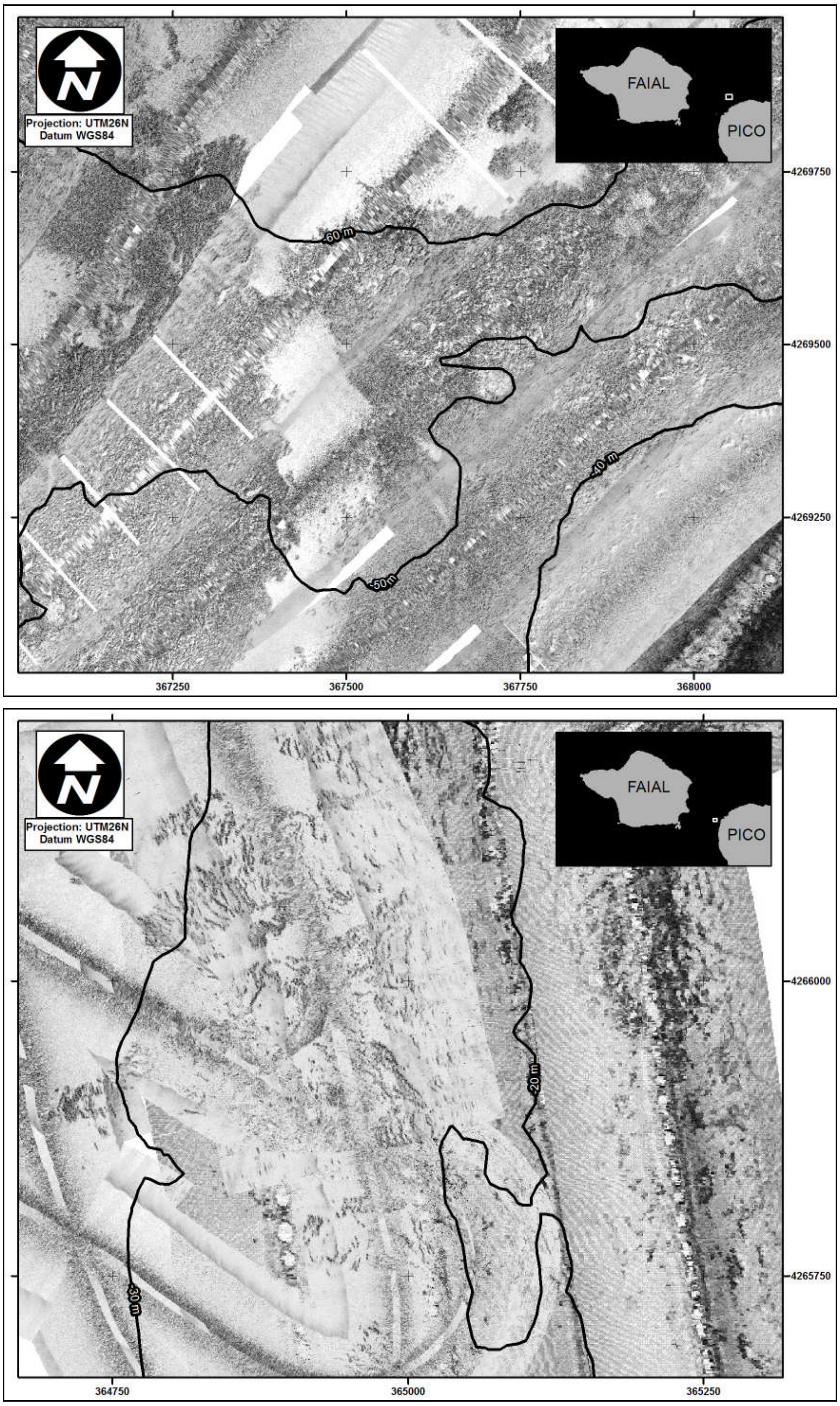

Figure 27: Backscatter aspect of different lava flow morphologies: A. Overlapping lava sheets of NW Pico with a small sediment deposit (brighter shades of grey) at the base of the upper lava front; B. Lava flow off Areia Larga (W Pico) displaying down-flow concentric compression ridges partially covered by sediment.

A

B

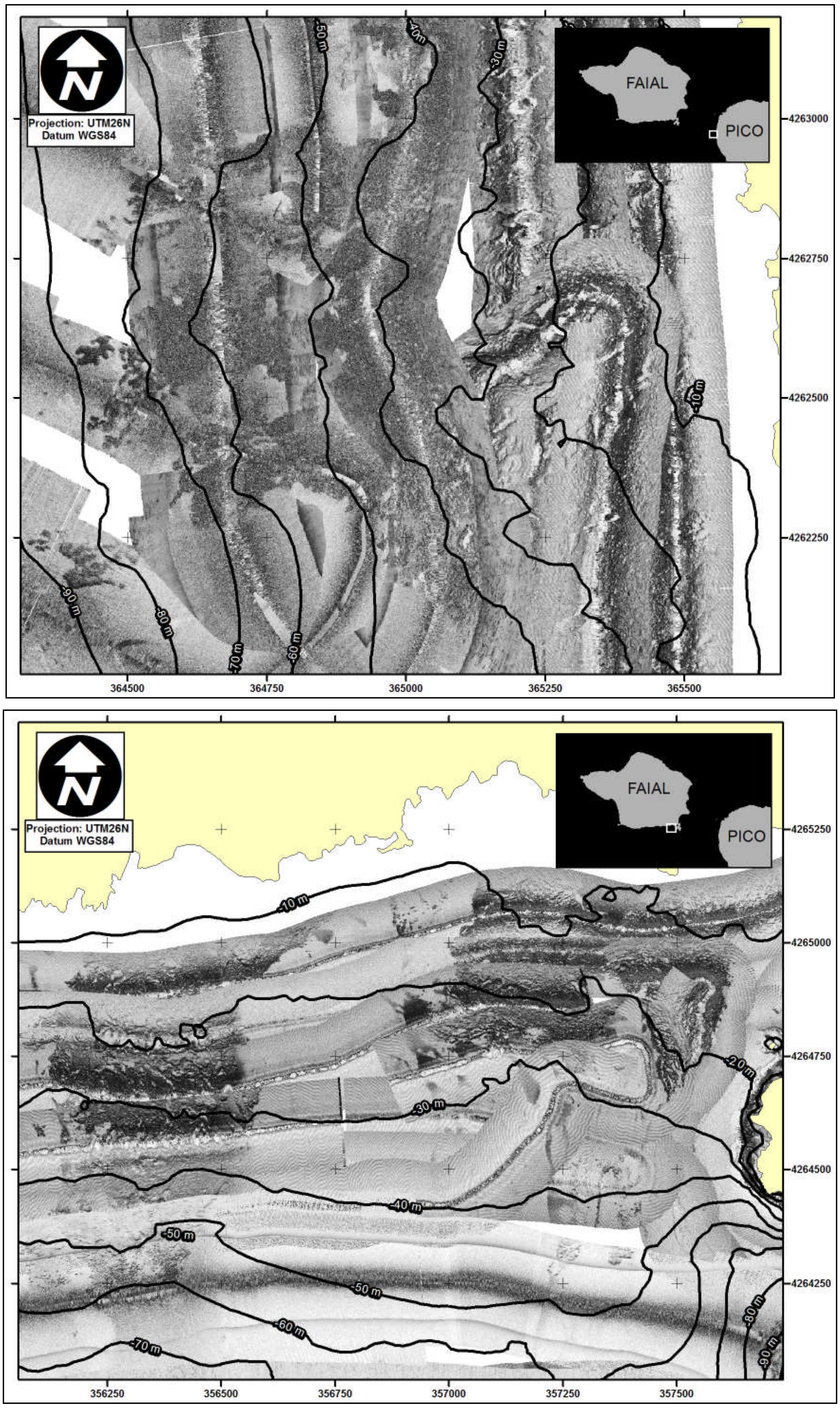

Figure 28: A. Lava sheets off Monte (W Pico) sourcing smaller dendritic lobes; B. Two lava flows off Pasteleiro (SE Faial) displaying compression ridges.

A

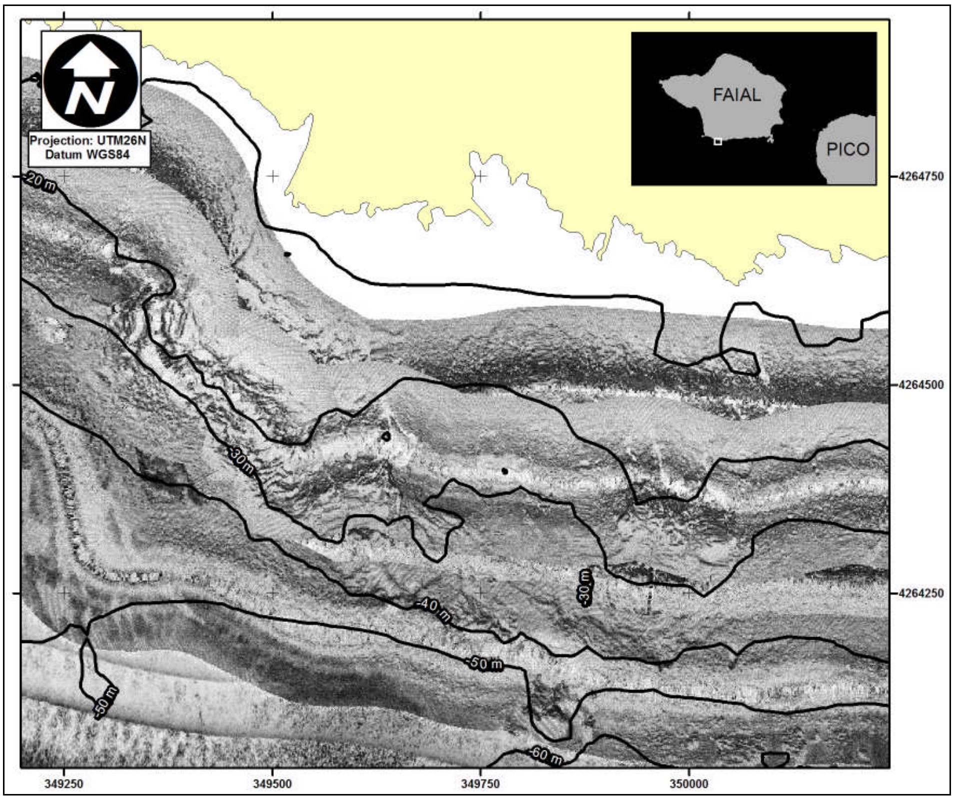

B

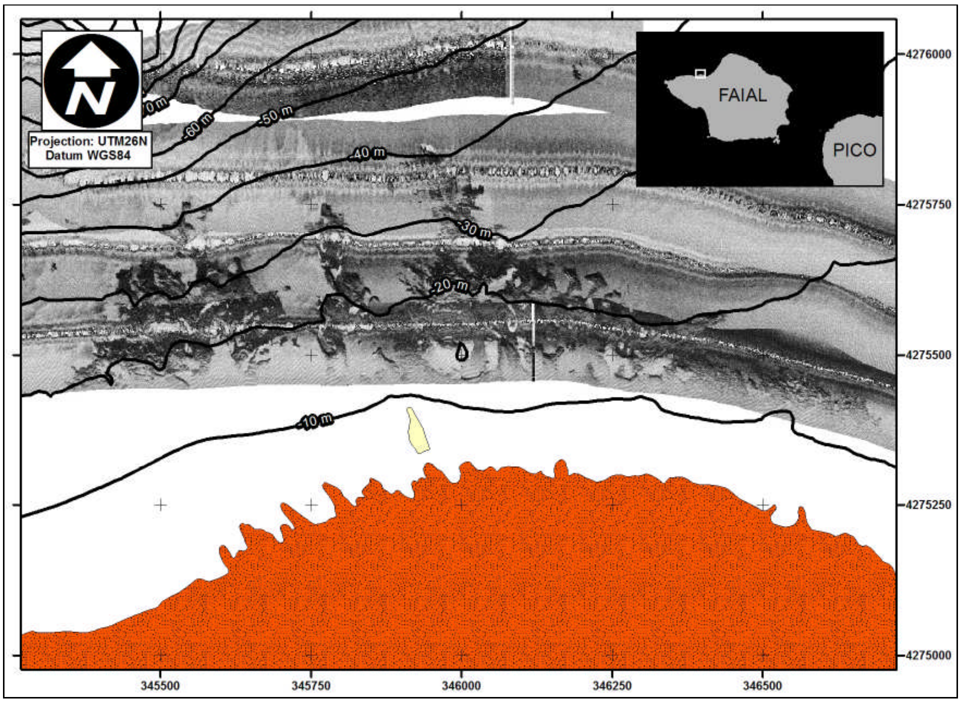

Figure 29: A. Lava flows off Faial's airport displaying large compression ridges; B. Northernmost underwater section of the 1672 lava flow to the north of the Capelo peninsula showing multiple lava fingers developing over a sediment bed.

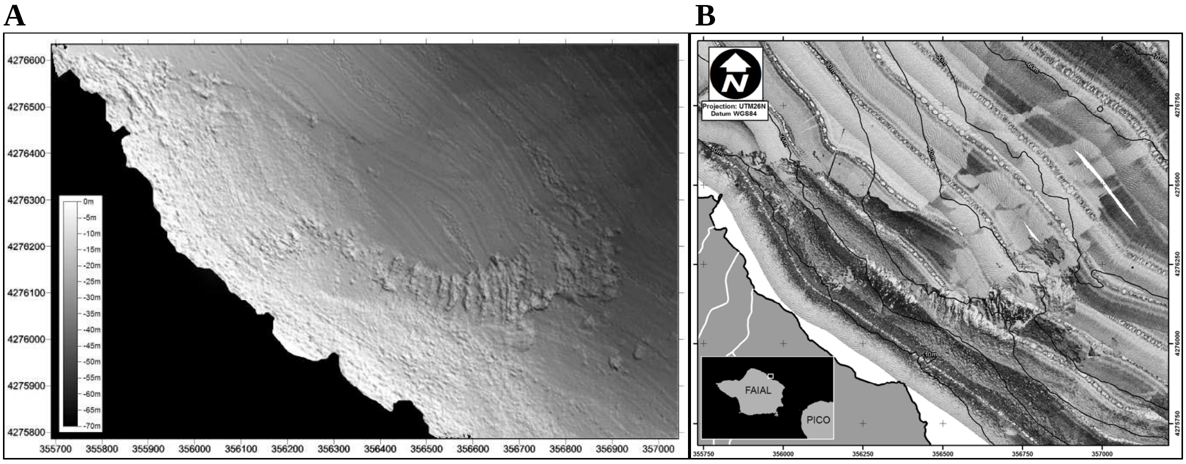

Figure 30: Lava flow cropping out at the base of the boulder slope (SE of Salão harbour) showing large down-flow convex compression ridges. A. Grayscale-coded bathymetry. B. Backscatter mosaic.

4.4.7. On-shelf faulting

The results from using underwater volcanic and tectonic lineaments to identify on-shelf fault extensions are presented in Figure 31. Fault extensions were most abundant in the inter-island passage either projecting from the Pedro Miguel graben (for a zoomed in view see also Figure 5) or associated with the Baixa do Sul ridge (for a zoomed in view see also Figure 6).

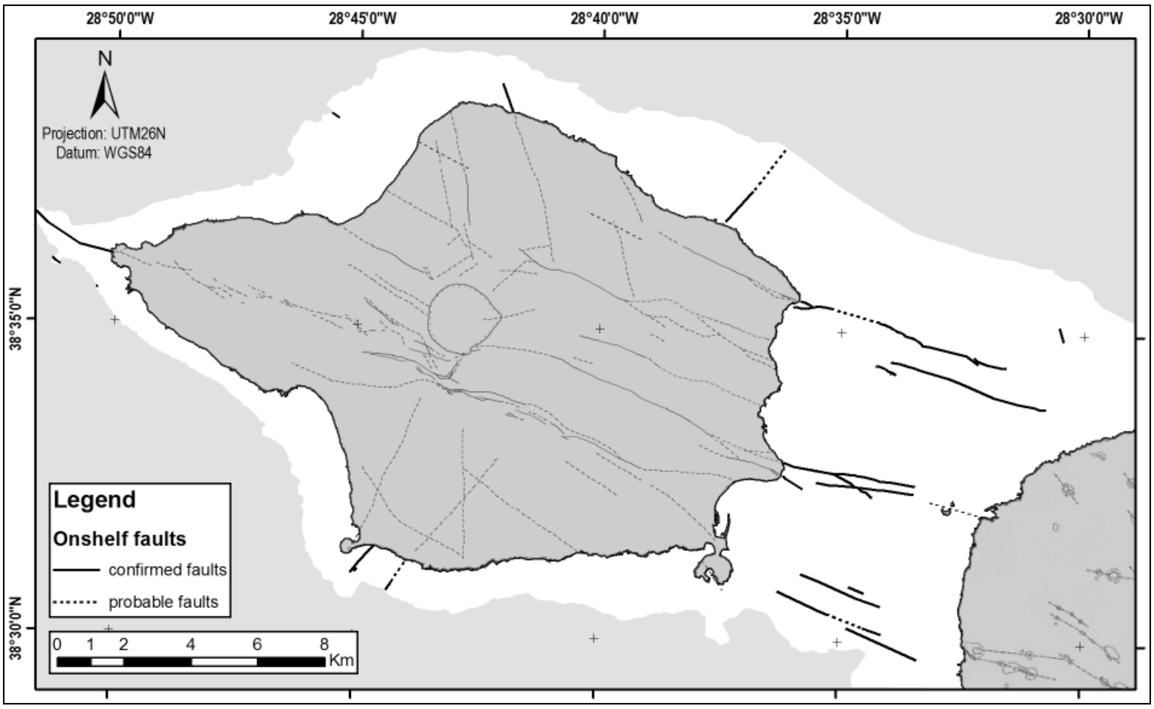

Figure 31: Faults identified from volcanic and tectonic on-shelf lineaments. Onshore tectonic maps are adapted from Madeira (1998), Nunes (1999) and Camacho et al. (2007).

The southernmost normal fault of the Pedro Miguel graben (known as the Espalamaca fault) was readily identified on the shelf with a prominent footwall which forms a ridge extending from the Espalamaca headland to Baixa do Norte (Figure 32). Of note along the ridge is also a dextral strike-slip fault (SSF1 in Figure 5) trending N55W. The continuation of this fault towards Pico is uncertain due to the masking by sediment. The lateral displacement produced by this fault between the two adjacent blocks is clear on the south side of the ridge and a small vertical component is also noticeable on the top of the ridge.

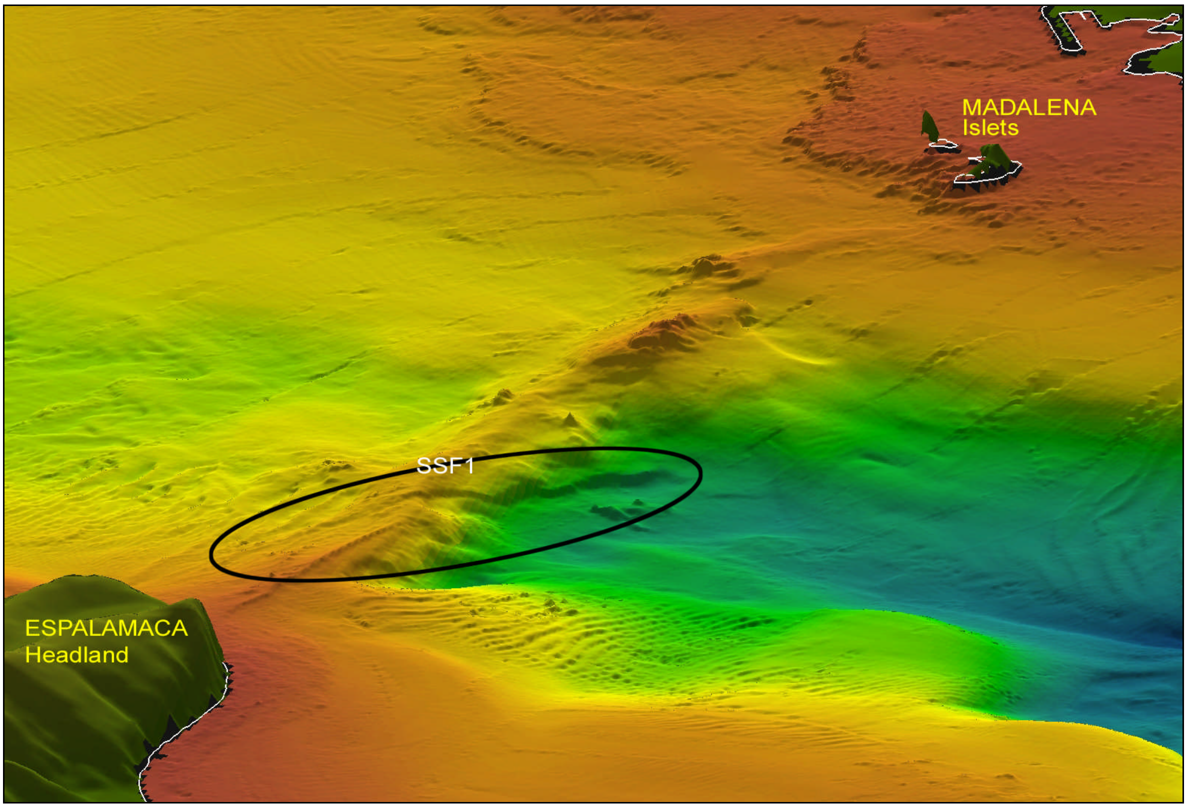

Figure 32: 3-D perspective emphasizing the vertical component of fault SSF1 which strikes diagonally on the Espalamaca-Madalena ridge. A crisp crest is also visible just off Espalamaca headland which was shown by ROV ground-truthing to be a sharp sand ridge, rather than a tectonic feature.

Other faults related to the Pedro Miguel graben resurface mid-passage (lineaments NF1 to NF4 in Figure 5). Scarp heights of these submerged sections were smaller than those found in their subaerial projections. It is likely that significant amounts of sediment accumulating at their basement are masking their full vertical relief. Other WNW-ESE lineaments suggested by Figure 5 should be disregarded as artefacts created by poor data quality at the margins of scarcely overlapping swaths.

There is ample evidence that volcanic activity is associated with the on-shelf faulting. The Baixa do Sul ridge appears as the most productive volcano-tectonic feature in the passage. The upper parts of the complex retain well-defined extrusive centres such as a Surtseyan cone and pillow lava stacks.

Along its extension, the Espalamaca-Madalena ridge exhibits probable eruptive centres on VC5 (Baixa do Norte) and VC6. Given that it looses surficial expression off the Madalena Islets and that the latter are slightly off its projection, it is uncertain whether the islets volcanic centre is associated with the same structure or a neighbouring radial fault from the Pico Mountain Complex. On the seaward projection of the Ribeirinha fault at least two eruptive centres (VC2 and VC3) are also discernible (see Figure 33 for a detailed illuminated view). A vertical offset of approximately 4 m was measured between the volcanic materials sitting either side of the fault in VC2 indicating movement since the eruptions.

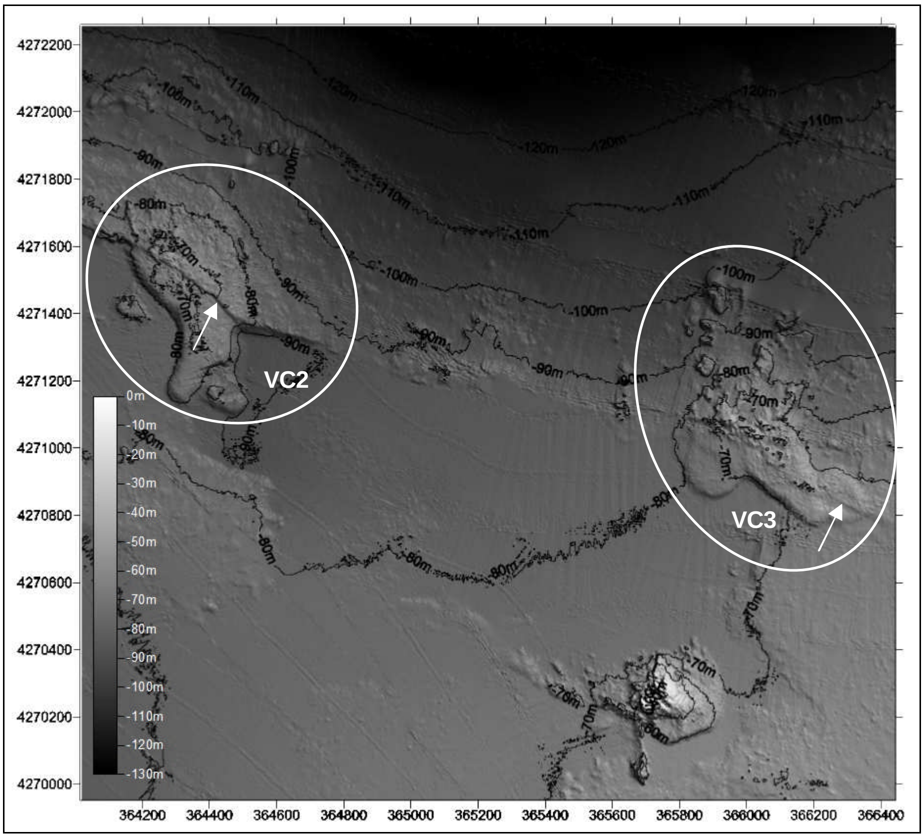

Figure 33: Evidence of fissural volcanic activity associated with the underwater prolongation of the Ribeirinha Fault. Note the vertical offset of the volcanic materials sitting either side of the fault in VC2 and VC3 (white arrows).

4.4.8. Southern passage basin

Nunes (1999) has reported that the bathymetric surveys done by the GeoAçores/89 expedition and existing nautical charts were insufficient to validate Zbyszewski et al. (1963) interpretation that the basin in the southern half of the passage might represent an underwater caldera. The results of the present study provided a high resolution image of this depression which does not support the existence of a caldera. Although it is acknowledged that oldest geomorphologic features may be covered and smothered by sedimentary deposits, the depression rather appears to represent the gap between the flanks of Faial and Pico islands. This gap became a small basin when the material from eruptions along the Baixa do Sul ridge blocked its southern entrance. The scarp featuring the northern side of Baixa do Sul ridge may be related to the Flamengos fault but the emplacement of the Almoxarife Formation conceals any surficial evidence of this connection. Given the steep slopes that surround this basin, it is suggested that it is gradually filling by sediment deposition derived from the surrounding island margins. The greater water depths found in the southern basin compared to the shelf area north of the Espalamaca-Madalena ridge suggests a young age for the Baixa do Sul ridge inasmuch as it represents the closure of the southern pathway allowing sediments to escape from the shelf towards the slope. The construction of a flatter and better defined shelf in the northern part of the passage likely resulted from a possible westward extension of the early Ribeirinha complex together with the material eroded from the surrounding islands being gradually trapped in the troughs created by a series of normal faults that over the last 73-40 kyr (Madeira, 1998) have straddled the inter-island gap. Fissural volcanism associated to these faults created not only additional construction material for this shelf but also enhanced barriers to downslope sediment run-off. A 3-fold discrepancy in the size of sediment-supplying watersheds (totalling 7,618 ha around the northern basin and 2,485 ha around the southern one) together with some diversion of streams towards Faial's south shore as a consequence of the Almoxarife Formation emplacement may represent additional limitations to sediment deposition in the southern basin.

4.4.9. Sediment covered areas

Areas interpreted as sediments in the backscatter mosaic represented 68% of the Faial and western Pico shelves. Backscatter amplitude variations indicated a variety of grainsizes from coarse sediments to fine sands. The transition between areas of different grainsizes was frequently gradational precluding a clear demarcation of the different sediments in the absence of high-resolution ground-truthing in the boundary region.

The sediment areas displayed a large range of bedform types, particularly in the Faial-Pico passage (Figure 5 and Figure 6). The predominant ones were fields of flow-transverse sand waves with a clear bathymetric expression. Sand waves reached a maximum height of 18 m and developed to depths of 180 m. A thorough analysis of these bedforms is provided in Chapter 4.

5. Discussion

The swath surveys executed around Faial and western Pico in 2003 and 2004 provided high resolution information about a variety of on-shelf geomorphologic patterns. Interpretations of the main features are presented below that relate them to tectonic, volcanic, erosional and sedimentary processes.

Whenever possible, underwater features are related to subaerial structures studied in the literature but dated stratigraphic information is limited to constrain the age of most structures.

5.1. Tectonics

5.1.1. Isostasy

Values obtained for the depth of the analytic shelf edge (ASE) off most sectors of the islands differed considerably from the global sea level lowstands in recent Glacial Maxima, suggesting thick on-shelf sediment wedges, different emplacement times and vertical crustal movements.

An examination of shore-normal sub-bottom profiles off the SW corner of the Almoxarife Formation (the only area where a few sub-bottom profiles effectively extended down to the beginning of the island slope) reveals a thick sediment wedge present over a sub-bottom reflector that intersected the seafloor surface at 114 m depth and constitutes a palaeo-shoreline (Figure 34). This reflector is interpreted as the palaeo-horizon planed by surf erosion on the island flank during past sea level fluctuations which has been buried by a sediment wedge with a maximum thickness of 35 m. The location of its distal palaeo-shoreline at 114 m depth further suggests that (if any) the area may have only suffered a minor uplift of ~16 m, rather than the massive ~75 m uplift suggested by the ASE location.

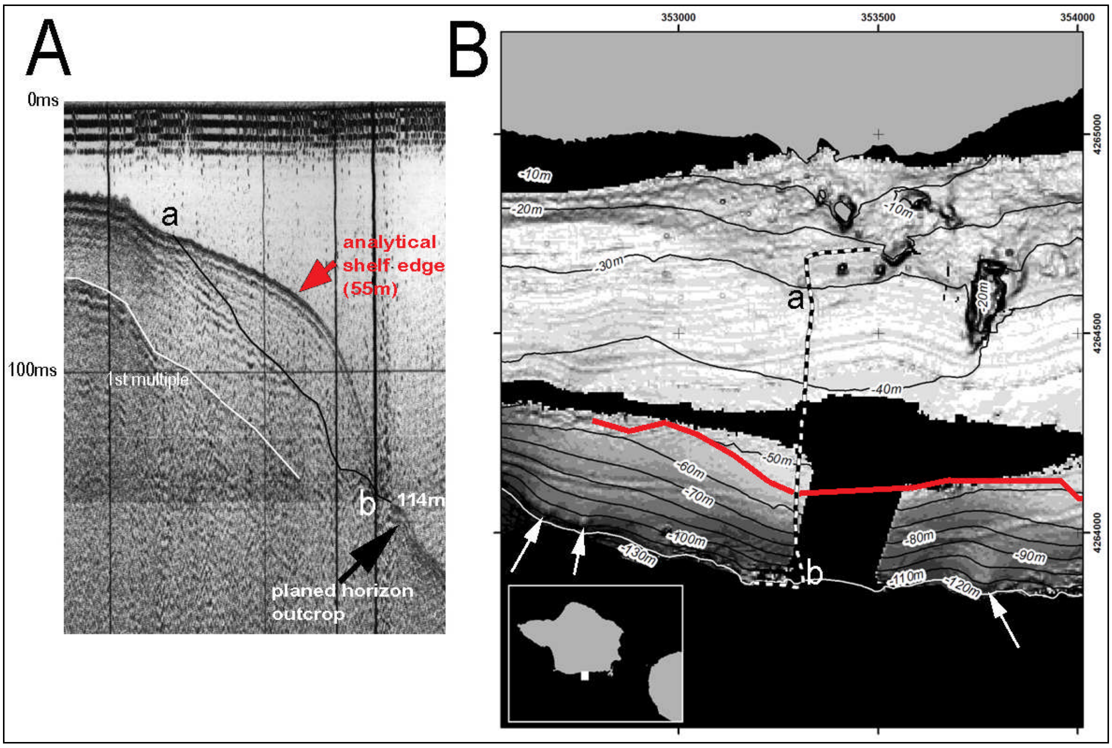

Figure 34: Sand wedge on southern Faial shelf. A. Seimic profile with delineated bedrock horizon (a-b). B: Location of the profile and local bathymetry. Note the location of the analytic shelf edge (55 m depth on A and red line on B) and the surfacing of the eroded bedrock horizon only at 114 m depth. Outcrops of this bedrock horizon are visible in the area along the 110-130 m depth stratum (white arrows).

The lack of outer shelf seismic data around the rest of the island precludes locating the edge of the planed bedrock and obtaining a more robust indicator of the isostatic behaviour.

Despite this data shortage, the presence of a thick sediment wedge likely accounts for the shallow location the ASE off the S and SW margins of the Cedros Complex, as suggested by the identification of mid-shelf sediment thicknesses of 40 m in Varadouro Bay (Quartau, 2002).

Contrastingly, the Ribeirinha complex and the northern margin of the Faial-Pico passage displayed ASEs (-170 m and -183 m, respectively) significantly deeper than the glacial maxima lowstands that occurred since the emergence of this edifice (800 kyr BP). The apparent continuity between these two sectors of the shelf edge suggests that they may represent the margin of an early shallow-water edifice straddling from north-eastern Faial (the oldest part of the island) to the northern half of the present Faial-Pico passage. In these circumstances, the seemingly planed structure on the northern margin of the Faial-Pico passage is interpreted as a subsided early shelf of this edifice (Figure 5).

Disregarding the sediment probably accreted on the outer shelf of an edifice of this age, a depth at edge of approximately 180 m implies that the edifice has subsided at least ~50 m since the Pleistocene lowstand where surf action planed it.

It is hypothesized that the sinking of this early edifice may be associated with crustal warping generated by sequential loading resulting from the formation of neighbouring islands (McNutt & Menard, 1978; Lambeck, 1981). In this particular case, subsidence could be a response to the emplacement of São Jorge island (~30 km to the NE), which emerged 200 kyr later than the Ribeirinha complex. If one assumes the loading has generated not only subsidence but also tilting of Faial towards the NE, the same process could also account for the excessive dip (12º) of the subaerial slopes of the Ribeirinha Complex pointed out by Pacheco (2001), which exceeds the typical sloping angle (<10º) of shield volcanoes (Cas & Wright, 1987; Francis, 1993).

A concurrent uplift of the opposite island margin is not absolutely necessary in the present case, as at least part of vertical movement may have been accommodated within the Pedro Miguel graben. However, the tilting process could help explain the minor uplift suggested by the location of the planed bedrock margin at 114 m.

The occurrence of the shelf edge at a mere 21-25 m depth off the Capelo peninsula is a consequence of the young age of this edifice rather than of tectonic or major sedimentation processes and will be discussed in 5.3.1.

The ASE of 134 m off the western sector of the Cedros Complex roughly matches the lowstand at the Last Glacial Maximum but the sample is too small to derive any sound conclusions and no seismics data exist to assess the thickness of the sediments accumulated on the outer shelf.

5.1.2. Faults

Whilst active faults are generally well known over the islands of Faial and Pico, the same is not true for the surrounding seafloor. The high resolution of swath data contributed to a more precise mapping of some of these structures, which were either expressed in displacements of the seafloor surface or in volcanic lineaments.

The faults with the best on-shelf expression were those projecting seaward from the Pedro Miguel graben on northeastern Faial, which confirms previous suggestions by Berthois (1953) and Nunes (1999). However, not all of the Pedro Miguel graben faults were topographically expressed on the seafloor surface along their seaward projections. Only those presenting headwalls that were not buried too deep by the coating of frequently reworked sediments could be pinpointed.

Often, these faults were clearer in the centre of the passage, where stronger currents appear to prevent thick sedimentation. Many of the fault extensions towards eastern Faial were capped by sediments, whilst towards Pico they were mostly covered by the lava flows.

A previously unreported dextral strike-slip fault straddles the Espalamaca-Madalena ridge and trends N55W. It does not strictly belong to any of Faial's dominant fault families (which strike N60-80W and N10-30W according to Madeira & Brum da Silveira (2003) and its connection to onshore faults could not be established from seafloor topography.

Volcanic activity is commonly associated with the faults and is manifest as small cones and possible fissural extrusions. Some older extrusions (e.g., VC5 and VC6 on the Espalamaca Fault) appear to have been heavily eroded by waves. The largest volcanic activity was associated with the faults underlying the Baixa do Sul ridge where a large edifice encloses a basin on the southern half of the passage (Figure 23).

With the exception of the NNW-SSE trending faults, the surficially-expressed faults identified in the Faial-Pico passage did not confirm the interpretation of the local submerged tectonics deduced by Dias & Matias (2006) from Faial's 1998 aftershock epicentre sequence.

5.2. Volcanic features

Based on the preliminary volcanologic map proposed by Nunes (1999) for the island of Pico, the large submerged lava field indentified off its NW shoreline represents the prolongation of the subaerial lava flows generated by the profuse effusive activity of the Pico Mountain Complex. However, it was seldom possible to directly match underwater and subaerial flows. This is due not only to the survey gap in the very nearshore but also to the fact that some of the underwater benches belong to older/deeper flows which subaerial counterparts have been partially or totally capped by more recent overlying eruptions.

Using Nunes (1999) stratigraphy, the position of the flows places them in the Lower Unit of the Pico Mountain Complex with ages between 40 and 240 kyr. Considering their shallow stratigraphical position as an indication that they belong in the latest part of this interval, it is possible that a significant part of the flows may have been emplaced during periods when the area was subaerially exposed (for a eustatic sea level curve for the period see e.g. Fleming et al., 1998). If this were the case, then it would explain the morphologic similarities between the submerged 2-3 m thick superimposed benches and the *pahoehoe* flows found onshore. The work also corroborates Nunes (1999) observation that the material extruded in this sector of Pico typically exhibits a very fluid nature and is extruded in small volumes.

Lava benches with fronts showing fine flow structures like dendritic terminus with no obvious signs of erosion suggest that emplacement occurred partially underwater at a time when Holocene transgression had already submerged parts of the shelf (see also Mitchell et al., 2008).

Only around the youngest complexes of Faial could onshore volcanic centres be related to the flows identified underwater. The Almoxarife Formation exhibits one flow to the east that is here related to the eruption of Monte Queimado. To the south it presents flows that are related to the eruptions of Monte das Moças and Monte Carneiro respectively from the east to the west (Figure 28-B).

The Capelo Peninsula is dominated by lava flows that cross the narrow shelf. Most of them display an abundance of gullies through which volcanic sand was observed flowing downslope. This topographic richness hindered the identification of the margins of individual flows. The submerged extension of the 1672 flow was clearly identifiable off both shores of the peninsula with its southerly arm crossing the narrow shelf on the southern flank of the peninsula. On the northern shore, the westerly arm of this flow also flowed onto the slope while the easterly arm penetrated to a maximum depth of 41 m but did not reach the island slope, which is located farther offshore in this area (Figure 29-B).

The cones of Capelinhos (W Faial) and Monte da Guia (SE Faial) did not display any submerged lava flows, confirming their essential Surtseyan nature.

The best examples of lava flows in the Cedros Complex are on the southern shore, off the airport (Figure 29-A), but a few small flows are also visible north of Morro de Castelo Branco. The northern shore of this complex exhibits bedrock outcrops scattered amongst the boulder slopes which were suggested to be heavily dismantled volcanic cones. They were significantly eroded and no clear flow-denoting features were readily identifiable on their surface.

A single lava flow was identified around the Ribeirinha complex to the SE of Salão harbour. The feature outcrops from amongst the boulders (Figure 30) and exhibits down-flow convex ridges that indicate an extrusion centre to the west. Although it is impossible to identify the related extrusion centre, it is possible that this is located in the Cedros complex.

A tentative dating is provided for VC2 based on the vertical displacement measured between the two blocks of this volcanic cone and the slip rate estimated by Madeira (1998) for the subaerial sections of the Ribeirinha fault. Given a normal fault height of 4 m and a minimum normal slip rate of 0.16 cm/yr a maximum age of 2,500 yr is obtained.

5.3. Erosional features

5.3.1. Shelf width

Menard (1983) has suggested that oceanic islands outside reef-forming seas are generally truncated by marine abrasion, resulting in the development of broad near-horizontal shelves. The width of these planed horizons depends primarily on the age of the edifices being dismantled and their exposure to swell, with larger shelves being associated with older and/or more exposed sectors.

The largest shelf extents around Faial and Pico were found off the oldest edifices of Cedros, Ribeirinha and the Pico Mountain. The fact that the shelves to the west of the 470 kyr-old Cedros complex or to the NW of the 230 kyr-old Pico Mountain Complex are broader than off the 800 kyr-old Ribeirinha complex may be a consequence of their different exposure to swells. While the coasts of western Cedros or NW Pico face prevailing swells directly, the northern shore of the Ribeirinha Complex will more often experience swells in the less erosive long-shore directions.

The definition of the roughly linear edge uniting the Ribeirinha complex (NE Faial) and the NW Pico margin (Figure 16-B) is also worth highlighting. South of this edge, located at approximately at 183 m, there is a sizeable terrace with a slope of less than 2º that extends to 142 m depth. This is hypothesized as a subsided relic shelf of an early edifice emplaced on the northern half of the passage prior to the development of the Pico Mountain Complex. The more recent northwestern margin of the later is superimposed on the eastern side of the alleged terrace. The fact that this sector of the relatively recent Pico Mountain Complex displays a shelf that is actually wider than that found off the almost 4 times older Ribeirinha complex, also suggests that the lavaflows produced during the emplacement of the Pico Mountain have capped a pre-existing shelf with a history of marine planation as long as or longer than the Ribeirinha complex.

An extremely narrow shelf (a mere 138 m wide) consistent with a very recent emplacement was identified on the SW of Pico (in front of Porto do Calhau), south of where the Baixa do Sul ridge meets Pico's southwestern flank.

A wider shelf was revealed off the Almoxarife Formation (30 ± 20 kyr-old) compared to that off the southern coast of the 470 kyr-old Cedros Complex. This suggests the Almoxarife Formation may have only superficially capped a pre-existing edifice and its already well-developed shelf. This is further supported by the thick sediment wedge present on this part of the shelf (as shown in 5.1.1) and lack of clear evidence of lava flows reaching the island slope.

The wider shelf of Varadouro Bay compared to the southern coast may be associated with differential exposure. The recent emplacement of the Capelo peninsula has diminished the exposure of Varadouro Bay to refracted NW swells but the presence of tall coastal cliffs is indicative of the strong sea erosion that has prevailed on this flank of the Cedros complex throughout most of its history.

The shelves present off either side of the Capelo peninsula also display an asymmetry that is likely related to exposure. In addition they are interesting for their narrowness and depth at edge. The average width of ~400 m is interpreted as reflecting the recent emplacement of the edifice which still displays active volcanism.

As denoted by the two historic eruptions recorded in the edifice, partial accretion over the shelf can still partially coat the incisions cut by the sea during periods of volcanic quiescence on both flanks of the peninsula. However, the presence of a shelf suggests that marine back-wearing may already exceed magmatic accretion.

The present depth at the edge of 21-25 m is a likely consequence of shelf incision beginning when Holocene transgression was already well underway. An approximation of the time when the net balance between marine backwearing and magmatic accretion tipped over towards the former was computed by considering that the outer shelf edge is mostly prone to active erosion while experiencing surf action and that these forces do not extend to more than 10 m below the surface (Dietz & Menard, 1951). In these circumstances, a depth at edge of 25 m suggests marine back-wearing began to prevail when sea level was approximately 15 m bpsl, which occurred approximately 8 kyr-ago (Fleming et al., 1998).

Menard (1983) obtained marine backwearing rates of 0.6 to 1.7 km/Myr for the initial erosional phase of the Canary islands. Although there is a shortage of geochronologic data that can be used to comprehensively understand the geological construction of the Faial and Pico edifices, the rates obtained in the present study seem much higher than those present by Menard. This may be explained by the lesser exposure of the Canary Islands to large swells and the broader age range in Menard's dataset, where very young edifices may be under-represented.

5.3.2. Mass wasting

It is speculated that the emplacement of the Monte da Guia cone very close to the shelf edge overloaded this section of the island margin and eventually led to the collapse which produced the incision extending across the shelf margin and slope. Likely, seismic activity and the fact that the heavy volcanic load was possibly emplaced over shelf sediment deposits may have facilitated the failure (see also Lodato et al., 2007).

As an indentation that locally removed the planed shelf area up to the shoreline, this scar currently represents a major interceptor of longshore-transported sediments (see Greene et al., 2002 and Normark, 1970 for analogous functional description of Californian canyons). Most of the sediments transported by currents either running eastwards along the south coast of Faial (see Youssef, 2005) or spilling westwards from the Faial-Pico passage are probably channelled into the scar and feed the downslope debris fan.

Other large gullies detected to the west of Praia do Norte on the Cedros complex margin, may have been generated by island margin collapses during times of lowered sea-level, when the extreme swells observed in the areas may have transported large quantities of sediments onto the outer shelf (see also Greene et al., 2002) which facilitated failures.

5.3.3. Palaeo-shorelines

The Faial shelf showed very limited palaeo-shoreline records. This is attributed to the covering of the shelf with unconsolidated sediment which may have been sufficiently thick to withstand a complete wash out during periods of regression and subaerial exposure and from which surface erosional records have been erased by swells and currents throughout postglacial transgression. In contrast, eastern Pico displayed good examples of probable palaeo-shorelines. This situation was likely facilitated by the abundance of geologically-young, and therefore uncoated by sediments, hard substrates prone to wave quarrying.

The most interesting result was that bathymetric horizons corresponding to sea level standstills actually show a lack of palaeo-shoreline records when compared to the horizons associated with a fast sea level rise throughout the Holocene. This suggests that good palaeo-shoreline records develop during periods of fast sea level rise and are preserved as sea level continues to rise and halts the erosion. It is postulated that standstills provide enough time for erosion to dismantle the lava benches in a way that does not leave cliff palaeo-shorelines.

Various palaeo-shorelines carved on the lava benches are exceptionally preserved (Figure 18 and Figure 19). Considering conventional coastal dynamics (Carter, 1999) and descriptions of basalt cliff erosion (McKenna, 2002; Borges, 2003), it is clear that the frontal scarps represent relic wake-quarried basaltic shorelines similar to the *type IV* coasts identified by Borges (2003). In fact, present shorelines found around Pico and other volcanic archipelagos like the Canary Islands exhibit similar plunging cliffs with narrow indentations (Figure 35).

Similar plan view morphologies could also be identified in sunken palaeo-shorelines off Kawaihae Bay (Hawaii Island, Hawaii) represented in a bathymetric grid (50 m resolution) produced from swath surveys (Figure 36).

A

B

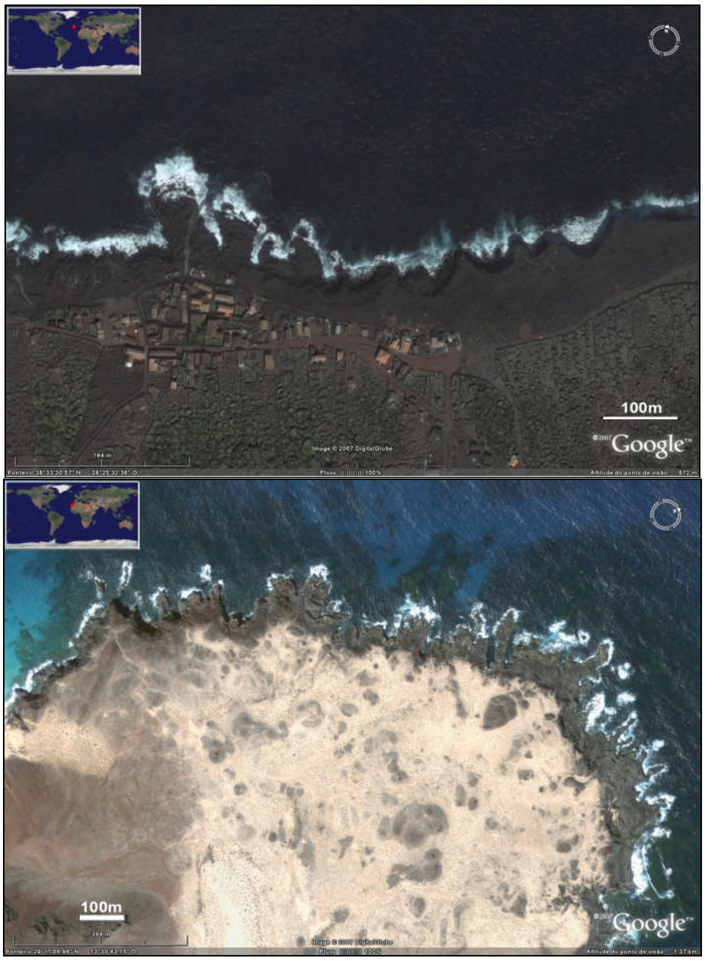

Figure 35: Aerial plan view of modern shorelines with a morphology comparable to the reported palaeshorelines. A. Lajido coast on northwestern Pico Island (Azores). B. Northern Graciosa (Canary Islands). Image credits: Google Earth © Digital Globe 2007.

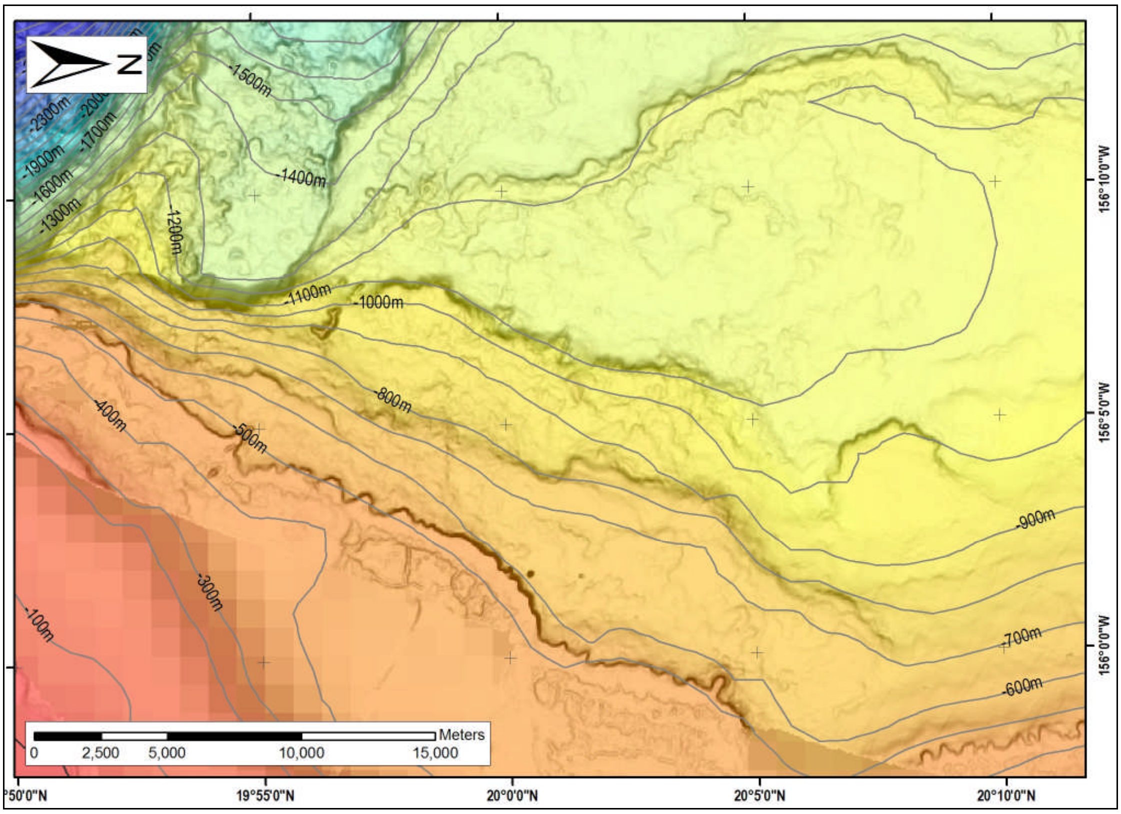

Figure 36: Sunken palaeo-shorelines off Kawaihae Bay (Hawaii Island, Hawaii) showing similar plan view profiles. Grid credits: Main Hawaiian Islands Multibeam Synthesis.

As marine transgression caused the level of low tides to rise above lava bench edges, the forces carving the palaeo-shoreline will have been significantly reduced (Davis, 1896, but see also Sunamura, 1991) thus preserving the palaeo-shoreline. Subsequently, a low sedimentation rate maintained the features exposed.

Preservation of features on transgression was such that even fine structures could often be seen such as compression ridges in the bench upper surfaces. The cobble and boulder-sized erosion debris found on the benches (Figure 37) are postulated as having been mostly produced by quarrying of the upslope lava front.

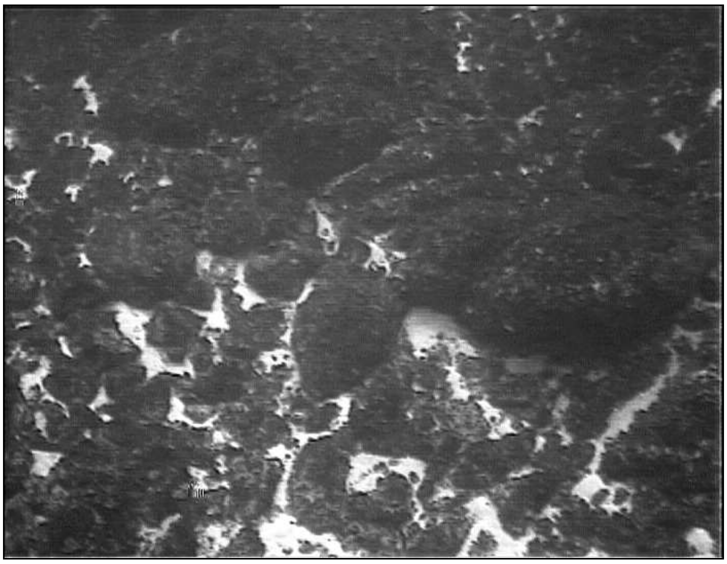

Figure 37: ROV image collected over a lava platform showing boulder and cobble-sized erosion clasts interspersed with a possible preserved patch of ropy lava. The white material is biogenic sediment originating from shelled fauna inhabiting the rocky surfaces.

5.3.3.1. Preservation of the bench morphology

A dominant characteristic of the area where the majority of the palaeo-shorelines is located is benched morphology found when following a nearshore to offshore transect. Rather than being associated with terracing of the island flank by marine erosion, this morphology is the result of the superimposition of succeeding lava flows that traverse the isobaths (Figure 38) and, in particular cases, still bear compression ridges and folding on their upper surfaces.

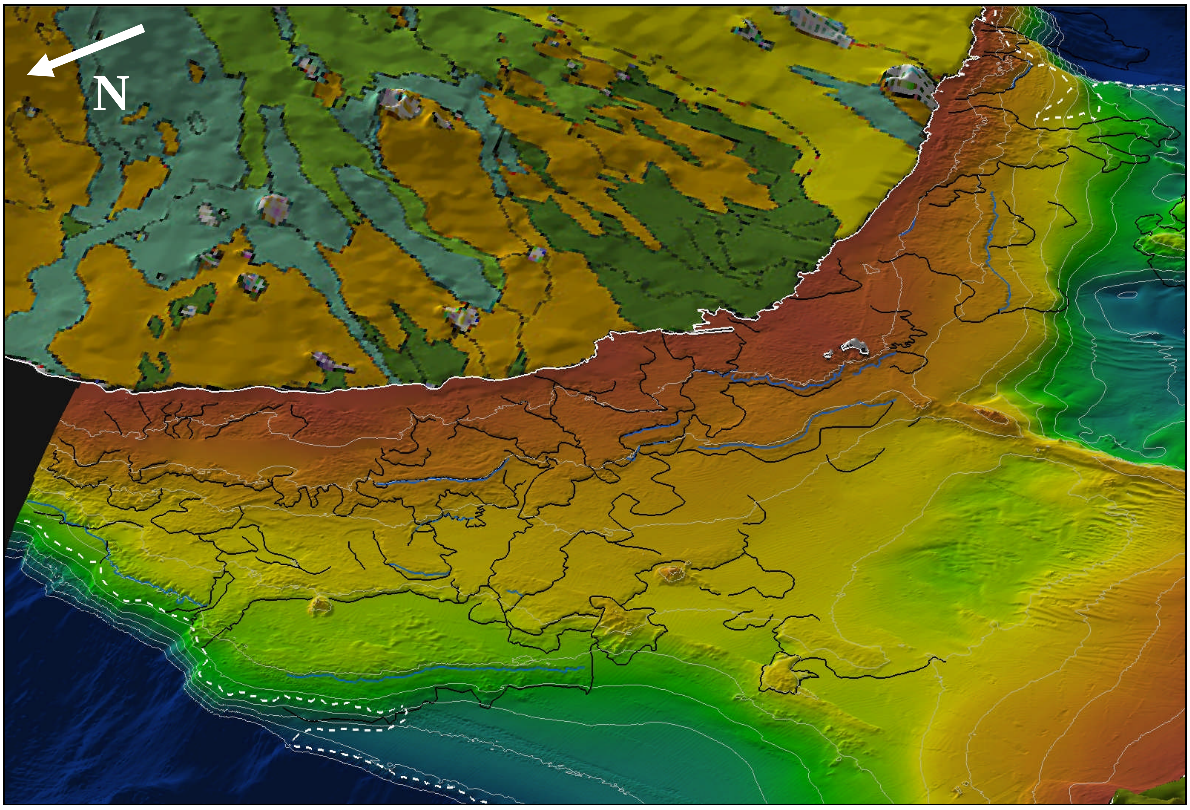

Figure 38: Perspective of the north-western Pico lava delta. Individual lava fronts are delineated in black whilst palaeo-shorelines are delineated in blue. Thin grey lines are isobaths spaced at 20 m intervals down to 200 m depth. Dashed white line represents the shelf edge. The volcanologic map published by Nunes (1999) is draped on the subaerial relief of the island to illustrate limitations in the linkage between lava flows identified onshore and underwater.

As discussed in section 5.3.3, the rapid sea level transgression is a major influence in the preservation of the benching. Most of the lava flows would have undergone submersion during the fastest period of postglacial transgression, where sea level was rising at rates of ~1.0 m/100 yr (Fleming et al., 1998). Considering that erosion is most active throughout the 3 meters represented by the average lava front thickness, plus or minus the local tidal range of 1.5 m, the time window where surf action would most actively erode each lava front would have been limited to approximately 6 centuries. Using the rate of 0.1 m/yr estimated by Borges (2003) for similar *type IV* shores, frontal recessions for a period of 6 centuries would have amounted to a total of 60 m only.

The structural quality of the flow emplacement may have further prevented extensive dismantling. Nunes (1999) reports that pyroclast deposits and/or soil are either absent or minimal in this sector of the island. This would lead to successive flows adhering directly to the surface of previous flows without intervening friable layers that would afterwards facilitate marine erosion.

5.3.4. Nearshore geomorphology

Boulder slopes dominate around Faial, which can be explained by the considerable age of the Cedros and Ribeirinha complexes and exposed regime of most of the coast. Contrastingly, lava flows are concentrated around the younger edifices of the Pico Mountain, Almoxarife and Capelo Peninsula.

Borges (2003) provides an explanation on how sea-erosion operates on the coasts of the Azores but does not describe the underwater morphologies generated by the rearrangement of the mass waste material long- and cross-shore. The dipping terraces found off the NE coast of Faial are interpreted as a trait of this action. The magnitude of the dip diagonally to the bathymetric contours would not suggest an association to erosional terracing by sea level standstills. Rather, it is hypothesized that they formed throughout transgression as prevailing swells spilt churned material onto the leeside of boulder protrusions. The major swells affecting this shore are from W and NW and wash along this coast oblique to the shoreline thus likely transporting boulders along a vector with a longshore and downslope component.

A significant narrowing of the boulder slope (from 900 to less than 175 m) occurs south of Ribeira de Joana Pires (Figure 10), despite the heightening of the seacliff, which reaches 300 m at Costa Brava. The wide boulder slope off the Cedros results from the dismantling of the block north of the Ribeira de Joana Pires – Ribeirinha lineament (see Madeira, 1998 for more information on this subaerial fault) which is interpreted as the subaerial section of a ridge extending northwestwards from the northwestern tip of the island. This ridge is mapped in Searle (1980) and its proximal part is visible in Figure 4.

6. Conclusions

The combination of high-resolution bathymetry and backscatter data with ground-truthing information from multiple sources (e.g., *in situ* imagery, grab samples and seismic profiles) proved to be a powerful tool in the completion of the first geomorphologic inventory of an Azorean island shelf.

The work revealed a diverse and complex mosaic of rocky and sedimentary geomorphologic structures associated with tectonic, volcanic, erosional and sedimentary processes. A preliminary map of surficial bottom types is presented that pioneers the high resolution mapping of Azorean island shelves.

The variation of shelf extent showed a relationship with the geologic age history of the related subaerial edifices. With exceptions off the Almoxarife Formation and SW Pico, wide shelves dominated the older edifices in comparison to extremely narrow shelves on the geologically young and active areas (e.g., Capelo complex). Using the geologic edifices present in the study area, a logarithmic curve was calculated that relates the age of edifices younger than 800 kyr and shelf widening rates.

Depth at the *analytic shelf edge* (ASE, defined as the boundary along the 5º slope contour), is presented as an appropriate indicator of the lowest bedrock horizon planed during glacial sea level lowstands in non-sedimented shelves showing evidence of no isostatic variation (e.g., northwestern Pico). The index was flawed around older edifices with thick sediment wedges, over which the 5º threshold was located at much shallower depths. In the latter case, seismic profiles were helpful in identifying the vertical location of buried planed bedrock horizons and for making inferences about the tectonic isostasy of the related subaerial edifice. Seismic profiles extending to the shelf edge revealed sediment wedges as thick as 40 m accumulated over planed bedrock horizons with distal edges emerging approximately at the level of recent glacial maxima lowstands. Although this limitation prevents direct use of ASE for drawing conclusions about the isostasy of the areas where the shelf appears to be uplifted, it can yield conservative subsidence rates in old edifices with ASE significantly below the sea level during recent glacial maxima. A rate of 0.75 mm/yr was obtained for the oldest edifice of Faial island (Ribeirinha complex). It is further suggested that this edifice extended east given the linear continuity of the Ribeirinha complex margin with the shelf edge of the northern half of the passage.

Faial's nearshore was dominated by boulder slopes and lavaflows that were better defined around the more recent edifices of the Capelo peninsula and Almoxarife Formation. Western Pico was dominated by lava flows, the most outstanding of them being a sequence located off the northwestern coast. Establishing relationships between individual flows and probable extrusion centres and eruptive events was hampered by subsequent subaerial events burying the upstream stretches of the underwater flows.

On-shelf palaeo-shorelines were also reported for the first time in the Azores and are especially well preserved. Their cliffed morphology is comparable to palaeo-shorelines found on volcanic island flanks in Hawaii and to modern shorelines found along the neighbouring Pico coast. The recorded palaeo-shorelines occur only in bathymetric strata corresponding to periods of fast sea level rise during the Holocene transgression and are absent in strata corresponding to Holocene sea level standstills. This suggested that in standstills erosion is given enough time to either dismantle the lava benches in a way that does not leave cliff palaeo-shorelines or that erosion deposits ends up covering the cliffs. Well-defined compression ridges observed in the upper surfaces of submerged lava fronts eroded into cliff palaeo-shorelines suggested that the benched morphology observed off northwestern Pico is primarily caused by the emplacement of succeeding lava flows rather than terracing of the island flanks by marine erosion. Furthermore it demonstrated that lava flows can preserve surface texture despite being traversed by the surf zone during sea level fluctuations.

Other new insight of on-shelf geomorphologic features includes (i) the mapping of the underwater prolongation of onshore faults, (ii) the submerged evidence of fissural volcanic activity associated with these faults, (iii) the clarification of the origin of the basin in the southern half of the passage which appears to originate from a portion of the inter-island gap being enclosed by the volcanic edifice of Baixa do Sul rather than from a large submerged caldera as originally claimed by Zbyszewski et al (1963) and for which Nunes (1999) could not provide a clarification based on the GeoAçores '89 data.

From a geologic perspective, the current results should be regarded primarily as an early geomorphologic account appealing to specialists from different fields to develop further investigation on the complex underlying processes. Given the wealth of information in the dataset, a thorough analysis of the different features reported is beyond the scope of this work.

Finally it should be highlighted that detailed descriptions of the seafloor such as the one presented in this paper are also important in building an understanding of the benthic ecosystem dynamics to support an informed stewardship of marine environments (Eittreim et al., 2002). This is particularly important in the present case in view of the various marine protected areas that have been declared (e.g., SACs) and proposed (e.g., Faial-Pico Passage Marine Park) for the study area. The high resolution seafloor maps presented hold great potential to inform the design of ecologically effective zoning schemes, support management decisions and provide benchmarks for monitoring studies. A particularly relevant task in the short term will be to convert the seafloor information into a biotope interpretation categorizing the relevance of the different bottom types for fishery resources and biodiversity.

7. References

Berthois, L. (1953). Contribution à l'étude lithologique de l'archipel des Açores. *Comunicações dos Serviços Geológicos de Portugal*, 34: 127-141.

Blondel, P., & B. Murton (1997). *Handbook of seafloor sonar imagery*. PRAXIS-Wiley, Chichester. 314 pp.

Borges, P. (2003). Ambientes Litorais nos Grupos Central e Oriental do Arquipélago dos Açores. *Ph.D. Thesis*. Universidade dos Açores, Ponta Delgada, Cdrom.

Camacho, A.G., J.C. Nunes, E. Ortiz, Z. França & R. Vieira (2007). Gravimetric determination of an intrusive complex under the Island of Faial (Azores): some methodological improvements. *Geophysical Journal International*, 171 (1): 478-494.

Cannat, M., A. Briais, C. Deplus, J. Escartin, J. Georgen, J. Lin, S. Mercouriev, C. Meyzen, M. Muller, G. Pouliquen, A. Rabain & P. da Silva (1999). Mid-Atlantic Ridge - Azores hotspot interactions: along-axis migration of a hotspot derived event of enhanced magmatism 10 to 4 Ma ago. *Earth and Planetary Science Letters*, 173(3): 257-269.

Carter, R.W.G. (1999). *Coastal environments: an introduction to the physical, ecological and cultural systems of coastlines*. 7th ed., Academic Press, London. 617 pp.

Carvalho, F. (2003). *Elementos do clima de agitação marítima no Grupo Central dos Açores (Mar Alto)*. Instituto de Meteorologia, Portugal. 98 pp.

Cas, R.A.F., & J.V. Wright (1987). *Volcanic Successions: modern and ancient: a geological approach to processes, products and sucessions*. George Allen & Unwin/Chapman & Hall, London. 528 pp.

Chovelon, P. (1982). Évolution volcanotectonique des îles de Faial et de Pico. *M.Sc. Thesis*. Paris-Sud University, Centre d'Orsay. 186 pp.

Coutinho, R. (2000). Elementos para a monitorização sismovulcânica da ilha do Faial (Açores): Caracterização hidrogeológica e avaliação de anomalias de Rn associadas a fenómenos de desgaseificação. *Ph.D. Thesis*. Universidade dos Açores, Departamento de Geociências, Ponta Delgada. 342 pp.

Davis, W.M. (1896). The outline of Cape Cod. *Proceedings of the American Academy for Arts and Sciences*, 31: 303-32.

Dias, N.A., & L. Matias (2006). Aftershock Sequence of July 1998 Faial and Pico Islands (Azores): An Analysis of Waveform Similarities, Seismic Anisotropy and Crustal Structure. *Eos*. Transaction of the American Geophysical Union, 87(52), Fall Meet. Suppl., abstract S53A-1311 (poster file at http://www.igidl.ul.pt/FMSantos/NewsLetter/Nuno_poster.pdf)

Dietz, R.S., & H. Menard (1951). Origin of abrupt change in slope at continental-shelf margin. *Bulletin of the American Association of Petroleum Geologists*, 35: 1994-2016.

DoD (2001). *Global Positioning System Standard Positioning Service Performance Standard*. Assistant Secretary of Defense for Command, Control, Communications, and Intelligence.

Duarte, R.M.M.D. (1997). Simulação Numérica de Correntes Induzidas pelas marés: O caso Faial-Pico no Arquipélago dos Açores. *Licenciatura Thesis*. Departamento de Física. Faculdade de Ciências da Universidade de Lisboa, Lisboa. 90 pp.

Eittreim, S.L., R.J. Anima & A.J. Stevenson (2002). Seafloor geology of the Monterey Bay area continental shelf. *Marine Geology*, 181: 3-34.

Faria, C., T. Ferreira, J.L. Gaspar & F. Sousa (2003). Tectonic structures revealed by CO_2 soil diffuse degassing anomalies at Faial Island (Azores). *Geophysical Research Abstracts*, 5: 13119.

Feraud, G., I. Kaneoka & C.J. Allegre (1980). K/Ar ages and stress pattern in the Azores: dynamic implications. *Earth and Planetary Science Letters*, 46: 275-286.

Fleming, K., P. Johnston, D. Zwartz, Y. Yokoyama, K. Lambeck & J. Chappell (1998). Refining the eustatic sea-level curve since the Last Glacial Maximum using far- and intermediate-field sites. *Earth and Planetary Science Letters*, 163: 327-342.

França, Z., J.V. Cruz, J.C. Nunes & V.H. Forjaz (2003). Geologia dos Açores: uma perspectiva actual. *Açoreana*, 10(1): 11-140.

França, Z., C.G. Tassinari, J.V. Cruz, B. Rodrigues, V. Araña & A. Aparício (2006). Petrology, geochemistry and Sr-Nd-Pb isotopes of the volcanic rocks from Pico island, Azores (Portugal). *Journal of Volcanology and Geothermal Research*, 156(1-2): 71-89.

Francis, P.W. (1993). *Volcanoes: a planetary perspective*. Oxford University Press, Oxford. 443 pp.

Gente, P., J. Dyment, M. Maia & J. Goslin (2003). Interaction between the Mid-Atlantic Ridge and the Azores hot spot during the last 85 Myr: emplacement and rifting of the hot spot-derived plateaus. *Geochemistry, Geophysics and Geosystems*, 4 (10): 1-23.

Greene, H.G., N. Maher & C.K. Paull (2002). Physiography of the Monterey Bay Marine Sanctuary and implications about continental margin development. *Marine Geology*, 181: 55-84.

Instituto Hidrográfico (2005). *Tabela de Marés 2006*. Instituto Hidrográfico, Lisboa. vi+196 pp.

Isidro, E., M. Ramos, C. Oliveira & L. Barcelos (2006). *Relatório Açores do Projecto "Aquicultura Marinha e Recifes Artificiais: novos modelos de produção integrada"* (MARINOVA ref. MAC/4.2/M11 - INTERREG III-B MAC). 5 pp + Anexos 24 pp.

Lambeck, K. (1981). Lithospheric response to volcanic loading in the Southern Cook Islands. *Earth and Planetary Science Letters*, 55: 482-496.

Ligi, M., N.C. Mitchell, M. Marani, F. Gamberi, D. Penitenti, G. Carrara, M. Rovere, R. Portaro, G. Centorami, G. Bortoluzzi, C. Jacobs, I. Rouse, C. Flewellen, S. Whittle, P. Terrinha, J. Freire Luís & N. Lourenço (1999). Giant volcanic ridges amongst the Azores islands. *Eos.* Transaction of the American Geophysical Union, 80, Fall Meet. Suppl., F913.

Lodato, L., L. Spampinato, A. Harris, S. Calvari, J. Dehn & M. Patrick (2007). The morphology and evolution of the Stromboli 2002-2003 lava flow field: an example of a basaltic flow field emplaced on a steep slope. *Bulletin of Volcanology*, 69: 661-679.

Lourenço, N., J.M. Miranda, J.F. Luís, A. Ribeiro, L.A.J. Mendes-Victor, J. Madeira, and H.D. Needham (1998). Morpho-tectonic analysis of the Azores Volcanic Plateau from a new bathymetric compilation of the area. *Marine Geophysical Researches*, 20(3): 141-156.

Lundblad, E., D.J. Wright, J. Miller, E.M. Larkin, R. Rinehart, D.F. Naar, B.T. Donahue, S.M. Anderson & T. Battista (2006). A Benthic Terrain Classification Scheme for American Samoa. *Marine Geodesy*, 29(2): 89-111.

Madeira, J. (1998). Estudos de neotectónica nas ilhas do Faial, Pico e S. Jorge: uma contribuição para o conhecimento geodinâmico da junção tripla dos Açores. *Ph.D. Thesis*. Universidade de Lisboa, Lisboa. 481 pp.

Madeira, J., & A. Brum da Silveira (2003). Active tectonics and first paleoseismological results in Faial, Pico and S. Jorge islands (Azores, Portugal). *Annals of Geophysics*, 46: 733-761.

McKenna, J. (2002). Basalt cliffs and shore platforms between Portstewart (Co Derry) and Portballintrae (Co Antrim). In Knight, J. (ed.). *Field guide to the coastal environments of Northern Ireland*. CERF/PB/IRTU/MI, Belfast, pp. 157-164.

McNutt, M.K., & H.W. Menard (1978). Lithospheric flexure and uplifted atolls. *Journal of Geophysical Research*, 83: 1206-1212.

Menard, H.W. (1983). Insular erosion, isostasy and subsidence. *Science*, 220: 913-918.

Mitchell, N.C., C. Beier, P. Rosin, R. Quartau, & F. Tempera (2008). Lava penetrating water: Submarine lava flows around the coasts of Pico Island, Azores. *Geochemistry, Geophysics and Geosystems*, 9(3): 29 pp.

Moore, J.G. (1987). Subsidence of the Hawaiian ridge. *U.S. Geological Survey Professional Paper*, 1350: 85-100.

Normark, W.R. (1970). Channel piracy on Monterey deep-sea fan. *Deep-Sea Research*, 17: 837-846.

Nunes, J.C. (1999). A actividade vulcânica na ilha do Pico do Plistocénico superior ao Holocénico: mecanismo eruptivo e hazard vulcânico. *Ph.D. Thesis*. Universidade dos Açores, Ponta Delgada. 357 pp.

Nunes, J.C. (2003). Estruturas de colapso gravítico lateral na Ilha do Pico (Açores): mecanismo, constrangimentos e idade. *In* García, F.G., & J.L.B. Valero, (eds.). *Actas da 3ª Assembleia Luso-Espanhola de Geodesia e Geofísica*, vol. II. Editorial de la UPV-Universidad Politécnica de Valencia, Valência. pp. 731-735.

Nunes, J.C., J.V. Cruz, Z. França, G. Sigvaldason, M.R. Carvalho, J. Garvin & J.L. Alves (1998). Production Rates and Age of Pico Stratovolcano (Azores Islands): An Estimation From Historical Eruptions Data. *In* J.M.G. Garcia-Garcia e M.D.R. Romacho (eds.). *Actas da 1ª Assembleia Luso-Espanhola de Geodesia e Geofísica*. Sesione S09-4 . Almeria. Espanha. Universidad de Almeria e Instituto Geográfico Nacional. CD-ROM.

Nunes J.C., A. Camacho, Z. França, F.G. Montesinos, M. Alves, R. Vieira, E. Velez, & E. Ortiz (2006). Gravity anomalies and crustal signature of volcano-tectonic structures of Pico Island (Azores). *Journal of Volcanology and Geothermal Research*, 156: 55-70.

Oliveira Pires, H., & F. Carvalho (1996). *Fundamento e características do modelo de terceira geração MAR3G*. Instituto de Meteorologia, Lisboa, Portugal. 38 pp.

Pacheco, J. (2001). Processos associados ao desenvolvimento de erupções vulcânicas hidromagmáticas explosivas na ilha do Faial e sua interpretação numa perspectiva de avaliação do Hazard e minimização do Risco, *Ph.D. Thesis*. Azores University. 330 pp.

Quartau, R., F. Curado, T. Cunha, L. Pinheiro & J. H. Monteiro (2002). Projecto Gemas – Localização e distribuição de areias em redor da ilha do Faial. *Relatório Técnico INGMARDEP*, 5/2002. Dep.to de Geologia Marinha, IGM, Lisboa. 37 pp., 30 figs.

Quartau, R., F. Curado, S. Bouriak, J.H. Monteiro & L. Pinheiro (2003). Projecto Gemas – Localização e distribuição de areias em redor da ilha do Pico. *Relatório Técnico INGMARDEP*, 16/2003. Dept. de Geologia Marinha, IGM, Lisboa. 49 pp., 33 figs.

Quartau, R., H. Duarte & P. Brito (2005). Projecto Gemas – Relatório da campanha de amostragem de sedimentos (FAPI-3) realizada na plataforma e na orla costeira das ilhas do Faial e do Pico. *Relatório Técnico INGMARDEP*, 2/2005. Dept. de Geologia Marinha e Costeira, INETI, I.P., Lisboa. 17 pp., 9 figs.

Richard, J. (1934). Liste générale des stations des Campagnes scientifiques du Prince Albert de Monaco avec notes et observations. *Résultats des campagnes scientifiques accomplies sur son yacht par Albert 1er prince souverain de Monaco.* 89: 1-471.

Searle, R. (1980). Tectonic pattern of the Azores spreading centre and triple junction. *Earth and Planetary Science Letters*, 51: 415-434.

Serralheiro, A., V.H. Forjaz, C.A. Matos Alves & B. Rodrigues (1989). *Carta Vulcanológica dos Açores – Ilha do Faial.* Serviço Regional de Protecção Civil, Universidade dos Açores & Centro de Vulcanologia (eds.). INIC, 4 sheets at 1:15.000 scale.

Simões, A., R. Duarte & M. Alves (1997). A pilot ocean monitoring site at Azores islands. pp. 444-454. In J.H. Stel, H.W.A. Behrens, J.C. Borst, L.J. Droppert & J.P. van der Meulen (eds.). Operational Oceanography: The Challenge for European Co-Operation. *Proceedings of the First International Conference on EUROGOOS*. Elsevier Science Ltd, The Hague.

Stephenson, W.J. (2000). Shore platforms: a neglected coastal feature? *Progress in Physical Geography*, 24(3): 311-327

Stretch, R.C., N.C. Mitchell, & R.A. Portaro (2006). A morphometric analysis of the submarine volcanic ridge south-east of Pico Island, Azores. *Journal of Volcanology and Geothermal Research*, 156(1-2), 35-54.

Sunamura, T. (1991). The elevation of shore platforms: a laboratory approach to the unsolved problem. *Journal of Geology*, 99: 761-766.

Tazieff, H. (1959). L'éruption de 1957-1958 et la tectonique de Faial (Açores). *Memórias dos Serviços Geológicos de Portugal*, 4: 71-88.

Tempera, F., P. Afonso, T. Morato, S. Gubbay, T. Dentinho, M. Silva, R. Prieto, F. Cardigos, M.J. Pitta & R. Serrão Santos (2001). Technical-Scientifical Management Proposal for the Faial-Pico Channel SACs (in Portuguese). Departamento de Oceanografia e Pescas da Universidade dos Açores, Horta. *Arquivos do DOP*. Série Relatórios Internos, nº 8/2001, viii+76 pp.

Todd, B.J., G.B.J. Faber, R.C. Courtney, & R.A. Pickrill (1999). Quaternary geology and surficial sediment processes, Browns Bank, Scotian Shelf, based on multibeam bathymetry. *Marine Geology*, 162: 165-214.

Youssef, W.B.H. (2005). Caractérisation *in situ* de l'environnement physique des habitats benthiques occupés par *Codium elisabethae* au sein de sites d'études particuliers (Faial, Açores). *Mémoire de D.E.A en Océanologie*. Université de Liège, Liège. 94 pp.

Zbyszewski, G., F. Moitinho de Almeida, O. Veiga Ferreira & C. Torre de Assunção (1959). *Geologic map of Faial (Azores).* Serviços Geológicos de Portugal, Lisboa, 1:25,000 scale map with 25 p text.

Zbyszewski, G., C.R. Ferreira, O.V. Ferreira & C.T. Assunção (1963). *Carta Geológica de Portugal na escala de 1:50000. Notícia explicativa da Folha A, Ilha do Pico (Açores).* Serviços Geológicos de Portugal, Lisboa. 23 pp.

8. Acknowledgements

This work has been supported by various funding sources including the Royal Society, the British Council (Germany), the Higher Education Funding Council for Wales, the Regional Directorate for Science and Technology of the Azores and projects MARINOVA (INTERREG IIIb/MAC/4.2/M11), MAROV (PDCTM/P/MAR/15249/1999) and GEMAS (DROTRH contract).

Fernando Tempera has been financed by a PhD grant (ref. SFRH/BD/12885/2003) from the Fundação para a Ciência e a Tecnologia.

Neil Mitchell is thanked for all his careful review of the chapter and suggestions that considerably improved the contents of this chapter.

Rui Quartau is acknowledged also for his suggestions and for the sharing of seismic data collected in the study area.

The use of the terrestrial relief maps produced by the Instituto Geográfico do Exército was conceded by the Regional Secretariat for the Environment under the scope of project MARÉ (Life Natureza B4-3200/98-509).

The masters and crews of RV *Arquipélago* and RL *Águas Vivas* are acknowledged for all their effort during the work at sea.

Thierry Schmitt, Frederico Cardigos and Eduardo Isidro are thanked for their collaboration throughout the surveys and in the processing of the data.

Paul Byham and Submetrix are thanked for the very useful support during operations with the Swathplus system and processing of the data collected.

Bernie Coakley and Russel Dodd (GSE Rentals) are thanked for their advice on and *in situ* support of the swath sonar installation.

Instituto Hidrográfico is acknowledged for facilitating the installation of the tide gauge in Horta's Tidal Gauge house.

Sónia Santos from Direcção Regional do Ambiente is acknowledged for the kind loaning a substitute DGPS during the 2004 survey.

Guilherme Soares (DRRF-Açores) is thanked for supplying files for DGPS post-processing.

CHAPTER 4

LARGE SEDIMENTARY BEDFORMS AND ASSOCIATED CURRENTS IN THE FAIAL-PICO PASSAGE (AZORES, NE ATLANTIC)

Abstract

Faial and Pico are the only islands in the Azores that are united by a shelf. New multibeam data has been recently collected for the inter-island passage. Analysis of the bathymetric and backscatter data has shown that 66% of the seabed is composed by sediments. An account is given in this paper of extensive current-induced bedforms identified on these sediment surfaces. These features include large fields of straight crested sand wave, linguoid coarse lag waves, celled crest arrangements and scour furrows. Bedforms extend to depths of 180 m with sand wave amplitudes up to 18 m suggesting high energy conditions.

The geometry of the bedforms is used to infer bottom current patterns and the induced on-shelf pattern of sediment transport in the inter-island passage. Partial recirculation of the sediments is shown for the enclosed basin located in the southern part of the inter-island passage.

Bedform surface freshness revealed by *in situ* imagery and bedform sharpness indicate that oceanographic conditions persist at present that maintain the bedforms. The currents necessary to maintain these sand wave fields are determined using fluid-dynamic relationships and bedform characteristics. The results are discussed with respect to new current measurements collected by a mid-passage mooring indicating that present currents of up to 90 cm/s may occasionally mobilize the bedforms. Longer observational series are required to obtain better estimates of the frequency of these events and the oceanographic and meteorological factors that regulate them.

Keywords: large bedforms; volcanic island shelf; impinging currents; Azores.

Table of Contents

1. Introduction

The typical "life history" of volcanic island shelf sediments can be described as a chain of events that begins with volcaniclastic and erosional sediments being either transported from the land surface or generated and emplaced by either shallow-water eruptions or surf erosion. Part of these sediments will be trapped by rugged volcano-tectonic topography and/or accrete over the shelf in the form of sediment wedges. Excluding mass wasting processes that cause portions of the shelf to collapse onto the island flanks and surrounding deep ocean floor, the majority of the sediment will slowly migrate offshore under the action of shelf currents and gravity. At the shelf edge the sediment tumbles down the slope either channelled through gullies and turbidity current channels, or by mass wasting events as the sediment wedge margin collapses under the weigh of increasing sediment loads.

Despite this can be assumed to be the general process, sedimentary patterns and processes occurring on volcanic island shelfs in mid to high latitude archipelagos (i.e., with non-reefal shelves) are still scarcely studied (Quartau, 2007).

Previous research of coastal sediments in the Azores has focused on intertidal and supralittoral deposits, most of it concerning coastal erosion issues brought about by excessive sand extraction on beaches and dunes (LNEC, 1987; Borges et al., 2002; Borges, 2003; Lafon et al., 2006). Investigation of submerged shelf sediments has chiefly developed over the last decade as access to modern acoustic surveying technology grew. Surveys using sub-bottom profilers have already been conducted around the islands of Faial, Pico, Flores and São Miguel (Quartau et al., 2002, 2003, 2005, 2006; Bates, 2005) to assess aggregate distribution and deposit volume, mostly motivated by the need to manage rising demands for underwater extraction.

In 2003-2004, surveys with beam-forming and phase-measuring swath sonars were conducted around Faial island and western Pico as part of a wider effort to characterize the geomorphology of the shelf and map the distribution of seafloor types for habitat mapping purposes. The site is unique in the Azores context for a shelf that unites two islands. Its good conservation status and particular ecological conditions also make the area of great relevance for nature conservation having received designations under the Natura 2000, the OSPAR and the BIOMARE networks. These designations should be further supported in the near future by the declaration of a Marine Park within the Azorean network of protected areas (Tempera et al., 2001).

The new high resolution multibeam bathymetry and backscatter revealed the geomorphology of the passage includes extensive fields of prominent sedimentary bedforms seemingly produced by powerful hydrodynamic conditions. These patterns are of interest to (i) geologists investigating the processes driving non-cohesive sediment movement in narrow shelf environments, (ii) ecologists involved in habitat mapping for marine protected area design and (iii) coastal managers for evaluation of sand extraction activities or underwater cable routing.

This paper concentrates on: (i) describing the general characteristics of these fields; (ii) inferring sediment transport patterns; (iii) estimating near-bottom current velocities based on bedform geometry; (iv) presenting new information on local currents derived from a mid-passage oceanographic mooring and CTD surveys; and (v) comparing estimated and actual currents in order to estimate the recurrence of bedform activity under the present oceanographic framework.

2. Study area

The Azores is an archipelago of nine islands situated in the Northeast Atlantic. The islands spread across an extent of 617 km and are aligned along major tectonic lineaments generally trending WNW-ESE (Figure 1). The study area is located between the islands of Faial and Pico (in the central island group) that are separated by a 6 km-wide passage.

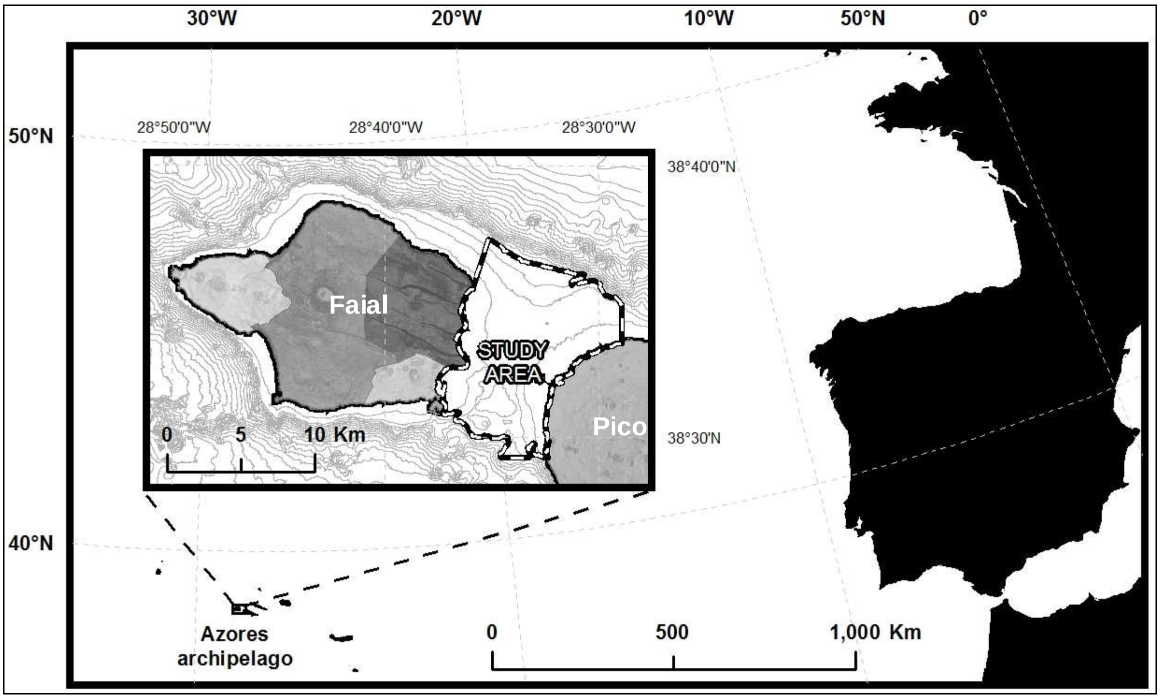

Figure 1: Location of the study area in the Faial-Pico passage (Azores, Portugal, NE Atlantic)

2.1. Geologic setting

The seafloor in the study area is composed of a submerged shelf with flanks rising from depths of 1500m on the north side and 900m on the southern side. Large expanses of the passage are shallower than 100m and a rocky ridge with a maximum depth of 63m straddles between the two islands from Espalamaca headland (on Faial island) to Madalena (on the Pico shore). Boulders produced by coastal erosion and lava flows generated by eruptions form most of the rocky seafloor areas, but sedimentary deposits dominate the shelf, locally reaching a thickness of up to 42 m (Quartau et al., 2002, 2003).

The islands of Faial and Pico are estimated to have emerged in the Pleistocene as eruptions generally associated with tectonic faulting build up tall volcanic edifices. The two islands are connected by a shallow shelf that, judging from the age of the subaerial edifices that surround (800kyr for Faial's Ribeirinha complex and 250 kyr for the Pico Mountain complex), was likely exposed and flooded repeatedly by the eustatic sea level fluctuations associated with Middle and Upper Pleistocene glacial periods. Concurrent tectonic displacements causing subsidence or uplift may have also affected the vertical location of the land masses, but the local isostatic history and its effects on shelf exposure are still poorly known.

2.2. Hydrodynamic setting

2.2.1. Geostrophic flows

Altimetric data averaged over several years show mean geostrophic flows in the area to be typically from North to Northwest with average speeds of 5-10 cm/s (AVISO dataset, 2007). Fine-scale studies aimed at resolving the pattern of flows in the vicinity of the island are ongoing (Bashmachnikov, unpublished data). However, anecdotal information indicates that the larger scale currents intensively interact with the complex seafloor topography in the area to produce sub-mesoscale oceanographic phenomena including narrow jets, trapped currents and localized upwelling (Ana Martins, pers. com.). This information also suggests that in the shelf areas the effects of geostrophic circulation is of secondary importance in comparison to that of the much stronger currents induced by tidal waves as they meet the shoaling and complex topography that surrounds the islands.

2.2.2. Tidal flows

Ocean tides in the Faial-Pico passage have a maximum amplitude of 0.75 m (Instituto Hidrográfico, 2005). Flood tidal currents are roughly to the North and ebb tidal flows are to the

South. Both suffer a significant acceleration within the passage by horizontal and vertical funnelling. A tidal-induced shallow-water current model produced by Duarte (1997) for the area suggested maximum vertically-averaged tidal currents of 0.6 m/s and indicated that flood currents would be first observed on the Pico side of the passage whilst ebb currents would first occur on the Faial side. Subsequent research by Simões et al. (1997) reported a good fit of these modelling results with observations collected by ADCP (Acoustic Doppler Current Profiler) throughout a tide cycle. The profiles acquired showed maximum currents of 1.10 m/s near the surface and 0.50 m/s near the seabed. Results also indicated that the currents decreased towards the shallow margins of the islands, indicating that the regime was not fully barotropic.

2.2.3. Swell induced flows

Data from Carvalho (2003) indicate that prevailing swells approach Faial from the Northwest and West (rel. freq. $_{NW+W}$ = 53%) while the largest average significant wave heights (~3m) are from West and Southwest (Figure 2). Despite most of the passage being partially fetch-shadowed from the prevailing swells by Faial, Pico and São Jorge (~30km to the Northeast), waves of considerable size may propagate to the area by refraction.

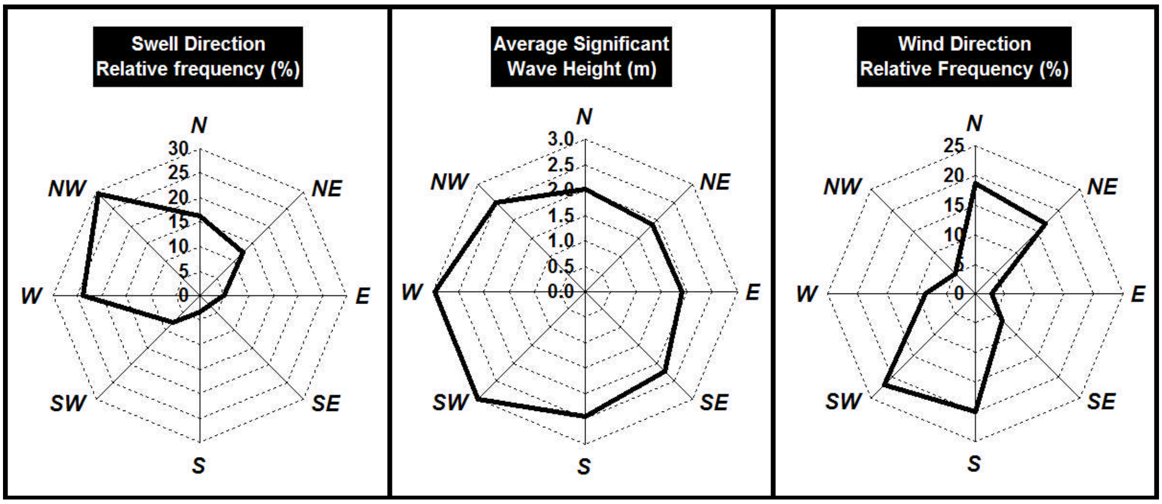

Figure 2: Swell and wind statistics for Faial Island (adapted from Carvalho, 2003 and data from the Horta Meteorologic Observatory provided by Instituto de Meteorologia)

No studies exist on the currents induced by winds and swells, but their effects may attain considerable intensity given the full meteorologic and oceanographic exposure of the islands. The discrepancy between the prevailing directions of swells and winds (Figure 2) suggests the two do not necessarily concur in their action.

3. Methods

3.1. Swath bathymetry

High resolution bathymetry and backscatter data were collected by swath surveys conducted in the autumn 2003 and summer 2004. A Reson 8160 beam-forming sonar system (50 kHz) mounted on the 25-m long RV *Arquipélago* was used to cover areas with bathymetry typically deeper than 40 m. A Submetrix 2000 phase-measuring sonar (117 kHz) installed on the 11m-long RV *Águas Vivas* was subsequently used to cover the nearshore areas.

Beam-forming sonar data were post-processed using CARIS HIPS & SIPS v. 5.4. (® CARIS). Phase-measuring sonar bathymetry was first post-processed using Swathplus v. 2.04 (© SEA Ltd.), where gross filtering of erroneous soundings was performed, and then using CARIS HIPS & SIPS ®.

Results of both surveys were binned in grids with resolutions of 20 and 5 m which were subsequently merged in a GIS environment. Beam-forming sonar data had priority over the swathe data due to less noise.

Backscatter (i.e., variations in the intensity of the reflected acoustic energy along and across the swath) was recorded in both surveys. CARIS HIPS & SIPS ® was used to process beam-forming sonar backscatter and produce seafloor mosaics at a resolution of 1 m^2. Processing included both geometric correction (bottom tracking, removal of altitude and slant range correction) and elementary radiometric compensation (beam angle). Phase-measuring sonar backscatter was processed in SONARWEB PRO v. 3.16 (® Chesapeake Technology, Inc.) where geometric corrections and time varied gain radiometric compensation were applied. Final swathe mosaics were assembled using the "shine-through" algorithm and a resolution of 1 m^2.

3.2. Seafloor validation

In situ information on sediment type, grainsize and structure was provided by both existing data and newly collected datasets. This information typically was consisted of shapefiles holding populated attribute tables that were integrated with the bathymetry and backscatter mosaics in the GIS.

Historic data were digitized from nautical charts (mostly derived from sampling executed in the 1940's) and expedition reports (Richard, 1934; for sampling in the late 19th and early 20th centuries). Some caution was exercised in the use of the historic data given the age of the surveys, lack of information about the sediment classification utilized, the sampling technique used for most sample collection (armed sounding leads) and the considerable bias of the sampling towards shallow areas in the vicinity of harbours.

New samples for sediment characterization were obtained using a Duncan box corer (Quartau et al., 2005) and a Van Veen grab (Isidro et al., 2006).

Additional *in situ* observations about the sediment and seafloor aspect were extracted from imagery collected in point surveys executed with a VideoRay Explorer ROV (summer 2004) and transect surveys carried out with a Tritech MD4000 drop-down camera (summer 2005). ROV and DDC deployments concentrated at representative locations where different physiographic and/or acoustic signatures had been identified in the bathymetric and/or backscatter maps.

A minimum of two representative locations per signature (e.g., coarse sediments, fine sediments, sand wave fields) was sampled.

3.3. Estimation of currents from sediment surface characteristics

3.3.1. Sediment movement threshold

A basic estimate of the threshold flow velocity required to entrain a particle of a certain grainsize (D<0.2cm) in water at 20ºC can be obtained by using the empirical relationship provided by Miller et al. (1977):

Equation 1 $$\overline{U}_{100} = 122.6D^{0.29}$$

where:

D is the grain size diameter measured in centimetres

$\overline{U}_{100}$ is flow velocity 1m above the bottom in cm/s

3.3.2. Fit of velocity profiles

In sedimentary systems the size of sand waves is a complex function of many variables and the literature discerning the process-response mechanisms that relate flow conditions, sediment transport and bedform development is extensive. The major principles are described in sedimentology reference works such as Allen (1985), Southard (1991) or Leeder (1999).

Relationships published in the literature were used to infer the vertical flow velocity profiles from a set of bedform characteristics that could subsequently be compared with results from previous oceanographic studies conducted in the study area. The method suggested by Kubo et al. (2004)

is used. This approach assumes that the bedform measurements are derived from straight-crested dunes in an equilibrium state with impinging flows that are predominantly unidirectional. This should approximate reasonably well the conditions in the studied wave fields, where bedforms were clearly asymmetric and often showed approximately linear crests

The estimates of the velocity of these flows are derived from the classic "law of the wall", which describes how the flow velocity of a fluid changes logarithmically with the distance to a friction-inducing surface. This relationship can be expressed as the von Kármán-Prandtl equation (von Kármán, 1934):

Equation 2 $$U_{(z)} = \frac{U_\tau}{k}.\ln\frac{z}{z_0}$$

where $U_{(z)}$ – flow velocity at height z above the bed

U_τ – friction velocity

k – von Kármán constant (assumed to be 0.41 in clear water)

z – height above the bed

z_0 – roughness length

Friction velocity (U_τ) is a critical parameter for calculations of the behaviour of flow moving over a rough surface. It is defined as $U_\tau = \sqrt{\tau_0/\rho}$, where τ_0 is the loss of momentum (friction) exerted on the flow by the texture and roughness of the surface and ρ represents the fluid density. Ideally U_τ should be measured locally but no profiles were available for the benthic boundary layer over the sediment wave fields. Alternatively, U_τ is here estimated by applying the threshold equation for the occurrence of dunes (Allen, 1972; Allen & Homewood, 1984):

Equation 3 $$\frac{U_\tau D}{v} = 1.117\left(\frac{gD^3}{v^2}\right)^{1/2} - 2.087 \Leftrightarrow U_\tau = \frac{v}{D}\left(1.117\left(\frac{gD^3}{v^2}\right)^{1/2} - 2.087\right)$$

where D – mean grain size diameter;

v – fluid kinematic viscosity (1.004×10^{-6} m^2/s);

g – gravity acceleration (9.801 m/s^2)

The friction induced by the seabed is influenced by two factors: the loss of momentum induced by the grain size (skin friction) and that generated by the roughness elements such as bedforms (form drag). There are various approaches to estimate the roughness length (z_0) depending on which of these factors is more important. Given that the studied seabed is covered by large bedforms, roughness was considered to depend essentially on the dimension of the sediment waves. Thus the equation proposed by Wooding et al. (1973) was adopted:

Equation 4 $$z_0 = 2H\left(\frac{H}{L}\right)^{1.4}$$

where H – height of the sediment wave;

L – length of the sediment wave.

Experimental work by Soulsby & Wainwright (1987) showed that using this approach a prediction of the order of magnitude of z_0 can be made, which is considered sufficiently accurate given that the parameter is logarithmised in Eq. 1 and a small inaccuracy in its estimation should not critically influence the result obtained.

By replacing *Eq. 3* and *Eq. 4* into *Eq. 2*, flow velocities can be obtained for any height above the fields by applying:

Equation 5 $$U_{(z)} = \frac{\nu}{D.k}\left(1.117\left(\frac{gD^3}{\nu^2}\right)^{1/2} - 2.087\right)\ln\left(\frac{z}{2H\left(\frac{H}{L}\right)^{1.4}}\right)$$

An additional current estimate was computed using the characteristics of field SW4 (the field located closer to the mooring) and a distance of 35m above the bed (U_{120}) that could be compared with the measurements acquired at the lowest current meter (located at 120m depth) installed in the mid-passage mooring. Another estimate was obtained for the surface velocity (U_0) over each field using z = *water depth* which could be compared to the near-surface ADCP measurements presented in Simões et al. (1997).

Bridge (2003) indicates that integration of the "law of the wall" over the flow depth yields that the depth-averaged flow velocity occur at a distance of 0.368*d* from the bed, *d* being the full depth of the flow. Using z=0.368*d* in *Eq. 5*, a depth-averaged flow velocity estimate (U_{DA}) for the water section above each field was obtained that can be compared with the maximum depth-averaged current estimated by Duarte's (1997) model which is forced by conditions similar to a spring tide.

3.4. Oceanographic measurements

3.4.1. Current velocity

In order to assess the actual occurrence of currents with the intensities estimated by the different methods described in 3.3.2, current measurements collected by a mid-passage oceanographic mooring were analysed. The mooring was deployed twice at the same location Lat: 38º32,148'N; Long 28º34,441'W (see yellow star symbol in Figure 3). The location is roughly in the centre of the Faial-Pico passage and presents a depth of 150m. Observations covered two periods corresponding to spring-summer and autumn-winter-spring. In the first deployment (April-July 2005; duration ≈ 3.5 months), three Aanderaa current meters were deployed at depths of 40m, 110m and 140m. The second deployment (November 2005-May 2006; duration ≈ 6 months) included only two current meters which were at depths of 86m and 117m.

In addition, another two moorings were deployed: one in the Pico-São Jorge passage to the north of the study area and another one to the south of Faial. Both contained 4 Aanderaa current meters which collected data down to depths of 1200-1500m depth.

The data acquired were screened for errors and analysed for the effect of biofouling. The latter was particularly strong in the passage mooring but screening revealed that only the conductivity measurements were significantly disturbed with valid information being retrievable only for the first month of observations. Temperature and current velocity measurements did not show significant bias (Bashmachnikov, unpublished data).

3.4.2. Density fields

Tidally-induced vertical mixing and upwelling within the channel results in a density increase of the surficial waters and a concurrent density decrease of the underlying waters. This process results in density gradients both within the channel and towards the non-mixed surroundings that can induce local currents.

Data about the density fields in the study area were supplied by four oceanographic cruises conducted in October-November 2003, March-April 2005, November 2006 and December 2006. The surveys included the collection of 101 CTD (conductivity-temperature-depth) profiles using SBE9, SBE19 and Midas-ECM profilers. The data were pre-processed using a standard SBE procedure and vertical binning with a resolution of 1 m.

The potential contribution of the density gradients to the mean flow is evaluated using the dynamic approach of the Csanady's method as in Sheng & Thompson (1996).

4. Results

A total of 620 km of survey tracks (365 km with multibeam + 255 km with swathe) was completed in the Faial-Pico passage, corresponding to an effective surveying time of 60h51m (39h17m with beam-forming sonar + 21h34m with phase-measuring sonar).

Interpretation of the backscatter mosaics showed that 66% of the Faial-Pico shelf was covered by sediment beds which were delimited where the backscatter featured finely grained texture and low to medium amplitude (Blondel & Murton, 1997).

Frequent adjustments of the sonar settings during the survey produced radiometric backscatter artifacts that could not be removed to produce a compensated amplitude mosaic. However, backscatter amplitude variations within individual tracks denoted the clear presence of patches of distinct grainsize. When imaged by the ROV and drop-down camera, low backscatter patterns revealed mostly volcanic sands occasionally coated with lighter biogenic particles. Strong finely-grained backscatter was mostly associated with gravels although some cobble surfaces featured a similar acoustic pattern when surveyed with the multibeam system. Transition between coarser and finer sediments was typically gradational within the passage which, along with backscatter artefacts, prevented the demarcation of sediment patches of different grainsize. Populations of the surface-dwelling polychaete *Ditrupa arietina* were commonly detected on fine sands. Some coarse-grained beds supported dense infauna assemblages as suggested by dense burrowing.

4.1. Fields of sand waves

Bedforms of considerable sizes were identifiable both in the backscatter record and in the bathymetry, being present on 29% of the sediment surfaces found in the Faial-Pico passage. Similar bedforms were absent from the rest of Faial's shelf. The predominant bedforms were fields of flow-transverse sand waves with a clear bathymetric expression. Other smaller features, such as ripple marks bore no microtopography discernable at the resolution provided by the multibeam systems but could be identified on the backscatter mosaics. The two sources of information were used in conjunction for mapping the patches of sedimentary bedforms within the passage. Asymmetry of the sediment undulations and scouring marks were then used to derive associated bottom currents. An overview of the study area and the distribution of the different bedform fields is presented in Figure 3. This map combines bathymetry grids (20m resolution) from the multibeam and swathe surveys. For completeness at this small scale, data holes on the shelf were filled with information digitized from official hydrographical charts (c46403 - Instituto Hidrográfico). Rotation-invariant “shading” is achieved using a slope map rendered in grayscale.

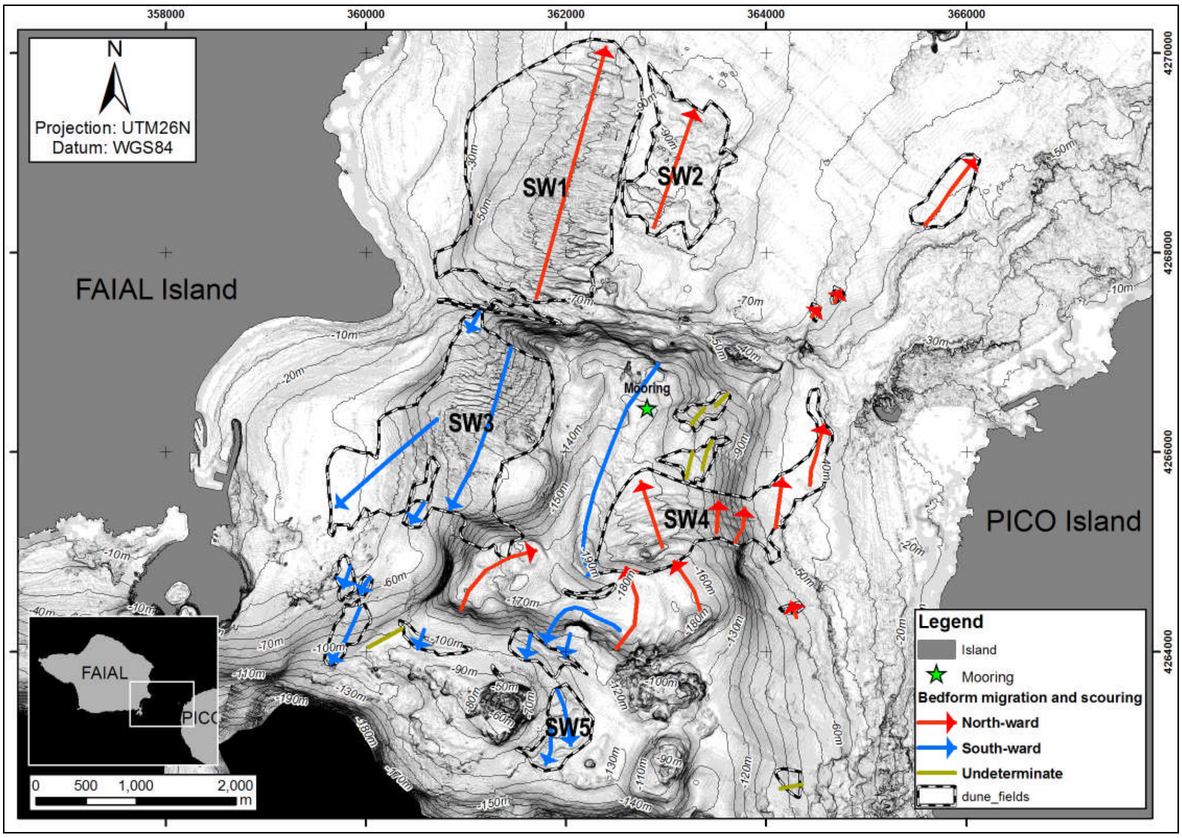

Figure 3: Fields of sedimentary bedforms and near-bottom current direction as derived from bedform asymmetry and scouring marks.

Detailed images of each major field are shown in Figure 4 to Figure **7**. Data holes were left blank in these figures as interpolation would have created conspicuously artificial surfaces within the wave fields. Some survey artefacts are visible such as linear across-track corrugations originated by insufficient attitude correction on the sonar system during acquisition and survey edge effects caused by deficient correction for sound velocity variation within the water column. Despite the holes and pervasive noise, seafloor features are easily discerned and morphologic interpretation is not compromised.

The most extensive fields were found on the western part of the passage (SW1 and SW3), developing both to the north and south of the Espalamaca-Madalena ridge.

Bedforms on the northern half of the passage all displayed lee faces facing the NNE indicating they result from bottom currents from the SSW. Bedforms on the southern half of the channel showed a more complex pattern. The features on the western part seem to be predominantly formed by southward currents while those on the east side seem a result of northward currents. Sediment waves in SW1 (Figure 4-A centre left & Figure 4-B) developed between water depths of 42 and 83 m and displayed long sharp asymmetric crests suggesting migration to the NNE. A clear decrease in wavelength occurred towards the shallower western margin of the field. The backscatter record of these shallow areas features ripple marks up to depths of 28 m but their topographically undulation only becomes noticeable in the swath bathymetry at depths greater than 42 m. The tallest waves in SW1 were located in the southwest corner of the field and attained a relief of 10 m (from trough to crest) and a maximum wavelength of 130 m. Nautical charts indicated a substrate dominated by fine sands, which was corroborated by ROV and drop down camera imagery (e.g., see Figure 9-A for image collected at the along DDC21).

Sediment waves in SW2 (Figure 4-A centre right & Figure 4-C) develop between depths of 88 and 97 m. The waves showed linguoid crests (Allen, 1968) on the northern part of the field and occasionally barchanoid shapes on the southern part of the field. Their asymmetric profiles suggest migration to the NNE. In areas where multiple lines of crests were present, an out-of-phase arrangement prevailed with maximum crest height at 3m and wavelengths of 70m. A drop-down camera lowering on the northern edge of this field showed a substrate composed of biogenic rubble with no noticeable fine fraction. This rubble featured shell and hard skeleton debris and live organisms such as branched bryozoans (Figure 9-B). Some patches of this rubble were densely burrowed indicating very active bioturbation.

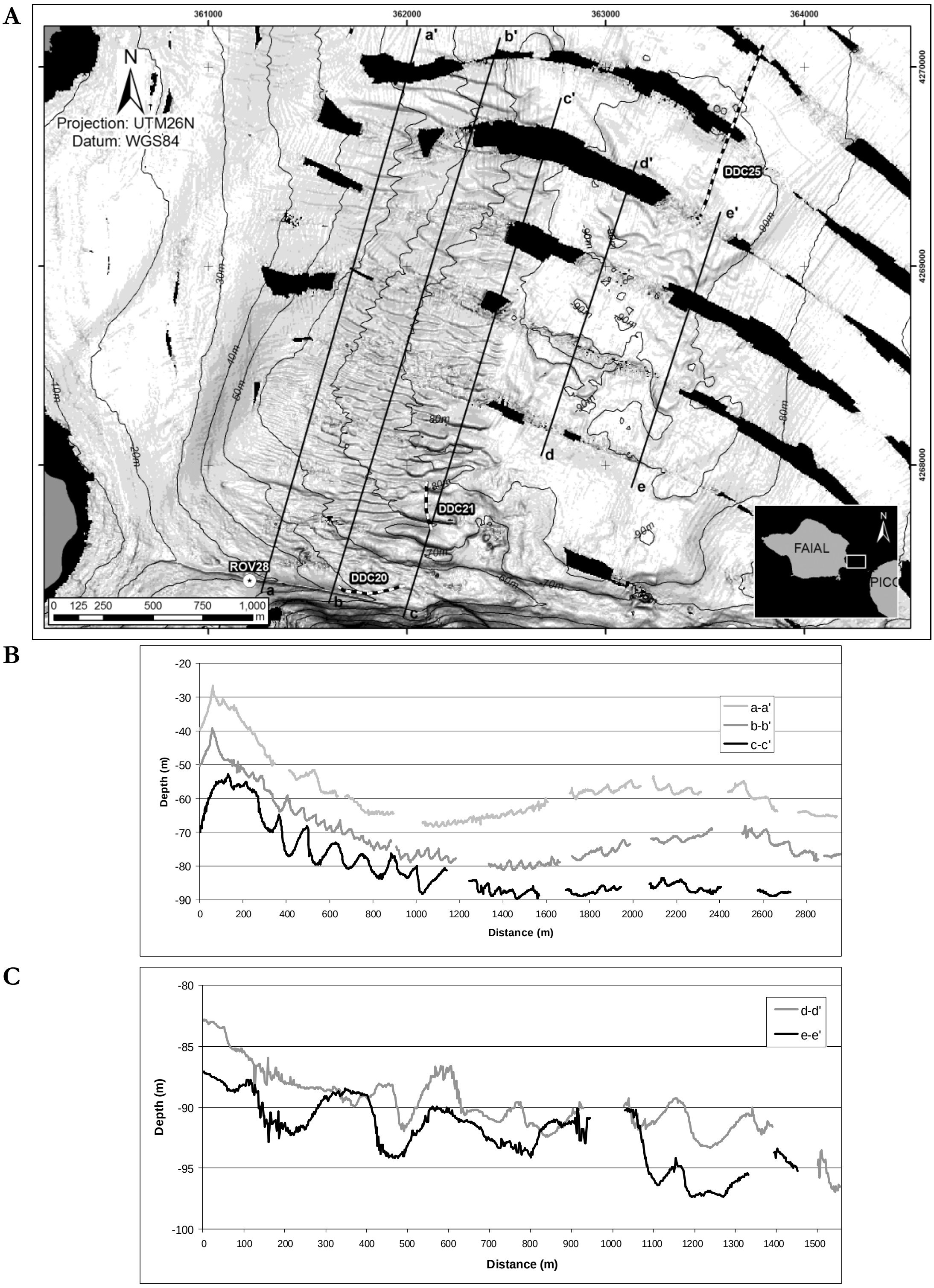

Figure 4: Sand wave fields SW1 (on the East) and SW2 (on the West). A. Plan view with shading provided by slope map. B. Profiles of SW1. C. Profiles of SW2.´

Sand waves in SW3 are at depths between 40 m and 122 m. Their asymmetric profiles indicate a SSW-ward migration (Figure 5). The main crests were continuous for lengths of almost 1,000 m and bore maximum heights of ~6 m and maximum wave lengths of ~60 m. Portions of SW3 displayed a celled morphology where the long-crested waves were divided transversely into cells by streamwise lines (named seams in Allen, 1984). The seams in SW3 were orientated at an angle of ~70º in relation to the large flow-transverse crests and bore maximum heights of ~3m and maximum wave lengths of ~40m. Their lee faces were roughly towards WNW and were clearest on the troughs of the flow-transverse waves.

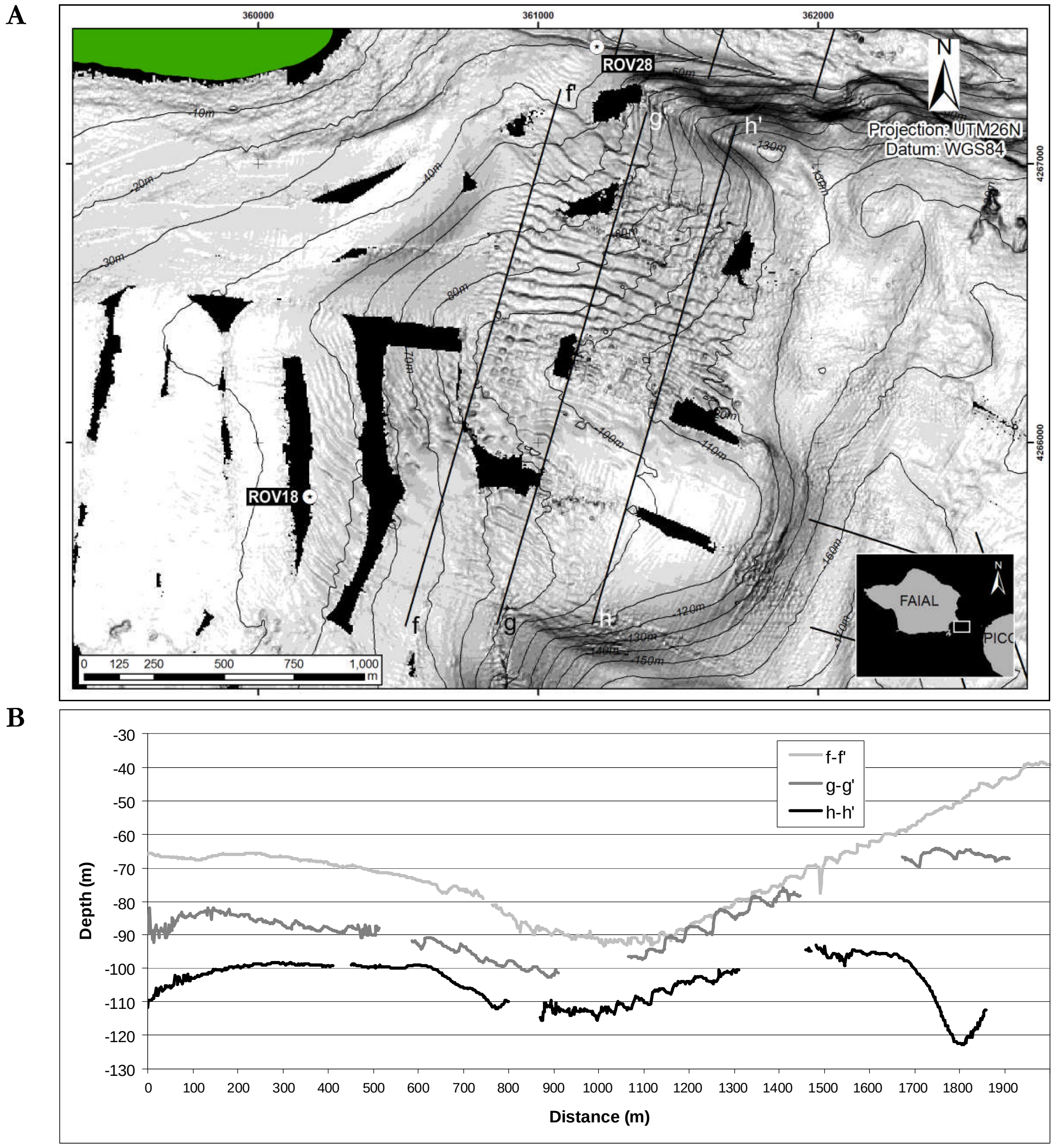

Figure 5: Sand wave field SW3. A. Plan view with shading provided by slope map. B. Profiles of SW3.

SW4 is shown in Figure 6 and is particularly interesting both for the depth at which it is found (between depths of 120m and 180m, with across-slope waves extending to a minimum depth of 60m) and the heights of its sediment waves. The first and southernmost of these waves is the tallest bedform recorded in the Faial-Pico passage. Its centre peaks 18m above its upstream base and its lee face is separated from the northern part of the field by a 16m-deep plunging pool. The northern part of the field displayed wave heights of 2m to 5m. Asymmetric crests indicated migration towards the NNW-NNE.

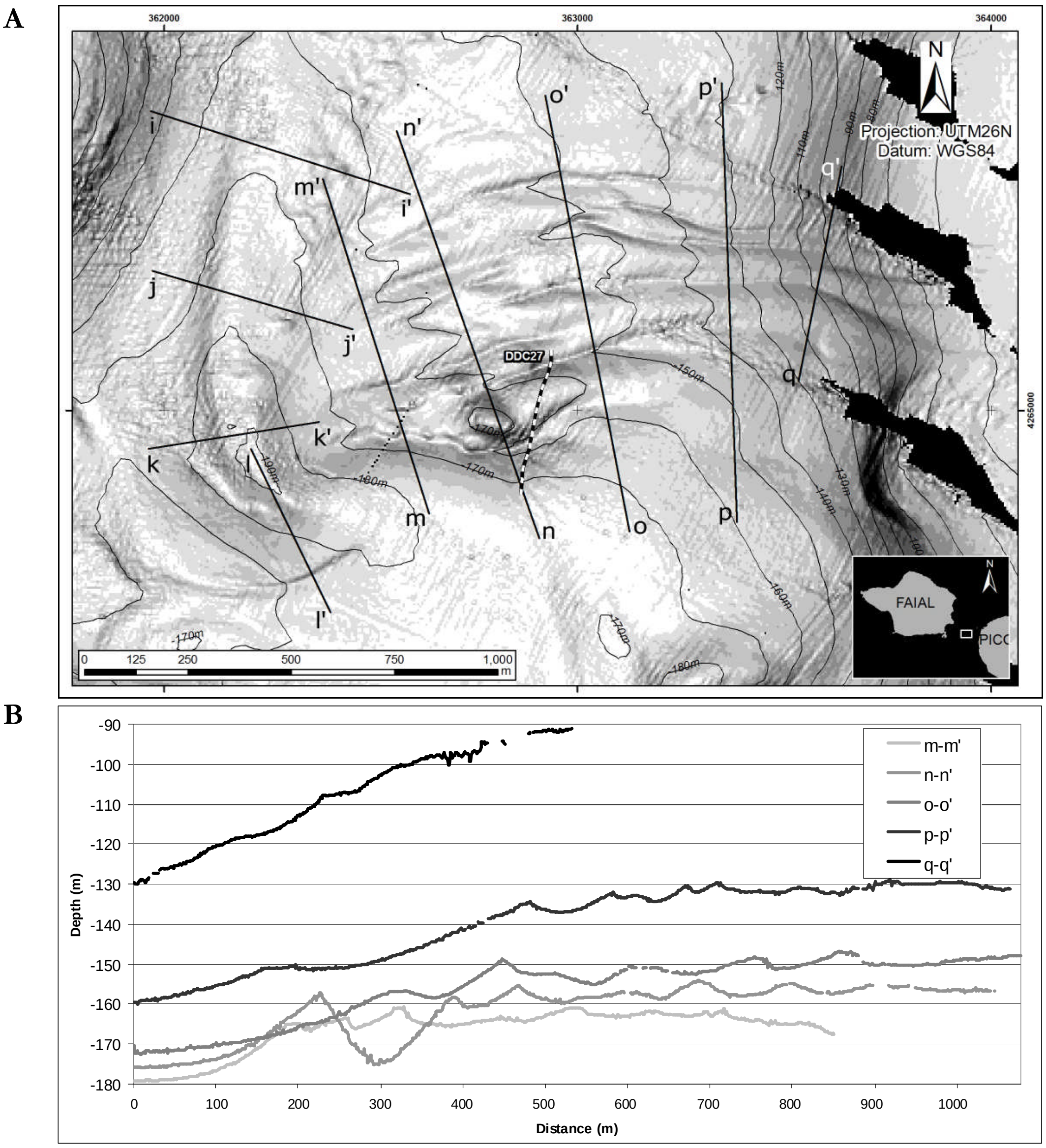

Figure 6: A. Plan view of sand wave field SW4 (on the right) and scoured furrow (on the left) with "shading" provided by slope map. B. Profiles of SW4. Note the 18-m height of the southern-most wave in SW4 and the plunging pool behind it. Profiles i-i', j-j', k-k' and l-l' are presented in Figure 8 and Figure 10.

SW5 was associated with a sediment body located on the eastern flanks of Baixa do Sul between 100 and 127 m depth. The asymmetry of the features indicates sediment transport to the SSE. The dunes displayed a low relief and slightly disordered crest morphology that suggests the substrate may be composed of coarse material similar to the SW2 field. As shown in Figure 7-B, the stoss side of these waves is nearly plane probably as a result of the sloping ground upon which they are moving. Maximum height of the lee sides is 5 m.

A

B

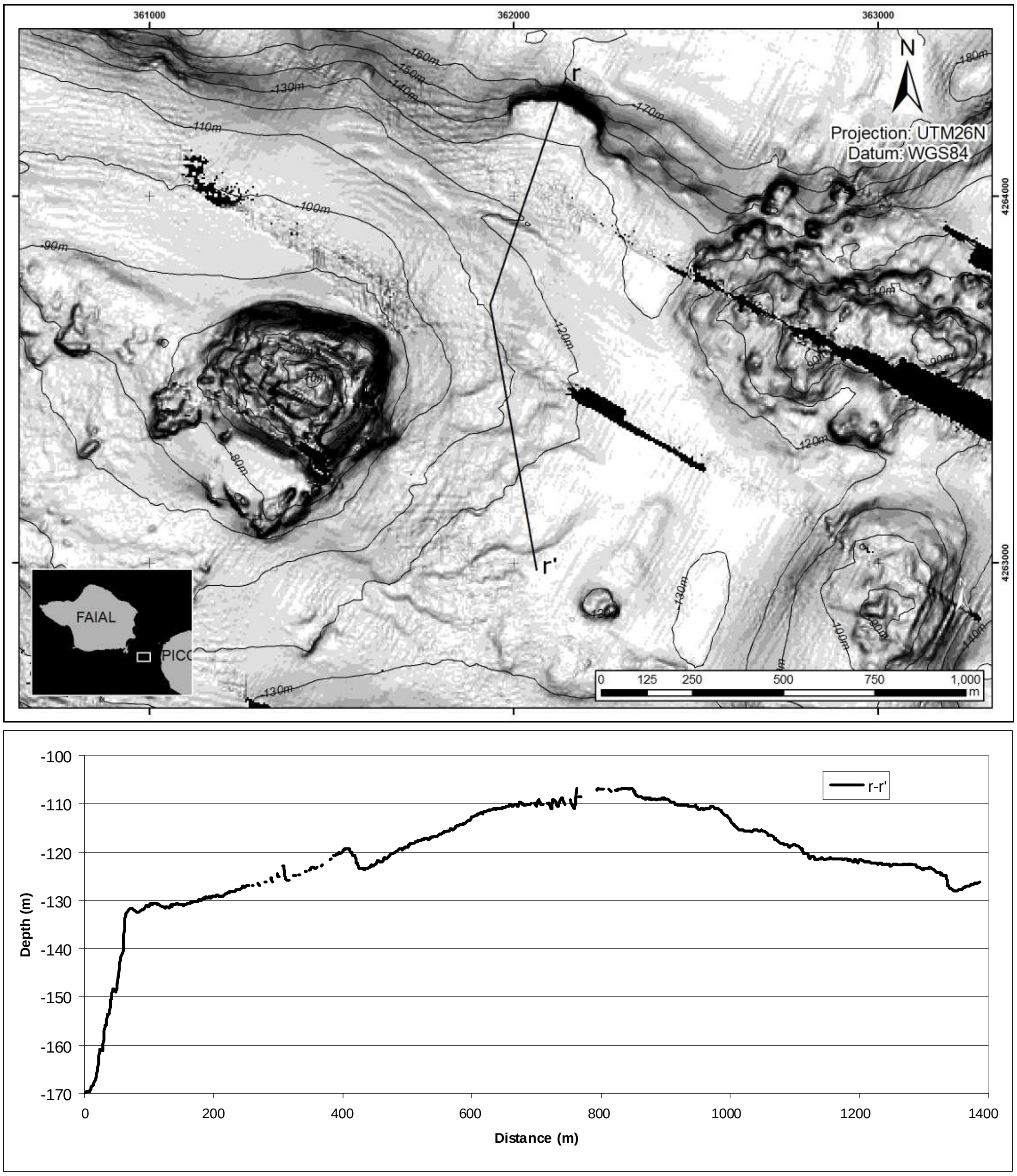

Figure 7: Sand wave field SW5. A. Plan view with shading provided by slope map. B. Profile from the scarp northeast of Baixa do Sul (r) to the southern boundary of SW5 (r').

Other large bedforms in the area include an isolated crescent-shaped sediment ridge to the north of the Baixa do Sul ridge northern flank (Figure 8) and a sharp-crested sand wave present over the western section of the Espalamaca-Madalena Islets ridge. Asymmetry of the latter feature was not well defined and the backscatter indicated that bedrock is exposed on both sides of the dune.

Figure 8: Profile of an isolated dune illustrated on the lower left of Figure 6.

The images collected with the ROV and the drop-down camera showed non-silted surfaces, ripple fans, and ebb lees indicating recent mobilization (Figure 9). These traces of recent activity extended to the deep SW4 field, which exhibited widespread fresh-looking highly asymmetric NNE-trending ripples (Figure 9-D). Field SW5 was not sampled.

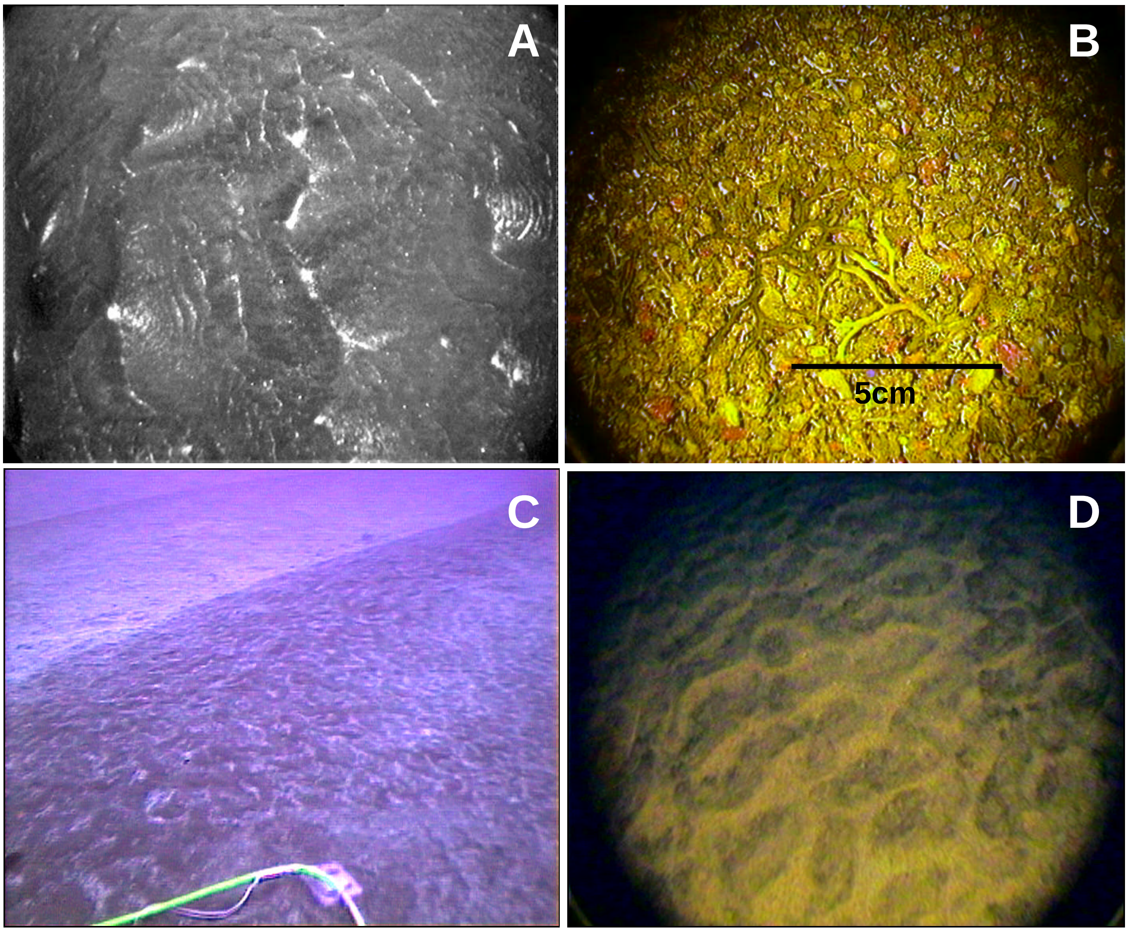

Figure 9: A - Ripple fans imaged on the stoss of a large sand wave in SW1 (imaged along the DDC21 track in Figure 4). B - Loose biogenic rubble on the north of SW2 (imaged along the DDC25 track in Figure 4). C - Megaripples in SW3 (imaged at ROV18 in Figure 5). D - Ripple marks imaged over a large sand wave in SW4 (imaged along DDC27 track in Figure 6).

4.2. Scour marks

The existence of scour-generated features is suggested by the concave deepening of the bathymetry along probable flow pathways. Backscatter in these areas indicated a coarser/harder seabed and *in situ* observations at the centre of the northern half of the passage (Figure 9-B) suggested that scoured beds are dominated by a lag of biogenic rubble.

The basin on the southern half of the passage contains a well developed scoured furrow with a N-S orientation narrowing to the south. This feature extends from the southern flank of the Espalamaca-Madalena ridge to the north flank of the Baixa do Sul ridge, where it inflects to the east (see Figure 3 and left-hand side of Figure 6). Profiles of this furrow are shown in Figure 10.

The flat plane observed in the southernmost profile (k-k' in Figure 10) and stronger backscatter of the area suggests scouring has reached a coarser/harder surface.

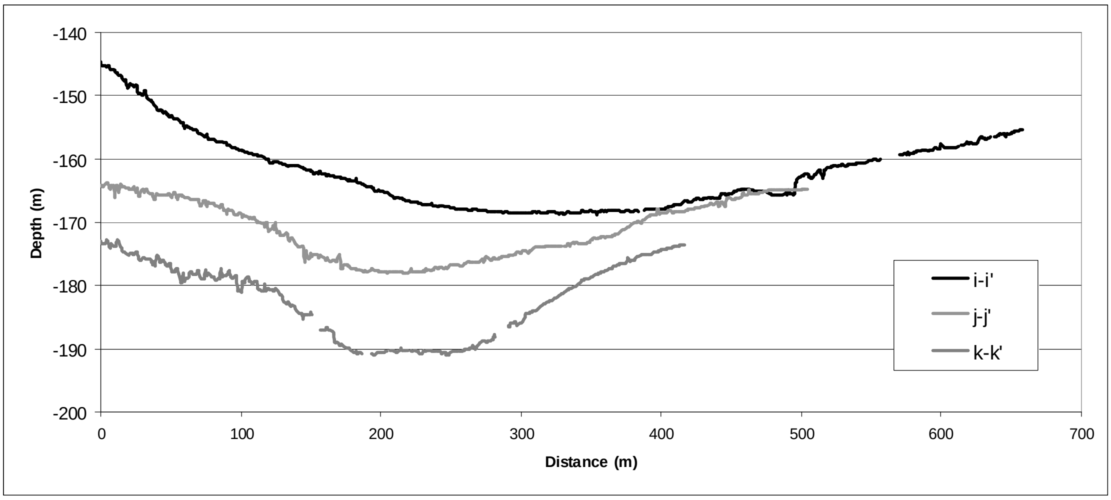

Figure 10: Profiles of a scour furrow illustrated on the left-hand side of Figure 6.

4.3. Estimation of currents from bedform characteristics

The characteristics of the different wave fields are summarized in Table 1. Measurements of extraordinary bedforms are shown in between brackets but they were ignored in the subsequent velocity profile reconstruction as they were not considered representative of the field.

The grainsize information is derived from recent sampling with a Duncan box corer in the vicinity of fields SW1, SW3 and SW4 (Quartau, 2007) These results were generally considered more reliable and indicate that these fields are probably composed of medium to coarse sands (D≈0.5 mm) rather than the fine sands suggested by the 1940's nautical charts, which do not document the methodology and classification used.

Table 1: Characteristics of the sediment wave fields.

Sediment wave field	Field characteristics						Representative bedform		
	Min. depth	Max. depth	Migrating towards	Grainsize (Wentworth where available)	Origin of grainsize information	Approx. grain diameter (mm)	Wave height (m)	Wave length (m)	Depth
SW1	(28) 42	83	NNE	Medium to coarse sands	Recent samples in the field margins	0.50	10	(130) 115	70
SW2	88	97	NNE	Biogenic rubble	Drop down camera	Insufficiently characterized	3	70	92
SW3	40	122	SSW	Medium to coarse sands	Recent samples in the field margins	0.50	6	(75) 60	75
SW4	(60) 120	180	NNW-NNE	Medium to coarse sands	Recent samples in the field margins	0.50	(18) 5	(212) 103	155
SW5	100	127	SSE	Biogenic rubble?	Extrapolated from SW2	Insufficiently characterized	5	97	125

Flow velocities were estimated based on the representative bedform in each sediment wave field using *Eq. 1* and *Eq. 5*. The results are presented in Table 2 which also compares them with points of reference drawn from the literature.

Table 2: Reconstruction of flow conditions from bedform characteristics in each sand wave field. Estimates are also obtained at 120m depth to compare with measurements from deepest current meter at mid-passage mooring.

Sediment wave field	***Eq. 1* threshold flow velocity for average grain entrainment** $\overline{U}_{100}$	**Point of reference:** maximum velocity measured at mid-passage mooring deepest current meter (~120m)
SW1, SW3, SW4	0.51 m/s	0.80-0.90 m/s
Sediment wave field	***Eq. 5* current estimate at 120m depth** U_{120}	**Point of reference:** maximum velocity measured at mid-passage mooring deepest current meter (~120m)
SW4	0.99 m/s	0.80-0.90 m/s
Sediment wave field	***Eq. 5* current estimate at surface** U_0	**Point of reference:** maximum near-surface velocity ADCP measurement in Simões et al. (1997)
SW1	0.84 m/s	1.10 m/s
SW3	0.91 m/s	
SW4	1.26 m/s	
Sediment wave field	***Eq. 5* depth-averaged current estimate** U_{DA}	**Point of reference:** maximum depth-averaged current estimated by Duarte's (1997) model
SW1	0.66 m/s	0.6 m/s
SW3	0.73 m/s	
SW4	1.08 m/s	

The mid-passage mooring deployed between April 2005 and May 2006 provides the best available dataset to assess the maximum intensity of the currents in the Faial-Pico passage over a reasonably long period. Its lowest current meter (placed at approximately 120m deep, 35m above the seabed) measured maximum velocities of 0.80-0.90 m/s which exceeds the flat bed sediment transport threshold ($\overline{U}_{100}$=0.51 m/s) computed from the grainsize of SW1, SW3 and SW4.

Surface flow velocities (U_0) estimated over fields SW1 and SW3 (ranging 0.84 to 0.91m/s) are below the maximum velocities of 1.0-1.1 m/s measured near the surface by the ADCP survey reported in Simões et al. (1997). However, the estimate 1.26 m/s obtained over SW4 is above the reported ADCP measurements. Finally, the depth-averaged estimates (U_{DA}) are all above the depth-averaged current presented by Duarte (1997).

4.4. Actual currents and potential drivers

In order to further investigate the conditions mobilizing the observed bedforms an account is given of the currents measured by a mid-passage mooring. This is followed by considerations on the potential contribution from tidal wave barotropic forcing, density-driven currents, regional geostrophic circulation and calculations for wind-induced currents and swell-induced currents based on textbook fluid dynamics.

4.4.1. Current measurements at oceanographic mooring

Only the data collected by the deepest current-meters installed in the mid-channel mooring are compared to the currents estimated from the bedforms characteristics. Data for the period November 2005–May 2006 were provided from the current meter deployed at 117m depth. Since no current meter was deployed at the same depth in the period April-July 2005, an average of the data collected by current meters installed at 140 m and 110 m depth was computed as an approximation that could be compared in the two periods. The results show that velocities averaged 0.20 m/s in the first period and 0.21 m/s in the second. Maximum velocities measured during spring tides were in the 0.80-0.90 m/s class. The distribution of current velocities obtained during the two periods is shown in Figure 11.

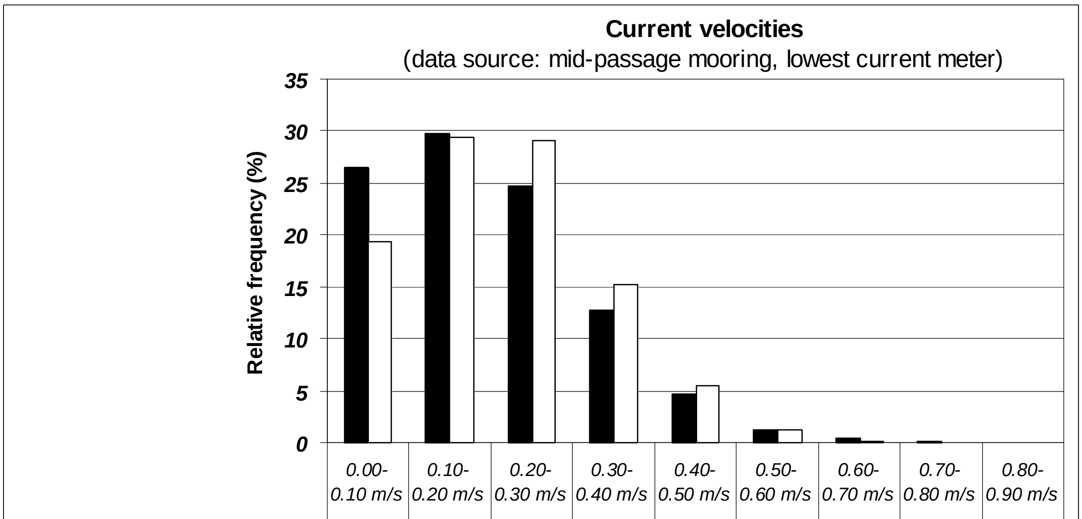

	0.00-0.10 m/s	0.10-0.20 m/s	0.20-0.30 m/s	0.30-0.40 m/s	0.40-0.50 m/s	0.50-0.60 m/s	0.60-0.70 m/s	0.70-0.80 m/s	0.80-0.90 m/s
■ Apr-Jul 2005 (140-110m average)	26.47	29.73	24.64	12.73	4.62	1.3	0.39	0.12	0.02
□ Nov 2005–May 2006 (117m)	19.34	29.38	29.06	15.26	5.49	1.24	0.18	0.05	0

Figure 11: Distribution of current velocity (%) at the Faial-Pico passage mooring in two observation periods. Measurements are from the current-meter nearest to the seabed.

The relative frequency and average current velocity directional spectra are shown in Figure 12.

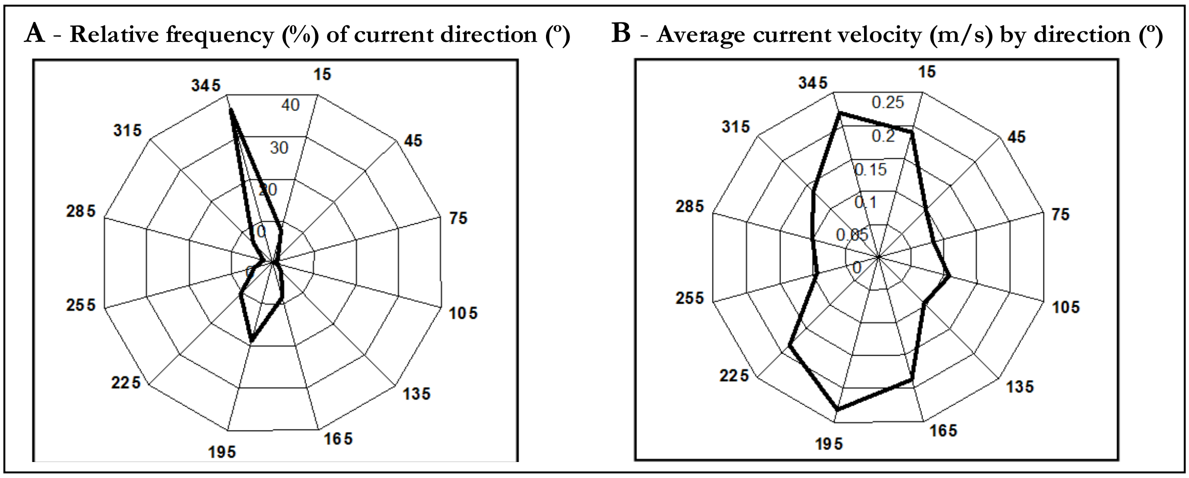

Figure 12: Direction spectra of currents measured at the Faial-Pico passage mooring by the current-meter nearest to the seabed (approx. 120m depth). A. Relative frequency. B. Average velocity.

The predominance of NNW and SSW directions is clear both in terms of relative frequency and current velocity. These directions were expected given the N-S orientation of the channel and match the migration direction shown by the neighbouring SW3 field (bound to SSW) and SW4 field (bound to NNW-NNE).

Data acquired at the mooring did not show significant vertical variability of the tidal flows suggesting that bottom friction may be restricted to a logarithmic benthic boundary layer as thin as 1-3 m (Bashmachnikov, pers. com.).

4.4.2. Tidal currents

Tides are the main driving force of flows within the Faial-Pico passage. The funnelling of the waters through a complex topography produce significant residual tidal currents, as a result of non-linearity of the tide and tidally-induced vertical mixing. The patterns and intensity of the tidal flows are presented by revisiting the barotropic model build by Duarte (1997) for the Faial-Pico passage.

The model uses shallow-water equations and is forced on the open boundaries by a single tidal wave approaching from south with an amplitude of 0.80 m. According to the author, these conditions should represent a spring tide dominated by the M2 component.

The pattern of residual currents is reproduced in Figure 13 and shows that residual flows in the southern half of the passage are generally directed to N-NW at the eastern side of the channel and to S-SW at the western side, forming a cyclonic vortex. Residual velocities reach approximately 0.20 m/s.

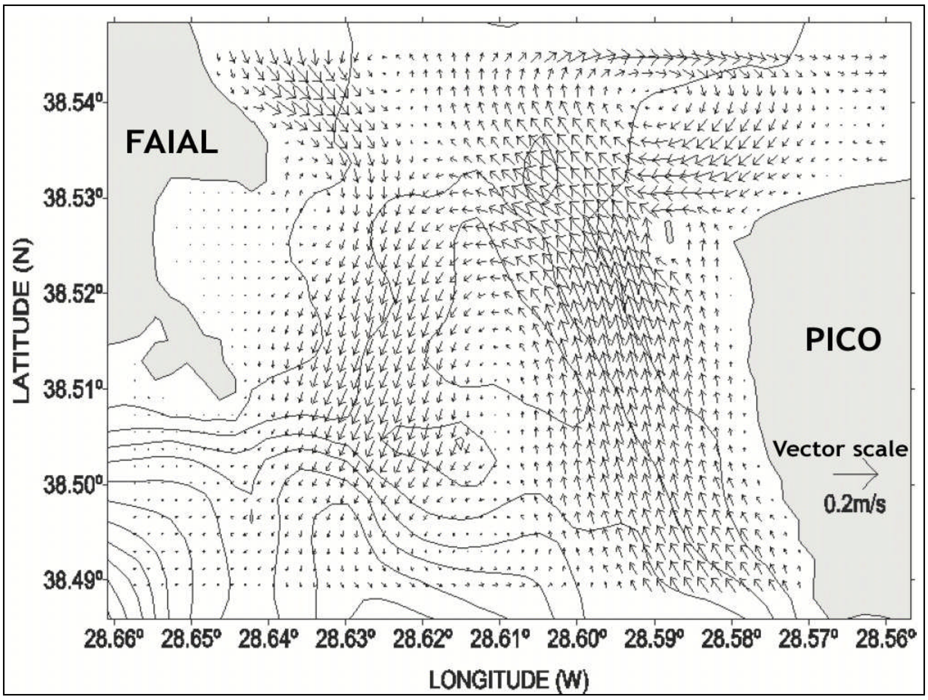

Figure 13: Residual currents along a tidal cycle in the Faial-Pico passage [Fig 4.2.22 in Duarte (1997)].

The model predicts maximum depth-averaged velocities of about 0.60 m/s (Duarte, 1997). Simões et al. (1997) reported a good fit between currents measured with an ADCP (Acoustic Doppler Current Profiler) throughout a tidal cycle and the estimates provided by the model.

4.4.3. Density-driven currents

CTD surveys showed that during summer and autumn (Aug, Oct, Nov) a significant stratification was observed in the upper 100 m that contrasted with the late autumn/spring surveys (Dec, Mar) (Figure 14).

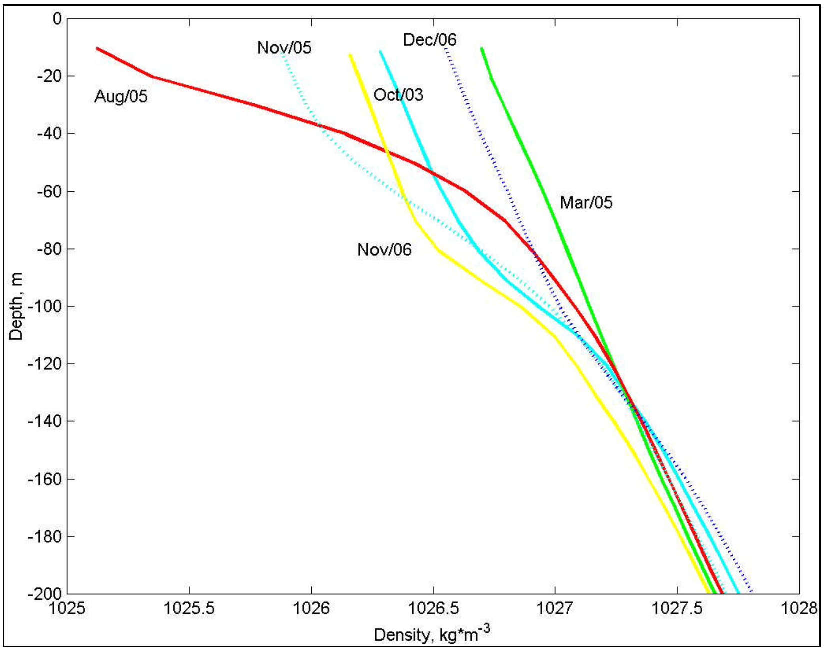

Figure 14: Mean vertical density profiles at the stations outside the channel (background).

Independently of the variation of the background vertical density distribution, density fields (Figure 15 and Figure 16) were characterized by low bottom density values inside the channel and increased density values at both edges.

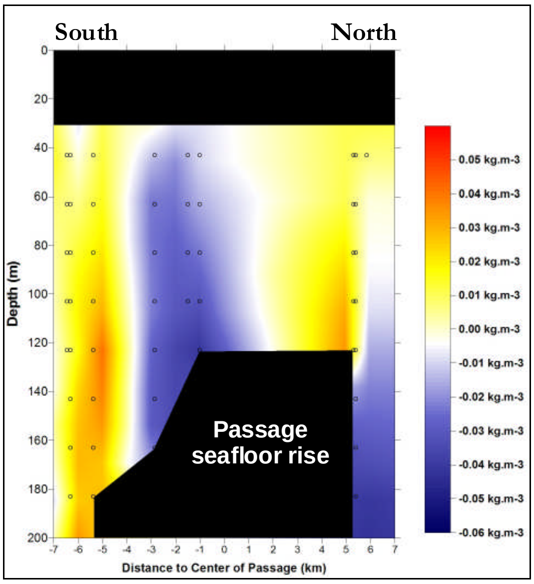

Figure 15: Density anomalies (kg.m^{-3}) from a composite South to North cross-section including all casts. Blue shades are lower than average densities whilst warm colours are higher than average densities. White is for values around the average density. Points represent measurements along CTD casts used in the interpolation.

This is also observed in the depth-averaged fields shown in Figure 16, particularly in the non-stratified conditions that prevail during the winter.

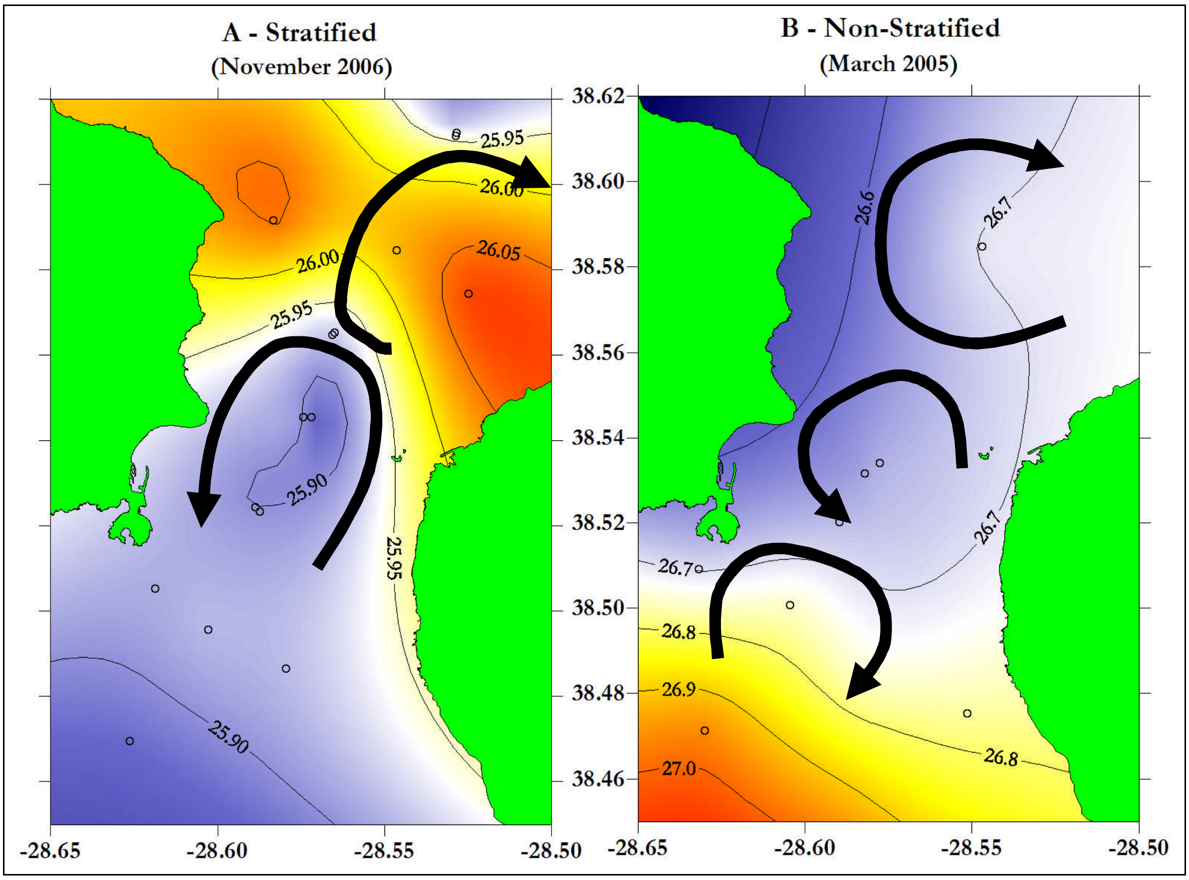

Figure 16: Faial-Pico passage depth-averaged density (σ_t) fields for the 10-90m depth layer in stratified and non-stratified conditions. Arrows represent the direction of the flows induced by these density gradients.

Interpretation of these density gradients suggests that the centre to southern part of the passage is an area of permanent bottom-accentuated cyclonic vortex whilst the northern part exhibits an anticyclonic vortex. The November 2006 survey suggested that this vortex was more accentuated at the eastern side of the channel. Both anticyclonic vortices are induced by deep water upwelling during the North-South oriented tidal incursions (Bashmachnikov, pers. com.).

The density data suggest that the geostrophic currents should be minimum near the surface, thus the 0-reference level can be put at the sea-surface when applying the Csanady's method (Sheng & Thompson, 1996). The resulting computations showed that density currents will reach velocities in excess of 0.50 m/s near the seafloor (Bashmachnikov, pers. com.).

4.4.4. Geostrophic drift

The spatial scale of the data provided by global datasets such as the AVISO dataset (2007) are too coarse to resolve the flows in the Faial-Pico passage. It is likely that the geostrophic drift, averaging an intensity of 5-10 cm/s, interacts with the seafloor as it approaches the islands and is diverted in an anti-cyclonic pattern. This should make the drift follow the northern slope of the Faial-Pico rise towards ESE. Most probably, there is a geostrophic flow which enters the Faial-Pico passage from the north but its contribution should be minimal and easily countered by the intense tidal flows, particularly during flood.

4.4.5. Wind-induced currents

Wind-induced currents may affect the shallow parts of the channel. Thickness of the water layer mobilized by the wind can be evaluated from the equation in Bowden (1983):

Equation 7 $D=4.3*W/(\sin(\varphi))^{1/2}$

where W - wind speed

φ - latitude

For the average 7.6 m/s (27km/h) wind observed in Horta (1960-1991 climatologic data), the maximum depth affected by the wind-induced current is of 41 m, whereas the majority of the bedforms investigated are below this depth. Even for strong winds of 70 km/h (19.4 m/s), when the Ekman layer can reach 106m depth, the predicted speed of the Ekman flow will only be 0.07-0.08 m/s at 50m depth, and approximately 0.02 m/s at 100-m depth.

4.4.6. Swell-induced currents

The orbital velocity of near-bottom wave-induced currents (u_b) can be estimated from the characteristics of waves observed at the sea surface. Deep water wave statistics are derived from Carvalho (2003) and used to estimate on-shelf "bottom-feeling" wave characteristics on the online wave calculator at *http://www.coastal.udel.edu/faculty/rad/wavetheory.html*. This facility was implemented from Dean & Dalrymple (1991) and is based on the dispersion relationship for progressive linear water waves and Snell's Law for straight and parallel offshore contours.

Calculations are presented for average conditions observed during northerly, southerly, and the south-westerly swells, which should represent maximum effects in the study area as they come to the passage without major interferences and approximately along its axis. In addition, results are presented for swells with significant heights (Hs) of 6m and 10m to illustrate the power of the oscillatory currents induced by storm swells. Swells impinging unhindered on the passage with Hs≥6m compose 1% of the swell observations and occur from the North, South and Southwest. Swells with Hs≥10m only occur 0.025% of the time and from the Southwest. The "bottom-feeling" velocities of these swells are represented as profiles in Figure 17.

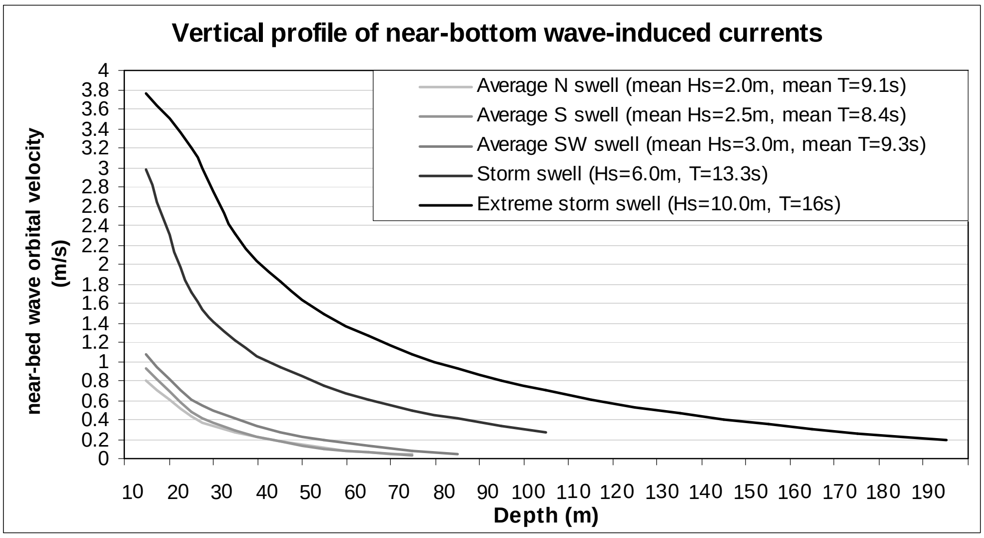

Figure 17: Vertical profiles of near-bottom oscillatory currents induced by oceanic swells approaching unhindered into the channel.

Only the velocities occurring deeper than 40m are of relevance for the maintenance of the sediment wave fields since this is where most bedforms are concentrated. Average swells generate velocities <0.3m/s at depths of 40m while storm swells can induce velocities of 1-2m/s at the same depth. A 10m storm swell can produce currents of 0.8m/s at depths of 90m, which is roughly the same intensity of the maximum tidal currents measured by the mooring.

5. Discussion

The discussion is focused on the transport patterns derived from the bedform morphology and on how existing information on local hydrodynamics corroborates the indicated migration direction of the large sediment waves.

5.1. Morphology and transport pattern

Bedform asymmetry is usually a good indicator of the net direction of sediment transport by unidirectional currents or by a reversing current with time-velocity asymmetry (Johnson et al., 1982). Given the poor knowledge of local currents, the information derived from the bedforms about bottom flow patterns is valuable.

The migration of features towards opposite directions within SW1 and SW3 indicates unequal effect of ebb and flood currents either side of the Espalamaca-Madalena ridge. This is a frequent feature in sills subject to non-uniform reversing flows (Gary Greene, pers. comm.). The water flowing into a narrowing section is less efficient in mobilizing the sediments than water moving out the same area. This is probably due to water mass stalling and turbulence dampening as the flow is horizontally and vertically funnelled.

Features within SW1 result from NNE-bound flood currents impinging on a sand deposit to the northeast of Espalamaca. The opposite is suggested for SW3, which seems to be primarily mobilized by SSW-bound ebb currents impinging on a sand deposit to the southeast of the Espalamaca headland.

The fact that both SW1 and SW3 fields stem from sources based upon the Espalamaca-Madalena Islets ridge raises the question of whether there is any replenishment of the sediment source. It is postulated that transport forces on the west of the passage are acting on sediment deposits which are being excavated at a greater rate than they are being replaced. Bedforms around these wave fields do not indicate any incoming sediment pathways. Instead the steep bathymetric contours to the northeast and southeast of the headland do suggest sidewalls of increased erosion areas. In this erosion context it is possible that SW2, directly along the longitudinal axis of the centrally depressed passage, represents a lag area winnowed of its fines by a longer and probably more forceful history of current scouring.

Both the north and southern half of the passage show the effects of a strong central flow. While on the northern half this flow shapes the linguoid and barchanoid beforms of field SW2, the pattern in the southern basin is more complex. In the centre of the southern basin, the sediment transport occurs along a scour furrow trending towards the SSW. On approaching the northern flank of the Baixa do Sul ridge, the near-bottom flow seems to be topographically obstructed by the northern flank of this obstacle and is deflected to the east. In this process the current shapes a hooked deposit topped by a narrow crescent-shaped crest. As a result, the scoured sediments are redirected towards the upstream area of SW4, on the northeast of the Baixa do Sul ridge. Bottom currents entering from the south, constricted between Baixa do Sul and Pico island, then push these sediments up SW4, re-circulating them towards the NNE-N. This bedform configuration corroborates the anticlockwise residual current pattern suggested by Duarte's current model for the southern half of the passage and its different sectors are activated at different stages of the tide cycle.

For the sake of completeness, the celled pattern visible on portions of SW3 should be mentioned. It likely results from spur-scour pit sequences developing on the troughs of the flow-transverse waves. According to Allen (1984) the scour pits form when successions of powerful vortices descending from the main flow form in the lee of the crests. Where the vortices "explode" against the trough surfaces, scoured depressions are formed that contain ripple fans radiating towards the crested reattachment spurs.

5.2. Impinging currents

The size of the sand waves and extension of the fields suggest strong near-bottom currents. The bedform features are therefore investigated with respect to knowledge about the oceanographic framework presently impinging on the area published in the literature, namely from Duarte (1997) and Simões et al. (1997), as well as new measurements using moored current meters deployed for approximately 9.5 months in the Faial-Pico passage (Bashmachnikov et al., unpublished data).

5.2.1. Current direction *vs.* migration patterns

The directions of the modelled residual tidal flows (Figure 13) show a good match with the directions of sediment transport in SW2, SW3, SW4 and SW5 (Figure 3). In all of them, migration direction is usually within one octant of the residual current direction. The exception to this is field SW1 which displays wave migration in the opposite direction of the residual flow. This is interpreted as being a consequence of Duarte's model poor performance near its northern open boundary, which precluded the extraction of accurate residuals. Similarly the residual are in opposite direction of the current deemed responsible for the scouring observed between the northern flank of the Baixa do Sul ridge and the south of the SW3 field. In any case, it is worth-noting that depth-averaged residual currents may represent poorly the actual near-bottom residual flows.

5.3. Current strength and wave feature size

According to the bedform stability field presented by Southard (1991), currents of the intensity measured at the mooring are sufficient to generate dunes in medium to coarse sands such as those in fields SW1, SW3 and SW4.

Estimates derived from the "law of the wall" following the work of Allen & Homewood (1984) and Kubo et al. (2004) show that bedforms in fields SW1 and SW3 should be active at present under extreme conditions. Even in the case of field SW4, where the current estimates exceeded (by ~0.3 m/s) any current measured during the 9.5 month series of mooring observations, it is postulated that the discrepancy is not sufficient to interpret the bedforms as relic features. In face of the current meter records and estimated currents, it is suggested that mobilization may be restricted to extreme events such as large storm swells and winds which generate near-bottom oscillatory currents that provide the additional drive for sediment transport. However, *in situ* observations collected in the summer suggested that this may occur more often than that as signs of recent activity such as non-silted surfaces and fresh secondary bedforms including fresh highly asymmetric ripples and ripple fans were clearly identifiable over the bedform surfaces.

The conditions in fields SW2 and SW5 were not estimated given the lack of information on the grainsize of the material, which were relevant for obtaining an estimate of the friction velocity U_τ from *Eq. 3*. Backscatter information suggested a seafloor composed of coarse material and *in situ* imagery showed a biogenic lag largely dominated by particles of grainsize >1cm. Bathymetry showed bedforms that attain 3m height and are lower than the bedforms observed on finer sediments. This corroborates the suggestion that sediment wave height augments as the grain size of the material increases to approximately 0.5mm, after which the wave height decreases as grain size continues to increase (e.g., Allen, 1984). Flood (1983) and Belderson et al. (1988) add that coarse sediments generally occur under bottom currents of >1.0m/s. Occasional flows of this magnitude are likely responsible for maintaining depressed hollows along the centre of the passage by promoting the winnowing of the finer fractions. Moreover, the same intense currents must shape the coarse lag left behind into linguoid and barchanoid waves on the northern half of the channel (SW2 field) and into a scour furrow on the southern basin.

Calculations conducted in the present work assumed bedform friction dominated the roughness configuration, corresponding to the condition of a fully turbulent flow. Since viscous forces produced near the wall by grain texture (skin friction) may also contribute to the overall flow resistance in transitional flows, this approach may underestimate the value of the currents necessary to produce the observed sand waves. However it is worth noting that bedform friction also weakens the viscous generation cycle. Because no velocity profiles were available to estimate actual friction velocity over the fields analysed, it was not possible to establish which factor is more important and whether the bedforms produce a transitional or fully turbulent flow.

5.4. Current drivers

Although barotropic flows may represent the largest driver of currents in the Faial-Pico channel, these may also be associated with reasonably strong density gradients. Calculations based on the density fields computed from CTD profiles indicated that near-bottom density-driven flows could reach velocities in excess of 0.50 m/s. The intensity of these flows could add to the barotropic flows and partially compensate for the frictional loss of energy occurring closer to the seafloor in the flow's benthic boundary layer. It is postulated that this could explain the small vertical variation of the flows reported along the mid-passage mooring. Barotropic and baroclinic processes should be concurrent in their action over the sediments as modelled residual tidal currents show directions similar to the density-driven currents. Both of these generally mirror the migration direction of the sediment waves.

Although the asymmetry of the dunes suggests that none of the fields are wave-dominated, it is worth-noting that waves are extremely efficient at stirring up bottom sediment due to the large velocity gradients they create in the boundary layer (Madsen, 1976). The superimposition of oscillatory currents induced by the swells on tidal flows can cause sediment movement threshold to be exceeded even under rather weak tidal currents (Allen & Homewood, 1984).

The unidirectional currents generated by the winds may further contribute to the overall flow observed over the fields. This significant action probably extends to the deepest parts of the shelf during extreme storms. It is suggested that even if the associated flows are not above the critical threshold for sediment motion, the motions they superimpose on tidal flows can contribute significantly to the overall near-bottom flow and help the threshold be exceeded. In the tidal-dominated Dover Strait, it has been shown that wind-induced currents can even prevail over tidal currents during strong wind periods (Idier et al., 2006) and induce periods of no tidal current

reverse, related either to flood or ebb periods according to the wind direction. Anecdotal information collated from local users of the area indicates this effect has also been observed in the Faial-Pico passage.
The relative significance of the main types of currents is summarized in Table 3.

Table 3: Significance of the main factors generating currents in the study area.

Type of flow	Significance
Tidal currents	High
Density currents	High
Swell-induced currents	Medium for the fields shallower than 100m during extreme storms
Wind-induced currents	Medium for the fields shallower than 100m during extreme storms
Geostrophic currents	Low

Despite the results presented in this paper, the analysis of more widespread observational series and the construction of a 3-D hydrodynamic model are still crucial to fully understanding which combination of tidal currents and other forces such as density currents, wind-induced currents, storm surges, internal waves and geostrophic currents are central in generating the flows required to mobilize the bedforms found in the various sediment wave fields.

6. Conclusions

Multibeam surveys aimed at mapping the habitats and geology of the Faial-Pico passage revealed that sediments accounted for 66% of the seafloor surface. Variations in backscatter indicated variability in grainsize whilst bathymetric data exposed prominent bedforms such as straight crested sand waves, waves with celled crest patterns, linguoid waves, barchanoid waves and scour depressions. The bedforms covered 29% of the sediment beds and are the first reported on shelves of the Azores islands.
Despite the fact that the Faial-Pico passage is only subject to a microtidal regime and is located over shelf areas younger than 800kyr, sediment deposits are extensive and display an abundance of signs substantiating sediment transport. Bedforms reaching a maximum height of 18m were recorded that extend to depths of 190m. Large bedforms were not found shallower than 40 m depth, although some rippled morphology locally persisted in the backscatter record to depths of 28m.
The dimensions of the wave fields and bedforms provide evidence for the occurrence of strong bottom currents which were partially attested by existing oceanographic observations. These

currents result from a unique combination of factors in the Faial-Pico passage which includes the funneling of oceanic tidal currents, density currents and seafloor morphology. The size of the bedforms is maximized by the presence of average grain sizes (~0.5mm) that are optimal for producing tall sediment waves.

A comparison between bedform-based current estimates and *in situ* measurements indicated that currents do occur under the present oceanographic conditions that are capable of maintaining many of the observed bedforms. Moored current meter data suggested the frequency at which this occurs on an annual basis to be minimal as bedform-based current estimates were towards the maximum of the measured current ranges. However, *in situ* observations suggested a higher frequency for this mobilization, as even summertime observations revealed signs of recent activity such as non-silted surfaces together with fresh secondary bedforms including highly asymmetric ripples and ripple fans were clear over the bedform surfaces of the deepest field.

Current measurements that are more intense in time and space and allow for the construction of fine-scale vertically-explicit hydrodynamic models are therefore necessary to assess which mechanisms actually generate the powerful flows that form and maintain the sediment wave dynamics in the passage. This should be done by long-term current flow monitoring using moorings, ADCP current profilers and repeated multibeam surveys. The expected insight is particularly relevant for cable routing issues, which have been deployed in the area for more than one century, as well as an understanding of sediment dynamics that can inform the management of aggregate extraction activities.

7. References

Allen, J.R.L. (1968). *Current ripples*. North Holland, Amsterdam. 433 pp.

Allen, J.R.L. (1972). Instability of an upper-phase plane bed: a test of Bagnold's criterion. *Sedimentary Geology*, 8: 309-316.

Allen J.R.L. (1984). Sedimentary Structures: Their Character and Physical Basis. *Developments in Sedimentology* 30, Vol. 1, 2nd ed., Elsevier, Amsterdam. 593 pp.

Allen, P.A., & P. Homewood (1984). Evolution and mechanics of a Miocene tidal sandwave. *Sedimentology*, 31: 63-81.

Allen, J.R.L. (1985). *The Principles of Physical Sedimentology*. George Allen and Unwin, London. 272 pp.

AVISO dataset. as in October 2007. Merged geostrophic currents. http://www.aviso.oceanobs.com/html/donnees/produits/hauteurs/global/msla_uk.html.

Bates, C.R. (2005). Sub-bottom profiling for sand resource assessment, Flores island, Azores. *TEAM Internal Report*, 05-04: 21 pp.

Belderson, R.H., J.B. Wilson & N.A. Holme (1988). Direct observation of longitudinal furrows in gravel and their transition with sand ribbons of strongly tidal seas. In: de Boer, P.L., A. van Gelder & S.D. Nio (eds.). *Tide-influenced Sedimentary Environments and Facies*. Reidel, Dordrecht, pp. 79-90.

Blondel, P., & B.J. Murton (1997). *Handbook of Seafloor Sonar Imagery*. PRAXIS-Wiley & Sons. 314 pp.

Borges, P., C. Andrade & M.C. Freitas (2002). Dune, bluff and beach erosion due to exhaustive sand mining – the case of Santa Barbara Beach, São Miguel (Azores, Portugal). *Journal of Coastal Research*, Special issue, 36: 89-95.

Borges, P. (2003). Ambientes Litorais nos Grupos Central e Oriental do Arquipélago dos Açores. *Ph.D. Thesis*. Universidade dos Açores, Ponta Delgada, CD-ROM.

Bowden, K.F. (1983). *Physical Oceanography of Coastal Waters*. Ellis Horwood Ltd., Chichester. 302 pp.

Bridge, J.S. (2003). *Rivers and Floodplains: Forms, Processes, and Sedimentary Record*. Blackwell, Oxford. 491 pp.

Carvalho, F. (2003). *Elementos do clima de agitação marítima no Grupo Central dos Açores (Mar Alto)*. Instituto de Meteorologia, Lisboa. 98 pp.

Dean, R.G., & R.A. Dalrymple (1991). *Water Wave Mechanics for Engineers and Scientists*. World Scientific Press. 353pp.

Duarte, R.M.M.D. (1997). Simulação Numérica de Correntes Induzidas pelas marés: O caso Faial-Pico no Arquipélago dos Açores. *Licenciatura thesis*. Departamento de Física. Faculdade de Ciências da Universidade de Lisboa, Lisboa. 90 pp.

Flood, R.D. (1983). Classification of sedimentary furrows and a model for furrow initiation and evolution. *Bulletin of the Geological Society of America*, 94: 630-639.

Idier, D., D. Astruc & T. Garlan (2006). Spatio-temporal Variability Of Currents And Sediment Fluxes Over A Dune Field In The Dover Strait. *Eos*. Transaction of the American Geophysical Union, 87(36), Ocean Sci. Meet. Suppl., Abstract OS53P-06.

Isidro, E., M. Ramos, C. Oliveira & L. Barcelos (2006). Relatório Açores do Projecto "Aquicultura Marinha e Recifes Artificiais: novos modelos de produção integrada" (MARINOVA ref. MAC/4.2/M11 - INTERREG III-B MAC). *DOP Internal Document*, 29 pp.

Instituto Hidrográfico (2005). *Tabela de Marés 2006*. Instituto Hidrográfico, Lisboa. vi+196 pp.

Johnson, M.A., N.H. Kenyon, R.H. Belderson & A.H. Stride (1982). Sand transport. *In*: Stride, A. H. (ed.) *Offshore tidal sands. Processes and deposits*. Chapman and Hall, London. pp. 58-94.

Julien, P.Y. (1998). *Erosion and sedimentation*. Cambridge University Press, Cambridge.

Kubo, Y., W. Soh, H. Machiyama & H. Tokuyama (2004). Bedforms produced by the Kuroshio Current passing over the northern Izu Ridge. *Geo-Marine Letters*, 24: 1-7.

Lafon, V., F. Jose, F. Tempera, L. Macedo, A. Martins, R.S. Santos & R. Bates (2006). Summertime Morphodynamics of Two Beaches Presenting Different Wave Exposure – Faial Island, Azores, Portugal. *Proceedings of Coastal Dynamics 2005 - 5th International Conference on Coastal Dynamics*. ASCE, New York. CD-ROM.

Leeder, M. (1999). *Sedimentology and Sedimentary Basins. From Turbulence to Tectonics*. Blackwell Science, Oxford. Xvi + 592 pp.

LNEC (1987). Areal de Santa Bárbara (ilha de S. Miguel): análise do problema das extracções de areias e de soluções alternativas. *Nota Técnica*, 11/87-NP. 14 pp.

Madsen, O.S. (1976). Wave climate of the continental margin: elements of its mathematical description. In: D.F. Stanley and D.J.P. Swift (Eds). *Marine Sediment Transport and Environmental Management*. John Wiley, New York. pp. 65-90.

Miller, M.C., I.N. McCave & P.D. Komar (1977). Threshold of sediment motion under unidirectional currents. *Sedimentology*, 24: 507-527.

Quartau, R. (2007). The insular shelf of Faial: Morphological and sedimentary evolution. *Ph.D. thesis*. University of Aveiro, Aveiro. 301 pp.

Quartau, R., F. Curado, T. Cunha, L. Pinheiro & J.H. Monteiro (2002). Projecto Gemas – Localização e distribuição de areias em redor da ilha do Faial. *Relatório Técnico INGMARDEP*, 5/2002. Dep.to. de Geologia Marinha, IGM, Lisboa. 37 pp., 30 figs.

Quartau, R., F. Curado, S. Bouriak, J.H. Monteiro & L. Pinheiro (2003). Projecto Gemas – Localização e distribuição de areias em redor da ilha do Pico. *Relatório Técnico INGMARDEP*, 16/2003. Dep.to de Geologia Marinha, IGM, Lisboa. 49 pp., 33 figs.

Quartau, R., H. Duarte & P. Brito (2005). Projecto Gemas – Relatório da campanha de amostragem de sedimentos (FAPI-3) realizada na plataforma e na orla costeira das ilhas do Faial e do Pico. *Relatório Técnico INGMARDEP*, 2/2005. Dep.to de Geologia Marinha e Costeira, INETI, I.P., Lisboa. 17 pp., 9 figs.

Quartau, R., F. Curado, H. Duarte & C. Pinto (2006). Projecto Gemas – Localização e distribuição de areias em redor da ilha de S. Miguel. *Relatório Técnico INGMARDEP*, 3/2006. Dep.to de Geologia Marinha e Costeira, INETI, I.P., Lisboa. 40 pp., 35 figs.

Richard, J. (1934). Liste générale des stations des Campagnes scientifiques du Prince Albert de Monaco avec notes et observations. *Résultats des campagnes scientifiques accomplies sur son yacht par Albert 1er prince souverain de Monaco*, 89: 1-471.

Sheng, J., & K.R. Thompson (1996). A robust method for diagnosing regional shelf circulation from scattered density profiles. *Journal of Geophysical Research*, 101(C10): 25647-25659.

Simões, A., R. Duarte & M. Alves (1997). A pilot ocean monitoring site at Azores islands. In J.H. Stel, H.W.A. Behrens, J.C. Borst, L.J. Droppert & J.P. van der Meulen (eds.). *Operational Oceanography: The Challenge for European Co-Operation.* Proceedings of the First International Conference on EUROGOOS. pp. 444-454.

Soulsby, R.L., & B.L. Wainwright (1987). A criterion for the effect of suspended sediment on near-bottom velocity profiles. *Journal of Hydraulic Research*, 25(3): 341-355.

Southard, J.B. (1991). Experimental determination of bed-form stability. *Annual Review of Earth and Planetary Sciences*, 19: 423-455.

Tempera, F., P. Afonso, T. Morato, S. Gubbay, T. Dentinho, M. Silva, R. Prieto, F. Cardigos, M.J. Pitta & R. Serrão Santos (2001). Technical-Scientifical Management Proposal for the Faial-Pico Channel SACs (in Portuguese). Departamento de Oceanografia e Pescas da Universidade dos Açores, Horta. *Arquivos do DOP*. Série Relatórios Internos, nº 8/2001, viii + 76 pp.

Von Kármán, Th. (1934). Turbulence and Skin Friction. *Journal of the Aeronautical Sciences*, 1: 1-20.

Wooding, R.A., E.F. Bradly & J.K. Marshall (1973). Drag due to regular arrays of roughness elements of varying geometry. *Boundary Layer Meteorology*, 5: 285-308.

8. Acknowledgements

This work has been supported by various funding sources including the Royal Society, the British Council (Germany), the Higher Education Funding Council for Wales, the Regional Directorate for Science and Technology of the Azores and projects MARINOVA (INTERREG IIIb/MAC/4.2/M11), MAROV (PDCTM/P/MAR/15249/1999), GEMAS (DROTRH contract), OPALINA and CIMBA.

Fernando Tempera has been financed by a PhD grant (ref. SFRH/BD/12885/2003) from the Fundação para a Ciência e a Tecnologia.

To Igor Bashmachnikov for sharing unpublished data and significantly contributing to produce a more complete chapter regarding the oceanography of the area. Neil Mitchell is acknowledged for all his suggestions that significantly permitted to improve this manuscript.

Fernando Tempera has been financed by a PhD grant (ref. SFRH/BD/12885/2003) from the Fundação para a Ciência e a Tecnologia.

Gary Greene is thanked for sharing his extensive experience on shelf geomorphology.

The use of the terrestrial relief maps produced by the Instituto Geográfico do Exército was conceded by the Regional Secretariat for the Environment under the scope of project MARÉ (Life Natureza B4-3200/98-509).

The masters and crews of the RV *Arquipélago* and RV *Águas Vivas* are acknowledged for all their effort during the work at sea.

Frederico Cardigos and Thierry Schmitt are thanked for their collaboration throughout the surveys and in the processing of the data.

Paul Byham and Submetrix are thanked for the very useful support during operations with and processing of data from the Swathplus system.

Bernie Coakley and Russel Dodd (GSE Rentals) are thanked for their advice on and *in situ* support of the multibeam installation.

Instituto Hidrográfico is acknowledged for facilitating the installation of a temporary tide gauge in Horta's Tidal Gauge house.

Sónia Santos from Direcção Regional do Ambiente is acknowledged for the kind loaning a substitute DGPS during the 2004 survey.

Guilherme Soares (DRRF-Açores) is thanked for supplying files for DGPS post-processing.

The AVISO altimetric products were produced by SSALTO/DUACS and distributed by AVISO with support from CNES.

Chapter 5

Rippled scour depressions and sorted bedforms on the volcanic island shelf of Faial (Azores, NE Atlantic)

Abstract

New multibeam sonar surveys reveal well-delimited coarse-sediment zones (CSZ) off eastern Faial Island (Azores, Northeast Atlantic). These CSZ conform to seabed features named “rippled scour depressions” and “sorted bedforms” which were hitherto unreported in the poorly investigated context of narrow volcanic island shelves. The CSZ were found in depths of 8 to 70 m and display cross-shore elongated shapes attaining lengths of approximately 1,100 m and widths of 280 m. Their flooring is composed of coarse sediments containing some scattered boulders that contrast with the finer sediments that prevail in the area. The gravel fraction is shaped into wave orbital mega-ripples that changed orientation in the course of a 9-month period.

High resolution bathymetry, backscatter images and *in situ* video grabs are presented, together with sub-bottom profile data and sediment grainsize information about the area.

Three CSZ morphologic types are identified from the general shape, relief, size and orientation to the shoreline: “broad depressions”, “small depressions” and “sorted bedforms”, all of which are described. “Broad depressions” plan view morphology and relief suggest sedimentary gravity flow scars along which cross-shore patches of the surficial stratum of fine sands were removed. The possibility of such on-shelf mass movements being triggered by cross-shore nearbed flows, seismic activity or submarine groundwater discharges is suggested. However, in view of the long-shore hydrodynamic mechanism recent literature implied in for the formation of the true “sorted bedforms”, the possibility of “broad depressions” forming from gradual enlargement and merging of “small depressions” is also discussed.

Typical sorted bedforms are reported for the shoaling convex area less than 30-m deep immediately off the rocky Pedro Miguel headland. These features are probably produced by enhanced bottom stresses likely associated with long-shore currents steered and intensified by the lateral restriction created by the coastal protrusion and the elevated topography off the promontory.

Sub-bottom profiles are used to explore the linkage of the coarse material found within the broad scars to the underlying stratigraphy. Possible sources for the coarse material include plinian-subplinian flows produced by the Caldera Formation in the last ~5500 kyr, among other discussed possibilities.

Historical surficial sediment information suggests that CSZ may have existed or recurred in the area for at least six decades, representing a new maximum for the persistence of these features.

Keywords: rippled scour depressions; sorted bedforms; volcanic island shelf; Azores

TABLE OF CONTENTS

1. Introduction

As a result of the dissemination of swath sonar systems, the seabed of world shelves is being disclosed at ever increasing resolutions. A class of features identified off many coasts in depths between 2 and 80 meters consists of elongate bands exhibiting low relief and containing sediment with high acoustic backscatter that contrasts with the surrounding finer sediments (Cacchione et al., 1984; Murray & Thieler, 2004; Ferrini & Flood, 2005; Garnaud et al., 2005). In this work we will generically refer to them as "coarse sediment zones", or CSZ (Goff et al., 2005). However, terms such as "rippled scour depressions" (Cacchione et al., 1984) and "sorted bedforms" (Murray et al., 2003) have also been used to describe subsets of these features. The genetical and morphological implications of each designation are quite distinct as reviewed below.

Typical CSZ display long-shore scales of tens to hundreds meters and across-shore scales of 100 to 5,000 m (Goff et al., 2005; Traykovski, 2005). Their axes generally trend at high angles to the shoreline, although similar structures that were unusually shore-parallel have been reported by Hunter et al. (1988). They are typically found in sediment-starved or low sedimentation settings where the deposition of new fine sediments or reworking of existing ones is insufficient to dilute or bury coarse material (Murray & Thieler, 2004).

CSZ are typically floored with coarse sand, gravel and/or shell hash and incise by up to ~1 meter into the adjacent fine sediment blankets (Garnaud et al., 2005). Their floor is commonly arranged in long straight-crested ripples with wavelengths of up to 1.7 m and heights of up to 40 cm (Cacchione et al., 1984). The interaction of the uncovered coarse sediments with strong near-bed oscillatory currents produced by surface waves and swells is considered responsible for this bedform pattern which is often oriented perpendicularly to the depression axis.

1.1. Forcing hydrodynamic mechanisms

Despite the renewed worldwide attention given to these features over the last few years, the scarcity of data on the fine-scale physical oceanographic conditions at CSZ sites has so far precluded a general consensus on the mechanisms that form and maintain these seabed features.

Early work implied strong scouring rip currents generated by large storm waves in the formation of CSZ (Reimnitz et al., 1976; Morang & McMaster, 1980; Needell et al., 1982; Aubrey et al., 1984). Cacchione et al. (1984) have further suggested that CSZ are flow-parallel features generated by strong near-bed cross-shore currents associated with storm-induced downwelling.

More recently, in contrast with the wave driving, Gutierrez et al. (2002, 2005) implied wind as the dominant influence on near-bed flows in some areas and correlated the direction of bedload fluxes with the main axis of the sorted bedforms.

These earlier conjectures generally converge in the concept that CSZ are *passive* features shaped by the spatial pattern of hydrodynamic forcing scouring localized windows through thin blankets of fine sand (Cacchione et al., 1984). Large-scale physiographic features such as protruding headlands or underwater ledges were suggested to assist in the seaward steering of these scouring flows.

1.2. Self-organization model

A model emerging from more recent studies of CSZ fine scale morphology and morphodynamics has fundamentally changed the conceptual framework used to explain how the coarse patches are supposed to form. The new framework postulates that these features develop primarily from long-shore currents and form on the up-drift sides of shore-normal highly asymmetric bathymetric undulations (hence the "sorted bedforms" designation used in Schwab et al., 2000; Murray et al., 2003; Murray & Thieler, 2004).

Contrasting with the earlier models, the results from these works provide no evidence of cross-shore sediment transport and authors further suggest that the coarse patches are not necessarily related to the broader physiography or the existence of buried strata of coarser material. According to them, the spatial segregation of different grain sizes results from a hydrodynamic process that *actively* winnows the fine fraction of poorly sorted sediments having a substantial coarse fraction and leaves localized lag concentrations (Thieler et al., 1998, 2001). Murray & Thieler (2004) suggest that after the early coarse concentrations are formed, CSZ grow and are maintained by a positive feedback process that promotes *self-organization*. They explain that the greater surface roughness inside the coarse patches effectively interacts with the wave-induced orbital motions and creates enhanced turbulence both at the grain and bedform scales (namely in the form of large oscillatory ripples) thereby promoting the winnowing process and inhibiting the deposition of fine sediments. This theory has been substantiated by modelling studies such as Sleath (1987), Fredsøe et al. (1993) and Laursen et al. (1994). Large-scale long-shore mean currents eventually carry the advected fines downstream of the coarse patches over to the less turbulent fine sediment domains. These differences in sediment transport over zones of coarser and finer bed material reinforce the spatial segregation of grain sizes (Murray et al., 2000, 2003, Murray & Thieler, 2004). The coarse lag regions end up protecting the underlying material from entrainment and asymmetric large-scale "sorted bedforms" develop that feature narrow coarsely-floored updrift-facing flanks armouring long gently-sloping fine sediment faces. Modelling studies by Murray & Thieler (2004) have indicated that this arrangement can develop spontaneously under virtually all combinations of wave, current and sediment characteristics tested.

1.3. Main objectives

This paper presents new observations of CSZ in a narrow shelf environment on mid-ocean volcanic islands - a poorly investigated setting where this type of seabed features had not hitherto been identified. The analyses focus on CSZ identified off the eastern coast of Faial Island (Azores, NE Atlantic) for which high resolution bathymetric and backscatter maps are presented. Imagery collected by an ROV and a drop-down camera illustrate *in situ* aspects of the features. Existing sub-bottom profiles are used to aid in the interpretations and provide novel elements for the discussion on stratigraphical conditions that may promote their formation.

2. Study area

The Azores is an archipelago of nine islands situated in the Northeast Atlantic. The islands spread across an extent of 617 km and are aligned along major tectonic lineaments generally trending WNW-ESE (Figure 1). Faial is located in the central group of islands and is separated from neighbouring Pico by a 5 km-wide shelf.

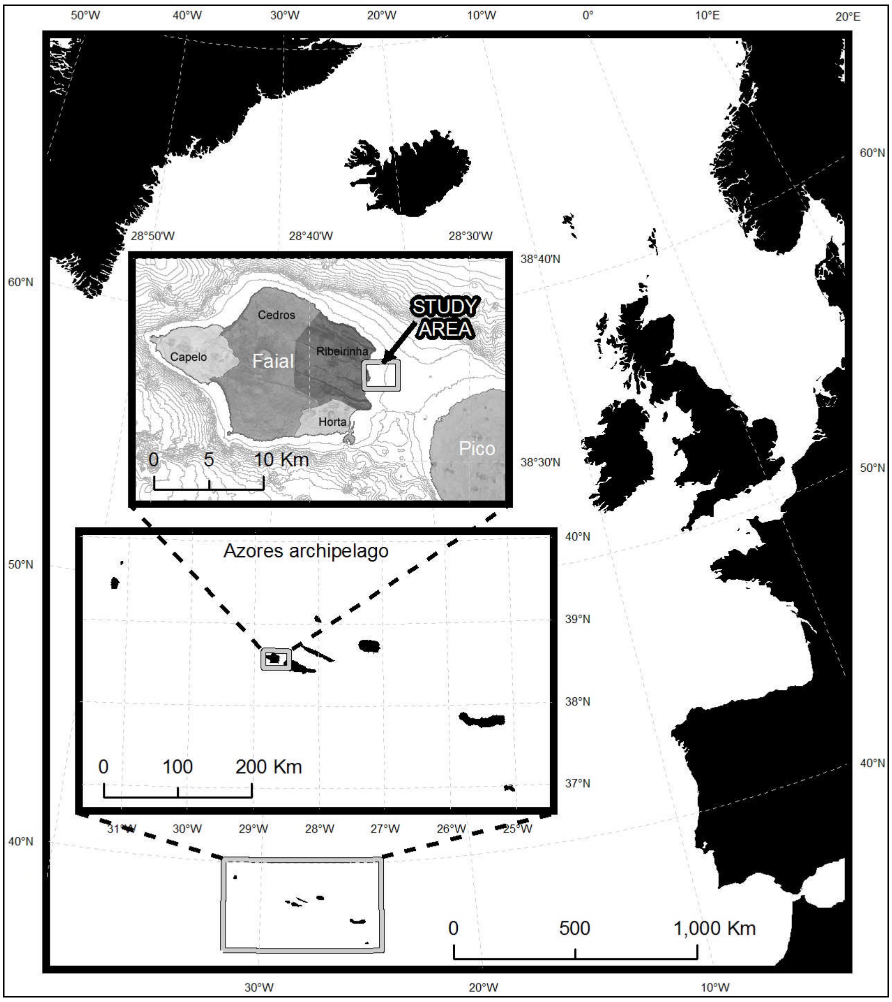

Figure 1: Location of the Pedro Miguel study area off eastern Faial Island (Azores, NE Atlantic).

2.1. Geologic setting

The scars reported in this paper are found off the Pedro Miguel headland on the eastern shore of the oldest and northeastern-most edifice of the island – the Ribeirinha complex (Figure 1). This unit is a composite volcano estimated to have emerged at about 800 kyr BP (Féraud et al, 1980). According to Pacheco (2001) the bulk of its subaerial construction extended to about 580 kyr BP and formed an emerged edifice with a diameter of ~8 km. Presently only residual traits of a caldera persist due to heavy erosion and tectonic processes associated with the Pedro Miguel graben. The faults associated with this distensile structure dominate the present subaerial morphology of the Ribeirinha complex and likely underlie the sediment wedge present off the Pedro Miguel headland.

Extensive areas of this complex are capped by trachyitic deposits of the uppermost sub-unit of the Cedros complex, the islands central volcano to the west. This sub-unit, named the Caldeira Formation consists of a sequence of deposits of plinian-subplinian eruptions produced over the last 16 kyr. A fine stratigraphy and distribution maps of the pumice airfall, surge, lahar and pyroclastic flow onshore deposits produced in this period can be found in Pacheco (2001). The most important pyroclastic flows and surges of this eruptive sequence happened at approximately 1 kyr BP and are associated with the opening of Faial's central caldera (Madeira, 1998).

The area where the CSZ have been found is probably a sediment-covered abrasion shelf carved on the flanks of the Ribeirinha complex and, given the age of the latter, must have undergone various exposures during Middle and Upper Pleistocene glacial periods.

Submerged sediment deposits in the area are considered of significant economic importance and in need of management. In this context, single-beam and sub-bottom profiling surveys have been recently conducted on the shelves surrounding Faial that resulted in maps of sediment distribution and assessment of sediment volumes down to 80 m depth (Quartau et al., 2002).

No stratigraphic sequence exists for these on-shelf sediments based on underwater coring. However, the existing sub-bottom profiles showed only highstand deposits suggesting sequences from previous sea-level oscillations were not preserved (Quartau, 2007).

Nearshore extraction pits have been imaged in Lafon et al. (2006) near the study area and further to the north, where a significant part of the extraction activity is conducted down to depths of 15 m.

2.2. Oceanographic setting

Faial Island experiences a microtidal environment (*sensu* Davies, 1964) with maximum spring tides ranging 1.5 m (Instituto Hidrográfico, 2005). Tides are semidiurnal and provide the chief hydrodynamic driver of the currents observed within the Faial-Pico passage, where flows are accelerated due to vertical and horizontal funnelling. Flood currents in the area are typically NNE-bound and ebb currents are SSW-bound. A tidal-induced shallow-water current model produced by Duarte (1997) for the passage between the two islands suggested maximum vertically-averaged tidal currents of 0.6 m/s. This has been substantiated by Simões et al. (1997) with observations collected with an Acoustic Doppler Current Profiler throughout one tide cycle which indicated that the currents decreased towards the shallow margins of the islands and the regime was therefore not fully barotropic. The effect of these currents on long- and cross-shore sedimentary transport is undocumented but the geometry of sand waves to the SE of the CSZ indicates a long-shore sediment drift towards NNE.

The prevailing swells approach Faial from the NW and W (rel. freq. $_{NW+W}$ = 53%) while the largest average significant wave heights (~3 m) are from W and SW (Figure 2). Despite Pedro Miguel being on the leeside from these swells and significantly fetch-shadowed by the neighbouring islands of Pico (7 km to the SE) and São Jorge (32 km to the NE), the shape and small size of the island permit waves of considerable size to propagate to the area by refraction when large swells occur during storms. Wave energy along this coast could therefore be classified as moderate to high.

The importance of swell-induced and wind-driven currents is unknown. However, the discrepancy between the prevailing directions of swells and winds suggests they do not often concur in their action (Figure 2).

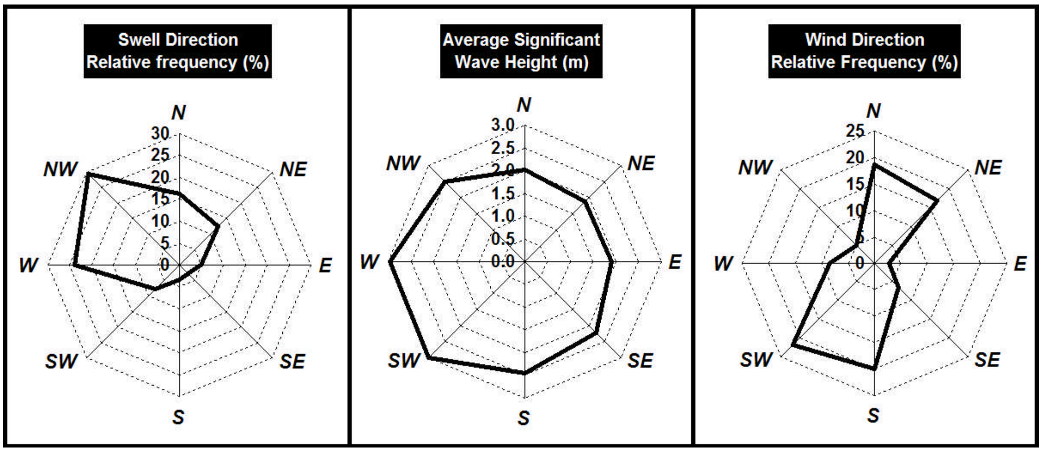

Figure 2: Swell and wind statistics for Faial Island (adapted from Carvalho, 2003) and wind data from the local Meteorologic Observatory (data credits: Instituto de Meteorologia).

3. Methodology

High resolution bathymetry and backscatter data were collected in swath surveys executed in the autumn 2003 (beam-forming sonar) and summer 2004 (phase-measuring sonar). The beam-forming system (Reson 8160; 50 kHz) was mounted on the RV *Arquipélago* and used to cover areas typically deeper than 25 m. The phase-measuring system (Submetrix 2000; 117 kHz) was installed on the RV *Águas Vivas* and used to cover the nearshore areas. The temporal distribution of the different surveys and sample collections described below is shown in Table 1.

Table 1: Timing of the different surveys and sample collections.

Month / Year	Jun	Jul	Aug	Sep	Oct	Nov	Dec
2001		SEI					
2003					BFSW		DBC
2004	PMSW	ROV, PMSW					
2005				DDC			

DBC – Duncan box coring for grainsize; DDC – groundtruthing with drop-down camera; BFSW – beam-forming swath sonar survey; PMSW – phase-measuring swath sonar survey; ROV – groundtruthing with Remotely Operated Vehicle; SEI – Seismic sub-bottom survey with boomer and chirp.

Limited parts of the shelf were surveyed with both systems and thus provided some data to verify short-term morphological changes. This assessment was limited to major changes because in parts of the phase-measuring swath sonar survey only regular GPS navigational accuracy was obtained, which after Selective Availability discontinuation displays and horizontal accuracy of ~8 m ($RMS_{95\%}$) according to DoD (2001).

3.1. Backscatter

CARIS HIPS & SIPS v. 6.0 (® CARIS) was used to process the beam-forming swath sonar backscatter, including both geometrical correction (bottom tracking, removal of altitude and slant range correction) and elementary radiometric compensation (beam angle). The backscatter from the phase-measuring swath sonar was processed in Sonarweb Pro® v. 3.16 (Chesapeake Technology, Inc.) where geometrical corrections and time varied gain (TVG) radiometric compensation were applied. No calibration between the backscatter intensities measured by the two sonar systems was performed. Final mosaics were produced at a resolution of 1 m^2.

3.2. Seismic data

Sub-bottom information was derived from a seismic survey where a number of predominantly shore-normal traverses were made around the island using an EG&G 230-1 Uniboom boomer (0.7-8 kHz) and a Datasonics CAP-6000W chirp sonar system (1.5-10 kHz sweep) (Quartau et al., 2002).

3.3. Grainsize information

Composition of surficial sediments was derived from grainsize analysis of samples collected in the area by means of Duncan box-corer (Quartau et al., 2005). The sampling site locations were determined using standard GPS. Data digitized from a 1942 nautical chart (ref: C184 – Instituto Hidrográfico) were used to complement this information. Additional *in situ* observations that illustrated sediment grainsize and seafloor aspect were provided by a VideoRay Explorer remotely operated vehicle (summer 2004) and a Tritech MD4000 drop-down camera (summer 2005).

4. Results

Coverage from the beam-forming and phase-measuring sonar surveys provided new high-resolution information on the seabed morphology and backscatter of the study area. CSZ of various morphologies were found to dominate an area of 2,000m×1,600m to the east and northeast of the Pedro Miguel headland. Figure 3 shows the oblique to shore-normal arrangement of these elongate features illustrating their expression as areas of low relief and high acoustic reflectivity.

The features were categorized according to their general shape, size, edge distinctiveness, relief and orientation to the shoreline. A classification of the coarse sediment zones in different physiographic types and the respective cross-sectional profiles are shown in Figure 4. The three morphological types are individually described and analysed below.

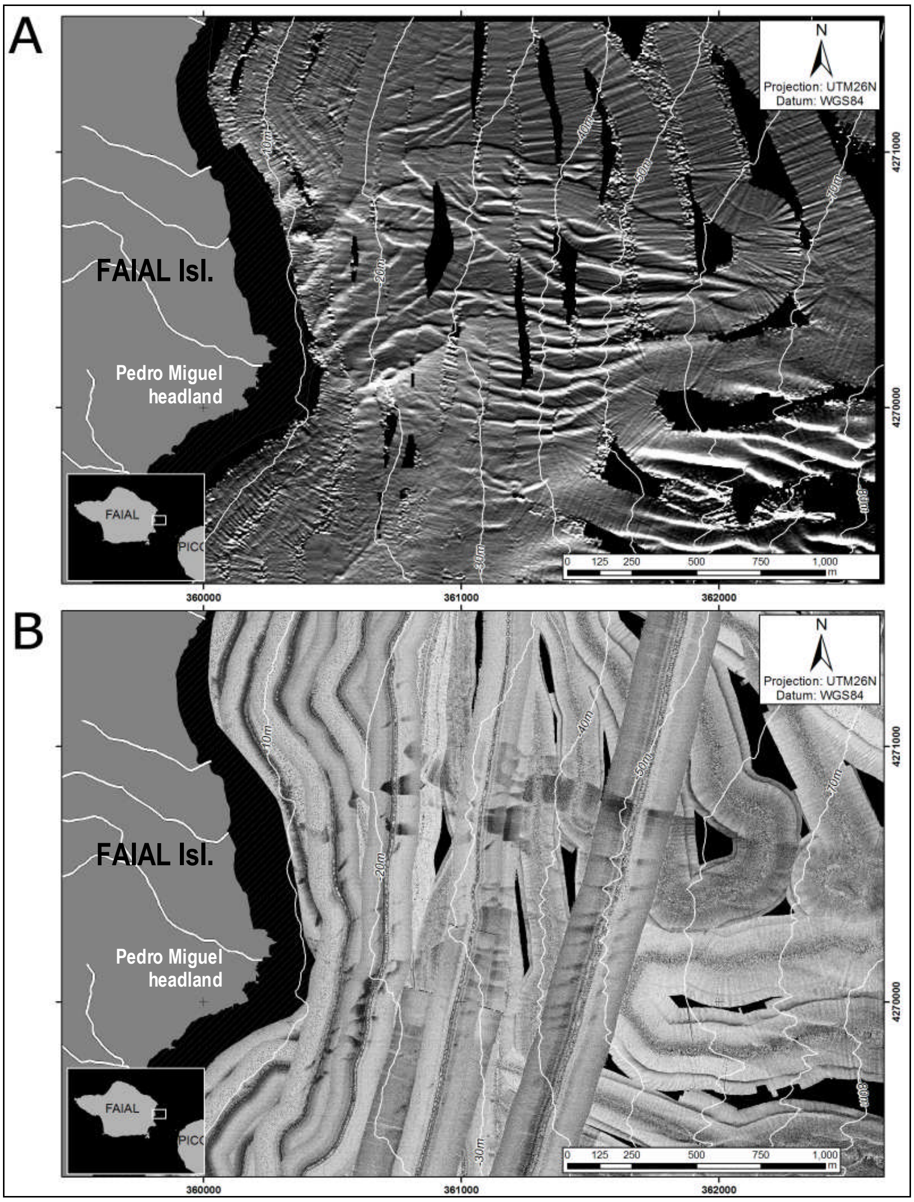

Figure 3: Shore-normal scars off Pedro Miguel headland. Black represents data gaps. A. Plan view with shaded relief and bathymetric contours. Some across-track artifacts generated by insufficient pitch or heave correction are particularly evident on the upper left of the figure and should be ignored. B. Acoustic backscatter mosaic highlighting the coarse sediment zones (dark tones trending normal and oblique to the shoreline) contrasting with the featureless adjacent bottom. The conspicuously strong backscatter visible along the centre of many surveys tracks should be discarded as an artefact.

A B

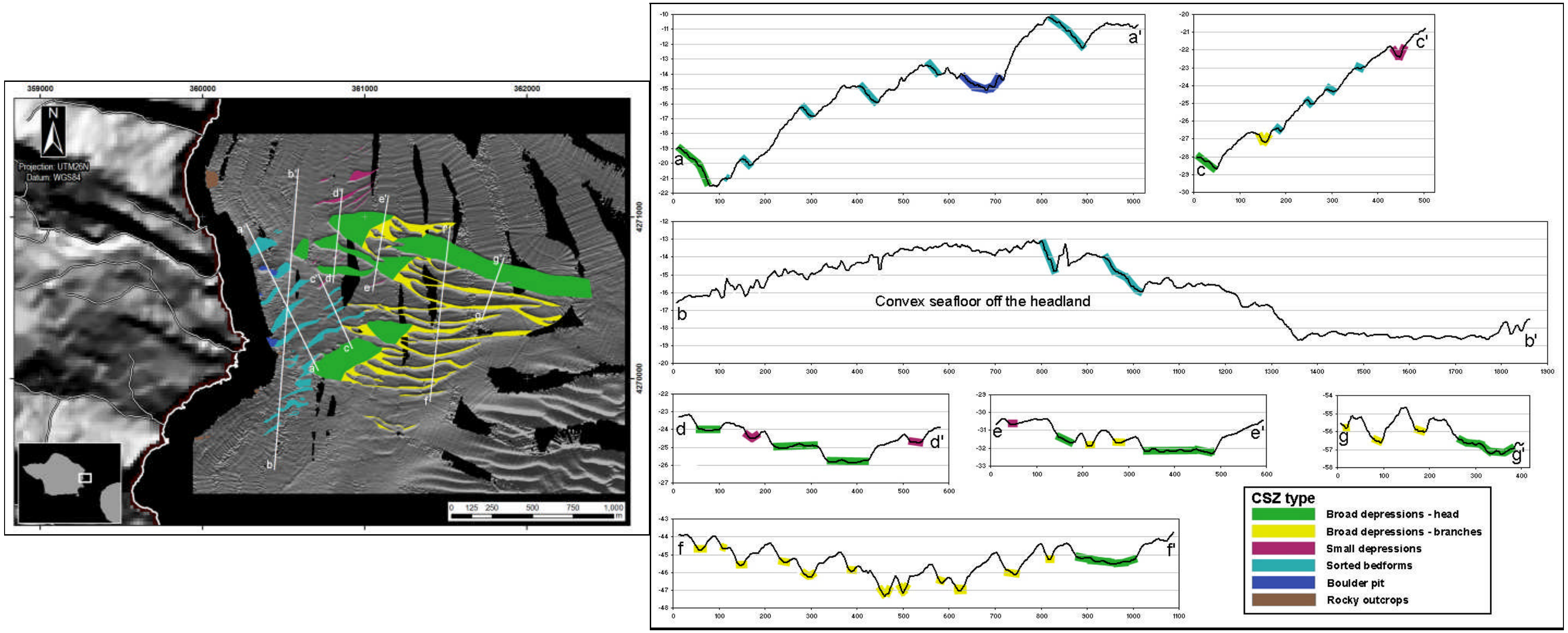

Figure 4: Classification of the coarse sediment zones in different physiographic types and bathymetric cross sections. Distance (*xx* axis) and depth (*yy* axis) are in metres. Black on map represents data gaps. Features of note include: the low wave-like bedforms trending normally to the shoreline on which the coarse areas are superimposed (a-a' and c-c'); the convex profile off the headland upon which the sorted bedforms develop (b-b'); the flat floor of the broad depressions (d-d' and e-e') which becomes slightly concave in the deeper areas (f-f' and g-g'); the vertical offset between the two neighbouring depressions (d-d'); the depressions in which the coarse material concentrates in the branching channels downslope of the broad depressions heads and their separation by a wave-like arrangement of the surficial sand veneer (f-f' and g-g'). Substrate undulations on the lower right corner are sediment waves.

4.1. Broad depressions

These features consist of sharply-edged depressed areas roughly perpendicular to the bathymetric contours. They are characterized by heads located at depths of 19 to 36 m (green areas in Figure 4) which broaden downslope and eventually divide into multiple narrower distributary-like branches (yellow areas in Figure 4). The depressed heads do not show any clear rhythmic long-shore distribution or lineament but they seem to cluster in a sub-area of 700 m × 400 m. The depressions develop from the heads and cut down along a gentle slope dipping between 3º and 1º to the east. The largest one is ~1,100 m long and the widest spans across ~280 m with forking branches at their lower end that are typically 10 to 30 m wide and separated by patches of finer sediment. On their seaward end, these branches merge with the downdrift tapering end of a sediment wave field in an area where the shelf gradient decreases and net deposition is probably occurring.

The depressed areas incise as much as 1 m into the surrounding finer sand blanket. Cross-sections (d-d', e-e', f-f' in Figure 4) suggest these depressions are not associated with any bathymetric undulations such as those typically associated with the sorted bedforms discussed in 4.2. Instead, broad depressions are flat floored and bound by steep sidewalls on both edges (maximum inclination ~8.5º in a 5-m resolution grid). The backscatter intensity and inclination of the sidewalls is slightly higher on the southern side of the depressions (Figure 6-D).

As the feature heads widen, some broad depressions are observed to merge into adjacent ones. In a few instances (profile d-d' in Figure 4-B), one of the depressions is noticeably deeper than the other by about 1 m.

Visual ground-truthing imagery collected at the head of one of these depressions at 23 m depth during the ROV#27 deployment showed that the strong backscatter acoustic signature was produced by coarse-grained gravel and some outcropping boulders that clearly contrasted with surrounding finer sediment blanket (Figure 5). The video imagery also revealed that the coarse sediment within the scars is arranged into well-developed, long-crested symmetric megaripples ~25 cm tall with a wavelength of ~1.5 m. This is comparable to the measurements obtained from a fine-scale analysis of the multibeam data over the depression heads, which shows megaripples with wavelengths between ~2.2 m (in a scar head at 22.5 m deep) and ~2.5 m (in a scar head at 25.2 m deep) with a height of ~20 cm. Video footage further showed that the finer sediments surrounding the depression's head ramped and graded into the coarse mega-ripples over distances of a few metres only, with fine sediments exhibiting small ripples with wavelengths in the order of 20-30 cm (Figure 5).

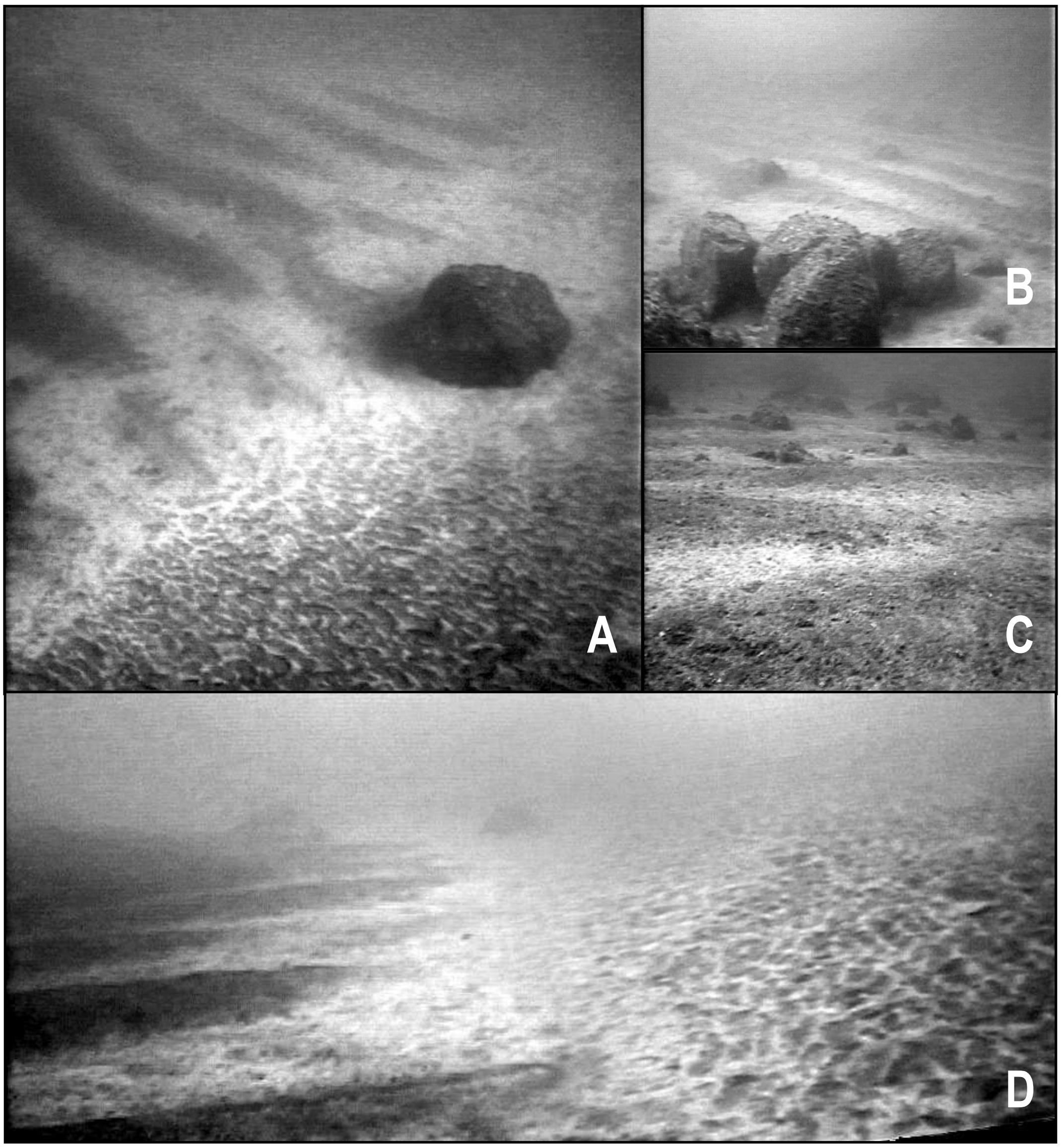

Figure 5: Frame grabs from ROV video footage collected on a broad depression head during the ROV deployment #27 (see location in Figure 8). A. Scar head. Note the discrepancy in ripple size and pattern between the surrounding fine sands (lower right) and the large ripples within the scar (top left); ripple crest pattern is distorted in the vicinity of the boulder. B. Boulders within the scar. C. Close-up of the gravel ripples with large cobbles and small boulders in the background. D. Ramping sidewall between the depression and the fine sediment. Note the inter-fingering of the fine sediments with the coarse sediment ripples near the edge. The white patches are collections of lighter biogenic particles segregated from the volcanic sediment matrix on the ripple troughs.

Drop-down camera traverses made in deeper areas in September 2005 (DDC 23 in Figure 8) confirmed that ripples inside CSZ extend to at least 29 m depth but are significantly less prominent (<10 cm tall) and display shorter wavelengths (~1 m). No cobble or boulder-sized material was detected. Biogenic mounds and fish foraging pits were frequent both within and outside the scars. Some algae (*Chaetomorpha* cf. *linum* and *Sporochnus pedunculatus*) colonized the coarser grains exposed on the ripple crests. The surrounding medium sands did not bear any recognizable rippling. One traverse at ~56 m depth (DDC 24 in Figure 8) showed no ripples either within or outside the depressions. Close-ups of the seafloor within the depressions at this depth suggested pumice granule to pebble gravel with well-rounded grains (Figure 9).

Parts of the scars surveyed with an interval of 10 months showed that harsh winter conditions did not significantly change the limits of existing depressions, recoat them or formed new ones. However, a significant change was observed in ripple orientation within the upper part of the depressions. Whilst beam-forming swath sonar backscatter obtained in October 2003 indicated ripple crests subparallel to the southern sidewall, i.e., trending approximately NW-SE (132º) (Figure 6-C & D), the ROV deployments in July 2004 showed mega-ripples trending approximately transverse to the sidewalls, i.e., aligned N-S (Figure 5).

4.2. Sorted bedforms

These are elongate bands of coarse sediment generally featuring less sharp edges both in the bathymetric and backscatter record. They are confined to depths shallower than 30 meters and trend obliquely (80º-60º) to the general angle of Pedro Miguel headland northern shore (turquoise areas in Figure 4). A narrowing of this angle is noticeable from the protruding part of the headland towards the coastal recess to the north of the headland.

Unlike "broad depressions", these CSZ bear no connection to heads and show a degree of rhythmic long-shore distribution. Locating them on the local bathymetry reveals they roughly overlie crescent-shaped sloping faces of large-scale seafloor undulations. These bedforms are subtle and highly asymmetric with wavelengths between 50 and 130 m and maximum amplitudes of approximately 1.5 m. Sorted bedforms in the shallowest areas tend to be wider and more widely spaced than those in deeper areas and to the SE of the headland.

4.3. Small depressions

These features (red areas in Figure 4) are narrow features with a relief identical to broad depressions (namely a flat floor and low relief edges). They locally merge into the broad depressions but display no identifiable head or downslope branching. They trend ENE-WSW (45º-70º), i.e., oblique to axis of the broad depressions, but within the trend range of their heads' northern edges. The largest one is approximately 460 m-long. Neighbouring small depressions seem to be arranged quasi-regularly with separations of 30-50 m but overall they appear irregularly scattered.

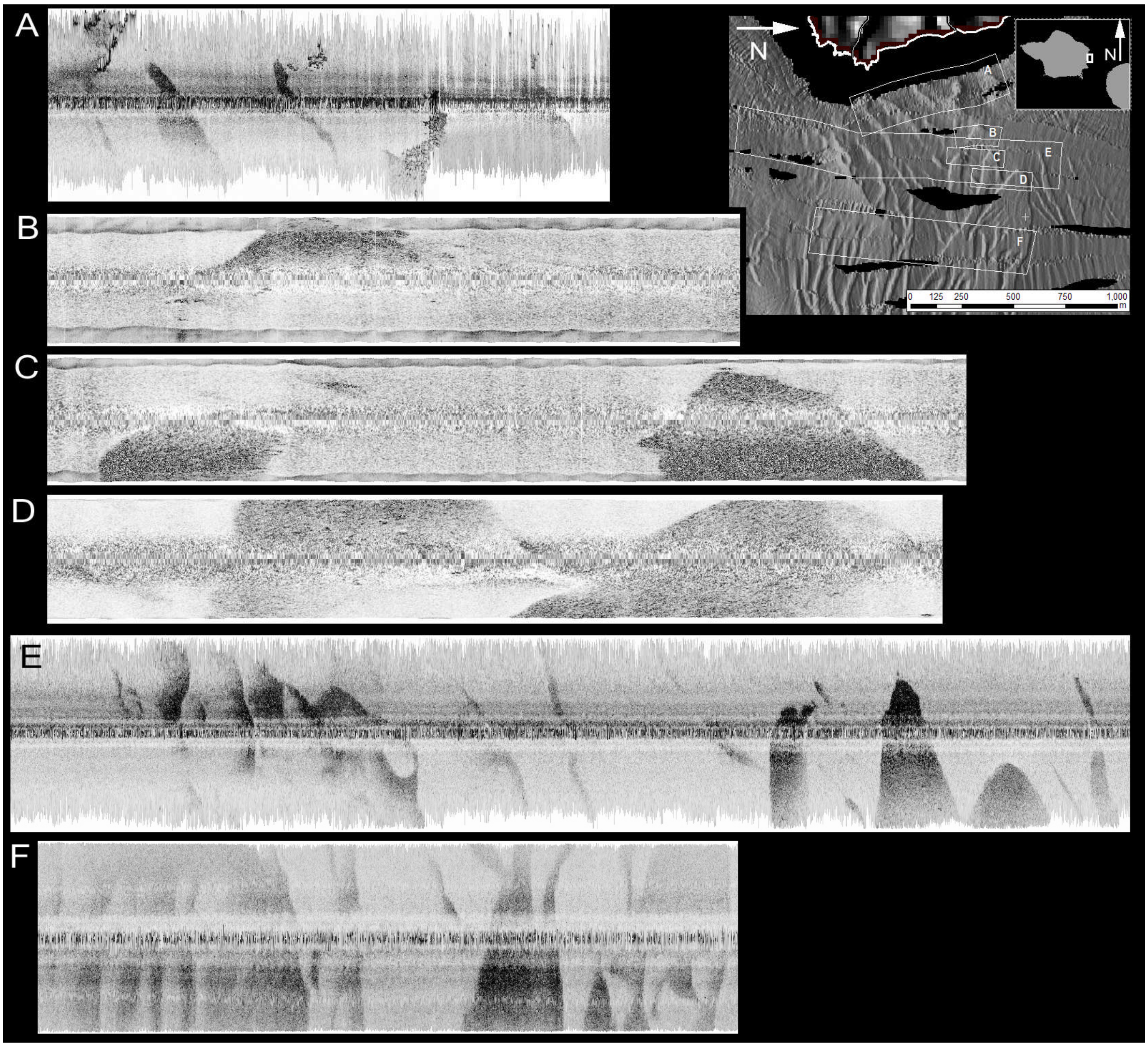

Figure 6: Detailed acoustic backscatter records of CSZ. Upper right inset shows geographical location of strips and scale. A, E & F backscatter is from a 117-kHz phase-measuring sonar. B, C & D backscatter is from a 50-kHz beam-forming swath sonar. To preserve maximum backscatter detail, strips are not drawn to common scale or geometrically corrected. A – Blocks, boulders and CSZ in the nearshore. Note that a cluster of boulder associates with a pit-like depression and extends seaward as a coarse sediment domain; B, C – Landward heads of some broad depressions. Note the sharp boundary between the backscatter of the coarse sediments in the depressions and the surrounding fine sands. The top (landward) edge of the right-hand scar head was visited in ROV deployment #27 (see Figure 5); D - Note the boulder-sized material scattered throughout the scars (dark targets with acoustic shadows) and the faint striated pattern created by the long-crested ripples. The latter are sub-parallel to the left-hand (southern) edge in the right-hand scar and oblique in the left-hand scar. Note the asymmetry between the sharp backscatter transition on the left-hand edge compared with the gradation into brighter shades of gray (and therefore finer grainsize) observed towards the right-hand edge; E, F - Varied morphology of the CSZ.

4.4. Sub-bottom profiles

Sub-bottom seismic sections are presented in Figure 7. Acoustic penetration was generally limited to 2-3 meters off the Pedro Miguel headland but still allowed sub-surficial horizons to be interpretable. The sections show a strong seismic reflector buried 1-2 m underneath the blanket of fine sands that dominates the area (Figure 7-B). This sub-bottom feature shows lateral continuity with the coarse material exposed in CSZ. Exploration of seismic sections acquired to the North of the Pedro Miguel area and penetrating slightly deeper (approximately 5 m) revealed multiple thin reflectors (Figure 7-C) which may indicate the processes producing coarser sub-surficial horizons may have re-occurred in time.

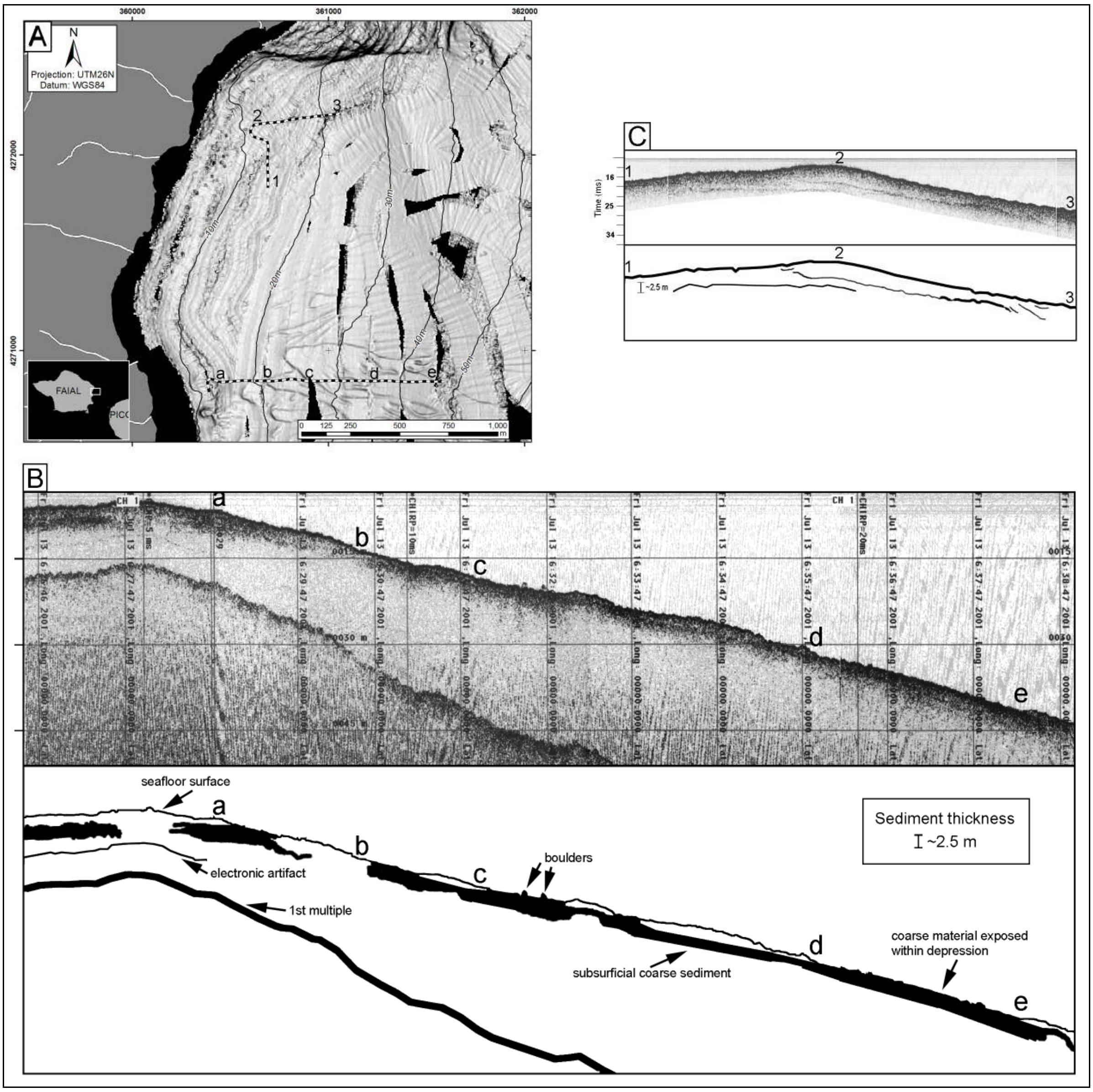

Figure 7: Sub-bottom profiles highlighting the sub-surficial structure of sediments in the area. A. Location of the profiles. B. Sub-bottom profile off Pedro Miguel revealing the shallow sub-surficial reflector exposed within the depressions. C. Sub-bottom profile off Ribeirinha showing multiple sub-surficial reflectors alternating with sediments of higher acoustic transparency. These reflectors are buried more deeply than the outcropping reflector detected off Pedro Miguel.

4.5. Grainsize

The location of surface sediment samples and respective texture is shown in Figure 8, which collates both historical and recent information.

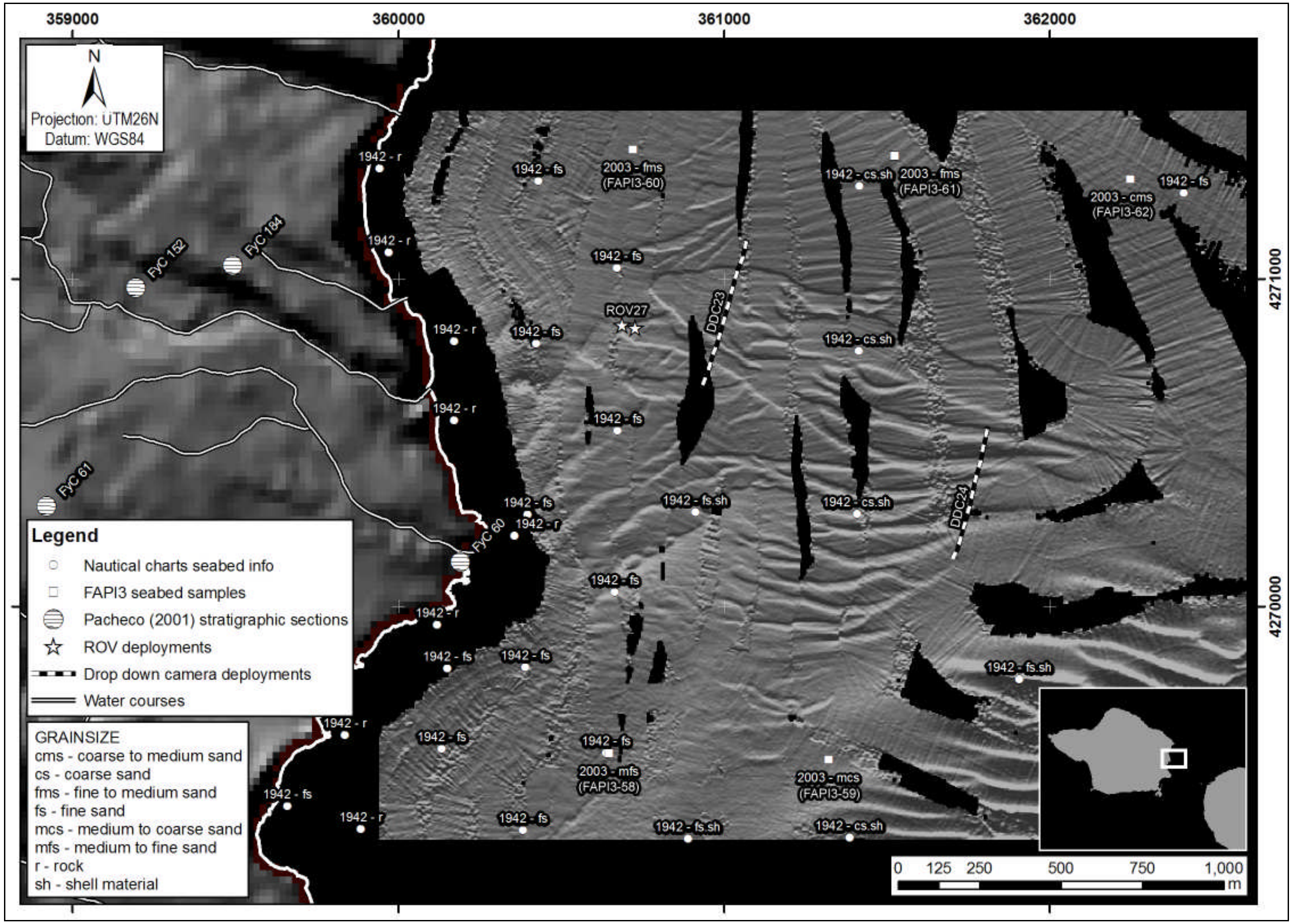

Figure 8: Location of surface sediment samples and respective texture. Samples are labelled with year of sampling and grainsize class (Wentworth for 2003 samples; unknown for 1942 samples). Sampling was conducted with armed leadline in 1942 (circles) and a Duncan box corer in 2003 (squares). Detailed grainsizes of 2003 samples are shown in Table 2. Data from Pacheco (2001) on-shore stratigraphic sections are shown on Table 3.

It is worth noting that samples characterized as coarse sand with shell material (cs.sh) in the 1942 dataset coincide with the present CSZ and that their grainsize is coarser than that of neighbouring grounds, which are dominated by fine sands. Together with the sediment interpretation derived from the imagery data (Figure 9), this information correlates well with the backscatter levels, which are lower over the finer sediments found outside the CSZ and strong over the coarser sediments found within the CSZ.

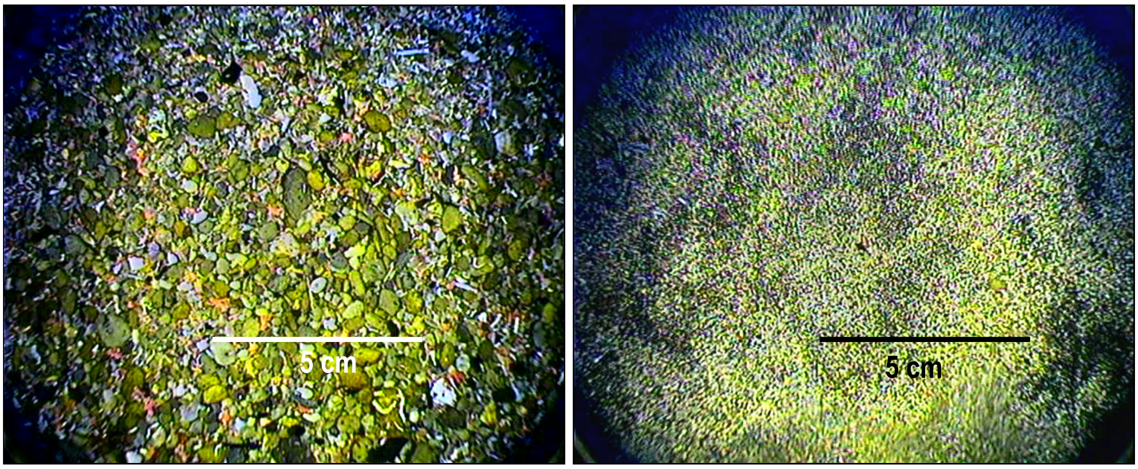

Figure 9: Drop-down camera close-up images showing grainsize of sediment patches along DDC24 track (Figure 8). A - Coarse gravel within the scars (rounded pumice? granule to pebble gravel). B - Finer sands outside the scars.

Grainsize information of sediment samples collected in the area during the FAPI3 mission are shown in Table 2, including classification and average weight percentages. This information indicates sediments outside the CSZ are dominated by slightly gravelly sands (Folk classification) poorly to moderately well sorted. Since the sampling was done in ignorance of CSZ, no core referred to a CSZ.

Table 2: Grain size (in weight percentage) of sediment samples collected in the study area with a Duncan box corer (2003 FAPI3 mission). The category of each sample in the Folk and Udden-Wentworth classifications is provided together with sorting. Data credit: Quartau (2007).

Station	Setting	Depth (m)	Date	Gravel Wt%	Sand					Silt wt%
					Very coarse wt%	Coarse wt%	Medium wt%	Fine wt%	Very fine wt%	
FAPI3-58	Non scar	57	1/12/2003	0	0	5	57	36	1	1
				Udden-Wentworth classification: medium to fine sand Folk classification: slightly gravelly sand Sorting: moderately well sorted						
FAPI3-59	Non scar	58	1/12/2003	0	11	23	46	19	1	0
				Udden-Wentworth classification: medium to coarse sand Folk classification: slightly gravelly sand Sorting: moderately sorted						
FAPI3-60	Non scar	43	1/12/2003	0	6	10	28	47	8	1
				Udden-Wentworth classification: fine to medium sand Folk classification: slightly gravelly sand Sorting: moderately sorted						
FAPI3-61	Non scar	45	1/12/2003	0	12	8	37	41	2	0
				Udden-Wentworth classification: fine to medium sand Folk classification: slightly gravelly sand Sorting: poorly sorted						
FAPI3-62	Non scar	58	1/12/2003	0	14	43	40	3	0	0
				Udden-Wentworth classification: coarse to medium sand Folk classification: slightly gravelly sand Sorting: moderately sorted						

5. Discussion

The identification of the role of CSZ in shaping the distribution of sediment in shoreface and nearshore environments is important to understand shelf sediment dynamics (Ferrini & Flood, 2005) and clarify how land-sea interfaces respond to storms, sea-level-rise or changes in sediment supply (Thieler et al., 2001).

The variation in orientation, underlying topography and general morphology of the CSZ identified off the Pedro Miguel headland suggests that they may represent expressions of distinct cross-shore and/or long-shore processes. Given the limited data available about the hydrodynamics impinging in this study area and its underlying stratigraphy, the discussion presented in sections 5.1 to 5.3 makes extensive use of models proposed by morphological and functional studies of CSZ in other parts of the world. Section 5.4 explores the different possibilities for the particular sub-surficial framework observed in association with the Pedro Miguel CSZ. Insight about the evolution of the features is dealt with in 5.5.

5.1. Broad depressions

Overall these features are characterized by (i) broadening with increasing distance from shore, (ii) downslope branching, (iii) low relief on both edges and (iv) lack of an underlying topographic undulation. Such morphology relates them to the features reported by Morang & McMaster (1980) and the Type II RSD's described in Ferrini & Flood (2005) and clearly makes them different from the typical "sorted bedforms".

Two interpretations which are not necessarily mutually exclusive are proposed for the formation of broad depressions, namely (i) sorting of grainsize grades by long-shore hydrodynamic forcing and (ii) sedimentary gravity flows. These hypotheses are discussed in further detail below.

5.1.1. Long-shore hydrodynamic forcing

Observational and modelling studies presented in recent literature have gathered more evidence pointing towards "rippled scour depressions" and "sorted bedforms" being associated with long-shore currents. In order to consider this genetic mechanism in the formation of the broad depressions identified, one must also assume that long-shore near-bed hydrodynamics experience important qualitative and quantitative alterations as the substrate deepens. These variations could explain why this type of depression grows unusually broad and does not show any underlying topographic undulation when compared to the typical "sorted bedforms" found in shallower areas.

Given that (i) narrow bands occur within the same depth range and area of the broad depression heads, (ii) they show a trend similar to one of the head's sidewalls, and (iii) they show an identical low relief at both edges, it is further postulated that broad CSZ are initiated as "narrow small depressions" which eventually grow and coalesce to produce broader depressions that resemble cross-shore turbidity flow scars. This could happen through the mechanism suggested by Green et al. (2004), where the expansion of the coarse domains is promoted by the advection of coarse grains from the CSZ during very high turbulence periods and subsequent deposition onto surrounding finer sediment areas. Through a "seeding effect", this dispersal of coarse sediment could favour the formation of new coarse patches in the vicinity of existing CSZ and promote their gradual expansion. Gradual contact and merging of small CSZ would eventually lead to a higher scale and degree of organization (Murray et al., 2003). The fact that the turbulence-induced erosion and enlargement process should operate not only on the long-shore edges but also at the shore- and seaward edges of the features (Ferrini & Flood, 2005) could explain the downslope extension of the broad depressions. This could be facilitated by this type of feature being farther from shore, in a setting where currents may not be constrained to move predominantly along a single direction (Murray & Thieler, 2004). The time frame for this evolution is unknown but could amount to decades or centuries.

In any case, this scenario would imply that the branching pattern found in the lower part of the broad scars represented a deceptive morphology actually unrelated to a cross-shore sediment transport process removing surficial fine sands along narrow strips. It is suggested that it could be created by the arrangement of residual amounts of fine sediment either left within broad depressions or transported onto them by long-shore currents and subsequently shaped into transverse bedforms. The NNE-bound sand wave field adjoining the SE part of the broad depressions area may then constitute the source for this fine sediment.

Under this model, for a given depth, the older CSZ should carve more into the fine sediment blanket because of their longer history of fines winnowing. Therefore, when two coalescing broad depression display a vertical offset in the intersection area, the deepest one should be older than the one showing less relief (e.g., in profile d-d' in Figure 4-B).

The irregular spatial distribution and morphology of these depressions is not straightforward to explain from a simple long-shore non-uniformity of flows and associated bottom stresses fields.

The emplacement of the broad scars may therefore involve a degree of conditioning by the underlying stratigraphy. A similar explanation was put forward in Schwab et al. (2000) and Thieler et al. (2001), who refer pre-existing cross-shelf extended collections of coarse sediment from palaeo-fluvial channels as promoters of CSZ formation. The large outcropping boulders detected at the heads of the broad depressions could represent identical material which would facilitate the initiation of the sediment winnowing process and the long term anchoring of the CSZ in the area (for a similar case see Hunter et al., 1988).

A major inconsistency with "long-shore current induction" is the well-defined orientation of broad depressions perpendicular to the bathymetric contours. Any shore-normal features induced by long-shore currents should show a seaward trending deviation due to likely changes in the trend and/or power of hydrodynamic forcing across the range of depths and distance from shore they span (Murray & Thieler, 2004).

5.1.2. Sedimentary gravity flow scars

The morphology of the broad depressions is also consistent with that of cross-shore turbidity flow scars developing from a shoreward-convex head and removing patches of surficial sediment from the nearshore into the mid shelf. The full saturation of the unconsolidated sediments and the momentum induced by the material set in motion should allow the flow to run for several hundreds of meters despite the gentle slope (1-3º) of the seabed. Lowe (1976) indicated that natural laminar liquefied flows of fine-grained sand will generally re-sediment after moving a kilometre or less, which would agree with the length of the broad depressions identified off Pedro Miguel.

The presence of various heads and overlap between neighbouring depressions further suggests that the scars originate from multiple events. Where two depressions intersect and display a vertical offset, the relative age interpretation is opposed to the one drawn under the long-shore hydrodynamic forcing hypothesis. In the case of gravity flows, more recent and powerful gravity flow will have carved further into previous ones (e.g., in profile d-d' in Figure 4-B).

The concentration of coarse sediments within the scars could be explained by that fraction re-sedimenting first, as the turbulent energy associated with the slide decreased and became insufficient to keep it in suspension. Alternatively, existing sub-surficial coarse layers could play a critical role in the facilitation of the mass movements by undermining the foundation of the surface layers and providing a detachment plain that was subsequently exposed.

Substantial sediment transport occurring along the channel, which is indicated by the sediment waves present to the SE of the depressions, could be responsible for erasing turbidite deposits at the downslope end of the scars.

5.1.2.1. Gravity flow origin

Four potential triggers are suggested for the initiation of these sedimentary flows: (i) freshwater surges percolating through the sub-surficial coarse layer; (ii) seaward down-welling currents induced by large swells or onshore winds; (iii) seismically-induced liquefaction (e.g., Lowe, 1976; De Groot et al., 2006) or (iv) hyperpycnal flows (Mulder et al., 2003; Parsons et al., 2001). The first possibility implies freshwater from onshore watercourses or aquifers partially percolating through layers of higher permeability underneath the seafloor (e.g., coarse sub-surficial layer). Such events could be promoted by intense rainfall events (a characteristic of the Azorean climate) overcharging onshore groundwater pathways and reservoirs (for a review of seabed fluid flows see Judd & Hovland, 2007). When emerging through the thin overlying fine sand blanket, the lower density waters could fluidise the unconsolidated surface and trigger small turbidity flows down the shelf surface.

An alternative hypothesis of seaward down-welling currents induced by large swells is inspired by the mechanism proposed by Cacchione et al. (1984). In this case, the detachment of surficial horizons and subsequent turbidity currents would be induced by the pressure created by cross-shelf near-bed currents. The area is regularly impinged by large N/NW swells coming through the northern entrance of the passage either directly or by diffraction around the Ribeirinha headland. Less frequently, the area can also be affected by large swells from S/SW coming in through the passage's southern entrance.

Since the study area is also subject to moderate seismic activity, it is also possible that these underwater mass movements are triggered by co-seismic fault movements. The most recent strong earthquake was in 9th July 1998 (Richter magnitude = 5.8; MMI=VIII; Costa Nunes et al., 1999), with an epicentre 12 km to the NNE of the study area. The whole north-eastern sector of Faial was significantly affected, particularly along the Pedro Miguel graben faults, which trend in a direction identical to the broad depressions and respective branches. Although coated by a sediment wedge, these faults extend beneath the neighbouring seafloor (some of them recover surficial expression in the middle of the passage) and their movement may have initiated turbidity flows in the overlying sediments.

Finally, it should be mentioned that hyperpycnal flows produced by the neighbouring water courses during intense rainfall events could be responsible for the near-bed cross-shore currents promoting the slides. The most likely source for such phenomena is the neighbouring watercourse of Ribeira de Pedro Miguel, which represents the second largest watershed in Faial, totalling 1,500 ha. As shown in Figure 10, the broad depressions are approximately in line with the on-shelf steepest paths that would be followed by gravity-driven flows starting at the mouths of current water courses.

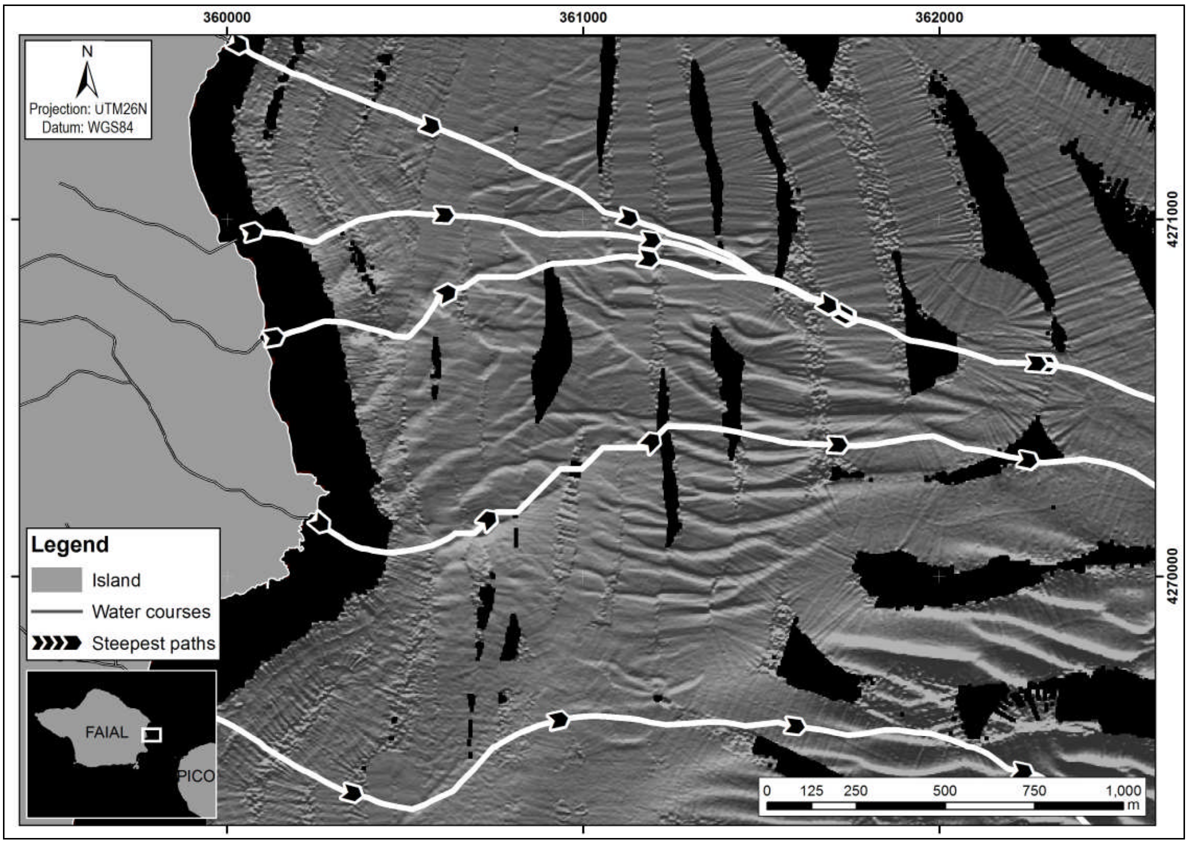

Figure 10: On-shelf steepest paths initiated at the mouths of current water courses. Note how most of them direct to the CSZ field.

5.2. Sorted bedforms

The sloping CSZ found in the nearshore of the Pedro Miguel headland are comparable to the "sorted bedforms" reported by Swift and Freedland (1978), Thieler et al. (1998, 2001), Schwab et al. (2000), Murray & Thieler (2004) or Ferrini & Flood (2005). Similarly, the coarse beds are found on narrow steep faces (interpreted as the updrift flanks) of low amplitude transverse bedforms featuring long gently sloping stoss flanks composed of finer sediment.

The concentration of this pattern in the shoaling convex area less than 30 m depth off a rocky promontory (Figure 4) indicates the mechanism is likely affected by local bathymetry (Ferrini & Flood, 2005). The lateral restriction created by the coastal protrusion and the elevated convex topography off Pedro Miguel headland is thought to steer and intensify long-shore currents and increase bottom stresses (Cacchione & Drake, 1990). The trend and sense of asymmetry of crests (with NW-facing coarse faces) suggest forcing currents moving towards SE with ebb tides steered around the headland representing their most likely and frequent driver. Alternatively, the currents could be associated with strong swells piling up large volumes of water against the headland and venting the set-up water through nearbed downwelling-induced flows (Cacchione, 2005). Swells generating currents fitting the transverse bedforms trend would probably be those impinge on the area through the northern entrance (directly or by refraction around the Ribeirinha headland).

Finally, the higher density of smaller CSZ observed farther from the headland could be a material occurrence of the steady-state narrower coarse domains expected according to the model developed by Murray & Thieler (2004) for current reversal conditions. Being farther from the buffering effect of the shoreline and shallow seabed, the area in question may be subject to a stronger influence of the periodic current reversals generated by the tides which would generate sorted bedforms with smaller wavelengths.

5.3. Wave-induced ripples

Mega-ripples imaged within the depressions by beam-forming swath backscatter and *in situ* video showed: (i) symmetry, (ii) long shore-parallel crests, (iii) height and wavelengths that reduced as depth increased.

All of these morphological traits are consistent with the explanation widespread in previous literature that ripples in CSZ stem from secondary rearrangement of the exposed coarse material by high-energy oscillatory bottom currents such as those generated by surface waves.

Since crests of wave induced ripples will be oriented perpendicular to the propagation direction of the waves that formed them, the reconfiguration observed on the ripple pattern between the beam-forming swath survey (October 2003) and ROV deployment #27 (July 2004) further shows these are active ripples that are probably mobilized and reshaped during large swells impinging from different directions. The patterns observed probably reflect the nearbed wave climate of the latest storm waning phase and were maintained in the interim by the ensuing fair weather wave climate (Reimnitz et al., 1976; Garnaud et al., 2005).

The higher mobility of finer sediments outside scars suggests they may be re-shaped more often and in much less energetic wave conditions than those within scars (Cacchione et al., 1984). The bedforms observed in the two areas may therefore show a geometry often reflecting disparate nearbed currents.

5.4. Sub-surficial coarse horizons

Due to the widespread occurrence of CSZ in very distinct geological contexts it has been suggested their formation and evolution results merely from oceanographic processes and is independent from factors such as the underlying stratigraphy or sediment supply (Murray & Thieler, 2004).

It is argued that a degree of control by the sub-bottom geology may be implied in the occurrence and concentration of the broad CSZ in the study area. This is mainly supported by the facts that: (i) the coarse sediments flooring the depressions contain coarse material up to boulder size; (ii) this material is exposed in areas distant from the shoreline; (iii) there is continuity between the exposed material and a strong shallowly buried acoustic reflector found on the margins of the scars; (iv) the coarse material apparently comprehends pumice gravel that could be directly related to the Holocene history of the area.

The origin of the coarse material within the CSZ remains unknown due to the lack of lithologic information about this horizon. A few hypotheses are explored below that comprehend both major geological events emplacing loads of coarse material and *in situ* generation of coarse material lenses by winnowing of a poorly-sorted matrix.

5.4.1. Palaeo-fluvial deposit

The cross-shelf collection of very poorly sorted coarse material is consistent with an exhumation of gravel lag associated with palaeo-fluvial channels or alluvium deposits (Schwab et al., 2000; Thieler et al., 2001). Several features may have facilitated the transport of very coarse material onto the shelf: (i) the torrential nature of onshore hydrologic activity, (ii) the fact that Ribeira de Pedro Miguel is fed by the second largest watershed in Faial island and (iii) the topographical emplacement of the adjacent streams over active normal faults. In these circumstances, the exhumed on-shelf deposit should represent an alluvium fed by rockfall from the headwall talus emplaced during the last glaciation shelf exposure. Mobilization of neighbouring sands by waves

and long-shore currents could presently be responsible for obscuring the nearshore of these deposits.
This possibility is further supported by the observation that the steepest paths from the present mouths of adjacent water courses come together in the area of the exhumed coarse horizons (Figure 10). However, it is acknowledged that determining former runoff patterns from the current bathymetry is conditioned not the least by the presence of the depressed CSZ themselves together with likely substrate rearrangements that took place throughout and after the Holocene transgression.

5.4.2. Plinian/subplinian deposits

Another likely candidate to produce shallow coarse deposits in the seabed off Pedro Miguel is the Caldera Formation. This is the most recent stratigraphic unit emplaced over the Ribeirinha complex and consists of pyroclastic flow, surge and lahar deposits from the plinian/subplinian eruptions occurring between 11 and 1 kyr BP, which eventually resulted in the creation of the current central caldera (Pacheco, 2001).
Geological subaerial sections analyzed by Pacheco (2001) in the vicinity of the scars revealed deposits of flows referenced C4, C3 and C11 which can exceed thicknesses of 100 cm (see stratigraphy in Table 3).

Table 3: Thickness of the Caldera Formation deposits present in stratigraphic sections studied in the onshore vicinity of the Pedro Miguel CSZ field (adapted from Pacheco, 2001). The location of these samples is shown in Figure 8.

Deposit / Section	C3 4790±50 yrs BP	C4 5500±60 yrs BP	C11 980±50 yrs BP
FyC 60	100 cm	128 cm	Absent
FyC 61	60 cm	70 cm	80 cm
FyC 152	Absent	Absent	170 cm
FyC 184	70 cm	34 cm	Absent

No sampling or dating has been made of the sub-surficial coarse strata so their nature is unknown. However, close-up images of the gravel in the scars do suggest rounded pumice (Figure 9) which would be consistent with this hypothesis (for similar examples see Hart et al., 2004). The coarser material (up to boulder size) could also have been emplaced by such catastrophic events which probably entailed enough energy to produce and roll down very coarse material onto pre-existing finer sediment deposits as observed in the seismic profiles.

Although only flows C4, C3 and C11 are present in the stratigraphy of this sector of the island, deposits of other Caldeira Formation plinian eruptions intersect the upstream areas of the watercourses running along the Pedro Miguel graben and discharging into the area of the scars. Therefore the presence of fluvial-transported loads from other eruptions from the Caldeira Formation in the stratigraphy of this part of the shelf should not be discarded either.

5.4.3. Transgressional lags

Transgression-generated coarse lags buried beneath Holocene sequences are a common feature in shelf sequences (e.g., Eittreim et al., 2002; Anima et al., 2001). The coarseness of the material found off Pedro Miguel is atypical of such deposits, chiefly because it contains boulder-sized material at more than 700 m from the present shoreline overlying considerably thick strata of finer material. It is unlikely that talus deposits from sea cliffs eroded throughout transgression would be found at such distances from the present shoreline.

5.4.4. Sorted bedform signature

Accepting the sorted bedforms model, CSZ would be sedimentary signatures produced by a process spatially sorting and segregating long patches of coarse sediments. As these features migrate long-shore, the trailing edges are progressively buried by the adjacent fine sediments (Thieler et al., 2001). Since the mobilization of these adjacent fines often occurs when currents are just energetic enough to suspend fine sand but not the coarser grains in the CSZ, this process goes on without grainsize mixing (Green et al., 2004; Garnaud et al., 2005). This mechanism leaves a sub-surficial coarse horizon (including ripple crests) that can be traced laterally for up to several meters. This scenario is not incompatible with the stratigraphic evidence found in the area which shows continuity of the coarse domains with the shallow reflector found underneath the adjacent fine sands and inter-fingering of the ripples with fine sand slithering at the CSZ edges. In case the migration occurs in both directions (e.g. as a result of strong oscillating tidal currents or of large storms impinging from both directions), the coarse horizon ought to extend underneath both margins (Murray & Thieler, 2004).
In this scenario, boulders inside the CSZ would simply represent the coarsest immovable fraction of the poorly sorted matrix from which fines are winnowed.

5.5. Evolution of CSZ

The relative persistence of CSZ is difficult to determine from the limited data presently available. Nonetheless, the absence of major changes (e.g., formation of new broad depressions; obliteration or migration of existing ones) in the areas where the two swath surveys coincided suggests that broad CSZ arrangement can remain stable over the course of several months and inclusively persist past energetic wintertime conditions.

The deep parts of the scars indicate an even lesser dynamics with sediment surfaces retaining widespread signs of prolonged biogenic activity (mounds and foraging pits) and permitting an unusual growth of macro-algae attached to the coarser grains.

Furthermore, a comparison with data on surficial sediments digitized from a 1942 nautical chart suggests that CSZ may have persisted or recurred in the area for more than six decades. This represents a new maximum in comparison with the nearly four decades hitherto reported by Goff et al. (2004) for CSZ at the Martha's Vineyard Coastal Observatory (MA, USA). Ferrini & Flood (2005) describe CSZ updrift edges that persisted for 5 years. Some workers indicate that some of the elongate narrow CSZ can be more ephemeral, forming and fading on time scales of less than 1 year (Ferrini & Flood, 2005) or in response to storms (Trembanis & Traykowski, 2005).

Thieler et al (2001) suggest these sediment-starved bedforms are either relatively stable or represents a recurring, preferential morphologic state to which the seafloor returns after storm-induced perturbations in an equilibrium between the sedimentary response and the long-term hydrodynamic forcing.

6. Conclusions

New multibeam sonar surveys reveal well-delimited coarse-sediment zones (CSZ) off eastern Faial Island (Azores, Northeast Atlantic). The features were located in depths between 8 and 70 m off Pedro Miguel headland in the Faial-Pico passage. This site differs from the narrow-shelf fully-open character of most Azores coasts for being placed on an inter-island shelf that is largely fetch-shadowed from prevailing swells but is nonetheless exposed to enhanced long-shore tidal currents funnelled through the Faial-Pico passage.

The variety of shapes, sizes and orientations of the features led to a division of CSZ in three categories: "broad depressions", "small depressions" and "sorted bedforms". Their characteristics match features described in previous literature as "rippled scour depressions" and "sorted bedforms”, which were hitherto unreported in the poorly investigated context of narrow volcanic island shelves.

“Broad depressions” plan view morphology features an upslope head which broadens downslope and eventually divides into multiple narrower branches. This morphology resembles a surficial mass movement scar developing and branching from a shoreward-convex head. Potential trigger mechanisms for these mass movements include: (i) submarine groundwater discharges, (ii) seismic activity and (iii) cross-shore nearbed flows. The explanation implying long-shore hydrodynamic forcing which is currently employed to explain “sorted bedforms” would be compatible with the long-shore rhythmic pattern of the branches exhibited by the lower part of the depressions. As far as “broad depressions heads” are concerned, this alternative scenario would imply they were formed from gradual enlargement and merging of “narrow depressions”, which are found in the same area.

Typical “sorted bedforms” were found in the shoaling convex area less than 30-m deep immediately off the rocky Pedro Miguel headland. These features are probably produced by enhanced bottom stresses likely associated with long-shore currents steered and intensified by the lateral restriction created by the coastal protrusion and the elevated topography found off the promontory (Cacchione & Drake, 1990; Ferrini & Flood, 2005).

Historical surficial sediment data suggests that CSZ persisted or recurred in the area at least since the early 1940’s, representing a new maximum for the persistence of these sort of features. A higher dynamics was detected in the mega-ripples found within the broad scar heads which changed orientation over a period of 10 months, indicating rearrangement by large surface swells. This was not as obvious in the deep parts of the scars where the CSZ surface presented signs of more prolonged immobility such as widespread biogenic mounds and fish foraging pits.

Beyond hydrodynamics, the formation of CSZ may also be controlled by a particular underlying stratigraphy. Sub-bottom profiles showed continuity of the coarse material with a sub-surficial reflector buried 1-2 m beneath the surrounding blanket of fine sands. The origin of the coarse material must lie on the geological history of this part of the shelf. Hypothesized sources for the coarse material (which includes material as large as boulders) include (i) plinian-subplinian flows produced by the Caldera Formation in the last ~5500 kyr, (ii) the latest sealevel transgression, (iii) palaeo-fluvial channels or (iv) sorted bedforms signature.

A programme dedicated to the monitoring of physical oceanographic conditions in the area of the CSZ is proposed to investigate the processes involved in the formation and evolution of these seabed features. The research should include measurements of the direction and intensity of nearbottom flows (specifically during storms) conducted in parallel with regular multibeam surveys (bathymetry + backscatter) that could determine the morphodynamics of the CSZ. Monitoring of nearbed salinity and temperature would further contribute to clarify whether groundwater discharge is involved in the creation of the "broad depressions".

The clarification of whether CSZ's in the study area are being controlled by catastrophic events or more gradual seabed evolution would be relevant to assess hazards to underwater cables and coastal engineering projects in the vicinity as well as plan sand extraction activities. From an ecological perspective it would be relevant for determining the spatial dynamics of biological communities depending on stable sedimentary beds.

7. References

Anima, R.J., S.L. Eittreim, B.D. Edwards & A.J. Stevenson (2001). Nearshore morphology and Late Quaternary geology framework of the northern Monterey Bay Marine Sanctuary, California. *Marine Geology*, 181: 35-54.

Aubrey D.G., D.C. Twichell & S.L. Pfirman (1984). Holocene sedimentation in the shallow nearshore zone off Nauset Inlet, Cape Cod, Massachusetts. *Marine Geology*, 47: 243-259.

Cacchione, D.A. (2005). Rippled Scour Depressions off Northern California - Processes and Patterns. *Eos*. Transaction of the American Geophysical Union, 86 (18), Jt. Assem. Suppl., abstract #OS31A-01.

Cacchione, D.A., & D.E. Drake (1990). Shelf sediment transport: an overview with applications to the northern California continental shelf. *In* B. LeMehaute & D. Hanes (eds.). *The Sea*, 9: 729-773. Wiley-Interscience, New York.

Cacchione, D.A., D.E. Drake, W.D. Grant & G.B. Tate (1984). Rippled scour depressions on the inner continental shelf off Central California. *Journal of Sedimentary Petrology*, 54 (4): 1280-1291.

Carvalho, F. (2003). *Elementos do clima de agitação marítima no Grupo Central dos Açores (Mar Alto)*. Instituto de Meteorologia, Portugal, 98 pp.

Costa Nunes, J., P.T. Costa & M.L. Senos (1999). Estudos de sismicidade no Arquipélago dos Açores-Aplicação ao sismo de 9 de Julho de 1998. In: C.A.P. Martins (ed.). *4° Encontro Nacional sobre Sismologia e Engenharia Sísmica*. Faro, Portugal, pp. 19-28.

Coutinho, R. (2000). Elementos para a monitorização sismovulcânica da ilha do Faial (Açores): Caracterização hidrogeológica e avaliação de anomalias de Rn associadas a fenómenos de desgaseificação. *Ph.D. Thesis*. Departamento de Geociências da Universidade dos Açores, Ponta Delgada. 342 pp.

Davies, J.L. (1964). A morphogenetic approach to world shorelines. *Zeitschrift für Geomorphologie*, 8: 127-142.

De Groot, M. B., M.D. Bolton, P. Foray, P. Meijers, A.C. Palmer, R. Sandven, A. Sawicki, & T.C. Teh (2006). Physics of Liquefaction Phenomena around Marine Structures. *Journal of Waterway, Port, Coastal, and Ocean Engineering*, 132(4): 227-243.

DoD (2001). *Global Positioning System Standard Positioning Service Performance Standard*. Assistant Secretary of Defense for Command, Control, Communications, and Intelligence.

Duarte, R.M.M.D. (1997). Simulação Numérica de Correntes Induzidas pelas marés: O caso Faial-Pico no Arquipélago dos Açores. *Licenciatura thesis*. Departamento de Física da Faculdade de Ciências da Universidade de Lisboa, Lisboa. 90 pp.

Eittreim, S.L., R.J. Anima & A.J. Stevenson (2002). Seafloor geology of the of Monterey Bay area continental shelf. *Marine Geology*, 181: 3-34.

Feraud, G., I. Kaneoka & C.J. Allegre (1980). K/Ar ages and stress pattern in the Azores: dynamic implications. *Earth and Planetary Science Letters*, 46: 275-286.

Ferrini, V.L., & R.D. Flood (2005). A comparison of Rippled Scour Depressions identified with multibeam sonar: evidence of localized sediment transport in inner shelf environments. *Continental Shelf Research*, 25: 1979-1995.

Fredsøe, J., B.M. Sumer, T.S. Laursen & C. Pedersen (1993). Experimental investigation of wave boundary layers with a sudden change in roughness. *Journal of Fluid Mechanics*, 252: 117-145.

Garnaud, S., P. Lesueur & T. Garlan (2005). Origin of sedimentary furrows associated with cohesive sediments on a shoreface setting (eastern Bay of Seine, France). *Geo-Marine Letters*, 1: 34-42

Gente, P., J. Dyment, M. Maia & J. Goslin (2003). Interaction between the Mid-Atlantic Ridge and the Azores hot spot during the last 85 Myr: emplacement and rifting of the hot spot-derived plateaus. *Geochemistry, Geophysics and Geosystems*, 4(10): 1-23.

Goff, J.A., L.A. Mayer, P. Traykovski, I. Buynevich, R. Wilkens, R. Raymond, G. Glang, R.L. Evans, H. Olson & C. Jenkins (2005). Detailed investigation of sorted bedforms, or "rippled scour depressions," within the Martha's Vineyard Coastal Observatory, Massachusetts. *Continental Shelf Research*, 25: 461-484.

Green, M.O., C.E. Vincent & A.C. Trembanis (2004). Suspension of coarse and fine sand on a wave-dominated shoreface, with implications for the development of rippled scour depressions. *Continental Shelf Research*, 24: 317-335.

Gutierrez, B.T., G. Voulgaris & E. Thieler (2002). Wind-driven flow and the maintenance of a Rippled Scour Depression: Wrightsville Beach, North Carolina, USA. *Eos*. Transaction of the American Geophysical Union, 83(47), Fall Meet. Suppl., abstract #OS52F-11.

Gutierrez, B.T., G. Voulgaris & E.R. Thieler (2005). Exploring the persistence of sorted bedforms on the inner-shelf of Wrightsville Beach, North Carolina. *Continental Shelf Research*, 25: 65-90.

Hart, K., S. Carey, H. Sigurdsson, R.S.J. Sparks & R.E.A. Robertson (2004). Discharge of pyroclastic flows into the sea during the 1996-1998 eruptions of the Soufriere Hills volcano, Montserrat. *Bulletin of Volcanology*, 66(7): 599-614.

Hunter, R.E., J.R. Dingler, R.J. Anima & B.M. Richmond (1988). Coarse-sediment bands on the inner shelf of southern Monterey Bay, California. *Marine Geology*, 80: 81-98.

Instituto Hidrográfico (2005). *Tabela de Marés 2006*. Instituto Hidrográfico, Lisboa. vi+196 pp.

Judd, A., & M. Hovland (2007). *Seabed Fluid Flow: The Impact on Geology, Biology and the Marine Environment.* Cambridge University Press, Cambridge. 492 pp

Laursen, T.S., J. Fredsøe & B.M. Sumer (1994). Numerical prediction of wave boundary layer over a bed with a change in roughness. *Coastal Engineering*, 24: 81-96.

Lafon, V., F. Jose, F. Tempera, L. Macedo, A. Martins, R.S. Santos & R. Bates (2006). Summertime Morphodynamics of Two Beaches Presenting Different Wave Exposure – Faial Island, Azores, Portugal. *Proceedings of Coastal Dynamics 2005 - 5th International Conference on Coastal Dynamics.* ASCE, New York. CD-ROM.

Lowe, D.R. (1976). Subaqueous liquefied and fluidized sediment flows and their deposits. *Sedimentology*, 23(3): 285-308.

Madeira, J. (1998). Estudos de neotectónica nas ilhas do Faial, Pico e S. Jorge: uma contribuição para o conhecimento geodinâmico da junção tripla dos Açores. *Ph.D. thesis.* Universidade de Lisboa, Lisboa. 481 pp.

Madeira, J., & A. Brum da Silveira (2003). Active tectonics and first paleoseismological results in Faial, Pico and S. Jorge islands (Azores, Portugal). *Annals of Geophysics*, 46: 733-761.

Madeira, J., & A. Ribeiro (1990). Geodynamic models for the Azores triple junction: a contribution from tectonics. *Tectonophysics*, 184: 405-415.

Morang, A., & R.L. McMaster (1980). Nearshore Bedform patterns along Rhode Island from side-scan Sonar surveys. *Journal of Sedimentary Petrology*, 50(3): 831-840.

Mulder, T., J.P.M. Syvitski, S. Migeon, J.-C. Faugères & B. Savoye (2003). Marine hyperpycnal flows: initiation, behavior and related deposits. A review. *Marine and Petroleum Geology*, 20(6-8): 861-882.

Murray, A.B., R. Thieler, A. Ashton & E. Tang (2000). *The importance of non-local effects in inner-shelf sediment transport and morphological development: Rip-current channels and rippled scour depressions.* Society of Engineering Science 2000, Columbia, SC.

Murray, A.B., & R. Thieler (2003). Inner continental shelf grain-size sorted patterns: instability and self-organization. *Geophysical Research Abstracts*, 5: 14631.

Murray, A.B., E.R. Thieler & B. Tighe (2003). Sorted sediment patterns on shallow shelves: Instability and finite-amplitude self-organization. *Proceedings of the 3rd International Symposium on River, Coastal, and Estuarine Morphodynamics*, Barcelona, Sept. 2003: 365-377.

Murray, A.B., & R.T. Thieler (2004). A new hypothesis and exploratory model for the formation of large-scale innershelf sediment sorting and "rippled scour depressions". *Continental Shelf Research*, 24: 295-315.

Murray, A.B., G. Coco, M.O. Green, T.M. Hume & E.R. Thieler (2005). A Refined Numerical Model for Sorted Bedform Formation and Evolution. *Eos.* Transaction of the American Geophysical Union, 86(18), Jt. Assem. Suppl., abstract #OS23B-06.

Needell, S.W., W.P. Dillon, & H.J. Knebel (1982). Erosional channels on the shoreface of Nauset Beach, Cape Cod, Massachusetts. *Geo-Marine Letters*, 2: 61-64.

Pacheco, J. (2001). Processos associados ao desenvolvimento de erupções vulcânicas hidromagmáticas explosivas na ilha do Faial e sua interpretação numa perspectiva de avaliação do Hazard e minimização do Risco. *Ph.D. thesis*. Azores University. 330 pp.

Parsons, J.D., J.W.M. Bush & J.P.M. Syvitski (2001). Hyperpycnal plumes with small sediment concentrations. *Sedimentology*, 48: 465-478.

Quartau, R. (2007). The insular shelf of Faial: Morphological and sedimentary evolution. *Ph.D. thesis*. University of Aveiro, Aveiro. 301 pp.

Quartau, R., F. Curado, T. Cunha, L. Pinheiro & J.H. Monteiro (2002). Projecto Gemas – Localização e distribuição de areias em redor da ilha do Faial. *Relatório Técnico INGMARDEP*, 5/2002. Dep.to de Geologia Marinha, IGM, Lisboa. 37 pp., 30 figs.

Quartau, R., H. Duarte, & P. Brito (2005). Projecto Gemas – Relatório da campanha de amostragem de sedimentos (FAPI-3) realizada na plataforma e na orla costeira das ilhas do Faial e do Pico. *Relatório Técnico INGMARDEP*, 2/2005. Dep.to de Geologia Marinha e Costeira, INETI, I.P., Lisboa. 17 pp., 9 figs.

Reimnitz, E.L., L.J. Toimil, F.P. Shepard & M. Gutierrez-Estrada (1976). Possible rip current origin for bottom ripple zones to 30-m depth. *Geology*, 4: 395-400.

Schwab, W.C., E.R. Thieler, J.R. Allen, D.S. Foster, B.A. Swift & J.F. Denny (2000). Influence of inner-continental shelf geologic framework on the evolution and behavior of the barrier-island system between Fire Island Inlet and Shinnecock Inlet, Long Island, New York. *Journal of Coastal Research*, 16: 408-422.

Simões, A., R. Duarte & M. Alves (1997). A pilot ocean monitoring site at Azores islands. pp. 444-454. In J.H. Stel, H.W.A. Behrens, J.C. Borst, L.J. Droppert, J.P. van der Meulen (eds.). *Operational Oceanography: The Challenge for European Co-Operation*. Elsevier Science Ltd, The Hague.

Sleath, J.F. (1987). Turbulent oscillatory flow over rough beds. *Journal of Fluid Mechanics*, 182: 369-409.

Swift, D.J.P., & G.L. Freeland (1978). Current lineations and sand waves on the inner shelf, Middle Atlantic Bight of North America. *Journal of Sedimentary Research*, 48(4): 1257-1266.

Thieler, E.R., W.C. Schwab, M.A. Allison, J.F. Denny & W.W. Danforth (1998). Sidescan-Sonar Imagery of the Shoreface and Inner Continental Shelf, Wrightsville Beach, North Carolina. *USGS Open-file Report*, 98-596. http://pubs.usgs.gov/of/1998/of98-596/.

Thieler, E.R., O.H. Pilkey, W.J. Cleary & W.C. Schwab (2001). Modern sedimentation on the shoreface and inner continental shelf at Wrightsville Beach, NC, USA. *Journal of Sedimentary Research*, 71: 958-970.

Traykovski, P. (2005). Observations of Sand Transport Processes Over Sorted Bedforms. *Eos*. Transaction of the American Geophysical Union, 86 (18), Jt. Assem. Suppl., abstract #OS23B-03.

Trembanis, A.C., & P.A. Traykovski (2005). Ripple and Morphologic Behavior of Sorted Bedforms. *Eos*. Transaction of the American Geophysical Union, 86 (18), Jt. Assem. Suppl., abstract #OS23B-01.

White, W.M., M.D.M. Tapia & J.-G. Schilling (1979). The petrology and geochemistry of the Azores Islands. *Contributions to Mineralogy and Petrology*, 69: 201-213.

8. Acknowledgements

To Neil Mitchell for all his suggestions that considerably improved the quality of this chapter.

Rui Quartau is acknowledged for sharing seismic and grainsize data collected in the study area.

Fernando Tempera has been financed by a PhD grant (ref. SFRH/BD/12885/2003) from the Fundação para a Ciência e a Tecnologia.

This work has been supported by various funding sources including the Royal Society, the British Council (Germany), the Higher Education Funding Council for Wales, the Regional Directorate for Science and Technology of the Azores and projects MARINOVA (INTERREG IIIb/MAC/4.2/M11), MAROV (PDCTM/P/MAR/15249/1999) and GEMAS (DROTRH contract).

The use of the terrestrial relief maps produced by the Instituto Geográfico do Exército was conceded by the Regional Secretariat for the Environment under the scope of project MARÉ (Life Natureza B4-3200/98-509).

The masters and crews of the RV *Arquipélago* and RL *Águas Vivas* are acknowledged for all their effort during the work at sea.

Frederico Cardigos and Thierry Schmitt are thanked for their collaboration throughout the multibeam survey and in the processing of the data.

Paul Byham and Submetrix are thanked for the very useful support during operations with and processing of data from the Swathplus system.

Bernie Coakley and Russel Dodd (GSE Rentals) are thanked for their advice on and *in situ* support of the multibeam installation.

Instituto Hidrográfico is acknowledged for facilitating the installation of the tide gauge in Horta's Tidal Gauge house.

Sónia Santos from Direcção Regional do Ambiente is acknowledged for the kind loaning a substitute DGPS during the 2004 survey.

Guilherme Soares (DRRF-Açores) is thanked for supplying files for DGPS post-processing.

CHAPTER 6

SPATIAL PATTERNS OF SEA SURFACE TEMPERATURE AND CHLOROPHYLL-*A* AROUND FAIAL ISLAND (AZORES, NE ATLANTIC) FROM SATELLITE IMAGERY

Abstract

Recent datasets of AVHRR and SeaWiFS satellite imagery are used to investigate the spatio-temporal variation of SST and chl-*a* around an oceanic island. The analysis focus on the yearly cycles and the spatial variation of Sea Surface Temperature (SST) and chlorophyll-*a* (chl-*a*) around Faial island (Azores, NE Atlantic). The study is conducted based on full resolution monthly composites derived from recent datasets extending more than five years.

Yearly and seasonally-averaged fields are obtained for both SST and chl-*a*. These fields show that SST is lower in the Faial-Pico passage and towards nearshore areas in general. This is explained by coastal upwelling and turbulent mixing of the water column by tidal currents in the topographically rich inter-island passage. Higher-than-average SST values (positive anomalies) prevail off the northern shores of Faial in spring and summer. Areas of predominantly lower-than-average SST values (negative anomalies) appear in the western and southwestern sectors in summer which may be related to leeside upwelling powered by the seasonal increase in the frequency of north and northeasterly winds.

Chl-*a* displays a more stable pattern throughout all seasons with the highest concentrations consistently found off the NW coast, in the Faial-Pico passage and in a narrow strip along the northern shore. The southern sector of the island and the offshore areas are dominated by lower values. In summer a small increase in chl-*a* concentration is found on the south-western sector of Faial that is concurrent with the establishment of the negative SST anomaly.

In view of the spatially consistent patterns obtained, the use of satellite imagery to assess spatial variability and derive fields for seawater temperature and primary productivity proxies is suggested as a first order approximation in areas where dense *in situ* oceanographic records at sufficient resolution are still lacking.

Keywords: SST; chlorophyll-*a*; spatio-temporal variability; Azores island shelves.

Table of Contents

1. Introduction

Studies of the major oceanographic patterns occurring near the Azores islands (Portugal, NE Atlantic) have been conducted since the 1980's. Most studies have targeted the Azores Current/Subtropical Front system which is located along latitudes 2º-3º to the south of the archipelago with a focus on mesoscale physical dynamics (e.g., Gould, 1985; Klein & Siedler, 1989; Cipollini et al., 1997; Alves & Verdière, 1999; Alves et al., 2002; Pingree, 2002) and associated biological dynamics (e.g., Macedo et al. 2000; Mouriño et al., 2005).

The installation of a High Resolution Picture Transmission (HRPT) satellite receiving station in the archipelago (ref.: HAZO) in 2001 represented an important low cost/high benefit contribution to the study of oceanographic patterns in this central part of the Atlantic at enhanced spatial and temporal resolutions. Studies by Martins et al. (2004), Bashmachnikov et al. (2004a,b); Lafon et al., (2004a,b) using AVHRR (Advanced Very High Resolution Radiometer) and SeaWiFS (Sea-Viewing Wide Field-of-View Sensor) imagery to study mesoscale temporal and spatial variability of sea surface temperature and ocean colour have since then contributed to a more precise and detailed knowledge of the Azores waters.

Despite these studies, investigations using satellite imagery to analyse the spatio-temporal variation of oceanographic patterns at an island scale have not been accomplished. Such knowledge is of particular importance for ecological studies applied to conservation and fishery management, namely those analysing factors regulating marine species distributions in the vicinity of the islands.

Although satellite measurements pertain to near-surface waters only, patterns displayed in satellite imagery are not always decoupled from the subsurficial layers that actual influence benthic assemblages on temperate shelves. For instance, during the winter, widespread convective and wind mixing ensures that the ocean surface is a close representation of the underlying mixed layer (which can extend to depths beyond the shelf edge). The same does not necessarily occur in summertime, because of strong warming of the surficial layer (down to 10-50 m depth), but subsurficial structure may still be detected at the surface in the presence of topographically-induced mixing or wind-induced upwelling.

The main aim of the study reported here is to investigate the potential of AVHRR and SeaWiFS satellite imagery for identifying thermal and ocean colour zonation at an island scale that may provide environmental proxies for studies of on-shelf benthic patterns (such as the goal ultimately presiding to this thesis). The study is carried out within a 5-km buffer around the coast of Faial and western Pico (Azores, NE Atlantic). This is an area of particular relevance for nature conservation which includes five marine Special Areas of Conservation

(SACs - Natura 2000 network), an OSPAR marine protected area and has been designated a long-term biodiversity research reference site under project BIOMARE.

On the basis of datasets extending more than 5 years and mainly acquired by the HAZO station, average anomaly fields of Sea Surface Temperature (SST) and chlorophyll-*a* (chl-*a*) distribution are extracted from AVHRR and SeaWiFS imagery, respectively, and the existence and magnitude of local SST and chl-*a* zonation are analysed. An effort is made to preserve the full resolution of the original imagery given the dimension of the study area.

A Geographic Information System (GIS) is used for (i) comparing data related in time and space, (ii) visualizing fields and (iii) overlaying complementary information. Meteorological patterns and seabed morphology are also provided in explanation of the spatial patterns identified.

1.1. Broader scope of the analyses

A number of projects have catalogued the variation of marine biological features (species and/or assemblages) at local and regional scales in the Azores (e.g., CLIPE, MARÉ, OGAMP, BIOTOPE, PARQMAR). The databases from these projects provide a good foundation from which to analyse spatial variations of species and assemblages at several scales but knowledge of the associated environment variation is required to interpret the variations and produce predictive models.

As reviewed in Menge et al. (1997, 2003) or Schiel (2004) temperature and plankton productivity regime are among the factors that interfere with the ecological requirements of individual species and regulate their biogeographic distributions, their abundance and ultimately the composition of the assemblages they constitute.

In the case of benthic studies on temperate shelves (such as the goal ultimately presiding to this thesis) information about environmental variability should ideally pertain to the near-bottom layer. However, data available to date (e.g., from sampling using *in situ* data-loggers and shipboard surveys) has insufficient resolution to produce a vertically-explicit spatio-temporal model of the thermal and ocean colour variability around Faial. The current paper aims at contributing to fill this lack by assessing spatial variability of SST and chl-*a* around Faial island based on satellite data. The specific scrutiny of whether provide valid proxies for the temperature conditions affecting benthic species, and therefore constitute significant explanatory variables, is conducted by the statistical modelling presented in Chapter 7.

2. Study area

2.1. Surface circulation

The Azores is an archipelago located on the northern edge of the North Atlantic Subtropical Gyre (Maillard, 1986) with islands situated between 39º 44’ N - 36º 55’ N and 31º 15’ W- 25º 00’W (Figure 1). The region is in an area of low wave/vortex activity (Fratantoni, 2001) and is bound between two eastward currents branching from the Gulf Stream: (i) the North Atlantic Current southern branch (NAC2) and (ii) the Azores Current (AzC) (Santos et al., 1995).

Differences in the thermo-haline properties of these flows promote the existence of quasi-permanent zonal fronts with varying position, meander development and eddy detachment. AzC meanders typically have wavelengths ranging between 160 and 450 km, periods from 40 to 250 days (occasionally up to 490 days) and westward propagation speeds of 0.9-3.0 cm/s (Gould, 1985; Cipollini et al., 1997; Alves & Verdière, 1999; Alves et al., 2002; Pingree, 2002).

On the northern flank of the meandering AzC, regular series of westward-propagating anticlockwise eddies develop as a rectification process of baroclinic instability (Onken, 1993; Pingree, 1997; Alves & Verdière, 1999). These eddies exhibit mean diameters in the order of 100 km (Le Traon & De Mey, 1994) and dominating periods of 200-250 days (Pingree, 2002). Over multi-annual scales, these eddies are perceived as a weak (1.8 cm/s) narrow (~200 km) westward counter-flow named the Azores Counter Current (AzCC). Despite the eddies being highly energetic, they move very slowly and the mean zonal transport associated with the AzCC averages a mere 2 Sv (Sv = 10^6 m^3/s) (Alves et al., 2002). The AzCC maximum intensity is observed in spring, concurrently with that of the AzC (Alves & Verdière, 1999).

Faial and Pico are located at a 38.6ºN latitude in the central group of Azores islands. Altimetric data averaged over several years show mean geostrophic flows in the area to be typically from N to NW with average speeds of 5-10 cm/s (AVISO dataset, 2007). Fine-scale studies aimed at resolving the pattern of flows in the vicinity of the island are ongoing (Bashmachnikov, unpublished data). Unpublished information indicates that the larger scale currents intensively interact with the complex seafloor topography of the area and produce submesoscale oceanographic phenomena including narrow jets, trapped currents and localized upwelling (Ana Martins, pers. com.). Observations suggest that in the shelf areas, the geostrophic circulation is of secondary importance compared to the stronger currents induced by the tides as they interact with the shoaling and complex topography that surrounds the islands. It should also be noted that the study area is regionally unique as it contains the only inter-island shelf in the Azores, which straddles the 5-km wide passage between eastern Faial

Island and western Pico Island. This shallow area produces particular oceanographic conditions (such as upwelling and tidal mixing) that can be shown to influence both the SST and chl-*a*.

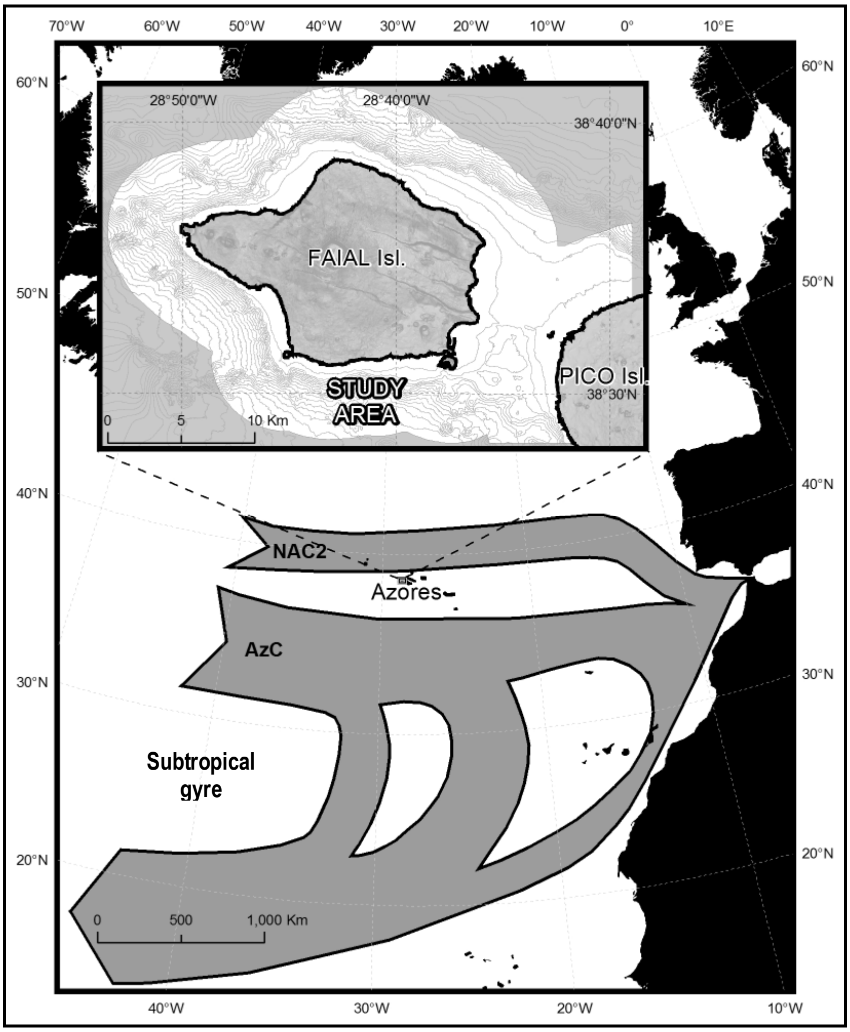

Figure 1: Location of Faial Island (Azores, Portugal, NE Atlantic) and general geostrophic surface transport. The study area is demarcated in the inset as a 5-km buffer demarcated around Faial and western Pico. NAC2 –North Atlantic Current southern branch; AzC – Azores current. Adapted from Siedler & Onken (1996).

2.2. Water characteristics

The vertical structure of temperatures in the upper ocean around the Azores is characterised by an oscillation between well-mixed and stratified conditions. During the winter, an upper mixed layer prevails to depths of approximately 150 m. During the summer months, stratification develops with the formation of a warm surficial layer that extends to depths of approximately 40 m. Below, a pronounced thermocline can extend to depths >100 m (Santos et al., 1995).

Surface waters in the region are generally oligotrophic, i.e., feature low nutrient levels (Santos et al., 1995). Locally, nutrient-rich sub-thermocline waters can be brought into the euphotic zone by frontal, topographical or vorticity effects (upwelling) and stimulate phytoplankton growth. These effects are typically associated with fronts that bound mesoscale eddies and areas where shoaling topography (e.g., seamounts, island shelves) accelerates the flow and generates vorticity that locally increases vertical mixing (OSPAR, 2000).

A 9-year dataset of daily *in situ* temperature measurements taken at Horta harbour (on the eastern coast of Faial) shows SST ranges from an average of 13.2ºC in January to 29.4ºC in July (Lafon et al., 2004). Salinity varies between 36.1 PSU in winter and 36.5 PSU in summer (Santos et al., 1995).

2.3. Phytoplankton production

Phytoplankton biomass around the Azores is normally low and exhibits an annual cycle close to that of temperate regions, which are delimited between 39ºN to 50ºN according to Longhurst (1998). This sort of cycle is highly dependent on the seasonal changeovers in the water column thermal stratigraphy (Campbell & Aarup, 1992) and features two annual blooms: (i) one in the spring, centred around April, where the annual chlorophyll-*a* maximum is reached, and (ii) another smaller one in the autumn, centred in October (Lalli & Parsons, 1997).

In subtropical latitudes south of the Azores, the upper ocean remains stratified throughout the year. Conditions are thus persistently oligotrophic which causes productivity to display a less marked seasonality. A small productivity maximum is reached in winter. Mean annual productivity is about half that of temperate waters and a greater proportion of the nutrients is recycled within the euphotic zone.

3. Methodology

The dataset used in the present study was supplied by the Department of Oceanography and Fisheries at the University of the Azores (DOP/UAç). Imagery was received at the HAZO HRPT Satellite Receiving Station (http://oceancolor.gsfc.nasa.gov/cgi/hrpt_station_info.pl?S=AZO) with the exception of a complementary set of SeaWiFS images concerning the period January 1999–March 2001, which was obtained from the Canary Islands HRPT Station (http://oceancolor.gsfc.nasa.gov/cgi/hrpt_station_info.pl?S=CAN).

The HAZO processing package (Figueiredo et al., 2004) was used to extract the monthly-averaged composites from *level-2* AVHRR and SeaWiFS for the study area. Despite the potential for spatio-temporal smearing of oceanographic structures, the averaging of the data at monthly scales was necessary to circumvent the cloudiness problem, which makes available information very patchy at higher temporal resolutions (Bashmachnikov et al., 2004a). The impact of cloudiness is particularly relevant in the Azores region where the percentage of cloud-free pixels in individual images averages only approximately 9% (Lafon et al., 2003). An effort was made to retain pixels immediately adjacent to the coastline as long as they survived the filtering processes detailed in 3.1 and 3.2.

The dataflow for the analyses is summarized in Figure 2.

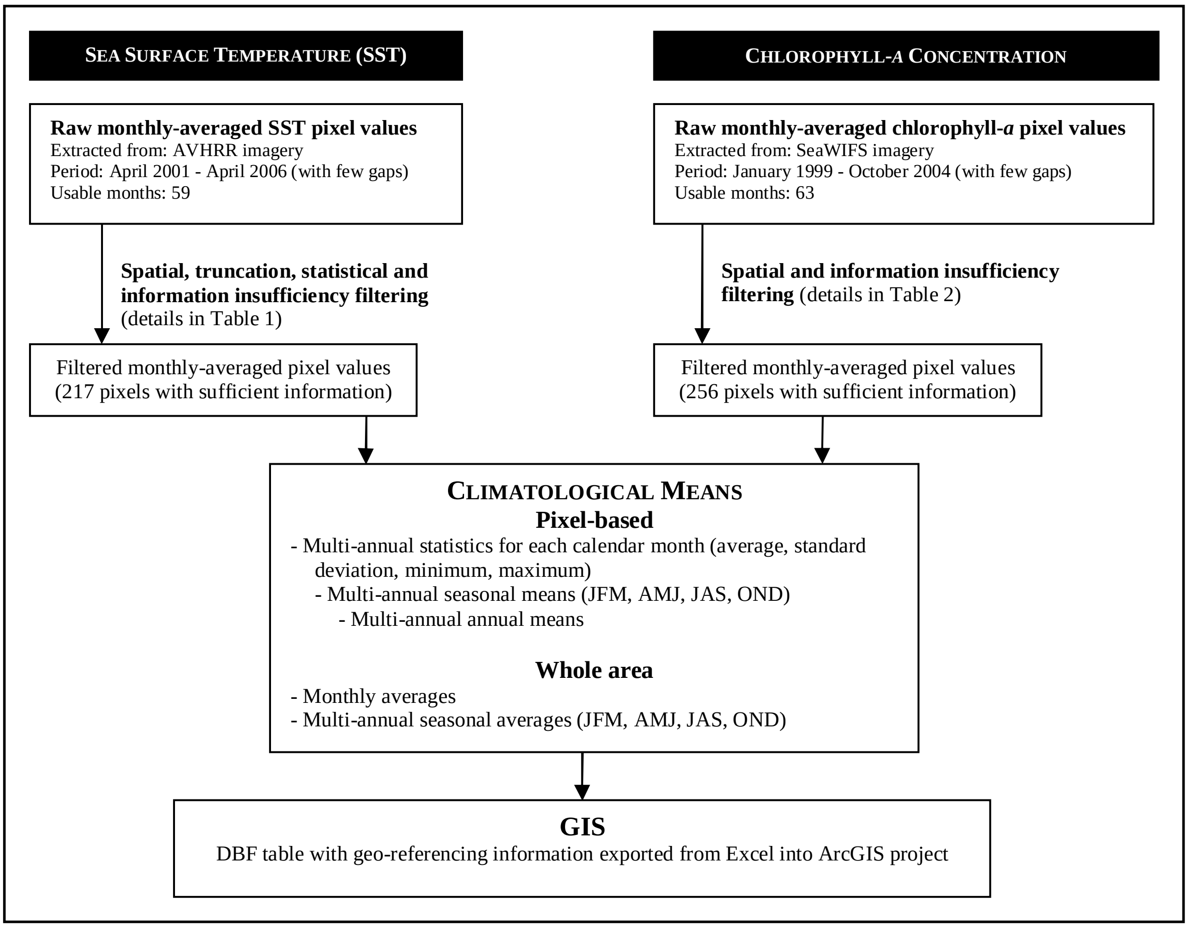

Figure 2: Dataflow scheme used in computing yearly and seasonal SST and chl-*a* climatology for pixels and study area.

3.1. AVHRR imagery

AVHRR imagery was received from satellites NOAA-12, NOAA-14, NOAA-16 and NOAA-17. Individual images were routinely processed in Seaspace Terascan v. 3.1 using the Multi-Channel SST algorithm (McClain et al., 1985), which includes the removal of clouds and corrections for a series of atmosphere-induced effects. Geo-referencing was accomplished manually due to limitations of the automatic routine in providing accurate locations in oceanic areas where the amount of cloud covering is often high and coastlines are limited.

The extraction master (fixed pixel grid) used to compile the data from the *level-2* imagery had a native resolution of 0.819’×0.684’ (Lat×Long). The monthly-averaged composites covered 59 months spanning from April 2001 to April 2006.

During the computation of these composites, no discrimination was made between day/night-time images, near-cloud pixels or different satellites. A series of filtering steps detailed in Table 1 was used to eliminate contaminated monthly-averaged pixels because they were either subject to probable contamination by land (spatial filtering) or their value showed considerable departures from the whole-area monthly mean (statistical $3\bar{\mu}$ thresholding as in Lafon et al., 2003). Only pixels for which a multi-annual average could be obtained for the full twelve months were finally kept to characterize the spatial regime in the study area.

Table 1: Steps used to filter out contaminated monthly-averaged SST pixels.

Step	Aim	Task summary	Software	Data format
1	Geographical delimitation of study area	Limitation of *level 2* AVHRR imagery dataset domain to rectangular geographical box	HAZO processing package	Internal table
2	Value-based band-pass truncation	Query of level 2 image dataset excluding pixel values outside the [+10ºC,+30ºC] interval; no discrimination between day & night images	HAZO processing package	Internal table
3	Computation of raw monthly-averaged dataset	Computation of monthly-averaged composite pixel values	HAZO processing package	dbf table with geo-referencing information
4	Limitation of analysis to fully marine pixels	Geographical exclusion of pixels within landmasses or partially contaminated by land areas	ArcGIS	Shapefile
5	Delimitation of pixel domain to 5-km buffer from island shoreline	Geographical exclusion of pixels farther than 5km from the coast and extraction of associated table	ArcGIS & MS Excel	Shapefile and excel file
6	Value-based high pass truncation of monthly-averaged pixels	Spreadsheet exclusion of pixel values <11.5ºC to remove remnant lower end contamination in monthly-averaged pixels	MS Excel	MS Excel file
7	Statistical filtering using value-based removal of outliers	1 – Computation of whole-area monthly averages and standard deviations 2 – within-month exclusion of pixels outside $]\bar{x}-3\bar{\mu}, \bar{x}+3\bar{\mu}[$ interval	MS Excel	MS Excel file
8	Exclusion of pixels holding insufficient data	Elimination of pixels where a multi-annual average could not be computed for at least one of the months	MS Excel	MS Excel file

The filtered dataset was used to study the spatio-temporal SST patterns, including the computation of whole-area statistics and the extraction of monthly, seasonal and annual fields. Anomalies were obtained as residuals by subtracting the whole-area monthly average from each monthly-averaged pixel. Multi-annual average fields (produced for “season” and “year” periods) were obtained by averaging the monthly anomalies for each pixel, ensuring that each of the relevant months contributed with equal weight.

3.2. SeaWiFS imagery

SeaWiFS imagery was received from SeaSTAR satellites and routinely processed using the SeaDAS software package. The procedure is fully-automated, including geo-referencing. The master used to extract the data from the *level-2* imagery had a native resolution of 0.412’× 1.130’ (Lat×Long). The monthly-averaged composites included 63 months spanning from January 1999 to October 2004.

The filtering applied to these composites is detailed in Table 2 and was aimed at eliminating pixels subject to probable land contamination or containing insufficient information to provide a 12-month weighted year average.

The filtering series did not include statistical $3_{\bar{\mu}}$ thresholding since the log-normal distribution of the data with a few very high but truthful values found amongst a background of many relatively low values (Campbell & O’Reilly, 1988) would have led to the exclusion of potentially good values.

Table 2: Steps used to filter out contaminated monthly-averaged chl-*a* pixels.

Step	Aim	Task summary	Software	Data format
1	Geographical delimitation of study area	Limitation of *level 2* SeaWiFS imagery dataset domain to rectangular geographical box	HAZO processing package	Internal table
2	Value-based band-pass truncation	Query of level 2 image dataset excluding pixel values outside the [0.01 mg/m^3, 6.00 mg/m^3] interval	HAZO processing package	Internal table
3	Computation of raw monthly-averaged dataset	Computation of monthly-averaged composite pixel values	HAZO processing package	dbf table with geo-referencing information
4	Limitation of analysis to fully marine pixels	Geographical exclusion of pixels within landmasses or partially contaminated by land areas	ArcGIS	Shapefile
5	Delimitation of pixel domain to 5-km buffer from island shoreline	Geographical exclusion of pixels farther than 5km from the coast and extraction of associated table	ArcGIS & MS Excel	Shapefile and excel file
6	Exclusion of pixels holding insufficient data	Elimination of pixels where a multi-annual average could not be computed for at least one of the months	MS Excel	MS Excel file

The filtered dataset was used to study the spatio-temporal chl-*a* patterns, including the calculation of monthly, seasonal and annual fields and whole area statistics.

Multi-annual average fields (produced for “season” and “year” periods) were obtained by averaging the monthly averages for each pixel, ensuring that each of the relevant months contributed with equal weight.

3.3. Inter-annual variability

The consistency/variability of the spatial patterns obtained either for SST or chl-*a* for the same month in different years was investigated using the Pearson correlation index based on one-to-one pixel correspondence.

3.4. Chl-*a* and STT spatial relationship

The existence of an inverse relationship between SST and chl-*a* at an island scale was investigated to confirm coastal upwelling (e.g., Solanki et al. 2001; Davenport et al., 2002; Joint et al., 2002;). The analysis was based on co-located synchronous chl-*a* and SST monthly averages. Since the masters through which SST and chl-*a* composite pixels were extracted did not fully coincide, the GIS was used to relate the two datasets using a spatial join technique. The appending of chl-*a* data to the attribute table of the SST shapefile was based on the "joining by spatial location" procedure and was performed on a monthly basis as this was the best available temporal scale at which some signal could be detected. Once joined, the Pearson correlation between the SST–Chl-*a* values in each month were computed using the statistical package StatSoft STATISTICA 6.0.

3.5. Neashore SST and chl-*a* extrapolation

As a result of pixels being eliminated by filtering aimed at avoiding land contamination, data holes are typically created in the nearshore that coincide with many of the sites sampled in the biological surveys (Chapter 7). In order to obtain estimates for these blank pixels, nearshore-offshore gradients are extracted to different sectors of the island. Regression lines (1^{st} degree polynomial) were then fit to the range of values found in each of these sectors and used as estimators of the gradients. Their statistical significance was assessed.

Nearest neighbour spatial joining based on the average annual field is firstly used to attach SST and chl-*a* values to the neashore blank pixels. In island sectors where statistical significance gradients were identified, the values are further corrected for the difference in distance to the shore between the centre of the nearest neighbouring pixel providing the value and the pixel being assigned the extrapolated value. Otherwise they are left unchanged.

4. Results

A total of 217 pixels emerged as valid from the filtering process of the SST composites while SeaWiFS composites produced 256 valid pixels. The difference in numbers is mostly due to the higher resolution of the masters used to extract the information from the SeaWiFS imagery.

4.1. Data for pixel-based climatology

The problem of retrieving valid pixels in a region heavily impacted by clouds is demonstrated in Figure 3 by displaying the average number of *level-2* image pixels used to compute each valid monthly composite pixel.

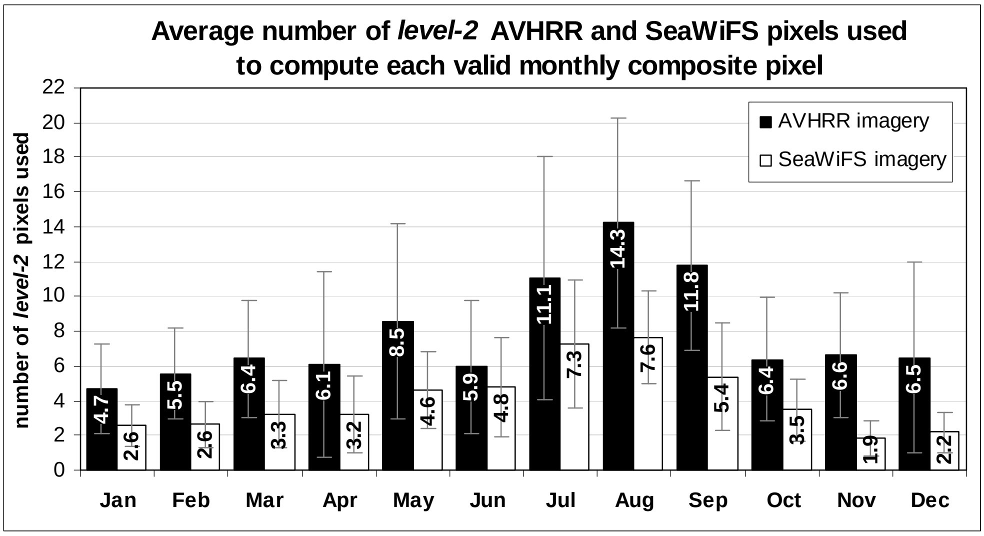

Figure 3: Multi-annual average number of *level-2* image pixels used to compute each valid monthly composite pixel in AVHRR (SST) and SeaWiFS (chl-*a*) imagery. Error bars are for one standard deviation.

In AVHRR composites, the number can be as low as 4.7 *level-2* pixels per composite pixel in a winter month such as January. However, summer records generally show higher number of acceptable pixels with averages for August of 14.3. The amount of information available from SeaWiFS imagery is roughly half of that available from AVHRR since the acquisition of ocean colour by the sensors is limited to periods of the day when the sea surface is properly illuminated by sunlight.

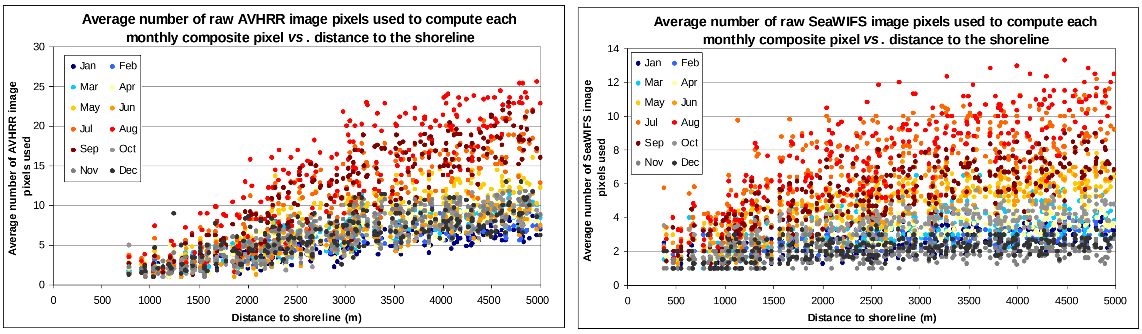

Figure 4: Scatterplots of the average number of *level-2* image pixels used to compute each valid monthly composite pixel *versus* distance to the shoreline. A. AVHRR. B. SeaWiFS.

Figure 4 illustrates the reduction of the amount of data available that occurs towards the shoreline in all calendar months.

4.2. Data for whole area climatology

The monthly variation of the number of valid pixels used in the calculation of whole area SST and chl-*a* concentration is shown in Figure 5. Only in two instances (December 2004 for SST and May 2001 for chl-*a* concentration) were averages computed from less than 50 composite pixels. These data amounts were considered suitable to extract the whole-area averages.

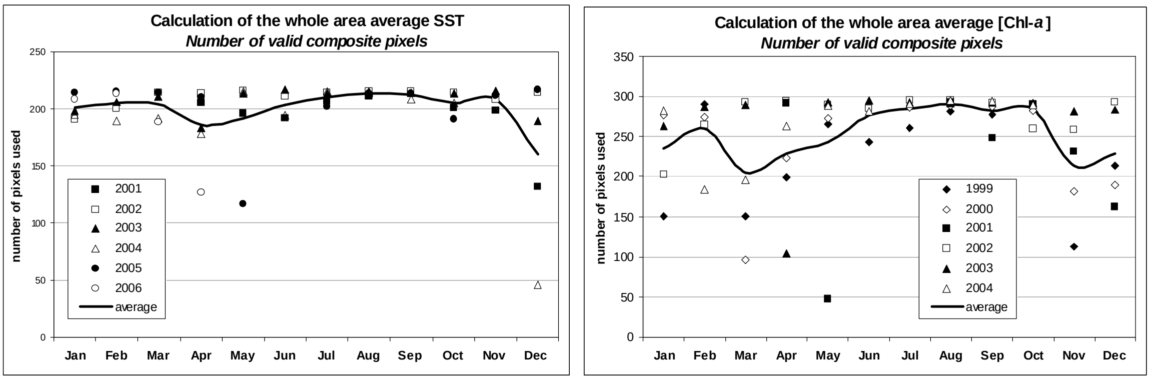

Figure 5: Monthly variation of the number of valid pixels used in the calculation of whole area SST (A) and chl-*a* concentration (B).

4.3. SST climate

The monthly oscillation of SST in the study area in the 5 years of data is shown in Figure 6.

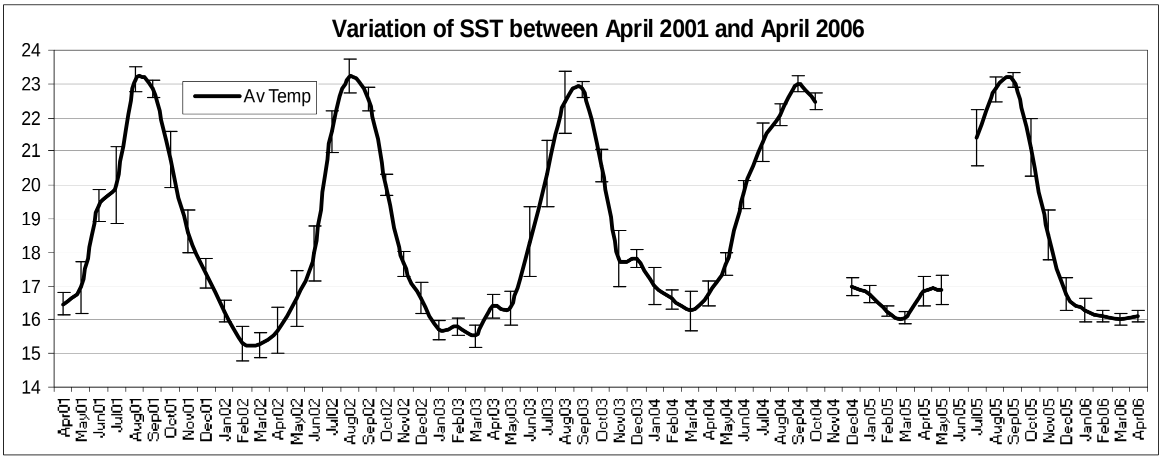

Figure 6: Monthly oscillation of SST around Faial island between April 2001 and April 2006. Vertical bars represent standard deviance.

Monthly average temperatures reached as high as 23.2ºC (August 2002) and as low as 15.3ºC (March 2002). A clear warming of winter temperatures was observed between 2002 and 2004 with warmer winters persisting through 2005 and 2006. Statistical differences were demonstrated ($p<0.05$) by performing a Univariate Test of Significance for the contrast between the two groups of winters (2002/2003 vs. 2004/2005/2004) and allowing for the effect of month (Statistica 6.0 © StatSoft) (Table 3).

Table 3: Results of Univariate Test of Significance for the contrast between the two groups of winters (2002/2003 vs. 2004/2005/2004).

	Sum of squares	df	Mean square	F	p
Effect	774,298.5	1	774,298.5	5,398,715	0.00
Error	428.8	2,990	0.1		

An average annual cycle composed using the combination of the more than 5 years of data is presented in Figure 7.

A **B**

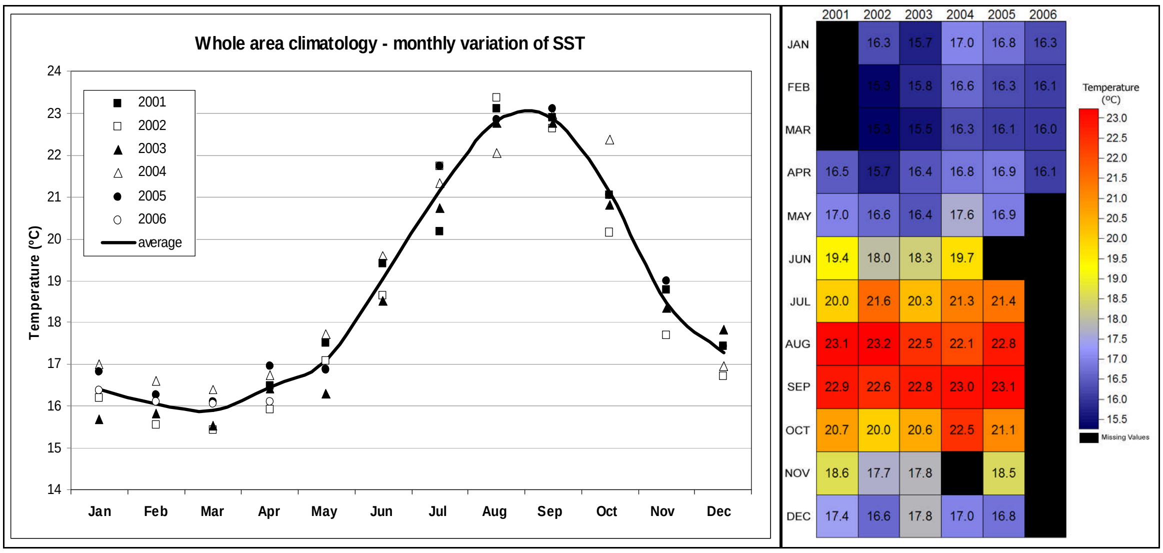

Figure 7: Whole-area climatology of SST. A. Average annual cycle; B. Colour-coded representation of the monthly averages indicating data gaps and highlighting intra and inter-annual variability.

Low winter temperatures (<16.5ºC) persist on average between January and April, the minimum being reached in March. Winter temperatures are on average 7ºC lower than those observed in summer. The highest temperatures are of approximately 23ºC and occur in August-September.

4.4. SST spatial patterns

The yearly-averaged anomaly field is shown in Figure 8. Each individual pixel is symbolised as a colour-coded circle located on the pixel centre and over a background with the underlying bathymetric contours. The yearly averaged values are displayed as values higher than average (termed positive anomalies) to those lower than average (termed negative anomalies). Negative anomalies concentrate within the passage between Faial and Pico and in the inshore-most pixels, while positive anomalies cluster in offshore patches.

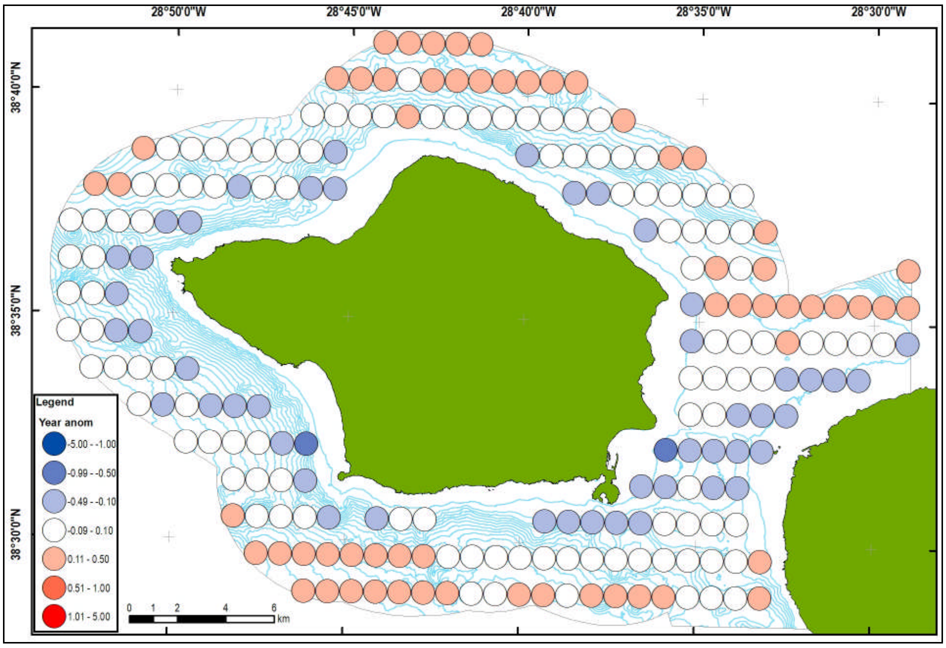

Figure 8: Yearly-averaged anomaly fields of SST around Faial Island.

The existence of a shore-normal gradient is noticeable in the anomaly field and is further analysed in Figure 9, which shows the monthly variation of the correlation between the monthly-averaged STT in each pixel and the distance of its centre to the shoreline. A statistically significant ($p<0.05$) Pearson correlation between these factors was found in 32 out of 57 months. In 30 of the statistically significant cases the correlation coefficient was positive.

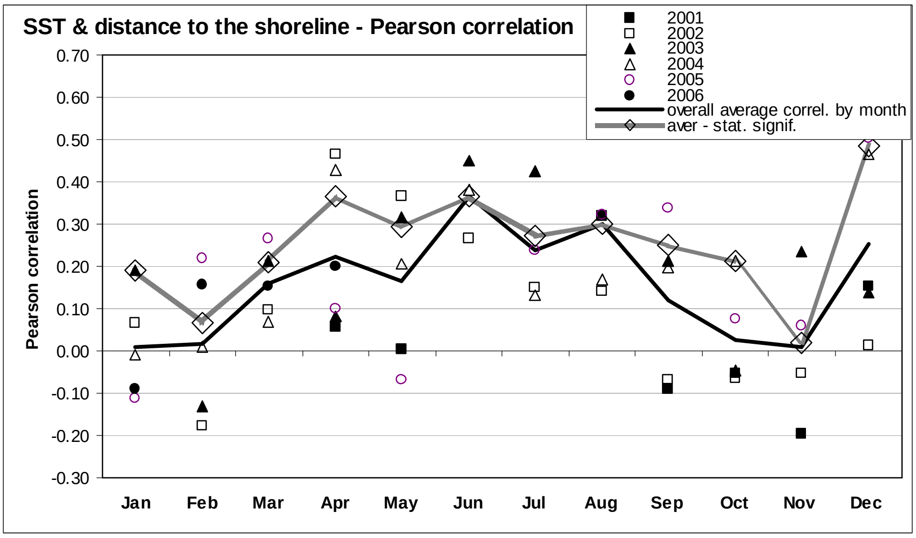

Figure 9: Monthly variation of the correlation between SST and distance to the shoreline.

The monthly correlation coefficients stay generally above 0.20 with the exception of January, February and November. The average of the correlation coefficients showing statistical significance was 0.26.

The monthly variation of the shore-normal SST gradient (as estimated by linear regression) is shown in Figure 10. Slopes of regression lines fit to the scatterplots in the months showing statistically significant correlation averaged 0.12 (i.e., an average increase of 0.12ºC per 1,000m increase in distance to the shoreline).

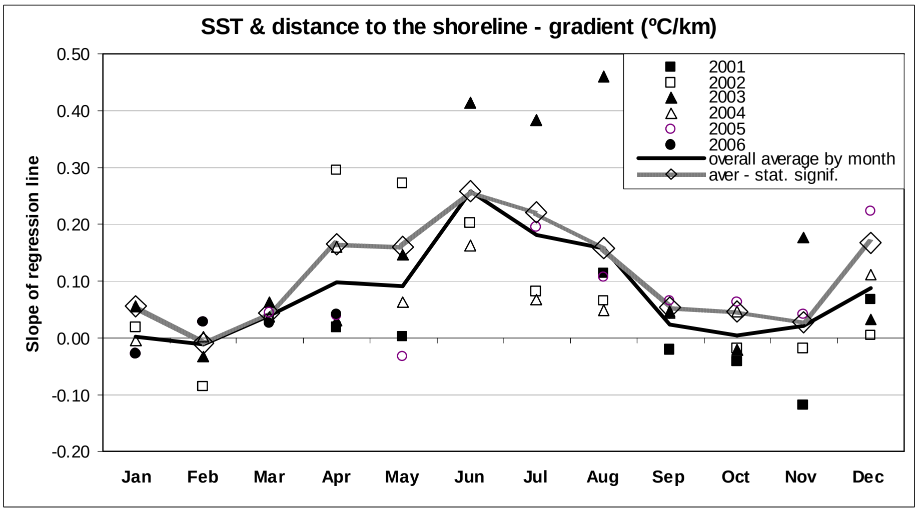

Figure 10: Monthly variation of the shore-normal SST linear gradients estimated from each monthly composite.

Sub-annual spatial patterns were investigated by analysing monthly and 3-month seasonal anomaly fields. The variation of the Pearson correlation between the patterns obtained by month in different years is shown in Figure 11. The results show that the correlations were consistently lower than 0.20 and averaged 0.08. Such low correlations indicate high inter-annual variability on a monthly basis and possibly the interference with high levels of small-scale noise. August was the month where most similar fields were obtained averaging a Pearson correlation of 0.37.

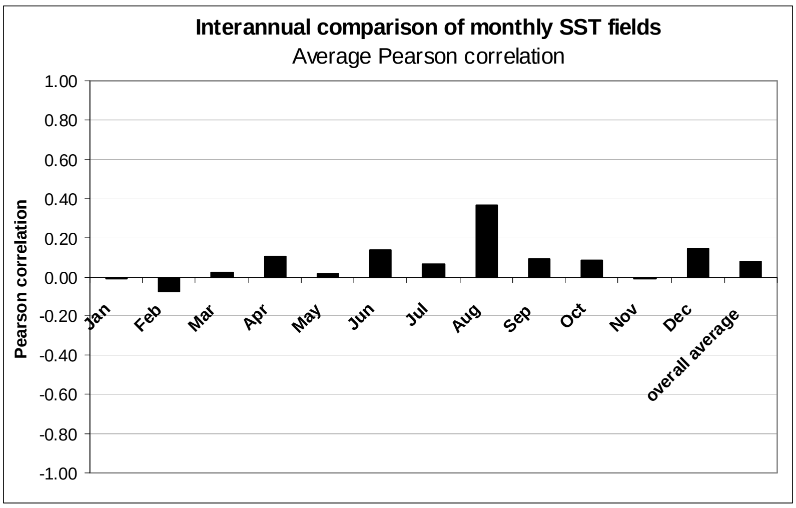

Figure 11: Pearson correlation between the monthly patterns obtained in different years.

Seasonal (3-month) multi-annual SST anomaly fields (Figure 12 to Figure 15) were used to illustrate the spatial patterns around the island as they are subject to lower levels of high-frequency noise than monthly fields. The radar diagram in the top right corner of each map illustrates a seasonally-averaged wind index calculated by multiplying the relative frequency of wind coming from each direction by its average velocity and standardizing the values obtained to the index maximum observed across all seasons. These local meteorological statistics were provided by Horta's Meteorological Observatory and concern the period 1960-1991.

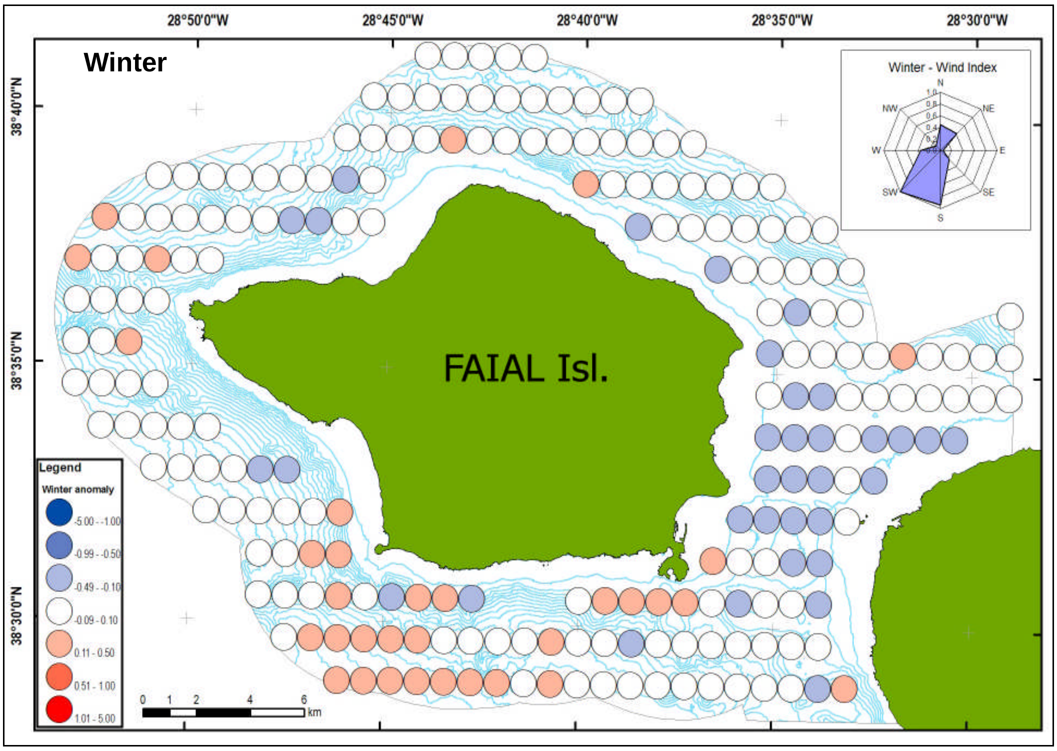

Figure 12: Winter (Jan/Feb/Mar) spatial pattern of SST anomalies around Faial Island. The radar diagram inset at the top right of each SST field represents a wind index (Rel. Freq. per octant × Aver. Vel. per octant) for each season.

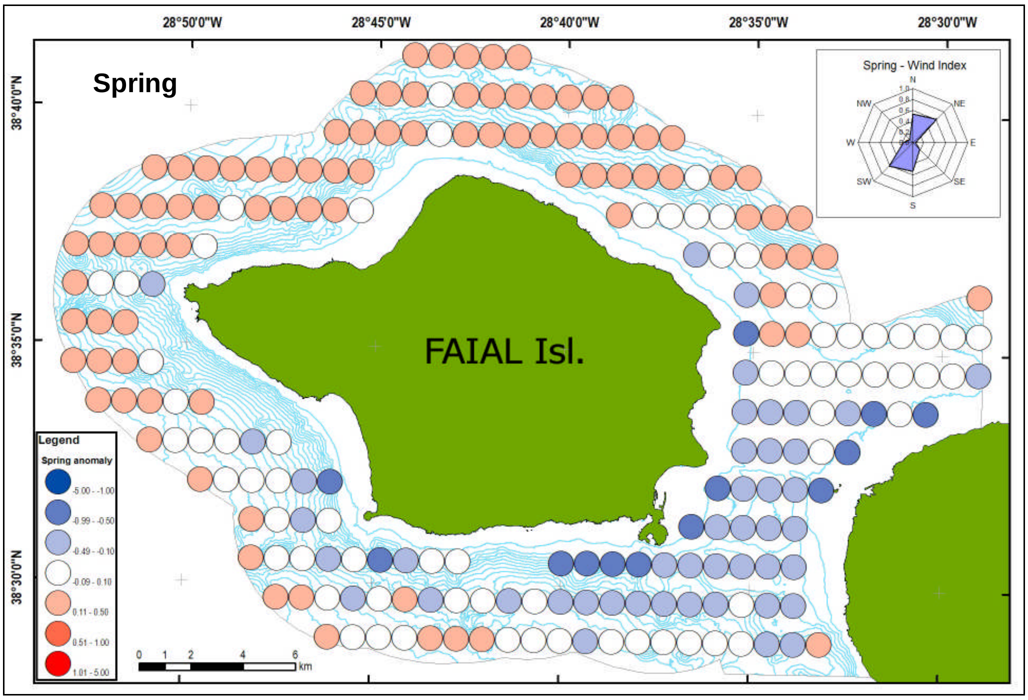

Figure 13: Spring (Apr/May/Jun) spatial pattern of SST anomalies around Faial Island.

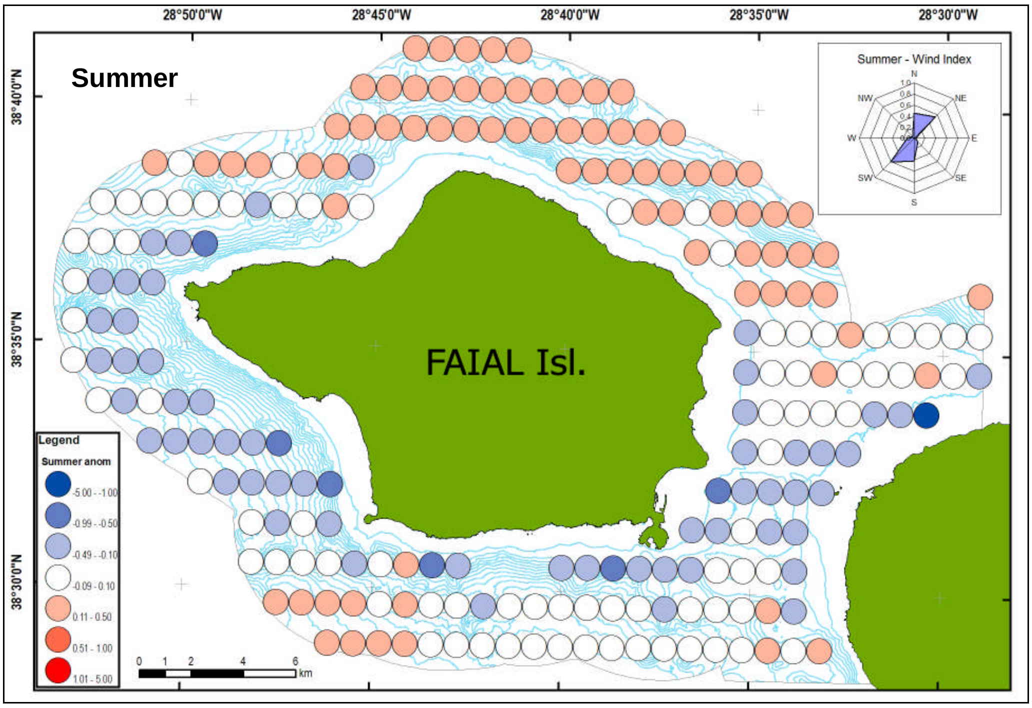

Figure 14: Summer (Jul/Aug/Sep) spatial pattern of SST anomalies around Faial Island.

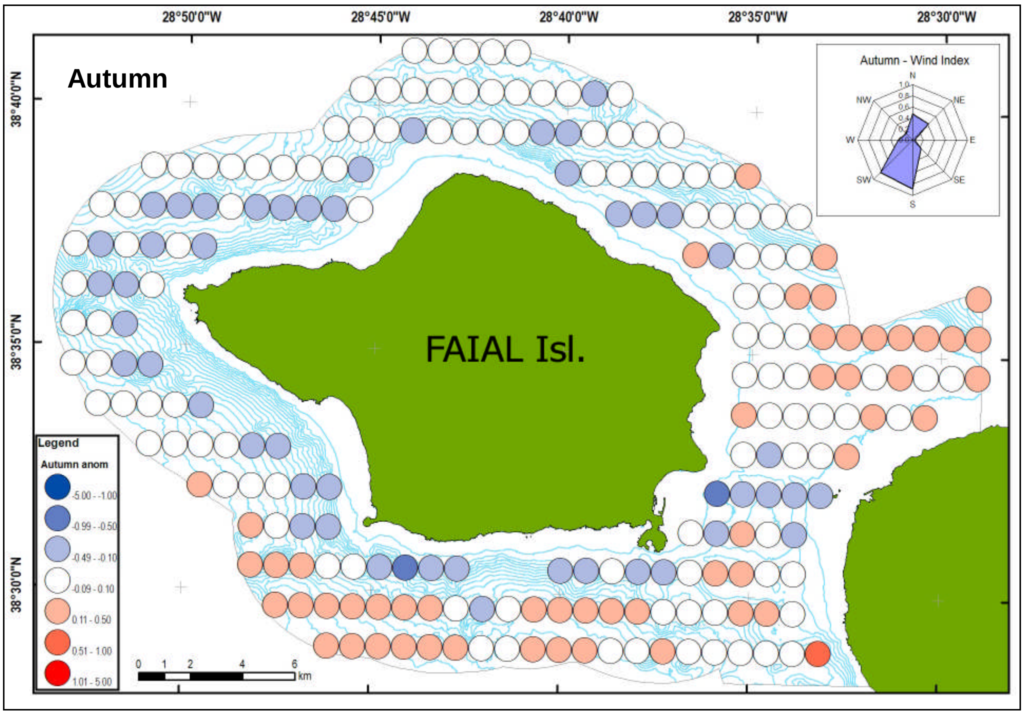

Figure 15: Autumn (Oct/Nov/Dec) spatial pattern of SST anomalies around Faial Island.

The anomaly fields show that the overwhelming majority of the SST pixels remained within 0.5ºC of the average throughout all seasons. Spring and summer periods exhibited the largest anomalies with a number of pixels (13 and 7 respectively) exhibiting values more than 0.5ºC below the average.

The sequence shows a clear seasonal variation in the location of positive and negative anomalies around the island. The winter is noteworthy for the lack of an extensive temperature zonation. However, it is worth-noting that negative anomalies persist in the centre of the passage between the islands and on various nearshore pixels. Small areas of positive anomaly are found off the southern coast and to the north of the passage.

Spring is noteworthy for the development of a clear concentration of positive anomalies off the northern and western coasts. The passage remains colder than average but the area of negative anomaly is extended with some nearshore pixels diverging further from the seasonal mean.

In summer, the positive anomaly persists off the northern shore but its westward extension is reduced. This occurs concurrently with the development of an area dominated by negative anomalies off the SW shore and western end of the island. The warmer patch off the northern sector of Faial disappears in the Autumn.

All seasonal patterns are consistent in showing that the passage pixels consistently display negative anomalies. The offshore-nearshore gradient is also clear throughout spring (0.2ºC per 1,000 m) and summer (0.1ºC per 1,000 m), with pixels closer to the shore showing in general lower temperature than the offshore ones. Autumn displays a gradient (0.07ºC per 1,000 m) that is one degree of magnitude smaller than spring and summer while the winter gradient (0.006ºC per 1,000 m) is negligible.

Small levels of residual noise are distinguishable in the seasonal fields as odd pixels clearly diverting from the anomaly trend of the surrounding patch. The low numbers of *level 2* pixels available for particular areas in some months together with the simplicity of the filters used while extracting the monthly composites are the most likely causes for these situations.

4.5. Chl-*a* climate

The monthly oscillation of chl-*a* concentration in the study area in more than 5 years of data is shown in Figure 16.

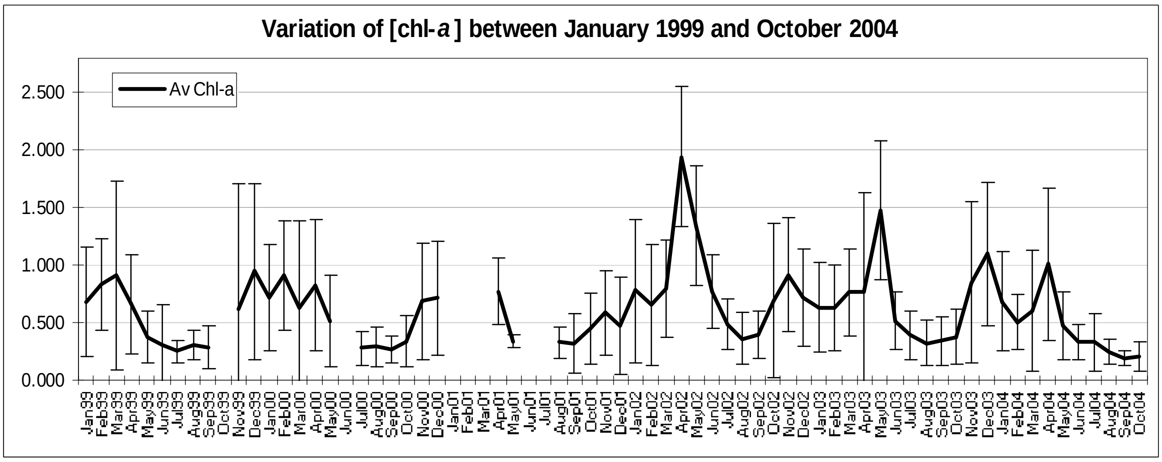

Figure 16: Monthly variation of chl-*a* concentration around Faial based on SeaWiFS imagery.

Years 2002 and 2003 show typical temperate region chl-*a* cycles with clear maxima in the spring. Despite the data gaps, it is perceptible that cycles in the period 1999-2001 show an affinity with subtropical cycles such as an enhanced chl-*a* concentration sustained throughout autumn and winter with barely discernible spring and autumn maxima.

Spring blooms in chl-*a* concentrations can be as high as 1.944 mg/m^3 (April 2002) but in most years peak concentrations are lower than 1.000 mg/m^3. September and October 2004 showed the lowest chl-*a* minima with average concentrations as low as ~0.200 mg/m^3.

An average annual cycle composed using the combination of the 5+ years of data is presented in Figure 17.

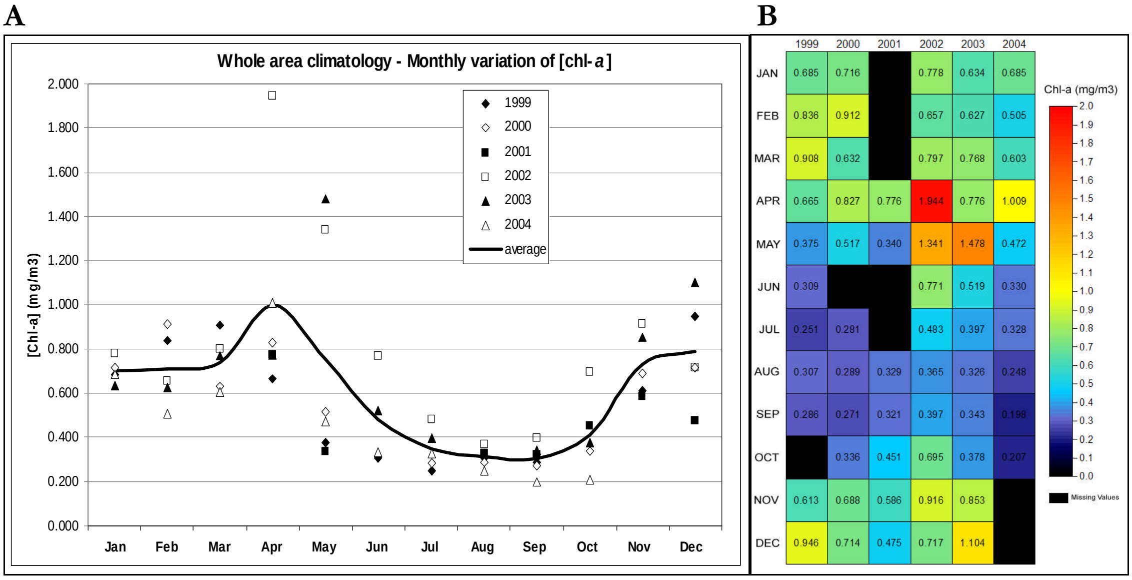

Figure 17: Whole-area climatology of chl-*a* concentration. A. Average annual cycle; B. Colour-coded representation of the monthly averages indicating data gaps as well as intra and inter-annual variability.

On average, the abundance of chl-*a* around Faial showed the two annual periods of increased chl-*a* typical of temperate zones. The major spring increase typically occurred in April while the autumn maxima occurred between November and December. Averaged values ranged from a maximum of 0.999 mg/m^3, during the spring maximum to a minimum of 0.302 mg/m^3 during the summer months. Average peak concentrations were ~1.8 times higher than the yearly average (0.607 mg/m^3). The autumn chl-*a* maxima averaged 0.818 mg/m^3, being 20% lower than the spring maxima. It is worth-noting the high inter-annual variability of the chl-*a* concentrations found in the spring and winter months.

4.6. Chl-*a* spatial patterns

The yearly-averaged chl-*a* field is shown in Figure 18. The pixels exhibit a clear zonation with highest concentrations found in an extensive area northwest of Faial, in the passage between the islands and in a narrow fringe along Faial's northern shore. The south and south-western sectors of the island and the more offshore pixels are dominated by lower than average values. Low values are also observed on the western and south-western sectors of Pico Island.

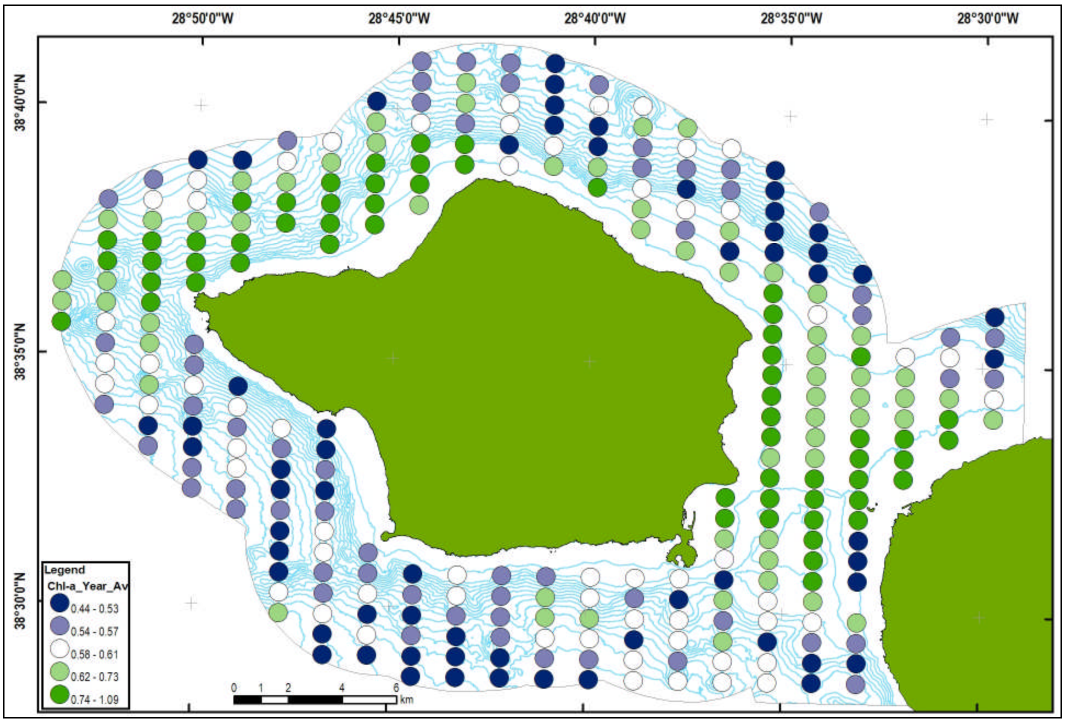

Figure 18: Yearly average chl-*a* concentration around Faial. Classes used are established from 20% quantiles due to a skewed data distribution.

Spatial patterns were investigated at monthly and seasonal (3-month) time scales. The monthly variation of the Pearson correlation between the monthly fields in different years is shown in Figure 19. The results show the correlations to average 0.11 and be consistently lower than 0.20. This indicates high inter-annual variability and possible interference with high levels of small-scale noise. The most similar fields were obtained in the months August, September and October which averaged Pearson correlations between 0.19 and 0.23.

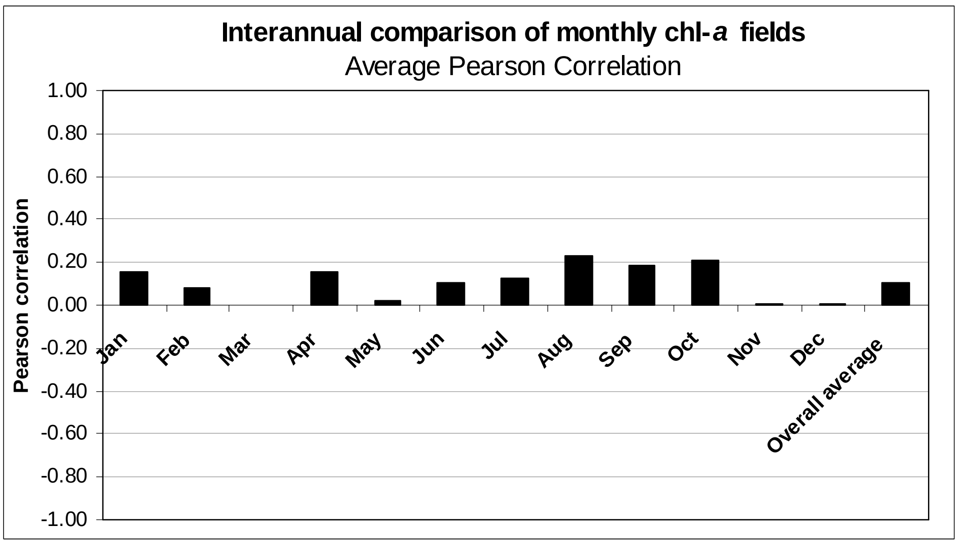

Figure 19: Pearson correlation between the monthly fields obtained in different years.

Seasonal multi-annual chl-*a* distribution fields (Figure 20 to Figure 23) were used to illustrate the spatial patterns around the island as they are subject to lower levels of high-frequency noise. The yearly-averaged field is fairly similar to mirrored in the patterns observed in the seasonally-averaged fields. The major exception to this general stability occurs in the areas off southwestern and southeastern Faial, which display a mild increase in chl-*a* concentration during the summer season. It is worth-noting that this concentration increase is concurrent with the summer negative temperature anomaly observed in the area (Figure 14).

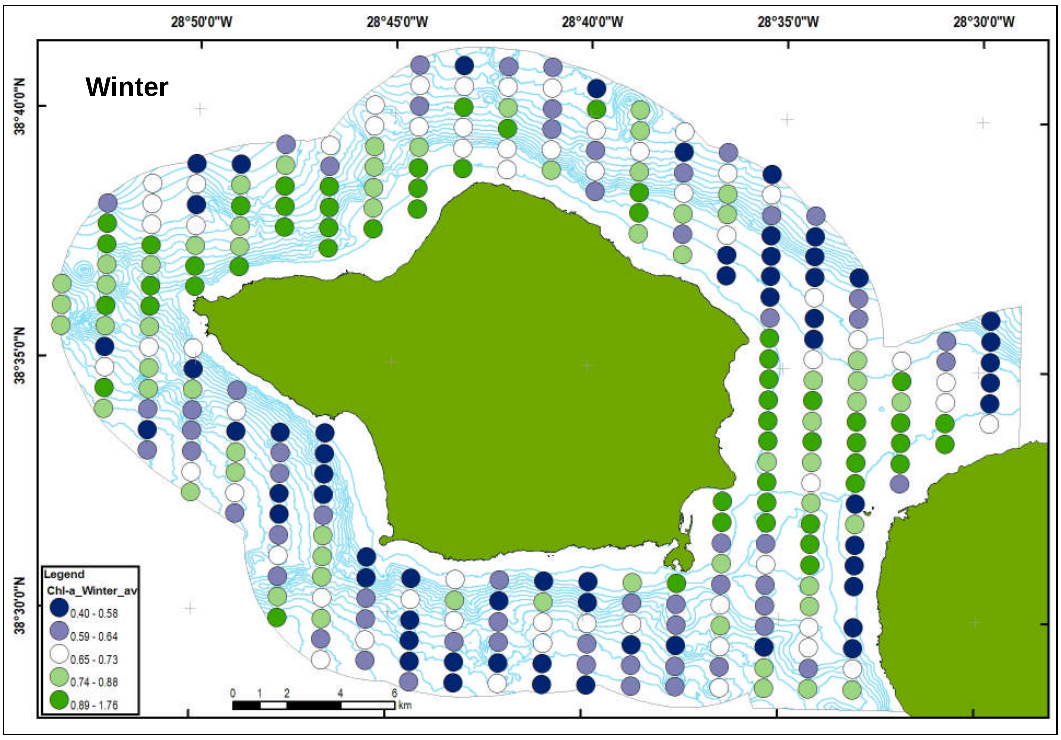

Figure 20: Winter (Jan/Feb/Mar) spatial patterns of chl-*a* concentration around Faial Island. Classes used are established from 20% quantiles due to a skewed data distribution.

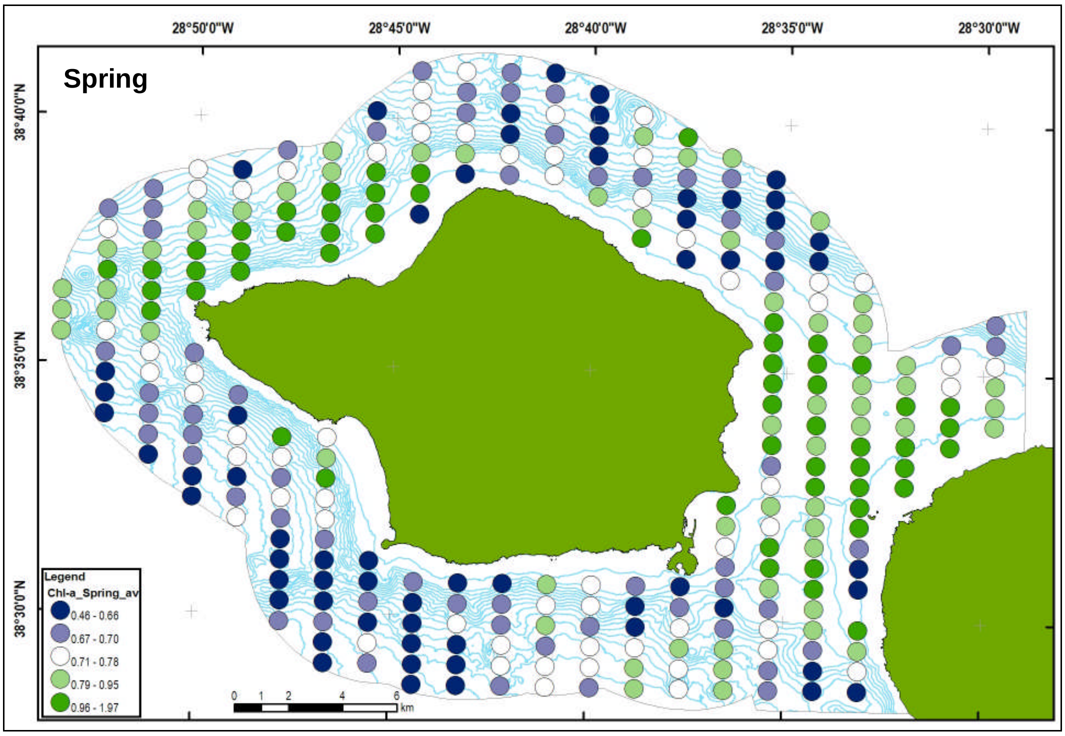

Figure 21: Spring (Apr/May/Jun) spatial patterns of chl-*a* concentration around Faial Island. Classes used are established from 20% quantiles due to a skewed data distribution.

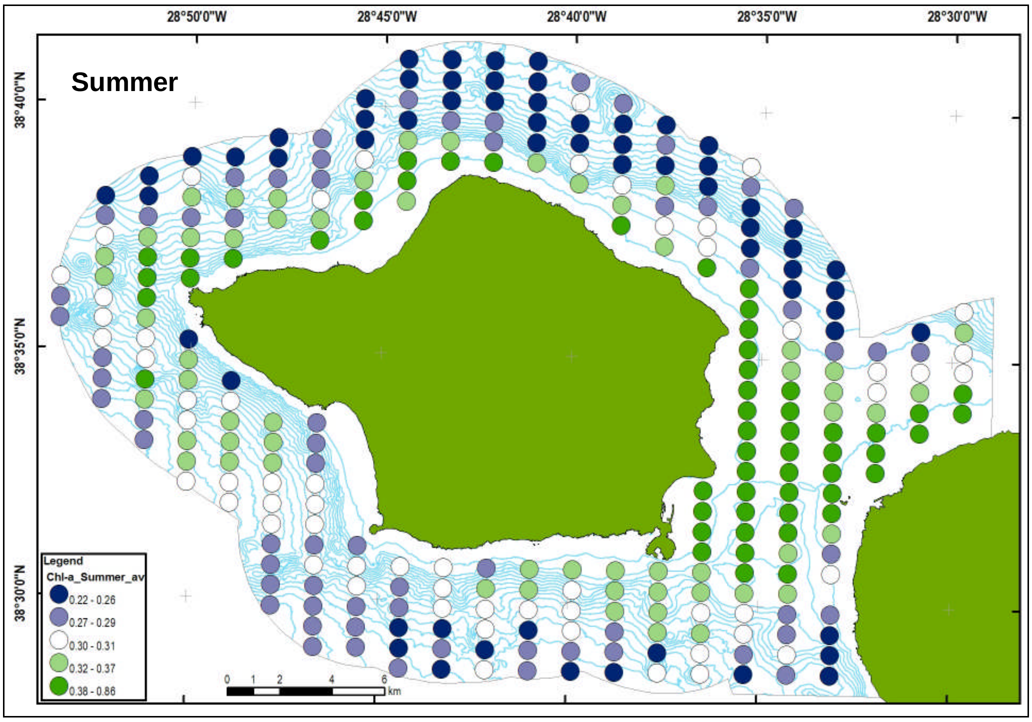

Figure 22: Summer (Jul/Aug/Sep) spatial patterns of chl-*a* concentration around Faial Island. Classes used are established from 20% quantiles due to a skewed data distribution.

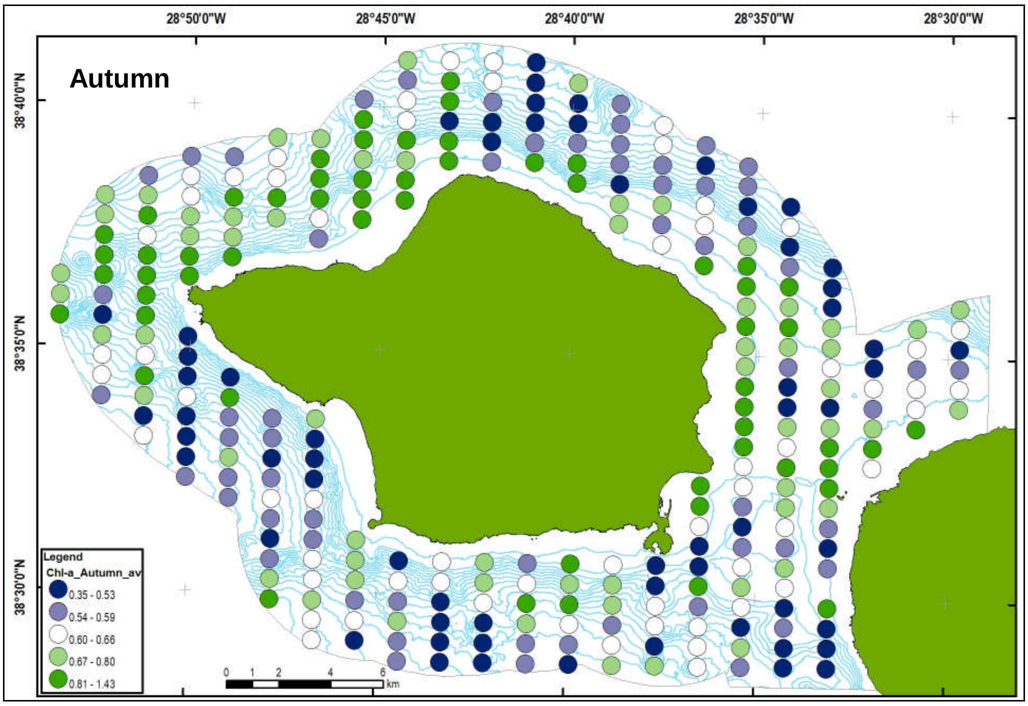

Figure 23: Autumn (Oct/Nov/Dec) spatial patterns of chl-*a* concentration around Faial Island. Classes used are established from 20% quantiles due to a skewed data distribution.

The existence of a shore-normal chl-*a* gradient is investigated through the Pearson correlation obtained from relating the chl-*a* concentration found in each pixel to the distance of the pixel centre to the shoreline (Figure 24). A statistically significant ($p<0.05$) correlation between the two parameters was found in 40 out of the 63 monthly composites available. The correlation averaged -0.23 in the months where statistical significance was found.

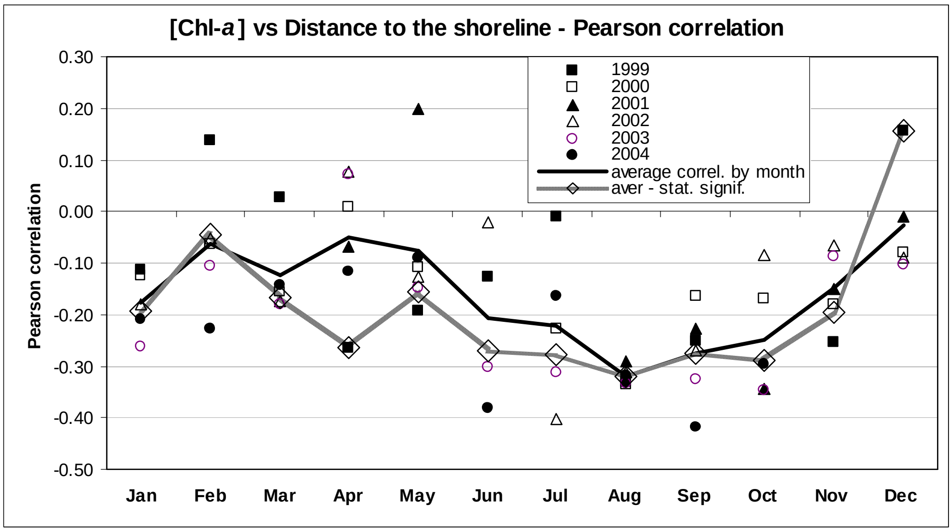

Figure 24: Monthly variation of the correlation between chl-*a* and distance to the shoreline estimated from each monthly composite.

Figure 25 shows the monthly variation of the slopes of regression lines fit to the chl-*a* vs. SST scatterplots obtained from each monthly composite. The overall average of the slopes measured in months where statistical significance was found (40 out of 63) was of -0.050 (i.e., an average decrease of 0.050 chl-*a* mg/m^3 per additional 1,000 m of distance to the shoreline).

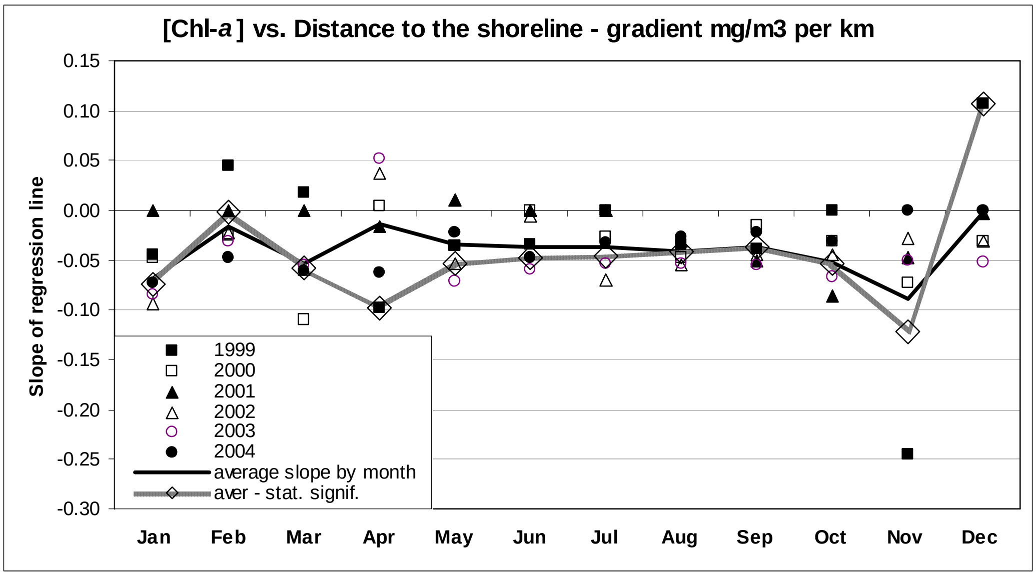

Figure 25: Monthly variation of the shore-normal chl-*a* gradients (linear fit) estimated from each monthly composite.

4.7. Chl-*a* and STT spatial relationship

SST pixels were geographically matched with chl-*a* concentrations by month. The distance between the co-located synchronous values obtained by the spatial join technique averaged a distance of 570 m. The Pearson correlation values between these pairs are plotted in Figure 26 as a function of the month. The calculations were undertaken with the assumption that each pixel represented an independent measure.

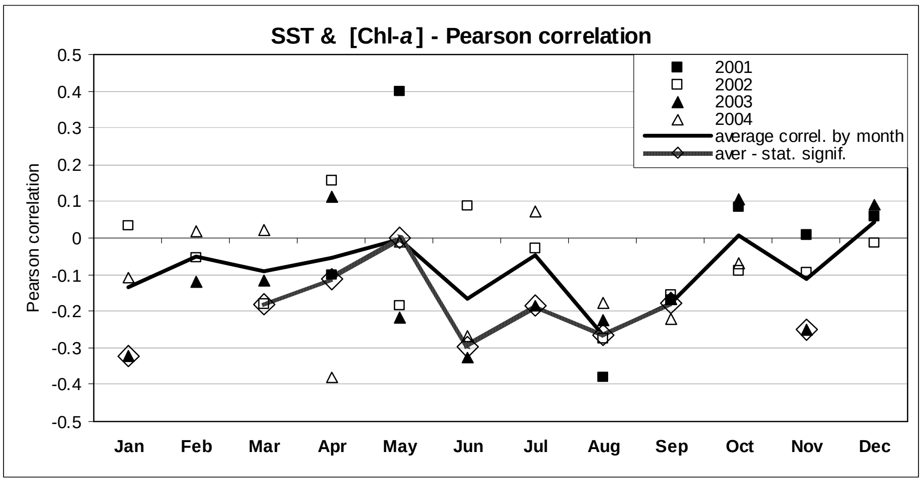

Figure 26: Correlation between SST and chl-*a* on a monthly basis.

Of the 41 months available, a statistically significant ($p<0.05$) correlation between the two parameters was shown in 19 cases. The average of the correlations showing statistical significance was -0.19. August and September showed a statistically significant negative correlation in all the years.

Slopes of regression lines fit to the scatterplots in statistically significant months averaged -0.129 (i.e., an average decrease of 0.129 chl-*a* mg/m^3 per 1ºC increase).

4.8. Neashore SST and chl-*a* extrapolation

Upon visual inspection of the seasonal and annual fields, five areas were recognized as being reasonably homogeneous in terms of pixels presenting comparable nearshore to offshore gradients: Faial N; Passage; Faial S; Faial SW and Faial NW

The scatter plots and regression line formulas obtained for the nearshore-offshore gradients at the different sectors are shown in Figure 27 and Figure 29. The fields with the completed nearshore blanks are shown in Figure 28 and Figure **30**.

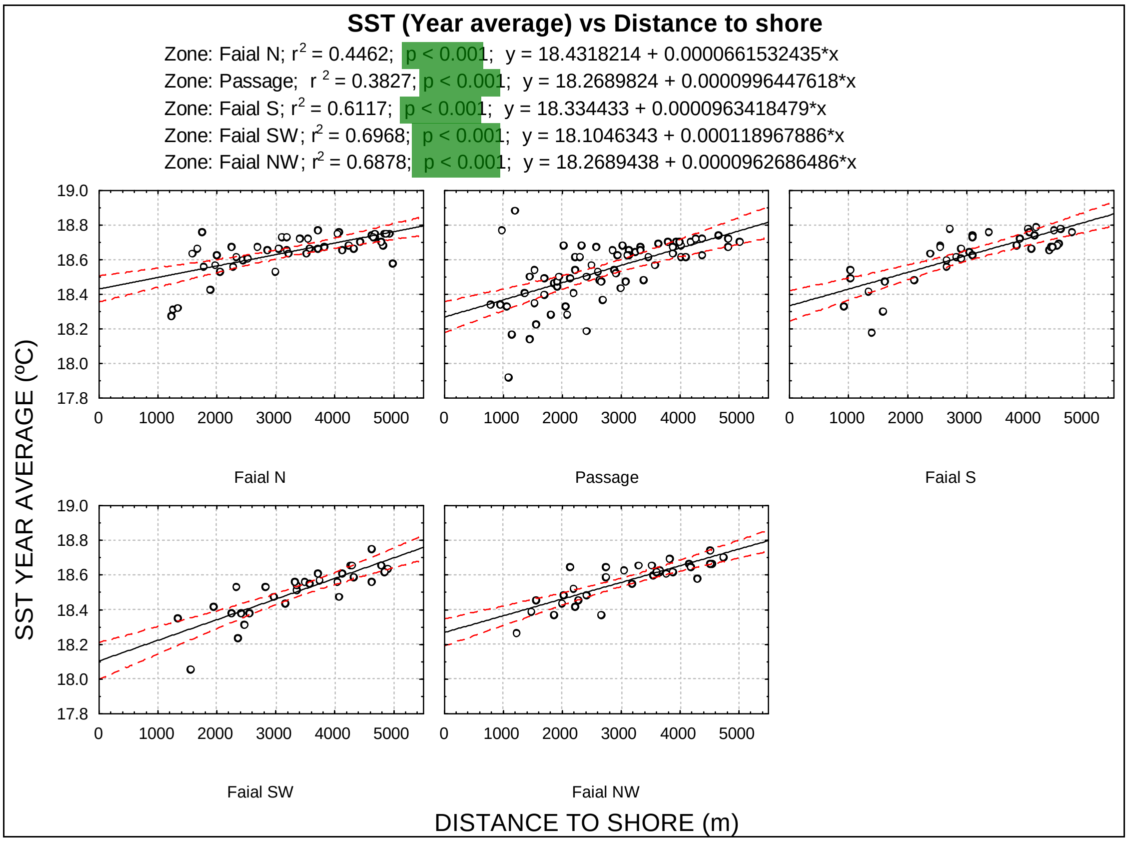

Figure 27: Nearshore-offshore gradients by island sector used to correct nearest neighbour spatial joining of SST values to pixels in nearshore blanks. Regression line formulas with respective goodness of fit index (R²) and statistical significance (p-value) are shown in the header preceding the scatterplots.

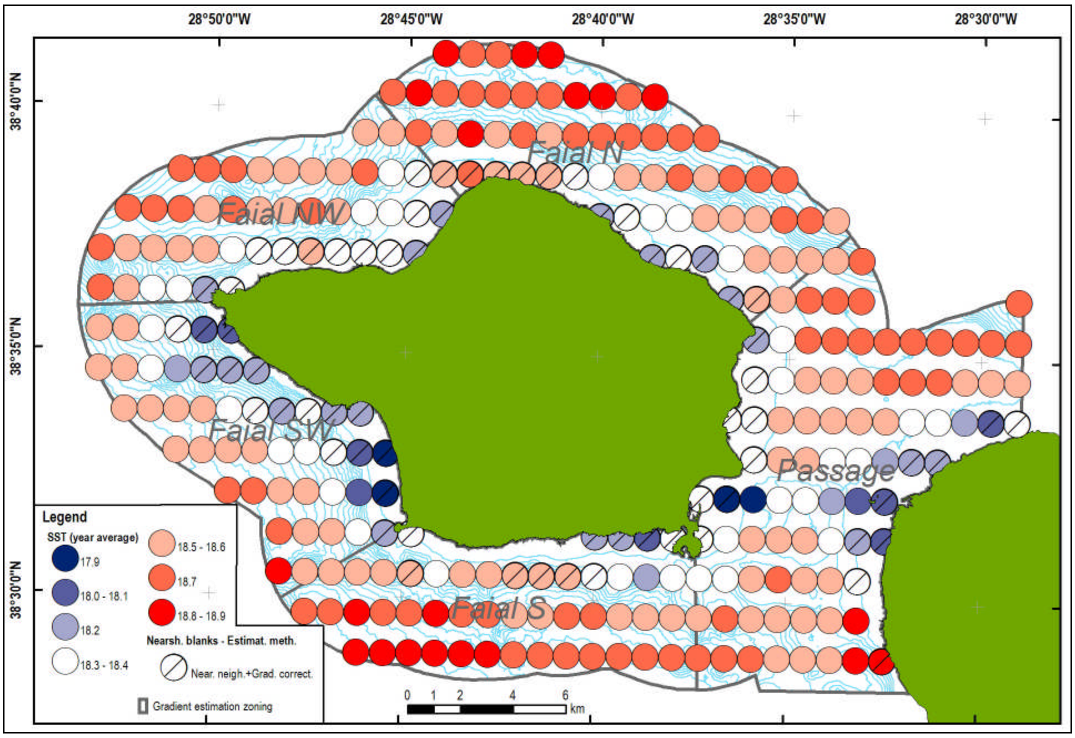

Figure 28: Yearly-averaged fields of SST around Faial Island with nearshore pixels filled by extrapolation. Sectors used to segment the island vicinity for gradient extraction are shown.

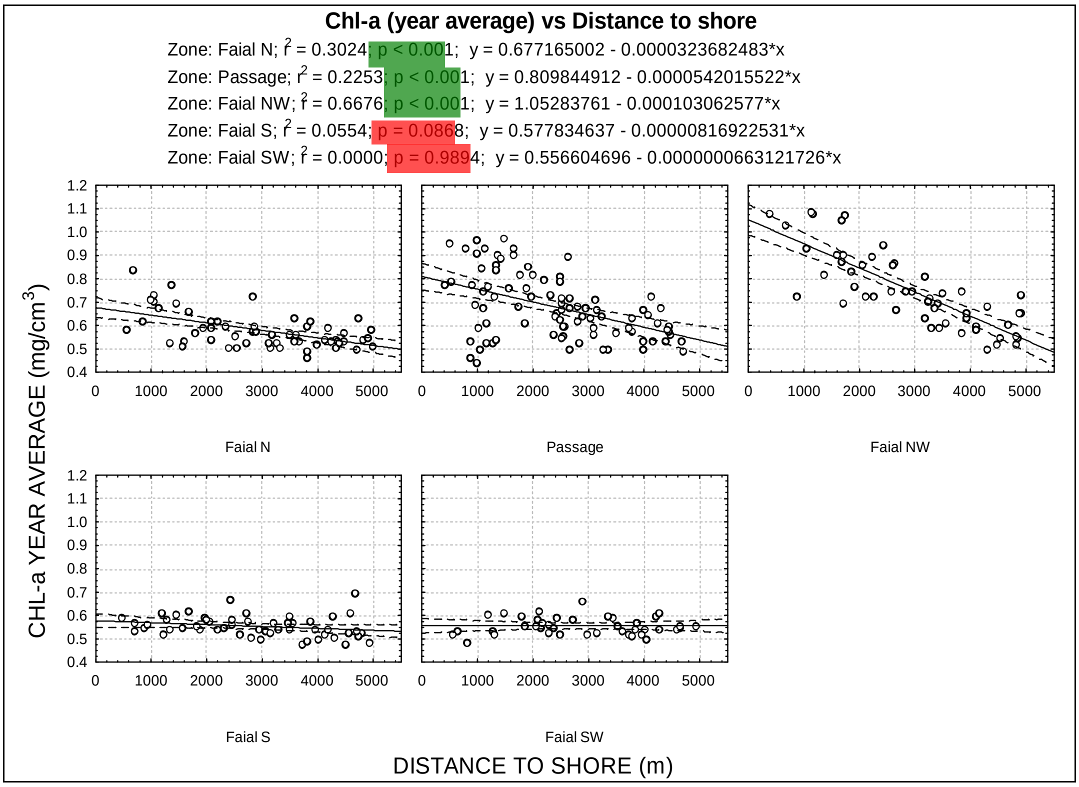

Figure 29: Nearshore-offshore gradients by island sector used to correct nearest neighbour spatial joining of SST values to pixels in nearshore blanks. Regression line formulas with respective goodness of fit index (R^2) and statistical significance (p-value) are shown in the header preceding the scatterplots.

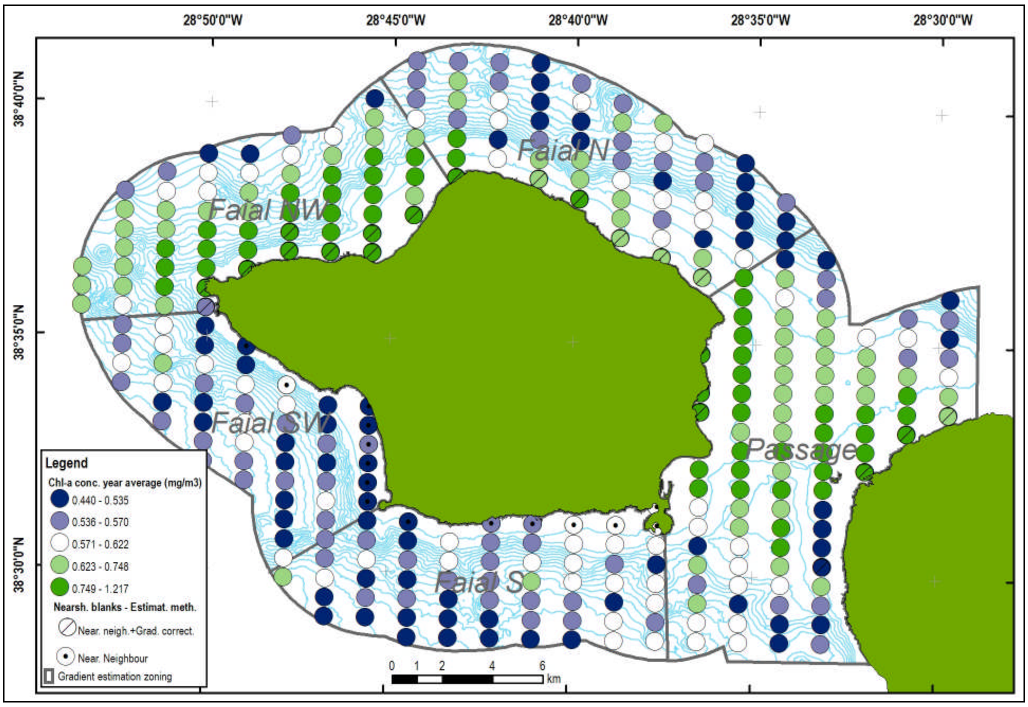

Figure 30: Yearly-averaged fields of SST around Faial Island with nearshore pixels filled by extrapolation. Sectors used to segment the island vicinity for gradient extraction are shown.

Whilst all SST nearshore-offshore gradients were statistically significant, the chl-*a* gradients were not statistical significant for Faial S and Faial SW. In the latter areas, the values obtained for the nearshore blank pixels using the nearest neighbour spatial join were therefore left unchanged.

5. Discussion

Satellite information about temperature and ocean colour around the Azores islands has been accumulating since 2001 as a result of the installation of a HRPT satellite receiving station. Despite the collection of *in situ* measurements of temperature and chlorophyll-*a* concentrations is important to validate the values extracted from satellite-measured radiance, good approximations of the spatial variability of SST and chl-*a* are generally provided by satellite imagery such as AVHRR (see e.g.: Eugenio et al., 2004; Lafon et al., 2004b for the Azores region) and SeaWiFS (Hooker & McClain, 2000; Gregg & Casey, 2004; D'Ortenzio et al., 2002; or Fuentes-Yaco et al., 2005 for general validation; Mendonça et al. (in revision) for validation in the Azores region).

5.1. Impact of clouds in data availability

A compromise between obtaining a good data coverage of the study area and maintaining some temporal resolution was achieved by extracting monthly composites both for SST and chl-*a* (see also Bashmachnikov et al., 2004a). Still the constraints of obtaining sufficient data in a cloud-ridden region could be realized from the average number of *level-2* AVHRR image pixels used to compute each valid monthly composite pixel (maximum: 14.3 in August; minimum: 4.7 in January). If one considers that on average 101 AVHRR images are received each month by the HAZO station (Lafon et al., 2004), the results obtained imply that in the less cloudy months information for each individual pixel is only obtained from 1 out of every 7 images. The issue is naturally amplified in SeaWiFS imagery, where the sensors can only acquire ocean colour data during daytime when sun elevation high enough to properly illuminate the sea surface but not too high to generate major glittering effects. Thus the fact that average *level-2* SeaWiFS pixels integrated in the monthly composite pixels are roughly half of those obtained in AVHRR composites and can reach averages as low as approximately 2 pixels per month in November.

Along with fine scale geolocation uncertainty, the non-application of advanced filtering methods to individual *level-2* images, such as near-cloud pixel erosion (Gonzalez & Woods, 1992; Casey & Cornillon, 1999; Lafon et al., 2004) or a more selective approach such as that of Jones et al. (1996) have introduced unrectified noise in the analysis (e.g., day-night variations, thin undetermined clouds, uniform atmospheric features, sensor biases). This was compensated by applying spatial and statistical filters to the monthly composites that were aimed at eliminating grossly contaminated pixels. The validity of the approach for extracting multi-annual seasonal and annual fields is confirmed by the unambiguous patterns identified, the reduced levels of high-frequency noise and the consistent whole-area annual cycles derived from the monthly data.

In summary, although the filtering used may have not have eliminated all thin cloud contaminated pixels, sensor errors and high SST daytime patches related to no-wind conditions in summer, the errors were probably minimized by the considerable amount of data averaged in the multi-annual seasonal fields (3 months × 5 years).

Since the fields obtained for these environmental factors are to be overlaid and related with biological occurrences in inner shelf environments, an effort was made to retain pixels adjacent to the coastline as long as they survived the filtering procedures. This was not fully successful as a 1 to 3-km wide data gap formed in the immediate nearshore. The decrease in data available towards the shoreline (Figure 4) is likely a combined result of orogenic clouds affecting nearshore pixels (which are eliminated by the cloud filters included in the MCSST algorithm) and/or of the geo-location uncertainty and infra-pixel clouds leading to contaminated composite pixels (which are eliminated by statistical filtering).

5.2. SST climate and inter-annual variations

The monthly oscillation of water temperature was clearly shown in the present study. August and September showed the warmest SST, reflecting the joint effects of summer warming of the upper ocean and reduced wind and wave stress produced by the establishment of the Azores High closest to the archipelago (typically July as indicated by the pressure dataset for Ponta Delgada, Azores at http://www.cru.uea.ac.uk/ftpdata/nao_azo.dat).

On the other hand, March showed the lowest average temperatures, a probable consequence of the preceding winter period when (i) the southern branch of the colder North Atlantic Current has moved closer to the islands, (ii) solar insulation has been restricted for several months and (iii) intense winter winds have produced upper ocean mixing and cooling of the sea surface.

The inter-annual comparison of monthly SST means showed significant variations. However, an investigation of the causes for this variability is beyond the scope of the present work as it would require the assessment of large-scale regimes and fluctuations (e.g., North Atlantic Oscillation) and dynamic oceanographic features (e.g., long-period Rossby waves) that should influence the oceanographic climate of the area.

5.3. SST spatial patterns

A pattern has been clearly identified in the spatial distribution of SST anomalies which should be of ecological importance despite a magnitude ranging only 1.5ºC.

The shallow and narrow passage between the islands of Faial and Pico was consistently noted as an area with temperatures lower than average. It is postulated that this anomaly is produced by intense tidal currents interacting with a rapidly shoaling bathymetry. The result is that cold water from deeper layers is regularly brought up and mixed with the surficial layers within the shallow passage. The vertically-mixed structure is confirmed by CTD profiles (Bashmachnikov, unpublished data). Although persistent throughout all seasons, this effect is particularly noticeable in the summer, when adjacent oceanic waters are typically stratified due to intense warming of the ocean surface layer.

Other negative anomalies (probably resulting from topographically-induced mixing/upwelling) are generally noticeable around Faial's shelf with lower than average values observed in the nearshore contrasting with the close-to-average or positive anomalies found in areas further offshore. This offshore-nearshore gradient was clear throughout spring and summer, but was disrupted in the autumn and winter months, likely as a result of widespread vertical mixing due to storm activity. The patterns formed by negative anomalies around Faial refine indications of topographically-induced cooling obtained at wider spatial scales by Bashmachnikov et al. (2004b).

Of particular note are the enhanced temperatures identified off the north coast of Faial in spring and summer. The establishment of this anomaly coincides with the period where meteorological averages show a balance between the north/north-easterly winds and the otherwise dominant south/southwesterlies. It is postulated that the absence of strong winds from the S-SW octants in spring and summer could relax leeside upwelling off the north and northwest sectors and allow the temporary establishment of warmer surficial waters. This hypothesis is partially supported by the negative anomaly that develops in the summer off SW Faial – possibly a result of upwelling driven by the north and north-easterly winds that become more common in this season. This situation contrasts with the autumn and winter periods when south and south-westerly winds are predominant in frequency and strength. During these periods, leeside upwelling should dominate to the north of the island but decline off the south and southwest sector. The north side would then be comparatively colder in relation to the S-SW sector. The waning of anomalies in value and in spatial extension during autumn and winter is likely a result of the generalized mixing associated with increased storminess and convection.

Due to the scarcity of valid on-shelf pixels and their size, it was not possible to investigate whether the degree of upwelling affecting nearshore areas could also related to differences in island shelf width and profile and in island flank topography.

The low correlations obtained between same month/different year fields is attributed to a combination of considerable interannual variability and high-frequency noise associated with limited data availability caused by island-induced cloud formations, particularly outside summer months. Despite this variance in the averaged-data, the seasonal and annual SST patterns exhibited zonal consistency, which was considered a good indication of the validity of the methodological approach used in extracting multi-annual anomaly fields at annual and seasonal timescales. Furthermore, it should be stressed that the anomalies noted are above the accuracy estimated for AVHRR-derived SST products which is in the order of 0.3ºC (Pichel, 1991; Donlon et al., 1999).

5.4. Chl-*a* climate

Two periods of increased chl-*a* were observed in the spring and autumn but they demonstrated high inter-annual variability. According to Neuer et al. (2007), the distinction between autumn and winter/spring blooms, which constitute the historically well-known seasonal production cycle in typical temperate regions of the North Atlantic, is not evident in subtropical regimes where a bloom in late autumn may merge with the winter maximum. Observations from the current study show that in some years cycles can feature (i) spring and autumn peaks that are barely discernible and (ii) enhanced productivity prevailing from November to March, supporting an interpretation that the Azores show a transitional character between temperate and subtropical regions.

Results that can be compared with those found in the current work are scarce given the focus of previous research in fully oceanic domains of the Azores Current/Subtropical Front system. However, some comparisons can be made with results from other work executed in the North and Northeast sectors of the North Atlantic Subtropical Gyre (Table 4).

Table 4: Comparison of whole-area surface chl-*a* averages (mg/m³) obtained in present study with values determined by previous literature.

Reference	Overall	Season				Measure
		Winter	Spring	Summer	Autumn	
This work						
Faial & Passage	0.60(±0.53)	0.72(±0.49)	0.82(±0.65)	0.32(±0.19)	0.64(±0.57)	Mean(±SD)
Teira et al., 2005						
Temperate (36ºN-44ºN)	0.13(±0.02)	–	0.16(±0.04)	0.05	0.10(±0.01)	Mean(±SE)
Fasham et al., 1985						
Azores Front	-		0.34-0.41			Min-Max
Macedo et al., 2000						
15º mode water domain				0.23(±0.04)		Mean(±SD)
Azores Front				0.18(±0.02)		Mean(±SD)
18º mode water domain				0.15(±0.03)		Mean(±SD)
depth < 25 m				<0.05		Mean(±SD)
Couto, 2004						
Sedlo seamount	0.35					Mean

From the table it can be noted that the surface chl-*a* concentrations derived from this study are 4 to 6 times larger than those obtained from *in situ* measurements reported for other parts of the Azores region. They are also higher than the average annual chl-*a* concentration reported in the study by Couto (2004) of the Sedlo Seamount, which was also based on analysis of SeaWiFS imagery.

Three main factors should explain this discrepancy. (1) The coastal waters around the island are possibly subject to more regular and intense upwelling than full oceanic waters (even if these represent frontal regions or are influenced by a seamount). Upwelling and tidal mixing can be as regular as the tides in the case of the interisland passage and protruding shelf areas. A sustained enhanced primary productivity should be induced by this permanent introduction of nutrients into the euphotic zone over shelf areas. (2) On a technical tier, it should be considered that methods applied to estimate pigment concentrations are not always accurate, particularly in coastal regions. Contamination by terrigenous or re-suspended sediments may induce artificially high radiance which the processing algorithm cannot spectrally differentiate from chl-*a*. (3) Last but not least, the discrepancy in spatio-temporal scales at which *in situ* and satellite-based sampling are made should be taken into account. While the literature data are drawn from studies based on single point instantaneous samples taken from a few litres of water, the satellite estimates are based on sensors that take averages over pixels representing a minimum area of approximately 1 km^2 (Holm-Hansen et al., 2004). In the present case these effects may have been further confounded by the fact that satellite data were composited at monthly scales and averaged at seasonal or annual scales.

An inter-annual comparison of spring chl-*a* maxima showed considerable variation, with the spring periods of 2002 and 2003 exhibiting the highest chl-*a* concentrations in the period analysed. The analysis of a longer time series is suggested to corroborate possible linkages between climate anomalies and oscillations in phytoplankton production. Further research should also collate contemporaneous weather observations and assess the potential role of winds/storms as regulating factors of bloom variability.

5.5. Chl-*a* spatial patterns

The existence of a zonation of surface chl-*a* is clear both in the annual and seasonal fields extracted from the monthly averages. Enhanced chlorophyll concentrations were found within the passage, to the NW of Faial and along a narrow fringe along the island's northern shore. Although these SeaWiFS-derived results are interpreted as reflecting mostly chl-*a* concentrations associated with phytoplankton, it has been previously noted that SeaWiFS data is limited with respect to resolving chl-*a* concentrations where they concur with suspended sediments (e.g., Wozniak & Stramski, 2004) or coloured dissolved organic matter (e.g.: Carder et al., 1989; Harding et al., 2005). Given the coastal context of the present study and absence of ground-truthing, the spectral interference of coloured materials with chl-*a* within the satellite imagery cannot be discarded, as the areas of alleged enhanced productivity coincide with those most exposed either to intense tidal currents (Faial-Pico passage and island corners) or to prevailing swells (NW and N coasts).

As with SST results, the low correlations obtained between same month/different year fields is attributed both interannual variability and high-frequency noise associated with limited data availability caused by island-induced cloud formations, particularly outside summer months.

5.6. Chl-a and STT spatial relationship

An indication that the enhanced chl-*a* areas identified around Faial's coast may not represent an artefact from swell or current-induced sediment re-suspension as suggested just above is provided by the inverse relationship between chl-*a* concentrations and SST prevailing in most months (section 4.7) and the temperatures gradients observed towards the shoreline (section 4.4).

The combination of these facts suggests a regime of coastal upwelling (induced by both tidal currents moving over rough and shoaling topography) and seasonal wind-induced leeside upwelling (when offshore winds lower the water surface on the island lee and subsurficial waters upwell to compensate for the loss of mass at the surface). The nutrients regularly input by these processes into shallow waters likely promote a sustained phytoplankton production in the island vicinity, explaining the persistence of higher chl-*a* concentrations in certain sectors of the study area throughout all seasons.

It is likely that the correlation level between the chl-*a* concentrations and SST would increase if this relationship was investigated using data with a higher temporal resolution (e.g., weekly-averaged pixels), as the upwelling episodes and the subsequent phytoplankton increases typically occur with one to several days difference (Lalli & Parsons, 1997). The fact that a considerable part of the signal was lost as data were temporally averaged at monthly scales may explain why statistically significant negative correlations were found in only 19 out of 41 cases.

Finally it is worth-noting that a possible mechanism involved in the retention of the plankton in certain sectors that are subject to potentially dispersive factors such as tidal and swell-induced currents has been presented by Mace and Morgan (2006). It consists of residual circular currents that form in the lee of coastal headlands thereby tending to maintain water masses and associated features in certain areas.

5.7. Nearshore gap extrapolation

Given the narrowness of the island shelves the nearshore gap typically precludes data being available for most shelf areas outside the interisland passage. An attempt to address this shortcoming was made by extrapolating the missing values of the nearshore pixels from the nearest neighbouring pixels and compensating for offshore-nearshore gradients.

The linear gradients used are a simplification that needs to be validated by *in situ* data as it is known that the shallower the water bodies get the higher surface to volume ratio they will have, which makes them more prone to faster air-sea heat changes, leading to enhanced cooling in winter and warming in Summer (e.g., Pearce et al., 2006). The scrutiny of whether the multiannual SST and chl-*a* fields with extrapolation of the nearshore blanks provide significant explanatory variables for the distribution of benthic species around Faial is conducted by the statistical modelling presented in Chapter 7.

6. Conclusions

The results obtained are of particular relevance given the spatio-temporal information they provide about oceanographic patterns that may be regulating the occurrence and composition of biological assemblages found in the vicinity of the island and are relevant in terms of ecological studies, conservation initiatives and/or fishery management.

This study has demonstrated that satellite imagery acquired at the HAZO station can be successfully used to derive information about oceanographic patterns in the island vicinity, where *in situ* oceanographic records are lacking to produce a spatio-temporal model of the thermal and ocean colour variability. Despite limitations of data availability at sub-monthly time scales caused by cloud cover, AVHRR and SeaWiFS monthly-averaged composites still provided enough data to identify consistent temporal cycles and first order approximations of the spatial variability of seawater sea surface temperature (SST) and chlorophyll-*a* (chl-*a*) concentration around shelf areas.

Yearly cycles of surface chl-*a* were consistent with the two-annual-blooms temperate regime. However, individual years showed some affinities with a subtropical regime by showing spring peaks barely discernible from winter levels and autumn maxima comparable to winter chl-*a* levels.

SST fields demonstrate that a negative temperature anomaly prevails within the inter-island passage throughout all seasons, with the strongest expression during the spring. Seasonal variations elsewhere were related to variations in the wind stress. Autumn and winter showed the least developed zonation because of the well-mixed conditions resulting from enhanced wind and swell stress. Contrastingly, spring and summer fields exhibited a more structured zonation. A negative SST anomaly forms off south-western Faial that is likely promoted by the relative increase of north and north-easterly winds observed during these months. On the opposite sectors of the island (N and NW) a wide positive temperature anomaly appears that is likely related to the coupled relaxation of south and southwesterly winds. This positive anomaly sector is broken up in autumn and winter when leeside upwelling is re-established off the northern shore.

Chl-*a* patterns were less variable throughout the year than SST ones. Enhanced chl-*a* concentrations were consistently observed in an extensive zone off northwestern Faial, the inter-island passage and in a narrow fringe along Faial's northern shore. The high chl-*a* concentrations generally coincided with areas of negative SST anomalies suggesting that mixing and upwelling effectively input nutrients into shallow waters which regularly stimulate a sustained phytoplankton production. These regimes are either (i) topographically-induced when tidal currents move over shoaling topography (such as over the shelf and in particular in the interisland passage) or (ii) wind-induced in the case of leeside upwelling. The mild enhancements of chl-*a* reported off SW and SE Faial in summer are suggested as a result of the latter case, as they appear in connection with a negative SST anomaly and a relative increase in the north and north-easterly winds.

Overall the SST and chl-*a* patterns suggest that effects usually associated with islands namely topographically-induced mixing/upwelling and wind-induced leeside upwelling are in operation on the immediate vicinity of Faial island and have a role in its oceanographic zonation.

Finally the need to conduct ground-truthing of the algorithms used to extract remotely sensed information around the Azores is noted as it would validate the data analysed, namely chl-*a* concentrations. The need to use imagery from sensors providing higher resolution is also highlighted since this would approach the scale at which biological data have been collected.

7. References

Alves, M., & A.C. de Verdière (1999). Instability dynamics of a subtropical jet and applications to the Azores front current system: eddy-driven mean flow. *Journal of Physical Oceanography*, 29: 837-864.

Alves, M., F. Gaillard, M. Sparrowm M. Knoll & S. Giraud (2002). Circulations patterns and transport of the Azores Front-Current system. *Deep Sea Research II*, 49: 3,983-4,002.

AVISO dataset (as in October 2007). Merged geostrophic currents. http://atoll-motu.aviso.oceanobs.com/?action=productdownloadhome&service=Aviso_dt&product=dt_ref_global_merged_madt_uv.

Bashmachnikov, I., V. Lafon & A. Martins (2004a). SST stationary anomalies in the Azores region. *Remote Sensing of Ocean and Sea Ice*. Proceedings of SPIE, 5569: 148-155.

Bashmachnikov I., V. Lafon & A. Martins (2004b). Sea surface temperature distribution in the Azores region. Part II: space-time variability and underlying mechanisms. *Arquipélago*. Life and Marine Sciences, 21A: 19-32.

Campbell, J.W., & J.E. O'Reilly (1988). Role of satellites in estimating primary production on the northwest Atlantic continental shelf. *Continental Shelf Research*, 8: 179-204.

Campbell, J.W., & T. Aarup (1992). New production in the North Atlantic derived from seasonal patterns of surface chlorophyll. *Deep-Sea Research*, 39: 1,669-1,694.

Carder, K.L., R.G. Steward, G.R. Harvey & P.B. Ortner (1989). Marine humic and fulvic acids: their effects on remote sensing of ocean chlorophyll. *Limnology and Oceanography*, 34: 68-81.

Casey, K.S., & P. Cornillon (1999). A comparison of satellite and *in situ*-based sea surface temperature climatologies. *Journal of Climate*, 12: 1,848-1,862.

Cipollini, P., D. Cromwell, M.S. Jones, G.D. Quartly & P.G. Challenor (1997). Concurrent altimeter and infrared observations of Rossby wave propagation near 34°N in the Northeast Atlantic. *Geophysical Research Letters,* 24(8): 889-892.

Couto, A. (2004). Estudo da Variabilidade Superficial em Mesoscala dos Montes Submarinos Sedlo e Seine (Nordeste Atlântico) através da Utilização de Imagens de Satélite NOAA (SST) e SeaStar (OC). *Licenciatura thesis*. University of the Azores, Ponta Delgada.

Davenport, R., S. Neuer, P. Helmke, J. Perez-Marrero & O. Llinas (2002). Primary productivity in the northern Canary Islands region as inferred from SeaWiFS imagery. *Deep-Sea Research II*, 49(17): 3,481-3,496.

D'Ortenzio, F., S. Marullo, M. Ragni, M. Ribera d'Alcalá & R. Santoleri (2002). Validation of empirical SeaWiFS algorithms for chlorophyll-a retrieval in the Mediterranean Sea: A case study for oligotrophic seas. *Remote Sens. Environ.*, 82: 79-94.

Efthymiadis, D., F. Hernandez & P. Le Traon (2002). Large-scale sea level variations and associated atmospheric forcing in the subtropical North-East Atlantic Ocean. *Deep Sea Research II*, 42: 3,957-3,981.

Eugenio, F., J. Marcello & E. Rovaris (2004). Validation of MODIS and AVHRR sea surface temperature using bulk measurements. *Remote Sensing of Ocean and Sea Ice*. Proceedings of SPIE, 5569: 78-86.

Figueiredo, M., A. Martins, P. Castellanos, A. Mendonça, L. Macedo, M. Rodrigues, V. Lafon & N. Goulart (2004). HAZO: A software package for automated AVHRR and SeaWiFS acquisition and processing. *Arquivos do DOP*. Série Relatórios Internos, no. 3/2004: 89 pp.

Fratantoni, D.M. (2001). North Atlantic surface circulation during the 1990's observed with satellite-tracked drifters. *Journal of Geophysical Research,* 106(C10): 22,067-22,094.

Fuentes-Yaco, C., E. Devred, S. Sathyendranath, T.Platt, L. Payzant, C. Caverhill, C. Porter, H. Maass & N. George (2005). Comparison of in situ and remotely-sensed chlorophyll-a in the Northwest Atlantic. *Indian Journal of Marine Science,* 34 (4): 341-355.

Gonzalez, R. & R. Woods (1992). *Digital Image Processing.* Addison-Wesley Publishing Company. 716 pp.

Gould, W.J. (1985). Physical Oceanography of the Azores Front. *Progress in Oceanography*, 14: 167-190.

Gregg, W. W. & N. W. Casey (2004). Global and Regional Evaluation of the SeaWiFS Chlorophyll Data Set. *Remote Sens. Environ.*, 93: 463-479.

Harding, L.W., A. Magnuson & M.E. Mallonee (2005). SeaWiFS retrievals of chlorophyll in Chesapeake Bay and the mid-Atlantic Bight. *Estuarine, Coastal and Shelf Science*, 62: 75-94.

Holm-Hansen, O., M. Kahru, C.D. Hewes, S. Kawaguchi, T. Kameda, V.A. Sushin, I. Krasovski, J. Priddle, R. Korb, R.P. Hewitt, B.G. Mitchell (2004). Temporal and spatial distribution of chlorophyll-*a* in surface waters of the Scotia Sea as determined by both shipboard measurements and satellite data. *Deep-Sea Research II*, 51: 1323-1331.

Hooker, S.B., & C.R. McClain (2000). The calibration and validation of SeaWiFS data. *Progress in Oceanography*, 45(3-4): 427-465.

Joint, I., S.B. Groom, R. Wollast, L. Chou, G.H. Tilstone, F.G. Figueiras, M. Loijens & T.J. Smyth (2002). The response of phytoplankton production to periodic upwelling and relaxation events at the Iberian shelf break: estimates by the ^{14}C method and by satellite remote sensing. *Journal of Marine Systems*, 32(1-3): 219-238.

Jones, M.S., M.A. Saunders & T.H. Guymer (1996). Global remnant cloud contamination in the along-track scanning radiometer data: Source and removal. *Journal of Geophysical Research*, 101(C5): 12,141-12,148.

Klein, B., & G. Siedler (1989). On the origin of the Azores Current. *Journal of Geophysical Research*, 94: 6,159-6,168.

Lafon, V., A. Martins, I. Bashmachnikov, F. José, M. Melo-Rodriguez, M. Figueiredo, A. Mendonça & L. Macedo (2004a). SST variability in the Azores region using AVHRR imagery: regional to local scale study. *Remote Sensing of Ocean and Sea Ice*, Proceedings of SPIE, 5569: 130-139.

Lafon, V., A. Martins, M. Figueiredo, M.A.M. Rodrigues, I. Bashmachnikov, A. Mendonça, L. Macedo & N. Goulart (2004b). SST distribution in the Azores. Part I: AVHRR imagery and *in situ* data processing. *Arquipélago*. Life and Marine Sciences, 21A: 1-18.

Lalli, C.M., & T.M. Parsons (1997). *Biological Oceanography: An Introduction.* 2nd ed. Butterworth-Heinemann for the Open University, Oxford. 314 pp.

Le Traon, P.-Y., & P. De Mey (1994). The eddy field associated with the Azores Front east of the Mid-Atlantic ridge as observed by the Geosat altimeter. *Journal of Geophysical Research*, 99(C5): 9,907-9,924.

Longhurst, A. (1998). *Ecological Geography of the Sea.* Academic Press, San Diego. 398 pp.

Mace, A.J., & S.G. Morgan (2006). Biological and physical coupling in the lee of a small headland: contrasting larval transport mechanisms in an upwelling region. *Marine Ecology Progress Series*, 324: 185-196.

Macedo, M.F., P. Duarte, J.G. Ferreira, M. Alves, & C. Valentina (2000). Analysis of the deep chlorophyll maximum across the Azores Front. *Hydrobiologia*, 441(1-3): 155-172.

Maillard, C. (1986). *Atlas hydrologique de l'Atlantique Nord-Est*. Publications IFREMER. 253 pp.

Martins, A., I. Bashmachnikov, V. Lafon, A. Mendonça, F. José, M. Figueiredo & L. Macedo (2004). Discovering the Azores Front/Current System with SeaWiFS Imagery. *Remote Sensing of Ocean and Sea Ice*. Proceedings of SPIE, 5569: 156-167.

McClain, E.P., W.G. Pichel & C.C. Walton (1985). Comparative performance AVHRR-based multichannel sea surface temperatures. *Journal of Geophysical Research*, 90: 11,587-11,601.

Mendonça A., A. Martins, M. Figueiredo, I. Bashmachnikov, A. Couto, V. Lafon & J. Aristegui (in revision). Evaluation of Ocean Colour and Sea Surface Temperature sensors algorithms using *in situ* data: A case study of temporal and spatial variability on two Northeast Atlantic seamounts. *Journal of Applied Remote Sensing*.

Menge, B.A., B.A. Daley, P.A. Wheeler, E. Dahlhoff, E. Sanford & P.T. Strub (1997). Benthic–pelagic links and rocky intertidal communities: Bottom-up effects on top-down control? *Proceedings of the National Academy of Sciences U.S.A.*, 94: 14,530-14,535.

Menge, B.A., J. Lubchenco, M.E.S. Bracken, F. Chan, M.M. Foley, T.L. Freidenburg, S.D. Gaines, G. Hudson, C. Krenz, H. Leslie, D.N.L. Menge, R. Russell & M.S. Webster (2003). Coastal oceanography sets the pace of rocky intertidal community dynamics. *Proceedings of the National Academy of Sciences*, 100(21): 12,229-12,234.

Mouriño, B., E. Fernández & M. Alves (2004). Thermohaline structure, structure, ageostrophic vertical velocity fields and phytoplankton distribution and production in the North East Atlantic subtropical front. *Journal of Geophysical Research*, 109(C04020).

Mouriño, B., E. Fernández, R. Pingree, B. Sinha, J. Escánez & D. Armas (2005). Constraining effect of mesoscale features on carbon budget of photic layer in the NE subtropical Atlantic. *Marine Ecology Progress Series*, 287: 45-52.

Neuer, S., A. Cianca, P. Helmke, T. Freundenthal, R. Davenport, H. Meggers & M. Knoll (2006). Biogeochemistry and hydrography in the eastern subtropical North Atlantic gyre. Results from the European time-series station ESTOC. *Progress in Oceanography*, 72: 1-29.

Onken, R. (1993). The Azores Countercurrent. *Journal of Geophysical Research,* 23: 1,638-1,646.

OSPAR (2000). *Quality status Report 2000, Region V – Wider Atlantic*. OSPAR Commission, London. 110 + xiii pp.

Pearce, A., F. Faskel & G. Hyndes (2006). Nearshore sea temperature variability off Rottnest Island (Western Australia) derived from satellite data. *International Journal of Remote Sensing*, 27: 2503-2518.

Pingree, R.D. (1997). The eastern subtropical gyre (North Atlantic): Flow rings recirculations structure and subduction. *Journal of the Marine Biological Association of the United Kingdom,* 77: 573-624.

Pingree, R.D. (2002). Ocean structure and climate (Eastern North Atlantic): *in situ* measurement and remote sensing (altimeter). *Journal of the Marine Biological Association of the United Kingdom*, 82: 681-705.

Santos, R.S., S.J. Hawkins, L.R. Monteiro, M. Alves & E.J. Isidro (1995). Marine Research, Resources and Conservation in the Azores. *Aquatic Conservation: Freshwater and Marine Ecosystems*, 5(4): 311-354.

Schiel, D.R. (2004). The structure and replenishment of rocky shore intertidal communities and biogeographic comparisons. *Journal of Experimental Marine Biology and Ecology*, 300: 309-342.

Siedler, G. & R. Onken (1996). Eastern Recirculation. In: Krauss, W. (ed.). *The Warmwatersphere of the North Atlantic Ocean*. Gebrüder Borntraeger, Berlin. pp. 339-364.

Solanki, H.U., R.M. Dwivedi & S.R. Nayak (2001). Synergistic analysis of SeaWiFS chlorophyll concentration and NOAA-AVHRR SST features for exploring marine living resources, *International Journal of Remote Sensing*, 22 (18): 3877-3882.

Teira, E., B. Mouriño, E. Marañón, V. Pérez, M.J. Pazó, P. Serret & E. Fernández (2005). Variability of chlorophyll and primary production in the Eastern North Atlantic subtropical gyre: potential factors affecting phytoplankton activity. *Deep-Sea Research I*, 52: 569-588.

Tempera, F., P. Afonso, T. Morato, S. Gubbay, T. Dentinho, M. Silva, R. Prieto, F. Cardigos, M.J. Pitta & R.S. Santos (2001). Proposta Técnico-Científica de Gestão dos Sítios de Interesse Comunitário do Canal Faial-Pico. Departamento de Oceanografia e Pescas da Universidade dos Açores, Horta. *Arquivos do DOP*. Série Relatórios Internos, nº 8/2001, viii+76 pp.

Wozniak, S.B., & D. Stramski (2004). Modeling the optical properties of mineral particles suspended in seawater and their influence on ocean reflectance and chlorophyll estimation from remote sensing algorithms. *Applied Optics*, 43: 3,489-3,503.

8. Acknowledgements

To Igor Bashmachnikov for his collaboration and suggestions, which improved significantly the quality of this chapter.

Ana Martins is acknowledged for providing the satellite imagery held at DOP/UAç and advise in remote sensing issues.

Miguel Figueiredo is acknowledged for extracting the satellite imagery and providing thorough information on the HAZO processing package.

Fernando Tempera was financed by a PhD grant from the Fundação para a Ciência e a Tecnologia (ref: SFRH/BD/12885/2003).

Others were supported by project DETRA (RAA-SRAPA/DRP 2000-2003) and own funds from the IMAR Centre at the University of the Azores.

The AVISO altimetric products were produced by SSALTO/DUACS and distributed by AVISO with support from CNES.

CHAPTER 7

PREDICTIVE MODELLING OF CHARACTERISTIC ALGAE DISTRIBUTIONS AROUND FAIAL ISLAND AND NEIGHBOURING PASSAGE (AZORES, NE ATLANTIC)

Abstract

Models that predict dominant species distributions based on a limited number of ecologic parameters are widely required to inform decisions regarding the conservation of both biodiversity and essential habitats for species of commercial or touristic interest. This work brings together for the first time quantitative species distribution information assembled under projects MARÉ, OGAMP and MARMAC by SCUBA diving, remote operated vehicle and drop down camera surveys executed on rocky infralittoral habitats in the archipelago of the Azores.

The chapter focuses on developing ordered logistic regression models for the variation of the abundance of a selection of macroalgae that dominate rocky infralittoral biotopes around Faial island. The combinations of major environmental variables (depth, slope, swell exposure, maximum tidal currents, sea surface temperature and chlorophyll-*a* concentration) that best explain the variation are found for six *taxa*: articulated Corallinaceae, *Codium elisabethae*, *Dictyota* spp., *Halopteris filicina*, *Padina pavonica* and *Zonaria tournefortii*.

Depth was consistently significant for all the species, highlighting its importance as a major environmental regulating factor for macroalgae. Slope was non-significant only for *P. pavonica*, confirming the influence of bottom physiography in the distribution of macroalgae. Exposure to swell was significant to articulated Corallinaceae and *H. filicina*. Exposure to currents was significant to articulated Corallinaceae, *C. elisabethae* and *P. pavonica*. Chlorophyll-*a* was significant for articulated Corallinaceae and *P. pavonica* and could indicate cases of "bentho–pelagic coupling". Sea surface temperature was non-significant for all the species, suggesting that either macroalgae abundance does not respond to water temperature at the range of variation found in the study area or that satellite-derived measurements may not provide a good proxy for temperature conditions at a benthic level.

Despite the generally low R^2 values that characterize the final models, the equations obtained are used to spatialize the distribution of the abundance of the six macroalgae for the rocky

seafloor around Faial on the basis of the raster fields of the environmental variables found to be statistically significant. A physical substrate map is used as the analysis mask to constrain representation of the results to rocky substrates. The continuous rasters obtained are the first maps that predict the distribution of infralittoral macroalgae abundances and facies around islands of the Azores.

Keywords: infralittoral dominant macroalgae, abundance, statistical models, predictive distribution maps, Faial island, Azores.

TABLE OF CONTENTS

1. Introduction

Due to the volcanic origin and young geologic age of the Azores archipelago, hard substrates are major components of the islands coastal areas. Their solid and often complex physiography typically correlates hard substrates with high levels of epibenthic biodiversity and attracts many mobile species, including most species of commercial interest. As a result, hard substrates are of great significance both to management of fishery resources and marine conservation, thus having been classified under Annex I of the EU Habitats and Species Directive as one of the habitats to protect (see "reefs" habitat - code 1170).

High resolution maps of the location and geomorphologic diversity of rocky habitats on the shelf around Faial island and western Pico were recently obtained from swath sonar surveys. This information provides a remarkable opportunity to map the distribution of benthic species, such as macroalgae, which are mostly limited to rocky seafloor areas.

Since the study of the marine algal flora of the Azores began around 150 years ago (Tittley & Neto, 1995), a total of 368 species of macroalgae has been recorded and further additions are under investigation (Tittley & Neto, 2005). An evolution in research lines is noticeable over the past two decades, with studies gradually changing from a taxonomic perspective to one with a more ecologic outlook, explicitly aimed at describing zonation patterns (e.g., Neto, 1992; Tittley & Neto, 1995; Neto, 1997; Tittley et al., 1998).

Menge et al. (1997a) have suggested that understanding the factors that determine, and ultimately help predict, community structure is a recurring challenge to ecologists in both natural and managed communities. This emphasis is clear in the most recent works conducted on the shore communities of the Azores, which focus on assemblage structure and on delineating algae-based biotopes (Tittley & Neto, 2000; Wallenstein & Neto, 2006; Wallenstein et al., 2007). Results indicate that only a limited number of species is relevant for biotope definition in the Azores and consequently interest has grown in producing models that predict macroalgae distributions based on a limited number of ecologic parameters (Azevedo et al., 2002). In relation to this, it is worth-noting that there is a strong case for making these statistical models of the distribution of species or algal-dominated assemblages spatially-explicit – an end result that has been virtually absent in the literature regarding the environments found around the Azores coasts.

By focusing on conspicuous characteristic species, quantitative visual surveys of benthic species can provide valid data for biotope analysis (e.g., Gamble, 1984; Connor & Hiscock, 1996; Kinsford & Battershill, 1998) and are most suitable to clear waters such as those of the Azores. However, the same conditions that favour water transparency also allow the belt dominated by frondose algae (i.e., the infralittoral zone) to extend down to depths greater than 40 m thus making these assemblages only partially accessible to direct observations by SCUBA divers (Holt & Sanderson, 2001a), whose work is severely limited at depths beyond 30m. Video-assisted technologies such as remotely operated vehicles, or ROVs (Howson & Davison, 2000), and drop-down camera (Holt & Sanderson, 2001b) are therefore required to survey the full infralittoral extent and collect observations of the conspicuous biota down to its deepest areas.

This work brings together for the first time the wealth of quantitative species distribution information assembled under projects MARÉ, OGAMP and MARMAC by SCUBA diving, ROV and drop-down camera surveys executed on infralittoral rocky bottoms. The comprehensive range of samples, in conjunction with information on several major environmental variables frequently involved in determining biologic communities, represent an exceptional opportunity to develop spatially-explicit predictive models of the distribution of species that dominate the composition of benthic infralittoral biotopes in the Azores.

For these reasons, the main objectives of this paper are:

- to identify which major environmental variables influence the distribution of six macroalgae characteristic of rocky infralittoral biotopes;
- to develop predictive models of the distribution of the selected six macroalgae based on these environmental variables;
- to spatially represent the predictive models for the rocky seafloor around Faial island and neighbouring passage using the statistical model equations upon continuous raster fields for the environmental variables found to be statistically significant.

From a review of possible statistical modelling approaches (namely Guisan & Zimmermann, 2000; Borooah, 2001; Ferrier et al., 2002; Guisan et al., 2002) ordered logistic regression models were chosen as an appropriate statistical modelling framework. The potential explanatory variables were collated from previous chapters (seafloor nature, depth, slope, SST and chl-*a* concentration) together with two additional variables introduced in this chapter that result from simple GIS analyses (swell exposure) and oceanographic models (maximum tidal currents).

1.1. Target species

Algal assemblages around Faial are dominated by calcareous red algae, brown algae and less frequently by green algae. Six *taxa* belonging to these algal groups and reaching their peak abundance at different depths were selected for the analysis. All of these *taxa* dominate the composition of some of the benthic infralittoral biotopes found in the Azores and, in cases such as that of the articulated Corallinacea, the species play an important functional role by providing the structural matrix around which the assemblage develops.

The species in question are all easily identified *in situ* and are conspicuous videographically, allowing comparable abundance information to be extracted from both SCUBA diving observations and ROV and drop-down camera surveys.

1.1.1. Articulated Corallinacea algal turf

Articulated Corallinaceae are calcareous red algae (Rhodophyta, Corallinales) with an erect habit that dominate one of the most common algal assemblages of the Azores infralittoral areas: the *coralline algal turf* (Tittley & Neto, 2000). Typically, articulated Corallinaceae form the rock-attached matrix for an algal turf composed of a mixture of different small-sized algal thalli growing in a dense, short and entangled mat, which is difficult to separate into its various components and externally uniform in appearance (Figure 1-A). This mat comprises Corallinaceae of the genera *Corallina, Jania, Amphiroa* and *Haliptylon*, as well as a variety of filiform Rhodophyta, Chlorophyta and Phaeophyta. The assemblage often dominates upper surfaces of rocks down to 30 m depth, with little variation in species composition and abundance (Neto & Tittley, 1995).

1.1.2. *Codium elisabethae*

Codium elisabethae O.C. Schmidt is a perennial green alga (Chlorophyta, Bryopsidales) endemic to the Macaronesia, where it can be found in the archipelagos of Azores and Madeira, as well as in the most northerly and easterly of the Canary Islands (Chacana, 2002).
Individuals are peculiarly shaped as dark green spongy globes (Figure 1-B) that may attain diameters of 40 cm (Neto et al., 2005). These globes may become irregularly shaped when developing in clusters and centrally depressed as they grow and reach several years old.
The species may form high biomass stands particularly in sheltered areas of horizontal or gently sloping bedrock between 10 and 25 m depth (Figure 1-C). It is commonly associated with *Halopteris filicina* and coralline crusts. The SE of Faial island seems to offer climatic conditions for the species, which reaches densities of up to 105 individuals/m^2 in places such as Caldeirinhas (Sirjacobs et al., 2004).

1.1.3. *Dictyota* spp.

Dictyota J.V. Lamouroux 1809 is a genus of brown algae (Ochrophyta, Dictyotales) for which at least 6 species are recorded in the Azores (Neto, 1994). The most common around Faial island are *Dictyota dichotoma* Suhr and *Dictyota bartayresiana* J.V. Lamouroux which occur predominantly down to depths of 20 m. Both of these species exhibit fronds with a regular dichotomous branching. *D. dichotoma* has an erect and bushy habit and may reach heights of up to 15 cm (Figure 1-D). It is typically more delicate than *D. bartayresiana* and may exhibit spirally twisted branches. Its colour is uniformly brown or green, sometimes with light blue shades. *D. bartayresiana* has a more prostrate habit and does not exceed heights of 5 cm. Its fronds are shorter and wider with a typical bluish green or brown colour. Both species exhibit iridescent shades when underwater.

The occurrences of these and other species of *Dictyota* were aggregated for the purpose of this analysis as they were not always recorded independently in the surveys and the taxonomic relationship between some species is still debated (Schnetter et al., 1987; De Clerck et al., 2001).

This *taxon* is considered by Tittley & Neto (2000) and Wallenstein et al. (2007) to characterize rocky mid-infralittoral biotopes in the Azores.

1.1.4. *Halopteris filicina*

Halopteris filicina (Grateloup) Kützing is an eastern Atlantic brown alga (Ochrophyta, Sphacelariales) that occurs from the British Isles to Angola, occurring also in the Mediterranean and the Macaronesian archipelagoes of the Azores, Madeira and Canary Islands. Its frond is stiff with dense dark brown feathery branchlets that can form tufts of up to 12 cm height (Figure 1-E). The species can live from eulittoral areas down to more than 40 m depth. In areas shallower than 20m its occurrence is often confined to vertical and sub-vertical shaded surfaces. Beyond 30m depth it usually becomes abundant in upper rocky surfaces. The species is considered by Wallenstein et al. (2007) to be co-dominant with *Stypocaulon scoparium* in one of the infralittoral biotopes identified for the Azores.

1.1.5. *Padina pavonica*

Padina pavonica (Linnaeus) Thivy is an eastern Atlantic brown alga (Ochrophyta, Dictyotales) that is distributed from the British Isles to Angola, occurring also in the Mediterranean and all the Macaronesian archipelagoes from the Azores to Cape Verde. The species is widespread in the archipelago and forms perennial populations. Its annual frond displays a characteristic twirl that gives it a trumpet-like shape (Neto, 1997). Typically the fronds grow to 2-7 cm height and 12 cm width. It presents a pale brown colour with concentric bands showing a light whitish calcification that is more intense on the upper surface. It has a photophile character and colonizes mainly sheltered and well lit areas usually below 20m depth. It grows in eulittoral pools and infralittoral rocks either in association with other species or forming dense stands with a monospecific appearance (Neto et al., 2005) (Figure 1-F). The species is considered by Tittley & Neto (2000) to be locally or seasonally predominant in some areas.

1.1.6. *Zonaria tournefortii*

Zonaria tournefortii (J.V. Lamouroux) Montagne is a brown alga (Ochrophyta, Dictyotales) widely distributed throughout the Atlantic. It presents elongate stipes developing into profuse lobed foliaceous blades marked by vague lines radiating from their base and by distant, rather indistinct, concentric zonations (Neto, 1997). These fronds can reach up to 30 cm length and are yellowish brown in colour (Figure 1-G).

The species inhabits infralittoral rocky bottoms usually below 15m depth, where it forms dense monospecific canopies overlaying crustose Corallinaceae that often extend to depths of more than 40 m (Figure 1-H). In particular situations, these stands have been recorded in shallow infrallitoral areas (see results for Flores island in Tittley et al., 1998), but more often in these conditions the species is confined to shaded microhabitats such as the intervals between large boulders or blocks. This species is considered by Tittley & Neto (2000) and Wallenstein et al. (2007) to typify one of the infralittoral biotopes identified for the Azores.

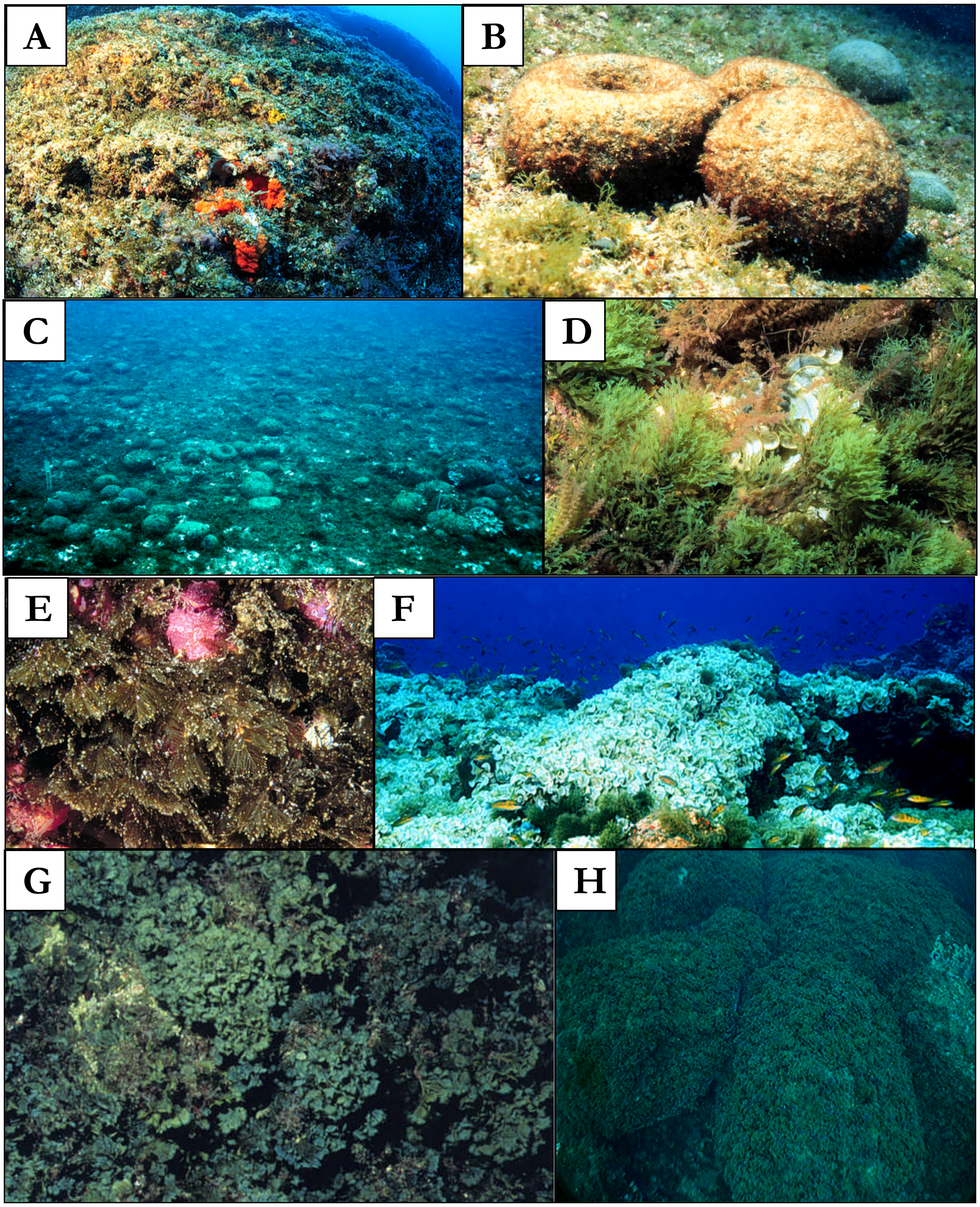

Figure 1. Aspect of rocky surfaces covered by the different species targeted by this study. A. Articulated Corallinaceae turf. B. *Codium elisabethae* plants. C. Climatic population of *Codium elisabethae* (23m depth; Monte da Guia SAC, Faial Island). D. Rocky surface dominated by *Dictyota dichotoma*. E. *Halopteris filicina*. F. Climatic population of *Padina pavonica*. G. Well-developed *Zonaria tournefortii* fronds. H. Climatic population of *Zonaria tournefortii* on deep infralittoral boulders.

2. Study area

The study focuses on rocky infralittoral grounds distributed around Faial island and on the neighbouring passage to Pico (Azores, Portugal, NE Atlantic) (Figure 2). These grounds extend throughout an area that is roughly 30 km West to East and 15 km North to South and encompass a wide range of physical environmental conditions. On-shelf depths fall quickly from the shoreline to the island margin, which can be located at distances from the shore between 140 m and 4 km.

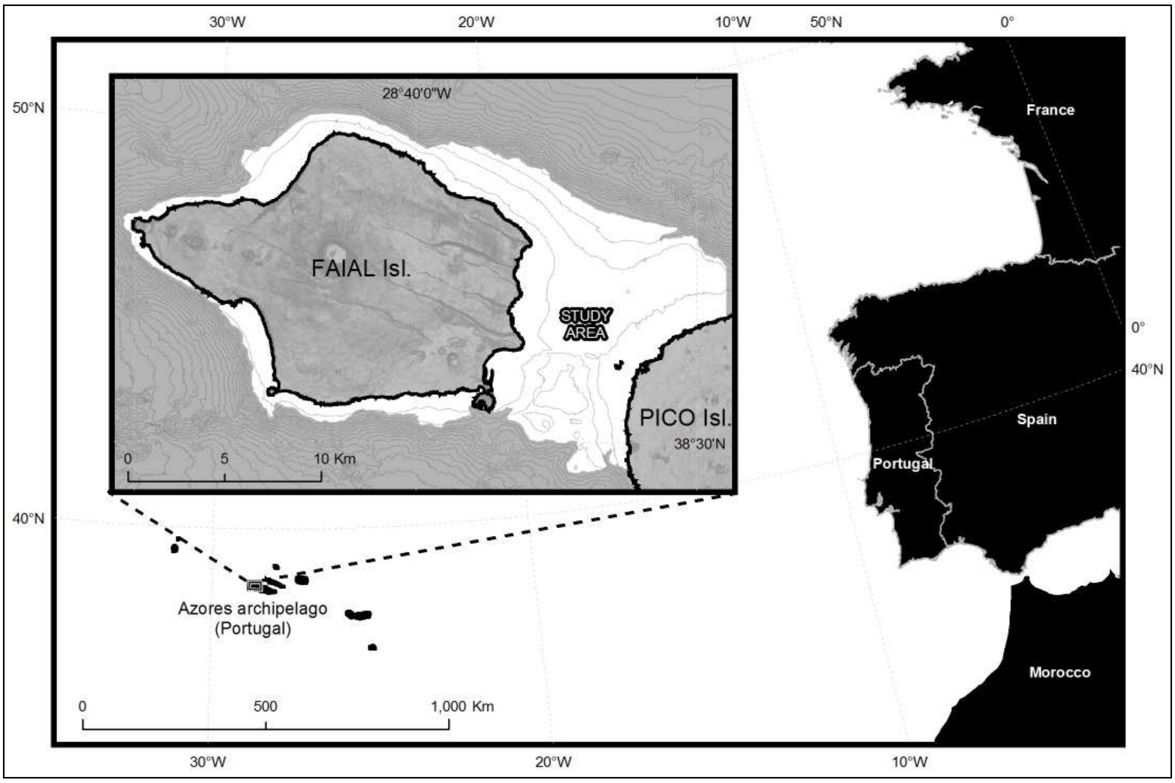

Figure 2. Location of Faial Island and neighbouring channel to Pico island. The study area is demarcated in the inset as a white area. Bathymetric contour spacing is 50 m.

The shelf seafloor includes boulder fields and bedrock expanses with varying degrees of complexity and slope. Exposure also varies substantially along the coast. Large sections are exposed to the full force of prevailing wind and swells whilst some embayments and leeward areas exhibit more sheltered conditions. These environmental variations result in a diverse set of representative habitats and associated species that offer varied ecologic research opportunities. The biodiversity of the area is well catalogued and substantial datasets have been accumulated on spatio-temporal variations in the occurrence and abundance of benthic species.

The area is also of great relevance for nature conservation and is in good conservation status (Tempera et al., 2001). Over the last two decades it has received marine conservation classifications that include zones designated under the Portuguese system of Protected Areas, five Special Areas of Conservation (SACs - Natura 2000 network), one OSPAR marine protected area and one long-term biodiversity research reference site (project BIOMARE).

3. Methodology

3.1. Biologic surveys

Geo-referenced species abundance data were collected mainly by SCUBA divers performing visual surveys down to 40m-depth. Beyond this limit for safe SCUBA diving with compressed air. Surveys of deep infralittoral areas were conducted with a remotely operated vehicle (ROV) and a drop down camera that collected video imagery down to 180m depth.

Table 1. Methodological sources of observations on algal abundance and their distribution in time.

Year / Method	1999	2000	2003	2004	2005
SCUBA	FT: 33	FT: 1	Others: 2	FT: 8	FT: 21 Others: 20
ROV				FT: 21	
Drop-down camera					FT: 11

FT – dives performed by Fernando Tempera; Others – dives performed by other observers

3.1.1. SCUBA diving surveys

Only an outline of the methodology used to survey the marine communities using SCUBA diving is presented. More detailed specifications can be found in Connor & Hiscock (1996) or Tempera et al. (2001).

The visual surveys focused on conspicuous species only, typically with sizes greater than 1 cm. The technique was applied by SCUBA divers trained to recognize the most common conspicuous benthic species and estimate their abundance *in situ*. The observations were collected along depth-transects approximately oriented perpendicular to the shore and located to cover the main physiographic types of coast present in the study area. Along each depth-transect, observers annotated the presence and abundance (by visually estimating the counts or percentage cover) of conspicuous sessile or sedentary species. Abundance of each species was recorded in facies presenting a well established physiognomic appearance. (i.e., avoiding transition areas). When a physiognomic discontinuity was perceived a record for a new facies was started and the transition depth band recorded. For a description of the semi-quantitative scale used for the estimates see 3.1.1.1.

Dives were temporally spread out through the summers of 1999, 2000, 2003, 2004 and 2005. Data collection was performed by 3 distinct observers. Sixty-three (63) dives were performed by Fernando Tempera and 22 other by the observers Vanessa Santos and Frederico Cardigos.

3.1.1.1. Abundance estimation

In situ abundance estimates were recorded using the MNCR percentage cover/density scales (Connor & Hiscock, 1996). These scales, also denoted SACFOR, provide a unified system for recording the abundance of marine benthic flora and fauna in biologic surveys that takes into account the regular size and growth form of the species. Six classes are used to categorize each species abundance: S – superabundant; A – abundant; C – common; F – frequent; O – occasional; and R – rare. An extract of the general SACFOR table provided by Connor & Hiscock (1996) is presented in Table 2, restricting growth forms to those relevant to the present study.

Table 2. SACFOR abundance scales relevant to the target species.

	GROWTH FORM	
	Turf-forming frondose algae	**Solitary plants with size >15cm**
SCORE	**PERCENTAGE COVER**	**DENSITY**
S	**≥40%**	**≥1/ 0.1 m²** (31.6cm × 31.6cm)
A	**20-39%**	**1-9 / 1 m²**
C	**10-19%**	**1-9 / 10 m²** (3.16m × 3.16m)
F	**5-9%**	**1-9 / 100 m²** (10m × 10m)
O	**1-5%**	**1-9 / 1000 m²** (31.6m × 31.6m)
R	**<1%**	**>1 / 10,000 m²** (100m × 100m)

Articulated Corallinacea, *Dictyota* spp., *Halopteris filicina*, *Padina pavonica* and *Zonaria tournefortii* were scored as "Turf-forming frondose algae" while abundance scoring for *Codium elisabethae* followed the scale presented under "Solitary plants with size >15cm".

To facilitate estimation of abundance, divers have occasionally used a quadrat consisting of a square frame of 1m × 1m subdivided into 25 smaller squares (20cm × 20cm) or alternatively counted plants in small strip transects.

The extraction of abundance estimates from the video footage collected in the ROV and drop-down camera surveys followed the same scale and was carried out by a single observer (Fernando Tempera).

3.1.2. ROV surveys

A VideoRay Explorer ROV was used for the deep infralittoral surveys in summer 2004. A total of 19 ROV deployments were executed over rocky seafloor which corresponded to

9h40min of usable video footage. The ROV operations were conducted to maximum depths of approximately 60 m, while the vessel was at anchor. A 2-3kg drop-weight was attached to the tether 11 m away from the ROV to minimize current-induced drifts and dampen swell movements. The observations conducted at each station were generally restricted to this radius around the drop-weight.

ROV dives concentrated on surveying representative locations where different physiographic/acoustic signatures had been identified in the bathymetric and backscatter maps. Given the spatial restriction of the observations around the drop-weight, only 2 to 3 habitats in the same depth band were generally sampled at each station (e.g., "horizontal and sub-horizontal surfaces"; "vertical and sub vertical surfaces"; "sediments"). Abundance estimates for each species were recorded separately in each of these habitats.

The ROV was deployed without any underwater positioning system (e.g., USBL) so the position of the system underwater was approximated using the position of the boat.

3.1.3. Drop-down camera surveys

A Tritech MD4000 drop-down camera was used during the summer 2005 to validate bottom types and estimate the abundance of conspicuous species fouling the substrates. These visual surveys covered from deep infralittoral locations to areas beyond the shelf edge (maximum 180 m depth).

The system comprised a video camera mounted on a metal frame which was suspended by a cable containing coaxial and light control elements. The enclosing frame was designed both to protect the camera in case of collision with the substrate and to keep its pitch and yaw attitude. This was achieved by a weigh of two kilos attached to the bottom of the frame (which approximately kept the camera mounting angle of 45º to the horizontal) and a rudder that kept the objective facing-forward (in the direction of the drift).

The drop-down camera was lowered to the seafloor by hand while the 11-m vessel was left to drift. These drifts were aimed at covering transects of representative seafloor types. The altitude of the system from the seafloor varied due to obstacle avoidance procedures and a hopping strategy aimed at obtaining both detailed close ups of the biologic benthic fouling (important for species identification and quantification) and wider views of the seabed. For most of the survey, the camera was positioned at approximately 2 m from the substrate which was close enough to easily describe the seafloor morphology down to depths of ca. 100 m as a result of good sunlight penetration (clear oceanic waters) and good performance of the camera in low light conditions. In deeper areas, illumination relied on two camera L.E.D.

lights (one either side of the lens) which provided sufficient light for distances to the ground smaller than 1m.

During the drifts, a computer logged time and position fed from the vessel GPS and depth from a single beam echosounder. The drop-down camera was deployed without an underwater positioning system.

The position of the system was approximated using the position of the boat when the cable was suspended directly beneath the boat. When cable drag and/or divergence between boat drift and current direction shift moved the camera away from the boat, annotations of the length of cable let out and a visual estimate of the cable slanting angle to the vertical were used to calculate a lag correction based on simple trigonometric formulae.

A total of 11 deployments were executed that covered rocky areas, corresponding to 12 hours of usable video footage.

Abundance estimates were conducted using the scale described in 3.1.1.1.

3.2. Sampling strategy

Instead of visiting a limited number of sampling stations multiple times, a decision was made to distribute more numerous sampling stations across the study area and guarantee that a wider range of combinations of environmental conditions was covered (though not repeatedly). On a first tier, coastal sectors subject to different degrees of exposure and presenting different coastal physiography were defined as basic sampling zones. Within each of these zones, a minimum of 3 random sampling stations were located that tried to cover the full depth range of macroalgae distribution. This strategy aimed to assess variations of the abundance of conspicuous species induced by the full range of environmental conditions in terms of depth, slope, exposure to currents and swell, water temperature and productivity regime found in the study area (attested in maps presented in section 3.6).

In order to sample the full extent of the infralittoral horizon down to the start of the circalittoral, observations were made using complementary means that included (i) randomly-placed depth-transects executed by SCUBA divers, (ii) ROV point deployments and (iii) drop-down camera transects.

Each surveyed location was subdivided into facies based on physiognomic perception. Each facies (e.g., "upper surfaces dominated by *Codium elisabethae* and *Halopteris filicina* between 25 and 16m depth" or "vertical surfaces dominated by *Halopteris filicina* between 20 and 14m depth") had specific species lists and abundance annotations. For the analyses carried out in this work, only the data from species occurring on rocky horizontal to sub-horizontal surfaces (0 to 45º inclination) were of interest, as they composed the most conspicuous biologic fouling for which comparable abundance estimates could be derived from the different sampling techniques used. For instance, observations made on microhabitats such as vertical to subvertical surfaces or pockets of frequently mobilized pebbles and cobbles were left out of the analyses.

All the observations were restricted to the period between 26^{th} June and 26^{th} September, which corresponds to the period when Sea Surface Temperature is highest (between 20 and 23 ºC) and seagoing conditions are more favourable.

3.3. Geographic Information System

A Geographic Information System (GIS) built within ArcGIS 9.1 ® ESRI was used to: (i) integrate the geo-referenced vectorial and raster information; (ii) overlay and visualize sampling locations and environmental variable maps; and (iii) extract matrices for statistical analysis by spatially intersecting the biologic data with the collocated values of the environmental variables (ArcGIS-embedded *spatial join* function and *Intersect Point Tool* in Hawth's Analysis Tools ArcGIS add-in).

3.4. Statistical modelling framework

Statistical models are ideally used to analyse how a response or independent variable (e.g., the abundance of a species) is influenced by a set of explanatory or independent variables (e.g., environmental parameters) expected to regulate its behaviour.

The different variables used are briefly presented in Table 3. Depending on the data available and/or the settings used in their modelling they exhibit different native resolutions.

Table 3. Summary of the variables used in the statistical models.

Response variable	Type	Observations	Time scale of observations
Abundance of selected infralittoral algae	Ordered categorical	SACFOR score attributed at every 1m interval along the transects	Summers 1999, 2000, 2003, 2004, 2005
Explanatory variable		-	
Depth	Continuous	Species abundance observations performed along the transects were allocated 1m-depth intervals from 0 to 58 m. Raster resolution used for spatialization: 5m	Surveys in autumn 2003 and summer 2004
Zonal slope	Continuous	Extracted in a GIS environment by intersecting the sampled point with a slope map. Raster resolution: 20m	Derived from combination of bathymetric surveys in autumn 2003 and summer 2004
Exposure to swell action	Continuous	Extracted in a GIS environment by intersecting the sampled point with the thematic raster resulting from a GIS-based fetch index weighted by swell statistics. Raster resolution: 200m	Multiannual average 1989-2002
Exposure to currents	Continuous	Extracted in a GIS environment by intersecting the sampled point with a thematic raster map resulting from a shallow water oceanographic current model. Raster resolution: 500m	Maximum spring tide model
Sea Surface Temperature	Continuous	Extracted in a GIS environment by intersecting the sampled point location with a thematic map of average SST. Raster resolution: 0.819'×0.684' (Lat×Long)	Multiannual weighted average from April 2001 to April 2006
Surface chlorophyll-*a* concentration	Continuous	Extracted in a GIS environment by intersecting the sampled point location with a thematic map of average surface chl-a concentration. Raster resolution: 0.412'× 1.130' (Lat×Long)	Multiannual weighted average from January 1999 to October 2004
Analysis mask		-	
Seafloor nature	Categorical	Raster layer representing the location of rocky seafloor with a 5m resolution and blanking out sediment surfaces	Derived from combination of seafloor surveys in autumn 2003 and summer 2004

The response variable was measured as a discrete number of mutually exclusive, collectively exhaustive and inherently ranked outcomes, i.e., it constitutes a categorical variable in which the categories have a natural order, e.g., from low to high (Borooah, 2001). In contrast, all explanatory variables are continuous. Depth, slope, SST and chl-*a* were computed from observational datasets obtained using a set of remote sensing techniques (acoustic echosounding and satellite imagery). Others (exposure to swell and currents) were proxies derived directly from GIS analysis and oceanographic modelling. The latter have undergone no *in situ* validation and are tentatively used in the absence of spatially-explicit observations of mechanical stresses induced by swells and currents.

3.4.1. Ordered logit method

The ordered categorical nature of the response variable determined that ordered logit methods (McCullagh, 1980) were most appropriate to investigate the relationship between the explanatory and response variables. Ordered logit models fit a logistic regression between the explanatory variables and an ordinal response variable exploiting the ordering in the estimation process, in contrast with multinomial models. In ordered logit models, the error term (ε_i) is assumed to be *logistically* distributed.

The STATA™ (v.10 from StataCorp LP) *ologit* module was used to perform maximum likelihood estimation of the parameters required by the models in this study.

3.4.2. Spatial autocorrelation

Spatial autocorrelation is an important source of bias in most spatial analyses. In this particular case, it is likely that (i) observations performed on adjacent depths at the same station and (ii) pseudo-replicates collected at the same station in different days or in neighbouring stations are more similar than observations made at stations located far apart. The exact spatial scale of this autocorrelation was not investigated, but clusters were defined that aggregated observations performed in the same area or in neighbouring areas for which the major environmental variables were deemed to be very similar. The correlation of the observations within clusters was computed using a Generalized Estimating Equations (GEE) approach and independence working correlation structure estimates were used in adjusting standard errors (robust clustering option in STATA™).

3.4.3. Non-linearity and explanatory variable transformation

Non-linearities in the relationship between the dependent variable and explanatory variables are an issue to model building (Sauerbrei et al., 2006). Ordered logit models assume a linear functional relationship between the response variable and each explanatory variable at the scale of the link function. However, this assumption may be incorrect, leading to model mis-specification.

A systematic approach to investigate possible non-linear functional relationships is available in STATA™ through multivariable fractional polynomial models (*mfp* command). This technique builds multivariable regression models for the relationships between response and each explanatory variable and selects the most appropriate polynomial transformation through a backward elimination procedure of the fitted polynomials using a significance level of 0.05 (p-value). Only 1^{st}, 2^{nd} and 3^{rd} order polynomials with a maximum of 6 degrees of freedom were tested as covariate transformations, since simple lines and curves were considered the most probable relationships from an ecologic perspective. By default, STATA™ performs a preliminary linear transformation to avoid the explanatory variables having negative and zero values.

3.4.4. Selection of significant explanatory variables

In fitting regression models data analysts are often faced with many predictor variables which may influence the outcome. Selection of the best model was initiated by fitting a full model with non-transformed variables. Since the relationship between the response variable and the explanatory variable was rarely linear and produced models that dropped too many predictors deemed important, more robust models were build by applying the *mfp* transformations described above to all explanatory variables. In the next step, *mfp*-transformed explanatory variables that still showed non-significant coefficients (p-value > 0.05) in the full model were dropped and new models were tested using only the explanatory variables with coefficients statistically different from 0. When only one statistically-significant parameter came out from this backward selection procedure, other alternative combinations were tested aiming at obtaining a model that include more than one parameter and presented a higher R^2.

The Akaikes Information Criterion (AIC) provided an additional measure to assess the fit of nested versions of the models tested for each species in order to determine the final acceptable model.

3.4.5. Goodness of fit

Several statistics have been proposed to replace the traditional coefficient of determination (R^2) which cannot be used to assess the performance of ordered logit regressions. A common substitute for this type of models is the MacFadden pseudo-R^2 (Hanemann & Kanninen, 1999) which is used in present study. A good fit is indicated when the pseudo-R^2 is above 0.2 whilst an R^2 approaching 0.4 is considered an extremely good fit (

3.5. Model spatialization

The multivariable models were spatialized based on the rasters of the explanatory variables found to be significant for each species. For this purpose a specific dataset containing the combination of values of the different explanatory variables observed in each raster cell was built. The dataset represented a 5-m resolution raster domain of 1,568,702 cells covering the rocky substrates down to 58 m depth below MSL (the bathymetric limit at which algae of the selected taxa were observed). Since the combination of values obtained from each raster cell was attached to individual geo-referencing information through X & Y columns, the prediction obtained from the model equation could be re-spatialized.

The prediction was done using the STATA command "*predict*", which calculates the predicted probabilities for each category of the dependent variable (abundance classes) based on a combination of explanatory variables. Before the command was applied, each of the significant covariates underwent the same polynomial transformation identified by the method described in section 3.4.3.

Since STATA™ does not create a single column containing the most probable category, but rather a number of columns containing the probabilities of each category possible for the response variable (i.e., each of the SACFOR abundance classes + absence category), the prediction spreadsheet had to be post-processed. To allow for the high number of rows involved, the SPSS® package (v. 14.0 from SPSS Inc.) was used. Additional columns were thereby produced that synthesized the most probable category predicted for each cell for each species. This spreadsheet was then imported into a Microsoft® Office Access 2003 *.mdb* file and re-spatialised in an ArcGIS environment.

The most probable category is used as the predicted abundance class in each predictive distribution map and its probability is shown in an associated map.

3.6. Presentation of the variables

3.6.1. Dependent variable

For modelling purposes, the ordered SACFOR categories were assigned ranked numerical values of 6 (superabundant) to 1 (rare). Given that the studied *taxa* are all conspicuous and easily recognized, it was assumed that cases where the experienced observers did not record the species effectively indicated that the species was searched and was effectively not found, therefore representing absence of the species for the purpose of abundance estimation. In the statistical modelling framework used (ordered logistic regression models), the absence class is as important as the ones representing the recording of the species with a specific abundance. A zero (0) was used to numerically represent the absence cases.

Finally it is worth-noting that the zero (0) to six (6) scale represent a simple ranking of the ordered categorical response variable and have no cardinal significance (Borooah, 2001). I.e., the difference in actual abundance between a score 1 and 2 is not equal to the difference between a score 5 and 6.

Table 4 summarizes the amount of observations used for each species as well as the number of clusters used in the working correlation structures.

Table 4. Number of observations per species

	Codium elisabethae	**Articulated Corallinacea**	*Dictyota* **spp.**	*Halopteris filicina*	*Padina pavonica*	*Zonaria tournefortii*
No. of observations	926	967	985	934	1020	1013
No. of clusters	104	104	104	109	111	113

The spatial distribution of each species observations and the respective abundance recorded in each station are shown in Figure 3 to Figure 8.

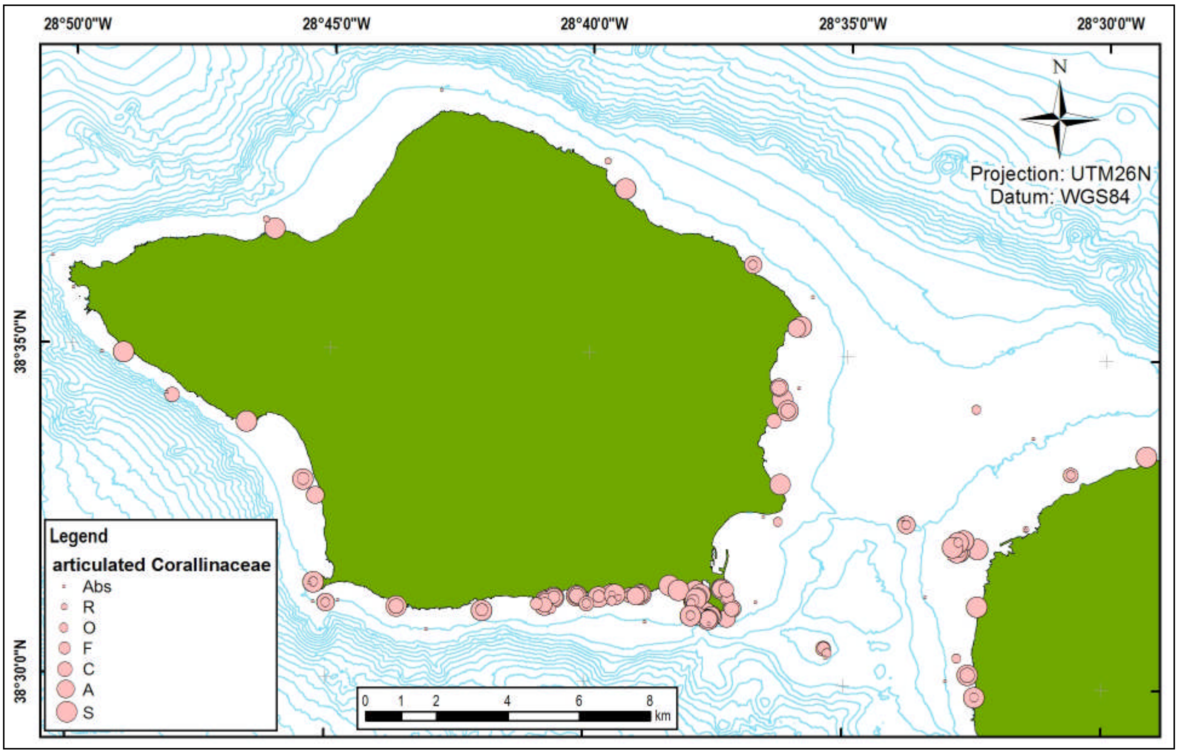

Figure 3. Spatial distribution of articulated Corallinaceae observations and respective SACFOR abundance score.

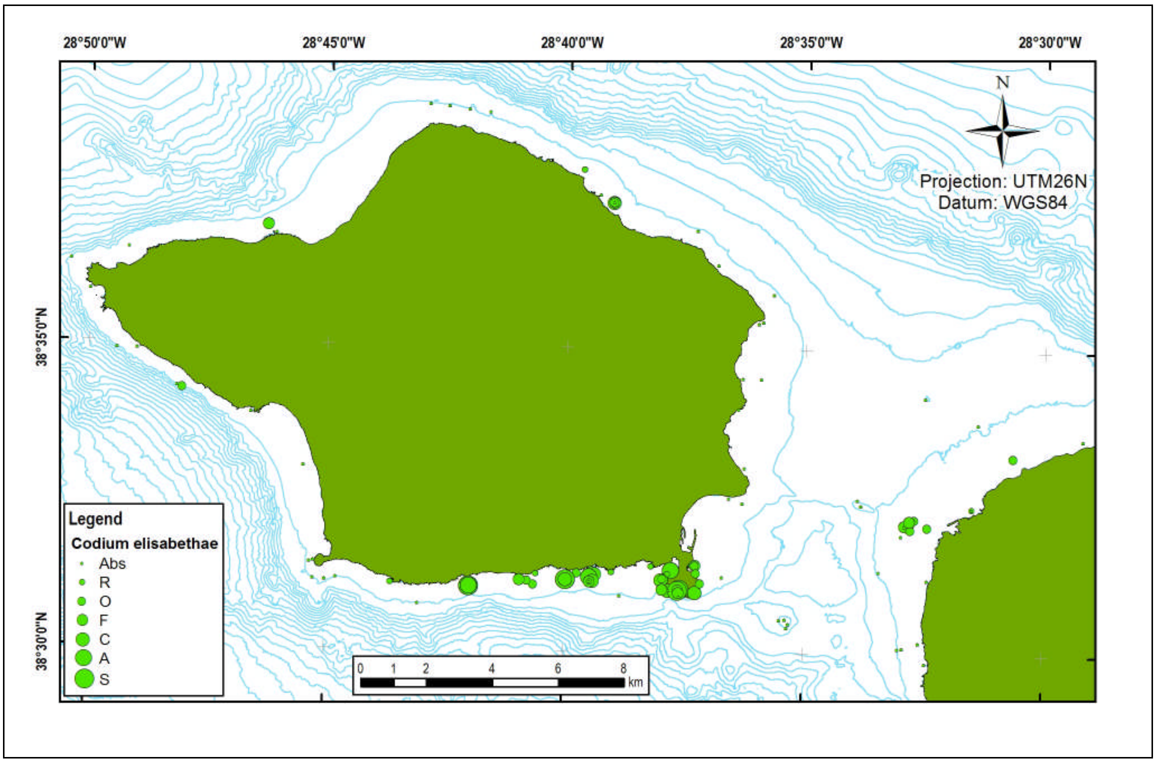

Figure 4. Spatial distribution of *Codium elisabethae* observations and respective SACFOR abundance score.

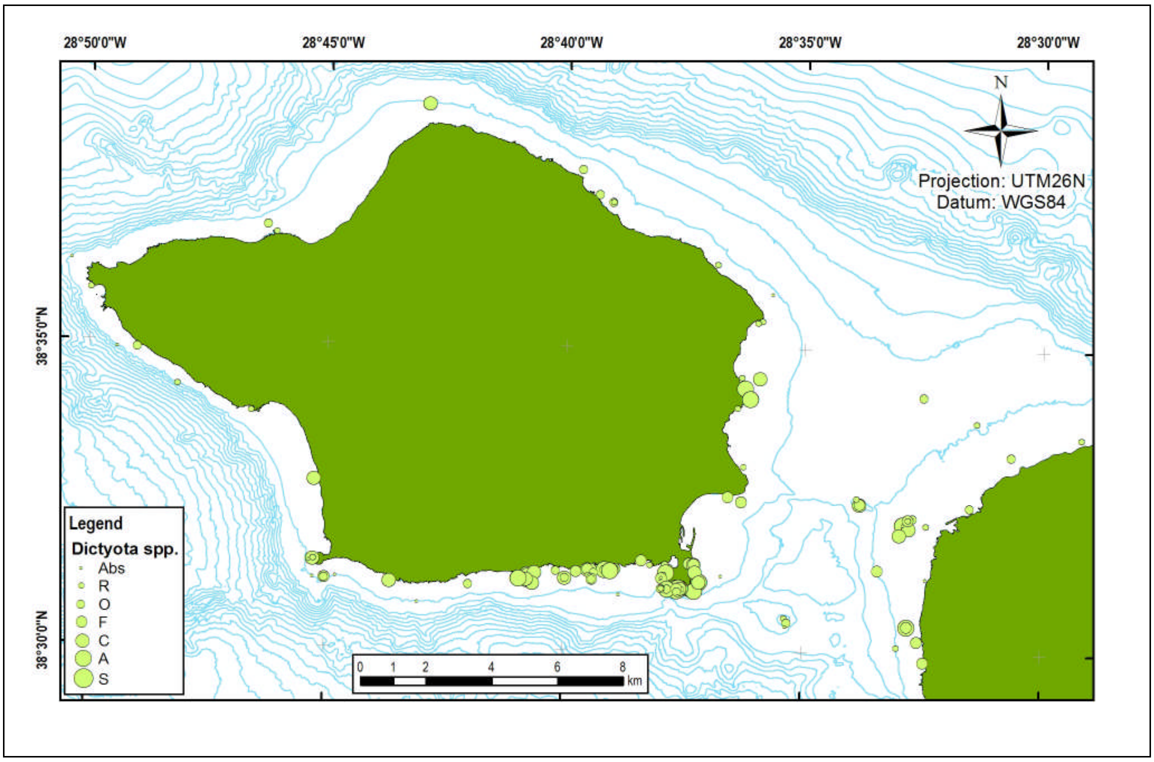

Figure 5. Spatial distribution of *Dictyota* spp. observations and respective SACFOR abundance score.

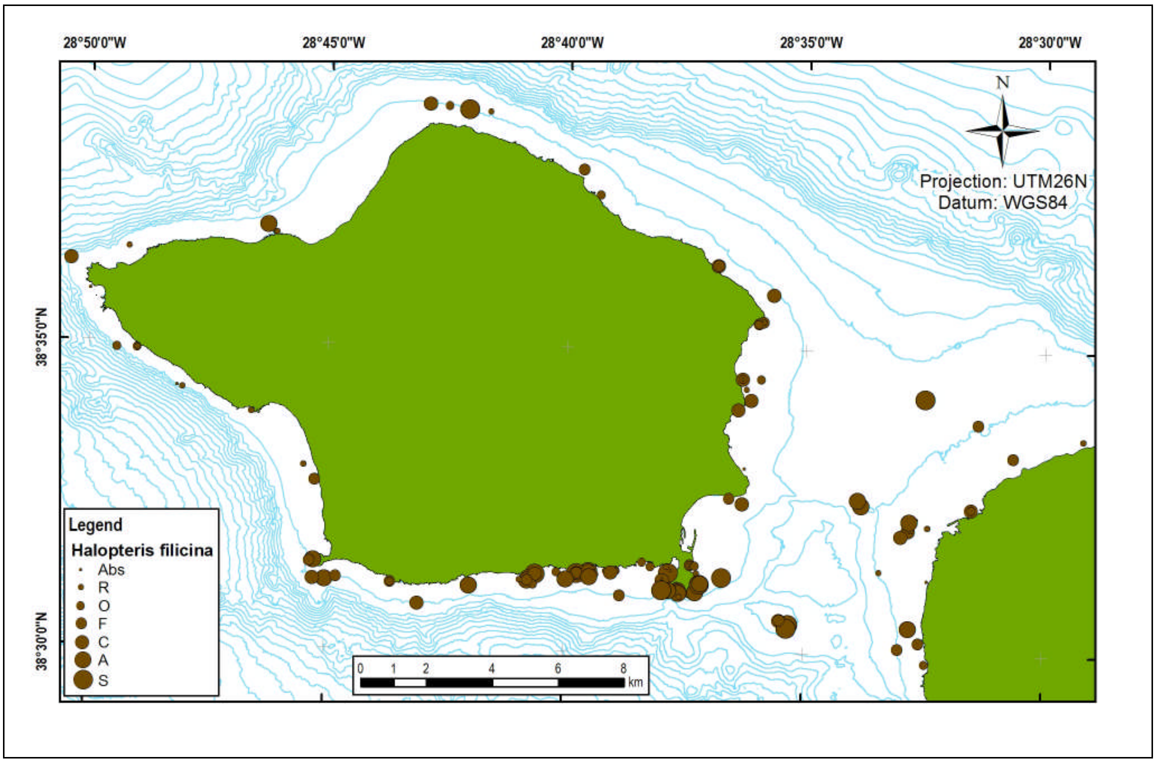

Figure 6. Spatial distribution of *Halopteris filicina* observations and respective SACFOR abundance score.

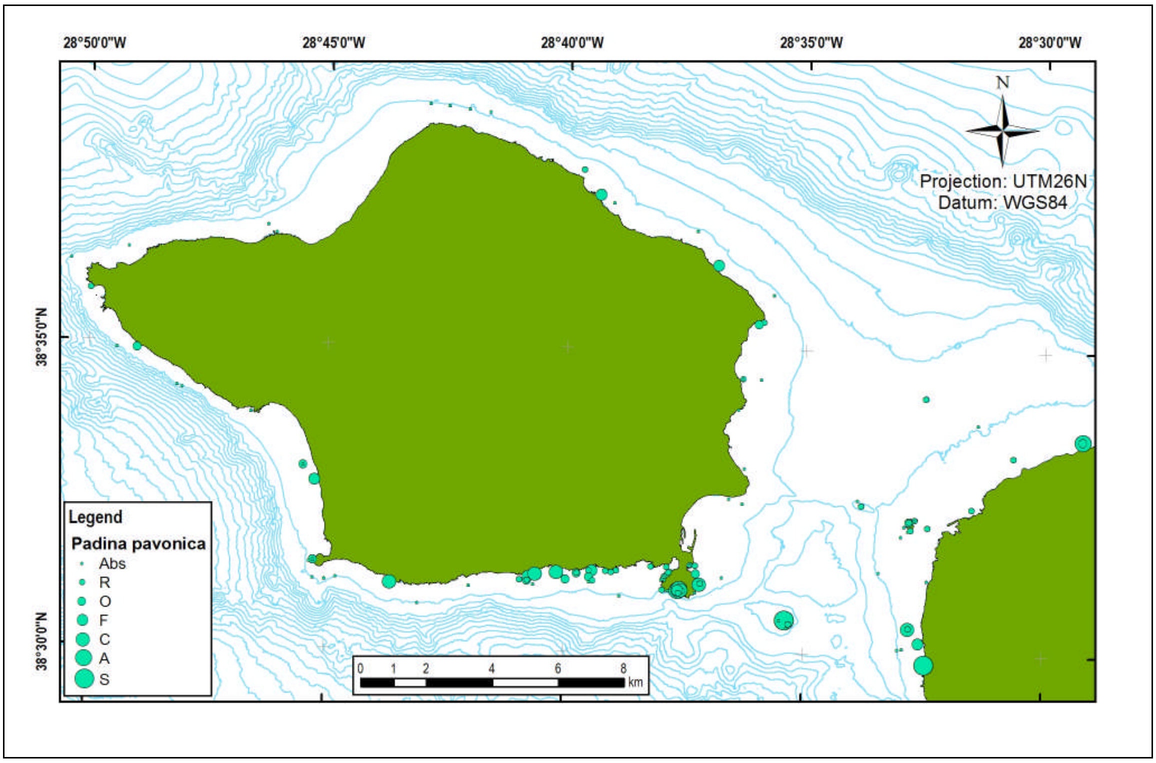

Figure 7. Spatial distribution of *Padina pavonica* observations and respective SACFOR abundance score.

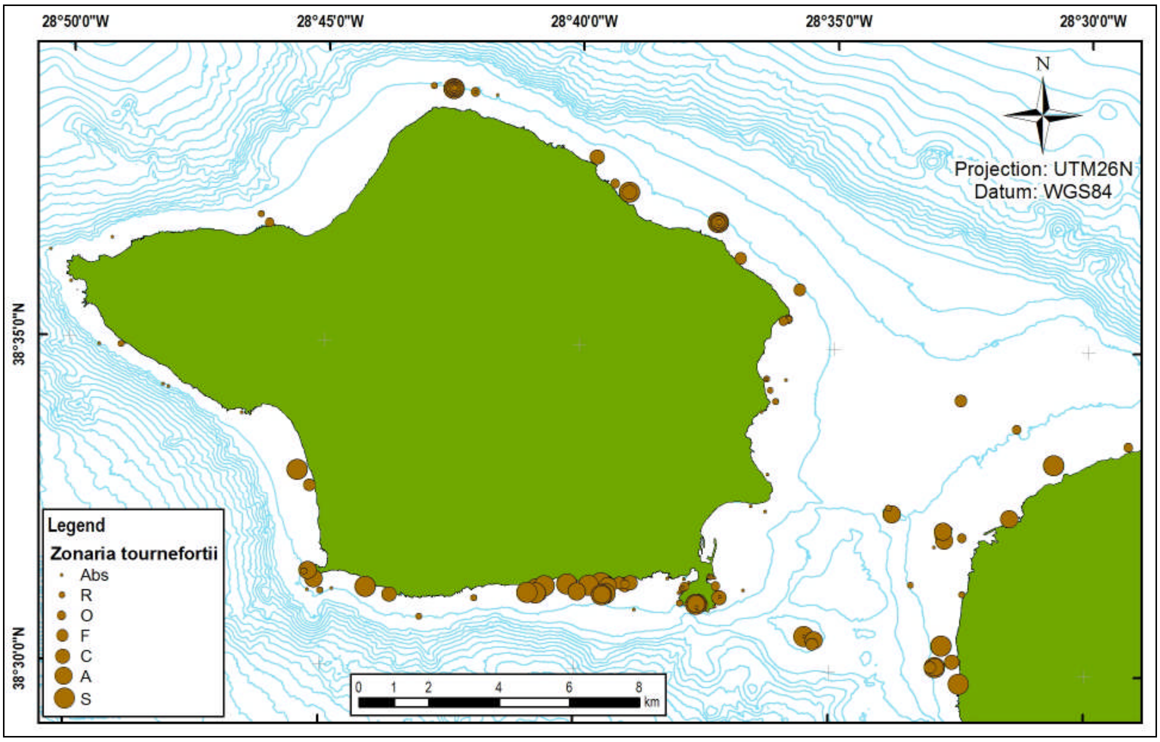

Figure 8. Spatial distribution of *Zonaria tournefortii* observations and respective SACFOR abundance score.

3.6.2. Independent variables

A summary is provided below of each environmental variable used as explanatory in developing the statistical models of abundance distribution. Raster fields used for each of the variables when intersecting the biological observations with environmental data and spatializing the final models are also represented.

3.6.2.1. Depth

The vertical reference of the observations was the Mean Sea Level (MSL). Considering that most dives were conducted irrespectively of the tidal stage and depths recorded for the observations were based on depth gauge readings and left uncorrected for tides, an average error of ±0.75 m (half of the maximum astronomic tide) should be attached to the vertical location of the underwater observations.

High resolution data from the swath sonar surveys were used to create the regular bathymetric grid representing the bottom topography. Data holes, which composed 27% of the rocky areas shallower than 58 m, were completed using bathymetric information digitized from official hydrographic sounding sheets, where available, or from published hydrographic charts. MSL was the vertical datum adopted for this bathymetry dataset which was used while spatializing the model. Mean Sea Level at Horta harbour is 1.08 m above the Hydrographic Chart Datum (José Gonçalves/C.M.H., pers. com.).

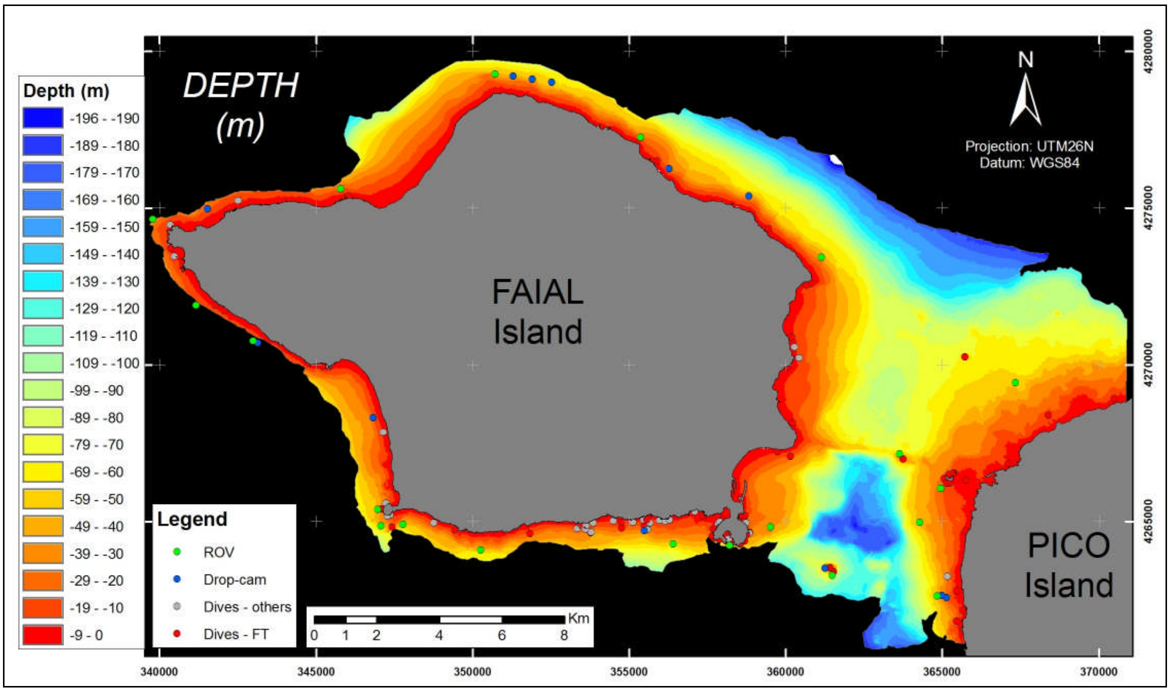

Figure 9. Bathymetry of the study area based on swath surveys represented at a 5 m resolution.

3.6.2.2. Slope

The map of onshelf slopes was generated from a regular bathymetric grid at a 20m resolution using ArcGIS 9.1 ® ESRI Spatial Analyst extension.

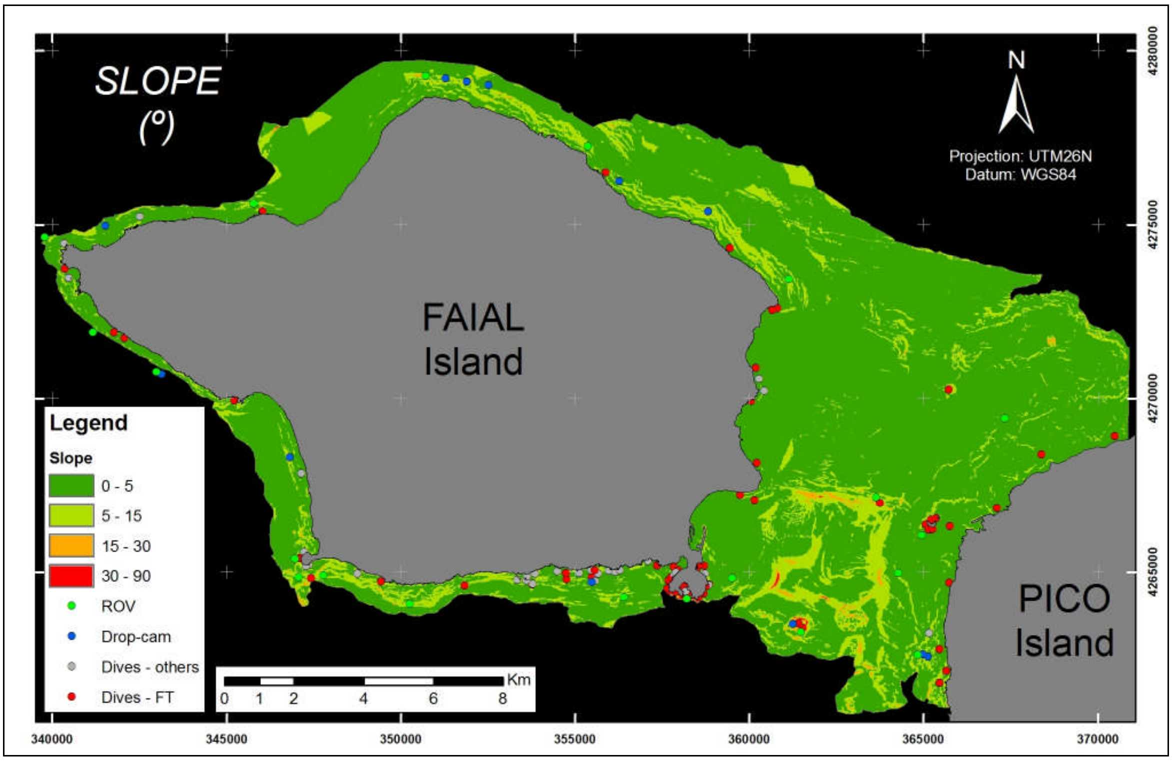

Figure 10. Onshelf slope map extracted from a bathymetry grid at 20m resolution.

3.6.2.3. Seafloor nature

Backscatter mosaics were integrated in the ArcGIS project and used as a basis for manual digitization of onshelf rocky seafloor areas. In instances where backscatter was of insufficient quality, topographic texture derived from high-resolution slope maps aided the demarcation of the rocky areas.

Visual data collected by SCUBA divers as well as ROV and drop-down camera deployments provided ground-truthing information to validate the classification.

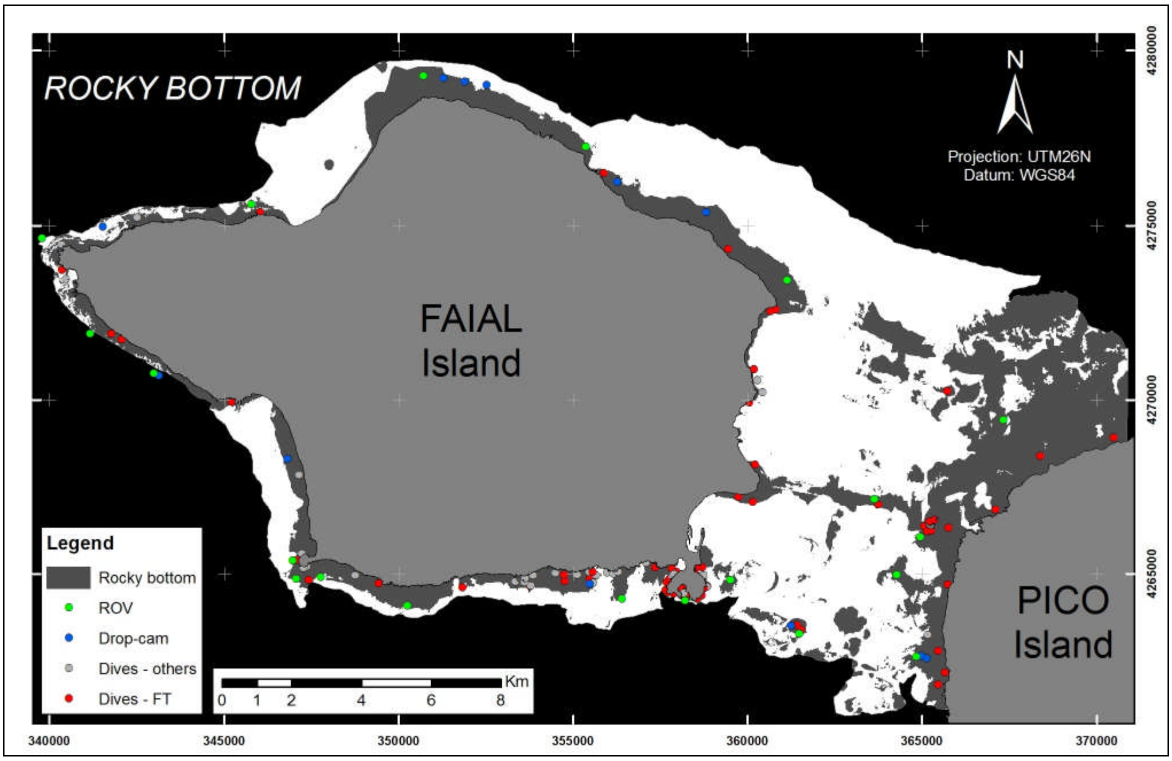

Figure 11. Segmentation of the shelf according to seafloor nature.

3.6.2.4. Sea surface temperature and chlorophyll-*a*

Reviews by both Menge et al. (1997a, 2003) and Schiel (2004) suggest that temperature and plankton productivity regimes are among the factors that interfere with the ecologic requirements of individual species and regulate their biogeographic distributions, their abundance and ultimately the composition of the assemblages they form.

In the case of benthic studies, information about these environmental variables should ideally pertain to the near-bottom layer. However, data available to date (e.g., from sampling using *in situ* data-loggers and shipboard surveys) had insufficient resolution to produce a vertically-explicit model of the thermal and ocean colour spatio-temporal variability at the scale of Faial island. As an alternative, surrogate average patterns were extracted in Chapter 6 for *sea surface temperature* (SST) and *surface chlorophyll-a concentration* (chl-*a*), respectively from AVHRR and SeaWiFS satellite imagery.

The average annual fields obtained and intersected with the biologic occurrences are shown in Figure 12 and Figure 13, both of which have resulted from multi-annual imagery datasets extending slightly in excess of 5 years.

Blanks on the nearshore were completed based on a nearest neighbouring spatial joining based on valid SST or chl-*a* concentration values found in adjacent pixels. The appended value was compensated for offshore-nearshore gradients in island sectors where nearshore-offshore gradients were found to be statistically significant (see Chapter 6).

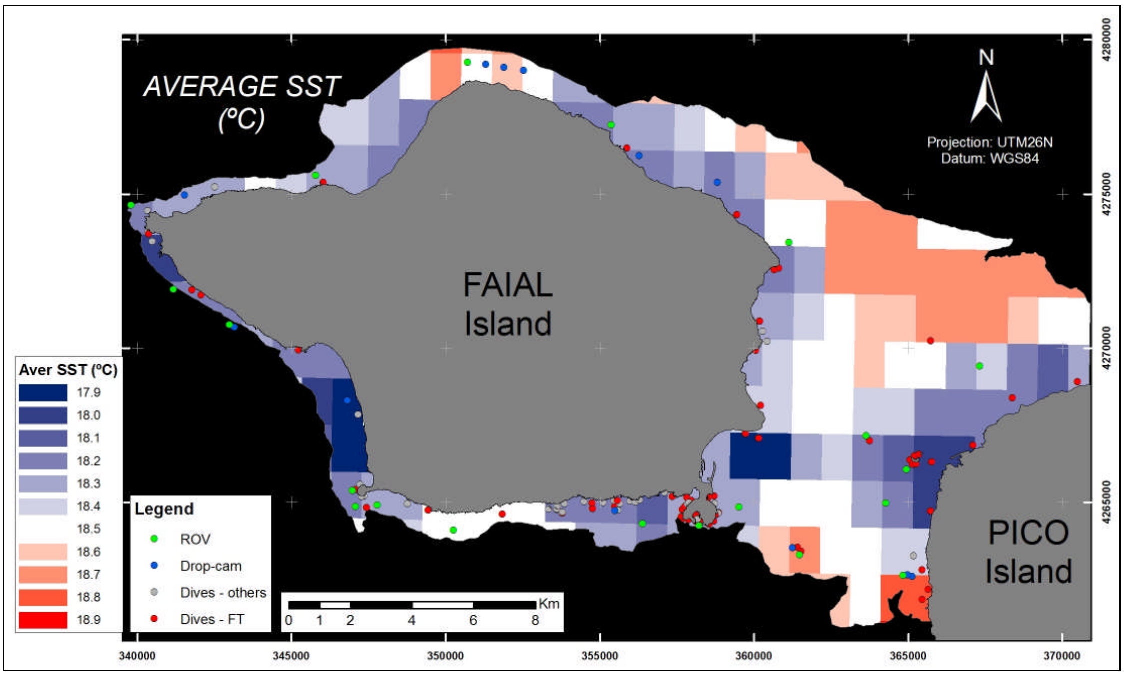

Figure 12. Yearly-averaged field of SST around Faial Island and neighbouring passage.

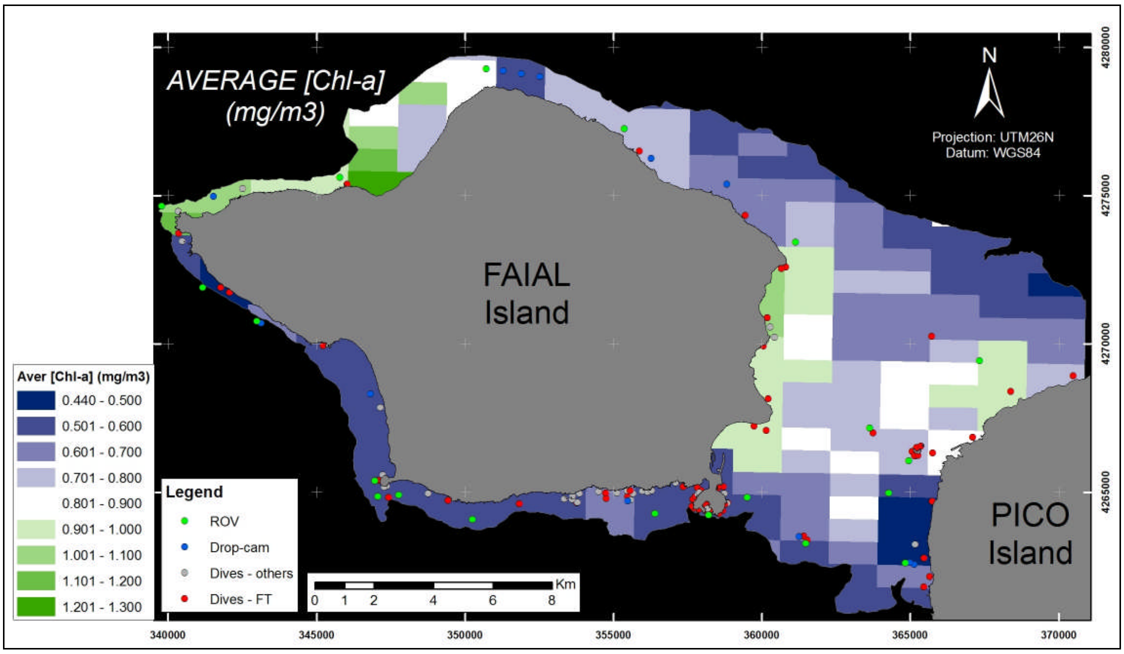

Figure 13. Yearly-averaged field of chl-*a* concentration around Faial Island and neighbouring passage.

The consistency of the spatial patterns and the reasonable magnitude of the differences between distinct sectors of the island suggest the existence of distinct surface temperatures and water properties favouring primary production which are postulated as being correlated with the subsurface regimes directly impacting on the benthic assemblages.

3.6.2.5. Swell exposure

Exposure to surface hydrodynamic events such as waves and swells is an important environmental factor that has been repeatedly implicated in the regulation of biologic assemblages, particularly in eulittoral and shallow infralittoral settings (e.g., Taylor & Schiel, 2003; Goldberg & Kendrick, 2004; Tuya & Haroun, 2006). For infralittoral benthic organisms, this effect is generally only relevant where the oscillating currents generated by passing waves effectively impinge on the seafloor. These effects typically impact more strongly on shallow water environments but with large oceanic swells regularly affecting the Azores islands, it is probable that swells can directly and indirectly impact marine biota to depths greater than 50 m.

A relative proxy of the distribution of wave energy affecting the biologic communities around the study area was built that assumes relative position of each location with respect to nearby islands and islets to play a major role in determining its exposure to waves approaching from each compass direction. A GIS script introduced by Puotinen (2005) was employed first to identify compass directions directly open to incoming swells. A spreadsheet computation was then used to weigh these windows with statistics of ocean swell direction and significant wave height obtained from Carvalho (2003). The numbers obtained at the directions each point is opened to are then summed to obtain an "absolute exposure index". Finally these "absolute" numbers are divided by the maximum absolute exposure obtained within the point domain (standardization by maximum) to obtain the relative exposure index. The method is further detailed in Appendix I.

The index computed using this method was re-spatialised in a GIS environment so that the spatial distribution of exposure could be visualized (Figure 14) and was available to intersect with the geo-referenced biologic data.

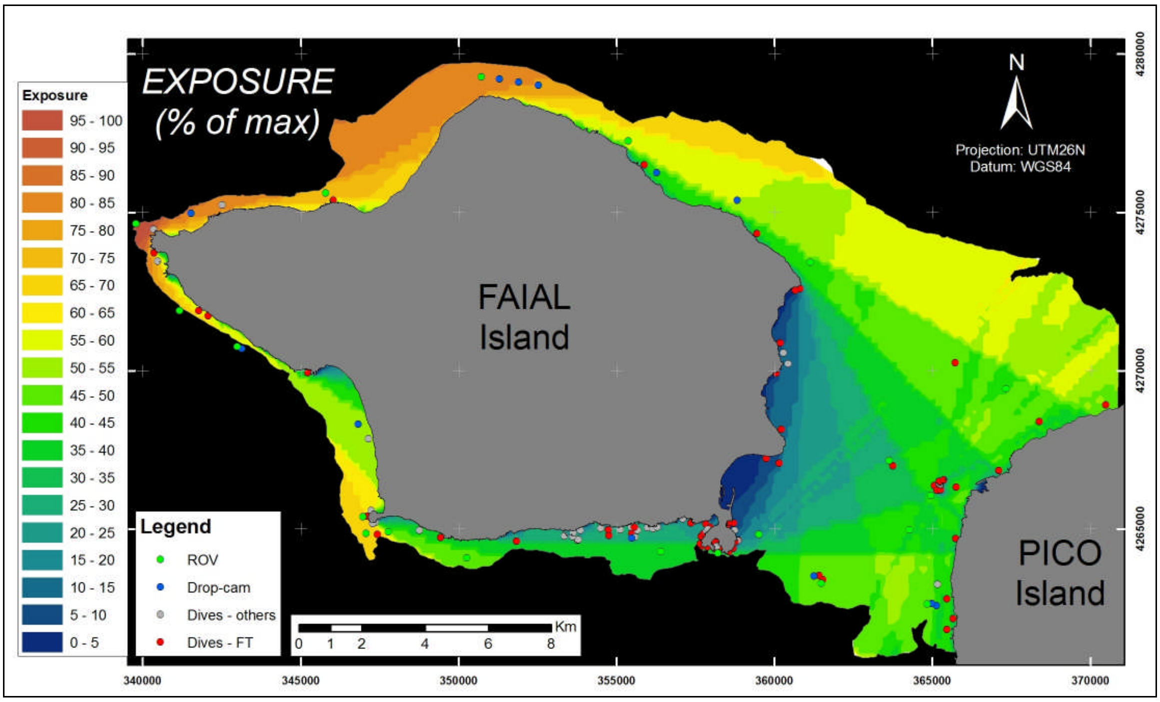

Figure 14. Swell exposure field for Faial Island and neighbouring passage.

A more sheltered character was found in eastern Faial, some small embayments (Porto Pim and Madalena harbour) or areas behind headlands (Varadouro beach, areas scattered along Faial southern shore) which contrast with the highly exposed character of NW Faial.

3.6.2.6. Exposure to currents

A proxy for the exposure of benthic communities to currents was developed from maximum currents induced by a maximum astronomic tide. The current fields were obtained from a simple shallow-water oceanographic model detailed in Appendix II. Computations of the free surface flows in the vicinity of Faial Island were executed within the TELEMAC (®EdF-LNH) software system. Current fields were extracted after the model stabilized, which was considered to happen at the end of 2 tidal cycles (90,000 sec). Vertically-averaged current velocity fields were then obtained for the next 3 tide cycles (93,750 sec to 225,000 sec) at a period of 3,750 sec (i.e., 1/12th of a complete tide cycle). A field of maximum current velocities observed at each node over this period was extracted and "absolute" currents were divided by the maximum absolute current velocity recorded by the model for the study area (standardization by maximum). This relative current exposure index was then used to build the field shown in Figure 15, which constituted the GIS layer that was intersected with the geo-referenced biologic data.

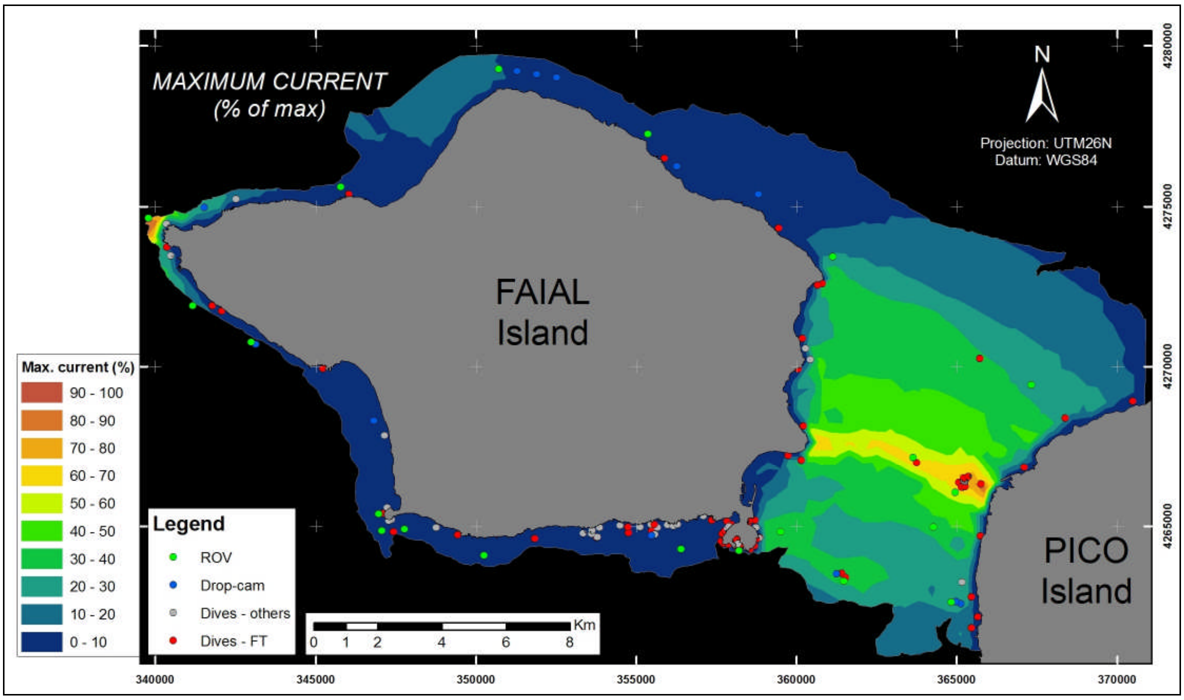

Figure 15. Swell exposure for Faial Island and neighbouring passage.

4. Results

The relationship between the raw abundance (dependent variable) and the potential explanatory variables is shown in Appendix III.

The final multivariable fractional polynomial models used to transform explanatory variables based on their non-linear relationship with the response variable are presented in Appendix IV.

4.1. Statistical models

A summary of the model configurations and fit measurements obtained for the different models tested are presented in Table 5.

The final models (highlighted in bold) show that depth was consistently significant for all the species. Slope was non-singnificant only for *P. pavonica*. Exposure to swell was significant to articulated Corallinaceae and *Halopteris filicina*. Exposure to currents was significant to *Codium elisabethae*, articulated Corallinaceae and *Padina pavonica*. SST was non-significant for all species, while chl-*a* was significant for the articulated Corallinaceae and *Padina pavonica*.

Table 5. Summary of model configurations and fit measures. Final accepted models are in bold.

Species	Dependent Variable Transformation	Depth	Slope	Expos. to swell	Expos. to current	SST	[Chl-*a*]	MacFadden pseudo- R^2	AIC	BIC	Deviance
Articulated Corallinaceae	None	X	X_{ns}	X_{ns}	X	X_{ns}	X	0.1866	2909.728	2968.219	2885.728
	MFP_{full}	X	X	X	X	X_{ns}	X_{pns}	0.2311	2767.667	2865.151	2727.667
	MFP_{red1}	**X**	**X**	**X**	**X**		**X**	**0.2202**	**2798.560**	**2876.547**	**2766.560**
Codium elisabethae	None	X_{ns}	X_{ns}	X	X_{ns}	X	X_{ns}	0.0544	2088.947	2146.917	2064.947
	MFP_{full}	X	X	X	X	X_{ns}	X_{ns}	0.2742	1624.979	1721.596	1584.979
	MFP_{red1}	X	X	X_{ns}	X			0.2577	1652.932	1730.226	1620.932
	MFP_{red2}	**X**	**X**		**X**			**0.1875**	**1798.222**	**1856.192**	**1774.222**
Dictyota spp.	None	X_{ns}	X_{ns}	X_{ns}	X_{ns}	X_{ns}	X_{ns}	0.0233	3476.049	3534.761	3452.049
	MFP_{full}	X	X	X_{ns}	X_{ns}	X_{ns}	X_{ns}	0.0973	3226.722	3314.789	3190.722
	MFP_{red1}	**X**	**X**					**0.0755**	**3289.660**	**3343.479**	**3267.660**
Halopteris filicina	None	X	X_{ns}	X_{ns}	X_{ns}	X_{ns}	X_{ns}	0.0872	3224.534	3282.608	3200.534
	MFP_{full}	X	X	X	X_{ns}	X_{ns}	X_{ns}	0.1658	2958.794	3041.065	2924.794
	MFP_{red1}	**X**	**X**	**X**				**0.1537**	**2991.285**	**3049.359**	-
Padina pavonica	None	X	X_{ns}	X_{ns}	X_{ns}	X_{ns}	X_{ns}	0.0508	2573.219	2632.35	2549.219
	MFP_{full}	X	X_{ns}	X_{ns}	X_{ns}	X_{ns}	X	0.1527	2317.388	2420.867	2275.388
	MFP_{red1}	X					X_{ns}	0.0878	2471.715	2525.918	2449.715
	MFP_{red2}	**X**			**X**		**X**	**0.1177**	**2397.595**	**2466.581**	**2369.595**
Zonaria tournefortii	None	X	X	X_{ns}	X_{ns}	X_{ns}	X_{ns}	0.0575	3203.617	3262.665	3179.617
	MFP_{full}	X	X_{pns}	X_{ns}	X_{ns}	X_{ns}	X_{pns}	0.1585	2878.795	2977.209	2838.795
	MFP_{red1}	**X**	**X**					**0.1115**	**3017.307**	**3066.514**	**2997.307**

Full . full model (all explanatory variables); red. - reduced model (keeping variables with coefficients significantly different from 0); ns – non-significant coefficients (p>0.05); pns - coefficients for some quadratic/cubic terms after transformation were non-significant (p>0.05);

4.1.1. Model parameterization

The final parameterizations of the ordered logit models build for the different species are presented in sections 4.1.1.1 to 4.1.1.6.

Figure 17 to Figure 21 present the relationships between the probability of the different abundance categories and each of the independent variables that were identified as statistically significant in the final model for each species. The effects of other environmental factors are removed when producing each individual graph.

4.1.1.1. Articulated Corallinacea

Number of obs = 967
Wald $\chi^2(10)$ = 157.18, Prob > χ^2 = 0.0000
Log pseudolikelihood = -1383.2801
MacFadden pseudo-R^2 = 0.2202
Deviance: 2766.560

Robust (Std. Err. adjusted for 84 clusters in clustalt)
Note: 10 observations completely determined. Standard errors questionable.

Abundance =	Coef.	Std. Err.	z	P>|z|	[95% Conf. Interval]	
Idep__1	-1.007833	.2075647	-4.86	0.000	-1.414652	-.6010132
Idep__2	1.285068	.3062478	4.20	0.000	.6848337	1.885303
Idep__3	-.4510909	.1184874	-3.81	0.000	-.6833219	-.2188598
Isl__1	-3.47707	1.316879	-2.64	0.008	-6.058105	-.8960359
Isl__2	3.612199	1.491819	2.42	0.015	.6882873	6.536111
Isl__3	-1.260505	.609738	-2.07	0.039	-2.45557	-.0654409
Iexps__1	.8530226	.3438322	2.48	0.013	.1791239	1.526921
Iexps__2	-.3641946	.1727511	-2.11	0.035	-.7027806	-.0256086
Iexpc__1	.0050942	.0013065	3.90	0.000	.0025335	.0076549
Ichla__1	-4.173645	1.415258	-2.95	0.003	-6.9475	-1.39979

(Ancillary parameters)

_cut1	-2.714525	.4846635
_cut2	-2.176556	.4540506
_cut3	-.2375432	.3447293
_cut4	.3823935	.3416814
_cut5	1.18893	.3546992
_cut6	2.467325	.3496625

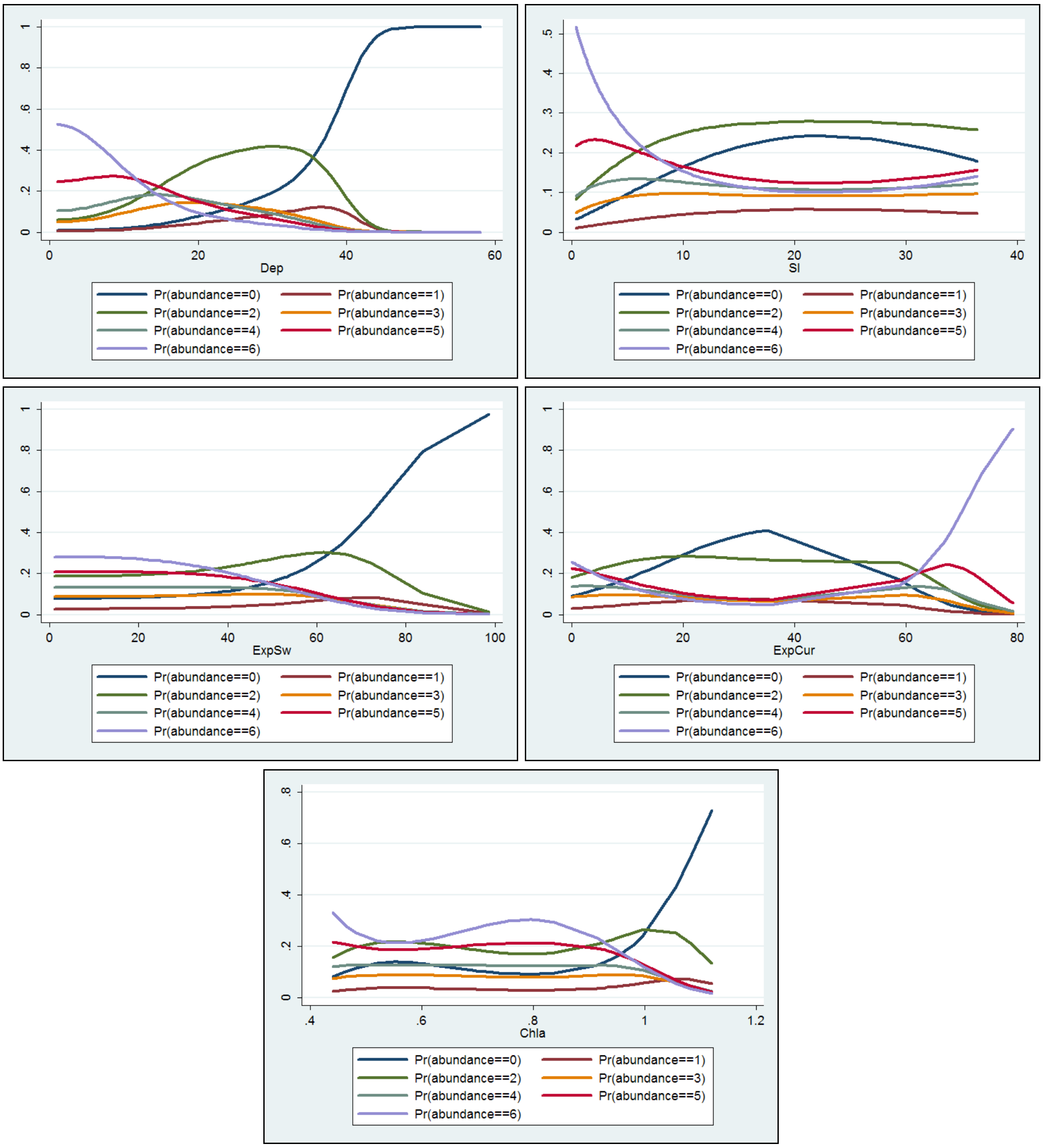

Figure 16. Articulated Corallinacea: probability of the different abundance classes (*yy* axis) *versus* significant explanatory variables Dep (depth), Sl (slope), ExpSw (exposure to swell), ExpCur (exposure to tidal currents) and Chla (chlorophyll-*a* concentration).

4.1.1.2. *Codium elisabethae*

Number of obs = 926
Wald $\chi^2(6)$ = 90.18, Prob > χ^2 = 0.0000
Log pseudolikelihood = -887.11089
MacFadden pseudo-R^2 = 0.1875
Deviance: 1774.222

Robust (Std. Err. adjusted for 84 clusters in clustalt)
Note: 19 observations completely determined. Standard errors questionable.

Abundance =	Coef.	Std. Err.	z	P>|z|	[95% Conf. Interval]	
Idep__1	1.933366	.3545979	5.45	0.000	1.238366	2.628365
Idep__2	-1.419202	.2633827	-5.39	0.000	-1.935423	-.9029818
Isl__1	-.9794122	.4025234	-2.43	0.015	-1.768344	-.1904808
Isl__2	.280488	.1084546	2.59	0.010	.0679209	.4930551
Iexpc__1	-1.391132	.3335477	-4.17	0.000	-2.044873	-.7373905
Iexpc__2	.0271913	.0056092	4.85	0.000	.0161975	.0381851

(Ancillary parameters)

_cut1	.8212923	.4262952
_cut2	1.35638	.4443274
_cut3	2.323708	.4254287
_cut4	3.672151	.6188751
_cut5	4.408702	.6867768
_cut6	5.528997	.6618321

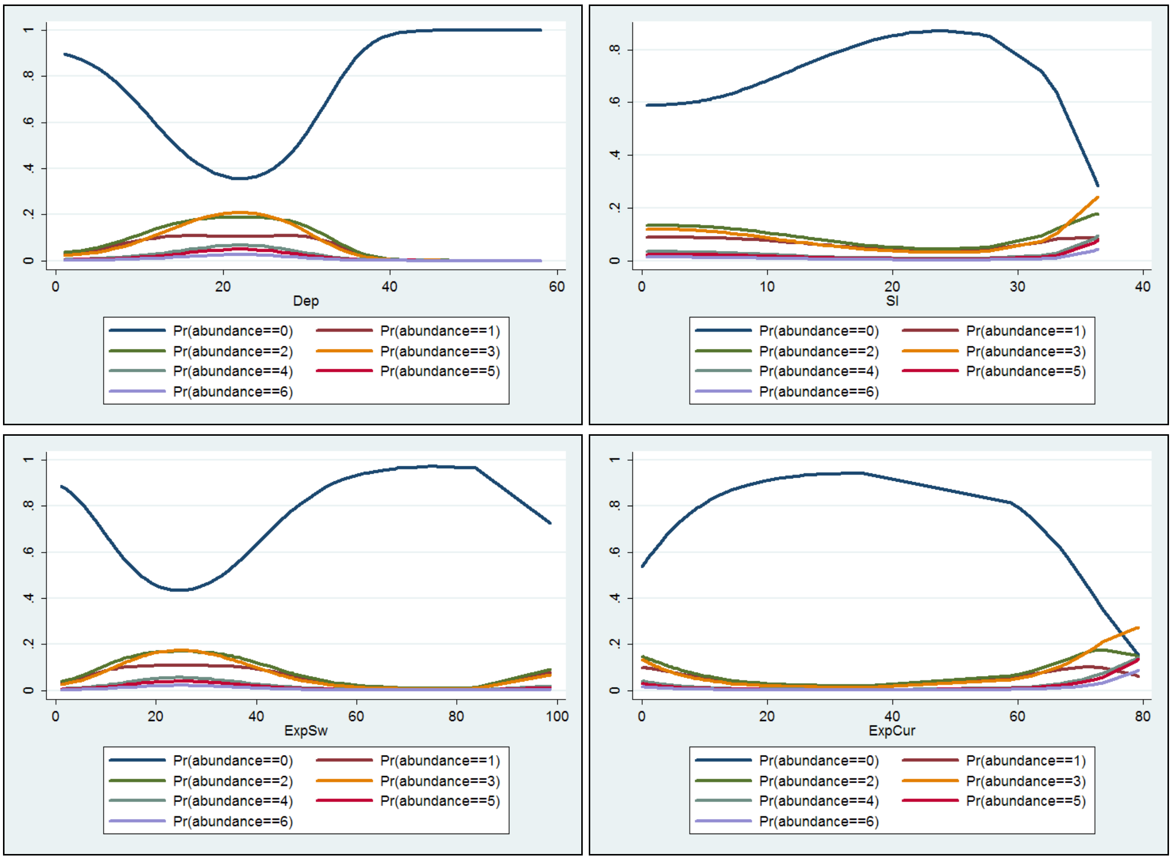

Figure 17. *Codium elisabethae*: probability of the different abundance classes (*yy* axis) *versus* significant explanatory variables Dep (depth), Sl (slope) and ExpSw (exposure to swell) and ExpCur (exposure to tidal currents).

4.1.1.3. *Dictyota* spp.

Number of obs = 985
Wald $\chi^2(5)$ = 58.36, Prob > χ^2 = 0.0000
Log pseudolikelihood = -1633.8302
MacFadden pseudo-R^2 = 0.0755
Deviance: 3267.660

Robust (Std. Err. adjusted for 85 clusters in clustalt)

Abundance =	Coef.	Std. Err.	z	P>|z|	[95% Conf. Interval]	
Idep__1	1.595986	.4205557	3.79	0.000	.7717119	2.42026
Idep__2	-2.17784	.5634169	-3.87	0.000	-3.282117	-1.073563
Idep__3	.7119265	.1962599	3.63	0.000	.3272641	1.096589
Isl__1	1.039181	.2425325	4.28	0.000	.563826	1.514536
Isl__2	-.8154786	.1892242	-4.31	0.000	-1.186351	-.444606

(Ancillary parameters)

_cut1	-3.184826	.3513949
_cut2	-1.831579	.3144959
_cut3	-.6241853	.2765847
_cut4	.043266	.2526344
_cut5	1.155507	.2641389
_cut6	3.783962	.993613

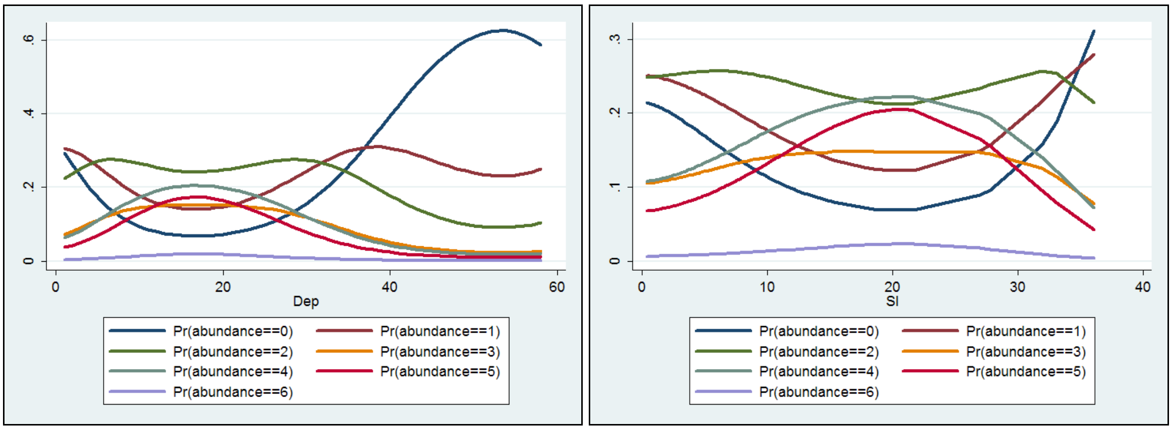

Figure 18. *Dictyota* spp.: probability of the different abundance classes (*yy* axis) *versus* significant explanatory variables Dep (depth) and Sl (slope).

4.1.1.4. *Halopteris filicina*

Number of obs = 934
Wald $\chi^2(6)$ = 86.47, Prob > χ^2 = 0.0000
Log pseudolikelihood = -1483.6426
MacFadden pseudo-R^2 = 0.1537

Robust (Std. Err. adjusted for 88 clusters in clustalt)

Abundance =	Coef.	Std. Err.	z	P>|z|	[95% Conf. Interval]	
Idep__1	.8710306	.2050167	4.25	0.000	.4692053	1.272856
Idep__2	-.8671836	.2794548	-3.10	0.002	-1.414905	-.3194622
Idep__3	.2136116	.0952064	2.24	0.025	.0270105	.4002128
Isl__1	-.2704756	.1273548	-2.12	0.034	-.5200863	-.0208648
Isl__2	.2483882	.0988193	2.51	0.012	.0547059	.4420706
Iexps__1	-.0198441	.0085247	-2.33	0.020	-.0365522	-.0031361

(Ancillary parameters)

_cut1	-1.782497	.2963483	-2.363329	-1.201665
_cut2	-.9696075	.2560866	-1.471528	-.467687
_cut3	-.2098087	.2723293	-.7435644	.323947
_cut4	.3853208	.2747062	-.1530935	.9237351
_cut5	1.246665	.309271	.6405055	1.852825
_cut6	3.251844	.402863	2.462247	4.041441

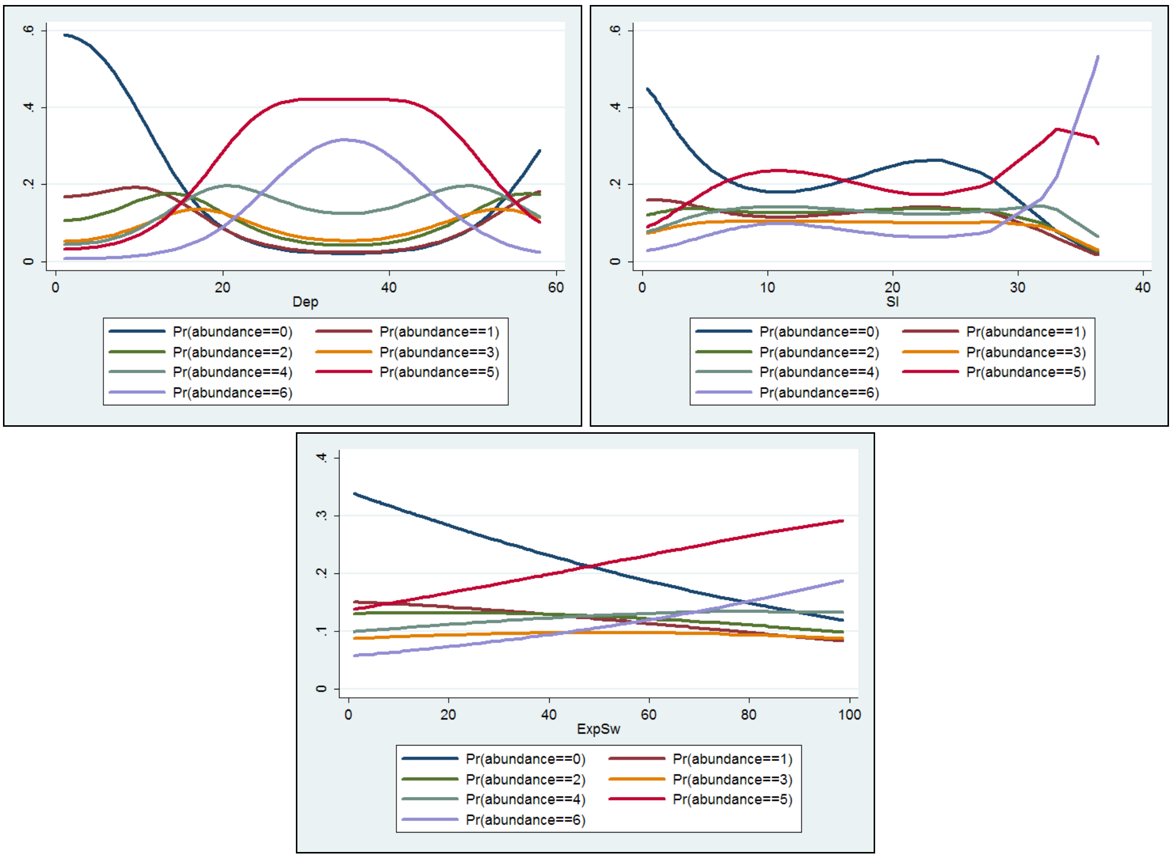

Figure 19. ***Halopteris filicina*: probability of the different abundance classes (*yy* axis) *versus* significant explanatory variables Dep (depth), Sl (slope) and ExpSw (exposure to swell).**

4.1.1.5. *Padina pavonica*

Number of obs = 1020
Wald χ^2 (8) = 23.40, Prob > χ^2 = 0.0029
Log pseudolikelihood = -1184.7976
MacFadden pseudo-R^2 = 0.1177
Deviance: 2369.595

Robust (Std. Err. adjusted for 88 clusters in clustalt)

Abundance =	Coef.	Std. Err.	z	P>|z|	[95% Conf. Interval]	
Idep__1	2.636937	.714174	3.69	0.000	1.237182	4.036692
Idep__2	-2.169703	.5230487	-4.15	0.000	-3.19486	-1.144547
Iexpc__1	.4964269	.1573274	3.16	0.002	.1880707	.804783
Iexpc__2	-.5238331	.1673854	-3.13	0.002	-.8519024	-.1957638
Iexpc__3	.1377875	.0448328	3.07	0.002	.0499169	.2256582
Ichla__1	10.05875	4.393044	2.29	0.022	1.448536	18.66895
Ichla__2	-36.68112	13.3111	-2.76	0.006	-62.7704	-10.59185
Ichla__3	118.3509	45.5516	2.60	0.009	29.07143	207.6304

(Ancillary parameters)

_cut1	-1.826633	.5058252
_cut2	-.2020621	.5049939
_cut3	.4783579	.5233125
_cut4	1.173244	.5203416
_cut5	1.903653	.5994212
_cut6	2.744483	.7860764

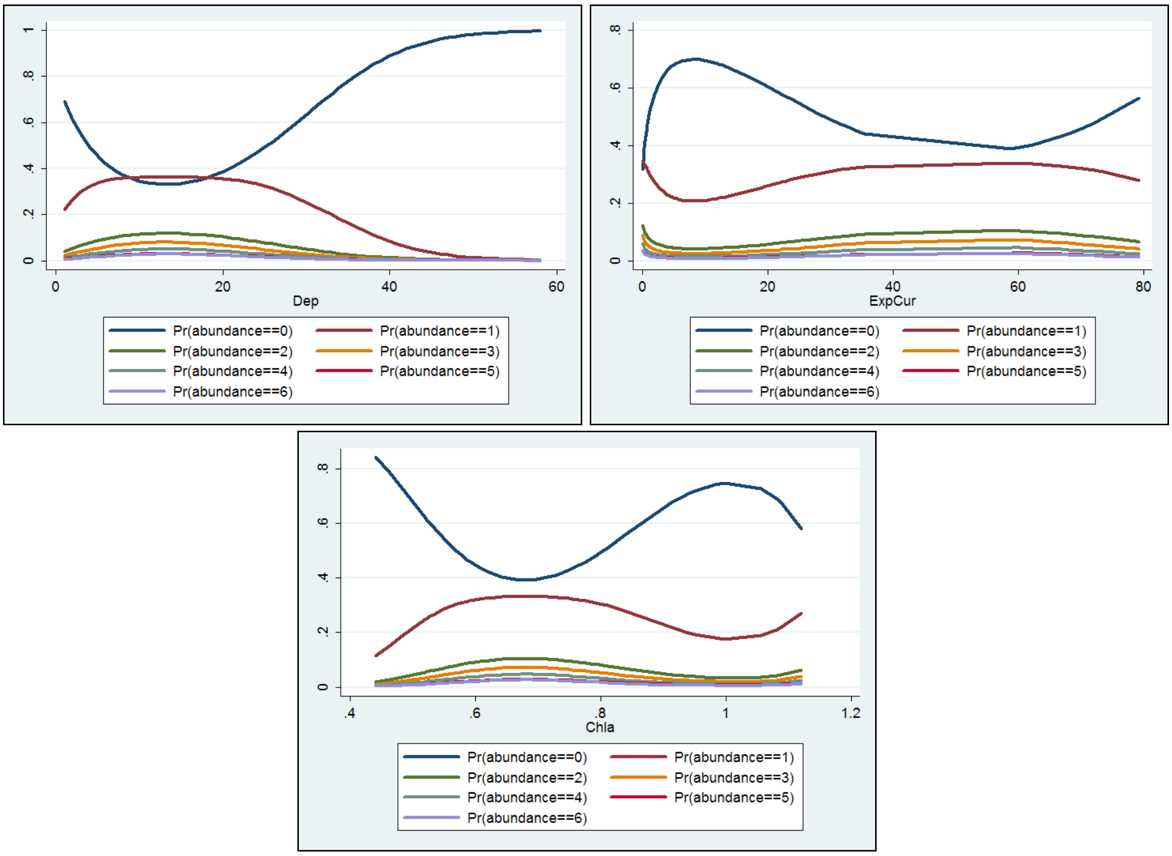

Figure 20. *Padina pavonica*: probability of the different abundance classes (*yy* axis) *versus* significant explanatory variables Dep (depth), ExpCur (exposure to tidal currents) and Chla (chlorophyll-*a* concentration).

4.1.1.6. *Zonaria tournefortii*

Number of obs = 1013
Wald χ^2 (4) = 57.24, Prob > χ^2 = 0.0000
Log pseudolikelihood = -1498.6536
MacFadden pseudo-R^2 = 0.1115
Deviance: 2997.307

Robust (Std. Err. adjusted for 91 clusters in clustalt)

Abundance =	Coef.	Std. Err.	Z	P>|z|	[95% Conf. Interval]	
Idep__1	1.116212	.170128	6.56	0.000	.7827676	1.449657
Idep__2	-.6561395	.1057902	-6.20	0.000	-.8634845	-.4487945
Isl__1	-1.069366	.4101216	-2.61	0.009	-1.87319	-.2655428
Isl__2	.6695263	.3060441	2.19	0.029	.069691	1.269362

(Ancillary parameters)

_cut1	-1.018697	.3617213
_cut2	-.0093288	.3516904
_cut3	.4095036	.3240473
_cut4	.7423474	.3146797
_cut5	1.060456	.3067934
_cut6	1.874625	.3265784

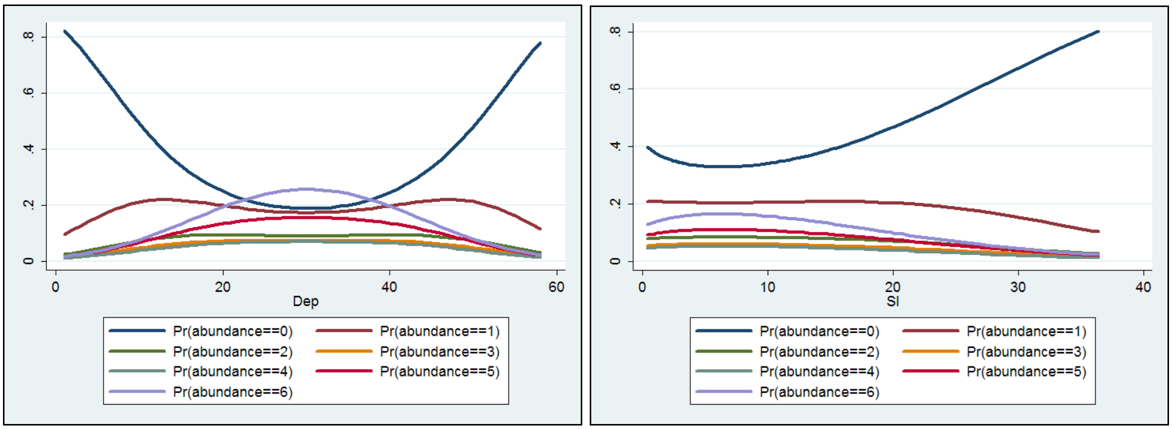

Figure 21. *Zonaria tournefortii*: probability of the different abundance classes (*yy* axis) *versus* significant explanatory variables Dep (depth) and Sl (slope).

4.1.2. Goodness of fit

The maximum fit (MacFadden pseudo-R^2 = 0.2202) was obtained for articulated Corallinaceae whilst the poorest fit (MacFadden pseudo-R^2 = 0.0755) was obtained for *Dictyota* spp. These values represent goodness of fit levels that can be considered good (articulated Corallinaceae, *Codium elisabethae*), intermediate (*Halopteris filicina*, *Padina pavonica*, *Zonaria tournefortii*) and poor (*Dictyota* spp.).

4.1.3. Spatialization of the models

The multivariable models obtained for each species are spatialized in Figure 23 to Figure 28. The most probable outcome derived from using the final model upon the rasters of the significant explanatory variables is used as the predicted abundance class (A). The probability of the predicted abundance class is shown in the associate figure (B). Due to variance in the data, a higher number of outcomes statistically compete when the species is present ("presence areas"). This explains the observed decrease in the probability of the predicted abundance class in the "presence areas" in comparison to the marginal areas of the distribution, where absence is predicted and usually presents a much higher probability than the other possible outcomes (e.g., see graphs for probability of the different abundance classes *versus* depth in Figure 17 to Figure 21).

In all maps, rocks beyond 58m depth are intrinsically masked as species absence as predictions were not conducted for raster cells with depth>58m. That was the bathymetric limit where the *taxa* analysed were observed.

A

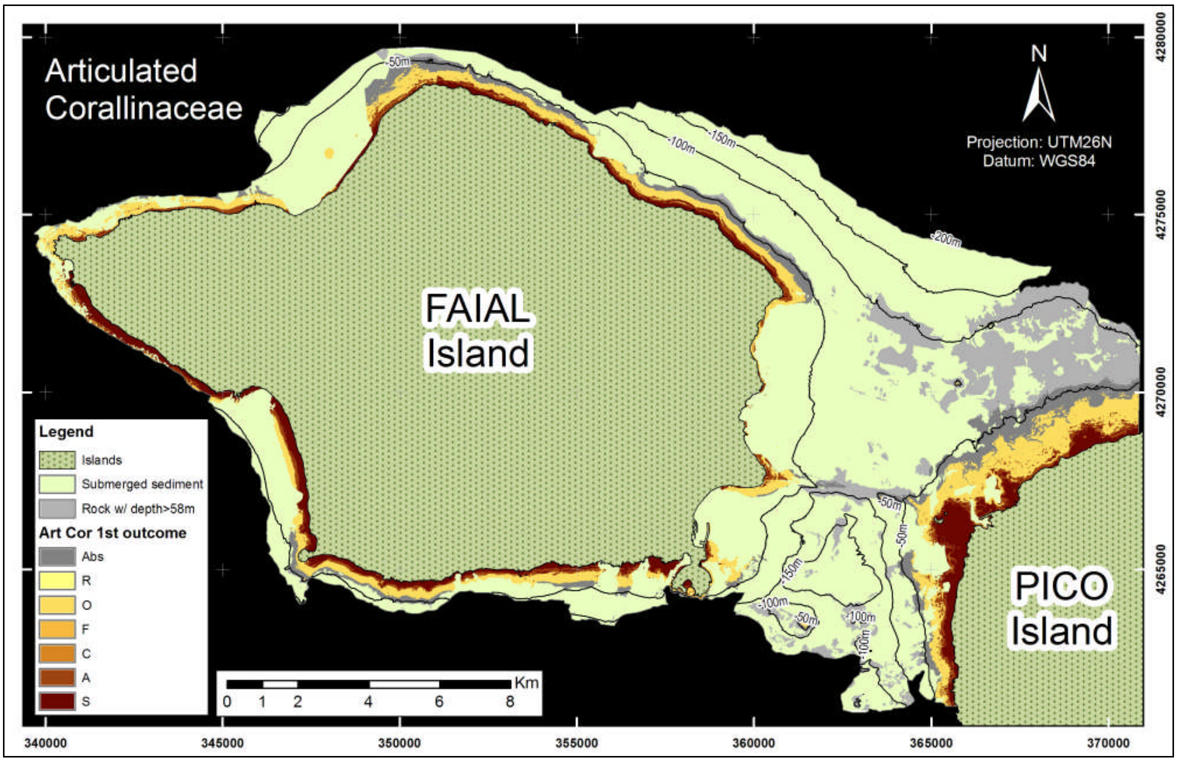

B

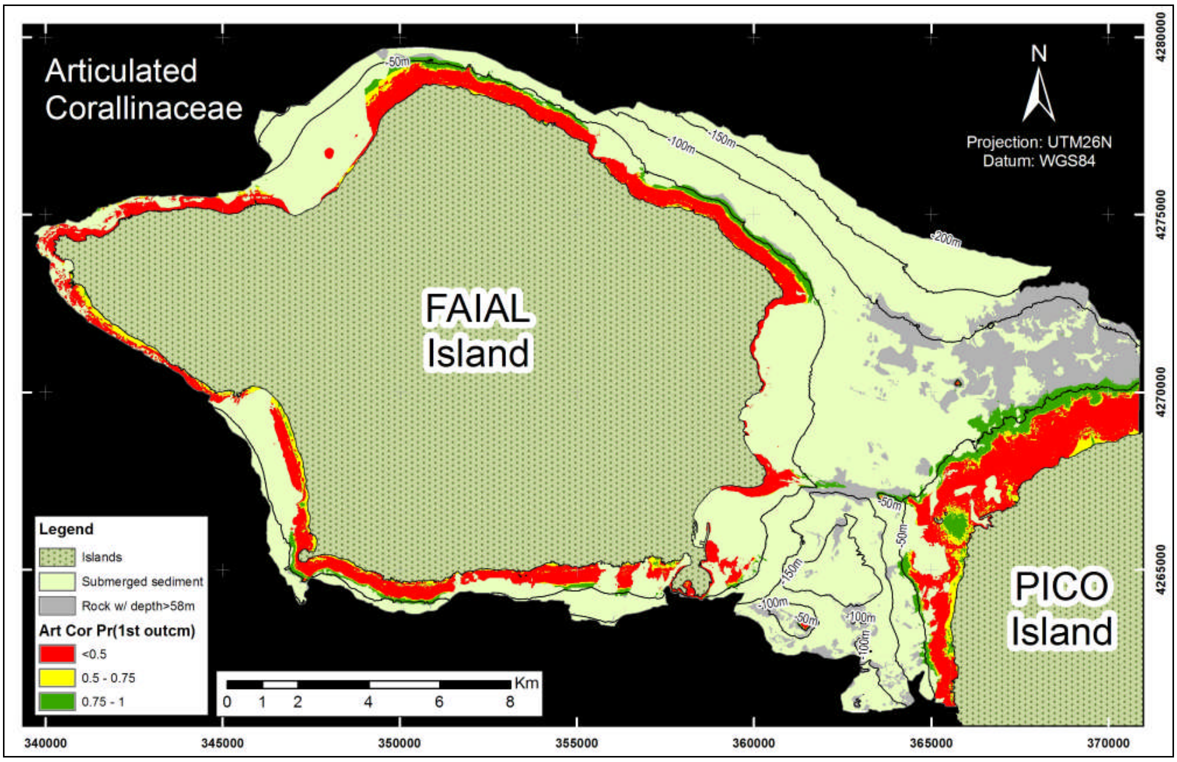

Figure 22. Articulated Corallinaceae: A. Spatialization of the abundance class prediction (most probable outcome) using the final model upon the rasters of the significant explanatory variables. B. Probability of the predicted abundance class.

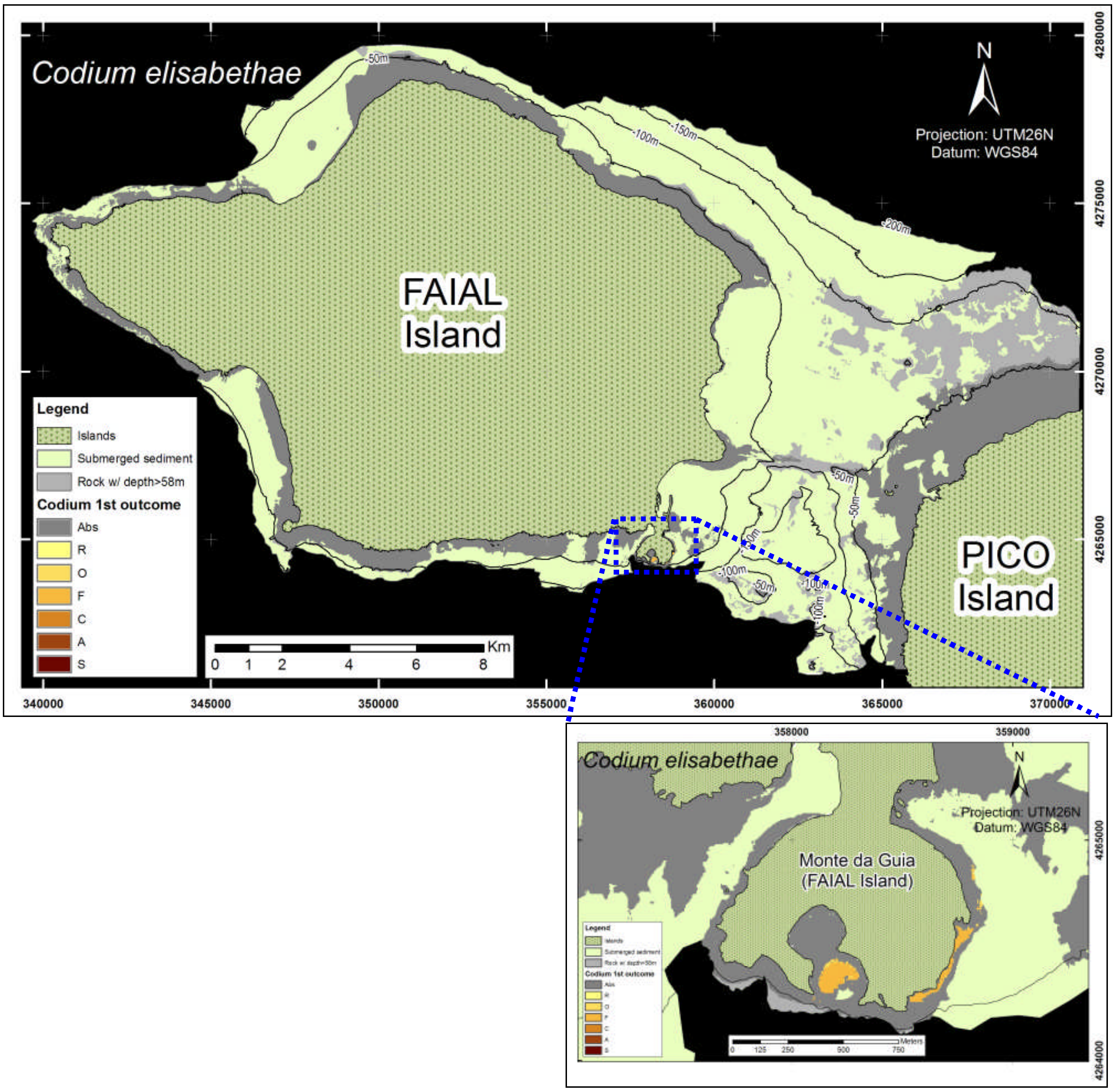

Figure 23. ***Codium elisabethae*****: Spatialization of the abundance class prediction (most probable outcome) using the final model upon the rasters of the significant explanatory variables.**

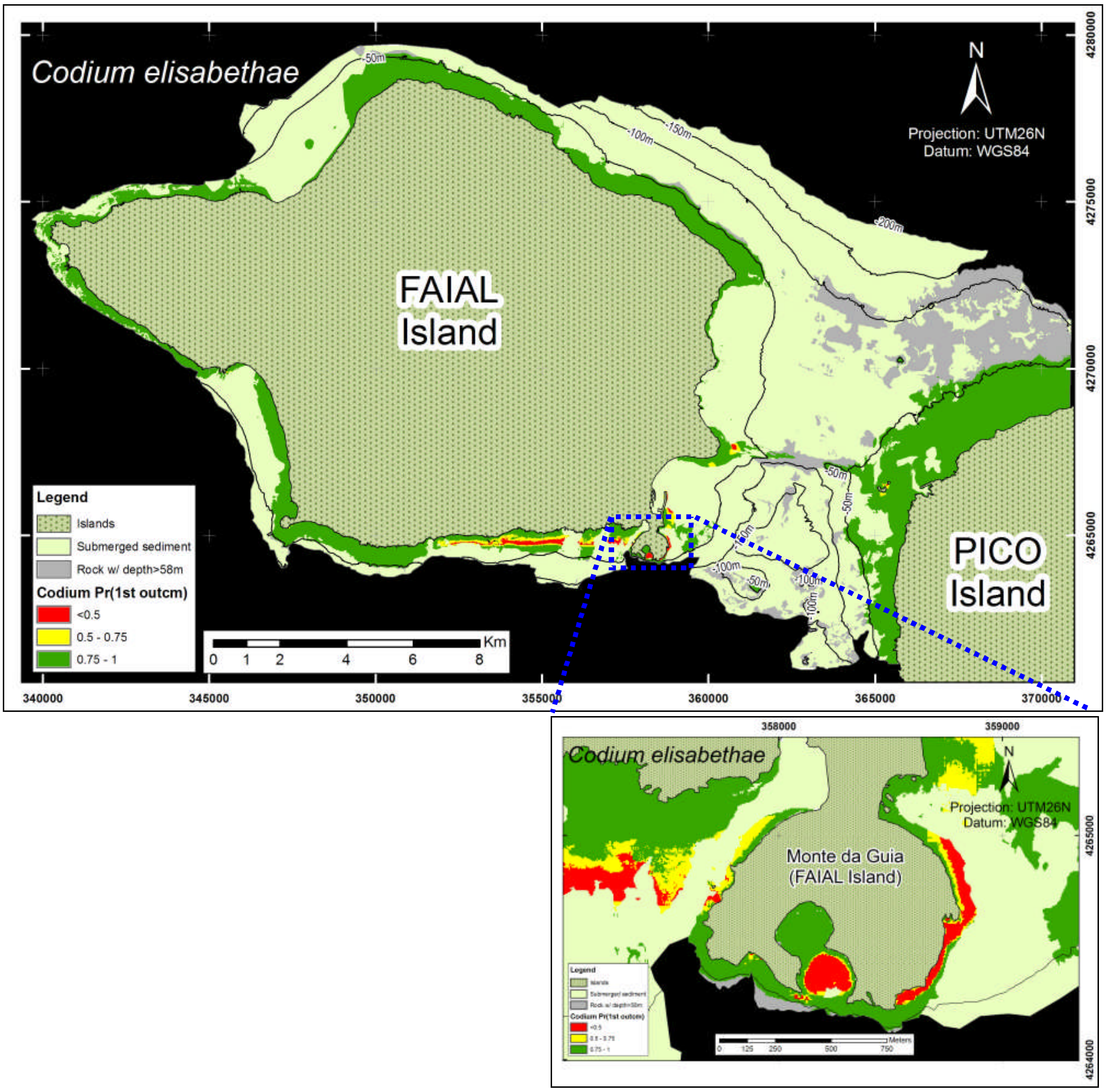

Figure 24. ***Codium elisabethae*****: Probability of the predicted abundance class.**

A

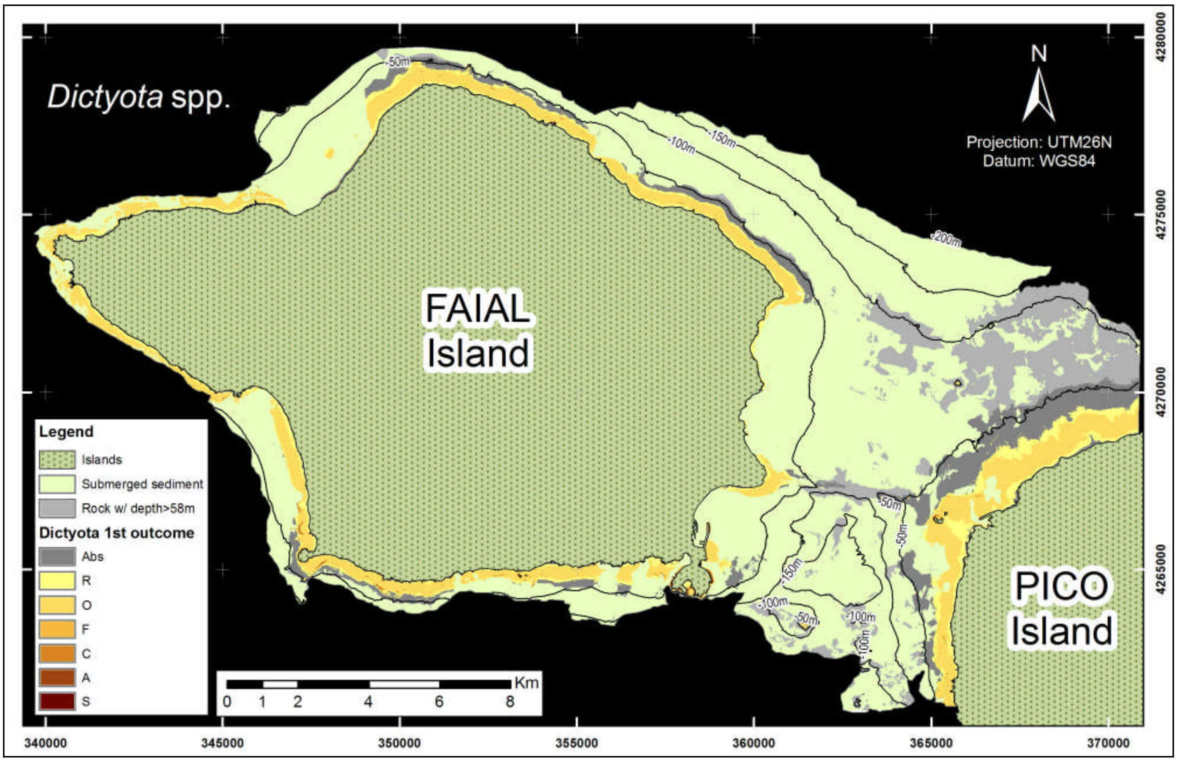

B

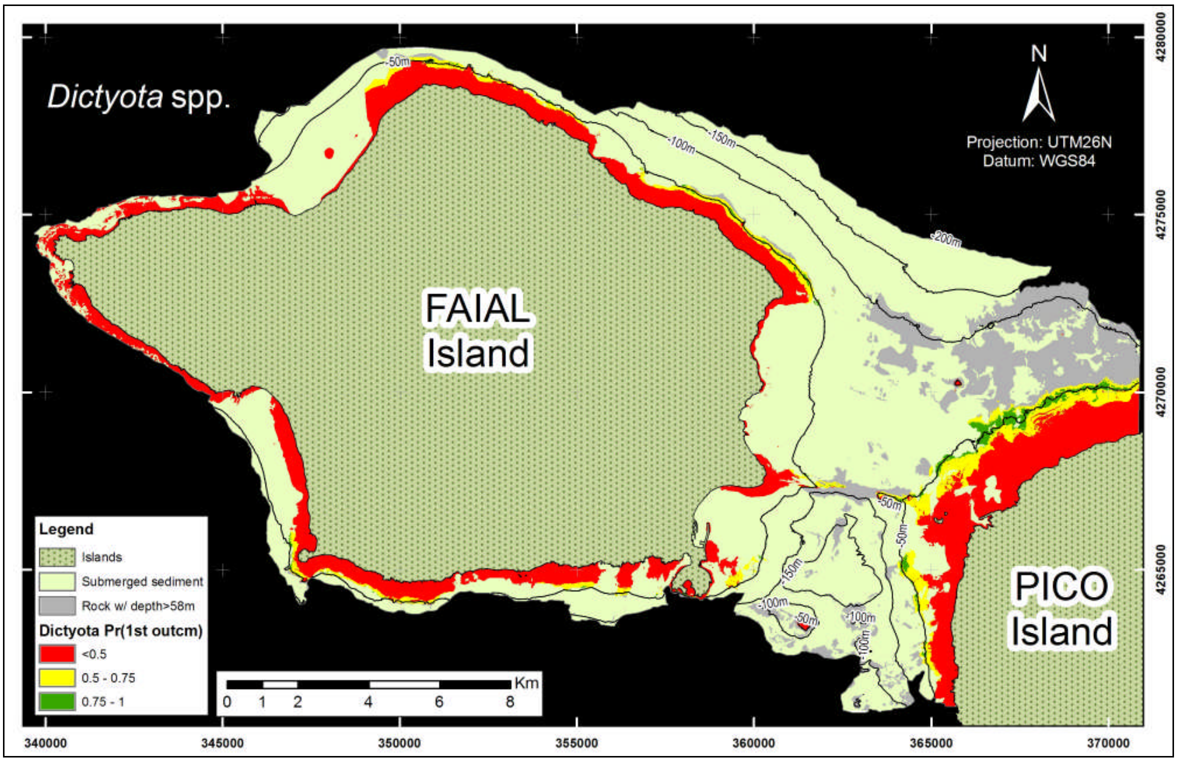

Figure 25. *Dictyota* **spp.: A. Spatialization of the abundance class prediction (most probable outcome) using the final model upon the rasters of the significant explanatory variables. B. Probability of the predicted abundance class.**

A

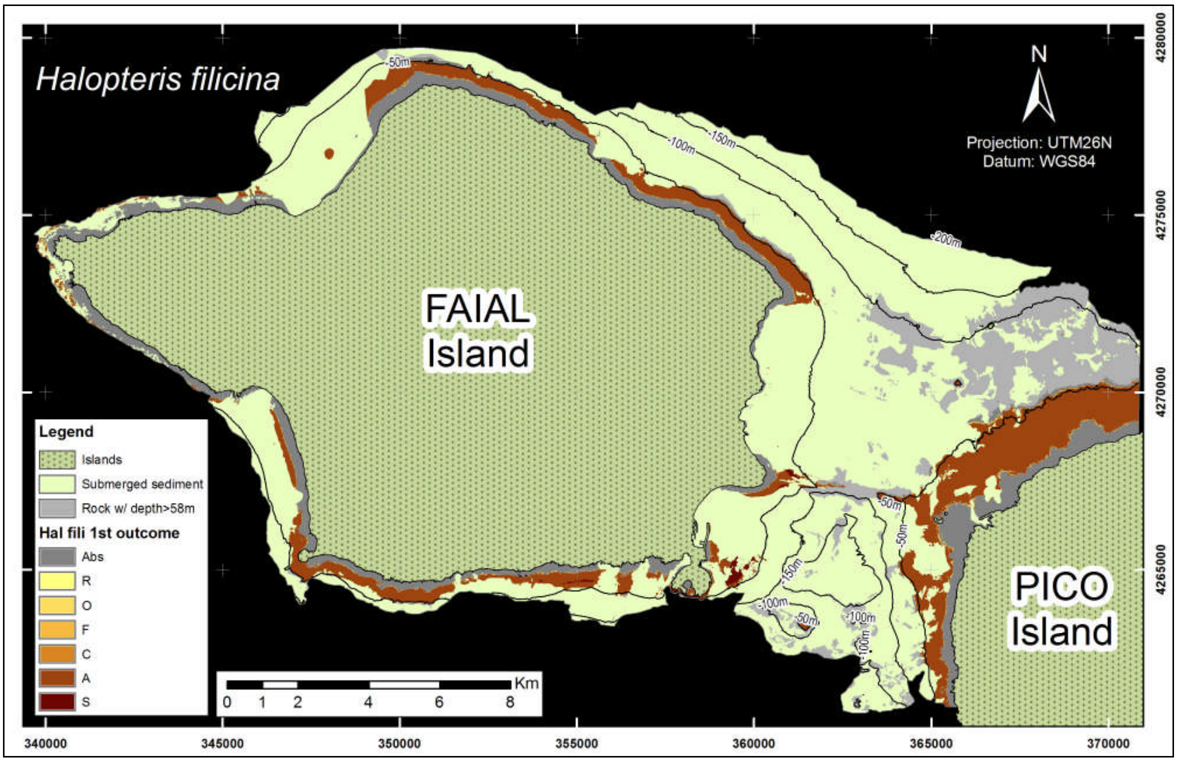

B

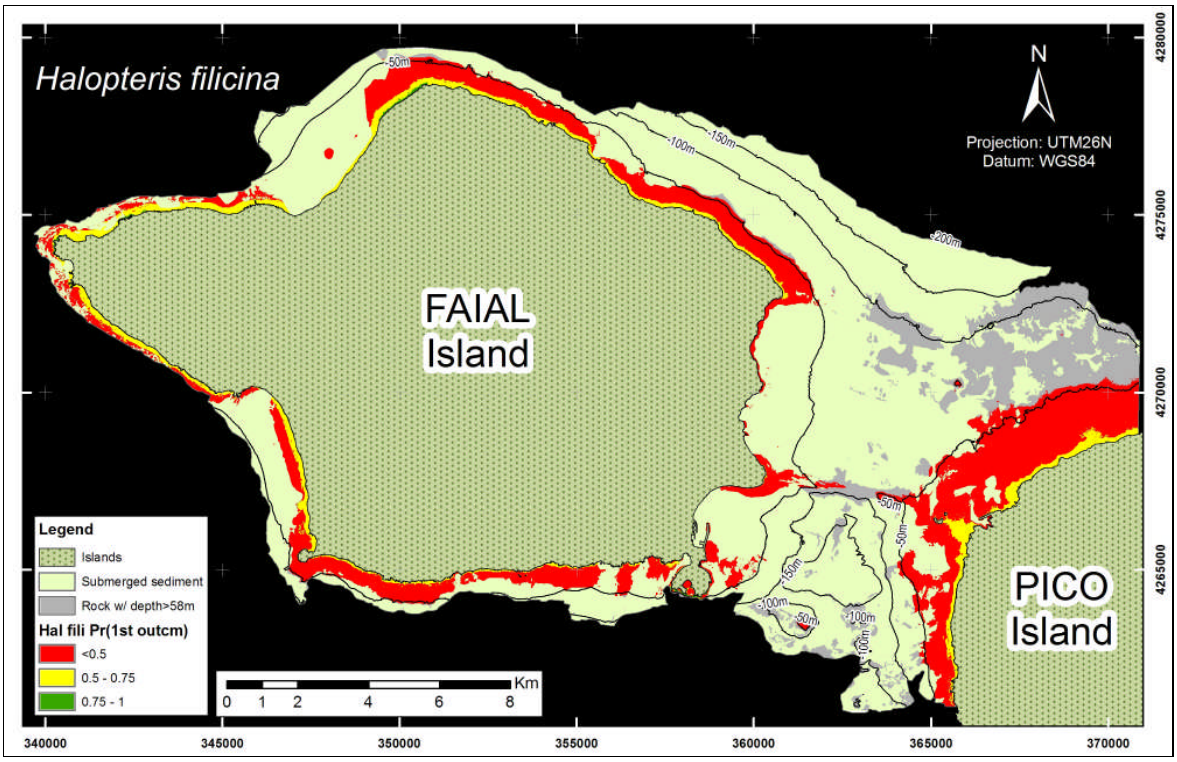

Figure 26. ***Halopteris filicina*****: A. Spatialization of the abundance class prediction (most probable outcome) using the final model upon the rasters of the significant explanatory variables. B. Probability of the predicted abundance class.**

A

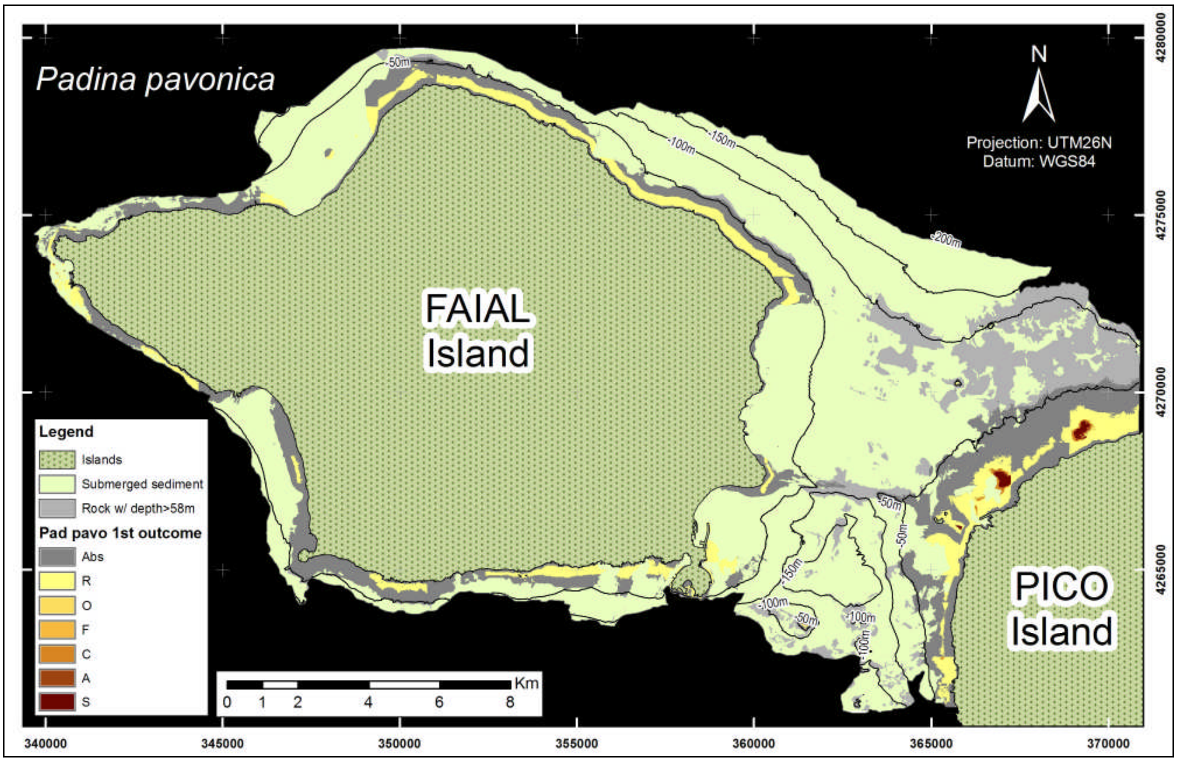

B

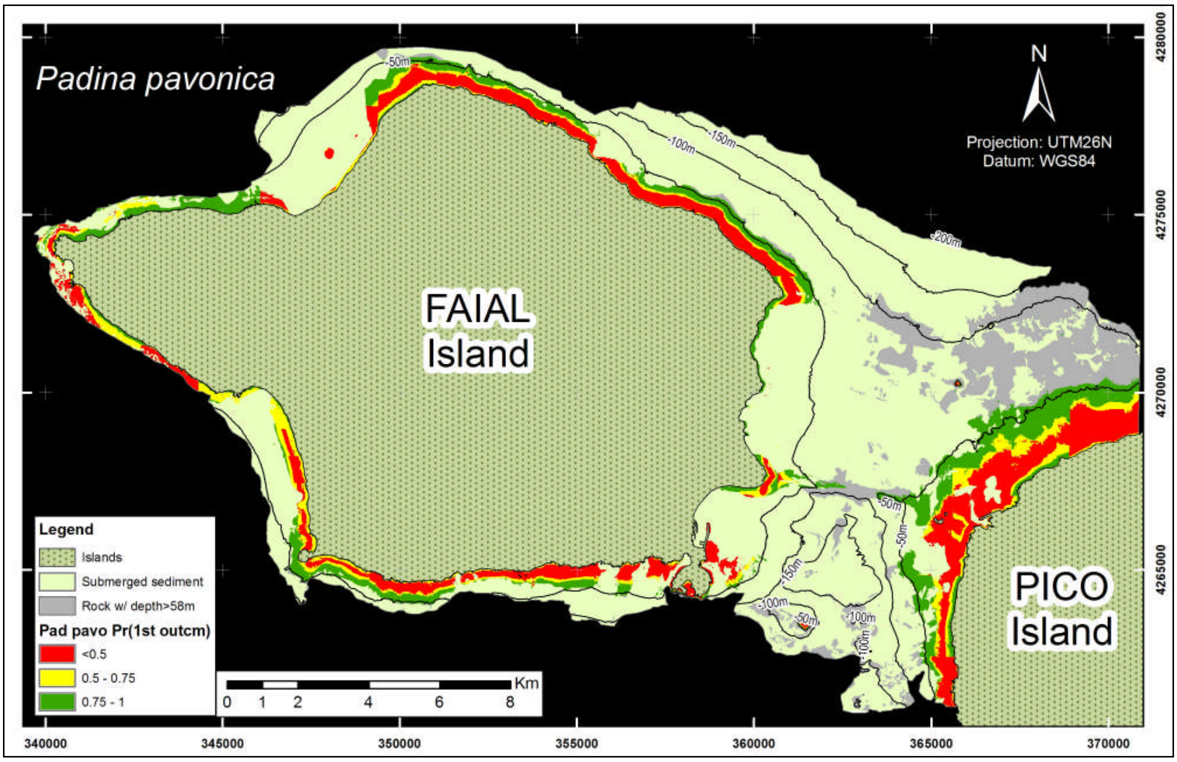

Figure 27. *Padina pavonica*: A. Spatialization of the abundance class prediction (most probable outcome) using the final model upon the rasters of the significant explanatory variables. B. Probability of the predicted abundance class.

A

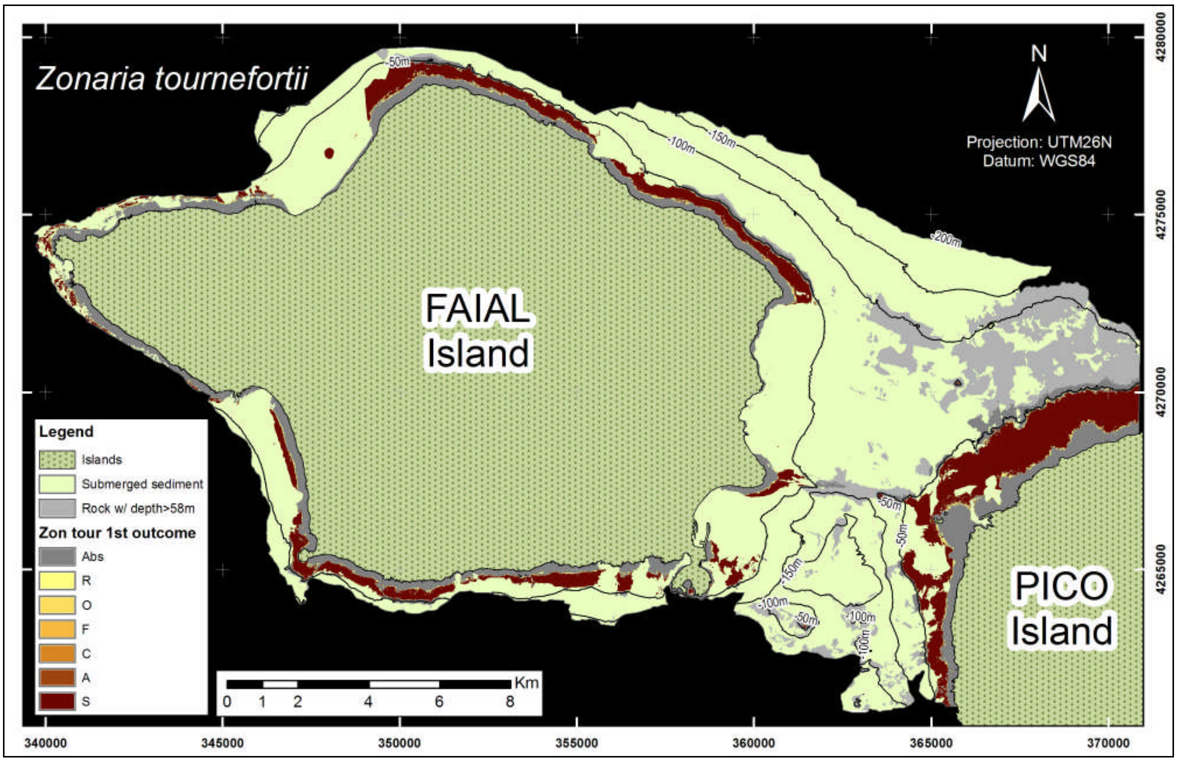

B

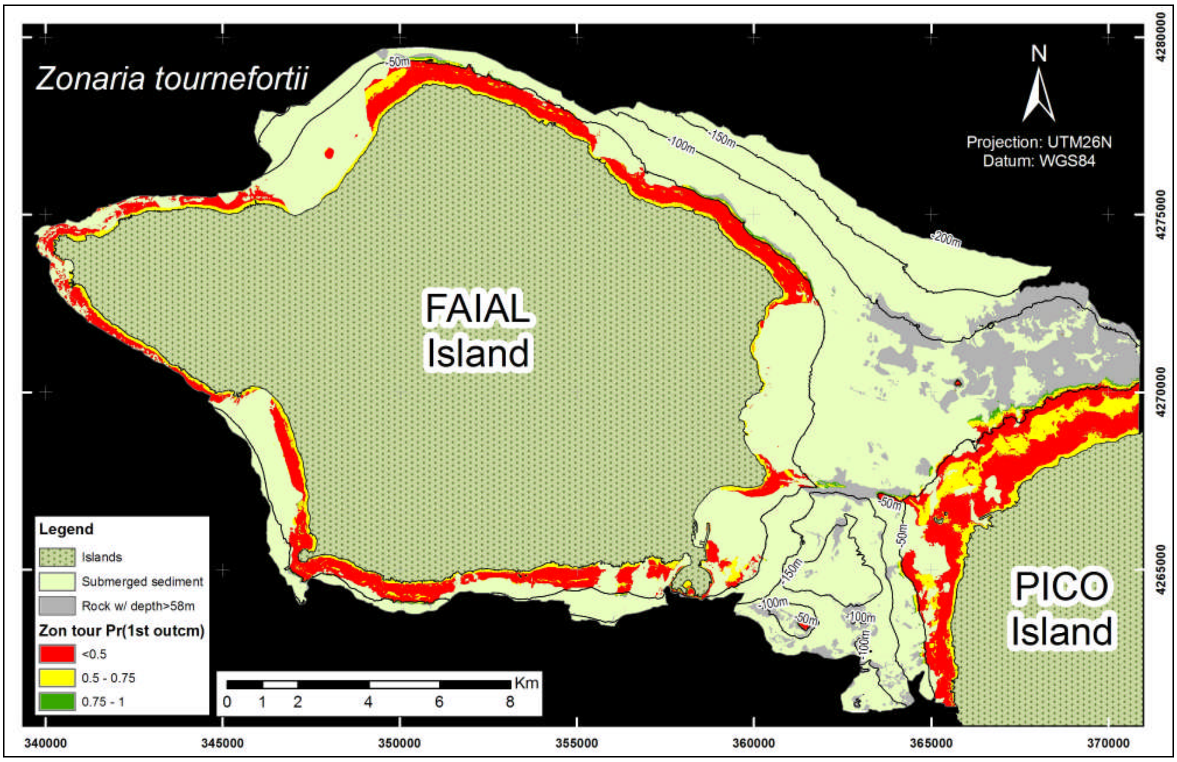

Figure 28. ***Zonaria tournefortii*****: A. Spatialization of the abundance class prediction (most probable outcome) using the final model upon the rasters of the significant explanatory variables. B. Probability of the predicted abundance class.**

4.1.3.1. Dominant species composite

A composite map where pixels dominated by different species are symbolized in different colours is shown in Figure 29. In some pixels, two or three species are co-dominant. The map demonstrates the spatial distribution of the different *facies* in the study area and is particularly successful in highlighting their succession along a shore-normal/depth-wise profile.

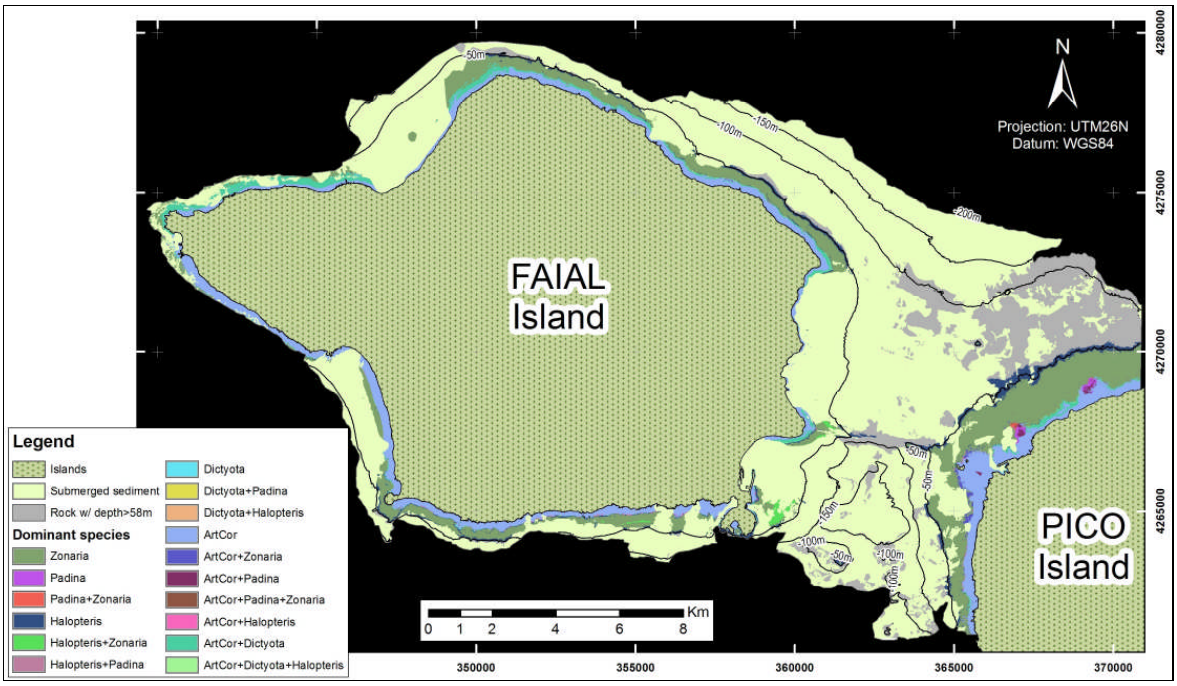

Figure 29: Spatial distribution of *facies* dominated by different species.

5. Discussion

The role of macroalgae in providing substrate, shelter, nesting and feeding grounds for a wide variety of microorganisms, epiphytic algae, invertebrates and fish makes them key ecologic forces regulating the structure of the associated infralittoral communities.

The results presented here demonstrate that the abundances of the six macroalgae *taxa* studied have a non-uniform distribution around the island of Faial. The different combinations of environmental variables providing the best explanation for the abundance variations observed in different species underline the complex interrelationships between macroalgae abundance and environmental variables.

As in any statistical modelling, inferences about pattern-process causal relationships underlying the variability observed would be speculative. Conclusions are based on spatial associations discussed in view of limited information presented in previous studies about the ecologic requirements of studied species in the biogeographic region of Macaronesia.

5.1. Depth

The fact that this parameter has been significant in all models highlights the prominence of depth in regulating the abundance of macroalgae in the Azores (Neto et al., 2000) as in other regions (e.g., Goldberg & Kendrick, 2004). From a modelling perspective, depth usually represents a proxy for other parameters such as light quantity and quality, wave and wind-induced hydrodynamics as well as temperature, all of which usually decrease with increasing depth. Identifying which of these individual factors causes the vertical variation in the abundance of the different target species would require additional information not available to this study.

The results support the association of the articulated Coralliaceae with shallow infralittoral levels and the association of *Dictyota* spp. and *Padina pavonica* with mid infralittoral depths (Neto et al., 2000, Tittley & Neto, 2000, Wallenstein et al., 2007). *Codium elisabethae* appears to reach a maximum slightly deeper than the later species but should also be included in the mid infralittoral.

The sciaphilous character of *Zonaria tournefortii* (Montañés et al., 2002) and *Halopteris filicina* (Augier, 1985) are also confirmed. Both these species can occur to shallower levels but in these situations they are usually confined to shaded microhabitats. They start colonising upper surfaces at depths greater than 25-30m and typically dominate the assemblages in the deep infralittoral to depths greater than 40m. Around Faial, *Halopteris filicina* is the last conspicuous frondose macroalgae to disappear before circalittoral assemblages establish, which can be considered to occur in areas deeper than 55m deep.

It is interesting to note that the vertical location of the facies of *Padina pavonica* (mid infralittoral in the Azores) vs. *Zonaria tournefortii* (deep infralittoral in the Azores) is inverted when compared to their relative position in Madeira Island (Augier, 1985; Bianchi et al., 1998).

5.2. Slope

Slope of the substratum has been shown to strongly influence many eulittoral and infralittoral organisms and be a major structuring factor in coastal communities (e.g.: Whorff et al., 1995; Gabriele et al., 1999; Somsueb et al., 2001; Toohey, 2007). Whorff et al. (1995) attributes this effect to the amount of sedimentation that affects the algal fronds.

With the exception of *Padina pavonica*, slope has been significant in all the models. This is interpreted as a confirmation of the influence of medium scale bottom physiography (as opposed to a micro-scale corresponding to, e.g., an analysis of upper surfaces of boulders vs. their flanks or undersides) in the distribution of studied macroalgae. Because the species observations that were used to build the models were inherently limited to horizontal and sub-horizontal rocky surfaces, the role of other aspects of bottom physiography on macroalgal distribution was not tested. However, it is worth-mentioning that rocky substrate categories (e.g., bedrock, boulders, cobbles) were not found to play a determinant role in influencing the infralittoral macroalgal assemblages studied by Wallenstein et al. (2007) in the Azores.

5.3. Exposure to swell and currents

Hydrodynamic conditions induced by swell and currents are two factors found to significantly regulate infralittoral communities in various parts of the world (e.g., Menge & Sutherland, 1976, 1987; Underwood & Chapman, 1998; Goldberg & Kendrick, 2004; Tuya & Haroun, 2006) and are key factors used in many biotope classifications (e.g., Stephenson and Stephenson, 1949; Connor et al., 1997).

These two variables are not necessarily spatially coincident around Faial. According to the proxy used for exposure to currents, the highest impact of tidal currents should concentrate in the Faial-Pico passage and off the Capelinhos headland. However, areas most exposed to swell are those between the North and Westernmost ends of the island. This separation of regimes provided a good opportunity to assess which species respond to each of the variables individually.

Results suggest that *Halopteris filicina* is influenced by exposure to swell alone, whilst *Codium elisabethae* and *Padina pavonica* respond to tidal currents instead. Articulated Corallinacea seem to respond to both types of hydrodynamic conditions. For *Dictyota* spp. and *Zonaria tournefortii* this parameter was non-significant and therefore not used in the model that produced the best explanation of the data variance.

The influence of hydrodynamic exposure in articulated Corallinaceae supports the differences in abundance of coralline turfs previously reported by Neto et al., 2000, Tittley & Neto, 2000 Tuya & Haroun (2006) between sheltered and exposed coasts. This infralittoral association is typically best developed on the leeward side of the Macaronesian islands.

As is both apparent from the raw data and the predictive map produced for *Codium elisabethae* (Figure 4 and Figure 24 respectively) the species occurs preferentially in areas sheltered from tidal currents and on the leeside to prevailing swells. The growth form and size attained by the species may make it prone to plants being easily detached from the substrate in highly hydrodynamic conditions. It is worth-noting that massive pull out events have been recorded under exceptional hydrodynamic conditions in the leeward coasts (personal observations) and this may play a significant role in the population dynamics of the species. The life strategy of the species, where asexual budding represents a non-negligeable reproductive contribution

(Sirjacobs et al., 2004), may further favour the persistence of denser populations in locations where individuals are present already.

From the raw data and predictive map produced for *Padina pavonica* (Figure 7 and Figure 27 respectively) it worth noting the association of the species to exposed habitats such as the mid-channel reefs and NW and SW coast of Pico. This does not support the inclusion of this species in a "photophylous infralittoral rock biocenosis subject to relatively calm conditions" as suggested by Augier (1985) for the other Macaronesian archipelago of Madeira. Together with the previous observation regarding the vertical distribution of the species, it appears that *Padina pavonica* in the Azores finds climatic conditions in habitat with distinct attributes from Madeira.

5.4. SST

It is likely that the lack of significance obtained for this environmental variable in all models indicates that macroalgae abundance may not respond to water temperature at the range of variation found in the study area. Alternatively it may suggest a lack of relationship between sea surface temperature and the water temperature at the near-bottom layer, rejecting the hypothesis to use satellite-derived SST as a proxy for shelf waters temperature regime. Ultimately it may also be that the extrapolation used for obtaining temperature data in the near shore data blanks, where most sampling concentrated, may not be valid and this has precluded the identification of statistical relationships.

5.5. Chlorophyll-*a* concentration

Finding chl-*a* concentration to be significant in the models for articulated Corallinaceae and *Padina pavonica* could be interpreted as an indication that these species respond to the same conditions (namely in terms of nutritional properties) that also regulate primary production in the water column. This could represent a case of "bentho-pelagic coupling", i.e., the interaction of benthic communities with the biologic and physical processes in the nearshore pelagic environment (cf., Menge et al., 1997a,b).

This type of trophic and nutrient-derived interactions in marine community structure is a relatively recent area of research in marine ecology and its understanding is still limited to studies performed on relatively few *taxa* (for a macroalgae review see Schiel, 2004). Typically they have been studied in fucoid and kelp species, which only exceptionally dominate biotopes in the Azores. Although functional studies are required, the statistical models suggest that in warm temperate/subtropical oceanic islands, other functional groups may exhibit similar influences.

Mesoscale oceanographic patterns such as island upwelling processes (associated with either prevailing wind patterns or differences in island shelf and flank topography) are the most probable drivers for these effects, influencing the quantity of nutrients and phytoplankton circulated to algae and filter feeders living in the shallow nearshore. As an example, Menge et al. (1997a) determined that, on central Oregon shores, chl-*a* concentration in the water column was consistently higher at specific locations along the coast and demonstrated that the significant scale of variation was of tens of kilometers. Results derived from satellite imagery indicate that SST and chl-*a* differences at the several kilometers scale also seem to occur at the scale of Faial island (see Chapter 6).

5.6. Low goodness of fit

Limited success in capturing the variance of the data is evident from the low goodness of fit (as measured by MacFadden pseudo-R^2) obtained in some of the models. It is suggested that this is partially caused by a failure to include major environmental variables, namely some that further describe resource availability and habitat attributes interacting with the life-history strategies and the biology of the species. Moreover additional variables should have been considered to describe biological regulators of algal distribution such as species competition and predation. However complementary work based on the abundance of invertebrate and fish herbivores is necessary to develop such variables for the study area.

Finally it should be highlighted that the datasets analysed result from the fusion of data collected from different years (1999-2005) and different platforms (namely, direct observation by divers and visualization of video footage). For this reason, sampling-related factors should have been included as tentative explanatory variables which could have highlighted additional factors responsible for data variance. Regarding interannual variability in algal abundance on eulittoral and shallow infralittoral grounds of the Azores it is worth referring that an assessment conducted on a time scale of just two years (Neto, 2000) did not find inter-annual changes to be too important. From the 30 dominant species investigated in that study, only one species (*Dictyota dichotoma*) showed statistically significant inter-annual changes in abundance. Coincidently, this species was included in the *taxon* for which the lowest goodness of fit was obtained (*Dictyota* spp.) and therefore it is hypothesized that temporal variability was partially responsible for the low predictive power of the *Dictyota* spp. model. An enhanced experimental design with temporal calibration of surveys would be required to assess and control the true influence of these factors. Furthermore, potential methodological variance introduced by different observers and visual surveying methods (namely scuba divers, ROV and drop-down camera) should also be investigated.

5.7. Cross-validation

The predictive power or accuracy of the statistical models was not independently assessed due to time shortages. Therefore the models should not be considered as fully validated by independent data. It is suggested that in the future this analysis is undertaken using a split-sample procedure (van Houwelingen & Le Cessie, 1990) that defines sets of test cases and excludes them from the samples used to estimate the model parameters (learning cases). This cross-validation analysis should be rerun a minimum of 200 times, each time leaving 20% of the cases out of the learning data. Since individual samples were partially auto-correlated within clusters, bootstrapping should involve sub-sampling of the clusters instead of samples.

The scores predicted for the test samples in each run should then be compared to the observed scores and accuracy percentages computed.

5.8. Future work

This study developed distribution models at an island scale but the intention for future research is to export these models to other islands and examine distributions at an archipelago scale. Tittley & Neto (2001) detected no strong floristic and biogeographic differences between individual islands or island groups within the 600 km spread of the archipelago – a probable consequence from (i) the small latitudinal variation of the archipelago, (ii) similar impinging climate conditions and (iii) lack of major differences in land-induced factors. This attribute is perceived as limiting the number of obvious gradients in the physical environment and will probably facilitate between-island extrapolations.

A few major challenges are envisaged in relation to up-scaling the results of this study to other areas:

- (1) *enhance the procedures used to obtain the oceanographic covariates*. At present oceanographic information is either the result of modelled proxies or is extracted from multiannually averaged satellite imagery fields with a non-validated method of nearshore interpolation. Ideally, results of enhanced oceanographic models that produce near bottom information about currents and swell exposure should feed this type of studies. In practice, the approach followed in this study may have failed to identify valid relationships and therefore show higher fit measurements either due to (i) the modelled exposure indices representing unsuitable proxies or (ii) the loss of inter-annual variation signal through working with multiannually-averaged SST and chl-*a* fields with disregard of the interaction between annual environmental differences and the field season when assemblages were sampled.

- (2) *complete the information about the fine scale distribution of bottom types and biological occurrences*. Island shelves in the Azores have only been surveyed in high resolution around Faial island. Spatializing the models taking into account the distribution of suitable substrate would therefore require further swath surveys. Concurrently, more biologic sampling data would have to be collected in some islands in order to guarantee validation of the model extrapolations. Finally, the importance of integrating information on the heterogeneity expected in infralittoral assemblages at different spatial scales in new surveys designs is highlighted. Indications derived from eulittoral studies in the Azores are presented in Martins et al. (2008).

- (3) *assess whether these taxon-specific distributions models provide suitable proxies for the distributions of the biotopes the target taxa dominate*. *Facies* map such as that presented in Figure 29 should be compared with biotope distribution maps. If the dominant species modelling provides accurate results, this approach could potentially reduce the expertise required for biotope surveys as well as data analysis costs.

- (4) *exploit alternative statistical modelling approaches*. Nested strategies that first develop presence/absence models for each species (binary logistic regression) and then model the abundance of the species in the areas were presence is predicted (ordered logit regression) could be tested. Alternatively, ecological niche factor analysis (ENFA) which dispense with using absence information could be trialed. The later would also allow for a more straightforward definition of environmental envelopes for each species.

- (5) *autecology studies* – research on the direct relationships between biological traits and abiotic/biotic forces is important to infer about cause-effect processes driving the variability observed and decide upon additional environmental variables to integrate in the models.

6. Conclusions

Results reveal that the approach used to collate environmental information from various sources and statistical analysis can be used to produce models that explain part of the variability observed in macroalgae distributions and can be used to develop predictive models at an island scale.

Depth was consistently significant for all the selected species, highlighting its importance as a major environmental regulating factor for macroalgae. Slope was significant for all species except *Padina pavonica*, confirming the influence of bottom physiography in the distribution of macroalgae. Exposure to swell was significant to articulated Corallinaceae and *Halopteris filicina*. Exposure to currents was significant to articulated Corallinaceae, *Codium elisabethae* and *Padina pavonica*. Chl-*a* was significant for articulated Corallinaceae and *Padina pavonica* and could be an indication of "bentho–pelagic coupling". SST was non-significant for all the target species, suggesting that either macroalgae abundance does not respond to water temperature at the range of variation found in the study area or that satellite-derived measurements may not provide a good proxy for temperature conditions at a benthic level.

Consistent predictive distribution maps were obtained for the rocky infralittoral substrate by spatializing the final model equations using the continuous raster fields for the environmental variables found to be statistical significant.

However, given that final models obtained for four of the six *taxa* show intermediate to low goodness of fit values, future efforts should concentrate on intersecting the biologic occurrences with additional or revised environmental variables including biological ones if available (e.g., herbivory pressure). Setting up additional controls of sampling-related variability during model development is also advised.

7. References

Augier, H. (1985). Première Contribution à l'Étude et à la Cartographie des Biocenoses Marines Benthiques de l'Ile de Madère. *Boletim do Museu Municipal do Funchal*, 37(168): 86-129.

Azevedo, J.M.N., A. I. Neto, A.C. Costa, H.I. Cepêda, R.P. Norberto, M.P. Henrique & M.I. Parente (2002). *Plano Regional da Água - Açores: Relatório da fase I.* Caracterização e diagnóstico da situação actual. Meio marinho. Departamento de Biologia, Universidade dos Açores. 70 pp. + annexes.

Bianchi, N., C. Morri, G. Sartoni & P. Wirtz (1998). Infralittoral epibenthic communities around Funchal (Ilha da Madeira, NE Atlantic). *Boletim do Museu Municipal do Funchal*, Sup. no. 5: 59-80.

Borooah, V.K. (2001). *Logit and Probit: Ordered and Multinomial Models*. Sage University Papers Series on Quantitative Application in the Social Sciences, 07-138. Sage, Thousand Oaks, CA. 97 pp.

Carvalho, F. (2003). *Elementos do clima de agitação marítima no Grupo Central dos Açores (Mar Alto).* Instituto de Meteorologia, Portugal. 98 pp.

Chacana, M. (2002). *Codium elisabethae* O.C. Schmidt, newly recorded from the Canary Islands. *Constancea*, 83(17).

Chapman, M.G. (2003). Paucity of mobile species on constructed seawalls: effects of urbanization on biodiversity. *Marine Ecology Progress Series*, 264: 21-29.

Connor, D., & K. Hiscock (1996). Data Collection Methods. In Hiscock, K. (ed.). *Marine Nature Conservation Review: Rationale and Methods*. Joint Nature Conservation Committee, Peterborough.

Connor, D.W., M.J. Dalkin, T.O. Hill, R.H.F. Holt & W.G. Sanderson (1997). Marine Nature Conservation Review: marine biotope classification for Britain and Ireland. Vol. 2. Infralittoral biotopes. Version 97.06. *Joint Nature Conservation Committee Report*, 230.

De Clerck, O., P. De Vos, M. Gillis & Eric Coppejans (2001). Molecular Systematics in the Genus *Dictyota* (Dictyotales, Phaeophyta): A First Attempt Based on Restriction

Patterns of the Internal Transcribed Spacer 1 of the rDNA (ARDRA-ITS1). *Systematics and Geography of Plants*, 71(1): 25-35.

Ferrier, S., G. Watson, J. Pearce & M. Drielsma (2002). Extended statistical approaches to modelling spatial pattern in biodiversity in northeast New South Wales. I. Species-level modeling. *Biodiversity and Conservation*, 11: 2,275-2,307.

Gabriele, M., A. Bellet, D. Gallotti & R. Brunnetti (1999). Infralittoral hard substrate communities of the northern Adriatic Sea. *Cahiers de Biologie Marine*, 40: 65-76.

Gamble, J.C. (1984). Diving. In: N.A. Holme & A.D. McIntyre (eds.). *Methods for the study of marine benthos. International biological programme handbook no. 16* (2nd ed.). pp. 99-139. Blackwell Scientifc Publications, Oxford.

Goldberg, N.A., & G.A. Kendrick (2004). Effects of island groups, depth, and exposure to ocean waves on subtidal macroalgal assemblages in the Recherche Archipelago, Western Australia. *Journal of Phycology*, 40(4): 631-641.

Guisan, A., & N.E. Zimmermann (2000). Predictive habitat distribution models in ecology. *Ecological Modelling*, 135: 147-186.

Guisan, A., T.C.J. Edwards & T. Hastie (2002). Generalized linear and generalized additive models in studies of species distributions: setting the scene. *Ecological Modelling*, 157: 89-100.

Hanemann W.M., & B. Kanninen (1999). The statistical analysis of discrete-response CV data. In: I.J. Bateman & K.G. Willis (eds.). *Valuing environmental preferences: theory and practice of the contingent valuation method in the US, EU and developing countries*. Oxford University Press, Oxford.

Holt R., & B. Sanderson (2001a). Procedural Guideline No. 3-3: *In situ* survey of subtidal (epibiota) biotopes and species using diving techniques. pp: 233-239. In J. Davies, J. Baxter, M. Bradley, D. Connor, J. Khan, E. Murray, W. Sanderson, C. Turnbull & M. Vincent (eds). *Marine Monitoring Handbook*. 405 pp.

Holt R., & B. Sanderson (2001b). Procedural Guideline No. 3-5: Identifying biotopes using video recordings. pp: 241-251. In J. Davies, J. Baxter, M. Bradley, D. Connor, J. Khan, E. Murray, W. Sanderson, C. Turnbull & M. Vincent (eds). *Marine Monitoring Handbook*. 405 pp.

Howson, C.M., & A. Davison (2000). *Trials of monitoring techniques using divers and ROV in Loch Maddy cSAC, North Uist*. Scottish Natural Heritage, Edinburgh.

Kingsford, M.J., & C.N. Battershill (1998). Subtidal habitats and benthic organisms of rocky reefs. pp. 84-114. In: M.J. Kingsford & C.N. Battershill (eds.). *Studying Temperate Marine Environments. A Handbook for Ecologists*. Canterbury University Press, Christchurch.

McCullagh, P. (1980). Regression models for ordinal data (with discussion). *Journal of the Royal Statistical Society*, Series B 42, 109-142.

Martins, G.M., R.C. Thompson, S.J. Hawkins, A.I. Neto & S.R. Jenkins (2008). Rocky eulittoral community structure in oceanic islands: scales of spatial variability. *Marine Ecology Progress Series*, 356: 15-24.

Menge, B.A., & J.P. Sutherland (1976). Species diversity gradients: synthesis of the roles of predation, competition, and temporal heterogeneity. *American Naturalist*, 110: 351-369.

Menge, B.A., & J.P. Sutherland (1987). Community regulation: variation in disturbance, competition, and predation in relation to environmental stress and recruitment. *American Naturalist*, 130: 730-757.

Menge, B.A., B.A. Daley, P.A. Wheeler, E. Dahlhoff, E. Sanford & P.T. Strub (1997a). Benthic–pelagic links and rocky eulittoral communities: bottom-up effects on top-down control? *Proceedings of the National Academy of Sciences of the United States of America*, 94: 14530-14535.

Menge, B.A., B.A. Daley, P.A. Wheeler & P.T. Strub (1997b). Rocky eulittoral oceanography: an association between community structure and nearshore phytoplankton concentration. *Limnology and Oceanography*, 42: 57-66.

Menge, B.A., J. Lubchenco, M.E.S. Bracken, F.T. Chan, M.M. Foley, T.L. Freidenburg, S.D. Gaines, G. Hudson, C. Krenz, H.M. Leslie, D.N.L. Menge, R. Russell & M.S. Webster (2003). Coastal oceanography sets the pace of rocky eulittoral community dynamics. *Proceedings of the National Academy of Sciences of the United States of America*, 100: 12,229-12,234.

Montañés, M.A., M. Sansón & J. Reyes (2002). Morfología, anatomía y distribución de *Zonaria tournefortii* en las islas Canarias (Phaeophyceae, Dictyotales). *Vieraea*, 30: 67-86.

Neto, A.I. (1992). Contribution to the Taxonomy and Ecology of the Azorean Benthic Marine Algae. *Biological Journal of the Linnean Society*, 46: 163-176.

Neto, A.I. (1994). Checklist of the Benthic Marine Macroalgae of the Azores. *Arquipélago*. Life and Marine Sciences, No. 12A: 15-34.

Neto, A.I.M.A. (1997). Studies on algal communities of São Miguel, Azores. *Ph.D. thesis*. Universidade dos Açores, Ponta Delgada. 309 pp.

Neto, A.I. (2000). Observations on the biology and ecology of selected macroalgae from the littoral of São Miguel (Azores). *Botanica Marina*, 43(5): 483-498.

Neto, A.I., & I. Tittley (1995). Stucture and Zonation of Algal Turf Communities on the Azores: a Numerical Approach. *Boletim do Museu Municipal do Funchal*, Sup. No. 4: 487-504.

Neto, A.I., I. Tittley, A. Levi & W.F. Farnham (2000). Structure and Zonation of Algal Communities in the Bay of São Vicente (São Miguel, Azores). *Arquipélago*. Life and Marine Sciences, Suppl. 2 (Part A): 63-69.

Neto, A., I. Titley & P. Raposeiro (2005). *Flora Marinha do Litoral dos Açores*. Secretaria Regional do Ambiente e do Mar, Horta. 156 pp.

Puotinen, M.L. (2005). Tropical cyclone impacts on coral reef communities: Modelling the disturbance regime in the Great Barrier Reef Region, 1969-2003. *Ph.D. thesis*. James Cook University, Townsville, Australia.

Sauerbrei, W., C. Meier-Hirmer, A. Benne & P. Royston (2006). Multivariable regression model building by using fractional polynomials: Description of SAS, STATA and R programs. *Computational statistics & data analysis*, 50 (12): 3,464-3,485.

Schiel, D.R. (2004). The structure and replenishment of rocky shore. eulittoral communities and biogeographic comparisons. *Journal of Experimental Marine Biology and Ecology*, 300: 309-342.

Schnetter, R., I. Hörnig & G. Weber-Peukert (1987). Taxonomy of some North Atlantic *Dictyota* species (Phaeophyta). *Hydrobiologia*, 151/152: 193-197.

Sirjacobs, D., F. Tempera, F. Cardigos, S. Gobert, G. Lepoint, J.-M. Bouquegneau & R.S. Santos (2004). Study of the structure, distribution and dynamics of *Codium elisabethae* populations in the reef ecosystem of Faial Island (Azores): use of submarine image analysis. In: *Proceedings of the 5th International Symposium on Fauna & Flora of Atlantic Islands*.

Somsueb, S., M. Ohno & H. Kimura (2001). Development of seaweed communities on suspended substrata with three slope angles. *Journal of Applied Phycology*, 13(2): 109-115.

Stephenson, T.A., & A. Stephenson (1949). The universal features of zonation between tide-marks on rocky coasts. *Journal of Ecology*, 37: 289-305.

Taylor, D.I., & D.R. Schiel (2003). Wave-related mortality in zygotes of habitat-forming algae from different exposures in southern New Zealand: the importance of "stickability". *Journal of Experimental Marine Biology and Ecology*, 290(2): 229-245.

Tempera, F., P. Afonso, T. Morato, R. Prieto, M. Silva, A. Cruz, J. Gonçalves & R. Serrão Santos (2001). Biological assemblages of the Faial-Pico Channel SACs (in Portuguese). Departamento de Oceanografia e Pescas da Universidade dos Açores, Horta. *Arquivos do DOP,* Série Relatórios Internos, no. 7/2001, vi+95 pp. http://www.horta.uac.pt/projectos/macmar/life/novidades/pdfs/SIC/Canal/Comunidades1.pdf

Tittley, I., & A.I. Neto (1995). The Marine Algal Flora of the Azores and its Biogeographical Affinities. *Boletim do Museu Municipal do Funchal*, Sup. No. 4: 747-766.

Tittley, I., & A.I. Neto (2000). A provisional classification of algal-characterised rocky shore biotopes in the Azores. *Hydrobiologia*, 440: 19-25.

Tittley, I., & A.I. Neto (2005). The marine algal (seaweed) flora of the Azores: additions and amendments. *Botanica Marina*, 48: 248-255.

Tittley, I., A.I. Neto & W.F. Farnham (1998). Marine algae of the island of Flores, Azores: Ecology and floristics. *Boletim do Museu Municipal do Funchal*, sup. no. 5: 463-479.

Toohey, B. (2007). The relationship between physical variables on topographically simple and complex reefs and algal assemblage structure beneath an *Ecklonia radiata* canopy. *Estuarine, Coastal and Shelf Science*, 71(1-2): 232-240.

Tuya, F., & R.J. Haroun (2006). Spatial patterns and response to wave exposure of 'shallow water' algal assemblages across the Canarian Archipelago: a multiscaled approach. *Marine Ecology Progress Series*, 311: 15-28.

Underwood, A.J., & M.G. Chapman (1998). Spatial analyses of eulittoral assemblages on sheltered rocky shores. *Australian Journal of Ecology*, 23: 138-157.

Van Houwelingen, J.C., & S. Le Cessie (1990). Predictive value of statistical models**.** *Statistics in Medicine*, 9(11): 1303-1325.

Wallenstein, F.F.M.M., & A.I. Neto (2006). Eulittoral rocky shore biotopes of the Azores: a quantitative approach. *Helgoland Marine Research*, 60: 196-206.

Wallenstein, F.F.M.M., A.I. Neto, N.V. Álvaro & C.I. Santos (2007). Algae based biotopes of the Azores (Portugal): spatial and seasonal variation. *Aquatic Ecology*. Online first paper. DOI: 10.1007/s10452-007-9134-y.

Whorff, J.S., L.L. Whorff & M.H. Sweet (1995). Spatial variation in an algal turf community with respect to substratum slope and wave height. *Journal of the Marine Biological Association of the UK*, 75: 429-444.

8. Acknowledgements

To Dr. Jack Jarvis (University of St. Andrews) for his critical support with setting up the TELEMAC current model.

To Dr. Marji Puotinen (University of Wollongong) for extracting the fetch data for vicinity of Faial data using her AML™ script for Arc-Info™.

To Monique MacKenzie, Peteke Feijten, Maarten Van Ham, Filipa Samarra, David Manley, Zhiqiang Feng and Robin Flowerdew for their support with Statistical Modelling techniques and software.

To Jorge Fontes, Frederico Cardigos, Vanessa Santos, Jaen Nieto Amat, Ricardo Delgado and Pedro Frade for their help with the dives.

To the crew of RV *Águas Vivas* Paulo Martins and Vítor Rosa for their competence and ability in ensuring the survey goals and safe returns to shore.

To all the various boat skippers from DOP's ribs and rented vessels, namely Filipe Goulart.

To Cláudia Oliveira, David Abecasis, Inês Seabra and Manuela Ramos for their help during the ROV and drop-down camera surveys.

Fernando Tempera was financed by a PhD grant from the Fundação para a Ciência e a Tecnologia (ref: SFRH/BD/12885/2003).

CHAPTER 8

MAIN CONCLUSIONS

The investigation conducted in the course of this thesis articulated various fields of geology, oceanography and ecology contributing to the understanding of processes affecting the shelf of Faial and neighbouring passage to Pico.

The main conclusions from each of these domains are summarized below.

1. Hard seafloor geology

The present work is the first to map and complete a geomorphologic inventory of an Azorean island shelf. This was only possible by combining high-resolution swath bathymetry and backscatter data with ground-truthing information from sources such as *in situ* imagery, grab samples and sub-bottom profiling.

The work revealed a diverse and complex mosaic of rocky and sedimentary geomorphologic structures associated with tectonic, volcanic, erosional and sedimentary processes. Maps of surficial bottom nature are presented that pioneer the high resolution mapping of Azorean island shelves.

1.1. Shelf extent

The variation of shelf extent showed a relationship with the geologic age history of the related subaerial edifice. With exceptions off the Almoxarife Formation and SW Pico, wide shelves prevailed off older edifices while extremely narrow shelves featured on the geologically young and active areas (e.g., Capelo complex). Using the geologic edifices present in the study area, a logarithmic curve was fit to the shelf widening rates in edifices younger than 800 kyr.

The two widest shelf sectors were found to the NW of Faial and NW of Pico, with widths of 2,817 m and 4,010 m. Around the Ribeirinha complex (the oldest edifice in the study area) the shelf averaged a width of 2,583 m. Capelo peninsula, the youngest part of Faial island, exhibited an extremely thin shelf with widths averaging 460 m on the more exposed north side and 337 m on the less exposed southern shore. The thinnest shelf, found on the SW of the Pico Mountain Complex, averaged a 138 m width.

Depths at the *analytical shelf edge* (ASE, defined along the 5º slope contour) varied significantly between the different margins. The deepest values were obtained off the Ribeirinha Complex and on the northern margin of the Faial-Pico passage where they reached between 170 and 180 m. Average depths south of Faial were between 59 and 70 m. ASE off the Capelo Peninsula were at depths as shallow as 21 to 25 m, reflecting the very recent emplacement (10 kyr) of this edifice. The shallowest ASE (averaging 14 m) was found on the SW of the Pico Mountain Complex. The edge off NW Pico averaged 122 m depth, roughly coinciding with sealevel during the most recent Glacial Maxima.

Depth at the *analytical shelf edge* (ASE) seemed an appropriate indicator of the lowest bedrock horizon planated during glacial sealevel lowstands in non-sedimented shelves (e.g., northwestern Pico). However, the index was flawed around older edifices where thick sediment wedges mask the eroded horizon and place the 5º slope contour (i.e., the ASE) at much shallower depths. In this case, seismic data were helpful to identify the vertical location of buried planated bedrock horizon in order to be able to make inferences about the tectonic isostasy of the related subaerial edifice. Sub-bottom profiles extending to the shelf edge on southern Faial revealed sediment wedges as thick as 40 m accumulated over planated bedrock horizons with distal edges emerging roughly at the level of recent glacial maxima lowstands. Although this limitation prevents direct use of ASE for drawing conclusions about the isostasy of the areas where the shelf appears uplifted, it can yield conservative subsidence rates in old edifices with ASE significantly below the recent glacial maxima lowstands. A rate of 0.75 mm/yr was obtained for the oldest edifice of Faial island (Ribeirinha complex). It is further suggested that this edifice extended further East given the roughly linear continuity of the Ribeirinha complex margin with the shelf edge of the northern half of the passage.

1.2. On-shelf geomorphology

It was revealed that the Faial nearshore is dominated by boulder slopes. Lavaflows are also abundant and better defined around the more recent edifices of the Capelo peninsula and Almoxarife Formation. Western Pico is equally dominated by lava flows, most of which are concentrated on a lava "delta" off the NW coast. Establishing relationships between the lowest individual flows and probable extrusion centers and eruptive events was not always possible due to subsequent subaerial flows that appear to bury the upstream sectors of the flows mapped underwater.

On-shelf palaeoshorelines are reported for the first time in the Azores, concentrating around western Pico. Their cliffed morphology is comparable to palaeoshorelines found on volcanic island flanks in Hawaii and to modern shorelines found along the neighbouring Pico coast. The recorded palaeoshorelines occur only in bathymetric strata corresponding to periods of fast sealevel rise during the Holocene transgression and are absent in strata corresponding to Holocene sealevel standstills. This suggested that in standstills erosion is given enough time to either dismantle the lava benches in a way that does not leave cliff palaeoshorelines or that erosion deposits end up covering the cliffs. Well-defined compression ridges observed in the upper surfaces of submerged lava flows displaying fronts eroded into cliff palaeoshorelines suggested that the benched morphology observed off northwestern Pico is primarily caused by the emplacement of succeeding lava flows rather than terracing of the island flanks by marine erosion. Furthermore it demonstrated that lava flows can preserve surface texture despite being traversed by the surf zone during sealevel fluctuations.

Further insight yielded by the analysis of the high resolution multibeam data included (i) the mapping of the underwater prolongation of onshore faults, (ii) submerged evidence of fissural volcanic activity associated with these faults, (iii) clarification of the origin of the basin in the southern half of the passage. The latter appears to be derived from a portion of the inter-island gap being enclosed by the volcanic edifice of Baixa do Sul rather than from a large submerged caldera as previously suggested.

2. Sedimentology

2.1. Bedforms

Multibeam surveys revealed that sediments accounted for 66% of the shelf surface of the Faial-Pico passage. Variations in backscatter indicated variability in grainsize whilst bathymetric data exposed prominent bedforms such as straight crested sand waves, waves with celled crest patterns, linguoid waves, barchanoid waves and scour depressions. These large bedforms covered 29% of the sediment beds and are the first reported in the shelves of the Azores archipelago.

Despite the fact that the area is only subject to a microtidal regime, bedforms reaching a maximum height of 18m extended to the deepest areas of the passage at 190m depth. Large bedforms were not found shallower than 40m, although some rippled morphology locally persisted in the backscatter record to depths of 28m.

The dimensions of the wave fields and bedforms provide evidence for the occurrence of strong bottom currents which were partially attested by existing oceanographic observations. These currents result from a unique combination of factors in the Faial-Pico passage which includes the funneling of oceanic tidal currents, density currents and seafloor morphology. The size of the bedforms is maximized by the presence of average grainsize (~0.5mm) that are optimal for producing tall sediment waves.

A comparison between bedform-based current estimates and *in situ* measurements indicated that currents do occur under the present oceanographic conditions that are capable of maintaining many of the observed bedforms. Moored current meter data suggested the frequency at which this occurs on an annual basis to be minimal as bedform-based current estimates were towards the maximum of the measured current ranges. However, *in situ* observations suggested a higher frequency for this mobilization, as even summertime observations revealed signs of recent activity such as non-silted surfaces together with fresh secondary bedforms including highly assymetric ripples and ripple fans over the bedform surfaces of the deepest field.

2.2. Coarse sediment zones

Coarse Sediment Zones (CSZ) which were hitherto unreported in the poorly investigated context of narrow volcanic island shelves were clearly identified and mapped using the high resolution multibeam data. The features were located in depths between 8 and 70 m in the Faial-Pico passage. This site differs from the fully open narrow shelf coasts of most Azores islands for being placed on an inter-island shelf that is extensively fetch-shadowed by the neighbouring islands of Pico and São Jorge. The location is exceptional within the study area in hydrodynamic terms because it is located on the lee side from prevailing swells but exposed to enhanced longshore tidal currents funnelled through the Faial-Pico passage.

The variety of shapes, sizes and orientations of the features led to a division of CSZ in three categories: “broad depressions”, “small depressions” and “sorted bedforms”. Their characteristics are described in Chapter 5 and match types of nearshore and inner shelf features described in previous literature as “rippled scour depressions” and “sorted bedforms” (Goff et al., 2005).

“Broad depressions” plan view morphology features an upslope head which broadens downslope and eventually divides into multiple narrower branches, suggesting surficial mass movement scars developing and branching from a shoreward-convex head. Potential trigger mechanisms for these mass movements include: (i) submarine groundwater discharges, (ii) seismic activity and (iii) cross-shore nearbed flows. However, an explanation implying long-shore hydrodynamic forcing such as the one currently employed to explain “sorted bedforms” would be partially compatible with the rhythmic longshore pattern of the branches in the lower part of the depressions. Under this scenario, it could be postulated that “broad depressions heads” form from gradual enlargement and merging of “narrow depressions”, which are found in the same area.

Typical sorted bedforms were found in the shoaling convex area less than 30m-deep immediately off the rocky Pedro Miguel headland. These features are likely produced by enhanced bottom stresses associated with long-shore currents steered and intensified by the lateral restriction created by coastal protrusion and the elevated topography off the promontory (Cacchione & Drake, 1990; Ferrini & Flood, 2005).

Historic surficial sediment data suggests that CSZ persisted or recurred in the area at least since the early 1940's, representing a new maximum in the persistence of these features (hitherto set at 4 decades by Goff et al., 2005). A higher dynamics was detected in the mega-ripples found within the broad scar heads which changed orientation in a period of 10 months, indicating rearrangement by large surface swells. This was not as obvious in the deep parts of the scars where the CSZ surface presented widespread signs of more prolonged immobility.

Sub-bottom profiles showed continuity of the coarse material within the CSZ with a sub-surficial reflector buried 1-2 m beneath the surrounding blanket of fine sands. Although further work is necessary to determine the exact origin of the coarse material (which includes material as large as boulders), potential sources are (i) plinian-subplinian flows produced by the Caldera Formation approximately in the last ~5,500 yr (considering only the deposits mapped in the Pedro Miguel region), (ii) the latest sealevel transgression, (iii) palaeo-fluvial channels or (iv) sorted bedforms signature.

3. Oceanography

3.1. Satellite imagery analysis

Satellite imagery acquired at the HAZO station was successfully used to derive information about oceanographic patterns in the island vicinity where *in situ* oceanographic records are lacking to produce a spatio-temporal model of the thermal and ocean colour variability. Despite limitations of data availability at sub-monthly time scales caused by cloud cover, AVHRR and SeaWiFS monthly-averaged composites still provided enough data to identify consistent temporal cycles and first order approximations of the spatial variability of seawater sea surface temperature (SST) and chlorophyll-*a* (chl-*a*) concentration in shelf areas.

Yearly cycles of surface chl-*a* were consistent with the two-annual-blooms temperate regime. However, individual years showed some affinities with a subtropical regime by showing spring peaks barely discernible from winter levels and autumn maxima comparable to winter chl-*a* levels.

SST fields demonstrate that a negative temperature anomaly prevails within the inter-island passage throughout all seasons, with the strongest expression during the spring. Seasonal variations elsewhere were related to variations in the wind stress. Autumn and winter showed the least developed zonation because of the well-mixed conditions resulting from enhanced wind and swell stress. Conversely, spring and summer fields exhibited a more structured zonation with a wide positive temperature anomaly appearing off N and NW Faial which was related to the relaxation of south and southwesterly winds. Seasonal changes in the wind pattern likely explain the shifting of leeside upwelling from the north of the island (autumn and winter) to the SW (summer). This effect is particularly evident during the summer, when a negative SST anomaly is clearly visible off SW Faial.

Chl-*a* patterns were less variable throughout the year. Enhanced concentrations were consistently observed in an extensive zone off north-western Faial, the inter-island passage and in a narrow fringe along Faial's northern shore. The high chl-*a* concentrations generally coincided with areas of negative SST anomalies suggesting mixing and upwelling that effectively input nutrients into shallow waters and regularly stimulate sustained phytoplankton production. These regimes are either (i) topographically-induced when tidal currents move over shoaling topography (such as over the shelf and in particular in the inter-island passage) or (ii) wind-induced in the case of leeside upwelling. The mild enhancements of chl-*a* reported off SW and SE Faial in summer periods are suggested as a result of the latter case, which should be promoted by the relative increase of north and northeasterly winds observed during this season.

Overall the SST and chl-*a* patterns suggest that effects usually associated with islands namely topographically-induced mixing/upwelling and wind-induced leeside upwelling are in operation on the immediate vicinity of Faial island and have a role in its oceanographic zonation.

3.2. Exposure to swell index

A proxy field for exposure to swell was build for the study area based on work by Puotinen (2005). The approach adopted is GIS-based and simplistically assumes that the relative position of each location with respect to nearby islands and islets determines its exposure to waves approaching from each compass direction. The computations weigh the open windows with published statistics of ocean swell direction and significant wave height and eliminate closed fetch windows.

The spatialization of the computed values showed the relative distribution of wave energy affecting the biologic communities. Sheltered conditions were predicted in eastern Faial, some small embayments and areas protected by headlands. This contrasts with the highly exposed character of NW Faial.

3.3. Exposure to currents

A simple shallow-water oceanographic model forced by the maximum astronomic tide was build in order to extract a proxy for the exposure of benthic communities to currents. The spatialization of the relative current exposure index, based on the maximum currents obtained for each model node throughout a tidal cycle after model stabilization, showed that tidal currents are more intense in the interisland passage and around the Capelinhos headland.

4. Habitat modelling

Major environmental variables collated from the previous analyses (depth, slope, swell exposure, maximum tidal currents, SST and chl-*a* concentration) were related to biologic data consisting of the abundance of six dominant macroalgae taxa characteristic of rocky infralittoral biotopes of the Azores (articulated Corallinaceae, *Codium elisabethae*, *Dictyota* spp., *Halopteris filicina*, *Padina pavonica* and *Zonaria tournefortii*).

Ordered logistic regression statistical models were used to identify which combinations of the environmental variables best explained the observed variations in the abundance of each species. Depth was consistently significant for all the species, highlighting its importance as a major environmental regulating factor for macroalgae. Slope was non-singnificant only for *P. pavonica*, confirming the influence of bottom physiography in the distribution of macroalgae. Exposure to swell was significant to articulated Corallinaceae and *H. filicina*. Exposure to currents was significant to articulated Corallinaceae, *C. elisabethae* and *P. pavonica*. Chlorophyll-*a* was significant for articulated Corallinaceae and *P. pavonica* and could be an indication of "bentho–pelagic coupling". SST was non-significant for all the species, suggesting that either macroalgae abundance does not respond to water temperature at the range of variation found in the study area or that satellite-derived measurements may not provide a good proxy for temperature conditions at a benthic level.

The models generally showed low R^2 values, suggesting that either other environmental variables should have been included in the analysis or that variation in sampling years, methods and observers introduced considerable levels of uncontrolled variability in the data.
Consistent predictive distribution maps were obtained for the rocky infralittoral substrate by spatializing the final model equations using the continuous raster fields for the environmental variables found to be statistical significant. This confirmed that provided models which explain a higher level of the variation observed in the data are achieved, the approach can be used to predict biologic distributions at an island scale in a spatially-explicit environment.

5. Geographic Information Systems

Though technically challenging, adopting a spatial approach to marine ecology mapping through the use of GIS provides a more realistic and intuitive framework. GIS-based analyses included data digitizing and editing, synthesis of multidisciplinary datasets from a variety of platforms, production of publication-quality graphics and implementation of spatial analysis and modelling. These functionalities provided a powerful interactive tool for managing, displaying and cross-analysing data. Furthermore, the fine-scale maps produced both for environmental variables and species distributions can be used to inform further ecologic studies and enhance the design of protective and management measure for marine environments and species that are of conservation and commercial interest.

6. References

Cacchione, D.A., & D.E. Drake (1990). Shelf sediment transport: an overview with applications to the northern California continental shelf. *In* B. LeMehaute & D. Hanes (eds.). *The Sea*, 9: 729-773. Wiley-Interscience, New York.

Ferrini, V.L., & R.D. Flood (2005). A comparison of Rippled Scour Depressions identified with multibeam sonar: evidence of localized sediment transport in inner shelf environments. *Continental Shelf Research*, 25: 1,979-1,995.

Goff, J.A., L.A. Mayer, P. Traykovski, I. Buynevich, R. Wilkens, R. Raymond, G. Glang, R.L. Evans, H. Olson & C. Jenkins (2005). Detailed investigation of sorted bedforms, or "rippled scour depressions," within the Martha's Vineyard Coastal Observatory, Massachusetts. *Continental Shelf Research*, 25: 461-484.

Puotinen, M.L. (2005). Tropical cyclone impacts on coral reef communities: Modelling the disturbance regime in the Great Barrier Reef Region, 1969-2003. *Ph.D. thesis*. James Cook University, Townsville.

CHAPTER 9

FINAL DISCUSSION

As an answer to an increasing demand for high-resolution geomorphologic information that could both contribute to geological hazard assessments and marine habitat mapping, this work presents the first high resolution maps of island shelf areas in the volcanic archipelago of the Azores. The current thesis innovatively uses the swath data as a basis for fine-scale geological mapping and subsequently articulates the results with information from complementary disciplines (namely oceanography, ecology and statistical modelling) in order to produce continuous fine scale maps of biological assemblages.

Given that the results obtained for the distinct subjects analysed have been discussed individually in each chapter and summarized in the previous chapter, this final discussion focuses on demonstrating that the objective of *developing an articulated multidisciplinary approach to the exploration and mapping of the seabed for geological and ecological studies* has been achieved.

The articulation made of multiple disciplines is considered to have the merit of allowing a broader understanding of geological, sedimentological and biological processes occurring on the shelf of Faial and neighbouring passage to Pico than would be possible from isolated investigation executed by researchers working vertically in specific subjects.

After a small introduction to the contents of the thesis (chapter 1) and a small review of the geological setting of the Azores islands (chapter 2), chapter 3 reflects the considerable effort put in processing the swath data and extracting the fundaments (high resolution bathymetry, seafloor slope and backscatter) from which fine-scale limits could be delineated not only for the study area (i.e., the shelves surrounding Faial island and western Pico) but also for the two main seafloor types: sediments and rocks. Given the intrinsically distinct nature of these seafloor types, this spatially-explicit information provided the most basic dichotomy in spatially defining marine biological interest.

In the scope of this thesis only rocky bottoms were targeted by studies that eventually lead to the production of biological distribution maps. However it was felt that the work ought not to ignore the information contained in the swath dataset about marked sedimentary patterns and therefore it contributed to the description of large bedforms dynamics (chapter 4) and coarse sediment zones (Chapter 5). This option not only permitted a more comprehensive geomorphological description of the study area but are also of interest from (i) a sedimentological perspective, (ii) future studies about the distribution of soft-bottom biological assemblages and (iii) to plan human activities such as aggregate extraction and cable routing.

An effort was made in every chapter and respective appendices to, while deriving the data that feed towards the final goal of establishing spatially-explicit statistical models for biological features, reflect the added understanding obtained about the geological and oceanographic analysis in question. This option to develop each subject more than strictly needed to extract simple thematic maps of the relevant environmental variables prevented establishing a linear sequence among chapters but improved the understanding of the processes and information contributed by the different disciplines. This contributed to more informed decisions while extracting significant information from the different datasets and revealed patterns and processes deserving further research from investigators interested in testing hypothesis in each fundamental field.

In order to develop statistical models of biological feature distribution on rocky areas, the work is considered to have derived legitimate surrogates of oceanographic variables factors that were considered as major regulating factors of the benthic assemblages (Chapter 6 and Appendices I and II) from both satellite imagery and spatially-explicit oceanographic and GIS modelling.

In the ultimate analytical chapter (Chapter 7) the different environmental factors (location of rocky seafloor, depth, slope, sea surface temperature, surficial chlorophyll-*a* concentration, exposure to swell and exposure to currents) were successfully collated and intersected with the information from the biological surveys on a GIS environment. The matrices thereby produced were analysed in statistical modelling framework that identified which combinations of parameters provided the best explanation of the biological occurrences and finally yielded spatially-explicit models of dominant macroalgae distributions at an island scale.

This ultimately permitted the achievement of an ecological study that makes use of specific products from different disciplines and eventually manages to test the importance of comprehensive combinations of environmental forces and yield innovative high-resolution spatially-explicit models. The insight obtained while deriving information in different fields allows for an enhanced reasoning why determinate environmental variables or models do not significantly explain the biological variability.

The biological distribution maps produced are hypothesized as preliminary proxies for benthic infralittoral facies and are of particular importance in a context of marine protected area (MPA) design. Further research on (i) the distribution of number of *facies* per geographical grid square, (ii) the definition a minimum facies area to protect, (iii) the intersection between benthic assemblage and commercial fish species movements is suggested as a practical contribution to establish MPA zoning schemes that robustly ensure the protection of biodiversity and commercial species essential habitats, tackling issues of spatial competition between multiple extractive and non-extractive activities.

Overall the knowledge acquired about geophysical and biologic surveying methods as well as modelling and mapping techniques is considered valuable to support the design and implementation of future seafloor mapping programmes in other areas of the Azores as well as in areas with similar characteristics (e.g., other Macaronesian archipelagos). Ideally these programmes should include the following tasks:

- swath surveys supplying fine-scale bathymetry and backscatter maps from which the main benthic habitats can be delimited and substrate variables (e.g., depth, slope, rugosity) extracted;

- production of island-scale fields of the spatial variation of seawater temperature and productivity regimes, ideally from coastal sampling and monitoring programmes given the poor performance of satellite imagery in nearshore areas;

- modelling of tidally-induced currents using shallow-water oceanographic models;

- modelling of an exposure to swell index ideally using wave propagation models fed by average swell/wave spectra; alternatively use GIS extraction of open windows weighted by swell statistics and substrate depth;

- production of fields representing the spatial variation of biotic factors such as predation (or herbivory in the case of modelling targeting macroalgae) and species competition;

- collection/collation of biological occurrence data from benthic surveys, preferably designed to take into account (i) depth and seafloor type variations, (ii) variability scales and ensure the sampling of the full range of environmental situations;

- intercalibration procedures that yield correction factors when multiple observers, complementary methodologies or multiannual surveys are used;

- intersection of biological occurrence data with environmental information and production of validated statistical models that can be spatialized in GIS environments.

CHAPTER 10

FUTURE WORK

Having in view issues that in the course of the study were identified as deserving more exhaustive analyses a number of useful avenues for future investigation are suggested.

1. Geology

Given the wealth of geomorphologic information in the swath dataset, a thorough analysis of the different features reported was considered beyond the scope of this work. Therefore, the results presented should be regarded as a preliminary geomorphologic account appealing to specialists from different fields to develop further investigation on the geologic processes underlying the complex geomorphologic shelf features identified. In particular, issues relating to volcanic island construction, shelf erosion and continuity between subaerial and submerged geologic features warrant further investigation. Some issues regarding the geomorphologic description of lava flows penetrating water around the coasts of Pico Island have already been addressed by Mitchell et al. (2008). In addition, a collaborative effort is ongoing to combine the data produced in this thesis with the results recently presented in Quartau (2007).

2. Sediment Dynamics

A future assessment of the mechanisms which generate the powerful current flows that form and maintain the sediment dynamics in the Faial-Pico passage is proposed. To accomplish this, current measurements with denser temporal and spatial coverage are necessary that can be used to validate future fine-scale vertically-explicit hydrodynamic models. This should be done by long-term current flow monitoring using moorings, regular ADCP current profiling and repeated multibeam surveys to record the changes of the sediment wave fields.

A dedicated project should also be established to investigate the processes involved in the formation and evolution of the Coarse Sediment Zones (CSZ) described in the eastern coast of Faial. The study should be aimed at assessing whether these features are controlled by catastrophic events (namely, gravity flows) or more gradual seabed evolution. The physical oceanographic conditions in the area should be monitored, including measurements of the direction and intensity of nearbottom flows (specifically during storms) with periodic multibeam surveys to investigate the morphodynamics of the CSZ. Monitoring of nearbed salinity and temperatures would further contribute to a clarification of whether groundwater discharge is important to the formation of the “broad depressions”. In both cases, the knowledge to be acquired would be relevant for planning the routing of communications cables, which have been deployed in the area for over a century, as well as managing aggregate extraction activities. From an ecologic perspective these studies would be relevant for determining the spatial dynamics of biologic communities associated with sedimentary beds.

3. Oceanography

A better knowledge of the oceanographic patterns and processes at an island scale is important for the continuation of coastal ecology studies applied both to conservation and fishery management.

3.1. Temperature and ocean colour

Data available to date from *in situ* sampling using dataloggers and moorings together with shipboard surveys has insufficient resolution to produce a spatio-temporal model of the thermal and ocean colour variability around Faial.

Although additional monitoring stations continue to be installed and the oceanographic cruise programme is becoming more intense, more information is still needed to understand variations in temperature and ocean colour at a benthic level in the island vicinity.

Since satellite measurements pertain mostly to near-surface waters, further investigation is suggested as to whether satellite-borne sensors with enhanced resolution (e.g., MODIS, MERIS) could provide more information about the shallow nearshore areas, where there are significant gaps in present knowledge.

Additional research is necessary on the imagery processing algorithms and their ability to produce accurate estimates of pigment concentrations in coastal regions of the Azores, whether local correction factors should be implemented and which algorithms are most valid to fill data blanks. *In situ* sampling is also required in order to test if ocean colour in exposed shelf areas is contaminated by terrigenous or ressuspended sediments that induce artificially high radiance that cannot be spectrally differentiated from chlorophyll-*a*.

The analysis of a longer time series is suggested to corroborate possible linkages between climate anomalies and oscillations in temperature and phytoplankton production. Further research should also collate contemporary weather observations and quantify the influence of winds/storms as factors regulating these two variables in the island vicinity.

3.2. Wave exposure models

Refining the index used for swell exposure should lead to better representation of the distribution of wave energy around the islands and eventually allow more effective predictive models that use swell-related effects as an explanatory variable.

In order to produce a model that realistically represents the spatial variability of wave exposure, it is suggested that wave models are developed that include the simultaneous effects of wave shoaling, refraction, and wave dissipation through bottom friction. Such an approach would permit a more accurate simulation of the way deep ocean waves approaching the coast are modified in their direction, height and other characteristics as they interact with the seafloor and coastline configurations. It is possible that could be done using MIKE 21 SW - a third generation spectral wind-wave model developed by DHI Water & Environment, where the annual average directional wave spectra (e.g., in Carvalho, 2003) would be used to recreate typical swell conditions incoming from each compass sector. An enhanced exposure index could then be computed from the weighted sum of the different sectorial wave conditions, where weight is provided by the relative frequency at which waves from each sector are observed in an average annual cycle.

With such an approach, refraction effects could be accounted, allowing for large swells to impinge on coastal sectors that are not directly exposed to the direction of incoming waves – an effect ignored by the GIS-based method using direct fetch only.

3.3. Current models

Refining the local current model would lead to a better representation of the spatial variability of currents and eventually allow more effective predictive models that use this as an explanatory variable. The results from the tidal-forced shallow-water oceanographic model implemented in this work provide some preliminary guidance for accomplishing this. It is suggested that a wider tidal-forced regional domain is run and used to feed the open boundary nodes of the local model, which could also be enhanced in bathymetric and node resolution. The modeled currents could be calibrated using *in situ* measurements and parameters such as friction at solid boundaries, diffusion model, turbulence model or Coriolis force action adjusted accordingly.

Eventually, vertically-explicit information should be extracted. Results for the near-bottom layer would be of particular interest to determine hydrodynamic forces impacting on sedimentary bedforms and benthic assemblages.

4. Habitat modelling

The results of the study indicate that the models built generally explain a limited but nonetheless important part of the variability shown by the observations. Models with a better fit will be important in order to export this approach to other islands and examine distributions at wider scales.

Several major challenges should be tackled while exporting or up-scaling this study.

(1) Procedures used to obtain the oceanographic covariates should be refined. At present, oceanographic information is either the result of modelled proxies or extracted from multiannual averaged satellite imagery fields with non-negligible nearshore interpolation. Ideally, environmental variables should be derived from enhanced oceanographic models that produce near-bed information about currents and swell exposure. Using modelled proxies or multiannual-averaged fields that show a limited correlation with the time when surveys were conducted or the conditions under which the assemblages developed can frustrate efforts to identify valid relationships and explain data variations.

(2) An enhanced experimental design with better survey calibration is required not only to assess the influence of time of survey, but to control sampling variation potentially introduced by multiple observers and visual surveying methods (e.g., scuba diving, ROV and drop-down camera). Information on the spatial scale of the heterogeneity expected for subtidal assemblages should also be incorporate in an ideal experimental design (for indications regarding intertidal eulittoral areas of the Azores, see Martins et al., 2008).

(3) Surveys of the fine scale distribution of bottom types and species in other island shelves should also be completed. Until now, only Faial shelf has been surveyed with modern hydrographic technologies such as swath sonars and is therefore properly mapped at a fine scale. Parallel efforts should be conducted to collate comparable biologic data acquired by different projects and teams that could be used to compile more comprehensive databases and identify gaps in model validation.

(4) It would also be useful to assess whether the *taxon*-specific distributions models will provide suitable proxies for the distributions of the biotopes that are dominated by the target *taxa*. If that is the case, this approach could potentially reduce the expertise required for biotope surveys as well as data analysis costs.

5. Geospatial information

One of the major challenges in setting up marine-related GIS projects in the Azores has been the scarce availability of even basic layers, such as bathymetry, coastlines representing the hydrographic chart datum at fine scales, bottom types or administrative units such as the EEZ, territorial waters, or boundaries of marine protected areas (for a review see Seabra et al., 2005). The establishment of an internet-based atlas of marine and coastal geographic data is suggested as a contribution to alleviate this problem. Such a digital infrastructure should involve a multi-institutional collaboration and would assist managers, researchers, and the public in general by providing standardized geo-referenced data. A resource for online uploading of new layers by registered users ("wiki" approach) would be an interesting feature for this atlas that could ensure its continuous and trustworthy development provided some metadata standards were guaranteed.

Regardless of all the plethora of tools already accessible in a GIS environment, characterizing the habitats of marine organisms highlighted some major technical limitations of current GIS software packages such as the lack of integration between the GIS and a number of standard software suites traditionally used in physical oceanography, remote sensing and hydrography. Uploading new data from these survey sectors and updating of GIS displays while working with geodatabases and routine protocols often require tedious intermediate and resourceful conversions as external formats were seldom directly readable into the GIS. Further streamlining of data importing procedures is required since the GIS will possibly never be able to perform remote sensing and statistical tasks and complementary software will always need be used in association.

The adoption of metadata standards and methodological descriptions for data resulting from a wide diversity of techniques and software is an additional challenge. Until a layer is finally ready to be imported into a GIS project, the original data must be processed through many steps requiring a complex sequence of technical decisions. Computerized automated logging would be an interesting development, if uncomplicated quality control and widespread informed use are to be promoted.

Finally, further integration or standardization of the format and design of databases used by different projects and workgroups is also desirable if analyses using broader data resources are to be performed. This requires an institution-wide effort to adapting historic and operational databases in order to make them promptly readable by GIS and allow geospatial information to be retrieved by specific queries.

6. Marine Conservation

Detailed descriptions of the seafloor such as the one presented in this paper are also important in building an understanding of the benthic ecosystem dynamics and implementing an informed stewardship of the marine environment. This issue is particularly important in the present case in view of the Marine Protected Area proposed for the Faial-Pico passage and the other conservation areas already designated around Faial and western Pico (e.g., SACs and limpet harvest refugia).

The information is considered instrumental in explaining local habitat preferences by fish and sea mammals. Work has already started that uses the habitat maps to interpret the movement patterns exhibited by a series of coastal fish species of commercial and conservation interest that have been targeted by active and passive telemetry studies ongoing in the area (Afonso et al., 2008; Afonso et al., accepted).

The high resolution seafloor and environmental variable maps produced hold therefore great potential to refine the design of ecologically effective zoning schemes, support management decisions and provide benchmarks for monitoring studies. A particularly relevant task in the short term will be to convert the seafloor information into a biotope interpretation categorizing the relevance of the different bottom types for fishery resources and general biodiversity.

7. References

Afonso P., F. Tempera & G. Menezes. 2008. Population structure and habitat preferences of red porgy (*Pagrus pagrus*) in the Azores, central north Atlantic. *Fisheries Research*, 93: 338-345.

Afonso P., J. Fontes, R. Guedes, F. Tempera, K.N. Holland & R.S. Santos. Accepted. A multi-scale study of red porgy movements and habitats use, and its application to the design of marine reserve networks. *Reviews: Methods and Technology in Fish Biology and Fisheries*.

Carvalho, F. (2003). *Elementos do clima de agitação marítima no Grupo Central dos Açores (Mar Alto).* Instituto de Meteorologia, Portugal, 98 pp.

Mitchell, N.C., C. Beier, P. Rosin, R. Quartau & F. Tempera (2008). Lava penetrating water: Submarine lava flows around the coasts of Pico Island, Azores. *G3 (Geochemistry Geophysics Geosystems)*, 9 (3): Q03024, doi:10.1029/2007GC001725.

Quartau, R. (2007). The insular shelf of Faial: Morphological and sedimentary evolution. *PhD thesis*. University of Aveiro, Aveiro. 301pp.

Seabra, M.I., F. Tempera & R.S. Santos (2005). Experiences in Applying Geographic Information Systems to Marine Conservation and Ecology in the Azores. *Geoinova*, 11: 139-159.

Appendix I

ESTIMATION OF SWELL EXPOSURE AROUND FAIAL ISLAND

TABLE OF CONTENTS

1. Introduction

The approach used to estimate the exposure to swell index assumed that the relative position of each place with respect to nearby islands and islets plays a key role in determining its exposure to waves approaching from a particular direction. An Arc-Info™ GIS procedure was used to compute open fetch windows. These windows were subsequently weighted in a spreadsheet environment using statistics of the ocean swell direction and significant wave height. The results produced a proxy of the distribution of wave energy affecting the biological communities around the study area.

2. Methodology

Open fetch windows to incoming wave energy for a point dataset within the island complex of Faial, Pico and São Jorge were estimated using a fully automated Arc-Info™ GIS script produced by Puotinen (2005a). For each point, the programme obtained fetch estimates at compass directions spaced 15º.

2.1. Domain

Figure 1 shows the extension of the 6,619 point dataset for which fetch distances were obtained. Points were spaced at 100 m intervals along the shorelines of Faial and western Pico shoreline and formed a regular grid with a 200 m resolution at sea. Only points located over the shelf were considered.

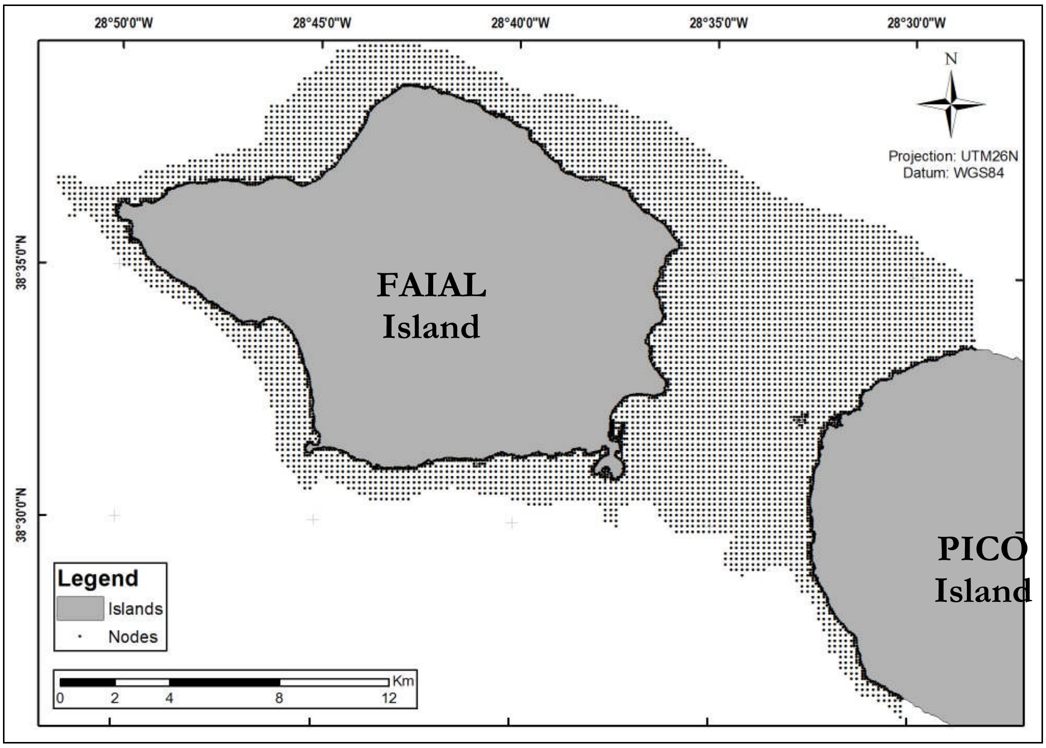

Figure 1: Point dataset for which fetch windows were extracted.

Figure 2 shows the configuration of coastlines in the island complex of Faial, Pico and São Jorge.

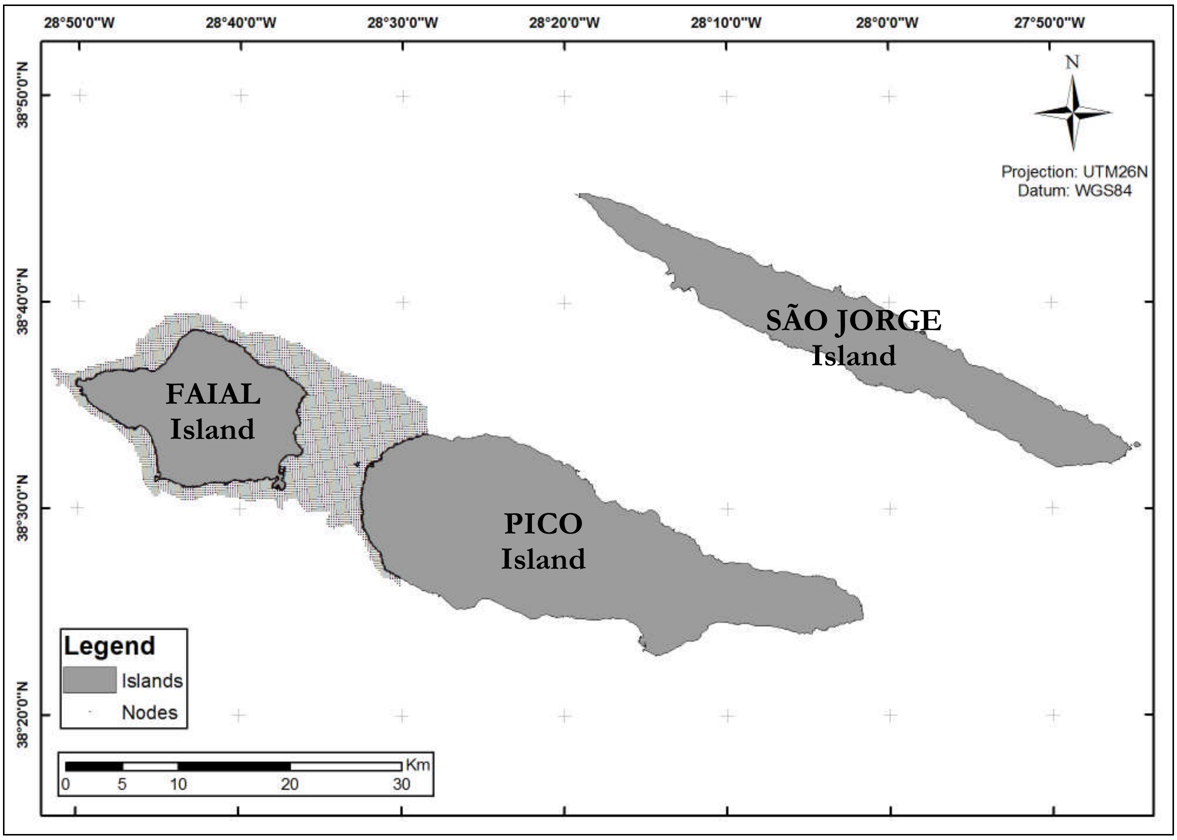

Figure 2: Coastline configuration used to extract fetch distances for the point dataset located on the left hand side of the picture.

Small islands located further away from the area but still in the path of swells approaching the study area (namely, Graciosa, Flores and Corvo) were consider too distant and/or small to significantly affect the exposure of the study area. Flores and Corvo are approximately 225-230 km to the NW of Faial, whilst Graciosa is 68km to the NE of Faial and is partially concealed behind São Jorge.

2.2. Extraction of fetch windows

The method used to extract fetch windows is detailed in Puotinen (2005a). The procedure is implemented by an AML™ Arc-Info™ script which can be found in Appendix 2 of Puotinen (2005b). The programme estimates fetch by calculating the straight-line distance between each point in the dataset and the nearest potential "wave-blocking" obstacle (i.e., island or islet coastline) along a series of equally spaced directions radiating from the point. In the present case, a fetch distance was obtained for each of the points in a total of 24 compass directions spaced at 15º intervals. The resulting measurements were recorded in the point file attribute table.

For each point, directions for which fetch distances were smaller than 85km (the maximum distance possible of any point in the dataset to its farthest "wave-blocking" obstacle) were considered as receiving no swell from that direction. Directions with fetches higher than 85km were used as fully open to incoming swells.

2.3. Swell data

The exposure degree index was calculated taking into account not only direct fetch windows but also multiannual-averaged directional spectra for relative frequency and significant wave height presented in Carvalho (2003) and corrected for an error in the directions on the table headers (Carvalho, pers. com.). This work presents long-term averaged swell data for the period 1989-2002 extracted from MAR3G – a wind-generated wave model described in Oliveira Pires (1993) and Oliveira Pires & Carvalho (1996). At the scale the data were extracted, MAR3G does not take into account effects of sheltering, refraction, heaving and energy dissipation due to friction. The swell statistics refer to a node off the Central Group (coordinates: 38ºN; 28ºW) considered to be representative of deep-ocean swell conditions.

The original data (at a 45º angular resolution) were used to interpolate directional spectra with a 15º resolution (Figure 3) that fitted the angular intervals at which fetch windows were computed.

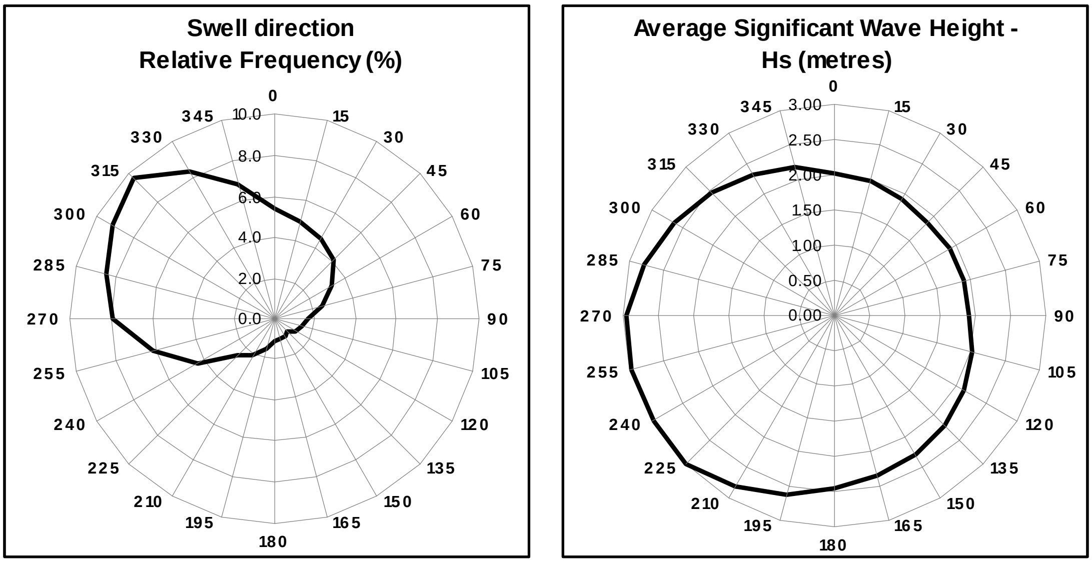

Figure 3: Direction spectrum and average swell height in Central Azores. A. Relative frequency of swell (percentage of days per year). B. Average significant wave height. All graphs use the meteorological convention ("from") for directions. Data credit: Carvalho (2003).

The data show that the Faial-Pico area is subject to prevailing swells from the NW and W, with the highest swells from the W-SW sector.

2.4. Computation of swell index

The fetch distances saved in the attribute table of the point shapefile were eventually exported into an Excel table. The exposure of each point to incoming waves was then computed by weighing each open direction with the average significant wave height ($\overline{H}_S$) incoming from that direction and the frequency (RF) at which waves come from that direction ($1\text{x}\,\overline{H}_S\,\text{xRF}$). Directions covered by obstacles were weighed with a 0 exposure. The numbers obtained at the directions each point is open to were then summed to obtain an "absolute exposure index". Finally these "absolute" numbers were divided by the maximum absolute exposure obtained within the point domain (standardization by maximum) to obtain the relative exposure index.

3. Results

The relative exposure index computed using the method detailed above was re-spatialised in the GIS environment so that the spatial distribution of exposure could be visualized and the new environmental layer could be intersected with the geo-referenced biological information. The exposure field produced is shown in Figure 4.

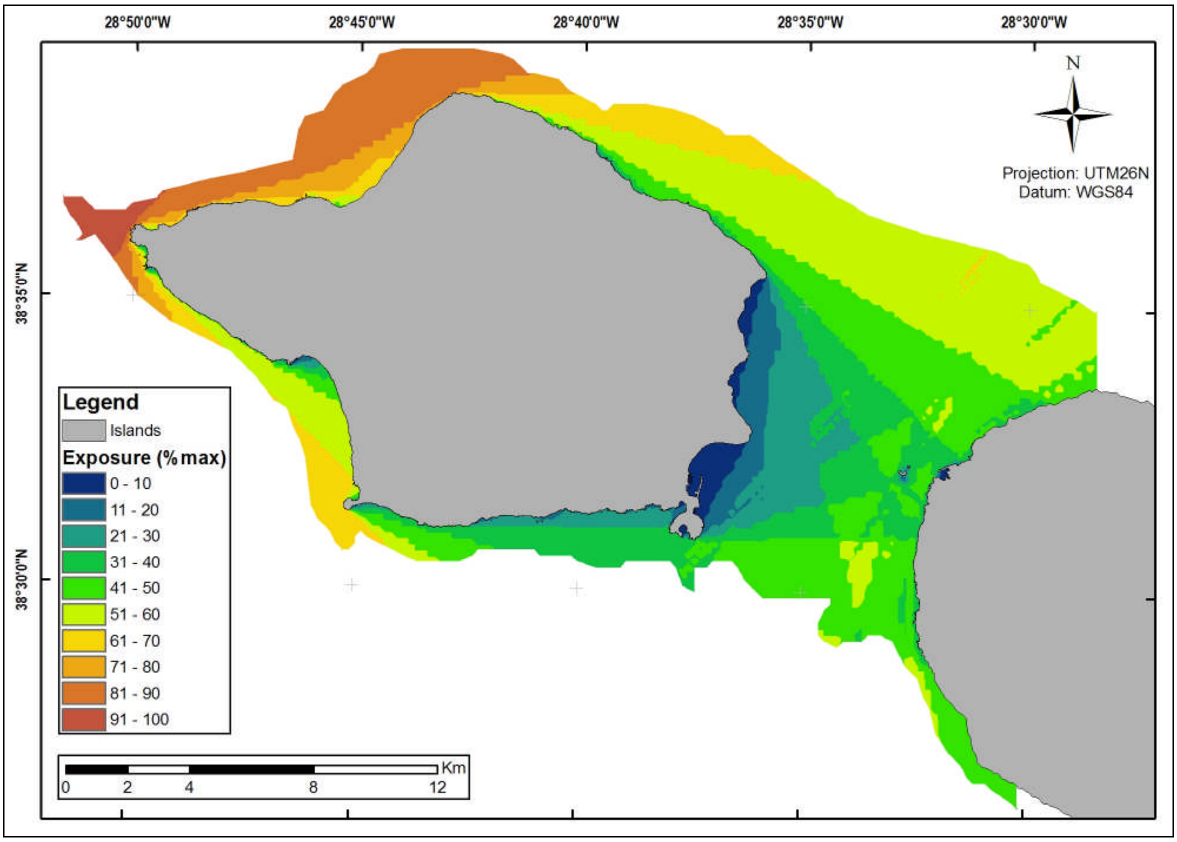

Figure 4: Swell exposure for Faial Island and neighbouring passage.

4. Suggestions for future enhancement

For a more realistic model it is suggested that a wave model is developed that includes the simultaneous effects of wave shoaling, refraction, and wave dissipation through bottom friction. Such approach would permit simulating how deep ocean waves approaching the coast are modified in their direction, height and other characteristics as they interact with the seafloor and coastline configurations. This could be done under MIKE 21 SW - a third generation spectral wind-wave model developed by DHI Water & Environment. This software system can simulate the growth, decay and transformation of swells in offshore and coastal areas.

The annual average wave conditions from each compass sector (e.g., directional spectra of wave height and period in Carvalho, 2003) could be used to recreate a typical swell incoming from each sector. An exposure index could then be computed from the weighed sum of the different sectorial wave conditions, where weight was represented by the relative frequency at which waves from each sector were observed in an average year cycle.

With such an approach, refraction effects could be accounted for, allowing for large swells to impinge on coastal sectors that are not directly exposed to the direction of incoming waves – an effect ignored by the GIS-based method using direct fetch only.

Refining the index should lead to better representation of the spatial variability of exposure to swell and eventually allow more effective predictive models that use swell-related effects as an explanatory variable.

5. References

Carvalho, F. (2003). *Elementos do clima de agitação marítima no Grupo Central dos Açores (Mar Alto).* Instituto de Meteorologia, Portugal, 98 pp.

Oliveira Pires, H. (1993). Modelação Numérica das Ondas Geradas pelo Vento. *PhD thesis*. IST, Universidade de Lisboa, 222pp.

Oliveira Pires, H. & F. Carvalho (1996). Fundamento e Características do Modelo de Ondas de Terceira Geração MAR3G. Instituto de Meteorologia, Lisboa, 38pp.

Puotinen, M.L. (2005a). An automated GIS method for modelling relative wave exposure within complex reef-island systems: a case study of the Great Barrier Reef. In: Zerger A, Argent RM (eds) Proceedings MODSIM05 International Congress on Modelling and Simulation. Modelling and Simulation Society of Australia and New Zealand, December 2005, p 1437–1443. Available at: www.mssanz.org.au/modsim05/papers/puotinen.pdf

Puotinen, M.L. (2005b). Tropical cyclone impacts on coral reef communities: Modelling the disturbance regime in the Great Barrier Reef Region, 1969-2003. *Ph.D. thesis*. James Cook University, Townsville, Australia.

6. Acknowledgements

To Pedro Maia and Dr. Fernando Carvalho (Instituto de Meteorologia, Portugal) for kindly providing the swell statistics dataset.

To Dr. Marji Puotinen (University of Wollongong) for her precious collaboration in extracting the fetch data for the vicinity of Faial using her AML™ Arc-Info™ script.

APPENDIX II

SPECIFICATIONS OF THE TIDAL-FORCED SHALLOW-WATER OCEANOGRAPHIC MODEL USED FOR FAIAL ISLAND

1. Introduction

Insight into current strength variability around Faial Island was required in order to implement the statistical modeling of biological communities. A proxy was developed for the maximum water current velocities impinging on benthic communities by setting up a simple shallow-water oceanographic model forced by the characteristics of a maximum astronomical tide. The construction of this model is detailed below.

1.1. Study area

Because of the volcanic origin of the archipelago, the oceanic islands of the Azores have very narrow shelves which abruptly break into island flanks. Shelf widths in the study area vary between 140 m and 4 km and the ensuing steep island flanks drop to depths beyond 1,300 m on the north and 800 m on the south.

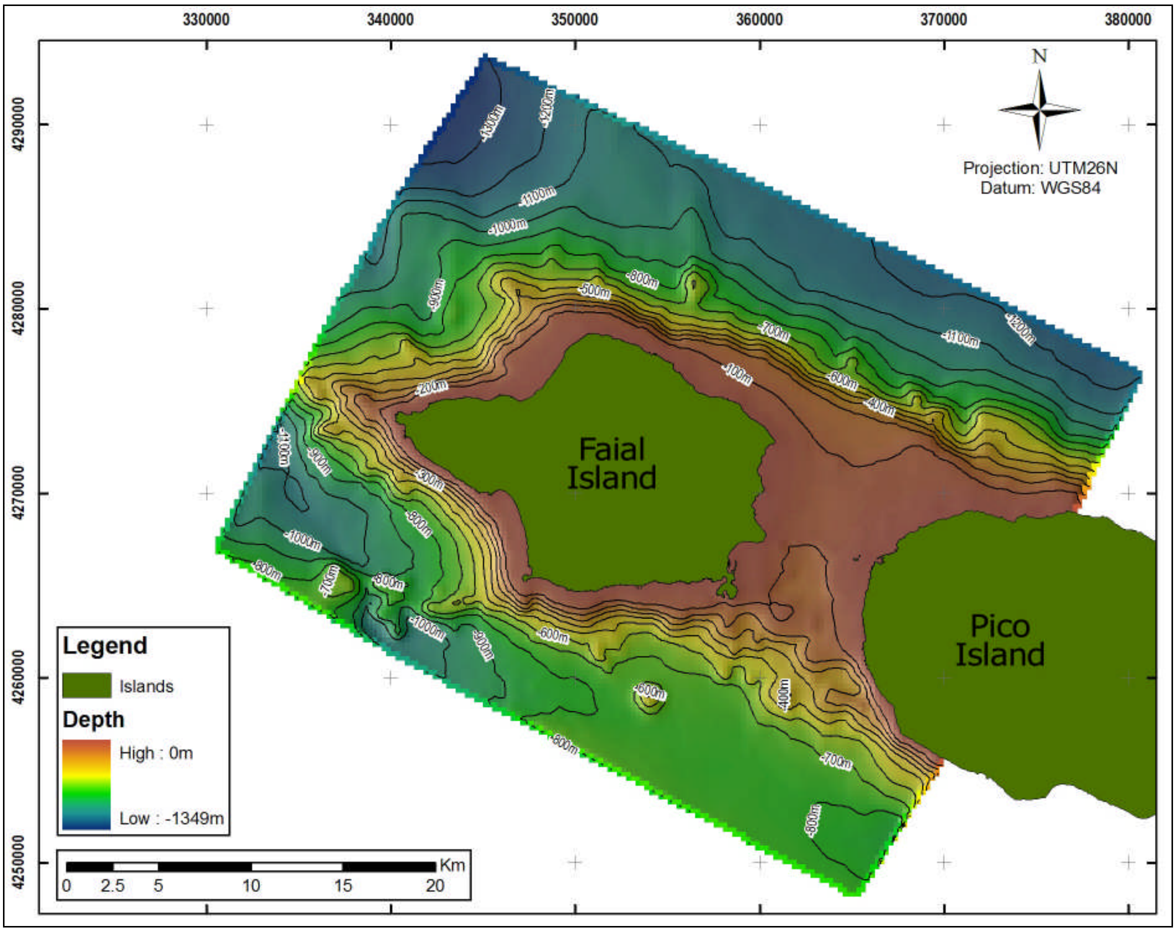

Figure 1: Physiography of the seafloor around Faial Island. Features of note include the inter-island shelf towards Pico and the steep drop of the island flanks.

Unlike the passages between other islands in the Azores, Faial island is separated from Pico island by a shallow 5km-wide passage which exhibits large expanses shallower than 100m. A sill straddling the narrowest section of this passage exhibits a maximum depth of 63m.
Although Faial island is subject to tidal ranging a maximum of 1.54 m, the passage physiography constrains tidal flows both vertically and horizontally, resulting in substantial current acceleration.

1.2. Objectives

The purpose of this work is to compute the free surface flow in the vicinity of Faial Island using a maximum astronomical tide as the forcing of water movements. Current fields are computed in TELEMAC and a field of the maximum currents observed at each node over a tide cycle is extracted after model stabilization.

2. Methodology

2.1. Cotidal chart

The interest in setting up the open model boundaries tangent to the cotidal contours required that a general cotidal chart was established for the vicinity of Faial. The relative differences between tidal times at a selection of Azorean harbours were used to interpolate the cotidal chart. From west to east, the harbours were: Lajes das Flores (Flores island), Horta (Faial isl.), Lajes do Pico (Pico isl.), Topo (São Jorge isl.), Angra do Heroísmo (Terceira isl.), Ponta Delgada (São Miguel isl.) and Vila do Porto (Santa Maria isl.). All of these stations are effectively or nearly open to the incoming tidal bulge.
The tidal times for the main harbours of Horta, Angra do Heroísmo, Ponta Delgada and Vila do Porto were extracted from the Portuguese Hydrographic Institute tide forecast webpage (as configured at http://www.hidrografico.pt/wwwbd/Mares/MaresPortosPrincipais). The relative time differences were standardized to the tide time in Horta harbour. The relative differences were obtained by averaging the time differences between them throughout a period of 12 lunar cycles (roughly one year). Relative time differences for the "secondary" harbours of Lajes das Flores, Lajes do Pico and Topo were obtained from Instituto Hidrográfico (2005).
The cotidal contours were obtained by interpolating the relative timings of the tides by using a bi-saddle polynomial in SURFER 8.0. The resulting field is shown in Figure 2, which illustrates how the tidal bulge arrives in the study area with a strike along a SSW-NNE axis (26° to the north in a UTM 26N WGS84 projection).

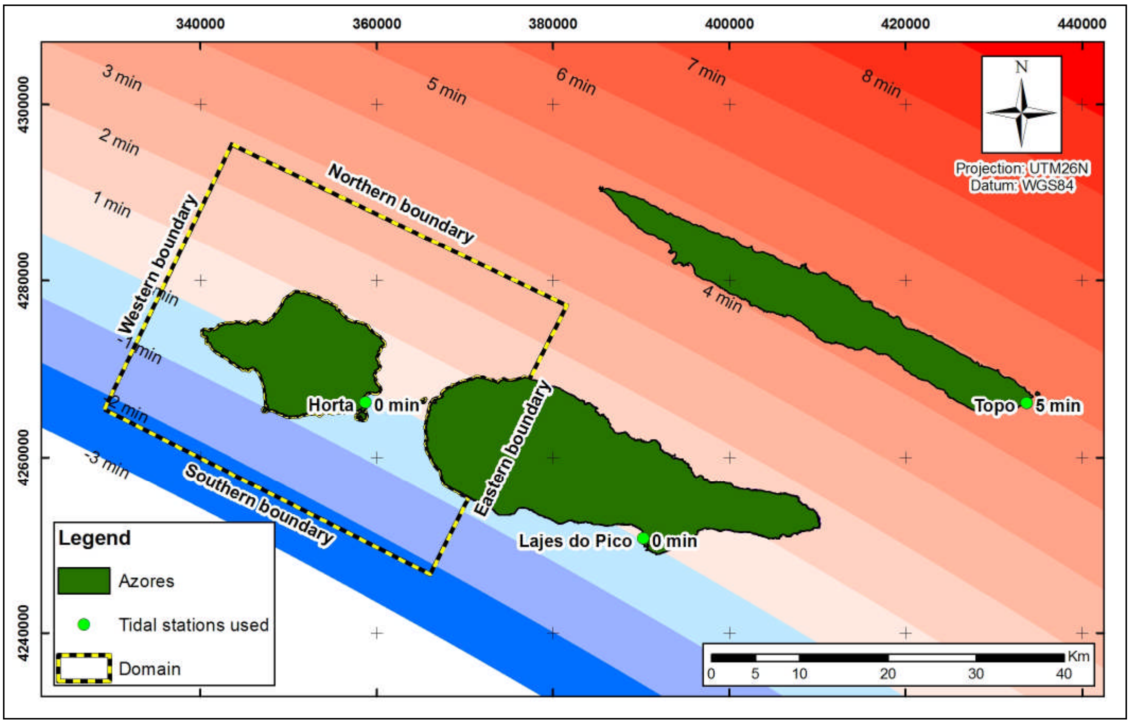

Figure 2: Cotidal chart for the study area.

2.2. TELEMAC software system

TELEMAC is a finite element-based, hydrodynamic software system developed by Electricité de France - Laboratoire National d'Hydraulique. The TELEMAC-3D module (release v.2P2) was used in the current work to solve fluid flow Navier-Stokes equations in a 3-dimensional space. The 3D space was subdivided in the form of an unstructured grid of triangular elements (the mesh). The software offers full flexibility to the user to introduce initial and boundary conditions and activate a variety of hydrostatic and non-hydrostatic options. Flooding and drying can be implemented, as well as atmospheric forcing such as through wind and pressure fields. A description of the TELEMAC model may be found at http://www.telemacsystem.com.

Due to a malfunction in the TELEMAC module used to visualize and extract vertically-discrete results, the results were extracted as vertically-averaged velocities using the TELEMAC RUBENS module (release v.4P1).

2.2.1. Model configuration

2.2.1.1. Mesh

The study domain was set as a rectangle defined around Faial at 500 m diagonal mesh resolution. Water depths at the mesh nodes vary between 0 m and 1,324 m.

2.2.1.1.1. 2D mesh

The 2D mesh was defined as follows :

- Number of 2D nodes: 5127
- Number of 2D elements: 9794
- Number of 2D boundary nodes: 460

2.2.1.1.2. 3D mesh

The 3D mesh was defined as follows :

- Number of vertical levels: 5 (equally spaced along the model's vertical extent)
- Number of 3D nodes: 25,635
- Number of 3D elements: 39,176
- Total number of boundary nodes: 12,554 (2,300 on the lateral boundaries + 5,127 on the surface + 5,127 on the bottom).

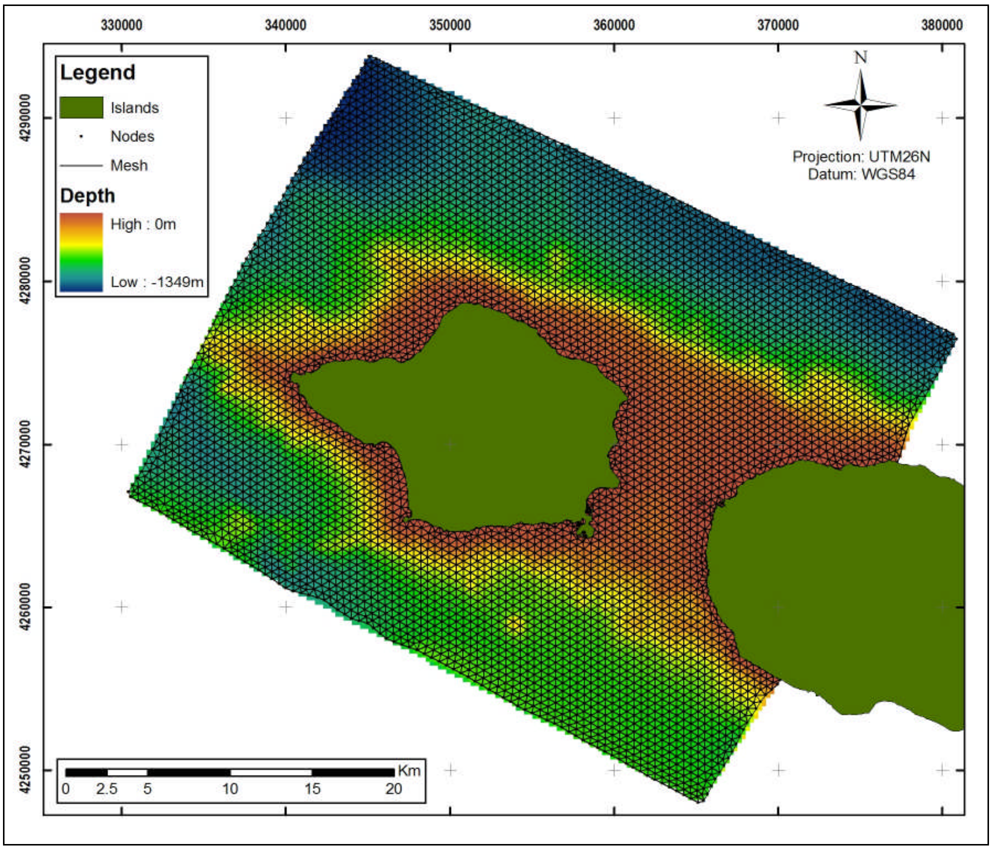

Figure 3: Diagonal mesh used for the vicinity of Faial Island. Resolution: 500m.

2.2.2. Boundary conditions

The southern and northern boundaries of the domain were set tangent to the cotidal lines modelled for the vicinity of Faial Island. They followed an angle of 116º to the north in a UTM 26N WGS84 projection. Such orientation is also close to that of the cotidal lines for the M2 harmonic component which dominated the semidiurnal tides in the area (FES2004 in Lyard et al, 2006). Such a setting permitted that no time differences had to be configured along each of the open tidal boundaries.

Both the oceanic and coastline lateral boundaries were set as solid closed boundaries (i.e., no flows were allowed across them) with sliding condition for velocities.

2.2.2.1. Characteristics of individual boundaries

- Southern boundary

  Type: open boundary with prescribed depth and free velocity (tidal)

  TELEMAC coding: LIHBOR=5 LIUBOR=4 LIVBOR=4 LITBOR=4

  Extension: between boundary point no. 1 and no. 80.

- Northern boundary

  Type: open boundary with prescribed depth and free velocity (tidal)

  TELEMAC coding: LIHBOR=5 LIUBOR=4 LIVBOR=4 LITBOR=4

  Extension: between boundary point no. 172 and no. 251.

- Western boundary

  Type: closed boundary (solid wall) with sliding condition defined by ϰ-ε model

  TELEMAC coding: LIHBOR=2 LIUBOR=2 LIVBOR=2 LITBOR=2

  Extension: between boundary point no. 252 and no. 312.

- Eastern boundary (including Pico island coastline)

  Type: closed boundary (solid wall) with sliding condition defined by ϰ-ε model

  TELEMAC coding: LIHBOR=2 LIUBOR=2 LIVBOR=2 LITBOR=2

  Extension: between boundary point no. 81 and no. 251.

- Faial island coastline

  Type: closed boundary (solid wall) with sliding condition defined by ϰ-ε model

  TELEMAC coding: LIHBOR=2 LIUBOR=2 LIVBOR=2 LITBOR=2

  Extension: between boundary point no. 313 and no. 460

2.2.3. Model driver

Faial island is subject to tides ranging a maximum of 1.54 m, as estimated from 2006 tidal tables (obtained from http://www.hidrografico.pt/wwwbd/Mares/MaresPortosPrincipais). A maximum astronomical tidal wave of amplitude=0.75m was therefore used to force the model. This wave was imposed at the southern border of the domain that forced the free surface to vary sinusoidally with a period of 12h30m (45,000 sec), as in a semidiurnal tide. The same free surface variation was imposed at the northern boundary but with a phase delay of 5 minutes (=300sec), as derived from the cotidal contours.

The following code was used in the FORTRAN file to impose the corresponding free surface fluctuations at the northern and southern boundaries of the model:

```
…
C****-------extra declarations ------****
      integer k, node1, node2, node3, node4
       double precision AT1,AT2, pi
C-------------------------------------------------------------------
       pi=3.141592653589D0
C
       AT1=AT/22500
       AT2=(AT+300)/22500
        node3 = 1
        node4 = 80
        node1 = 172
        node2 = 251
        do 10 k = node1, node2
      HBOR(K) = -zf(nbor(k)) - 0.75 + 0.75*COS(PI*AT1)
         HBOR(K) = DMAX1(0.D0,HBOR(K))
 10   CONTINUE
      do 11 k = node3, node4
      HBOR(K) = -zf(nbor(k)) - 0.75 + 0.75*COS(PI*AT2)
         HBOR(K) = DMAX1(0.D0,HBOR(K))
 11  CONTINUE
 …
```

2.2.4. Steering file

The synthax of the TELEMAC-3D steering file is show below.

```
/---------------KEYWORD STEERING FILE FOR TELEMAC3D -------------
/------------------FILES --------------------------------
FORTRAN FILE                  : './azore4.f'
STEERING FILE            : './azor-tide75cm7.str'
BOUNDARY CONDITIONS FILE : './azore.bdy'
GEOMETRY FILE              : './azore.geom'
COMPUTATION CONTINUED = YES
PREVIOUS COMPUTATION FILE   : './azor3D-tide75cm6'
3D RESULT FILE          : azor3D-tide75cm7
2D RESULT FILE          : azor2D-tide75cm7
TELEMAC-3D RELEASE: V2P2
NUMBER OF HORIZONTAL LEVELS :5
/--------------------------------------------------------------------/
/                   OPTIONS GENERALES
/--------------------------------------------------------------------/
TITLE = 'TELEMAC 3D: Faial Isl., +-75cm sine tide with high tide at CD'
VARIABLES FOR 2D GRAPHIC PRINTOUTS : 'U,V,H,B,E,D,S,M'
VARIABLES FOR 3D GRAPHIC PRINTOUTS :
'U,V,W,K,EPS,NUX,NUY,NUZ,RHO'
TIME STEP = 30.0
NUMBER OF TIME STEPS = 4500
GRAPHIC PRINTOUT PERIOD = 125
LISTING PRINTOUT PERIOD = 10
CORIOLIS = NO
TIDAL FLATS : YES
/--------------------------------------------------------------------/
/    PROPAGATION
/--------------------------------------------------------------------/
PRECONDITIONING FOR DIFFUSION OF VELOCITIES : 2
TURBULENCE MODEL : 3
SOLVER FOR PROPAGATION : 7
MAXIMUM NUMBER OF ITERATIONS FOR PROPAGATION : 250
NUMBER OF SUB ITERATIONS FOR NON LINEARITIES : 2
&ETA
&FIN
```

The most important non-default configurations are the choice of a κ-ε turbulence model (TURBULENCE MODEL=3), the use of diagonal preconditioning for the diffusion of velocities (PRECONDITIONING FOR DIFFUSION OF VELOCITIES=2) and the selection of a generalised minimum residual (GMRES) solver for the propagation (SOLVER FOR PROPAGATION=7).

All the other major configurations (most of them left in default) are summarized below:

DEPTH
TIDAL FLATS = YES (This treatment removes elements which are not entirely wet from the calculations, avoiding the creation of parasitic driving terms in the shallowest areas from each water is absent in certain periods of the tide)
TREATMENT ON TIDAL FLATS FOR VELOCITIES = 0 (forced to zero)
TREATMENT ON TIDAL FLATS FOR K-EPSILON = 0 (forced to zero)
CLIPPING DE H= YES
MINIMAL VALUE FOR DEPTH = 1.000000E-02
VALEUR MINIMUM DE H = 1.0E-07
MEAN DEPTH FOR LINEARIZATION = 0
INITIAL GUESS FOR DEPTH = 1 (Initial guess for the solver in the propagation step. This makes it possible to modify the initial value of C, upon each iteration in the propagation step, by using the ultimate values this variable had in the earlier time steps. Thus, the convergence can be speeded up when the system is being solved)

OTHER EFFECTS
CORIOLIS = NO (no effects from the Coriolis force)
WIND = NO (no wind effects)
COEFFICIENT OF WIND INFLUENCE = 0
AIR PRESSURE = NO (no effects from the atmospheric pressure)

PROPAGATION
TIME STEP FOR PROPAGATION = 30.0 (seconds)
NUMBER OF TIME STEPS = 45000
SOLVER FOR PROPAGATION = 3 (Generalised minimum residual; Default would be "conjugate gradient on a normal equation")
SOLVER OPTION = 3 (size of the Krylov space) (with solver option 7 one can define also this parameter setting it between 2 and 7)
PRECONDITIONING FOR PROPAGATION = 2 (diagonal)
MAXIMUM NUMBER OF ITERATIONS FOR PROPAGATION = 250 (NOT DEFAULT. Note: Default would be 60)
ACCURACY FOR PROPAGATION = 0.1000000E-03
LINEARIZED PROPAGATION = NO
TIME STEP FOR CONSOLIDATION = 1200.000
NUMBER OF SUB ITERATIONS FOR NON LINEARITIES = 2 (Used for updating, within one time step, the advection and propagation field upon the first sub-iteration, these fields are given by C and the velocity field in the previous time step. At subsequent iterations, the results of the previous sub-iteration are used to update the advection and propagation field. Non-linearities can be accounted for through this technique)

DIFFUSION
DIFFUSION = YES
TYPE DE SOLVEUR POUR LA DIFFUSION = 1
TYPE DE PRECONDITIONNEMENT POUR LA DIFFUSION = 7
SCHEME FOR DIFFUSION OF VELOCITIES = 1 (implicit)
SOLVER FOR DIFFUSION OF VELOCITIES = 1 (conjugate gradient)
IMPLICITATION FOR VELOCITIES = 1 (fixes the values of the implicitation coefficient in the propagation step)
PRECONDITIONING FOR DIFFUSION OF VELOCITIES = 2 (diagonal; Default would be 7 (crout))
COEFFICIENT FOR HORIZONTAL DIFFUSION OF VELOCITIES = 0.1000000E-03
MAXIMUM NUMBER OF ITERATIONS FOR DIFFUSION OF VELOCITIES = 60
ACCURACY FOR DIFFUSION OF VELOCITIES = 0.1000000E-05

CONVECTION
CONVECTION= YES
CONVECTION DE U ET V= YES
SCHEME FOR ADVECTION OF VELOCITIES = 1 (characteristics method)
SCHEME FOR ADVECTION OF DEPTH= 5 (conservative; variants of the Streamline Upwind Petrov-Galerkin, or SUPG, scheme are applied to the continuity equation)

VERTICAL VELOCITY
SOLVER FOR VERTICAL VELOCITY= 1 (conjugate gradient)
COEFFICIENT FOR VERTICAL DIFFUSION OF VELOCITIES = 1.0E-04
PRECONDITIONING FOR VERTICAL VELOCITY = 2 (diagonal)
ACCURACY FOR VERTICAL VELOCITY = 1.0E-04
MAXIMUM NUMBER OF ITERATIONS FOR VERTICAL VELOCITY = 100
IMPLICITATION FOR DEPTH = 0.55

K-EPSILON
DIFFUSION OF K-EPSILON = YES
SCHEME FOR DIFFUSION OF K-EPSILON = 1 (implicit)
SOLVER FOR DIFFUSION OF K-EPSILON = 1 (conjugate gradient)
MAXIMUM NUMBER OF ITERATIONS FOR DIFFUSION OF K-EPSILON = 60
PRECONDITIONING FOR DIFFUSION OF K-EPSILON= 7 (crout)
ACCURACY FOR DIFFUSION OF K-EPSILON = 1.0 E-06
ADVECTION OF K-EPSILON = YES
SCHEME FOR ADVECTION OF K-EPSILON = 1 (characteristics)

TURBULENCE AT BOUNDARIES
TURBULENCE MODEL FOR THE BOTTOM = 3 (rough with Chézy coefficient)
FRICTION COEFFICIENT FOR THE BOTTOM = 60
TURBULENCE MODEL FOR LATERAL SOLID BOUNDARIES = 3 (rough with Chézy coefficient)
FRICTION COEFFICIENT FOR LATERAL SOLID BOUNDARIES = 60

PHYSICAL CONSTANTS
GRAVITY ACCELERATION= 9.810000
DENSITY FOR STANDARD VALUE= 1025.000
AIR TEMPERATURE = 10.00000

3. Results

3.1. Field extraction

Current fields were extracted after the model was stabilized. This was considered to happen at the end of 2 tidal cycles (*t=90,000 sec*). Vertically-averaged current velocity fields were then extracted for the next 3 tide cycles (*t=93,750 sec to t=225,000 sec*) at a period of 3,750 sec (i.e., 1/12th of a complete tide cycle).

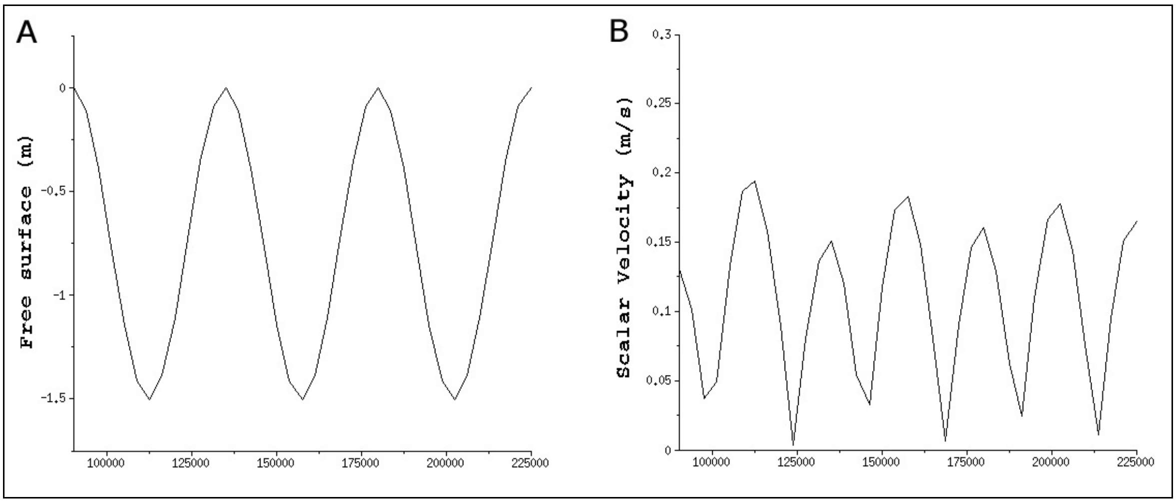

Figure 4: Variation of free surface height (A) and current velocity (B) between *t=90,000 sec* (i.e., 25h after the initiation of the model) and *t=225,000 sec* (i.e., 62h30m after the initiation of the model) in a mid passage node (coordinates; X=362,937m; Y=4,266,350m).

Figure 5 to Figure 8 show current velocity fields extracted at different modeling steps.

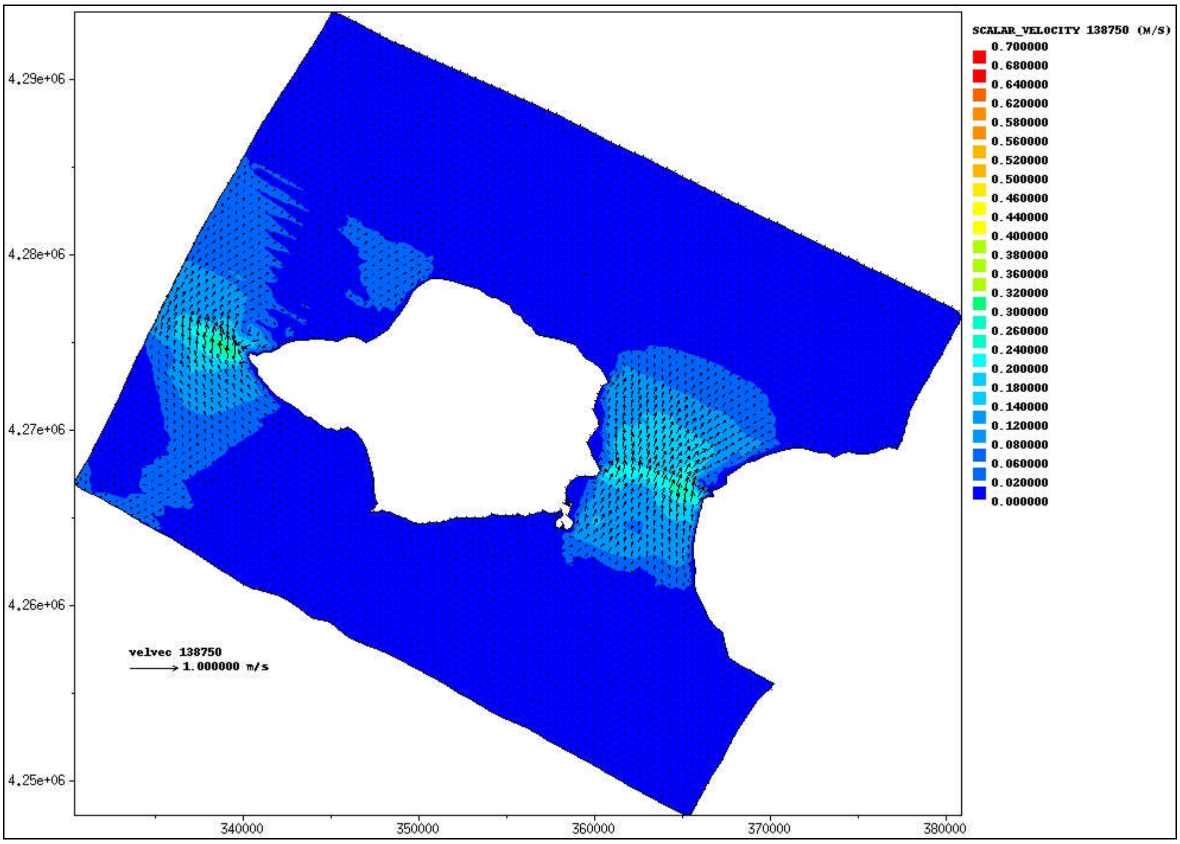

Figure 5: Vertically-integrated current velocity field at *t = 138,750 sec*. Flooding tide.

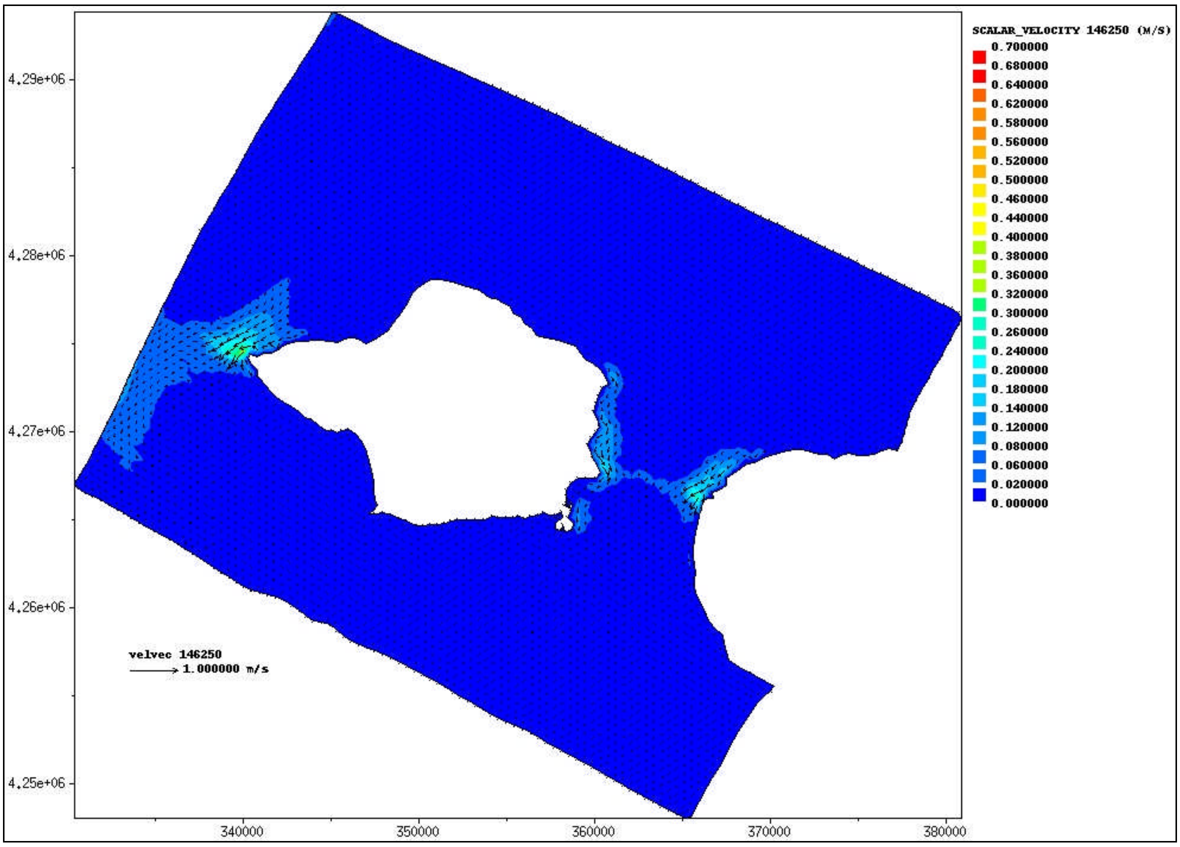

Figure 6: Vertically-integrated current velocity field at *t = 146,250 sec*. End of high tide.

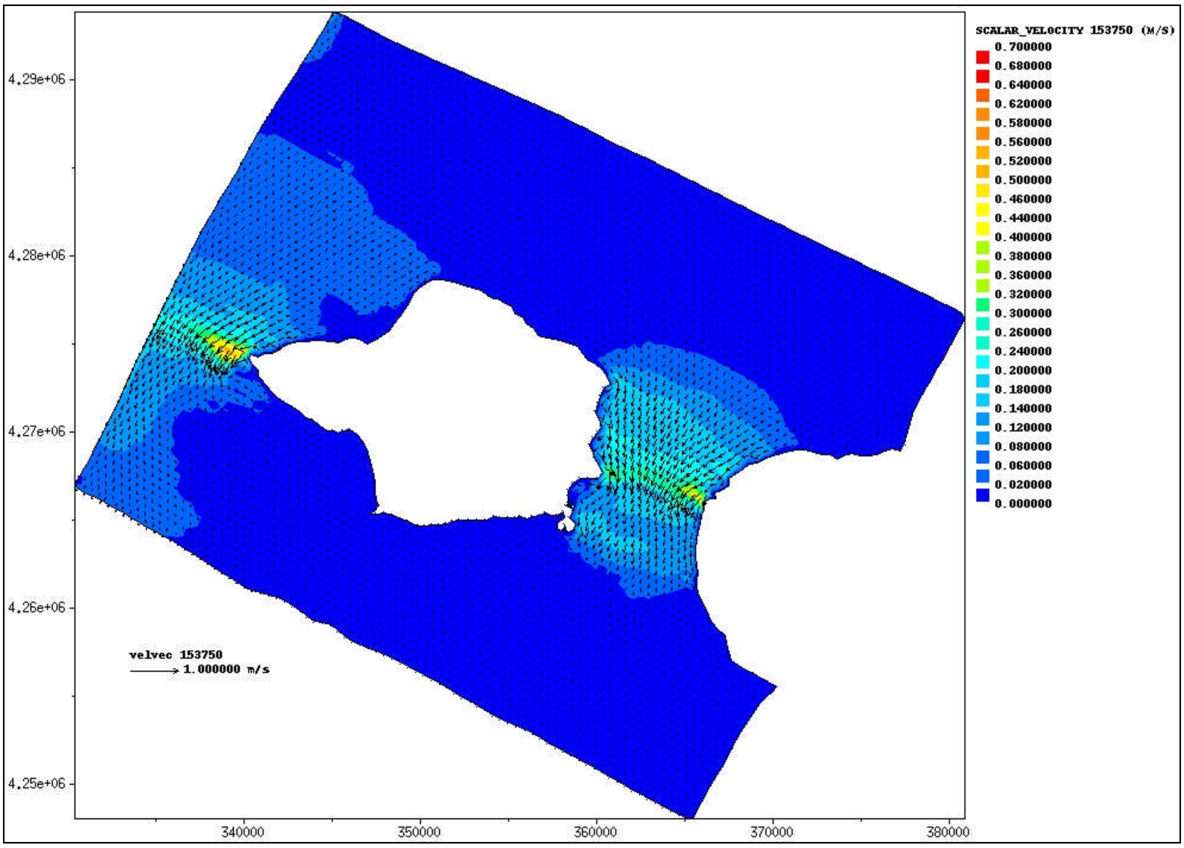

Figure 7: Vertically-integrated current velocity field at *t=153,750 sec*. Ebbing tide.

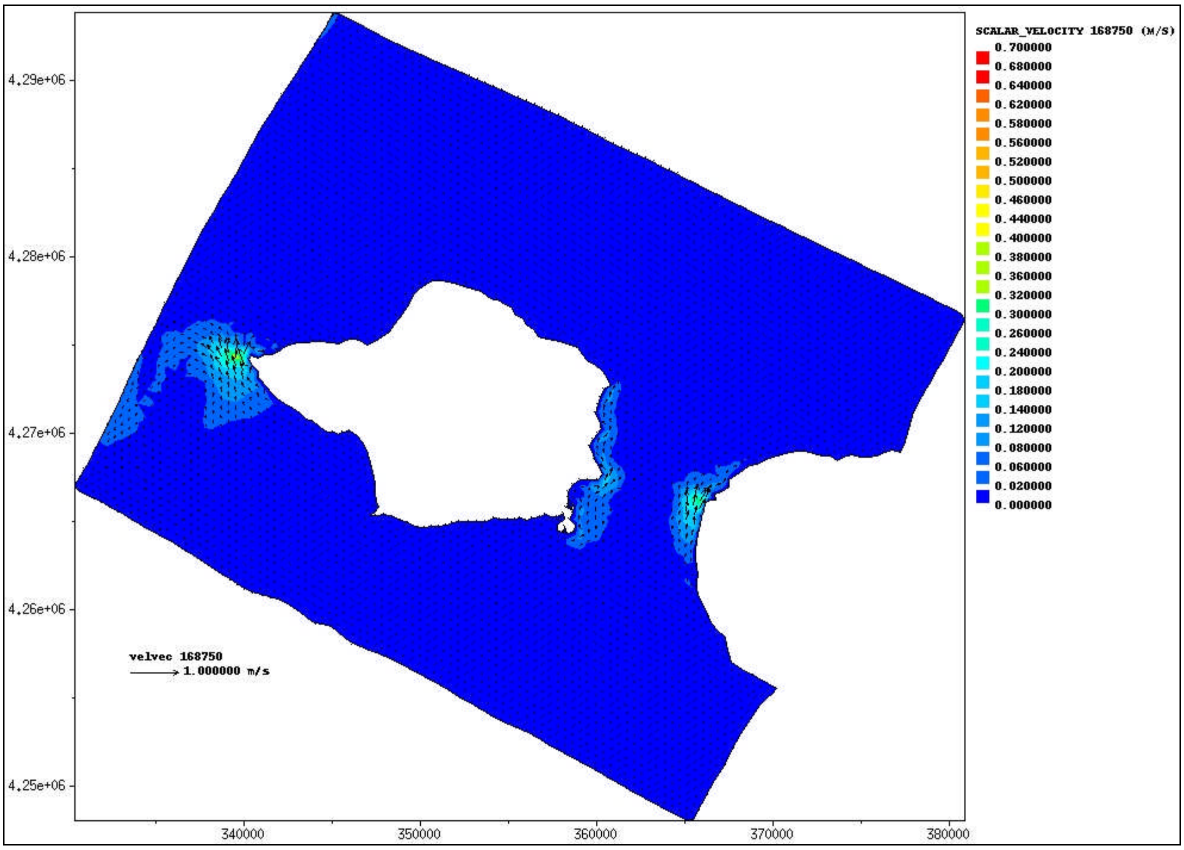

Figure 8: Vertically-integrated current velocity field at *t=168,750 sec*. End of low tide.

Maximum current velocities observed at each node between *t=93,750 sec* and *t=225,000 sec* were extracted and used to build the field shown in Figure 9.

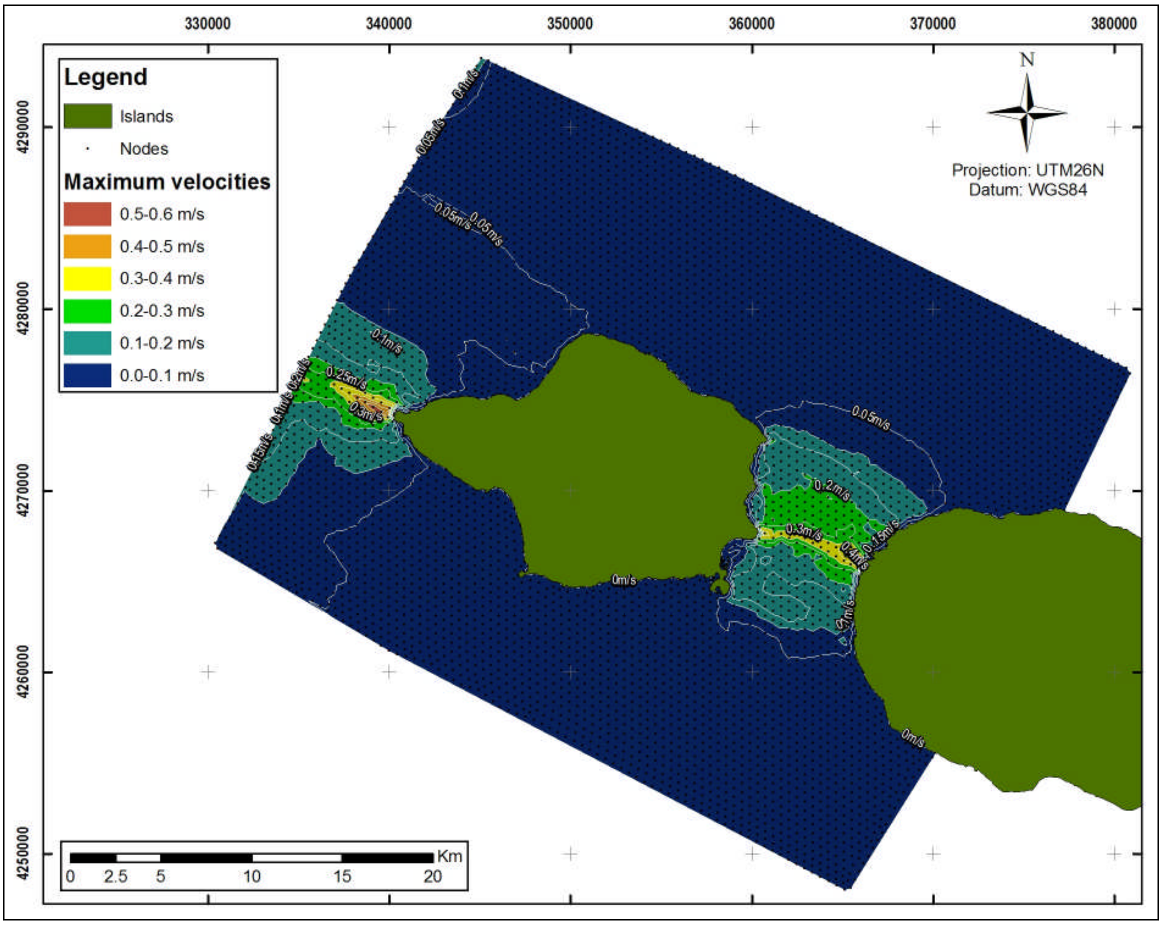

Figure 9: Maximum current velocity field.

3.2. Model Validation

No vertically-integrated *in situ* observations were available at the time of model validation that could be used to compare simulated currents to field measurements. If available this would have allowed for a calibration of the model configuration (e.g., friction coefficients) and would likely enhance the model performance.

It is noted that the maximum depth-integrated current velocities predicted by the model (0.54 m/s) underestimate the actual currents observed in the passage, which preliminary data provided by a recently deployed mid-passage mooring showed could reach 0.8-0.9 m/s at 120 m depth (Bashmachnikov, unpublished data).

In light of this comparison, the results were rather considered in their relative form, i.e., by standardizing the values obtained by the maximum. This maximum current layer produced was then intersected with the locations of biological sampling stations in the GIS environment to provide information about the maximum currents impinging on each site that could have an influence on biological occurrences.

Although the option to use a standardized by maximum current index rather than absolute current velocities prevented tying the statistical models of species abundance to actual current velocities, it was considered that the standardized index did provide a more robust proxy of how the current strength is distributed around the island in relative terms.

3.3. Suggestions for future model refinement

Refining the current model should lead to a better representation of the spatial variability of currents and eventually allow more effective predictive models that use this as an explanatory variable. In order to achieve this, some suggestions are listed below:

- Attach the tidal fluctuations to the mean sealevel (Note: in the current version of the model tides were made to fluctuate around a datum set 1.83m below mean sea level to avoid the appearance of artificial currents across solid boundaries when higher sea levels were used);
- Develop a wider tidal-forced regional domain and use it to feed the nodes of the local model at its open boundaries;
- Use the results of this regional model to feed the western and eastern oceanic boundary nodes and avoid establishing them as solid walls;
- Calibrate the model with *in situ* measurements;
- Extract vertically-explicit information, namely for the near-bed stratum;
- Enhance the resolution of the underlying bathymetric mesh;
- Obtain a stabilized model that takes into account the Coriolis acceleration;
- Consider bottom type zonation and the respective effect on bed-generated friction.

4. References

Instituto Hidrográfico. 2005. *Tabela de Marés 2006*. Instituto Hidrográfico, Lisboa. vi+196 pp.

Lyard, F., F. Lefèvre, T. Letellier & O. Francis. 2006. Modelling the global ocean tides: modern insights from FES2004. *Ocean Dynamics*, 56: 394-415. With respective grid data at http://www.aviso.oceanobs.com/html/donnees/produits/auxiliaires/fes_uk.html.

5. Acknowledgements

To Dr. Jack Jarvis for his critical support with setting up the model in TELEMAC.

To Dr. Igor Bashmachnikov for sharing current meter data collected in the mid-passage mooring.

The AVISO products are produced by SSALTO/DUACS and distributed by AVISO with support from CNES.

Appendix III

RELATIONSHIP BETWEEN DEPENDENT AND INDEPENDENT VARIABLES

The relationship between the abundance (dependent variable) and the potential explanatory variables is shown in Figure 1 to Figure 6. Quadratic regression curves with confidence intervals are fitted simply to facilitate the identification of the dominant trend. Where data overlap in the scatterplot, the size of the points increases to convey a sense of data density.

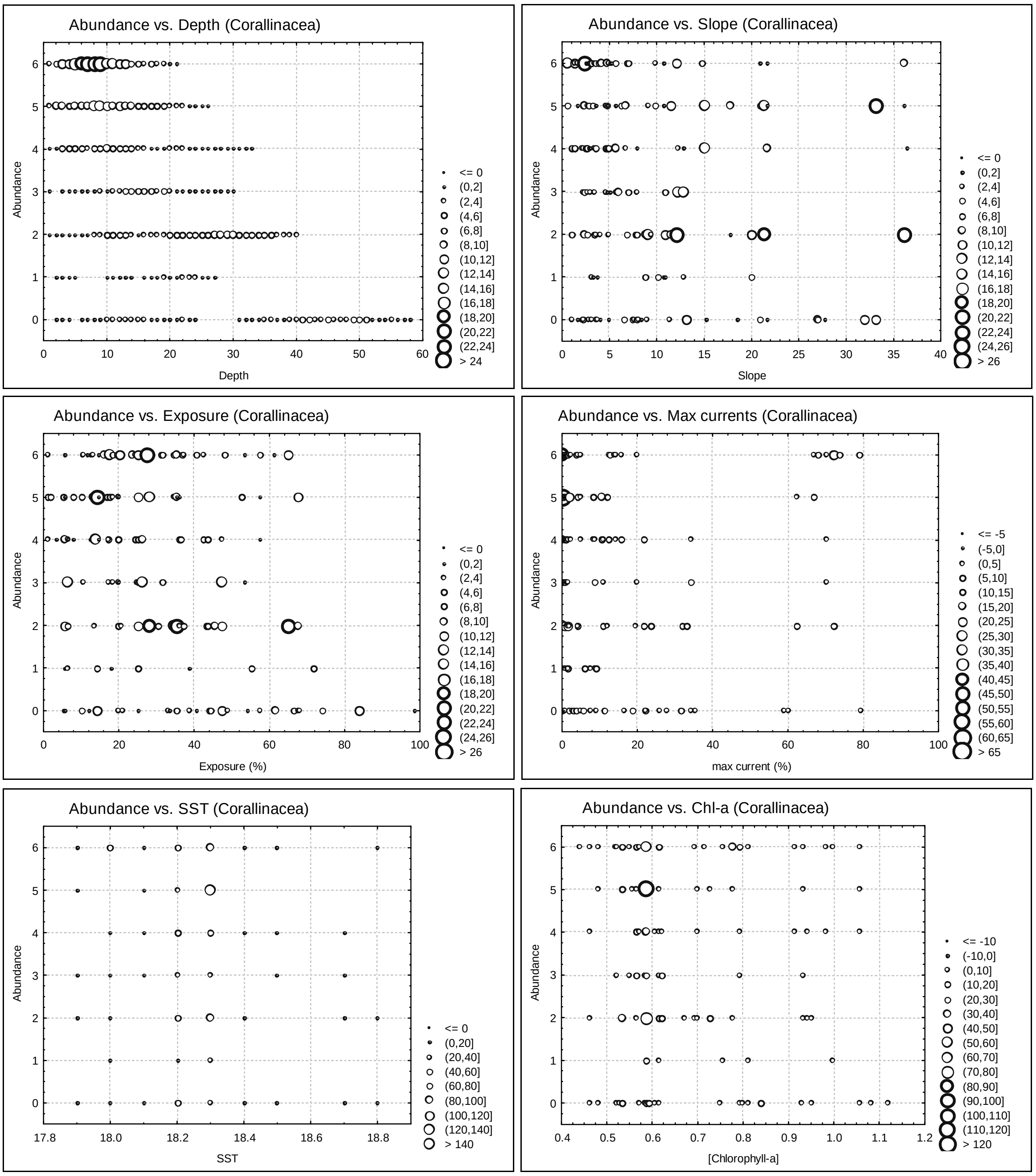

Figure 1. Articulated Corallinacea: frequency scatterplots of abundance (YY axis) *vs.* potential explanatory variables (XX axis).

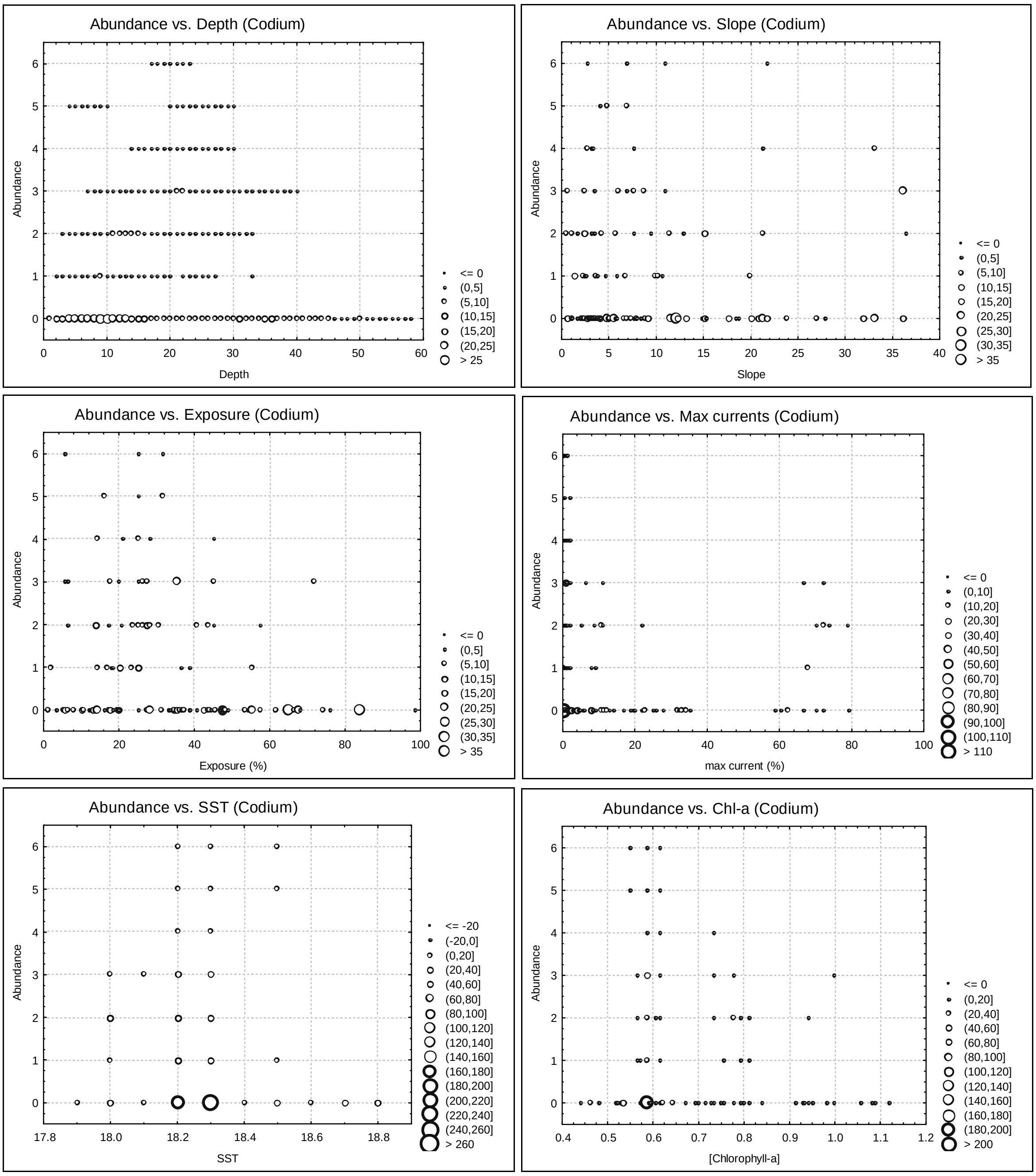

Figure 2. ***Codium elisabethae*****: frequency scatterplots of abundance (YY axis)** ***vs*****. potential explanatory variables (XX axis).**

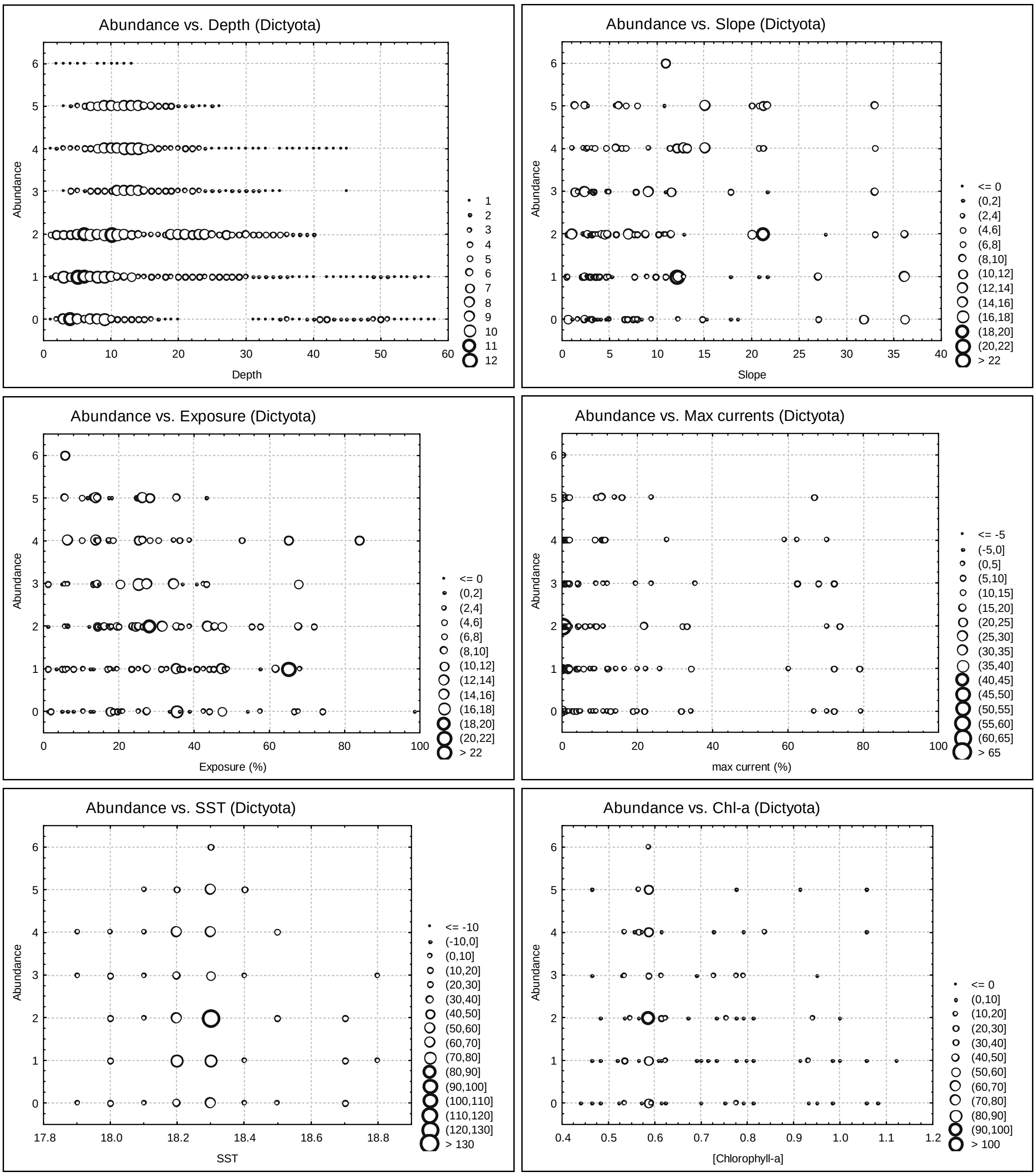

Figure 3. ***Dictyota*** **spp.: frequency scatterplots of abundance (YY axis)** ***vs.*** **potential explanatory variables (XX axis).**

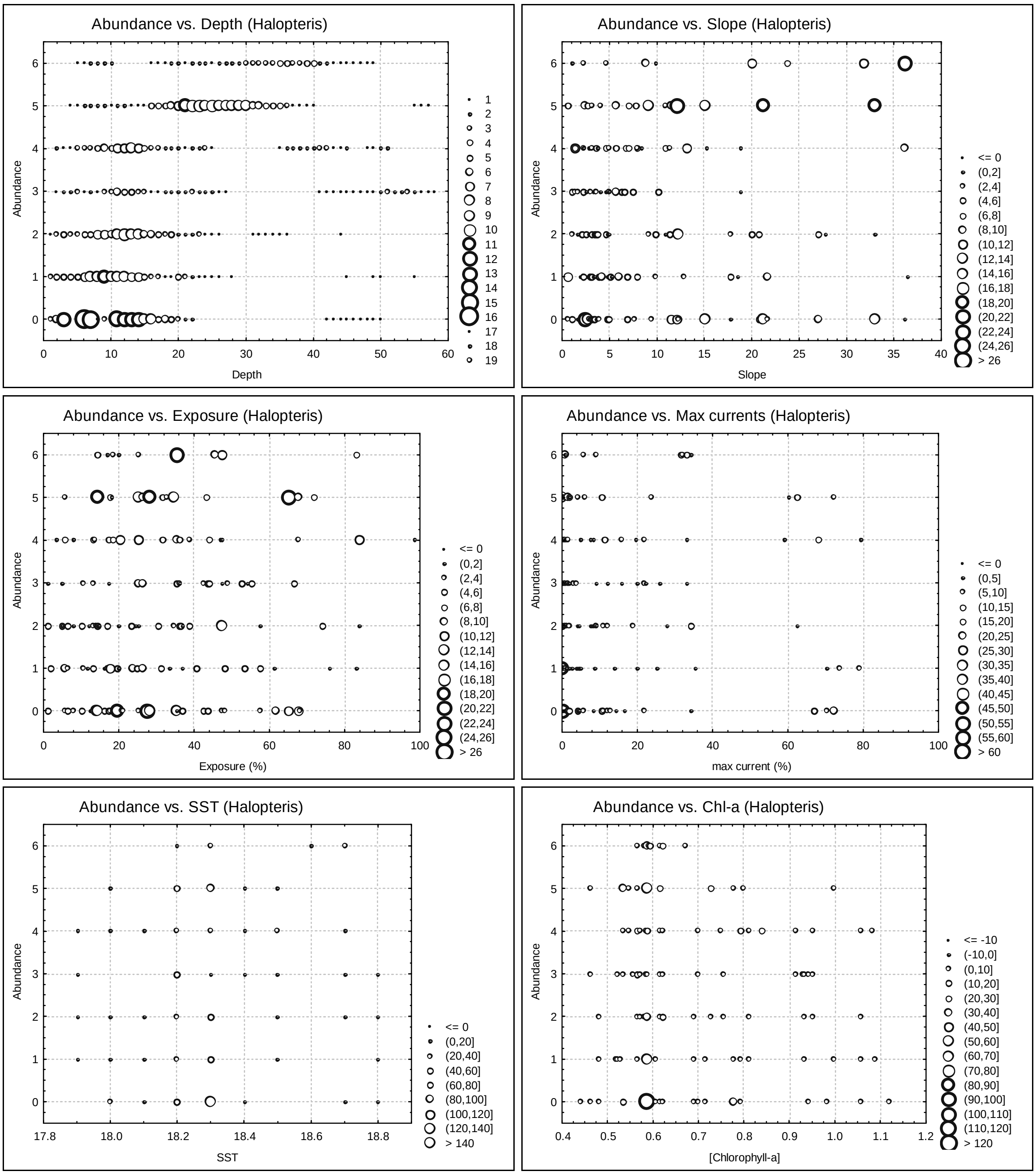

Figure 4. ***Halopteris filicina*****: frequency scatterplots of abundance (YY axis)** ***vs*****. potential explanatory variables (XX axis).**

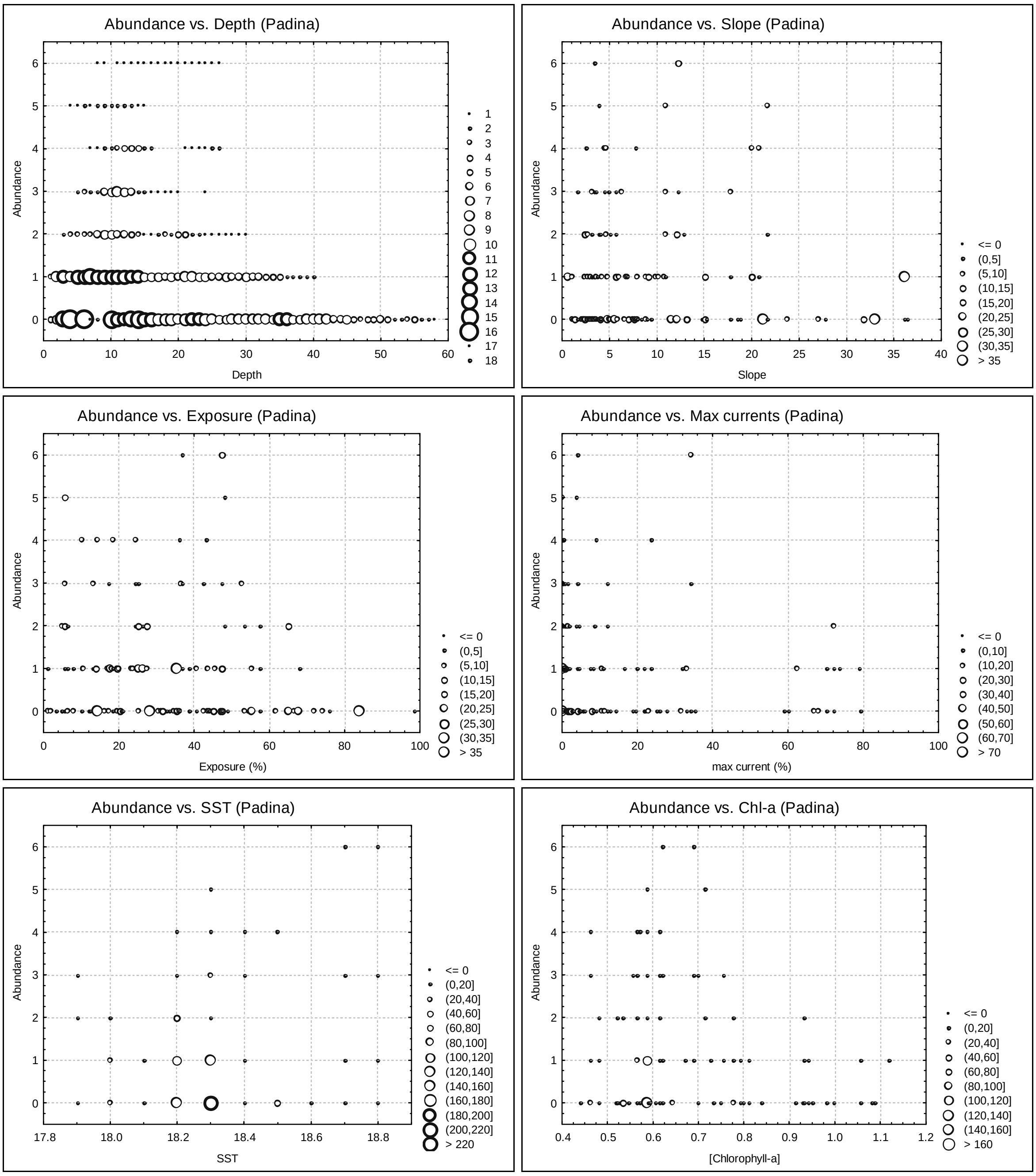

Figure 5. ***Padina pavonica*****: frequency scatterplots of abundance (YY axis)** ***vs*****. potential explanatory variables (XX axis).**

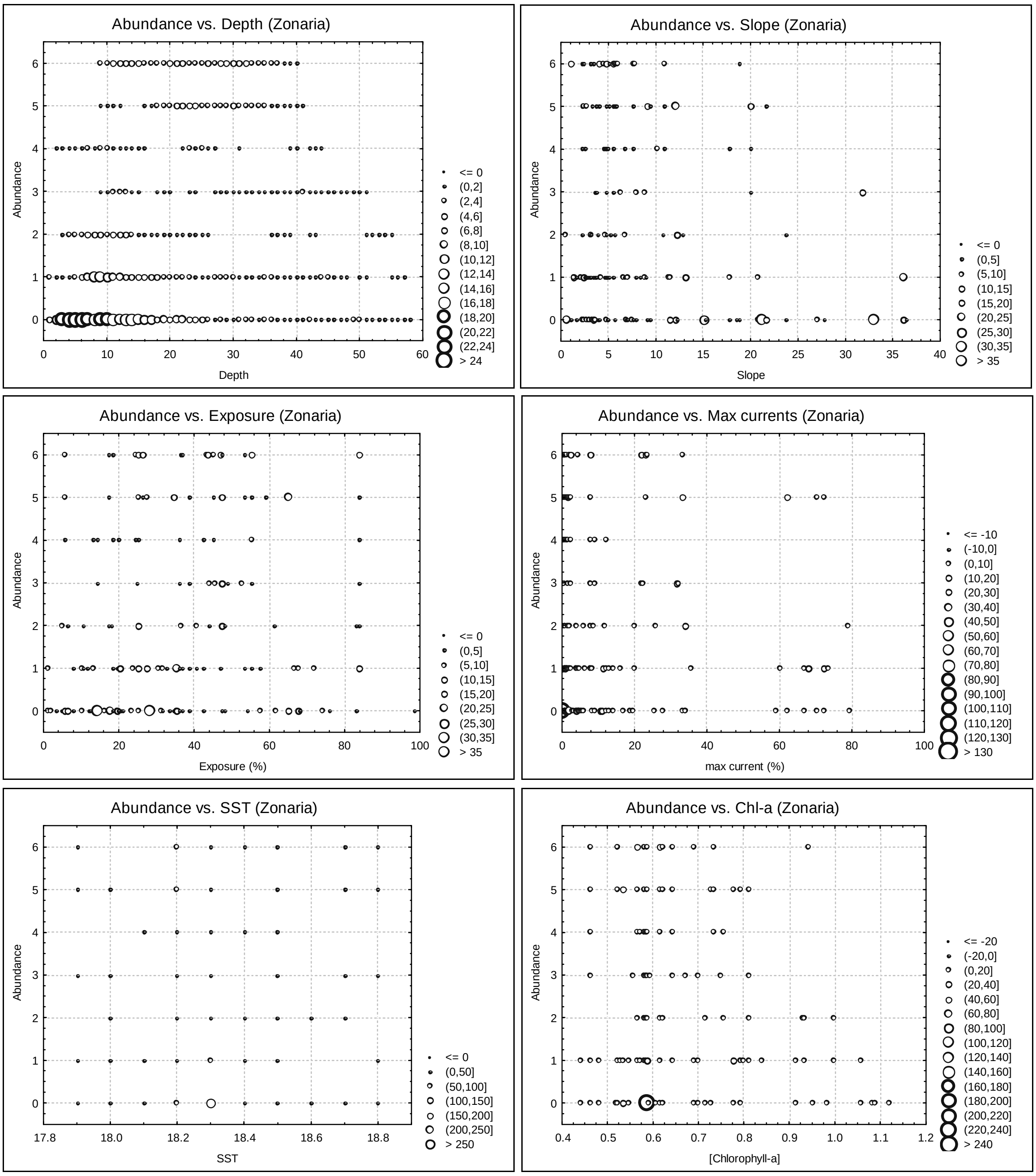

Figure 6. *Zonaria tournefortii*: frequency scatterplots of abundance (YY axis) *vs.* potential explanatory variables (XX axis).

Appendix IV

TRANSFORMATION OF THE EXPLANATORY VARIABLES

The final multivariable fractional polynomial models used to transform explanatory variables based on their non-linear relationship with the response variable are presented in Table 1 to Table 6.

Table 1. Articulated Corallinacea: fractional polynomial transformations applied to explanatory variables.

Variable	Depth (dep)	Slope (sl)	Exposure to swell (expsw)
Alpha	0.05	0.05	0.05
Status	in	in	in
Df	6	6	4
Powers	3 3 3	1 1 1	1 1
Transformation	Idep__1 = X^3-4.943547063 Idep__2 = X^3*ln(X)-2.633399676 Idep__3 = X^3*ln(X)^2-1.402797175 (where: X = dep/10)	Isl__1 = X-1.032461206 Isl__2 = X*ln(X)-.0329824612 Isl__3 = X*ln(X)^2-.0010536403 (where: X = sl/10)	Iexps__1 = X-3.033981354 Iexps__2 = X*ln(X)-3.367342287 (where: X = expsw/10)

Variable (continuation)	Exposure to current (expcur)	Chlorophyll-*a* concentration (chla)
Alpha	0.05	0.05
Status	in	in
Df	2	1
Powers	3	1
Transformation	Iexpc__1 = X^3-2.393203142 (where: X = (expcur+.0999999046325684)/10)	Ichla__1 = chla-.6434632895

Table 2. *Codium elisabethae*: fractional polynomial transformations applied to explanatory variables.

Variable	Depth (dep)	Slope (sl)	Exposure to currents (expcur)
Alpha	0.05	0.05	0.05
Status	in	in	in
Df	4	4	4
Powers	2 2	2 3	1 3
Transformation	Idep__1 = X^2-3.902118123 Idep__2 = X^2*ln(X)-2.656404986 (where: X = dep/10)	Isl__1 = X^2-1.103520727 Isl__2 = X^3-1.159233017 (where: X = sl/10)	Iexpc__1 = X-1.420993498 Iexpc__2 = X^3-2.869302072 (where: X = (expcur+.0999999046325684)/10)

Table 3: *Dictyota* spp.: fractional polynomial transformations applied to explanatory variables.

Variable	Depth (dep)	Slope (sl)
Alpha	0.05	0.05
Status	in	in
Df	6	4
Powers	2 2 2	2 2
Transformation	Idep__1 = X^2-2.884479796 Idep__2 = X^2*ln(X)-1.527829005 Idep__3 = X^2*ln(X)^2-.8092486804 (where: X = dep/10)	Isl__1 = X^2-1.068232393 Isl__2 = X^2*ln(X)-.0352545068 (where: X = sl/10)

Table 4. ***Halopteris filicina*: fractional polynomial transformations applied to explanatory variables.**

Variable	Depth (dep)	Slope (sl)	Exposure to swell (expsw)
Alpha	0.05	0.05	0.05
Status	in	in	in
Df	6	4	1
Powers	3 3 3	3 3	1
Transformation	Idep__1 = X^3-5.794615499 Idep__2 = X^3*ln(X)-3.393576244 Idep__3 = X^3*ln(X)^2-1.987424313 (where: X = dep/10)	Isl__1 = X^3-1.183273455 Isl__2 = X^3*ln(X)-.0663756108 (where: X = sl/10)	Iexps__1 = expsw-31.83865064

Table 5. ***Padina pavonica*: fractional polynomial transformations applied to explanatory variables.**

Variable	Depth (dep)	Exposure to current (expcur)
Alpha	0.05	0.05
Status	in	in
Df	4	6
Powers	1 1	3 3 3
Transformation	Idep__1 = X-1.890686275 Idep__2 = X*ln(X)-1.204253472 (where: X = dep/10)	Iexpc__1 = X^3-2.242996916 Iexpc__2 = X^3*ln(X)-.603973933 Iexpc__3 = X^3*ln(X)^2-.1626326408 (where: X = (expcur+.0999999046325684)/10)

Variable (continuation)	Chlorophyll-*a* concentration (chla)
Alpha	0.05
Status	in
Df	6
Powers	3 3 3
Transformation	Ichla__1 = chla^3-.260604999 Ichla__2 = chla^3*ln(chla) +.1168161414 Ichla__3 = chla^3*ln(chla)^2 -.0523628133

Table 6. ***Zonaria tournefortii*: fractional polynomial transformations applied to explanatory variables.**

Variable	Depth (dep)	Slope (sl)
Alpha	0.05	0.05
Status	in	in
Df	4	4
Powers	2 2	2 2
Transformation	Idep__1 = X^2-3.690343403 Idep__2 = X^2*ln(X)-2.409276703 (where: X = dep/10)	Isl__1 = X^2-1.012695493 Isl__2 = X^2*ln(X)-.0063878711 (where: X = sl/10)